LCH

Communication 14

Wall Roughness Effects on Flow and Scouring in Curved Channels with Gravel Bed

Daniel S. Hersberger

Communications du Laboratoire de constructions hydrauliques
Ecole Polytechnique Fédérale de Lausanne
Editeur: Prof. R. Sinniger

N°	1	1986	W. H. Hager Discharge measurement structures
N°	2	1988	N. V. Bretz Ressaut hydraulique forcé par seuil
N°	3	1990	R. Bremen Expanding stilling basin
N°	4	1996	Dr R. Bremen Ressaut hydraulique et bassins amortisseurs, aspects hydrauliques particuliers
N°	5	1997	Compte-rendu du séminaire à l'EPFL Recherche dans le domaine des barrages, crues extrêmes

Communications du Laboratoire de constructions hydrauliques
Ecole Polytechnique Fédérale de Lausanne
Editeur: Prof. Dr A. Schleiss

N°	6	1998	N. Beyer Portner Erosion des bassins versants alpins suisse par ruissellement de surface
N°	7	1998	G. De Cesare Alluvionnement des retenues par courants de turbidité
N°	8	1998	J. Dubois Comportement hydraulique et modélisation des écoulements de surface
N°	9	2000	J. Dubois, J.-L. Boillat Routing System - Modélisation du routage de crues dans des systèmes hydrauliques à surface libre
N°	10	2002	J. Dubois, M. Pirotton Génération et transfert des crues extrêmes - Le logiciel Faitou
N°	11	2002	A. Lavelli, G. De Cesare, J.-L. Boillat Modélisation des courants de turbidité dans le bassin Nord du Lac de Lugano
N°	12	2002	P. de Almeida Manso Stability of linings by concrete elements for surface protection of overflow earthfill dams
N°	13	2002	Erik Bollaert Transient water pressures in joints and formation of rock scour due to high-velocity jet impact
N°	14	2002	Daniel S. Hersberger Wall Roughness Effects on Flow and Scouring in Curved Channels with Gravel Bed

PREFACE

Flow behaviour and scouring in bends of sediment-transporting rivers is a topic on which researchers all over the world have focussed for some time. Scouring in river bends is the result of a rather complex, 3-dimensional flow pattern, which is normally assessed in practice by analytical-empirical methods derived mainly from laboratory tests. Most of these tests were carried out for almost uniform grain size distribution and rather small bed slopes. With the research described in the present communication, Dr. Daniel Hersberger filled up a considerable gap towards a better scientific understanding of the scouring process in bends of rather steep mountain rivers. A large number of systematic tests were performed using a wide and coarse grain size distribution in a 90°-curved channel. Furthermore, for the first time, the effect of a macro-roughness placed on vertical walls along a bend on the scour formation was considered.

The systematic tests carried out with a sophisticated test facility and novel data acquisition revealed that a considerable grain sorting process occurs across the cross section in the bend, which influences the scour process. The flow velocity measurements confirmed the presence of a main and a secondary circulation cell in the cross section. These tests proved and showed, that the maximum scour depth is considerably reduced by vertical ribs placed at an optimal spacing on the outer wall of the bend.

A new scour formulae derived by innovative methods, predicts the maximum scour depth as well as the cross section shape better than the known relationships. It also takes into account the grain size distribution and the effect of macro-roughness elements (vertical ribs) placed on the outer wall. Finally, Dr. Daniel Hersberger gives helpful recommendations for design engineers, which allow for the appropriate estimation of the maximum scour depth, the transversal bed slope and the locations of the scour as well as the choice of the optimum spacing of the vertical ribs on the outer wall with the purpose of reducing scour depth.

Prof. Dr. Anton J. Schleiss

PREFACE

L'écoulement et l'érosion dans les courbes de rivières à lit mobile est un sujet de recherche traité depuis un certain temps par de nombreux chercheurs à travers le monde. L'affouillement en courbe est le résultat d'un écoulement-3D assez complexe. La profondeur et l'extension de cette érosion sont en général estimées en pratique à l'aide de formules empiriques, obtenues essentiellement par des essais en laboratoire. La plupart de ces essais sont effectués avec une granulométrie quasi-uniforme et pour des faibles pentes du lit. Par la recherche décrite dans la présente communication, le Dr Daniel Hersberger a comblé une lacune importante, permettant de mieux comprendre scientifiquement le processus d'affouillement en courbe des rivières de montagne à pente élevée. Un De nombreux essais systématiques ont été effectués dans un canal caractérisé par une courbe à 90°, en utilisant un gravier grossier à granulométrique étendue. Pour la première fois, l'influence sur l'écoulement et l'érosion de nervures verticales disposées contre le mur de la rive extérieure a été considérée.

Les essais systématiques effectués dans une installation équipée d'un système d'acquisition de données très sophistiqué ont montré un tri granulométrique important dans la section en courbe, qui influence le processus d'affouillement. Les mesures de vitesse ont confirmé la présence de deux cellules d'écoulements secondaires dans la section transversale. Les essais ont également montré que la profondeur maximale d'érosion le long du mur de rive extérieur est réduite de manière significative par des nervures disposées avec un espacement optimal.

Une nouvelle formule empirique obtenue par des méthodes innovatrices a été proposée. Elle permet de prédire les érosions maximales et la topographie des sections concernées avec plus de réalisme et de précision que les formules existantes. Elle tient également compte d'une granulométrie étendue et de l'effet des éléments de macro-rugosités (nervures verticales) fixés sur le mur extérieur. Finalement le Dr Daniel Hersberger propose des recommandations utiles pour les ingénieurs praticiens, qui permettent d'estimer d'une manière appropriée l'affouillement maximal, le profil en travers du lit et l'emplacement de l'érosion ainsi que le choix de l'espacement optimal des nervures verticales à placer contre le mur extérieur dans le but de réduire la profondeur d'érosion.

Prof. Dr Anton Schleiss

Abstract

Wall roughness effects on flow and scouring in curved channels with gravel bed

In the narrow valleys in Alpine regions, rivers frequently flow across constructed zones, passing through villages and cities. Due to limited space, the protection from high floods often needs to be ensured by protection walls. During floods, these protection walls may be endangered by scour phenomena, especially if they are located in bends. In the past, the potential danger of under-scoured structures was reduced by sufficient foundation depth.

By providing roughness elements such as vertical ribs at the surface of walls located at the outer side of river bends, the local erosion along the foot of the wall can be considerably decreased, reducing the cost of wall foundations. Such observations were made during the review and optimization of several flood protection projects with hydraulic model tests in Switzerland. A literature review showed, that no systematic study of the influence of these ribs on scour and flow in bends was performed up to this day (§ 2). This research project covers this gap by investigating the development of the scour as a function of main parameters.

The study is based on an experimental investigation in a 90° bend with a radius of 6 m including measurements of the velocities, the water level, the bed topography, the sediment characteristics, the grain size distribution of the armoring layer, the discharge and the bed load (§ 4 and 5). The large set of tests covers a wide range of discharges, bed slopes, rather high Froude numbers, but in subcritical regimes, many rib spacings and depths. The formation of two scour holes was observed. Without macro roughness, a first scour hole occurs in the prolongation of the inner sidewall of the entry reach at the outer wall and a second scour hole appears at the end of the 90° bend.

The analysis of the performed tests results in the following conclusions:
- Most existing scour formulae considerably underestimate the scour depth in mountain rivers with coarse gravel bed (§ 3).
- Significant oscillations, both of the free water surface (stationary waves) and of the scour depth were observed, especially for the second scour hole.
- The two scour holes have different reasons. The first one is essentially due to the change of the main flow direction (impact on the wall) and the induced secondary current, whereas the second one is mainly due to increased velocity fluctuations after the point bar formed at the inner side of the channel (§ 6).
- In the average flow field in a bend, the highest main velocities are shifted from the center-line close to the surface toward the outer wall and then towards the bottom (§ 6). At the first scour, the highest main velocities are found next to the ground.
- A significant grain sorting process is observed over the cross-section due to the use of coarse gravel mixture, resulting in the accumulation of coarse sediments at the outer wall and depositions of fine material on the inner bank.

Abstract

By applying vertical ribs on the outer sidewall, an important impact on the scour process and on the flow field can be observed (§ 6). The macro-roughness has the following effects:

- The scour depth along the outer sidewall is significantly reduced and the prominent scours almost disappear.
- With increasing wall roughness, the first scour hole shifts in the downstream direction whereas the second one remains at about the same position.
- Significant oscillations of the water surface and the scour depth, observed without macro-roughness, are reduced by about 50% and the scour develops in a "smoother" way.
- The flow field undergoes a pronounced modification: the highest velocities are kept away from the outer sidewall, reducing the scour at the bottom of the outer wall foundations.
- Along the outer wall at the free surface, an secondary flow cell at the outer bank can be observed. The importance of this cell shows an important correlation with the bank protection effect.
- Optimum rib spacing is essential since an inappropriate spacing may lead to an important increase in scour depth.
- The transport capacity in the bend is reduced. In natural rivers, this phenomenon is compensated by a steepening of the bed slope.
- The upstream and downstream extremities of the bend are influenced by the ribs: upstream of the bend, the water depth increases due to the head losses in the bend, and downstream, some additional erosion is found in the center of the channel.
- The grain sorting process is not significantly influenced by the presence of the ribs beside an increase of the area of the coarse sediment zone.

This report furthermore presents a new empirical scour formula for the estimation of the maximum scour depth for mountain rivers with wide grain size distribution (§ 7), established with physically based parameters, which are the ratio mean water depth to channel width, a dimensionless ratio combining the mean velocity with the hydraulic radius and finally the friction angle of the bed material. The lateral bed profile in the maximum scour cross section can also be computed with this equation.

An estimation of the maximum scour depth in the presence of macro-roughness on the outer wall can be obtained with a formula depending on the rib spacing, the hydraulic radius, the Froude number and the difference between the dimensionless shear stress and the critical Shields parameter (§ 7).

Finally recommendations for hydraulic engineers (§ 8.3) are given to facilitate the application of vertical ribs on outer banks serving as macro-roughness.

Keywords:

Sediment transport in curved channels, scouring in bends, mountain rivers, laboratory tests, grain sorting process, coarse gravel bed, wide grain size distribution, armoring, mean velocity flow field, macro-roughness, vertical ribs

Résumé

Influences de la rugosité des murs de rive sur l'écoulement et l'érosion de canaux courbes avec lit de gravier

Dans les vallées étroites des Alpes, des rivières traversent fréquemment des zones construites. En raison des surfaces limitées, la sécurité contre les crues doit être assurée par des murs de protection. Pendant les crues, ces murs peuvent être mis en danger par l'érosion, plus particulièrement s'ils se situent en courbe. Dans le passé, cette menace a été contrecarrée par une profondeur de fondation suffisante.

La présence de macro-rugosités sur les rives extérieures des méandres dans les rivières de montagne permet de réduire fortement la profondeur d'érosion et ainsi le coût des fondations. Ce phénomène a déjà pu être observé sur des modèles réduits reproduisant des murs de rive nervurés. La revue bibliographique montre qu'il n'existe à ce jour pas d'étude systématique de l'influence de ces nervures sur l'érosion et l'écoulement en courbe (§ 2). La présente recherche comble cette lacune par l'étude du développement de l'érosion en fonction des paramètres hydrauliques et géométriques principaux.

L'étude se base sur des expériences effectuées dans une courbe à 90° avec un rayon à l'axe de 6 m, dans lequel les paramètres suivants ont été mesurés: le champ de vitesse, les niveaux d'eau, la topographie du lit, les caractéristiques des sédiments, la distribution granulométrique de la couche de pavage, les débits liquides et de charriage (§ 4 et 5). Le grand nombre d'essais couvre une large gamme de débits, de pentes longitudinales à des nombres de Froude proche de 1, mais toujours en régime fluvial ainsi que de nombreux espacements et profondeurs de nervures. La formation de deux fosses d'érosion a pu être observée. Sans macro-rugosité, une première fosse apparaît dans la prolongation du mur de rive intérieur à l'intersection avec le mur extérieur; une deuxième fosse se forme à la sortie du virage.

L'analyse des tests effectués aboutit aux conclusions suivantes:
- La plupart des équations d'érosions existantes sous-estime la profondeur d'érosion de manière significative pour des rivières de montagnes avec un lit grossier.
- Des oscillations importantes de la surface libre (ondes stationnaires) et de la profondeur d'érosion ont été observées, particulièrement au droit de la deuxième fosse d'érosion.
- Les deux fosses résultent de phénomènes différents. La première est due au changement de la direction principale de l'écoulement (impact sur la paroi) et du courant secondaire qui en résulte. La deuxième est essentiellement due à l'accroissement des fluctuations de vitesse derrière le banc de gravier qui se forme sur la rive intérieure du canal (§ 6).
- Dans le champ de vitesse en courbe, les vitesses les plus élevées se déplacent de la surface libre au centre du canal vers le mur extérieur où elles plongent vers le fond (§ 6). Dans la première fosse d'érosion, les vitesses tangentielles sont les plus importantes à proximité du fond.
- Un tri granulométrique important peut être observé dans le profil en travers dû à l'utilisation d'une granulométrie étendue avec des gros graviers: les gros particules s'accumulent vers la paroi extérieure et des fines sur le banc en rive intérieure.

Résumé

En disposant des nervures verticales sur le mur de rive extérieur, une influence marquante sur le processus d'érosion et sur l'écoulement peut être observée (§ 6). La macro-rugosité a les effets suivants:

- La profondeur d'érosion le long du mur de rive extérieur est réduite de manière significative et les fosses d'érosion sont considérablement atténuées.
- En augmentant la rugosité du mur de rive, la première fosse d'érosion se déplace vers l'aval, tandis que la deuxième reste à peu près au même endroit.
- Les oscillations considérables de la surface libre et de la profondeur d'érosion, observées sans les nervures, sont réduits de 50% environ et l'érosion de développe d'une manière plus douce.
- Le champ de vitesse subit des modifications importantes: les vitesses les plus élevées sont éloignées du mur extérieur, ce qui réduit l'érosion au pied de fondation de murs de protection.
- Le long du mur de rive extérieur, une cellule secondaire peut être observé près de la surface libre. Sa taille montre une corrélation significative avec la réduction d'érosion.
- Un espacement des nervures optimal est primordial, puisqu'une distance entre nervures non adaptée peut conduire à une augmentation de l'érosion.
- La capacité de transport en courbe est réduite. Dans des rivières naturelles, ce phénomène est compensé par une augmentation de la pente longitudinale.
- Les extrémités amont et aval du virage sont également influencées par les nervures: à l'amont, la hauteur d'eau augmente due aux pertes de charge en courbe et à l'aval on trouve de l'érosion supplémentaire à l'axe du canal.
- Le tri granulométrique n'est pas influencé de manière significative. Seule la taille de la surface sur laquelle les gros graviers s'accumulent augmente.

Hormis ces observations, le rapport présente une nouvelle équation d'érosion empirique, basée sur des paramètres physiques, pour l'estimation de la profondeur d'érosion maximale dans des rivières de montagne avec une granulométrie étendue (§ 7). Ces paramètres sont la hauteur d'eau moyenne rapportée à la largeur du canal, un paramètre combinant la vitesse moyenne de l'écoulement au rayon hydraulique et finalement l'angle de frottement des sédiments composant le lit. La topographie du profil en travers à l'endroit de l'érosion maximale peut être approchée par la même équation.

L'estimation de la réduction de l'érosion due à la présence de la macro-rugosité peut être effectuée à l'aide d'une relation dépendant de l'espacement entre les nervures, du rayon hydraulique, du nombre de Froude et de la différence entre la tension de frottement adimensionnelle effective (paramètre de Shields) et sa valeur critique (§ 7).

Finalement des recommandations pour les ingénieurs praticiens (§ 8.3) sont données afin de faciliter la mise en place de nervures sur des murs de rive, comme éléments de macro-rugosité.

Mots clés

Transport de sédiments en courbe, érosion en courbe, rivières de montagne, essais en laboratoire, tri granulométrique, lit formé de gros graviers, pavage, champs de vitesses moyennes, macro-rugosité, nervures verticales

Zusammenfassung

Einfluss der Wandrauhigkeit auf Strömung und Kolke in Kurven geschiebeführender Kanäle

In den engen Tälern des Alpenraumes durchqueren Fliessgewässer häufig Siedlungsgebiete. Ufernahe Infrastrukturanlagen und Gebäude entlang dieser Gebirgsflüsse sind keine Seltenheit. Wegen den engen Platzverhältnissen muss die Hochwassersicherheit der Anlieger oftmals mit Ufermauern gewährleistet werden. Diese Ufermauern sind während extremen Hochwasserereignissen durch Unterkolkung gefährdet, insbesondere wenn sie sich in einer Flusskrümmung befinden. In der Vergangenheit wurde dieser Kolkgefahr mit einer genügenden Fundationstiefe begegnet.

Erste Erfahrungen bei Hochwasserschutzprojekten haben gezeigt, dass die Kolktiefen entlang gekrümmter Ufermauern sehr wirksam durch Anordnung von Makrorauhigkeitselementen vermindert und damit kostspielige Aushübe für tiefliegende Mauerfundamente vermieden werden können. Dies konnte im Rahmen von systematischen Laborversuchen bestätigt werden, die im Folgenden beschrieben werden. Ein Literaturstudium hat aufgezeigt, dass der Einfluss von senkrechten Rippen auf Kolk und Strömung noch nie systematisch untersucht wurde (§ 2). Dieses Forschungsprojekt schliesst diese Lücke indem der Kolkprozess in Abhängigkeit der grundlegenden Parameter untersucht wird.

Die Studie basiert auf Experimenten in einem 90° gekrümmten Kanal mit einem Radius von 6 m bei welchen das 3D-Geschwindigkeitsfeld, die Wasserspiegellagen, die Sohlentopographie, die Sedimentcharakteristika, die Kornverteilung der Deckschicht, der Abfluss sowie die Geschieberaten gemessen wurden (§ 4 und 5). Die umfangreichen Tests decken ein weites Spektrum an Abflüssen, Gefällen bei recht hohen Froudezahlen, jedoch fliessenden Strömungsbedingungen sowie verschiedenen Rippenabständen und -tiefen ab. Ohne Makrorauhigkeit entsteht ein erstes Kolkloch in der Verlängerung der inneren Seitenwand des Einlaufs, ein zweites tritt am Bogenende auf.

Die Analyse der Versuche erlaubt folgende Schlussfolgerungen:
- Die meisten bestehenden Kolkformeln unterschätzen die Kolktiefen in Gebirgsflüssen mit grober Kornverteilung deutlich (§ 3).
- Grosse Oszillationen des Wasserspiegels (stationäre Wellen) sowie der Kolktiefen wurden - speziell im zweiten Kolk - beobachtet.
- Die beiden Kolklöcher entstehen aufgrund verschiedener Mechanismen. Das erste wird hauptsächlich durch die Richtungsänderung der Hauptströmung und der daraus folgenden Sekundärströmung verursacht (Aufprall auf der Aussenwand), während das zweite hauptsächlich durch die zunehmenden Geschwindigkeitsschwankungen hinter der Geschiebebank an der Kanalinnenseite hervorgerufen wird (§ 6).
- In Fliessrichtung bewegen sich die höchsten mittleren Geschwindigkeiten von der Kanalachse Richtung Aussenwand und anschliessend gegen die Sohle hin (§ 6). Im ersten Kolkloch werden die höchsten Geschwindigkeiten in Bodennähe beobachtet.

Zusammenfassung

- Ein markanter Sortierungsprozess aufgrund der breiten Kornverteilung lässt sich in Querrichtung beobachten. Grobe Komponenten sammeln sich an der Aussenwand im Kolkloch an, während feine Körner die innere Bank bilden.

Durch Anbringen von senkrechten Rippen entlang der Kurvenaussenseite kann der Kolkprozess sowie die Strömung markant beeinflusst werden. Die Makrorauhigkeit hat folgende Auswirkungen:

- Die Kolktiefe entlang der Aussenwand wird stark reduziert und die ausgeprägten Kolklöcher verschwinden praktisch vollständig.
- Mit steigender Wandrauhigkeit bewegt sich das erste Kolkloch flussabwärts, während das zweite ungefähr an gleicher Stelle verbleibt.
- Die ohne Rippen beobachteten Oszillationen des Wasserspiegels und der Kolktiefe werden durch die Makrorauhigkeit in etwa halbiert und der Kolk entwickelt sich gleichmässiger.
- Die Strömung wird stark beeinflusst: die höchsten Geschwindigkeiten werden von der Aussenwand ferngehalten und somit der Kolk am Fuss von Schutzmauerfundationen reduziert.
- Entlang der Aussenwand kann an der Wasseroberfläche eine sekundäre Strömungszelle beobachtet werden. Die Grösse dieser Zelle ist proportional zur Reduktion der Kolktiefe.
- Ein optimaler Rippenabstand ist von grosser Bedeutung, da ein schlecht gewählter Abstand die Kolktiefe sogar vergrössern kann.
- Die Sedimenttransportkapazität wird durch die Rippen reduziert. In natürlichen Flüssen wird dies durch eine Zunahme des Gefälles kompensiert.
- Auch die beiden Enden der Kurve werden durch die Makrorauhigkeit beeinflusst: oberhalb der Kurve nimmt die Wassertiefe infolge Energieverlust in der Kurve zu und unterhalb kann eine geringe Zunahme des Kolks in Kanalmitte beobachtet werden.
- Der Geschiebesortierungsprozess wird durch die Rippen kaum beeinflusst. Einzig die Ausdehnung der groben Ablagerungen entlang der Aussenwand wird vergrössert.

Nebst den erwähnten Beobachtungen präsentiert dieser Bericht eine empirische Kolkformel zur Abschätzung der maximalen Kolktiefe in Gebirgsflüssen mit grober Sohle und breiter Kornverteilung (§ 7), die auf physikalischen Parametern beruht. Diese sind das Verhältnis von mittlerer Abflusstiefe zu Flussbreite, eine dimensionslose Grösse, die die mittlere Geschwindigkeit mit dem hydraulischen Radius verbindet und schliesslich der Gleitreibungswinkel des Sohlenmaterials. Im maximalen Kolk kann das Querprofil der Sohle mit dieser Gleichung angenähert werden.

Die durch senkrechte Rippen erzeugte Kolkreduktion kann mit einer Beziehung ermittelt werden, die vom Rippenabstand, dem hydraulischen Radius, der Froudezahl und der Differenz zwischen effektiver und kritischer dimensionsloser Sohlenschubspannung abhängig ist (§ 7).

Empfehlungen für Wasserbauingenieure (§ 8.3) zur Abschätzung der durch die senkrechten Rippen erzeugte Kolkreduktion runden den Bericht ab.

Stichworte

Sedimenttransport in gekrümmten Gerinnen, Kurvenkolk, Gebirgsflüsse, Laborversuche, Geschiebesortierungsprozess, grobes Kiesbett, breite Kornverteilung, Deckschichtbildung, gemitteltes Geschwindigkeitsfeld, Makrorauhigkeit, senkrechte Rippen

Table of contents

Table of contents

x

CHAPTER 1

INTRODUCTION

1.1 Context

The floods of 1987 in the Reuss River Valley, 1987 and 1993 in the Rhone River Valley and 1997 at Sachseln in Switzerland caused catastrophic damages in villages and on infrastructures in these densely populated areas. Due to the limited space, the banks of mountain rivers crossing settlements and villages have often to be protected with walls against dangerous bank erosions. Compared to the riverbed, these walls are rather smooth; therefore high flow velocities occur along the walls and cause deep scouring near their foundations. At extreme floods the foundation of the bank walls can be undercut by scouring which results in failure of the protection wall. Especially walls in river bends are endangered because of the increased scouring action in bends. Failure of the foundation and consequently of the protection wall, will allow uncontrolled lateral bank erosion, which will result in serious destruction of buildings and infrastructures. If the endangered walls at the river banks are furnished with roughness elements as vertical ribs, scouring along the walls can be reduced considerably.

This fact was observed during the design of the protection measures in the Reuss River Valley (flood event of 1987) and Saas Valley (flood event of 1993). The protection walls at Gurtnellen-Wiler (Reuss River in Canton Uri) were equipped with vertical ribs, tested and optimized with qualitative scale model tests (KUSTER, JÄGGI, BEZZOLA, 1992 and JÄGGI, BEZZOLA, KUSTER, 1996, SCHLEISS, 2000).

Figure 1.1:   Hydraulic scale model of the Reuss River, Gurtnellen, Switzerland [Kuster et al., 1992]

1.2 Aim of the present research

The roughness elements are reducing the flow velocities along the wall at the outer side of the bend. Therefore the driving force of the scouring, namely the intensity of the secondary flow in lateral direction of the channel section is also reduced. Furthermore, the roughness elements are diverting the flow along the outer side of the bend toward the center of the channel; consequently the capacity of erosion of the flow at the wall foundation is reduced. Systematic laboratory test, described in the present study, confirm these observations.

Based on the laboratory tests one can further state that there exists an optimum spacing of macro-roughness elements for given flow conditions. The use of a wide grain size distribution, as it is present in gravel transporting mountain rivers, causes an important grain sorting in the cross-section of the channel, which itself has an important influence on the sediment transport and the scouring process in the curve.

Theoretical considerations, which allow the quantitative description of these phenomena and which take into account the governing parameters are established in this research study. It is now possible to estimate the scour depths along the walls roughened with vertical ribs as well as to determine the influence on the grain size sorting.

The present research study was carried out focusing on the following objectives:
- to investigate systematically the development of the scour as function of the roughness elements applied to the walls in a physical model;
- to derive a generally applicable formula for the quantitative estimation of the scour depth;
- to highlight the effect of grain sorting to the transport and the scouring process in the bend;
- to give design recommendations for design engineers;

The project supplies the scientific base to answer the following important question for practical considerations: Which roughness elements have to be applied to the wall to reduce the depth of scour along its foundation most effectively?

This research was carried out at the *Laboratoire de Constructions Hydrauliques* (LCH, Prof. A. Schleiss) in collaboration with the *Laboratoire d'Hydraulique Environnementale* [1] (LHE, Prof. W.H. Graf). Both laboratories investigated the problem of scour in bends from a different but complementary point of view. At LCH (this present project), the effect of applying roughness elements at the outer bank of channel bends on the flow and the scouring was investigated. At LHE, research was done on the hydrodynamics of flow in open-channel bends by Koen Blanckaert.

---

1. Former: *Laboratoire de Recherche Hydraulique* (LRH).

CHAPTER 2

STATE OF THE ART

2.1   Flow in bends

The water particles in the bend near the surface of an open channel are moved by acceleration forces, which are most significant near the surface, towards the outer side of the bend. Consequently the water surface at the outer side of the bend is higher than at the inner side. This difference in pressure head induces a flow near the bottom of the channel towards the inner side of the bend. This secondary flow in lateral direction is superimposed to the main flow in longitudinal direction. A spiral flow is created by these two flow components. Such a flow differs considerably compared to a flow in a straight channel in view of flow resistance and sediment transport. Therefore the following aspects were investigated in various research programs:

- inclination of water surface in lateral direction,
- spiral flow,
- head losses in bends,
- sediment transport in bends.

One of the oldest investigations was carried out by SHUKRY (1950), who measured in an rectangular deep channel with fixed bed the three flow components, the water surface elevation in lateral sections and the energy gradient in the curvature.

A different approach of the description of the flow was developed by GARBRECHT (1953); he explained the phenomenon by local impact and deviation of the flow. His experiments were performed at relatively steep slopes and sharp curvatures.

On the other hand the classical work of ROZOVSKII (1957) is based on a potential flow theory, because his measurements were carried out in channels and rivers with very low bed slopes.

DE VRIEND (1976, 1981) developed a numerical model for bend flow. Based on a logarithmic main velocity profile and its acceleration he derived the vertical and radial velocity components of the secondary flow.

More recent research concentrated mainly on the interaction between the flow and the bed topography (YEN, 1970 and HECKEL, 1978). The head losses in the bend were investigated in detail by ONISHI ET AL. (1976).

BATHURST ET AL. (1979) carried out field measurements of secondary currents and boundary shear stresses at bends of rivers with coarse alluvial beds. Other field experiments in a river bend were undertaken by HABIB (1986). He measured the velocity components in longitudinal, lateral and vertical direction and determined the bed topography as well.

A recent literature review on the research works on flow in bends has been given by BLANCKAERT & GRAF (2001). Blanckaert performed laboratory experiments in a strongly curved 120° bend. He observed an secondary cell at the outer bank close to the water surface. This outer-bank cell and a reduced turbulent activity are shown to have a protective effect on the outer bank.

2.2 Sediment transport

2.2.1 General transport formulae

Many textbooks give a good overview over the sediment transport processes and formulae like for example GRAF (1971, 1984) and GRAF & ALTINAKAR (1998), BILLI ET AL. (1992) and YALIN & DA SILVA (2001). SLEATH (1984) gives an overview of bedload and total load (bedload & suspended load) transport formulae including the formulae of DU BOYS (1879), DONAT (1929), RUBEY (1933), SCHOKLITSCH (1934), SHIELDS (1936), MEYER-PETER & MÜLLER (1948), BROWN (1950), EINSTEIN (1950), BISHOP ET AL. (1965), BAGNOLD (1966), ENGELUND & HANSEN (1967), ACKERS & WHITE (1973) and many others.

The first important study on sediment transport was performed by DU BOYS (1879). Based on observations on the Rhone River in France, he established his drag force theory and his bedload formula (§ 3.4.2/1).

SHIELDS (1936) performed laboratory tests with uniform grain size. Based on his tests and theoretical considerations, he established a criterion for inception of sediment motion (§ 3.4.2/2).

MEYER-PETER & MÜLLER (1948) performed a large test series at bed slopes between 0.1 and 2.3% and established a first bedload formula. SMART & JÄGGI (1983) extended this formula to channels with steeper slopes (up to 20%). Furthermore they introduced the influence of a wide grain size distribution in their formula. In the frame set of his study on fraction wise sediment transport, HUNZIKER (1995) proposed a modified bedload formula based on the one of Meyer-Peter & Müller.

ACKERS & WHITE (1973) established a bedload formula, based on dimensional analysis with empirically determined exponents. The main parameters are the discharge, the flow conditions (velocity and flow depth) and the sediment characteristics (mean diameter of the sediments, particle Froude number, friction velocity and sediment density).

WALLBRIDGE ET AL. (1999) experimentally measured threshold conditions for sediment entrainment for uniform and mixed sand under steady and unsteady flow conditions. They concluded that the sand grain pivoting angle and the entrainment thresholds are higher for a grain size acting as the finer fraction in a sediment mixture than for the same size in a uniform sediment. Likewise, entrainment thresholds are lower than for a uniform sand when the grain size acts as the coarse fraction in a mixture and mean sizes in a mixture behave as in uniform sediments

With the aim to determine the transport capacity, WANG (1999) carried out experiments and studied the erosion rate and river bed inertia.

CHILDS (2001) proposed a numerical model and criterion for incipient motion of a single sediment grain for the basic movements (translation and rotation).

2.2.2 Recent research on sediment transport related parameters

Some recent works deal with parameters related to the sediment transport, like e.g. the shear stress, the bed surface roughness.

MCEWAN, JEFCOATE & WILLETTS (1999) established a model to calculate explicitly the modification of the velocity profile and the reduction of the fluid shear stress due to moving grains. Their laboratory tests showed that moving grains can significantly contribute to flow resistance if there is no static roughness. They further showed the limitation of the sediment transport rate by the availability of the sediments.

MASSON & MARTINEZ (2001) observed the shear stress in a mixture of 1050 cylinders at different densities. The analyzed movements (horizontal and vertical translation and rotation) showed on a macroscopic scale that the plasticity is independent of the initial density, of the peak stress and of the dilating or contracting behavior. On a microscopic scale a different behavior between dense and loose samples was observed.

A rather academic study was performed by PAPANICOLAU ET AL. (2001). They analyzed the influence of surface roughness on near-bed turbulence and conclude that the time-averaged flow characteristics (Reynolds stresses and mean flow velocities) do not completely explain the roughness effect on flow characteristics. Furthermore they found a clear correlation between the sediment transport and the streamwise velocity for super critical flow conditions.

Considering a large data set of medium and large alluvial rivers, MOLINAS & WU (2001) pointed out the difficulty of laboratory measurements to obtain flow depth of more than 50 cm and very small slopes. These difficulties lead to rather low Reynolds numbers (~50'000) compared to field measurements (~500'000) and to higher Froude numbers compared to field data. To account for this fact, they developed an energy concept for sediment transport, which is based on the gravitational theory of VELIKANOV (1954), on the stream power theory by BAGNOLD (1966) and previous works of their research team (YANG, 1973 and YANG & MOLINAS, 1982). Their formula mainly applies for sand-bed rivers.

2.2.3 Transport formulae considering the grain size distribution

EINSTEIN (1950) proposed to compute the sediment transport rate for each sediment fraction instead of computing the average based on one characteristic diameter. The total sediment transport rate is obtained as the sum of the fractional rates. To take into account the interaction between the different grain size fractions, Einstein introduced a hiding function, correcting the shear stress of the given sediment fraction.

EGIAZAROFF (1965) chose another approach. He made theoretical considerations on near bed velocities and on the exposure of the grains and introduced a correlation function correcting the (average) critical shear stress.

Many authors (e.g. ASHIDA & MICHIUE, 1971) proposed power functions for Einstein's hiding function and Egiazaroff's correlation function. RIBBERINK (1987) introduced the study of Ashida & Michiue in Meyer-Peter & Müller's sediment transport formula and extended it to compute sediment transport rates of sediment mixtures.

Based on field measurements of MILHOUS (1973) at Oak Creek in Oregon, USA, PARKER (1990) extended the previously established formula (PARKER ET AL, 1982) for the sediment transport rate from a uniform grain to sediment mixtures. Their correction function depends on the diameter of the considered sediment fraction and the mean diameter of the armoring layer. They corrected the mean diameter of the armoring layer and not (like most other authors) the diameter of the considered sediment fraction.

MISRI, GARDE & RANGA RAJU (1984) developed a model for computing the bed load transport taking into account the interaction between the different grain sizes. Since small grains are sheltered by bigger ones, they will need higher velocities and velocity fluctuations than without sheltering effect. Misri et al. analyzed EINSTEIN'S (1950) sheltering factor and concluded that the scatter is important. While most models consider either the lift or the drag force to be predominant for incipient motion, Misri et al. assumed that the lift force is predominant for small particles (smaller than the mean diameter) and that the lift and drag forces act on the bigger grains. Their equation is based on data sets of various authors and obtained by curve fitting. They proposed to compute the sediment transport rate with the composition of the bed material without taking into account the armor layer, nor the fact that the transported sediment can be slightly coarser if the bed material is formed by a wide grain size mixture.

HUNZIKER (1995) gives a good overview over the studies, which allow a computation of the sediment transport rate of wide sediment mixtures. In the frame set of his work on fractionwise sediment transport, he performed a series of laboratory tests and analyzed the results of MEYER-PETER & MÜLLER (1948). He observed a systematically too high sediment transport rate (already documented by JÄGGI, 1995) due to the fact that Meyer-Peter & Müller overestimated the influence of the bedforms. That's why JÄGGI (1995) proposed to reduce the shear stress by 15 to 20 %. His modification leads to the desired correction of the sediment transport rates for high shear stresses, but it induces important differences for small shear stresses, since the transport starts at an effective dimensionless critical shear stress of $\theta_{cr} = 0.06$.

Therefore HUNZIKER (1995) proposed to modify MEYER-PETER & MÜLLER'S formula by replacing the factor 8 in their equation (see eq. 3.44) by a factor 5. HUNZIKER'S modification is confirmed by propositions of other authors like LUQUE & VAN BEEK (1976) who proposed a factor of 5.7 instead of 8. Finally HUNZIKER established a transport model allowing the computation of the sediment transport rate for each sediment fraction. A comparison with data sets of MEYER-PETER & MÜLLER (1948), ZARN (1997) showed a good correlation between computed and measured transport rates. The prediction of the bed armoring was tested against laboratory data of GESSLER (1965) and GÜNTER (1971) with good agreement.

With the aim to quantify the total load of a river, MOLINAS & WU (1998) determined a correction coefficient for rivers with a wide grain size distribution for the formulae of ENGELUND & HANSEN (1967), ACKERS & WHITE (1973) and YANG (1973). The corrected formulae were tested against a large set of experimental and field data.

2.3 Scouring

A state-of-the-art report of scouring in general was given by RAUDKIVI (1967), BREUSERS & RAUDKIVI (1991) and HOFFMANS & VERHEIJ (1997). But scour in bends is treated only in a summarized way. Only a few of the known formulae have been developed and verified for coarse gravel rivers. Most of them are valid only for small bed slopes where the influence of impact forces is still insignificant. Furthermore they are not verified for wide grain size distributions.

2.3.1 Scour in bends

At steady state conditions most models are based on equilibrium considerations at the particles of the bed. Usually, the transversal bed slope β is given as a function of the (local) flow depth h, the (local) radius r, and a factor of proportionality K. Most known models differ by the derivation of this factor of proportionality.

$$\sin(\beta) \, = \, K \cdot \frac{h}{r} \tag{2.1}$$

If $\sin\beta$ is replaced by dh/dr and the above equation is integrated, the following relationship for the bed topography can be obtained:

$$h \, = \, h_m \cdot \left(\frac{r}{R_c}\right)^K \tag{2.2}$$

FARGUE (1868) (cited in WILLIAMS, 1899) was probably the first to establish a formula for the maximum scour. His equation depends essentially on the geometry of the bend (radius, width) and furthermore on the flow velocity and the bank roughness.

Some more recent formulae are based on the equilibrium of a sediment grain:

VAN BENDEGOM (1947) was the first investigator to derive a relationship in the form as described above. In his equilibrium considerations the body force, the buoyancy force, as well as the drag force have been considered. Hence, the factor of proportionality was found to depend on the particle Froude number. With a somewhat modified approach BRIDGE (1976) obtained similar results but valid only for flat rivers in plains.

ENGELUND (1974) introduced the dynamic uplift as additional force, which is opposite to the gravity forces. He considered the particles to be transported in layers. His factor of proportionality K is found to be constant. This approach combined with the flow model proposed by ENGELUND makes it possible to compute the bed topography in the whole bend for constant and variable radii. The flow model is based on a rectangular cross-section with a fixed bed. Furthermore it is assumed that the ratio of width to depth is large and that the radius of curvature is significantly larger than the flow depth.

Based on detailed observations and descriptions of the scouring process KIKKAWA, IKEDA & KITAGAWA (1976) developed a formula for the estimation of scour depth at bends, which has been applied in practice frequently. The velocity distribution in the bend has been determined by

resolution of the momentum equation in radial direction combined with a simplified flow function. Therefore the assumption of a constant vortex viscosity and a modified logarithmic velocity profile have been made. They found that the factor of proportionality depends on the Froude particle number, the shear velocity and the flow velocity. REINDL (1994) established a scour formula based on the same approach. He added a sediment saturation parameter, quantifying the volume of sediments available for bedload. Reindl examined the influence of a backwater curve on the scour process.

Other investigators have developed slightly modified formulae based on the equilibrium of a control volume:

ZIMMERMANN (1979) worked out an analytical model and related the rotation moments in the curvature – the source of the boundary shear stresses, the curvature of the stream lines and the vertical velocity – to each others. FALCON & KENNEDY (1982) adopted the old approach of DU BOYS (1879), who assumed that the material is transported in layers.

ODGAARD (1981) developed a similar formula as Zimmermann, but valid for coarse bed load. ODGAARD & KENNEDY (1982) compared the results of VAN BENDEGOM's formula with data observed in flumes and rivers. He noted that the transversal slope estimations agreed only for weak longitudinal slopes with measured data. This can be explained by the fact that van Bendegom's assumption of a spherical, completely exposed particle is rather conservative and leads to an underestimation of the transversal slope. Odgaard also compared flume and prototype data with the results of Engelund's approach and observed a relatively poor concordance. He stated that the approach of Engelund more likely applies to slightly meandering rivers.

PETER (1986) reviewed the validity and the applicability of the different formulae by varying a lot of parameters in new series of physical model tests. He established en empirical scour formula giving quite good results for mountain rivers, depending on the width to depth ratio, the width of the grain size distribution and the channel slope.

The above mentioned scour formulae are analyzed in detail in section 3.5. Some additional works of interest are presented hereafter.

ZARN (1997) has analyzed the influence on the width of a river on the interaction between flow, morphology and sediment transport capacity. He developed two methods allowing to determine the mean and "maximum"[1] erosion depth.

For the determination of the transport capacity of a river, MOLINAS & WU (1998) have presented a correction coefficient for non-uniform grain size distributions for the transport equations of ENGELUND & HANSEN (1967), ACKERS & WHITE (1973), and YANG (1973). The corrected equations have been tested with numerous flume and field data. With the same aim WANG (1999) performed experimental studies on the ratio of erosion and the inertia of the riverbed.

---

1. The "maximum" erosion depth is defined as the 95% fractile.

2.3.2   Scour around structures in the river bed

An overview of scour around structures placed in river beds like spur dikes, bridge abutments and sills, can be found e.g. in BREUSERS & RAUDKIVI (1991) and HOFFMANS & VERHEIJ (1997).

a)   *Spur dikes / groyne fields*

Spur dikes deflect the main river current away from an erodible bank. In general they constrict the flow in a river and increase both, the local velocities and the mean velocity in the stream. BREUSERS & RAUDKIVI (1991) and HOFFMANS & VERHEIJ (1997) give an overview of the influences on scour due to spur dikes. The most important ones are the angle and the location at which the spur dyke is placed in the river, the shape of the dyke, the discharge and the roughness of the bed.

ODGAARD ET AL. (1982, 1983, 1984, 1987) studied the impact of groyne fields on scouring in Laboratory tests and in two rivers in Iowa. They showed, theoretically and by a physical model, that short, vertical, submerged vanes installed at incidence to the channel axis in the outer half of a river-bend significantly reduce the secondary currents and reduce the high-velocity attack of the outer bank.

KUHNLE, ALONSO & SHIELDS (1999) investigated the scour behind a spur dike placed on the wall of a flume. They propose a technique to predict the volume of scour.

In numerical models, groyne fields are generally considered as dead zones. A recent study of UIJTTEWAAL ET AL. (2001) analyzed the exchange process between a groyne field and the main stream. They identified two types of exchanges: a first one, induced by large eddies at the mixing layer and a second one over the whole groyne field induced by an important gyre at the upstream corner of the groyne field. After examination of their laboratory data, they concluded that it is correct to consider the groyne field as dead zone.

b)   *Bridge abutments*
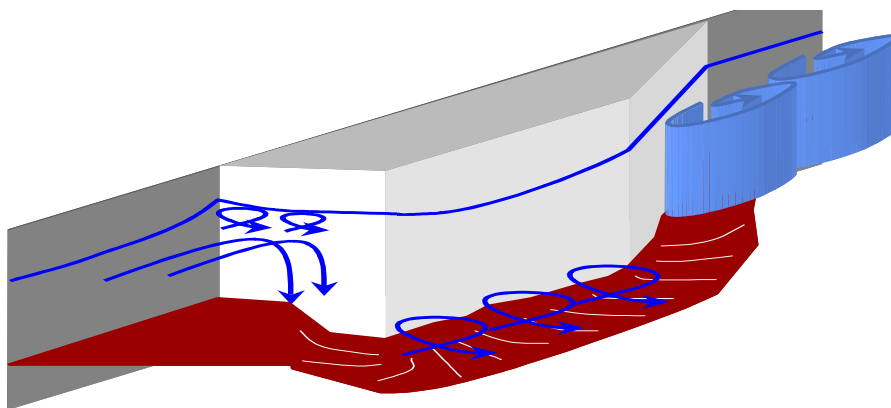
Figure 2.1:   Flow structure around a bridge abutment

The research done on bridge abutments is of interest for this research study since one isolated vertical rib can be compared to a bridge abutment even if the scale and therefore the effects are less important. Unfortunately only few literature is available in this area. Bridge abutments create a

complex flow structure (Figure 2.1). On the upstream face of the abutment the flow plunges down towards the bottom, where the principal vortex along the scour hole is located. Behind the abutment, the wake vortex can be found. Some small surface rollers can be seen upstream of the obstacle.

MELVILLE & RAUDKIVI (1984) summarized studies performed at the University of Oakland. An important result of their study is the conclusion that the abutment scour depth can be up to 2 to 5 times the mean flow depth.

Semi-empirical formulae to estimate the equilibrium scour depth are given by INGLIS (1949), AHMAD (1953), LIU ET AL (1961) and many others. Inglis found the scour depth to depend on the flow characteristics (mean water depth and discharge) and the with of the channel. Ahmad introduced correction factors depending on the channel bend, the shape of the abutment structure, the angle of attack and the porosity of the abutment. Liu et al. found the abutment scour to depend also on the Froude number. A recent review of local abutment scour equations is presented in PRZEDWOJSKI ET AL. (1995).

MOLINAS, KHEIRELDIN & WU (1998) determined the necessary rip-rap size for protection of bridge abutments. The phenomenon at the downstream side of such a narrow cross-section can be compared to the one observed behind an element of macro-roughness. From their results, it can be supposed that the elements of macro-roughness might have a significant influence on the flow structure. However, it is important to note that these experiments were not carried out in a bend.

c) Bed sills

GAUDIO ET.AL. (2000) performed experiments on scour downstream of bed sills in uniform sediment and obtained empirical formulae to predict the dimensions of the scour hole. An important result is that the Froude number does not seem to influence the dimensions of the scour hole.

2.3.3 **Bridge scour**

An overview of the phenomena influencing bridge scour related formulae can be found in textbooks like BREUSERS & RAUDKIVI (1991), MELVILLE & COLEMAN (1999). The large number of studies on bridge scour identified the following main parameters to influence the maximum scour depth: the particle Reynolds number, a particle Froude number, the ratios mean water depth to channel width and characteristic grain size to channel width and the ratio of sediment to water density. Furthermore the pier dimensions and placement in the flow field and the sediment grading play a role.

Some recent studies on scour in cohesive material were undertaken by TING, BRIAUD,& CHEN (2001) who found that the equilibrium scour depth in cohesive material is of the same order of magnitude as the one in a sand bed.

2.4 Macro-roughness of banks

Roughness elements are reducing the flow velocities along the wall at the outer side of a bend. Therefore the driving forces of the scouring are also reduced. Furthermore the roughness elements are diverting the flow from the outer side of the bend toward the center of the channel. As a consequence, the capacity of erosion of the flow at the wall foundation is diminished.

The interaction of flow and scouring in bends of natural channels, whose banks are protected by walls equipped with roughness elements, is mainly governed by the following parameters: curvature of the bend, slope of the river bend, opening angle of the bend, bed material (distribution and size of particles), flow characteristics, bed load, geometry and spacing of the roughness elements and the inclination of walls.

Almost no research has been performed on macro-roughness on outer side walls in bends. The works on abutment scour may help to understand the local flow field around one macro-roughness element (see § 2.3.2).

The first research on macro-roughness on outer side walls that could be found was performed by ATSUYUKI (1992). He placed different roughness elements on the outer wall: small blocks (5 x 5 mm) placed on a 16 x 16 mm grid, a so called ladder strip (a 10 cm high ladder with traverses every 10 cm placed in the upper part of the outer wall), and a slanting strip (some kind of inclined ribbon) with two different inclinations.[1] One important observation is that the maximum resistance to flow is obtained if the depth of the roughness e_d is of about 10 times the spacing e_s between elements.

GAIROLA (1996) studied the flow past rectangular obstructions of various aspect ratios placed on a flat bed. He obtained the velocity distribution and the length of the downstream separation bubble, using the finite element technique, and compared his results with available experimental data. The influence of the macro roughness on the flow structure can be deduced, at least partly, based on these studies, while keeping in mind that they were not made on a bend.

SCHERL (1996) reported recent experimental runs in bends. He studied the influence of the roughness of the walls on the scour in a trapezoidal sinuous channel. His work is based on the study of REINDL (1994) as well as the precise description of the phenomenon reported by KIKKAWA ET AL. (1976). In his study, grain particles glued at the inclined wall surface created the wall roughness. Scherl used uniform grains with an average diameter of 2.5 mm and compared the results to tests of Reindl with roughness created by uniform grains with 6.1 mm diameter. The tests showed that scouring started earlier and that the maximum scour depth was increased (for tests without point bar formation) due to the decreased wall roughness.

CHOI (2000) discussed the impact of riblets, beside other devices, in the modification of turbulent flow near a wall and reported a reduction of the turbulence intensity near the wall.

---

1. The depth of the roughness elements could not be found in the article.

ORLANDI & LEONARDI (2000) carried out numerical simulation of wall bounded flows and showed how a change of the boundary conditions near the wall brings about changes in the near wall turbulence structure. Of interest is the case of flow past cavities, typical of rough walls.

RHODES & SENIOR (2000) carried out a numerical study using CFD on rib roughness on side walls of a straight channel. They replaced small and large scale roughness with an equivalent roughness plane wall stating that the variation of equivalent roughness (ε) and the channel width are independent of the rib roughness height and spacing when scaled appropriately. The tests were performed for rather small roughness ribs (about 3 to 4 mm).

The effect of macro-roughness elements, as for example vertical ribs with a trapezoidal cross-section on the outer vertical wall of a bend, on the process of scouring has not been investigated so far. Furthermore the effect of wide grain size distributions on the scouring process is rarely explored.

2.5 *Grain sorting and armoring*

HARRISON (1950) was probably the first to perform a systematic study on bed armoring. He performed three test series with different sediment mixtures but at the same discharge. At a first stage, he recirculated the sediments in the channel. Then he cut the sediment feeding. For all tests he observed a parallel erosion of the whole bed and a coarsening of the surface layer. The erosion stopped after a certain time due to armoring for the tests with coarse sediments.

GESSLER (1965) examined the sediment transport of various sediment mixtures under normal flow conditions. He observed that the sediment transport stopped for all tests due to the formation of an armoring layer. Linking the dynamic lift to the shear stress by means of KEULEGAN'S log-velocity law, Gessler finally gave the probability that a grain does not move. Gessler assumed that a grain starts moving if the bed shear stress acting on it gets more important than a critical value and that the bed shear stress acting on a grain is not constant but fluctuating due to turbulences of the flow around an average value. These shear stress fluctuations are distributed statistically with a Gaussian (normal) law.

GÜNTER (1971) performed laboratory test to determine the critical shear stress of sediment mixtures with a special emphasis on the influence of shear stress fluctuations on the incipient motion criterion. The tests of Günter were conducted in the same channel as Gessler's (1965) experiments. Each test had a duration between 4 and 6 weeks with only short breaks to allow the measurement of the evolution of the bed topography. Günter finally proposed a method to determine the critical bed shear stress of a sediment mixture.

HUNZIKER's (1995) work on fractionwise sediment transport has already been described in section 2.2.3.

2.6 *Measurement technique and data treatment*

The present section is not exhaustive. It presents a small selection of articles concerning different measurement techniques and data treatments.

a) *Bed level measurement*

SMART (1999) studied velocity profiles and the bed friction in gravel bed rivers. He proposed to define the water depth based on the analysis of a logarithmic velocity profile. This can be particularly useful with mobile beds if the channel ground cannot be clearly determined.

YANKIELUN & ZABILANSKY (2000) developed a measurement device to dynamically record the evolution of scour in site and in the laboratory. The device is based on the propagation time of a frequency modulated signal (as used in radar applications, but directional) captured by burried sensors.

b) *Sediment sampling*

SIBANDA ET.AL. (2000) presented a new sampling technique for determination of the composition of the surface and subsurface of a sediment bedformed during flume experiments. This technique called wax coring was used in two flume experiments and showed good results but at a considerable effort compared to the sampling technique that will be used in the present study (see 4.4.6 e) on page 90)

c) *Velocity measurement technique*

ROLLAND (1995) (see also LEMMIN & ROLLAND, 1997 and ROLLAND & LEMMIN, 1997) developed an ultrasonic velocity profiler based on the Doppler effect. The instrument allows the simultaneous measurement of the velocity fluctuations in 3 directions. His study gives a detailed overview of the governing equations and the measurement technique.[1]

d) *Dimensional analysis*

The similitude and approximation theory of KLINE (1965) presents the basics of dimensional analysis. Furthermore he regrouped and extended works of various authors to establish his approximation theory. Based on considerations of the main influences on a physical process, the resulting forces are combined with each other to obtain physically correct dimensionless parameters.

e) *Genetic algorithm*

KEIJZER & BABOVIC (1999) developed a genetic algorithm allowing to search for functions fitting to a given data sets. The big advantage of this genetic algorithm is a dimensionally aware treatment of the data allowing to facilitate physical interpretation of the results and enhance the search efficiency. RODRIGUEZ AGUILERA (2000) gave an overview of the program using this genetic algorithm. Applications in hydraulic engineering were documented by BABOVIC ET AL. (2001).

1. The used velocity-measurement device is documented in § 4.4.4 and in METFLOW (2000).

2.7   Conclusions

In conclusion, it can be stated that the flow structure in bends, especially for fixed beds (§ 2.1) is a fairly well documented phenomena. But for mobile beds and particularly for mobile beds with wide and coarse grain size distributions - as found in mountain rivers - almost no research has been done.

Sediment transport in general as well as its mechanisms were widely discusssed and studied in previous works (§ 2.2). The same observation can be made concerning scour formulae (§ 2.3). Quite an important number of equations were established to determine the maximum scour depth, but most of them were developed for sand bed rivers (or uniform grains) in plains and not for rather steep mountain rivers with coarse sediment and wide grain size distribution.

Only little work has been done to study the influence of bank macro-roughness on flow and scouring in bends. Some studies with rather small roughness elements, formed e.g. by big stones and blocks, are known. However, roughness created by vertical ribs on outer side walls has not yet been systematically investigated.

The influence of a wide grain size distribution on the grain sorting and armoring process is only partially known. Some methods which compute the composition of the armoring layer do exist.

Additional research in the field of scour formulae that are applicable to mountain rivers with a bed formed of coarse gravel and a wide grain size distribution, is necessary. Furthermore, research on the influence of macro-roughness on flow and scouring needs to be encouraged.

CHAPTER 3

THEORETICAL CONSIDERATIONS

3.1 Introduction

3.1.1 Bed constitution and material

a) Constituting sediment layers in a gravel bed

In a natural mountain river, the bed material is usually formed of gravel, big stones and blocks. A sediment sample has different characteristics depending on where in the river it is taken. A sample taken in the sub layer will be constituted of coarse and fine sediments whereas a sample in the armoring layer (upper layer) will be mainly composed of coarse grains due to the wash out of fine sediments. If the sample is taken on a point bar (e.g. at the inner bank of a river bend) the sediments will be much finer than the sediments of the sub layer. The grains of the armoring layer are oriented in an overlaying pattern. (Fig. 3.1)
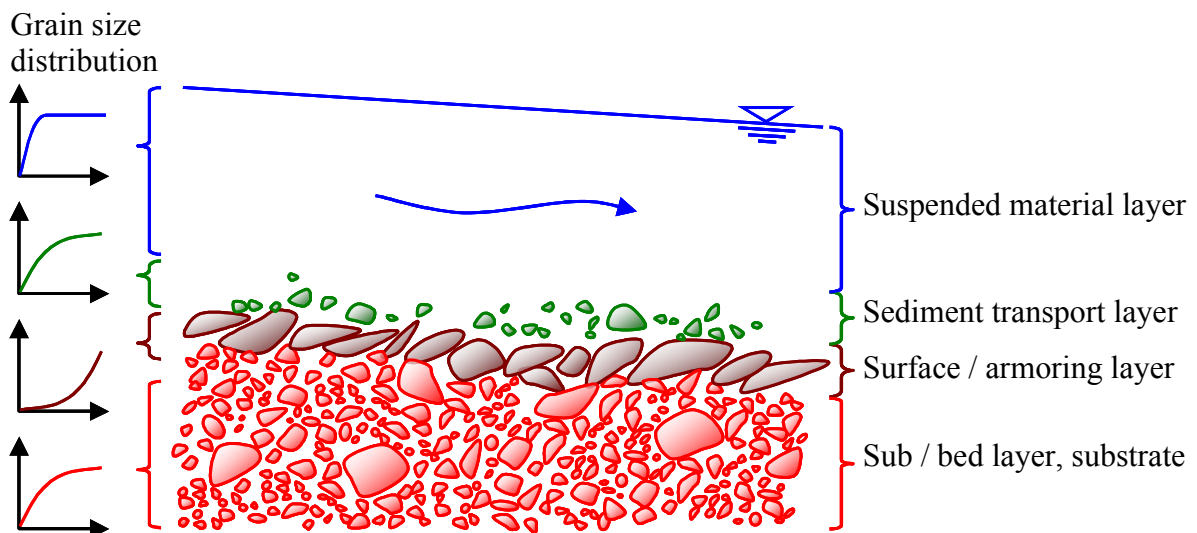
Figure 3.1:   Layers in a coarse gravel bed river submitted to armoring

b) Sieving and analysis of the grain size distribution

The geometry of a gravel grain can be approached by an ellipsoid (Fig. 3.2). The longest axis is defined as a, the longest dimension perpendicular this axis b and the shortest main dimension c. Generally b is considered as the main characteristic, since it is the dimension that is most perpendicular to the flow direction and therefore determinant for the erodibility of the bed.

For practical sieving considerations, the axis b limits the passing through a sieve with circular openings. If one uses a sieve with quadratic openings (as in the present study), the diameter remaining on the sieve is systematically too small. In general, the grain diameter remaining on a

sieve with circular opening can be considered to be 1.25 bigger than the one obtained with a quadratic opening.
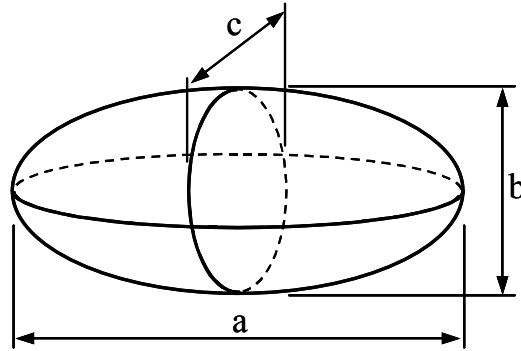
Figure 3.2:   Approximation of a sediment grain by an ellipsoid

c)   Minimum size of a sediment sample

In order to obtain a representative volume sample of the bed it is standard to extract a volume[1] of:

$$V[m^3] > 2.5 \cdot d_{max}[m] \qquad (3.1)$$

where the Volume V is measured in m^3 and the maximum grain size d_{max} in m.

For a representative surface sample the following minimum surface should be extracted[1]:

$$S > (10 \cdot d_{max})^2 \qquad (3.2)$$

where the surface of the sample S is measured in m^2. In the present study the armoring samples were marked with a color spray in order to obtain only the first layer of stones at the surface; afterwards the colored grains were taken out and sampled by sieving (quadratic openings). The surface for one sample was 15 x 60 cm (30 x 30 cm for the preliminary tests).

To convert a surface sample into a volume sample or vice versa, the following relationship can be used (FEHR, 1987):

$$\frac{\Delta p_{2i}}{\Sigma \Delta p_{2i}} = \frac{\Delta p_{1i} \cdot d_i^n}{\Sigma (\Delta p_{1i} \cdot d_i^n)} \qquad (3.3)$$

where d_i is the characteristic diameter of the considered fraction and p_i its volumetric part of the sample. Δp_{1i} gives the fractions of the initial sample and Δp_{2i} the fractions of the converted one.

To convert a surface sample into a volumetric sample (if there is no hydraulic sorting as for example in the armoring layer), the exponent n is 0.5.

---

1. According to the ISO 9001 manual of the Laboratory of Traffic Facilities (LAVOC) and (FEHR, 1987)

d) Characteristic diameters

The following characteristic diameters are commonly used to describe a grain size distribution: d_{10}, d_{16}, d_{30}, d_{50}, d_{65}, d_{84} or d_{90}.

- d_{65} and d_{90} are used to characterize the determinant roughness element of the bed and as approximation of the mean diameter of the armoring layer;
- d_{50} is used as approximation of the determinant grain size of the sediment transport;
- d_{16} and d_{84} are used to characterize the scatter of the grain size distribution. The width of the distribution is given with:

$$\sigma = \sqrt{d_{84}/d_{16}} \tag{3.4}$$

The mean diameter d_m is frequently used to describe the sediment transport rate:

$$d_m = \int_0^1 d_i dp = \frac{\Sigma(\Delta p_i \cdot d_i)}{\Sigma \Delta p_i} = \frac{\Sigma(\Delta p_i \cdot d_i)}{1} = \Sigma(\Delta p_i \cdot d_i) \tag{3.5}$$

p_i is the part (weight) of the sediment sample corresponding to the grain size d_i.

e) Density of the sediment

The sediment density usually ranges between $\rho_s = 2630$ and $2680 \ kg/m^3$. Measurements for the present study gave the following sediment density:

$$\rho_s = 2635 \ kg/m^3. \tag{3.6}$$

f) Porosity

The porosity p is defined as:

$$p = \frac{V_p}{V} = \frac{V_p}{V_p + V_s} \tag{3.7}$$

where V_p is the volume of the porosity and V_s the volume of the sediments (LANG, HUDER & AMANN, 1986, DYSLI, 1993). Three tests with the used bed material were performed. The resulting average porosity will be used in the present study:

$$n = 33.6 \ \% \tag{3.8}$$

with a standard deviation of 2.9 %. The error due to the measurement technique (size of the basket, precision of the balance) was estimated to be about 1 %.

g) Friction angles

Different friction angles can be distinguished:
- the static friction angle of repose of a soil,
- the dynamic friction angle, which is some degrees smaller than the static friction angle
- the bedload friction angle, used in some scour formulae is of the same order as the static friction angle (BAGNOLD, 1966) (see also Paragraph 3.5.2/4)).

The present paragraph describes a method to determine the static friction angle φ. If the *static* friction angle of a cohesion less soil cannot be determined by a laboratory test, the following method proposed by DHAWAN with the corrections of BRINCH HANSEN (COSTET & SAN-GLERAT,1981 and LANG, HUDER & AMANN,1986) can be used. The friction angle φ is determined with the following formula:

$$\varphi = \varphi_0 + \varphi_1 + \varphi_2 + \varphi_3 \qquad (3.9)$$

where the uncorrected friction angle $\varphi_0 = A + B + C + D$ is composed by the sum of

- $A = 1/7$ of the grain size fraction weight in % of the grains < 0.002 mm,
- $B = 1/5$ of the grain size fraction weight in % of the grains from 0.002 to 0.01 mm,
- $C = 1/3$ of the grain size fraction weight in % of the grains from 0.01 to 0.2 mm,
- $D = 1/2.5$ of the grain size fraction weight in % of the grains > 0.2 mm,

The correction factors are summarized in the following table

PARAMETER	SYMBOL	DESCRIPTION	VALUE
Compacity	φ_1	uncompacted normal dense	-6° 0° +6°
Form and grain roughness	φ_2	sharp angles normal rounded spheric	-1° 0° -3° -5°
Grain size distribution	φ_3	uniform normal wide	-3° 0° +3°

Table 3.1:   Correction factors for the determination of the friction angle φ

Sometimes φ_0 is put to 36°, 37° and 38° for sand, fine gravel and coarse gravel. For the tests performed in the present study, the friction angle determined with this method is of $\varphi = 37\,°$ assuming that the gravel is normally compacted with rounded grains and a normal grain size distribution. If we use the second possibility putting φ_0 equal to 38° (coarse gravel), the resulting friction angle is 35°.

Measurements of this friction angle performed on a tilting table gave the following friction angles fitting well with the predicted values. The precision of the measurement is estimated to be ±1 °.

GRAIN MATERIAL	RANGE*	AVERAGE
armoring layer	36 to 40°	38°
substrate (initial mixture)	36 to 40°	38°
fine (point bar) material	33 to 38°	37°

Table 3.2:   Measured friction angle for the used sediment
* The range gives the zone where the grains moved

The comparison between the measured and the analytically determined friction angle show a good agreement. Therefore the method of DHAWAN can be recommended for the determination of the friction angle if no measurements are available.

3.2 Flow equations and flow resistance

The flow resistance is influenced by the structure of the surface layer and the presence of sediment load and suspended load transport. The roughness of the surface layer is due to the characteristics of the surface layer and the presence of bedforms. Many works and textbooks give an overview over the different flow equations and the flow resistance, like e.g. DUBOIS (1998), SINNIGER & HAGER (1989), HUNZIKER (1995), ZARN (1997).

3.2.1   Flow resistance and friction laws

In his pioneer work, CHEZY (1768) related the average flow velocity to the bed slope and the water depth.

$$V = C \cdot \sqrt{h \cdot S} \tag{3.10}$$

For the friction coefficient C, CHEZY made important simplifications. About 100 years later, GANGUILLET & KUTTER published a formula, which allowed the computation of C as a function of the bed roughness. Authors like CHÉZY, GAUKLER, FORCHHEIMER, MANNING, CHRISTEN, (see SINNIGER & HAGER, 1989, §2.2) and many others published velocity power laws.

In Switzerland, the formula of STRICKLER (1923) found a wide application:

$$V = K_s \cdot R_h^{2/3} \cdot S^{1/2} \tag{3.11}$$

The relation between STRICKLER'S roughness coefficient K_s and the size of the characteristic roughness ε (usually the mean diameter of the surface layer d_m) is given by

$$K_s = \frac{Cst}{\sqrt[6]{\varepsilon}} \tag{3.12}$$

STRICKLER put the value of the constant Cst to 21.1 and used as characteristic roughness ε the mean diameter. MEYER-PETER & MÜLLER (1948) used a value of $Cst = 26$ combined with $\varepsilon = d_{90}$ (of the substrate). The higher constant Cst is partially compensated by the bigger grain diameter. MEYER-PETER & MÜLLER justified the increased constant with a better fit to the results of NIKURADSE. JÄGGI (1984) and HUNZIKER (1995) analyzed the constant Cst for the computation of the bed friction. They concluded that the initially proposed value of STRICKLER fits better to the observed values than the one of MEYER-PETER & MÜLLER. SCHÖBERL (1981) performed a series of tests and proposed an intermediate value of 23.5. In the present study a value of $8.2\sqrt{g} = 25.7$ is used in combination with d_{90}.

DARCY-WEISSBACH (VANONI, 1975) proposed the following friction law:

$$V = \sqrt{\frac{8 \cdot g \cdot R_h \cdot S}{f}} \tag{3.13}$$

Another frequently used velocity law was established by KEULEGAN (1938). Based on the theoretical analysis of VON KARMAN (1921) and PRANTL (1926) and the experiments of NIKURADSE (1933), KEULEGAN derived a logarithmic velocity distribution:

$$\frac{v(z)}{V_*} = \frac{1}{\kappa} \cdot \ln\left(\frac{z}{\varepsilon}\right) + B \tag{3.14}$$

The depth averaged velocity consequently writes as

$$V = V_* \cdot \frac{1}{\kappa} \cdot \ln\left(e^{\kappa \cdot B - 1} \cdot \left(\frac{h}{\varepsilon}\right)\right) \tag{3.15}$$

For water without suspension, the VON KARMAN constant is $\kappa \approx 0.4$. B is a function of the Shear Reynolds number Re^*. In the hydraulically rough domain ($Re^* \geq 70$) $B = 8.5$ and in the hydraulically smooth domain ($Re^* \leq 5$) $B = 1/\kappa \cdot \ln(Re^*) + 5.5$. For the transition, the following function can be used $B = 8.5 + (2.5 \cdot \ln Re^* - 3) \cdot \exp[-(0.127 \cdot [\ln(Re^*)]^2)]$ (YALIN, 1992).
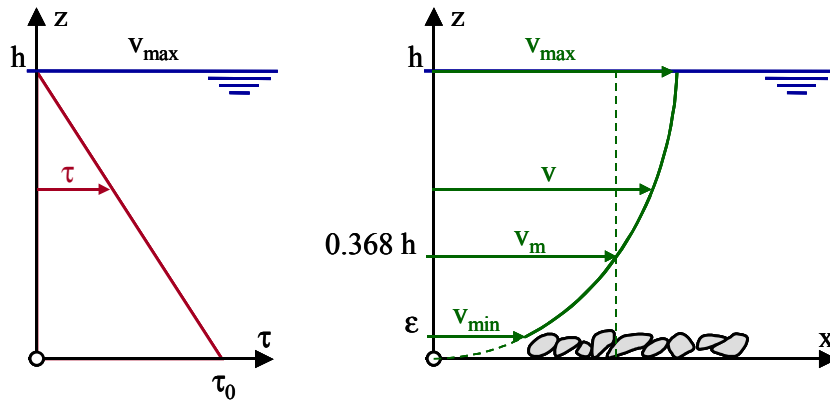
Figure 3.3: *Time averaged boundary shear and velocity distribution in an idealized channel for uniform flow and* $\varepsilon \ll h$

In the hydraulically rough domain, the velocity at a given distance from the ground can be obtained from equation 3.14:

$$\frac{v(z)}{V_*} = \frac{1}{\kappa} \cdot \ln\left(\frac{30.1 \cdot z}{\varepsilon}\right) = \frac{1}{\kappa} \cdot \ln\left(\frac{z}{\varepsilon}\right) + 8.5 \tag{3.16}$$

The minimum velocity $v(\varepsilon) = 8.5 \cdot v_*$ is given at $z = \varepsilon$. The average velocity writes:

$$V = 5.75 \cdot V^* \cdot \log\left(\frac{12.27 \cdot R_h}{\varepsilon}\right) \tag{3.17}$$

3.2.2   Flow resistance due to bedforms

Since no bedforms occurred during the tests[1], the present paragraph briefly summarizes the methods to compute bedforms. The best known theory to compute the friction losses due to bedforms was established by EINSTEIN (1950). He proposed to subdivide the average bed shear stress τ in a

part taking into account the grain roughness τ_{grain} and another one accounting for the losses due to bedforms τ_{bf}.

$$\tau = \tau_{grain} + \tau_{bf} \tag{3.18}$$

EINSTEIN assumed that the average velocity is proportional to the shear stress induced by the grain roughness τ_{grain} since the bedforms present in general a flat upstream slope. Therefore he assumed the logarithmic velocity law to remain valid which allows to subdivide the hydraulic radius in a part which is due to the grain roughness and another one due to the bedform roughness.

$$R_h = R_{h, g} + R_{h, bf} \tag{3.19}$$

JÄGGI (1983) pointed out that this subdivision is quite arbitrary.

3.2.3   Sediment transport parameters

a)   Boundary shear stress and friction velocity

Considering an isolated volume element ($\Delta x \times \Delta B \times h$) of the fluid (neglecting the influence of the side walls and $\varepsilon \ll h$) the time averaged boundary shear stress can be calculated as a gravity component in the following way (see Fig. 3.4):

$$\tau_0 = \frac{G_x}{\Delta x \cdot \Delta B} = \frac{\rho_w \cdot g \cdot h \cdot \sin\alpha \cdot \Delta x \cdot \Delta B}{\Delta x \cdot \Delta B} \cong \rho_w \cdot g \cdot h \cdot S_e \quad \left[\frac{kg}{m \cdot s^2}\right] \tag{3.20}$$

For not idealized channels, h has to be replaced by R_h.

If not especially mentioned, τ designates the boundary shear stress in the inlet reach. An approximated local shear stress was computed based on measured near bed velocity profiles. Using the log-velocity law of KEULEGAN (§ 3.2.1), the near bed friction velocity in the hydraulically rough domain can be written as:

$$v^* = \frac{v(z)}{\frac{1}{\kappa} \cdot \ln\left(\frac{z}{\varepsilon}\right) + 8.5}, \text{ and } V^* = \sqrt{\frac{\tau_0}{\rho_w}} = \sqrt{g \cdot R_h \cdot S} \quad \left[\frac{m}{s}\right] \tag{3.21}$$

Based on the velocity measurements within the near bed zone (one or two times the characteristic grain size diameters, which is d_{90} in the present study) an approximate friction velocity and consequently an approximate bed shear stress can be determined.

---

1. Bedforms were only observed temporarily during test C01b (at an initial bed slope of 0.7%, without macro-roughness at a discharge of 150 l/s) in the outlet reach. These were probably due to a too high inlet bed slope inducing higher Froude numbers in the channel. As soon as the bed slope in the inlet reach stabilized at the initially built in value, the bedforms disappeared.
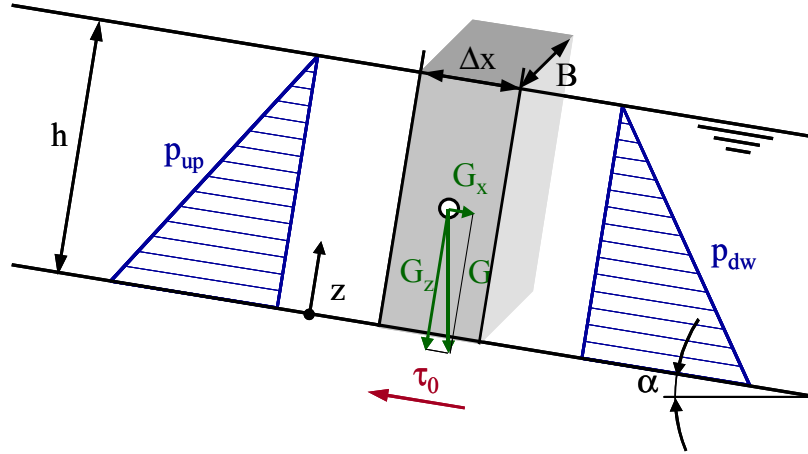
Figure 3.4:   Definition of the boundary shear stress as a gravity component

At a given distance z of the ground, the shear stress can be obtained with:

$$\tau = \tau_0 \cdot \left(1 - \frac{z}{h}\right) \tag{3.22}$$

b) Shear Reynolds number

The Shear Reynolds number is composed in analogy to the Reynolds number. The velocity is replaced by the shear velocity and the flow depth by the size of the roughness ε.

$$Re^* = \frac{V^* \cdot \varepsilon}{\nu} \tag{3.23}$$

c) Densimetric and sediment Froude number

In analogy to the Froude number, two dimensionless numbers are defined to characterize the sediment transport capacity of a river. The densimetric Froude number Fr_d[1] and the sediment Froude number Fr^* are distinguished by the used velocity:

$$Fr_d = \frac{V}{\sqrt{(s-1) \cdot g \cdot d}} ; \quad Fr^* = \frac{V^*}{\sqrt{(s-1) \cdot g \cdot d}} = \sqrt{\theta} \tag{3.24}$$

---

1. The densimetric Froude number - combining the flow velocity with sediment related characteristics - is frequently used in literature despite a less explicit physical meaning (compared to Fr^*).

3.3　*Wall influence and armoring*

HUNZIKER (1995) gives a good overview over the work performed in the domain of armoring. A summary of some possibilities to compute the composition of the armoring layer is given hereafter. The present study used GESSLER'S (1965) method to predict the grain size distribution of the armoring layer.

GESSLER (1965) examined the sediment transport of sediment mixtures. He performed an important number of tests, covering bed slopes between 0.195 and 0.4 %, and discharges from 10 to 86.7 l/s. The initially built in sediment mixture had a maximum diameter of 6, respectively 12 mm. A gate at the outlet of the test facility was regulated to obtain normal flow conditions over the whole length of the channel (40 x 1.0 m and 5 x 0.4 m for the steep slopes). Gessler observed that the sediment transport stopped for all tests due to the formation of an armoring layer.

GESSLER based his approach on the study of EINSTEIN & EL SAMNI (1949) who found that the dynamic lift of a sediment grain depends on the shear stress fluctuations and that the shear stress fluctuations are distributed according to a Gaussian (normal) distribution. Linking the dynamic lift to the shear stress by means of KEULEGAN'S log-velocity law, GESSLER and EINSTEIN & EL SAMNI finally obtained the following probability that a grain does not move:

$$q_{\text{no mvt}} = \frac{1}{\sigma \cdot \sqrt{2\pi}} \cdot \int_{-\infty}^{(\tau_c/\tau - 1)} \exp\left(\frac{-x^2}{2\sigma^2}\right) dx \tag{3.25}$$

GESSLER assumed that

- a grain starts moving if the bed shear stress acting on it exceeds the critical value, which depends on the grain size and the particle Reynolds number $Re*$.
- the bed shear stress acting on a grain is not constant but fluctuating due to turbulences of the flow.

He tested his theory with armoring tests for different sediment mixtures and different discharges. For tests performed at a constant discharge without sediment supply, GESSLER analyzed the formation of an armor layer. All these tests showed, that the bed eroded regularely over the whole length of the channel, till it finally stabilized at its final position. GESSLER observed that the armoring layer developed in the following way: In a first stage, the eroded material was transported in dunes with a height of about 1 to 1.5 times the maximum grain size diameter. These dunes appeared all over the channel at the beginning of the test. In a second stage - at lower sediment transport rates - the dunes disappeared. Secondary flow cells regrouped the coarse and fine sediments in separate longitudinal stripes. Finally a regular armor layer formed.

a) Wall influence

The wall influence is taken into account based on EINSTEIN (1934) and the friction coefficient of the bed can be computed according to Table 3.3 for the straight inlet reach.

	Measured data					Calculated data for subareas								Target cells				Shear stress
							A_0			A_w			A_{tot}	based on subsections			avg	
Test	Q	S_e	h	A	U	P_0	f_0	R_{h0}	P_w	$d_{w,90}$	f_w	R_{hw}	f_m	R_{h0}/f_0	R_{hw}/f_w	R_{hm}/f_m	R_{hm}/f_m	τ_0
-	m3/s	%	m	m2	m/s	m	-	m	m	mm	-	m	-	m	m	m	m	N/m2
(1)	(2)	(3)	(4)	(5)	(6)	(7)	(8)	(9)	(10)	(11)	(12)	(13)	(14)	(15)	(16)	(17)	(18)	(19)
B01b	0.15	0.82%	0.15	0.15	0.98	1.00	0.10	0.15	0.15	0.1	0.02	0.03	0.08	1.48	1.48	1.48	1.48	11.8
B01c	0.18	0.96%	0.17	0.17	1.07	1.00	0.11	0.16	0.17	0.1	0.02	0.03	0.08	1.51	1.51	1.51	1.51	15.2
B01d	0.21	0.82%	0.19	0.19	1.09	1.00	0.10	0.18	0.19	0.1	0.02	0.03	0.08	1.84	1.84	1.84	1.84	14.6
C01b	0.15	0.97%	0.15	0.15	1.00	1.00	0.11	0.14	0.15	0.1	0.02	0.03	0.09	1.32	1.32	1.32	1.32	13.6
C01c	0.18	0.90%	0.17	0.17	1.05	1.00	0.10	0.16	0.17	0.1	0.02	0.03	0.08	1.57	1.57	1.57	1.57	14.3
C01d	0.21	0.94%	0.19	0.19	1.11	1.00	0.11	0.18	0.19	0.1	0.02	0.03	0.08	1.68	1.68	1.68	1.68	16.4
D01b	0.15	0.59%	0.16	0.16	0.93	1.00	0.08	0.15	0.16	0.1	0.02	0.03	0.07	1.84	1.84	1.84	1.84	8.8
D01c	0.18	0.61%	0.19	0.19	0.99	1.00	0.08	0.17	0.19	0.1	0.02	0.04	0.07	2.06	2.06	2.06	2.06	10.2
D01d	0.21	0.76%	0.20	0.20	1.08	1.00	0.09	0.18	0.20	0.1	0.02	0.04	0.07	1.94	1.94	1.94	1.94	13.5

Table 3.3:   Computation of the friction factor solving simultaneously for all hydraulic radii (Tests without macro-roughness)

The discharge Q, the energy slope S_e as well as the characteristic wall roughness size $d_{w,90}$ are supposed to be known. The wall roughness was chosen $d_{w,90} = 0.1$ mm to obtain the roughness of the plastic walls. The cross-section $A = B \cdot h$, the velocity $V = Q/A$, and the wetted perimeters $P_0 = B$, $P_w = h$ were computed first.

GESSLER proposed to compute the wall friction with KEULEGAN'S (1938) relationship and to admit a hydraulically smooth bed. Since the walls in the used channel are much smoother than the bed, the bed friction factor was determined in the present study with KEULEGAN'S (1938) relationship:

$$f_0 = \left[2.21 + 2.03 \cdot \log\left(\frac{0.0251}{S_e}\right)\right]^{-2} \tag{3.26}$$

The friction factor for smooth walls is computed with:

$$\frac{1}{\sqrt{f_w}} = -2 \cdot \log\left(\frac{2.51}{Re_w \cdot \sqrt{f_w}}\right) \tag{3.27}$$

For rough walls or banks the following friction factor can be used:

$$f_w = \left[2.21 + 2.03 \cdot \log\left(\frac{R_w}{d_{w,90}}\right)\right]^{-2} \tag{3.28}$$

The average bed friction based on the previously computed bed and wall friction can be obtained with:

$$f_m = \frac{P_0 \cdot f_0 + 2 \cdot P_w \cdot f_w}{P_0 + 2 \cdot P_w} \tag{3.29}$$

Gessler made the assumption that the average velocity as well as the energy slope are constant over each sub-area[1]; the ratios R_{h0}/f_0, R_{hw}/f_w, R_{hm}/f_m (computed in Table 3.3 with equations 3.27 to 3.29) have to be equal to each other and equal to:

$$\frac{R_{hm}}{f_m} = \frac{V^2}{8 \cdot g \cdot S_e} \tag{3.30}$$

Finally the Shields parameter $\theta_0 = R_{h0} \cdot S_0 / ((s-1) \cdot d_{90})$ and the bed shear stress $\tau_0 = \theta \cdot (\gamma_s - \gamma_w) \cdot d_{90} = R_{h0} \cdot S_0 \cdot \gamma_w$ can be computed.

b) Armoring layer

GESSLER'S (1965) method to determine the grain size distribution of the armoring layer needs the energy slope, the water depth, the discharge and the grain size distribution of the substrate to be known. The computation procedure is based on the assumption that all subareas (the two areas acting on the side walls or banks and the one acting on the bed) have the same friction slope S_e and the same mean velocity V (GESSLER, 1965).

1. The grain size distribution of the substrate material needs to be known. d_i is the sieve opening, d_{gi} the mean diameter between two sieves associated to the part (weight) p_i remaining on the sieve d_i.

2. The critical shear stress τ_{cr} for each sediment fraction is determined based on the Shields diagram ($Re^* \rightarrow \theta_c \rightarrow \tau_{cr}$).

3. Determine the probability that the sediment fraction will not move with equation 3.25 (determine the probability of τ_{cr}/τ with a normal distribution centered on $\mu = 1$ with standard deviation $\sigma = 0.57$)

4. The part of the sediment fraction i of the armoring layer is established with

$$p_{i,\,arm} = \frac{\displaystyle\int_{d_{min}}^{d_i} (q_i \cdot p_i) dd}{\displaystyle\int_{d_{min}}^{d_{max}} (q_i \cdot p_i) dd} \tag{3.31}$$

5. GESSLER (1970) suggested to use a stability coefficient of the armoring layer defined as the mean probability for the armor layer grains to stay:

$$\overline{q_{arm}} = \frac{\displaystyle\int_{d_{min}}^{d_{max}} (q_i \cdot p_i) dd}{\displaystyle\int_{d_{min}}^{d_{max}} (q_i \cdot p_i) dd} \tag{3.32}$$

GESSLER compared measurements in the Aare River, upstream the Lake of Brienz in Switzerland at discharges between 95 and 215 m^3/s with his computational method and obtained a good

---

1. This simplifying assumption is quite common, despite the fact that the velocity near to the boundaries are decreasing. Nevertheless, the results obtained with this simplification give satisfactory results.

agreement. Additional measurements in irrigation channels in San Luis Valley in Colorado did not fit very well with the predicted values.

He concluded that

- a self-stabilization of the bed occurs, due to armoring of the bed surface
- the armoring layer is found to be essentially constituted of the biggest grain size fraction, but some small and smallest fractions are found yielding behind the coarse grains.
- the grain size distribution of the armor layer depends on the grain size distribution of the substrate and the average bed shear stress to which the bed was submitted.
- for too high bed shear stresses (about $2 \cdot \theta_{cr}$), no self-stabilization takes place.

3.4 Sediment transport capacity

3.4.1 Introduction

Many textbooks and documents give a good overview of the sediment transport formulae, like e.g. GRAF (1971, 1984) GRAF & ALTINAKAR (1998), JÄGGI (1999), RAUDKIVI (1982), YALIN (1977), ZANKE (1982), SCHEUERLEIN & SCHÖBERL (2001).

In general, the bed load transport rate Q_b is given as a function of the difference between the shear stress τ acting on the river bed and a critical shear stress τ_{cr} at which the sediment transport starts, or in dimensionless form as the sediment transport rate as a function of the difference between dimensionless shear and its critical value.

$$Q_b = fct(\tau - \tau_{cr}) \quad or \quad \Phi = fct(\theta - \theta_{cr}) \tag{3.33}$$

The dimensionless transport rate can be used to compare different sediment transport formulae:

$$\Phi = \frac{q_b}{\rho_s \cdot \sqrt{(s-1) \cdot g \cdot d^3}} \tag{3.34}$$

where
$$q_b = \frac{Q_b}{B}; \quad s = \frac{\rho_s}{\rho_w} \tag{3.35}$$

The dimensionless shear stress or Shields parameter θ is described in paragraph 3.4.2/2)

3.4.2 Transport formulae based on a uniform grain diameter

The present paragraph gives some transport equations which are based on a single grain size diameter. Often, the presence of an armor layer is introduced in the scour formulae by using the mean diameter of the armoring layer instead of the mean diameter of the substrate. The mean diameter of the armoring layer is often chosen equal to d_{90} of the substrate. To predict the sediment transport rate in the present study, the extended formula of MEYER-PETER - MÜLLER established by SMART & JÄGGI (1983) was used.

1) Du Boys (1879)

Based on observations of a 115 km long reach of the Rhone River between the bridge of St-Vallier and the Ardèche River in France, DU BOYS (1879) developed his drag force theory, which is still the base for some actual sediment transport formulae. His formula considers the product of the flow depth and the bed slope as the main parameter of sediment transport. He formulated the drag force as:

$$D = \frac{\rho_w \cdot h_m}{g} \cdot g \cdot S = \rho_w \cdot h_m \cdot S \tag{3.36}$$

Du Boys gave the thickness of the considered moving sediment layer for a unit surface ($1 \ m^2$):

$$e \leq \frac{1000 \cdot h_m \cdot S}{(s-1) \cdot \tan\phi} \qquad (3.37)$$

This sediment layer is subdivided in horizontal slides. Each of these slides moves with a different velocity decreasing from the bed surface. Du Boys gives the sediment transport rate with:

$$q_s = \chi \cdot D \cdot (D - D_{cr}) \qquad (3.38)$$

where $D = 1000 \cdot h_m \cdot S$ is the drag shear force according to Du Boys in kg/m^2, D_{cr} the critical drag shear force and χ a transport coefficient in $m^6/kg^2/s$. D_{cr} and χ need to be determined for each grain size.

The direct correlation between the sediment transport rate Q_s and the factor $h \cdot S$ can be found in most actual formulae. Though the validity of this correlation had been contested by Meyer-Peter et al. (1934), they finally introduced it in their formula of 1948.

2) *Shields (1936)*

Shields (1936) compared the "force of the flow on the grain" to the "resistance to the movement of the grain" based on tests with uniform grain size. Based on theoretical considerations and on laboratory tests he showed that the inception of the movement is a function of the Shear Reynolds number $Re^* = (V^* \cdot d)/\nu$ (see Fig. 3.5).

$$\frac{\rho_w}{\rho_s - \rho_w} \cdot \frac{R_h \cdot S}{g \cdot d} = fct(Re^*) \qquad (3.39)$$
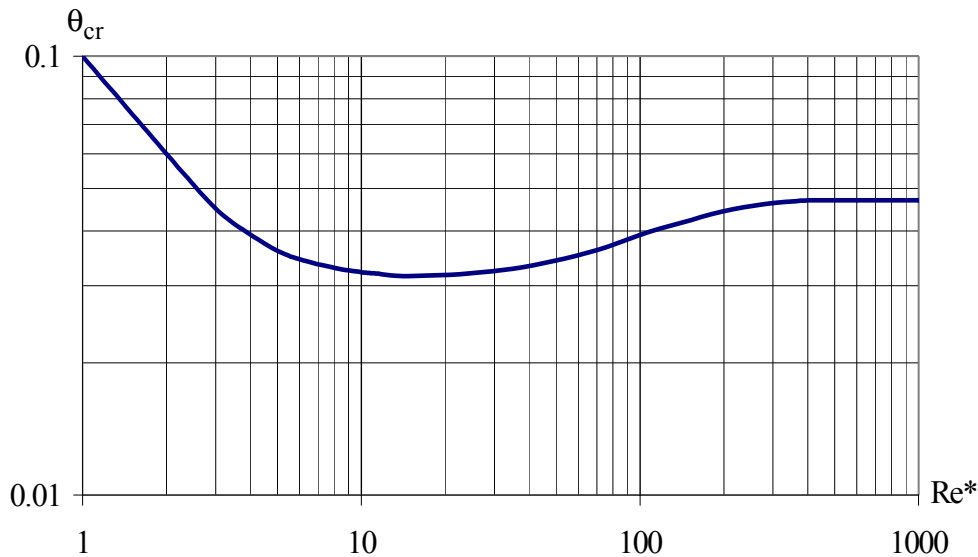
Figure 3.5:   Shields diagram [Günther, 1971, Fig. 6]

In the fully turbulent area, Shields assumed $\theta_{cr} = 0.050$. Meyer-Peter & Müller reduced the critical shear stress to $\theta_{cr} = 0.047$. Gessler (1965) pointed out that the critical value for the dimensionless shear stress given by Shields is systematically too high because he based his work on tests where bedforms occurred. His values include the effect of theses bedforms.

In the second part of his work, SHIELDS gave a dimensionless relation for the sediment transport rate:

$$\frac{Q_b}{Q} = fct\left(\frac{\tau - \tau_{cr}}{(\rho_s - \rho_w) \cdot g \cdot d}\right) \tag{3.40}$$

where Q_b and Q are the bed load transport rate and the discharge; the shear stress is given by

$$\tau = \rho_w \cdot g \cdot R_h \cdot S \quad \text{and} \quad \tau_{cr} = \theta_{cr} \cdot (\rho_s - \rho_w) \cdot g \cdot d_{50} \tag{3.41}$$

The dimensionless shear stress, also called Shields parameter is defined as

$$\theta = \tau^* = \frac{\tau}{(\rho_s - \rho_w) \cdot g \cdot d} = \frac{R_h \cdot S_0}{(s - 1) \cdot d} \tag{3.42}$$

If the influence of the side wall is considered, the hydraulic radius is replaced with the part of the hydraulic radius, acting on the bed R_{h0}.

3) *Meyer-Peter & Müller (1948) (MPM)*

MEYER-PETER, FAVRE & EINSTEIN (1934) performed an important test series between 1930 and 1934 on sediment transport with uniform grain size distributions, which served to establish a first bedload formula. A big series of additional tests was carried out by MEYER-PETER & MÜLLER (1948). These tests, performed with different sediment mixtures in 0.15 to 2.00 m wide channels at bed slopes between 0.1 and 2.3 %, allowed to show that the shear stress is a main parameter for the sediment transport rate. MEYER-PETER & MÜLLER'S formula was established for normal flow conditions and for conditions where the grain size distribution of the transported material is equal to the one of the sub-layer.

In 1948 they published their well known formula:

$$\left(\frac{K_0}{K_S}\right)^{1.5} \rho_w \cdot g \cdot R_{h0} \cdot S_e = 0.047(\rho_s - \rho_w) \cdot g \cdot d_m + \frac{1}{4} \cdot \rho_w^{1/3} \cdot [(\rho_s - \rho_w) \cdot g \cdot q_b]^{2/3} \tag{3.43}$$

The above equation can be written as "equilibrium of the forces acting on the grain", since all terms have the unit of a shear stress: $\tau_{delta} = \tau - \tau_{cr}$.

τ is the shear stress induced by the flow, τ_{cr} the critical shear stress that is necessary to get the grain moving and τ_{delta} the additional shear stress keeping the grain moving. Equation 3.43 can be rewritten in another form as

$$\Phi = 8 \cdot (\theta - \theta_{cr})^{3/2} \tag{3.44}$$

where $\quad \Phi = \dfrac{q_b}{\sqrt{(s-1) \cdot g \cdot d^3}}; \quad \theta = \left(\dfrac{K_0}{K_S}\right)^{1.5} \cdot \dfrac{R_{h0} \cdot S_e}{(s-1) \cdot d_m}; \quad \theta_{cr} = 0.047 \tag{3.45}$

Frequently, the formula of MEYER-PETER & MÜLLER is also written as:

$$Q_b = \frac{8 \cdot \rho_s \cdot B \cdot \sqrt{g}}{s-1} \cdot \left[\left(\frac{K_0}{K_S}\right)^{1.5} \cdot \frac{Q_0}{Q} \cdot h \cdot S - \theta_{cr} \cdot (s-1) \cdot d_m\right]^{1.5} \tag{3.46}$$

where Q_0 is the part of the discharge acting on the bed. The term $(Q_0/Q) \cdot h$ accounts for the influence of the side walls. This term can be replaced by R_{h0}. The coefficient $(K_0/K_S)^{1.5}$ introduces the bedforms in the equation. MEYER-PETER & MÜLLER did not give a formula to determine K_0. If the water depth h and the discharge Q are known, the influence of the bedforms can be computed with

$$K_0 = \frac{K_S \cdot K_w \cdot B^{0.67}}{[B \cdot K_w^{1.5} + 2 \cdot h \cdot (K_w^{1.5} - K_S^{1.5})]^{0.67}} \tag{3.47}$$

K_S is the roughness coefficient computed with Strickler's formula (eq. 3.11)

4) *Smart & Jäggi (1983)*

SMART & JÄGGI (1983) extended the method of MEYER-PETER & MÜLLER (1948) to channels and rivers with steeper slopes. They based their study on an additional set of tests in a 10 and 20 cm wide flume with bed slopes between 3 and 20 %. Based on their results and on the tests of MEYER-PETER & MÜLLER, they proposed the following relation to compute the sediment transport capacity:

$$Q_b = B \cdot \frac{4 \cdot \rho_s}{s - 1} \cdot \left(\frac{d_{90}}{d_{30}}\right)^{0.2} \cdot R_0 \cdot V \cdot S^{1.6} \cdot \left(1 - \frac{\theta_{cr} \cdot (s - 1) \cdot d_m}{R_0 \cdot S}\right) \tag{3.48}$$

which is equivalent to

$$\Phi = 4 \cdot \frac{V}{V*} \cdot \left(\frac{d_{90}}{d_{30}}\right)^{0.2} \cdot S^{0.6} \cdot \theta^{0.5} \cdot (\theta - \theta_{cr}) \tag{3.49}$$

With $\theta_{cr} = 0.050$, the authors used a slightly higher value compared to MEYER-PETER & MÜLLER (1948). The sediment transport rate depends only weakly on the coefficient $(d_{90}/d_{30})^{0.2}$. Neglecting this coefficient (put to 1.05) and assuming a relative sediment density of $s = 2.68$, the sediment transport rate can be computed with the following simplified formula:

$$Q_b = 2.5 \cdot B \cdot q \cdot S^{0.6} \cdot \left(S - \frac{d_m}{12.1 \cdot h_m}\right) \tag{3.50}$$

The correlations of equations 3.48 and 3.50 are of $r^2 = 0.97$ respectively $r^2 = 0.95$ and standard errors of $s_E = 66$ % respectively $s_E = 22$ % compared with the tests of MEYER-PETER & MÜLLER.

HUNZIKER (1995) performed another extension of MEYER-PETER & MÜLLER'S formula, allowing the computation of the sediment transport rate for each sediment fraction of the bed material (see 3.4.3/5)).

5) *Hunziker (1995)*

In the frame set of his study on sediment transport by grain size fractions, HUNZIKER (1995) analyzed the results of ZARN (1997) which were performed in a 3 m wide and 26 m long channel. He further analyzed the results of MEYER-PETER & MÜLLER (1948) and observed a systematic over-

estimation of the sediment transport rate which was already observed by JÄGGI (1994). This is due to the fact that MEYER-PETER & MÜLLER overestimated the influence of the bedforms. JÄGGI proposed to reduce the shear stress by 15 to 20 % which yields:

$$\phi = 8 \cdot (0.8 \cdot \theta - \theta_{cr})^{1.5}; \quad \theta = \frac{R_h \cdot S_0}{(s-1) \cdot d_m}; \quad \theta_{cr} = 0.047 \tag{3.51}$$

This modification leads to the desired correction of the sediment transport rates for high shear stresses, but it induces important differences for small shear stresses, since the transport starts at an effective critical shear stress of $\theta_{cr} = 0.06$. Therefore HUNZIKER (1995) proposed the following modification of MEYER-PETER & MÜLLER'S formula:

$$\phi = 8 \cdot (0.73 \cdot (\theta - \theta_{cr}))^{1.5} \quad \text{or} \quad \phi = 5 \cdot (\theta - \theta_{cr})^{1.5} \tag{3.52}$$

HUNZIKER'S modification is confirmed by propositions of other authors like LUQUE & VAN BEEK (1976) who proposed a factor of 5.7 instead of 8.

Finally, HUNZIKER established a transport model allowing the computation of the sediment transport rate for each sediment fraction. The total transport rate is given as the sum of the transport rates of the sediment fractions:

$$q_b = \Sigma q_{bi} \tag{3.53}$$

A comparison with data sets of MEYER-PETER & MÜLLER (1948), ZARN (1997) showed a good correlation between computed and measured transport rates. The prediction of the bed armoring was tested against laboratory data of GESSLER (1965) and GÜNTER (1971) with good agreement.

3.4.3   Summary of mentioned sediment transport equations

AUTHOR(S)	EQ.	CHARACTERISTIC DIAMETER (MM)	DOMAIN OF VALIDITY	REMARKS
Du Boys (1879)	3.38	Rhone River in France		Fields data
Shields (1936)	3.40			Lab data
Meyer-Peter & Müller (1948)	3.44, 3.46	$d_{ug} = 5.2 \div 28.6$	$S = 0.1 \div 2.3\%$	$\theta_{cr} = 0.047$; 74 lab tests
Smart & Jäggi (1983)	3.48, 3.49	$d_{ug} = 4.2 \div 10.5$	$S = 3 \div 20\%$	$\theta_{cr} = 0.050$, 40 lab tests and tests of MPM
Hunziker (1995)	3.52	see Meyer-Peter & Müller; Smart & Jäggi		extension MPM $\theta_{cr} = 0.050$

Table 3.4:   Comparison of sediment transport equations

3.5 *Bed topography in the bend*

3.5.1 Introduction

In general scour formulae are established based on equilibrium considerations of the forces acting on a grain. Taking the water depth h (free water surface to bed surface) and the radius r as variables, the local lateral bed slope is usually given by:

$$\sin\beta = K \cdot \frac{h_s}{r} \tag{3.54}$$
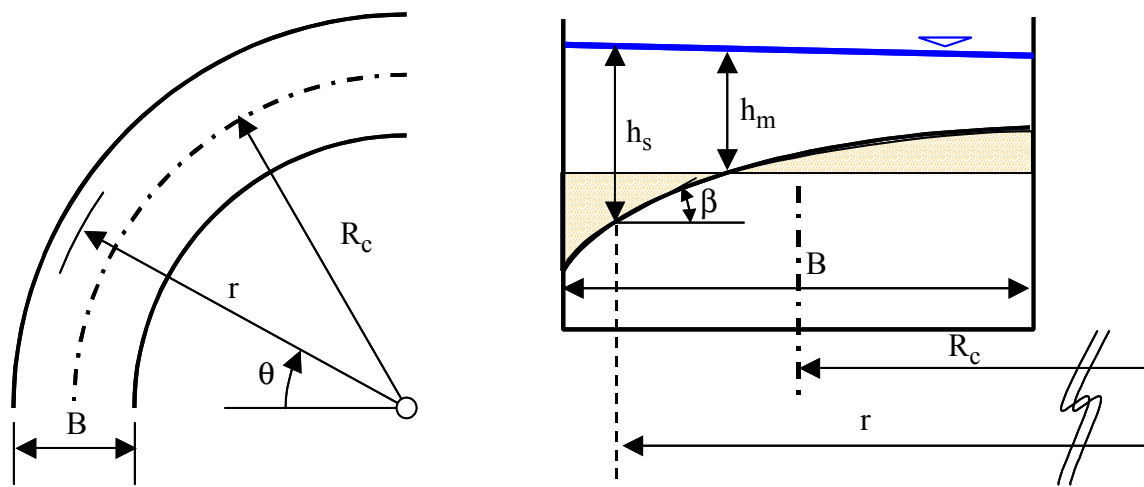
Figure 3.6: Definition sketch; situation and cross-section

In order to obtain the cross-section at the location of maximum scour, $\sin\beta$ is approached with $\sin\beta \approx \tan\beta = dh/dr$ and yields (after integration):

$$\frac{h_s}{h_m} = \left(\frac{r}{R_c}\right)^K \tag{3.55}$$

3.5.2 Scour formulae

1) *Fargue (1868) and Williams (1899)*

Louis Jérôme Fargue (1872-1910) (cited in Fargue, 1868 and in Williams, 1899) was probably the first to establish a scour formula for river bends. He established six laws based on observations of a 22 km long reach of the Garonne River in France, derived with momentum considerations. Two of them are given hereafter:

1. Law of displacement: The deepest and the highest point of the bed topography in a bend are located towards half the opening angle between beginning and end of the bend or in downstream direction of this point.

2. Law of depth: The greater the curvature, the greater the depth.

WILLIAMS (1899) gives a derivation of FARGUE's laws using his own shock pulse surface theory. This theory of shock pulse surfaces does not only allow the computation of the maximum scour depth, but also the location of the scour holes even for meandering rivers (see Fig. 3.7)
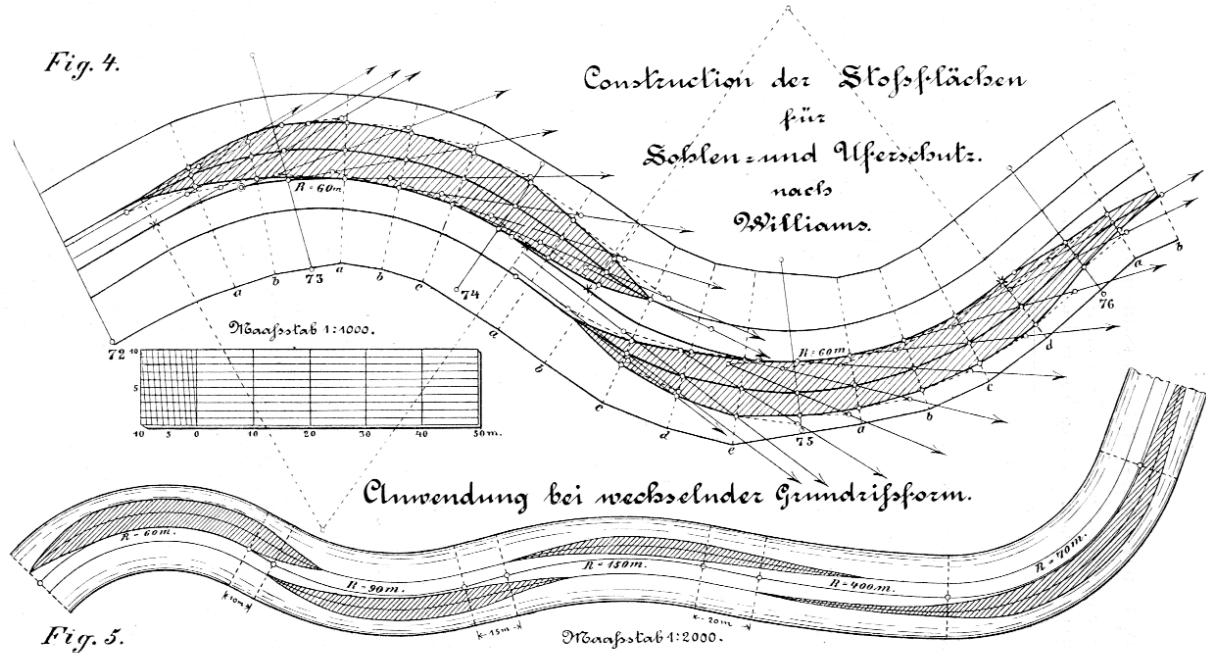
Figure 3.7:   Location of scour holes by means of the shock pulse surface theory [Williams 1899, Fig. 4 and 5]

Based on impulse consideration on the stream bank WILLIAMS demonstrates the validity of FARGUE's equation for the maximum scour depth given by the following equation:

$$h_{s,\,max} \;=\; c \cdot \sqrt{1 + m^2} \cdot \sqrt{\left(1 - \left(\frac{R_c}{R_c + B/2}\right)^2\right)} \;=\; c \cdot \sqrt{1 + m^2} \cdot \sin\frac{\phi}{2} \qquad (3.56)$$

with
$$c \;=\; \left(1 + \frac{V_0^2}{V_m^2}\right) \cdot \frac{1}{\sqrt{1 + m^2}} \cdot \mu \cdot \frac{A_{shock} \cdot V_m^2}{2 \cdot g} \qquad (3.57)$$

The coefficient c depends on the size of the shock surface A_{shock}, its roughness μ, the average flow velocity V_m, the flow velocity on the ground V_0 and the bank slope m : 1 (m = 0 for vertical side walls). ϕ is the angle between the tangents at the beginning and the end of the bend (= the opening angle between beginning and end of the bend). The maximum scour is supposed to be located at about $\phi/2$.

For a test section at the white Elster in Eastern Germany, WILLIAMS admitted that c = 0.5 is constant. Equation 3.57 depends on the radius of curvature, the geometry of the cross-section (B, m) and the velocity distribution (V_0, V_m)

2)   *Van Bendegom (1947)*

VAN BENDEGOM (1947) (given in ODGAARD (1981) based his equation on equilibrium considerations on a grain. A grain on an inclined plane (angle β between horizontal surface and inclined plane, see Fig. 3.8) is submitted to its weight, the buoyancy and the stream force. Weight and buoyancy can be summarized by the vertical force:

$$G' = (\rho_s - \rho_w) \cdot g \cdot k_1 \cdot d^3 \tag{3.58}$$

ρ_s and ρ_w are the densities of the sediment and the fluid, g is the gravity constant and d the characteristic grain size diameter. The proportionality factor k_1 corresponds to the ratio between the volume of the grain and d^3.

The dynamic stream force can be split in two components: the drag force D acting in the plane of the bed surface and the lift force L acting normally to it. The normal projection D of the dynamic stream force on the bed surface corresponds to the direction of the flow velocity on the bed surface. The drag force can be split in a component D_θ in stream direction and a component D_r in radial direction. δ is the opening angle between D and D_θ (see Fig. 3.8).
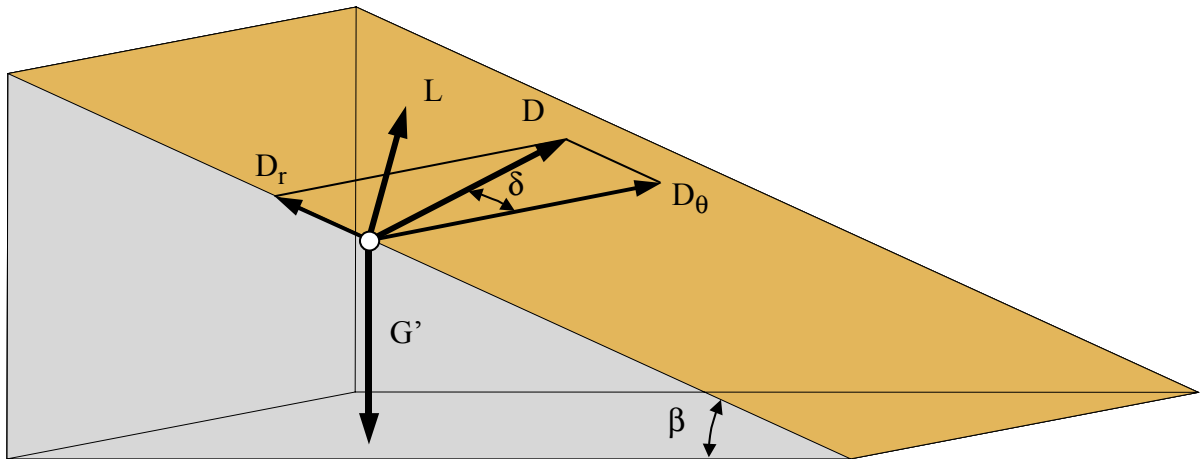
Figure 3.8:   Forces acting on a grain on an inclined plane

VAN BENDEGOM assumes that at equilibrium state, the grain moves only in stream direction, that the radial components of the forces compensate each others and that the dynamic lift force L, can be neglected. The equilibrium of the forces in radial direction consequently writes:

$$D_r = G' \sin\beta \tag{3.59}$$

VAN BENDEGOM put for D_θ the relation:

$$D_\theta = \frac{\rho_w \cdot g \cdot V^2 \cdot A_\perp}{C^2} \tag{3.60}$$

In this equation V designates the depth averaged flow velocity, $A_\perp$ the projection of the surface of the grain which is exposed to the flow in perpendicular direction to D_θ and C is the CHEZY coefficient which is assumed to take a value of 50 m$^{1/2}$/s.

VAN BENDEGOM further determined the deviation angle δ between the direction of the shear stress D (respectively the velocity) on the bed surface and the longitudinal axis of the channel D_θ as $\tan\delta = 10 \cdot h/r$. Taking into account that $D_r = D_\theta \cdot \tan\delta$, he obtained:

$$D_r = \frac{10 \cdot g}{C^2} \cdot \rho_w \cdot g \cdot V^2 \cdot A_\perp \cdot \frac{h}{r} \tag{3.61}$$

Replacing $A_\perp$ with $A_\perp = k_2 \cdot d^2$, where k_2 is a factor similar to k_1 for the volume of the grain in equation 3.57, he obtained after introducing equation 3.61 in equation 3.59:

$$\sin\beta = \frac{10 \cdot g}{C^2} \cdot \frac{V^2}{(s-1) \cdot g \cdot d} \cdot \frac{k_2}{k_1} \cdot \frac{h_s}{r} = \frac{10 \cdot g}{C^2} \cdot Fr_d^2 \cdot \frac{k_2}{k_1} \cdot \frac{h_s}{r} = 0.0589 \cdot Fr_d^2 \cdot \frac{h_s}{r} \tag{3.62}$$

where $s = \rho_s/\rho_w$. For spheres $k_1 = \pi/6$ and if the grain is completely exposed to the stream force (sphere on a smooth surface) $k_2 = \pi/4$.

This formula is based on spherical grains which are completely exposed to the flow. The equilibrium state is reached if no transport in radial direction occurs, i.e. if the grains only move in stream direction.

The assumption of a complete exposure of the grains is conservative and leads to underestimated values for β - therefore the lateral bed slope will be too small. The omission of the buoyancy causes an overestimation of the radial force in the downwards direction. This leads to an additional underestimation of the lateral bed slope β.

ODGAARD (1981) compared the predicted lateral bed slope of different formulae and compared them with laboratory and field data. For small slopes (only), a good correlation with the formula of VAN BENDEGOM can be obtained if the constant in equation 3.62 is increased from 0.059 to about 0.20 for laboratory data and even to 0.8 for field data.

3) Engelund (1974)

ENGELUND (1974) also established his formula considering the forces acting on a sediment grain. He assumed that the dynamic lift force L acts in vertical direction and that the grain slips on the bed. He expressed the equilibrium state, at which the grain just moves, by means of the slide friction law as:

$$(G' - L) \cdot \cos\beta \cdot \tan\phi = D_\theta \tag{3.63}$$

$(G' - L) \cdot \cos\beta$ corresponds to the force acting on the grain perpendicularly to the bed, $\tan\phi$ is the coefficient of friction and ϕ is the dynamic shear angle. The equilibrium condition in radial direction can be expressed as:

$$(G' - L) \cdot \sin\beta = D_r \tag{3.64}$$

Dividing equation 3.64 by equation 3.63, yields:

$$\frac{\tan\beta}{\tan\phi} = \frac{D_r}{D_\theta} = \tan\delta \tag{3.65}$$

ENGELUND determined the deviation angle δ based on a simple analytical model of the flow in a bend, which partially takes into account the roughness of the bed.

$$\tan\delta = 7 \cdot \frac{h_s}{r} \tag{3.66}$$

From equations 3.65 and 3.66, ENGELUND finally obtained:

$$\tan\beta = 7 \cdot \frac{h_s}{r} \cdot \tan\phi \tag{3.67}$$

Putting $\tan\beta = \partial y / \partial r \approx \partial h_s / \partial r$ and after integration, he got:

$$h_s = a \cdot r^{7 \cdot \tan\phi} \tag{3.68}$$

describing the flow depth (and consequently the bed topography) in radial direction. The factor a is an integration constant. By comparing his equation to model tests performed by HOOK (1974), Engelund found values for the dynamic shear angle ϕ ranging between 27° and 33°.

ENGELUND'S formula, combined with the proposed flow model, does not only allow the determination of the radial bed profile, but also a general computation of the bed topography in a bend. ENGELUND extended his approach to bends with variable radius of curvature. It has to be mentioned that his flow model is based on a rectangular cross-section with a fixed horizontal bed. Furthermore, the flow model is restricted to channels with a high width to depth ratio and the radius has to be significantly larger that the flow depth.

Under these mentioned conditions, $\tan\delta$ depends only insignificantly on the roughness of the bed and can be assumed to be almost constant. Consequently, equation 3.67 shows that the radial bed slope depends only on the dynamic shear angle ϕ, which is constant for a given bed material. Consequently, the radial bed topography depends only on the ratio h/r.

Results of laboratory tests and field observations (HOOK, 1974) show that $\tan\beta / (h/r)$ is not constant (ODGAARD, 1981). ODGAARD compared ENGELUND's formula with lab and field data. The correlation is relatively poor. According to Odgaard, this is due to the fact that ENGELUND's formula was established for weakly meandering channels, whereas his data sets were based on a fully developed flow in bends for which the assumptions of ENGELUND are no longer valid.

4) *Bridge (1976)*

BRIDGE'S (1976) formula is similar to the one of ENGELUND, but using $\tan\delta = 11 \cdot h_s / r$ based on the work of ROZOVSKII (1957) which is resumed in the present paragraph. The end of this paragraph gives an overview of the study of BAGNOLD (1966) concerning the friction factor, which ranges between $\tan\phi = 0.375 \div 0.75 = \text{fct}(\theta, Fr_d)$.

ROZOVSKII (1957), showed theoretically that the deviation angle δ can be expressed for smooth channels by:

$$\tan\delta \;=\; \frac{v_r}{v_\theta} \;=\; \frac{1}{\kappa^2} \cdot \frac{F_1(z) - \dfrac{\sqrt{g}}{\kappa \cdot C} \cdot F_2(z)}{1 + \dfrac{\sqrt{g}}{\kappa \cdot C} \cdot (1 + \ln z)} \cdot \frac{h_s}{r} \;=\; k \cdot \frac{h_s}{r} \tag{3.69}$$

and for rough channels by:

$$\tan\delta \;=\; \frac{v_r}{v_\theta} \;=\; \frac{1}{\kappa^2} \cdot \frac{F_1(z) - \dfrac{\sqrt{g}}{\kappa \cdot C} \cdot [F_2(z) + 0.8 \cdot (1 + \ln z)]}{1 + \dfrac{\sqrt{g}}{\kappa \cdot C} \cdot (1 + \ln z)} \cdot \frac{h_s}{r} \tag{3.70}$$

where z is the elevation above bed level and the functions F_1 and F_2 are given with:

$$F_1(z) = \int \frac{2 \cdot \ln z}{z - 1} dz \ \text{ and } \ F_2(z) = \int \frac{\ln^2 z}{z - 1} dz \tag{3.71}$$

In both equations (3.69, 3.70), a variation of the Chezy coefficient has only a small influence on the deviation angle δ. Approaching these equations by a linear equation, the coefficient k (eq. 3.69) takes the value of 10 to 12 for smooth and of 11 to 11.5 for rough surfaces.

ROZOVSKII compared his equation with a factor $k = 11$ against laboratory data of nine other authors and his own laboratory data, covering a large range of parameters ($V = 0.01 \div 0.68 \ \text{m/s}$, $Fr = 0.03 \div 0.68$, $Re = 3\,000 \div 300\,000$, $h/B = 0.02 \div 1.20$, $h/R_c = 0.01 \div 2.40$) with rectangular, triangular and parabolic cross-sections. He completed his data set with measurements on the Desna River in a reach located between Chernigov (Ukraine) and the confluence with the Dnjepr. The Desna has a very tortuous course flowing through sandy alluvial bed material ($R_c \approx 400 \ \text{m}$). Comparisons show an excellent agreement between measured and computed values (see Fig. 3.9).
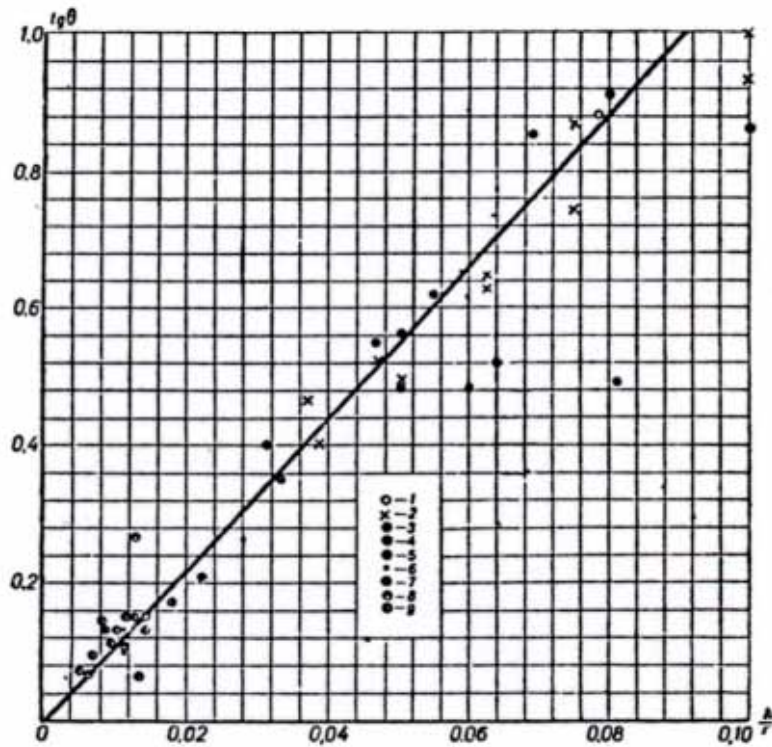
Figure 3.9: *Comparison of* $\tan\delta = 11 \cdot h/r$ *with laboratory and field data*
1-5: Rozovskii's tests no. I, II, VI, VII, IIX; 6: polygonal channel; 7: sand model;
8: Snov River; 9: Desna River, [Rozovskii. 1957, Fig. 81, p.194]

Therefore BRIDGE proposed the following formula:

$$\tan\beta = 11 \cdot \frac{h_s}{r} \cdot \tan\phi \qquad (3.72)$$

which yields after replacement of $\tan\beta \approx dh_s/dr$ and after integration:

$$h_s = a \cdot r^{11 \cdot \tan\phi} \qquad (3.73)$$

BRIDGE used the friction angle given by BAGNOLD (1954, 1956, 1966). Based on tests with small spheres with diameter 1.3 mm, BAGNOLD indicated that the friction angle $\tan\phi$ is of the same order as the 'static' friction coefficient for granular solids (see also § 3.1.1 g). If the grains are sheared over the surface, $\tan\phi$ ranges from 0.32 (for completely inertial conditions) to 0.75 (for completely viscous conditions). He found $\tan\phi$ to be depending on a Reynolds number, but finally assumed that within the limits 0.32 to 0.75, $\tan\phi$ was a function of the grain size only. In a later study on saltation, BAGNOLD (1973) gave an approximation for $\tan\phi$, for a rolling movement. For grains of normal shape and roughness in lower flow regime bed load transport, this constant value is 0.63. He admitted that $\tan\phi$ can be as small as 0.32 for fully inertial conditions in natural streams and greater than 0.63 if viscosity effects are more significant.

The given limit of 0.63 is equivalent to a friction angle of 32°, corresponding well with the friction angle of sand or finer components. Since the present study analyses gravel bed rivers, the friction angle is somewhat bigger (see 3.1.1 g).

Based on the works of ALLEN (1970), BRIDGE further gave a relation for the size of moving bed particles. The formula was established, neglecting the lift force.

$$d = \frac{3 \cdot \rho_w \cdot S_e \cdot h_s}{2 \cdot \tan\phi \cdot (\rho_s - \rho_w)} \tag{3.74}$$

Finally, BRIDGE compared his formula to field data, measured in the River Endrick in Scotland (BLUCK, 1971), in the River Desna, USSR (ROZOVSKII, 1957) and the River South Esk in Glen Clova, Scotland. Cross-sections were chosen in areas of fully developed spiral flow. All the rivers had ripples and dunes, indicating that the flow is in the lower flow regime. The grain size of River South Esk is of 1 mm, the one of River Endrick is coarser, whereas the one of the Desna River is finer. The longitudinal bed slope of River Esk is of 0.025 to 0.030 %. Bridge used values of $\tan\phi$ between 0.4 and 0.5 in order to obtain a good prediction. He further proposed to adjust the values of $\tan\phi$ to increase the precision of the prediction of the radial bed topography.

5)   *Kikkawa, Ikeda & Kitagawa (1976)*

KIKKAWA ET AL. (1976) defined the velocity distribution based on the equation of motion in radial direction, by means of a simplified stream function of the secondary flow. They assumed a constant eddy viscosity and a logarithmic velocity distribution, which is modified in radial direction with a special distribution function. Their equation was established for sand bed rivers and tested against laboratory data on fixed and mobile bed ($Fr = 0.56 \div 0.63$; $B/h = 16 \div 20$). The velocity distribution in stream direction at the location with flow depth h_m is described by:

$$\frac{v_\theta}{V*} = \frac{V}{V*} + \frac{1}{\kappa} \cdot \left(\ln\frac{z}{h_m} + 1 \right) \tag{3.75}$$

where v_θ is the velocity in stream direction at level z, $V*$ the shear velocity averaged in radial direction and V the average velocity in the cross-section $(V = Q/A)$.

The velocity profile at the location r in the cross-section becomes after introduction of a distribution function $f(r)$:

$$\frac{v_\theta}{V*} = f(r)\left[\frac{V}{V*} + \frac{1}{\kappa} \cdot \left(\ln\frac{z}{h_m} + 1 \right) \right] \tag{3.76}$$

where h is the local flow depth. The distribution function $f(r)$ corresponds to the velocity distribution v_θ normalized by the average velocity V.
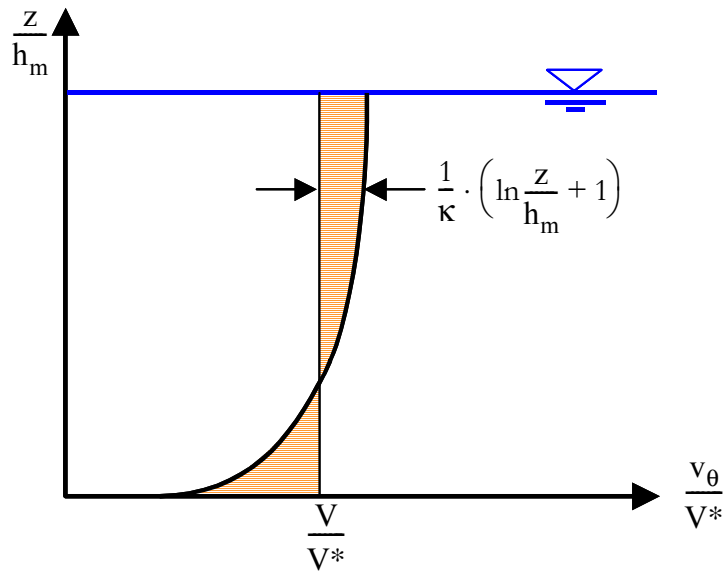
Figure 3.10: Velocity distribution at the location of the average flow depth h_m

For the ratio between radial and average velocity in the cross-section, KIKKAWA ET AL. found an analytical solution

$$\frac{v_r}{V} = (f(r))^2 \cdot \frac{h}{r} \cdot \frac{1}{\kappa} \cdot \left[F_A(\xi) - \frac{1}{\kappa} \cdot \frac{V^*}{V} \cdot F_B(\xi) \right] \tag{3.77}$$

with

$$F_A(\xi) = -15 \cdot \left(\xi^2 \cdot \ln\xi - \frac{1}{2}\xi^2 + \frac{15}{54} \right)$$

$$F_B(\xi) = \frac{15}{2} \cdot \left(\xi^2 \cdot \ln^2\xi - \xi^2\ln\xi + \frac{1}{2}\xi^2 - \frac{19}{54} \right) \tag{3.78}$$

where $\xi = z/h$. Putting $\xi = 0$, the radial velocity component at the bed can be given:

$$\frac{v_r(0)}{V} = (f(r))^2 \cdot \frac{h}{r} \cdot \frac{1}{\kappa} \left[-4.167 + 2.639 \cdot \frac{1}{\kappa} \cdot \frac{V^*}{V} \right] \tag{3.79}$$

The velocity vector on the bed surface is given by equations 3.76 and 3.77 depending on V, V^* and the forced vortex distribution $f(r)$.
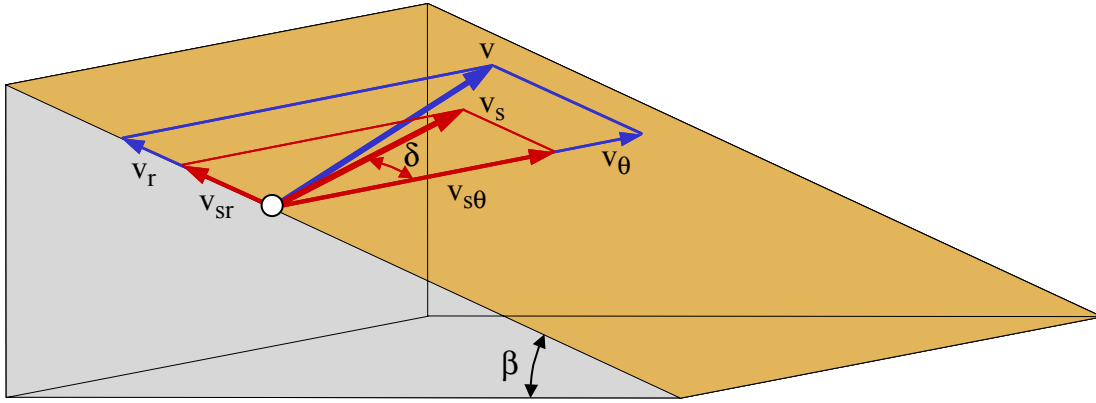
Figure 3.11: Velocity components of the flow and of the grain

According to figure 3.11, the flow velocity on the bed is noted v, the velocities in stream and radial direction are v_θ and v_r. The velocity of the grain is v_s with the corresponding components $v_{s\theta}$ and v_{sr}; δ is the deviation angle of the grain from the stream direction.

The components of the stream force acting on the grain are:

$$D_\theta = \frac{\rho_w}{2} \cdot C_D \cdot k_2 \cdot d^2 \cdot (v - v_s)^2 \cdot \frac{v_\theta - v_{s\theta}}{|v - v_s|}$$

$$D_r = \frac{\rho_w}{2} \cdot C_D \cdot k_2 \cdot d^2 \cdot (v - v_s)^2 \cdot \frac{v_r - v_{sr}}{|v - v_s|} \tag{3.80}$$

$$L = \frac{\rho_w}{2} \cdot C_L \cdot k_2 \cdot d^2 \cdot (v - v_s)^2$$

Assuming that the grain slips on the surface[1] and neglecting the longitudinal bed slope the components of the equilibrium of the grain write:

$$D_\theta - \mu \cdot (G' \cdot \cos\beta - L) \cdot \frac{v_{s\theta}}{|v_s|} = 0 \tag{3.81}$$

$$D_r - G' \cdot \sin\beta - \mu \cdot (G' \cdot \cos\beta - L) \cdot \frac{v_{sr}}{|v_s|} - \frac{G}{g} \cdot \frac{v_s^2}{r} \cdot \frac{v_{s\theta}}{|v_s|} = 0 \tag{3.82}$$

where $G = \rho_s \cdot g \cdot k_1 \cdot d^3$ is the weight of the grain, $G' = (\rho_s - \rho_w) \cdot g \cdot k_1 \cdot d^3$ the weight of the grain submitted to buoyancy and $\mu = \tan\phi$ the dynamic friction coefficient.

Since the intensity of the secondary flow on the bed is small compared to the main flow and if the lateral bed slope is small, the following simplifications can be made:

$$\frac{v_{s\theta}}{|v_s|} \approx 1; \quad \frac{v_\theta}{|v|} \approx 1; \quad \frac{v_\theta - v_{s\theta}}{|v - v_s|} \approx 1; \quad \cos\beta \approx 1; \quad \sin\beta \approx \tan\beta = \frac{\partial h}{\partial r} \tag{3.83}$$

1.This assumption is not confirmed by the tests performed in the present study. The observed movement of the transported grains has to be qualified as saltation.

Introducing equations 3.80 in 3.81 and 3.82 and applying the simplifications 3.83 yields

$$|v - v_s| = \sqrt{\frac{2 \cdot k_1 \cdot d \cdot g \cdot \mu}{k_2 \cdot (C_D + \mu \cdot C_L)} \cdot \frac{(\rho_s - \rho_w)}{\rho_w}} = \sqrt{\frac{4}{3} \cdot \frac{d \cdot g \cdot \mu}{(C_D + \mu \cdot C_L)} \cdot \frac{(\rho_s - \rho_w)}{\rho_w}} \quad (3.84)$$

and

$$\frac{\rho_w}{2} \cdot C_D \cdot k_2 \cdot d^2 \cdot (v - v_s)^2 \cdot \frac{v_r - v_{sr}}{|v - v_s|} - (\rho_s - \rho_w) \cdot g \cdot k_1 \cdot d^3 \cdot \frac{\partial h}{\partial r} \quad (3.85)$$

$$- \mu \cdot \left[(\rho_s - \rho_w) \cdot g \cdot k_1 \cdot d^3 - \frac{\rho_w}{2} \cdot C_L \cdot k_2 \cdot d^2 \cdot (v - v_s)^2 \right] \cdot \frac{v_{sr}}{|v_s|} = 0$$

In this equation, the last term - the centrifugal forces - has been neglected since it is an order of magnitude smaller compared to the other forces acting on the grain. The longitudinal bed slope has also been neglected.

Combining equation 3.84 with 3.85, KIKKAWA ET AL. finally obtained a relation giving the direction of the particle movement:

$$\tan\delta = \frac{v_{sr}}{|v_s|} = \frac{v_r}{|v|} - \frac{\dfrac{\partial h}{\partial r}}{\sqrt{\dfrac{k_2}{2 \cdot k_1} \cdot \dfrac{\mu \cdot C_D}{1 + \mu \cdot \dfrac{C_L}{C_D}}} \cdot \dfrac{|v|}{\sqrt{(s-1) \cdot g \cdot d}}} \quad (3.86)$$

At stable state, they assumed that $v_{sr} = 0$, which leads to $\tan\delta = 0$; therefore

$$\frac{dh}{dr} = \sqrt{\frac{k_2}{2 \cdot k_1} \cdot \frac{\mu \cdot C_D}{1 + \mu \cdot \dfrac{C_L}{C_D}}} \cdot \frac{v_r}{\sqrt{(s-1) \cdot g \cdot d}} \quad (3.87)$$

At the bottom, v_r is given by equation 3.79. Now KIKKAWA ET AL. introduced a logarithmic velocity distribution for rough walls ($|v| = v_\theta(d) = A_r \cdot f(r) \cdot V^*$) at the particle level $z = d$ with $k_s = d$ and $A_r = 8.5$ for rough boundaries. The drag and lift coefficients for spherical sand particles were measured by CHEPIL (1958). They are given for a wide range of shear Reynolds numbers Re^*. The friction coefficient μ was measured by IKEDA (1971). The sheltering coefficient λ_0, accounts for the sheltering effects due to other particles. A study of IWAGAKI (1956) showed that the tractive force on a particle is reduced to 35% of the tractive force without sheltering if sediment transport occurs over the whole cross-section. Since this sheltering effect is defined for the square root of the tractive force, i.e. for $V^* / \sqrt{(s-1) \cdot g \cdot d}$, λ_0 is:

$$\lambda_0 = 0.592; \quad \frac{C_L}{C_D} = 0.85; \quad C_D = 0.4; \quad \mu = 0.43 \quad (3.88)$$

By substituting these values in equation 3.86, KIKKAWA ET AL. obtained:

$$\tan\delta = \frac{v_{sr}}{|v_s|} = -f \cdot \frac{V}{A_r \cdot V^*} \cdot \frac{h_s}{r} \cdot \frac{1}{\kappa} \cdot F(0) - \frac{\dfrac{\partial h}{\partial r}}{\sqrt{\dfrac{k_2}{2 \cdot k_1} \cdot \dfrac{\mu \cdot C_D}{1 + \mu \cdot \dfrac{C_L}{C_D}}} \cdot \dfrac{f \cdot A_r \cdot \lambda_0 \cdot V^*}{\sqrt{(s-1) \cdot g \cdot d}}} \quad (3.89)$$

The bed profile at equilibrium state and the maximum scour depth are obtained based on equation 3.87:

$$\frac{dh_s}{dr} = -\sqrt{\frac{k_2}{2 \cdot k_1} \cdot \frac{\mu \cdot C_D}{1 + \mu \cdot \frac{C_L}{C_D}}} \cdot \frac{V}{\sqrt{(s-1) \cdot g \cdot d}} \cdot \frac{1}{\kappa} \cdot (f(r))^2 \cdot \frac{h_s}{r} \cdot \left(-4.167 + 2.640 \cdot \frac{1}{\kappa} \cdot \frac{V^*}{V}\right) \quad (3.90)$$

This equation can be integrated if the function f is known. Assuming that f is given by the forced vortex distribution and determining the integration constants with the boundary condition $R = R_c$; $h_s = h_m$ they found:

$$\frac{h_s}{h_m} = \exp\left(\frac{A}{2} \cdot \left(\frac{r^2}{R_c^2} - 1\right)\right) \quad (3.91)$$

with $\quad A = -\sqrt{\dfrac{k_2}{2 \cdot k_1} \cdot \dfrac{\mu \cdot C_D}{1 + \mu \cdot \dfrac{C_L}{C_D}}} \cdot \dfrac{V}{\sqrt{(s-1) \cdot g \cdot d}} \cdot \dfrac{\lambda_0}{\kappa} \cdot \dfrac{V}{V^*} \cdot \left(-4.167 + 2.640 \cdot \dfrac{1}{\kappa} \cdot \dfrac{V^*}{V}\right) \quad (3.92)$

After introduction of different simplifications (eq. 3.88), the constant A becomes:

$$A = \left(1.8955 - 3.0023 \cdot \frac{V^*}{V}\right) \cdot Fr_d \quad (3.93)$$

6) *Zimmermann (1983)*

ZIMMERMANN (see ZIMMERMANN & KENNEDY, 1978; ZIMMERMANN & NAUDASCHER, 1979 and ZIMMERMANN, 1974, 1983) developed a relationship for the boundary shear stress in radial direction τ_r averaged over the wetted perimeter. He compared the transverse drag on a sediment particle (computed with τ_r) with the corresponding opposing component of the weight of the submerged particle (centrifugal force).

His formula is based on the vertical distribution of the streamwise velocity v given by the power law:

$$v(z, r) = v_{surf}(r) \cdot \left(\frac{z}{h}\right)^{1/n} \quad (3.94)$$

where $v_{surf}(r)$ is the velocity at the free surface and $1/n$ a dimensionless exponent. The mean velocity is obtained by integration:

$$V(r) = \int_0^h v_{surf}(r) \cdot \left(\frac{z}{h}\right)^{1/n} = \frac{n}{n+1} \cdot v_{surf}(r) \quad (3.95)$$

The centrifugal force is not constant over the depth because of the velocity gradient. The induced force T_c (due to the centrifugal force) in the center of the channel on the flow for an angular increment of $d\phi$ is

$$dT_c = \int\limits_{r_i}^{r_o}\int\limits_0^h \left(\rho_w \cdot \frac{v^2(z, r)}{r} \cdot \left(z - \frac{h}{2}\right) \cdot r\right) d\phi \, dz \, dr \tag{3.96}$$

Introducing equations 3.94 and 3.95, Zimmermann obtained:

$$dT_c = \frac{\rho_w}{2} \cdot \frac{n+1}{n \cdot (n+2)} \cdot (R_o - R_i) \cdot h^2 \cdot V^2 d\phi \tag{3.97}$$

The centrifugal force is primarily balanced by the momentum T_r induced by τ_r. Assuming that the shear stress τ_{cr} is uniformly distributed around the channel perimeter and that the cross-section is rectangular, ZIMMERMANN got:

$$dT_r = -\tau_r \cdot \left[R_o \cdot (R_o - R_c) \cdot d + R_i \cdot (R_c - R_i) \cdot d + (R_o^2 - R_i^2) \cdot \frac{d}{4}\right] d\phi \tag{3.98}$$

in which $R_c = (R_o - R_i)/2$. Combining 3.97 and 3.98 he finally obtained the boundary shear stress in radial direction:

$$\tau_r = \frac{\rho_w}{3} \cdot \frac{n+1}{n \cdot (n+2)} \cdot \frac{h_m}{R_c} \cdot V^2 \tag{3.99}$$

Considering now the balance of the forces acting in radial direction on a spherical particle moving along the inclined bed plane (β) upwards toward the inner bank, ZIMMERMANN obtained:

$$\frac{dh}{dr} = \alpha_z \cdot \frac{n+1}{2 \cdot n \cdot (n+2)} \cdot \frac{h_m}{R_c} \cdot Fr_d^2 \tag{3.100}$$

α_z is the ratio of the projected surface of sediment particle to the projected area of a sphere. Integrating v given by the logarithmic velocity defect law in streamwise direction (between 0 and h) $((v - v_s)/V^* = 1/\kappa \cdot \ln(z/h))$, and putting this relation equal to equation 3.95, yields:

$$\frac{n}{n+1} = 1 - \frac{V^*}{\kappa \cdot v_s} \tag{3.101}$$

Eliminating v_s from the previous relation and introducing the definition of the Darcy-Weissbach friction factor f lead to:

$$\sqrt{f} = \sqrt{8} \cdot \frac{\kappa}{n} \tag{3.102}$$

After introduction of $\kappa = 0.4$, Zimmermann found $\sqrt{f} = 1.13/n$, which can be compared to the experimental relation of NUNNER (1956): $\sqrt{f} = 1/n$

ZIMMERMANN finally gave the following formula for the lateral bed slope:

$$\sin\beta = \frac{f + \sqrt{f}}{2 \cdot (1 + 2 \cdot \sqrt{f})} \cdot Fr_d^2 \cdot \frac{h_s}{R_c} \tag{3.103}$$

ZIMMERMANN assumed a fully developed secondary flow, which is not always found in natural river bends. Furthermore, his formula gives a straight line for the transverse bed slope which does not really correspond to laboratory and field observations.

7)   *Falcon & Kennedy (1983)*

FALCON & KENNEDY (1983) (see also FALCON, 1979) used DU BOYS approach of a sediment transport in layers. They considered a control volume in the armoring layer at equilibrium state. Based on the work of KARIM (1981), the authors gave the thickness of the control volume (thickness of the armoring layer) with:

$$z_b = d_{50} \cdot \frac{V^*}{V^*_{cr}} \tag{3.104}$$

Based on a vertical distribution of radial shear stresses, the primary flow velocity given by the power law $v(r, z)/V = (n+1)/n \cdot z^{1/n}$ and the definition of the exponent $1/n = \sqrt{f/8}/\kappa$, their equation for the lateral bed profile writes:

$$\sin\beta \approx \frac{dh_s}{dr} = \frac{\sqrt{8 \cdot \theta}}{(1-p)} \cdot \frac{1 + \sqrt{f}}{1 + 2 \cdot \sqrt{f}} \cdot Fr_d \cdot \frac{h_s}{r} \tag{3.105}$$

with p, the porosity of the armoring layer, $f = 8 \cdot g \cdot h_m \cdot S_e/V_m^2$, where V_m is the local depth averaged velocity. They assumed that $\kappa = 0.354$ and therefore $n = \sqrt{f}$ (see eq. 3.102).

The approach of FALCON & KENNEDY is similar to the one of ZIMMERMANN. The difference resides in the fact that FALCON & KENNEDY considered a vertical control volume, while ZIMMERMANN considered the whole cross-section. The formula of Zimmermann also accounts for the vertical shear stresses.

8)   *Odgaard (1986)*

ODGAARD (1981, 1982, 1984 and 1986) considered the forces acting on a control volume in a stable armoring layer, without any sediment transport (nor in radial, nor in stream direction). Taking into account the equation of FALCON (1979) and FALCON & KENNEDY (1983) for the radial drag force, the following formula is obtained:

$$\sin\beta \approx \frac{dh_s}{dr} = \frac{3 \cdot \alpha}{2} \cdot \frac{\sqrt{\theta}}{\kappa} \cdot \frac{n+1}{n+2} \cdot Fr_d \cdot \frac{h_s}{r} \tag{3.106}$$

where $\alpha = 1/k_2$ is the ratio of the projected area of a sediment grain normalized by d^2, $\kappa = 0.4$ the von Karman constant, C the Chezy coefficient and n is given with:

$$n = \frac{\kappa}{\sqrt{8/f}} = \frac{\kappa \cdot C}{\sqrt{g}} \tag{3.107}$$

Putting $\alpha = 4/\pi$, $\kappa = 0.4$ and $(n+1)/(n+2) \approx 1$, an earlier version of the same formula given in ODGAARD (1984) can be obtained:

$$\sin\beta \approx \frac{dh_s}{dr} = 4.8 \cdot \sqrt{\theta} \cdot Fr_d \cdot \frac{h_s}{r} \tag{3.108}$$

ODGAARD indicated that his formula may not apply in channels with heavy sediment load. Both equations 3.106 and 3.108 are valid for fully developed secondary flows in bends.

ODGAARD (1984) also developed an equation for the lateral bed slope in the development region, that is the zone where the bed slope in radial direction passes from a horizontal bed to the maximum scour bed profile. He used the exponential function given by ROZOVSKII (1957) for the growth of the secondary flow. ROZOVSKII assumed that the bed shear stress depends linearly on the radial velocity component at the free surface and on the lateral bed slope.

The lateral bed slope in the zone between the beginning of the bend and the first scour (called *development region*) is consequently given by:

$$\sin \beta \approx \frac{dh_s}{dr} = 4.8 \cdot \sqrt{\theta} \cdot Fr_d \cdot \left[1 - \exp\left(-\frac{2 \cdot \kappa^2}{n} \cdot \frac{R_c}{h_c} \cdot \phi \right) \right] \cdot \frac{h_s}{r} \tag{3.109}$$

9) *Bazilevich (1982)*

BAZILEVICH (1982) simplified a model established by the Institute of Fluid Mechanics, Academy of Science of the Ukrainian SSR[1]. He defined the equilibrium condition of scour as the absence of noticeable deepening of the bottom. At this state, the friction velocity $V*$ at the bottom has to be equal to the friction velocity $V*_{dest}$ corresponding to the destruction of the erosion pavement. $V*_{dest}$ is given for a gravel-bed channel (with $d \geq 1.5$ mm) by:

$$V*_{dest} = \frac{0.189 \cdot \sqrt{(s-1) \cdot g \cdot d_m}}{(d_{25}/d_{75})^{1/4}} \tag{3.110}$$

The friction velocity at the bottom at the given point is determined by:

$$V* = \frac{V \cdot \sqrt{g}}{C} = \frac{V \cdot \sqrt{g} \cdot f}{h^{1/6}} = \frac{V \cdot \sqrt{g}}{K_S \cdot h^{1/6}} \tag{3.111}$$

BAZILEVICH recommended to use the CHEZY-MANNING relation $n = (h_m^{2/3} \cdot S_0^{1/2})/V$ to determine the depth averaged velocity at the maximum scour location:

$$V_{h_{max}} = \sqrt{\frac{1-A}{1+A} \cdot V^2 + 2 \cdot g \cdot \Delta z} \tag{3.112}$$

where $$A = \frac{g \cdot \ln^2 \beta}{h_m^{4/3}}, \text{ and } h_m = \frac{1}{2} \cdot (h_{in} + h) \tag{3.113}$$

The length of the calculated reach is given as a function of the local water depth h and the one at the inlet h_{in}:

$$L = 10 \cdot (h - h_{in}) \tag{3.114}$$

---

1. He does not give any reference to this complete model. Unfortunately the translated paper does not allow a detailed analysis.

The superelevation of the free water surface is computed with:

$$\Delta z = L \cdot S_b \cdot \left(\frac{R_o}{R_c} \right) \tag{3.115}$$

Based on the analysis of field data with $h_{s,\,max}/h_m = 1.03 \div 3$, BAZILEVICH established the following equation for the lateral bed slope. If the value of $h_{s,\,max}$ is not known, he proposed to use $h_{s,\,max} = 1.6 \cdot h_m$ for mountain rivers (leading to a $\beta = 1.09 = 62°$).

$$\beta = 0.155 \cdot \frac{h_{s,\,max}}{h_m} + 0.845 \tag{3.116}$$

Finally, BAZILEVICH compared his formula against a small set of laboratory (TALMAZA & KROSHNIN, 1968 and VLASENKO[1]) and field data (Tisa River near Khust, Ukraine, below the mouth of the Boroyavka River). The configuration of all data sets was a 180° meander. The results of the comparison are satisfying. PETER (1985) indicated that BAZILEVICH'S formula is quite sensitive to numerical instability and to the choice of the bed roughness.[2]

10) *Peter (1986)*

PETER (1986) compared different scour formulae. He performed a large series of laboratory tests in a 135° bend with rectangular and trapezoidal cross-sections on a mobile bed. He varied the radius of curvature, the width of the channel, the discharge, the sediment mixture and the bed slope. Based on a dimensional analysis of his test data, PETER established an empirical formula for channels with a rectangular cross-section. The following equation gives the maximum scour depth, which can be located either at the first or second scour:

$$\frac{h_{s,\,max}}{h_m} = 5.23 - 13.0 \cdot \frac{h_m}{B} - 0.379 \cdot \sigma + 68.4 \cdot S_e \tag{3.117}$$

Since the parameter R_c/B is not a part of this equation, the application has to be limited to examined ratios of $R_c/B = 2 \div 6$. Furthermore, this equation does not take into account the grain size diameter; therefore a critical attitude towards this formula is necessary.

For channels with a trapezoidal cross-section, PETER found:

$$\sin\beta = \left(2.95 \cdot \frac{R_c}{B} - 0.7 \cdot \sigma - 29.3 \cdot \frac{h_m}{B} + 2.7 \cdot Fr + 3.4 \right) \cdot \frac{h_s}{r} \tag{3.118}$$

PETER also established formulae to locate the position of the first and the second scour, yet with a rather poor correlation ($r_{\alpha_1}^2 = 0.55$ and $r_{\alpha_2}^2 = 0.12$):

$$\alpha_1 = 20 \cdot \sqrt{\sigma} - 0.138 \cdot d* + 28 \tag{3.119}$$
$$\alpha_2 = 104 + 5.66 \cdot \sigma$$

---

1. Bazilevich does not give any reference for this data set.
2. Bazilevich based the determination of the bed roughness on the work of Altunin & Kurganovich, which could not be found in any library.

If the formula for α_1 is applied to field data, d^* becomes very (too) important. Therefore PETER proposed to use the following approximation:

$$\alpha_1 = 26.3 \cdot \sqrt{\sigma} + 11 \tag{3.120}$$

for engineering applications.

11) *Reindl (1994)*

REINDL (1994) established his analytical scour formula taking into account his own laboratory tests in a meandering channel with two successive 60° bends. The channel had a trapezoidal cross-section. He used a continuous sediment supply with different sediment sand mixtures $d = 2 \div 8$ mm. The tests were performed on fixed and mobile bed. In a second part of his study, special attention was paid to the influence of the backwater curve on the scour process.

REINDL established his scour formula based on the equilibrium of forces acting on a sediment grain similar to the approach of KIKKAWA ET AL. Based on the comparison of the near bed flow velocities obtained with different formulae (KIKKAWA ET AL, 1976, ZANKE, 1982, HJULSTRÖM, 1935, YANG, 1973, SHIELDS, 1936, MAVIS & LAUSHEY, 1948) and with his own measurements, he concluded that KIKKAWA ET AL. obtained a near bed velocity which is significantly too small. The computed velocities need to be corrected by a factor of 1.6 to 2.0 in order to fit to the computed values of other formulae and even with a factor of 2.2 compared with his measurements. Therefore he replaced KIKKAWA'S velocity distribution with Zanke's equation for the critical near bed flow velocity. He also modified the radial distribution function $f(r)$ of the normalized velocity in stream direction.

REINDL solved the following differential equation:

$$\frac{dh_s}{dr} = A \cdot (f(r))^2 \cdot \frac{h_s}{r} \tag{3.121}$$

and obtained:

$$\frac{h_s}{h_m} = \exp\left(\frac{A}{6} \cdot G_s \cdot \left(\frac{r^6}{R_c^6} - 1\right)\right) \tag{3.122}$$

where
$$A = -\frac{3}{2} \cdot C_D \cdot \frac{V}{\sqrt{(s-1) \cdot g \cdot d}} \cdot \frac{1}{\kappa} \cdot \left(-4.167 + 2.640 \cdot \frac{1}{\kappa} \cdot \frac{V^*}{V}\right) \tag{3.123}$$

and
$$G_s = 0.63 \cdot \frac{Q_b}{Q_{b,\,satt}} + 0.37 \tag{3.124}$$

REINDL concluded that the bed profile does not only depend on the dimensionless parameters V/V^* and Fr_D, but also on the sediment saturation G_s, especially for river reaches influenced by backwater curves.

3.5.3 Comparison of the scour formulae

The authors of the scour formulae used different approaches which are based on:

1. momentum considerations on banks and bed (Fargue),
2. equilibrium considerations of the forces acting on a sediment grain (van Bendegom, Engelund, Bridge and Kikkawa et al, Reindl with a different velocity distribution),
3. considerations based on forces acting on a control volume (Zimmermann, Falcon & Kennedy, Odgaard and Bazilevich) and finally
4. empirical formulae (Peter).

The characteristics of the different scour formulae are summarized in Table 3.5 (see also HERSBERGER & SCHLEISS, 2002).

AUTHOR	YEAR	EQ NO	$K = \text{fct}$	USED DATA *	ESTABLISHMENT OF EQUATION	REMARKS
Fargue	1868	3.56	R_c/B , roughness, V	F	analytical, momentum on bank and bed	formula for max. scour only
van Bend.[1] Engelund[2] Bridge	1947 1974 1976	3.62 3.67 3.72	Fr_d $7 \cdot \tan\phi = cst$ $11 \cdot \tan\phi = cst$		analytical, equilibrium of a grain	[1] valid for small slopes, big B/h , r » h [2] not established for fully dev. flow
Kik et al. Reindl[3]	1976 1994	3.91 3.122	Fr_d , V*/V , n Fr_d , V*/V , n, Gs	L L	analytical, equilibrium of a grain; velocity distribution	[3] introduced sed. saturation parameter
Zimmerm. Falc.&Ken. Odgaard	1978 1983 1986	3.103 3.105 3.106	Fr_d^2 , n Fr_d , n, θ , p Fr_d , n, θ	L+F L+F L+F	analytical, equilibrium of control volume	established for sand bed rivers
Bazilevich	1982	3.116	h_m/h_{max}	L+F	control volume	quite sensitive to chosen values
Peter	1986	3.118	R_c/B , σ , h_m/B , Fr	L	empirical, dimension analysis	valid for $R_c/B = 2 \div 6$; use with care since d not in formula

Table 3.5:   *Comparison of characteristics of discussed scour formulae*
       * F = Field data, L = Lab data

a) Formulae based on momentum considerations

The oldest examined scour formula of FARGUE considered the momentum equation on the bank and on the river bed. He simplified the scour process, assuming that the near bed velocity is submitted to little changes with varying discharge. Therefore the scour depth depends essentially on the river geometry and the computed value for a given river reach is almost constant.

b) Formulae based on equilibrium considerations

The analytical formulae of VAN BENDEGOM, ENGELUND AND BRIDGE are valid for small bed slopes, high width to depth (B/h) ratios and for small curvatures of the bend $(R_c \gg h)$. VAN BENDEGOM and ENGELUND established their equations for partially developed secondary flow conditions. The equation of van Bendegom is based on equilibrium conditions of spherical grains which are completely exposed to the flow. This leads to an underestimation of the bed slope in radial direction. Furthermore the static lift was neglected leading to an additional underestimation of the lateral bed slope. The formula of Engelund considered a rectangular cross-section with a fixed bed and slightly meandering bends. Bridge adjusted the formula of Engelund, integrating the results of the research works of Rozovskii; he assumed the ratio between tangential and radial velocity components to be equal to 11.

KIKKAWA ET AL. introduced a flow model, which allows to determine the drag and lift force as a function of characteristic flow and bed parameters. REINDL observed that the maximum flow also depends on the sediment saturation Gs for river reaches influenced by a backwater curve. He modified KIKKAWA'S formula, in order to take into account the quantity of sediment available for transport.

c) Formulae based on control volume considerations

ZIMMERMANN, FALCON & KENNEDY and ODGAARD considered control volumes of different size, but always with the thickness of the armoring layer. ZIMMERMANN used the whole cross-section at the maximum scour location, while FALCON & KENNEDY and ODGAARD used a local control volume. Since ZIMMERMANN'S equation is a function of h / R_c, the bed geometry in the cross-section is a straight line, which does not fit with the observed geometry of the cross-section. All three formulae were established for sand bed rivers.

BAZILEVICH'S formula is very sensitive to the chosen parameters (see PETER, 1985). Since the flow and geometric characteristics of a river often contain (considerable) uncertainties, this equation does not seem very appropriate for engineering practice.

d) Empirical formula

PETER gives an empirical formula based on a dimensional analysis. In general, his formula gives good results for alpine rivers (see PETER, REINDL). But unfortunately, it does not take into account the sediment size. Therefore the formula should be used with care within the authorized domain of radius to with ratios $R_c/B = 2 \div 6$.

3.5.4 Comparison with experimental data

In this paragraph, the mentioned scour formulae are compared to laboratory experiments for smooth walls performed in the frame set of this study (also published in HERSBERGER & SCHLEISS, 2002). The laboratory tests of PETER (1986), performed at the VAW (ETHZ) were added to this data set. The so obtained extension of the data set (39 tests) to 71 tests covers a wide

range of different parameters. Some of them, computed in the straight inlet reach, are given in the following table:

	THIS STUDY	PETER (1986)
Radius to width R_c/B	6	2 and 3.5
Grain size distribution (d_m;σ)	d_m = 8.5 mm ; σ = 1.82	1.7 ... 5.1 mm ; 1.19 ... 3.21
Froude- ; Reynolds number	0.68 ... 0.97 ; 44'000 ... 63'000	0.3 ... 1.2 ; 700 ... 4100

Table 3.6:   Characteristics of the laboratory tests of the present study and Peter's (1986) data

a) Maximum scour depth

Figure 3.12 gives a comparison of the mentioned formulae with the laboratory tests.

Despite important simplifications, the oldest formula of Fargue allows an estimation of the order of magnitude of the scour depth.

Most scour formulae - except the one of BRIDGE, PETER and REINDL - clearly underestimate the maximum scour depth. This may have various reasons: VAN BENDEGOM and ENGELUND used small slopes, whereas the laboratory tests were performed at rather steep slopes (0.3 ÷ 1.1 %). As mentioned in the previous paragraph (§3.5.3), the fact that the static lift was neglected and that a complete exposure of the spherical grains was assumed gives additional explanations.

The resluts of computations with BRIDGE's formula show a good agreement with measured scour depths, yet with an significant scatter. This is not surprising, since the factor K is constant and the only considered parameter is the friction factor ϕ.

KIKKAWA ET AL. underestimate the scour, too. The difference is probably due to the wide grain size distribution with rather coarse grain, which results in significant grain sorting across the cross-section (see § 6.5 and SCHLEISS & HERSBERGER, 2001). The scour depths computed with REINDL's formula are clearly overestimated compared to the laboratory tests. The important difference between measured and computed values (especially compared to the tests of Peter) could be due to the fact that the sediment saturation introduced by REINDL was not known for the tests of PETER and was put therefore equal to one.

The formulae of ZIMMERMANN, FALCON & KENNEDY and ODGAARD were established for sand rivers based on laboratory and field data. They all underestimate the scour depth in a gravel river by a factor close to 2. One reason is that the lateral bed slope of coarse gravel bed rivers is submitted to armoring phenomena, allowing a steeper transversal bed slope. Furthermore the measurement of the final scour depth is difficult for field experiments, since the hole is filled up with sediments with decreasing discharge at the end of the flood.

ODGAARD's formula was developed for a coarse sediment bed. He adjusted his formula on the field data of a bend of the Sacramento River (R_c ≈ 1 km, h_m ≈ 3 m) with a ratio of R / h ≈ 300. In the present study this ratio has a value of about 30. The longitudinal slope of the Sacramento River bend was estimated to be of 0.03 %, compared to 0.5% in our flume. The stronger curvature in the flume and the bigger longitudinal slope could explain the important underestimation of the transversal bed slope as well as the much wider grain size distribution for the experiments.
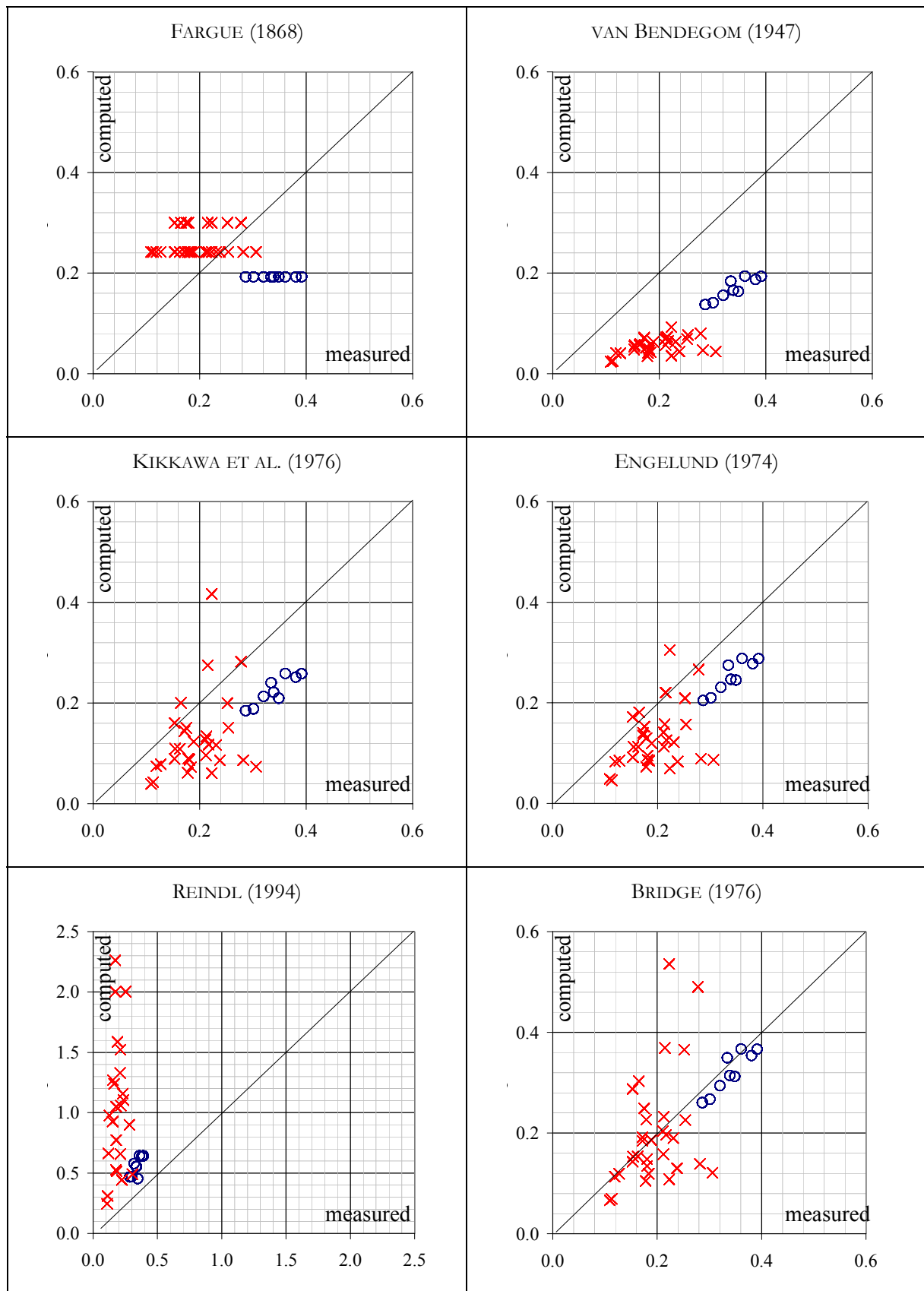
Figure 3.12: Comparison of computed maximum scour depth with experimental data
(continued on next page)
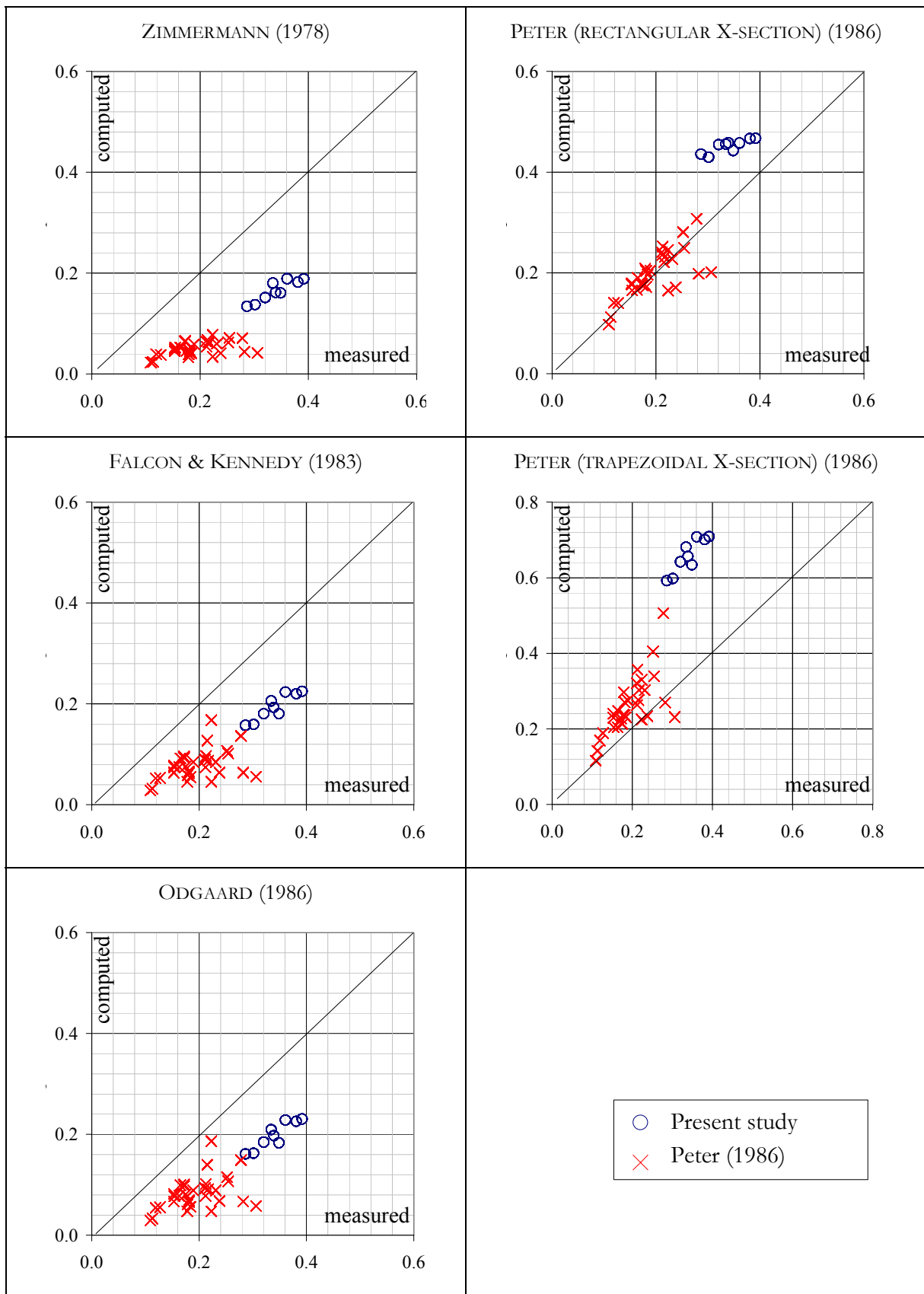
Comparison of computed maximum scour depth with experimental data
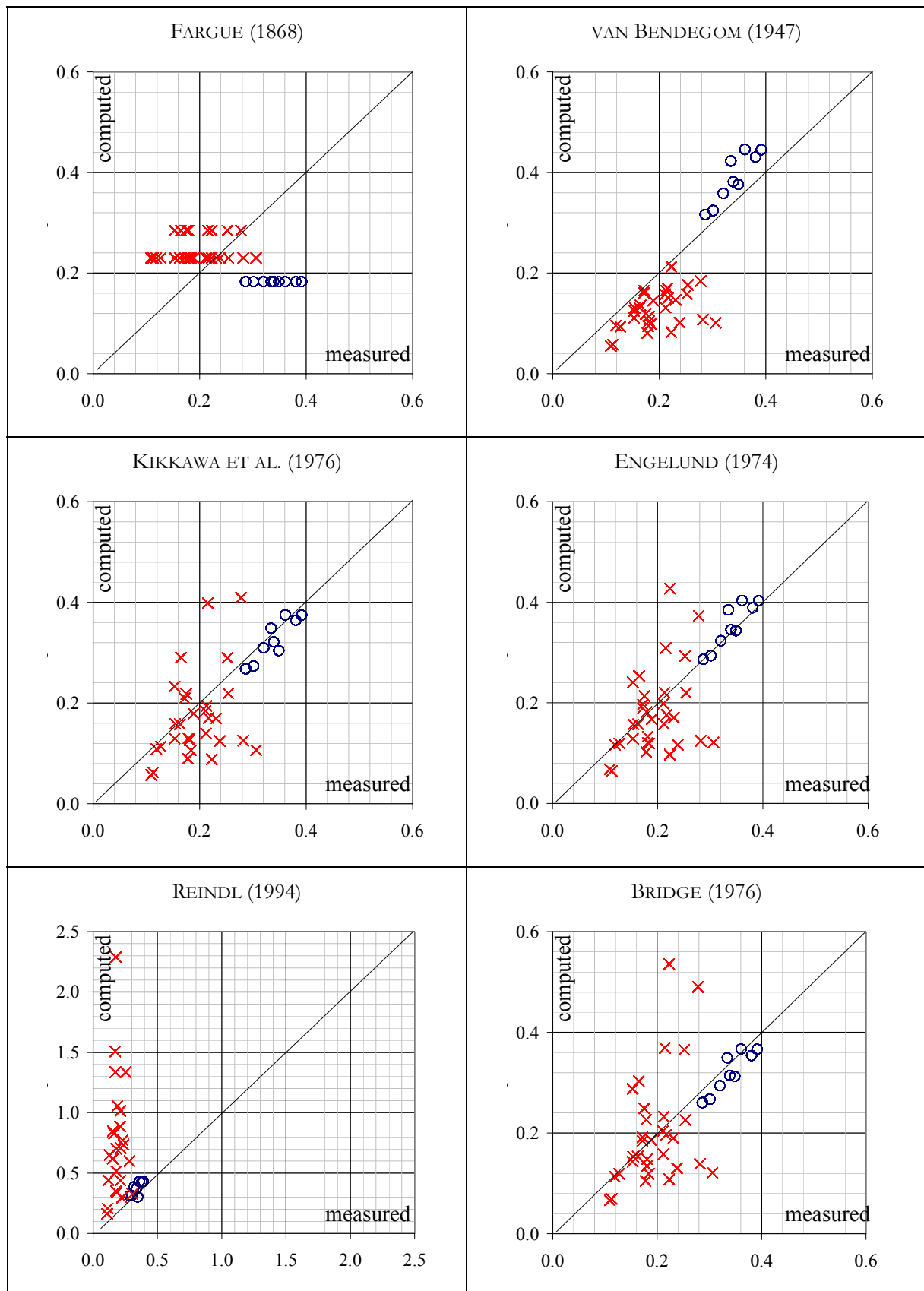
*Figure 3.13: Comparison of corrected computed maximum scour depth with experimental data
(continued on next page)*
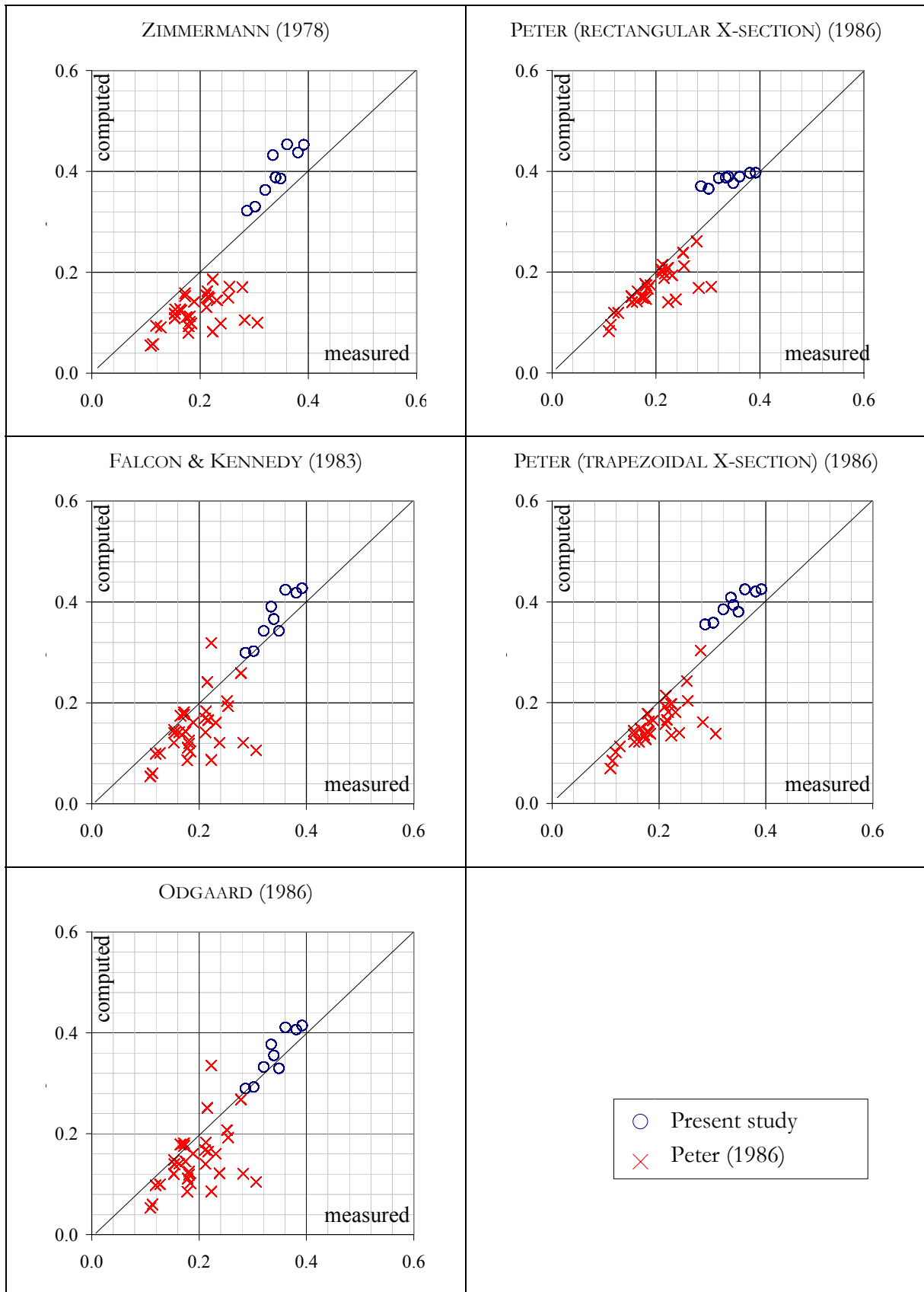
Comparison of corrected (with F_C) computed maximum scour depth with experimental data.

PETER slightly overestimates the scour compared to the lab tests of the present study. Since Peter neglects the grain size, the overestimation may be due to the coarser grain size.

In order to obtain a better fit between computed and measured values (see Fig. 3.12), the computed maximum scour depth can be adjusted with a correction factor F_C. To estimate the quality of the different scour formulae the regression coefficient R^2 is also given in Table 3.7.

Scour formula	F_C	R^2
Fargue	0.95	0.41
van Bendegom	2.3	0.79
Engelund	1.4	0.54
Bridge	1.0	0.29
Kikkawa et al.	1.45	0.32
Reindl	0.67*	0.21
Zimmermann	2.4	0.79
Falcon & Kennedy	1.9	0.75
Odgaard	1.8	0.73
Peter (rectangular)	0.85	0.87
(trapezoidal X-section)#	0.60	0.85

Table 3.7:   Correction factors for scour formulae and correlations with lab experiments
*   * compared only to our tests (LCH), # compared to rectangular X-section data*

Figure 3.13 compares the maximum scour depth[1], computed with the correction factors F_C of Table 3.7 to the measured ones.

---

1. definition sketch of h_s on Fig. 3.6 on page 40

b)   *Lateral bed geometry*
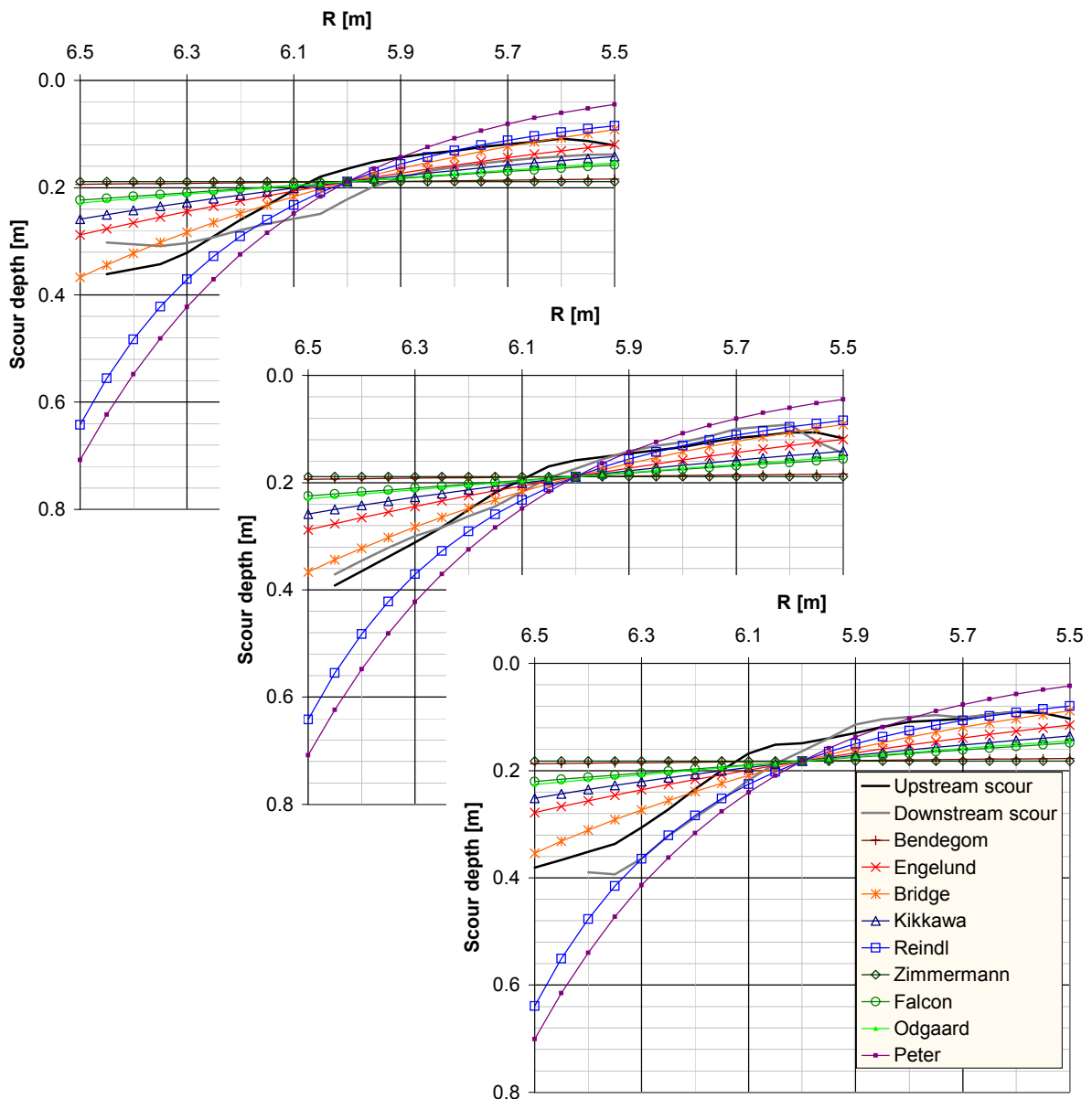
Figure 3.14: Comparison of different formulae with the measured bed topography (upstream, downstream) with Q = 210 l/s and S$_0$ = 0.35%, 0.5%, 0.7%, (from left to right) R$_c$ = 6.0 m, B = 1.0 m

The shape of the predicted bed topography in radial direction (Fig. 3.14) fits in general quite well with the measured one in the center region. Especially towards the outer bank, an important difference between predicted and measured bed geometry can be observed. This is due to the fact that most equations use an exponential cross-section profile, except ZIMMERMANN whose profile is linear. The tests show that the lateral bed geometry is rather s-shaped.

3.5.5 Conclusions

There exists a fair number of scour formulae. The comparison of scour formulae with laboratory tests show that most of them underestimate the scour depth in an mountain rivers with a coarse sediment mixture. The formulae of PETER and REINDL overestimate the scour and the formula of BRIDGE gives on average a good prediction of the scour, yet with a significant scatter. If the maximum scour depth computed with existing scour formulae are corrected with a correction factor F_C, good results can be obtained with the following equations: Peter, Zimmermann, van Bendegom, Falcon & Kennedy and Odgaard who all obtained correlations of more than $R^2 = 0.70$. The correlations of the other formulae are smaller than $R^2 = 0.60$. The correction factors as well as the correlations of the different formulae are given in Table 3.7.

Despite a very good correlation, the formula of PETER should be used with caution, since it does not take into account the grain size. It is interesting that the frequently preconized formula of KIKKAWA ET AL. shows an important lack of prediction capability when applied to mountain rivers.

The formula of BRIDGE needs no correction factor (1.0). This shows that, over a large number of tests, the average scour depth is quite well predicted. But the scatter of the different individual measurements is considerable and therefore the correlation is only 0.3. This shows that some essential parameters are neglected, despite good theoretical bases.

Most formulae assume an exponential cross-section profile. But the tests show that the bed topography in radial direction is rather s-shaped.

CHAPTER 4

EXPERIMENTAL SETUP AND TEST PROCEDURE

4.1   Description of the experimental setup

The present section gives an overview over the experimental setup, which had to be built especially for this research study. The works included the construction of the test platform and of the channel (described in the present section), the equipment with the data acquisition devices as well as the programming of the data acquisition and the data treatment (see § 4.4).

4.1.1   Geometry and nomenclature

The testing facility (Fig. 4.1) was mounted on a platform (14), approximately 3 m above the ground level of the experimental hall.

1. Sediment supply	8. Bend (R_c = 6 m, 90°)
2. Conveyor belt (10 m)	9. Exit reach (6.0 m)
3. Conveyor belt (2 m)	10. Tilting gate
4. Water supply pipe	11. Sediment sampling device
(in inlet box)	12. Outlet pipe
5. Perforated cylinder	13. Filtering basket
6. Assembly of small pipes	14. Test platform
7. Entry reach (7.5 m)	15. Measurement frame
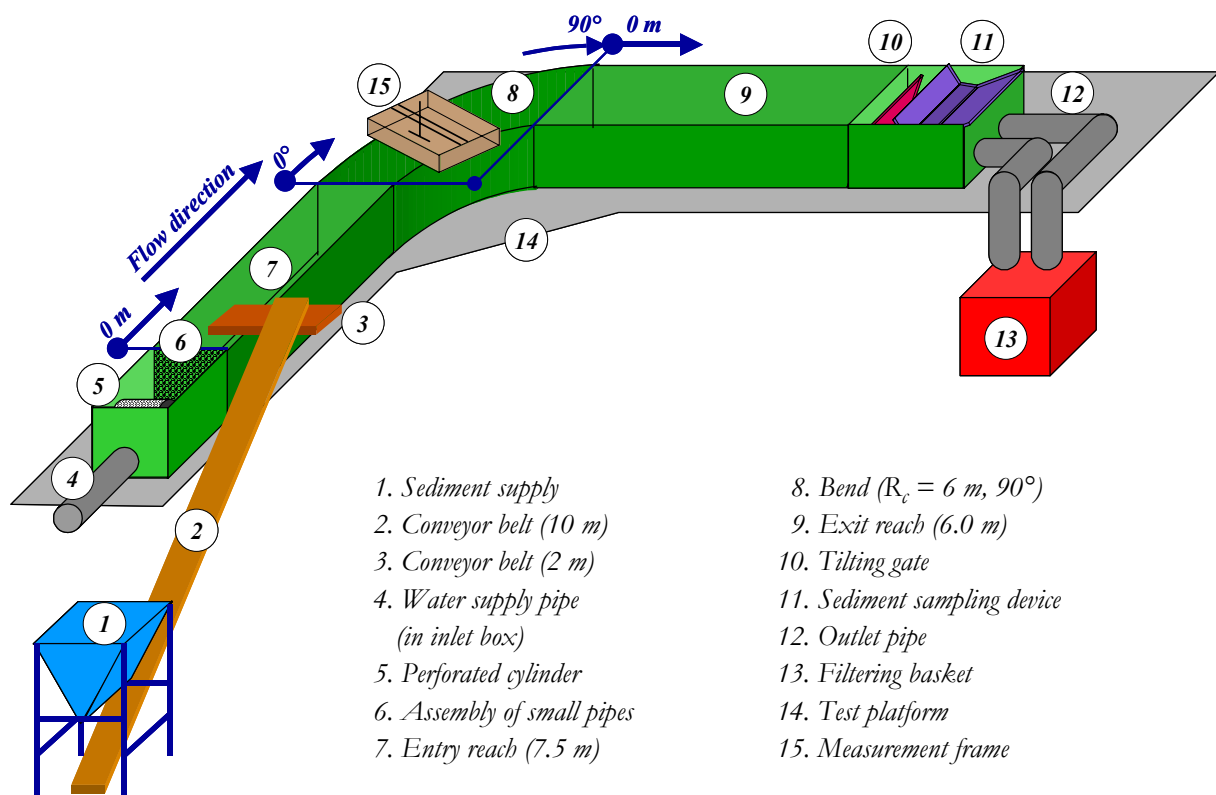
Figure 4.1:   Schematic view of the testing facility with definition of locations

The channel is composed of a 7.50 m long straight entry reach (7), followed by a 90° bend (8) with a radius of 6.00 m at the center line, ending with a 6.00 m long straight exit reach (9). The channel width and height are 1.00 m. The outer side wall is transparent in order to allow the observation of the flow and of the bed evolution.

A water supply pipe was mounted to a perforated cylinder ($\varnothing$ = 400 mm) (5) located in the upstream inlet box (1.00 m wide, 2.00 m long, 1.10 m deep).

For the preliminary tests, an assembly of small pipes (6) calmed the inflowing water (see §4.1.3). Due to the significant head losses caused by these pipes, they were replaced by a floating polystyrene plate in the main test series to obtain better flow conditions.

The sediment supply (1), described in detail in paragraph 4.1.2, allowed to store half a cubic meter of sediments in a conic tank. On the bottom of the reservoir, a rotating cylinder with a longitudinal slide controlled the sediment rate. The sediments were transported by two conveyor belts (2 and 3) into the channel where they were distributed by an inclined plate (see Fig. 4.2).

Figure 4.2:   Sediment inlet (left) and sediment sampling at the outlet (center and right)

At the outlet, a restitution basin collected the water and the sediments. The basin was equipped with a tilting gate (10) which allowed to control the water level at the outlet. The tilting gate was only used during filling and emptying of the channel to avoid bed erosion. During the tests, the gate was lowered. The flow conditions on the exit overfall were critical. A sediment sampling device (11) was located in the restitution basin (see Fig. 4.2 center and right). Two outlet pipes (12) collected the water and the sediments and lead them to an easily interchangeable filtering basket (13) which retained the sediments. The water was collected in the general basin (800 m^3) of the Hydraulics Laboratory and recirculated in the experimental channel.

1. Inlet	4. Entry reach (7.5 m)
2. Perforated tube	5. Bend (R$_{center}$ = 6 m, opening = 90°)
3. Assembly of small pipes (pipe grid)	6. Exit reach (6 m)

Figure 4.3:   Testing facility during construction

For the representation of the measurements, the elements of the channel were indicated in the following way (see Fig. 4.1):

- in the entry reach: distance to the channel entry in m (after the pipe grid)[1].
- in the bend: opening angle in degrees or distance from the channel entry in m along the central axes (e.g. 0° = 7.50 m; 90° = 16.92 m).
- in the exit reach: distance starting from the end of the curve (90°) or distance from the channel entry in m along the central axes.
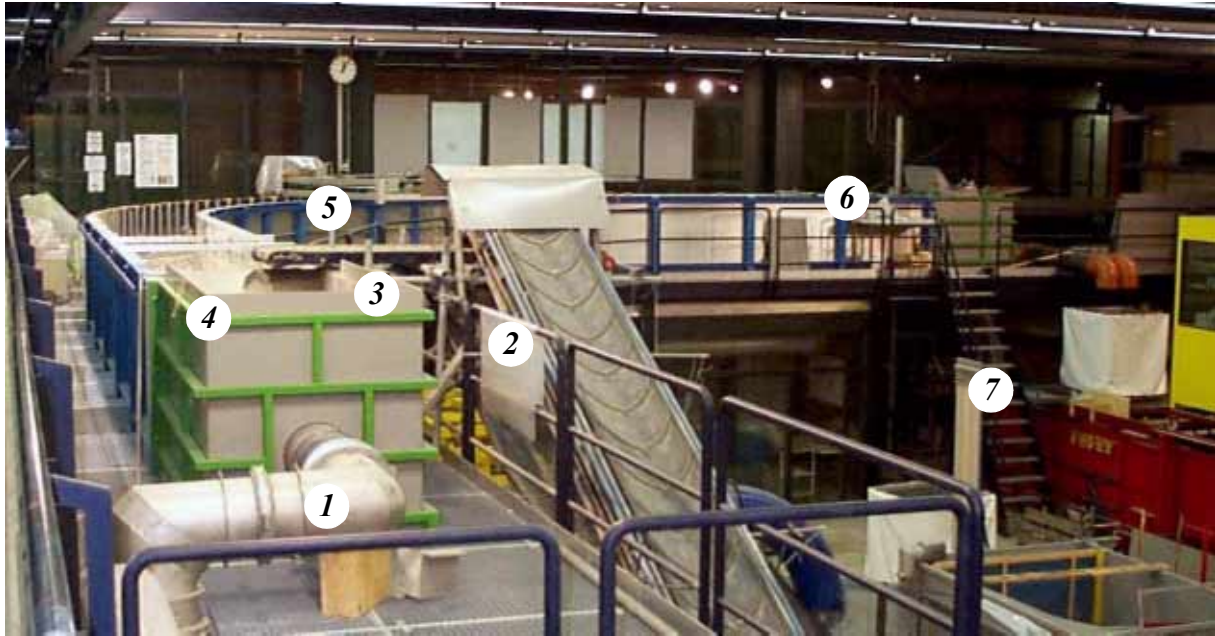
1. Inlet	5. Measurement frame
2. Conveyor belt (10 m)	6. Outlet
3. Conveyor belt (2 m)	7. Filtering basket
4. Sediment distribution	

Figure 4.4:   Operational experimental set-up

---

1. Sometimes the location in the entry reach is indicated as (negative) distance to the beginning of the bend.

4.1.2   Sediment supply machine

There are mainly 3 possibilities to obtain an automatic and continuous sediment supply in an experimental channel depending on the grain size of the used sediments:

1. Figure 4.5 shows on the left side a sediment supply used in the food industry working well with dry sand and for rather small transport rates. The discharge controller can be for example a vibrating device with a variable intensity or a screw with a variable rotation speed adjusting the sediment transport rate based on weighting of the sediment on the conveyor belt.

2. The scheme on the right side works well for rather fine gravel (a few mm of diameter) with a uniform grain size distribution. The opening gate (4) can be adjusted to different sediment sizes.

3. Another possibility consists in recirculating the sediments. Up to a diameter of about 10 mm, commercial solutions can be found at a reasonable price.
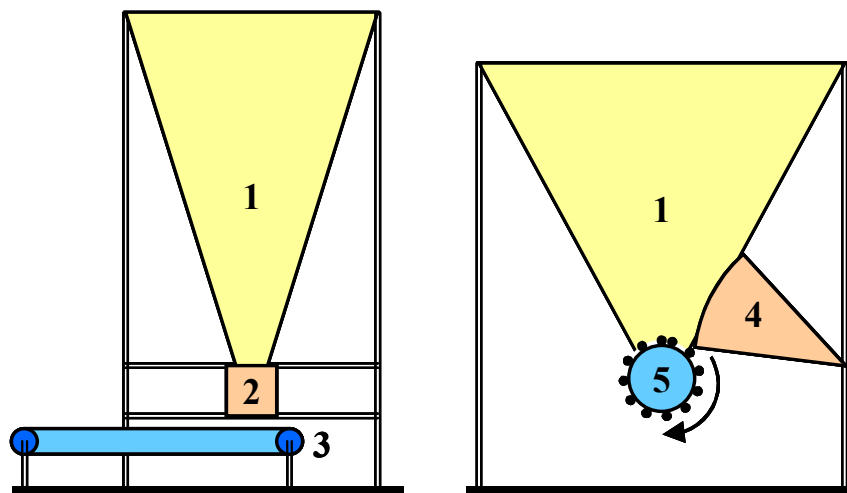
1. Reservoir, 2. Discharge controller, 3. Transport belt, 4. Variable opening, 5. Rotating cylinder with

Figure 4.5:   Different types of sediment supplies

The following reasons made it impossible to use one of the existing sediment supply types:

- The used sediments are recovered at the outlet and are reinjected in the channel. Due to the big amount of sediments used during one test, the time needed to dry all the sediments before reintroducing them into the circuit is too important. Therefore solution 1 was eliminated.
- Since a wide grain size distribution is used for the tests, device 2 is not appropriate, either.
- The fact that the coarsest used grain has a size of 32 mm makes it impossible to recirculate the sediments (solution 3).

Therefore it was necessary to develop a special sediment supply. The retained solution is presented in the following scheme (Fig. 4.6).
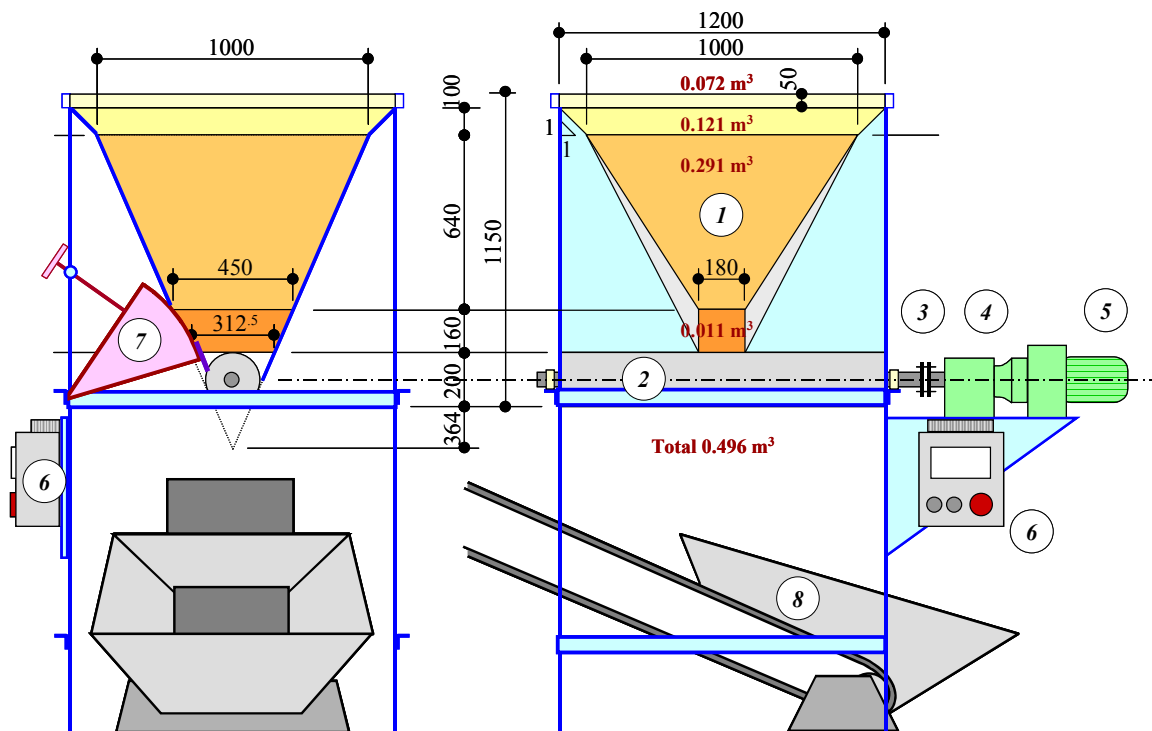
1. Sediment reservoir, 2. Rotating cylinder (with a slide opening), 3. Fuse to prevent rotating cylinder from damage, 4. Mechanic step-down gear, 5. Motor, 6. Electronic Frequency Modulator, 7. Gate to adjust the opening with thick plastic lip, 8. Conveyor belt

Figure 4.6: Scheme of the used sediment supply

The sediment reservoir (1) had a storage volume of 0.50 m^3. On its bottom, a rotating cylinder with a slice opening (2) continuously pushed the sediments through a thick plastic lip to drop on the conveyor belt (8). It was no problem to obtain high sediment rates. In order to get also low transport rates, several speed reducing devices were mounted to the motor (5): a mechanic step-down gear (4) reduced the rotation rate by a factor 20 and an electronic frequency modulator (6) allowed to reduce the initial rotation rate of the motor considerably. The axis was protected by a mechanic fuse (3) from damage. A gate with a thick plastic lip (7) allowed the control of the opening of the sediment supply (adjustment to the grain size and of the sediment supply rate). The precision of the time-averaged sediment supply rate is estimated to be at about 10 to 15%.
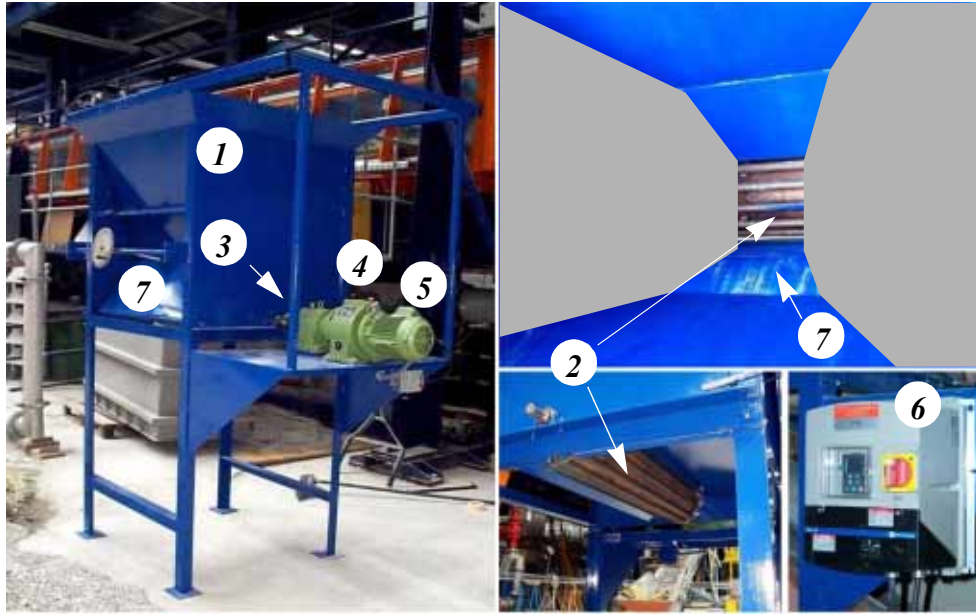
LEFT: general view, RIGHT TOP: view from inside the reservoir
CENTER BOTTOM: view from below the machine,
CENTER RIGHT: electronic frequency modulator

Figure 4.7:   Sediment supply machine (explanations see Fig. 4.6)

4.1.3 Inlet box

At the upstream end of the channel a water supply pipe ($\varnothing$ = 30 cm) was connected to the inlet box (1 m wide, 2 m long and 1.10 m high). The connection was made through a 80 cm long perforated cylinder ($\varnothing$ = 40 cm). This cylinder (2) had about 2000 holes with a diameter of 10 mm (Fig. 4.3 and Fig. 4.8). An overfall at the inlet (between the inlet box and the entry reach) prevented the sediments of the channel to fall back into the inlet box. For the preliminary tests, an assembly of 25 cm long small pipes (3) was put on top of the overfall (4) to direct the flow; they had a diameter of 40 mm in the upper half and 20 mm in the lower part. The battery of small pipes was removed for the main tests and replaced by a floating polystyrene plate to quieten the water surface.
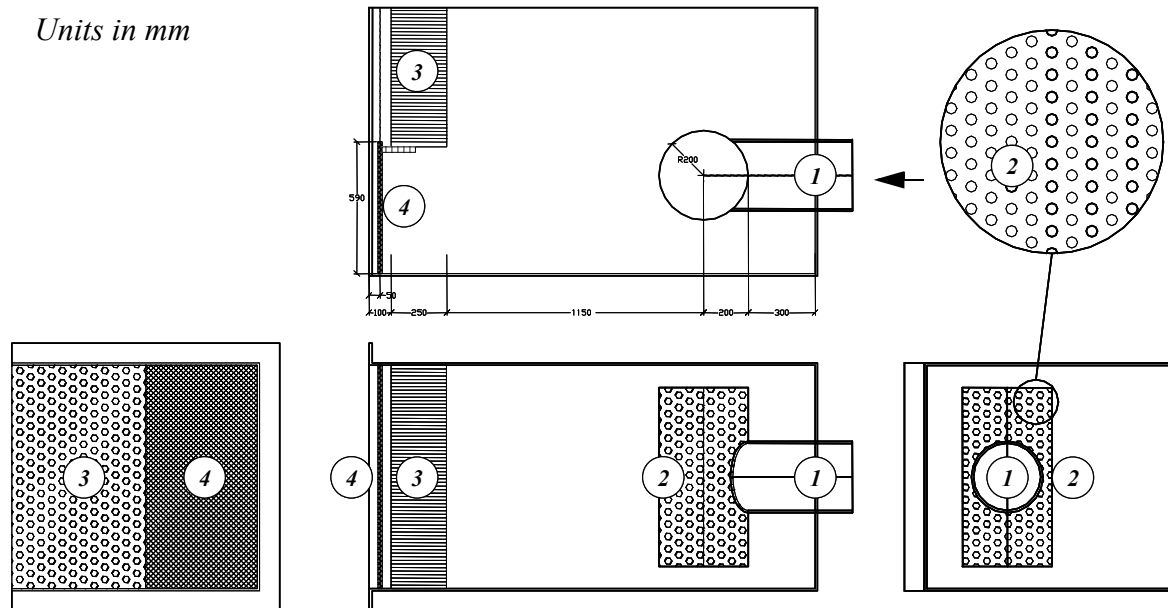
1. Water supply pipe, 2. Perforated cylinder, 3. Assembly of small pipes, 4. Overfall
(CENTER TOP: elevation, CENTER BOTTOM: situation, LEFT: downstr.-view, RIGHT: upstr.-view)

Figure 4.8:   Inlet box with perforated cylinder and assembly of small pipes

4.1.4   Outlet box with tilting gate and sediment sampling device

At the end of the channel, an outlet box was built assuming different functions (see Fig. 4.9):

- The control of the bed and water level at the outlet was ensured by a weir (1) between the exit reach and the outlet box; the flow condition over the weir was critical.
- A smooth filling and emptying of the channel was enabled by a tilting gate (2) which was completely lowered during the tests.
- The sediment sampling was performed by means of a big "L" covered with a fine grid (1 mm openings). The sampling device (3) is articulated at the downstream end of the outlet box. It can be operated with a crank lever.
- Finally, the water and the sediments were collected and lead to two outlet pipes (4).

Units in mm

1. Overfall, 2. Tilting gate, 3. Sediment sampling device, 4. Outlet pipes
(CENTER TOP: elevation, CENTER BOTTOM: situation,
LEFT: upstream-view, RIGHT: downstream-view)
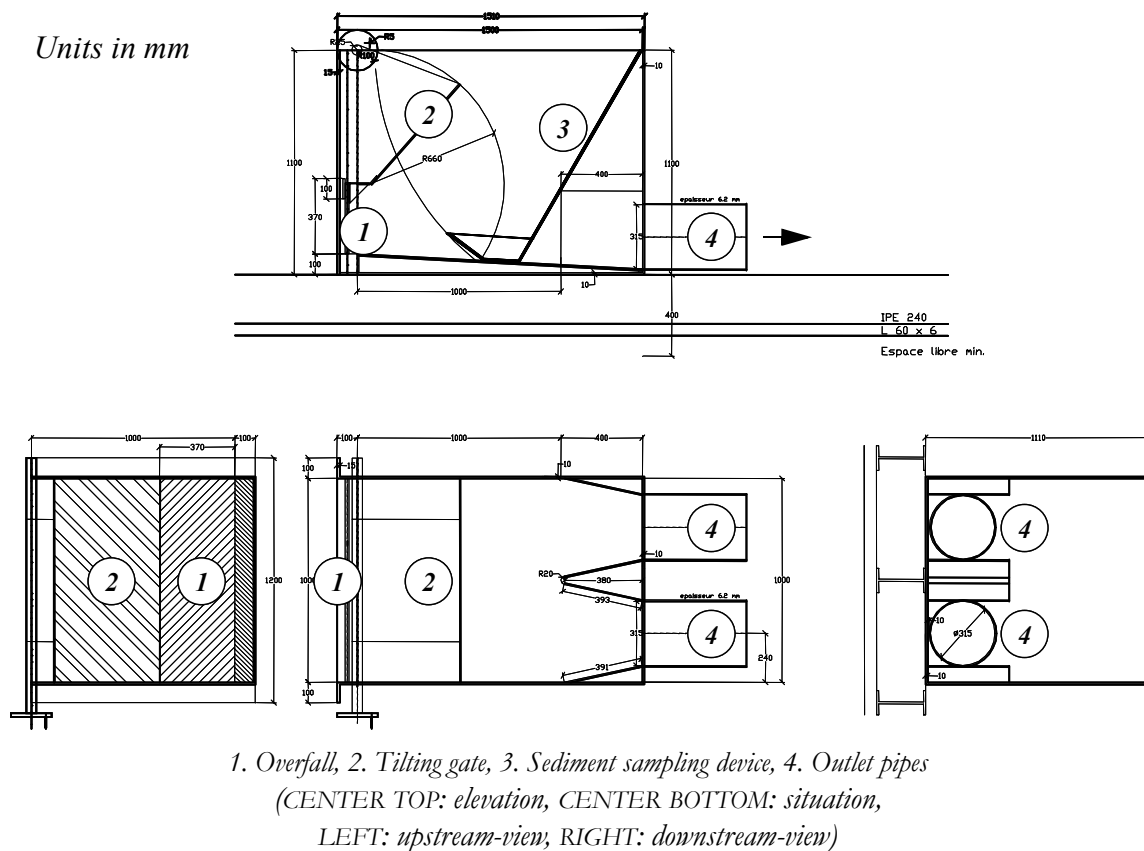
Figure 4.9:   Outlet box with tilting gate and sediment sampling device

4.1.5 Filtering basket

After the outlet pipes, the mixture water-sediments was filtered in a basket (see Fig. 4.10). The basket is a cube of 1.00 x 1.00 x 1.00 m covered on the sidewalls and on the ground with a doubled grid layer (openings 1 mm wide). The bottom can be opened to allow a fast emptying. A skirt was mounted around the basket to prevent the lab from a general inundation. Four small steel wheels allowed to position the basket at the right position on rails below the two outlet pipes.

LEFT-TOP: Structure of the filtering basket, LEFT-BOTTOM: view from inside, CENTER: Basket with the skirt, RIGHT TOP: Closing mechanism, RIGHT-BOTTOM: wheel and back flap

Figure 4.10: Pictures of the sediment filtering basket

4.2 *Parameters of the experiments*

4.2.1 General test parameters

The following paragraph gives an overview over the general test parameters. The chosen indicative[1] geometric scale is of 1:30.

a) *Channel geometry*

The bend radius at the centerline is 6.00 m. The channel is composed of a 2 m long inlet box, a 7.50 m long entry reach, followed by a 90° bend with a radius of 6.00 m at the centerline, a 6.00 m long exit reach and finally a 1.5 m long outlet box. The cross-section is rectangular (1.00 m wide and 1.00 m high). The ratio bend radius at the centerline to channel width (R_c/B) is 6.0 (see also § 4.1.1).

Before a test serie, the bed was levelled to fit the desired initial longitudinal bed slope; in every cross-section the bed was horizontal (perpendicular to the centerline of the channel). During the test, the sediment supply was adjusted to keep the longitudinal bed slope in the straight inlet reach as constant as possible.

b) *Flow conditions (discharge, bed slope)*

The used discharges ranged between 70 and 210 l/s: 70 l/s were used for the initial armoring of the bed (before the test started properly); 150, 180 and 210 l/s were used for the main tests. These discharges correpond to propotype discharges of about 350, 750, 890 and 1040 m3/s at a model scale of 1:30. The flow regime was maintained subcritical.

The bed slope in the inlet reach was maintained as constant as possible (as close to the initial bed level), by adjusting the sediment supply.

c) *Sediment transport*

The tests were performed for a constant discharge at equilibrium conditions in the straight entry reach. The sediment transport balance in the channel depends on the sediment supply, the transport capacity and the equilibrium conditions. The quantity of sediments introduced in the channel was variable to maintain the desired longitudinal bed slope in the entry reach (see also § 4.3) except for the preliminary tests where it was maintained at a constant rate.

The ratio of water depth to mean sediment diameter is of about $h_m/d_m \approx 15$.

Since the slope S_0 and sediment density coefficient s are the same for the laboratory experiments and a test reach in nature, the Shields parameter (eq. 3.42) will be proportional to R_h/d. In order to have the same transport characteristics, this ratio needs to be the same for the prototype and

---

1. The present study does not test a specific site. But if we consider prealpine rivers, the following set of parameters is quite representative: width of the river = 30 m, with a radius of about 200 m (e.g. the Emme River close to Wolhusen LU, Switzerland)

the model. Consequently, the grain size diameter can be chosen according to the geometric model scale.

d) Geometry of the macro-roughness

Macro roughness was created by trapezoidal ribs, placed vertically on the outer wall (Fig. 4.11) with a spacing of 1° (or 114 mm), 2° (227 mm), 4° (454 mm) and 8° (908 mm). The curved part of the channel as well as 1 m of the entry reach and 2 m of the straight exit reach were equipped with these macro roughness elements. In the straight (entry and exit) reaches, the spacing of the ribs was incremented by a factor $\sqrt{2}$ compared to the previous spacing with increasing distance to the bend (Fig. 5.3 on page 111).
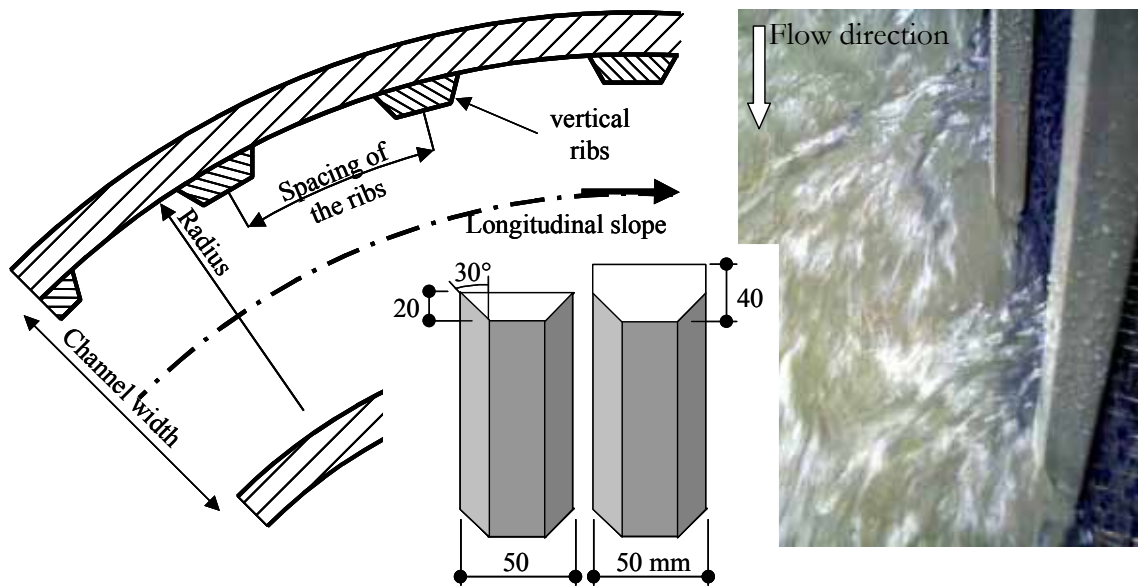
Figure 4.11: Scheme of the macro-roughness elements and picture of the flow around ribs

Figure 4.12: Macro-roughness on the protection wall, Reuss River in Gurtnellen (Switzerland)

4.2.2   Measured parameters
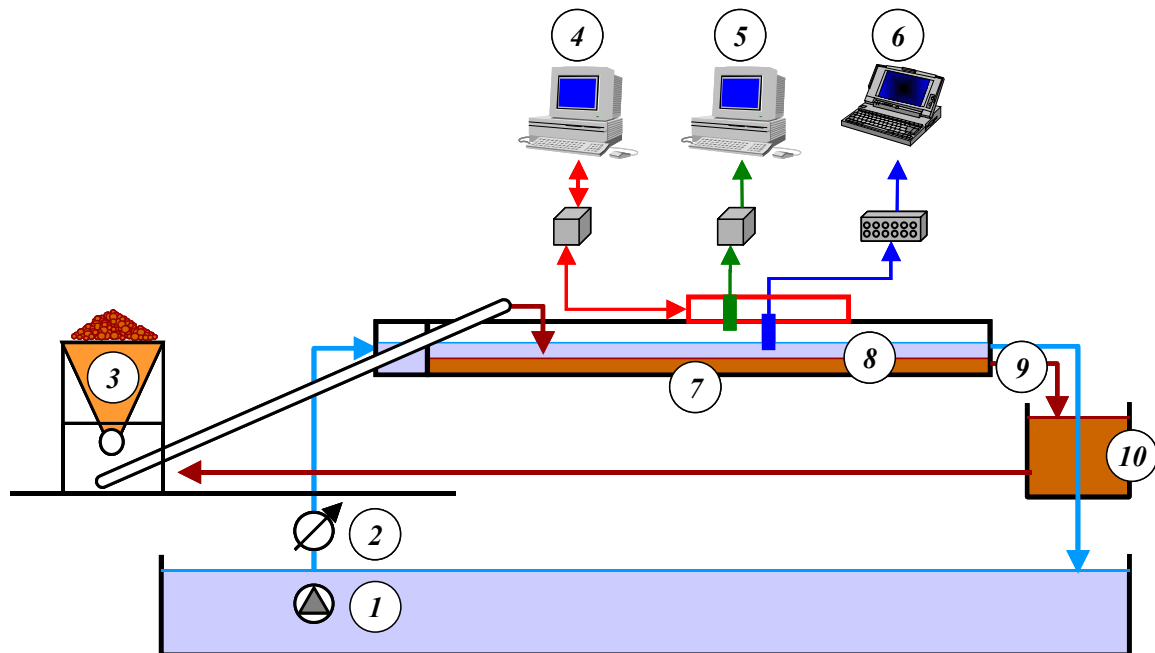
1. Pump
2. Electromagnetic discharge meter
3. Sediment supply (volumetric meas.)
4. Measurement frame command
5. Water level and bed topography
    measurement

6. Velocity measurement (UVP)
7. Armoring samples
8. Manual readings of water and bed
    levels on side wall
9. Sediment samples at the outlet
10. Total weight of sediments

Figure 4.13: Scheme of the experimental setup with circulations

On the experimental setup (Fig. 4.13) the following parameters were measured (see also § 4.4):

- The water level was recorded with an ultrasonic gauge (5) (see § 4.4.3 and Appendix 2.1.1).
- The bed topography was measured with the same ultrasonic gauge (5) (§ 4.4.3 and Appendix 2.1.1) at the end of the test once the channel emptied. The water was drained from the channel smoothly to avoid any alteration of the bed topography.
- A manual reading on the side walls (8) allowed the description of the evolution of the water and bed levels during the tests (every 30 or 60 min).
- The discharge was measured with an electromagnetic flow meter (2) which is part of the fixed laboratory equipment (see § 4.4.5).
- The bed load was measured at the inlet (3) (introduced volume) and at the outlet (10) (weight of the filtering basket). For most of the tests, sediment samples (9) were taken at a regular interval (every 30 minutes) and weighted to allow the analysis of the evolution of the bedload during the test.
- The velocities were measured with an Ultrasonic Velocity Profiler UVP (6) provided by Metflow SA, Lausanne, which is based on the Doppler effect. The measurement device is described in detail in paragraph 4.4.4 and in Appendix 2.1.2.

- The grain size distribution of the armoring layer (7) (surface samples) was analyzed after every test at four locations: in the upstream and downstream scour at the inner and outer sidewall (usually the same as the lowest and highest point of the cross-section) (§ 4.4.6). Another sediment (volume) sample was taken in the end of the test at the outlet of the channel in order to compare the initial grain size distribution with the one of the transported sediment.

4.2.3   Boundary conditions

The flow was stabilized in the inlet box (§4.1.3). An additional element to quieten the flow was the assembly of small pipes (Fig. 4.3), used for the preliminary tests. For the main tests the small pipes were replaced by a floating polystyrene plate, which increased the uniformity of the flow conditions at the inlet. The sediment supply was made approximately 50 cm downstream from the beginning of the channel.

At the outfall, the bed level of the channel was controlled by a step at the outlet (see table below). During the tests, the tilting gate at the exit was completely lowered leading to critical flow conditions on the step. The steps at the inlet and outlet were adjusted to fit to the initially built in bed slope (Table 4.1).

Tests	Slope*	Inlet step (a)	Outlet step (b)
A	0.50%	485 mm	370 mm.
B	0.50%	485 mm	370 mm .
C	0.70%	460 mm	300 mm*
D	0.35%	480 mm	400 mm.
E	0.50%	485 mm	370 mm.

*Table 4.1:   Heights of the step (above channel bottom) at the inlet and outlet for the different tests
* built in initial longitudinal bed slope*

** The step was fixed at 285 mm but leveled at
300 mm in the beginning of each test.*
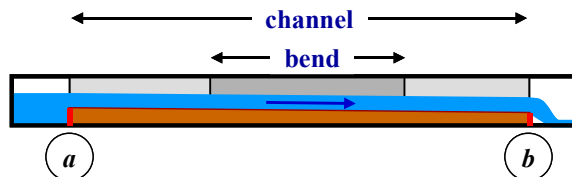
Since the Froude numbers were quite high, the water depths were close to critical flow depth. Therefore the influence of the backwater curve (see Fig. 4.14) was limited to a short distance, especially for the highest slope (< 4 mm at a distance of 1 m of the outlet); but it increased for the intermediate and lowest slope. For the two highest slopes the difference between water depth and normal water depth was less than 5 mm at the exit of the bend (6 m from the outlet). For the lowest slope, the backwater curve can have an influence on the second scour.
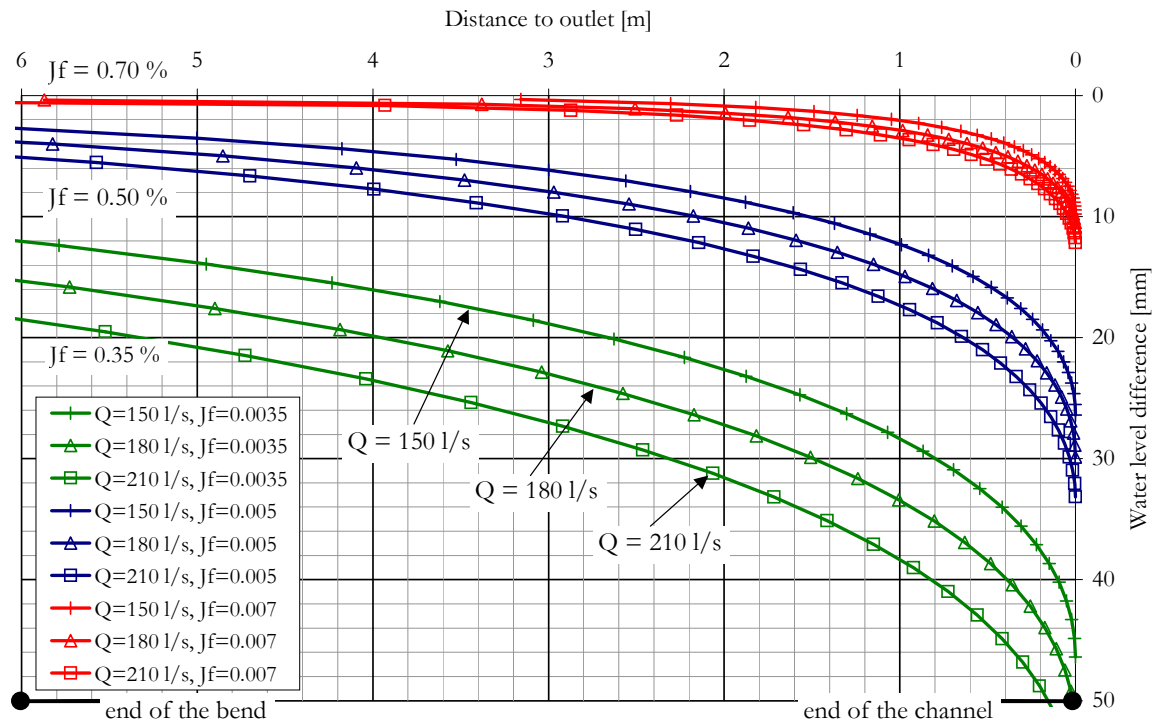
Figure 4.14: Computed backwater curve in the outlet reach - difference between computed water level and normal water depth

The bed load depends on the sediment supply, the transport capacity of the flow as well as on the corresponding equilibrium conditions. The tests were carried out with constant discharge, in situation of balance in the straight entry reach. Regarding duration, the tests were run until a global dynamic equilibrium was obtained (equality between fed sediments and sediment quitting the channel - in volume and grain size distribution - and stable bed levels along the outer side wall).

4.3   Properties of the used sediment mixture

a)   Grain size distribution

The bed of the flume was composed of a coarse sediment mixture. The mixture was selected according to common grain size distributions of alpine rivers (see Fig. 4.15) with the following characteristics:

d_{min} [mm]	d_{max} [mm]	d_{mean} [mm]	d_{10} [mm]	d_{35} [mm]	d_{50} [mm]	d_{75} [mm]	d_{90} [mm]
2	32	8.5	3.2	4.4	5.3	9.1	14.8

Table 4.2:   Characteristics of the used sediments

The part of fine sediments was left out for practical reasons (to reduce suspended load in the general water circuit of the laboratory and to keep the water transparent) and due to the fact that the fine parts are not significant for the bed load transport in the case of a wide grain size distribution in gravel bed rivers.
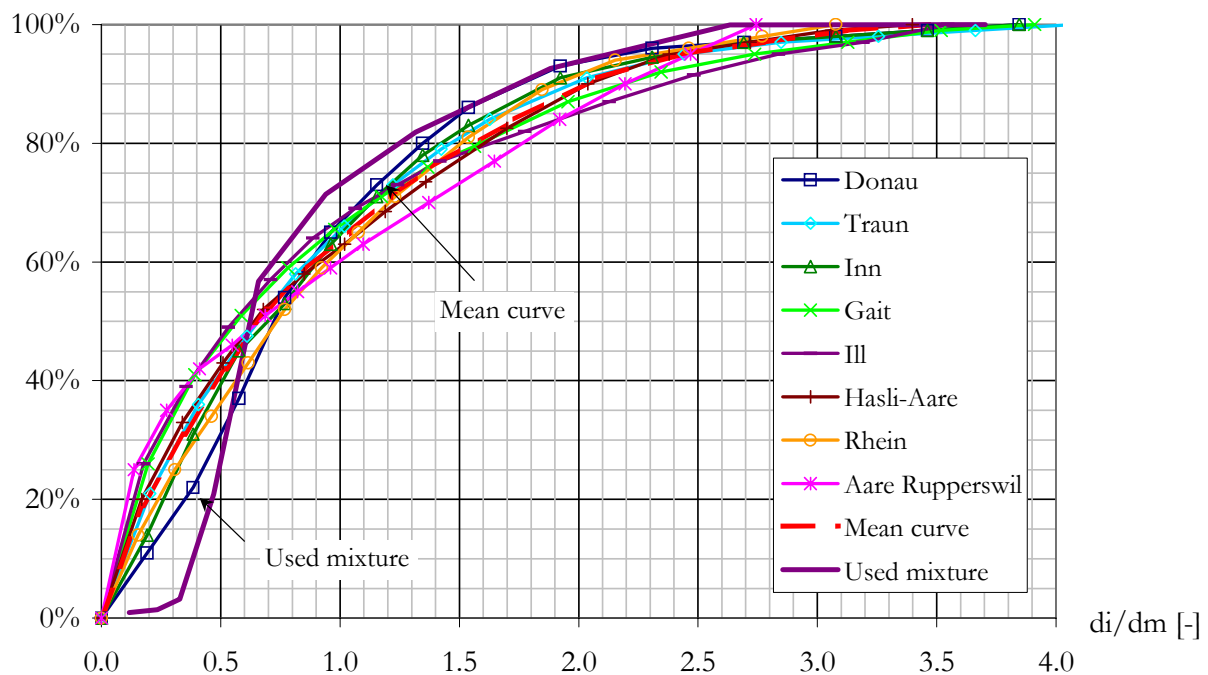
Figure 4.15: Grain size distributions of some mountain rivers and of the used sediment mixture

b)   Other parameters

Other parameters related to the sediment mixture like the density of the sediments, the porosity and the friction angle can be found in § 3.1.1.

4.4 *Measurement technique and data acquisition*

4.4.1 Overview

Fig. 4.16 gives a scheme of the automatic measurement devices. The whole data acquisition device[1] had to be programmed to suit the needs of the present research study (Appendix 2.2). The central command unit controls the following devices:

- The frame command unit, moved the probe support to the desired positions and allowed a semi-automatic data acquisition[2] (§ 4.4.2).
- The leveling unit performed the acquisition of the water and bed levels in the channel (§ 4.4.3).
- The velocity measurement unit - an ultrasonic velocity profiler, based on the Doppler effect - acquired the velocity profiles over the whole channel depth along 3 axis (giving the 3D velocity distribution) with an acquisition frequency of about 80 Hz (§ 4.4.4).
- These automatic measurements were completed with manual recordings of the sediment transport rate and the water levels and bed topography along the outer side wall (§ 4.4.6).
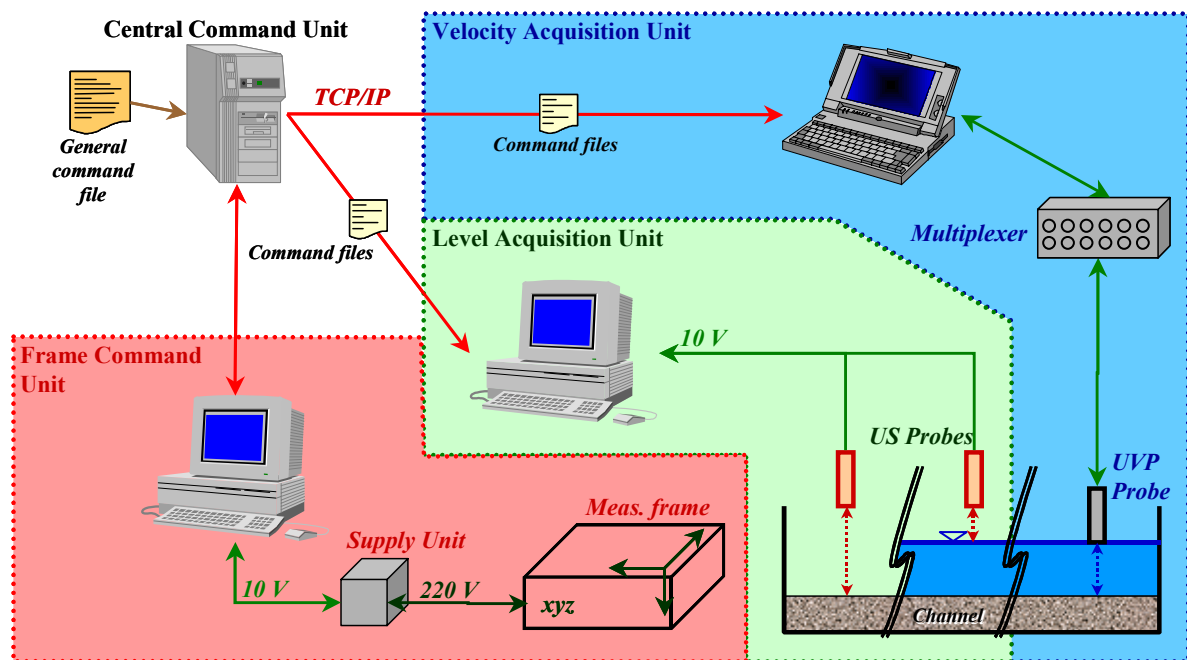
Figure 4.16: Scheme of the data acquisition

---

1. Including the *Central Command Program* and the *Chef Program*
2. The acquisition frame (traversing system 2 x 2 m) was moved manually to 8 predefined positions (every 15°). At each position, the frame automatically acquired the data within the frame area on a 9 x 9 cm grid (about 1500 automatic measurement points over the whole channel).
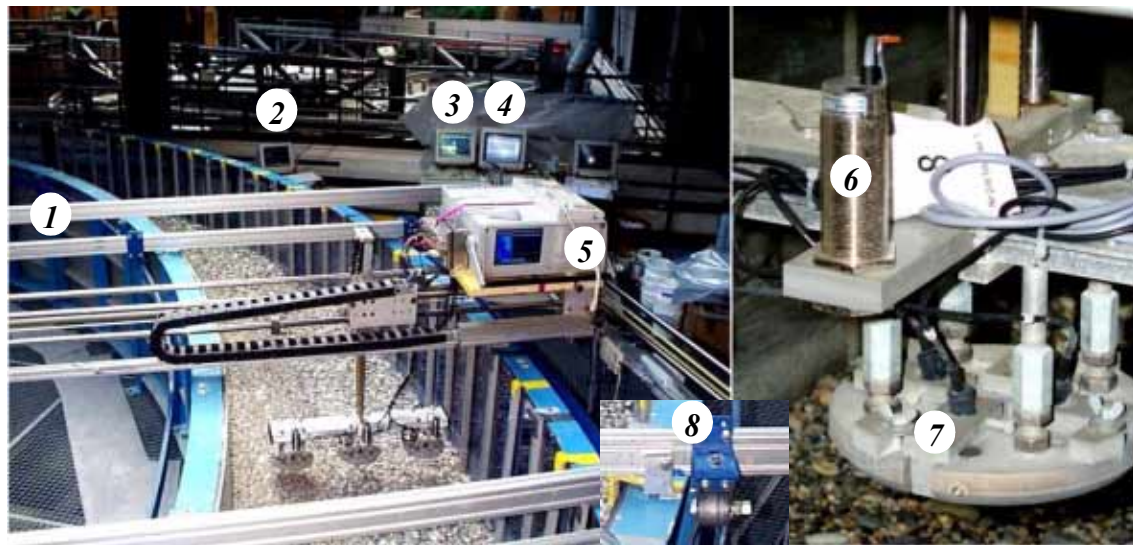
1. Measurement frame   5. Velocity acquisition
2. Discharge controller   6. Levelling probe
3. Frame controller   7. Velocity probe and support
4. Level acquisition   8. Fixation of the frame

Figure 4.17: Picture of the data acquisition system and the used probes

4.4.2 Central command unit and frame command unit

The central command unit (Appendix 2.2.1) read a command file and executed the instructions like the frame position, measurements to perform (water or bed levels, velocities) and duration of each measurement (see Fig. 4.18). A track of the executed commands as well as the reached frame positions were written to a log file. The central command program (Labview 5.1) sent small data packages with the instructions to the different computers, where the information was introduced by means of a small Visual Basic program (VB 5.1) into the final data acquisition program. It was possible to track the overall progress of the data acquisition on a remote computer.

The frame positions are given on Fig. 4.19. The automatic measurements were limited to the bend (positions 4 to 9) and the first 2 meters next to the curve (positions 3 and 10).
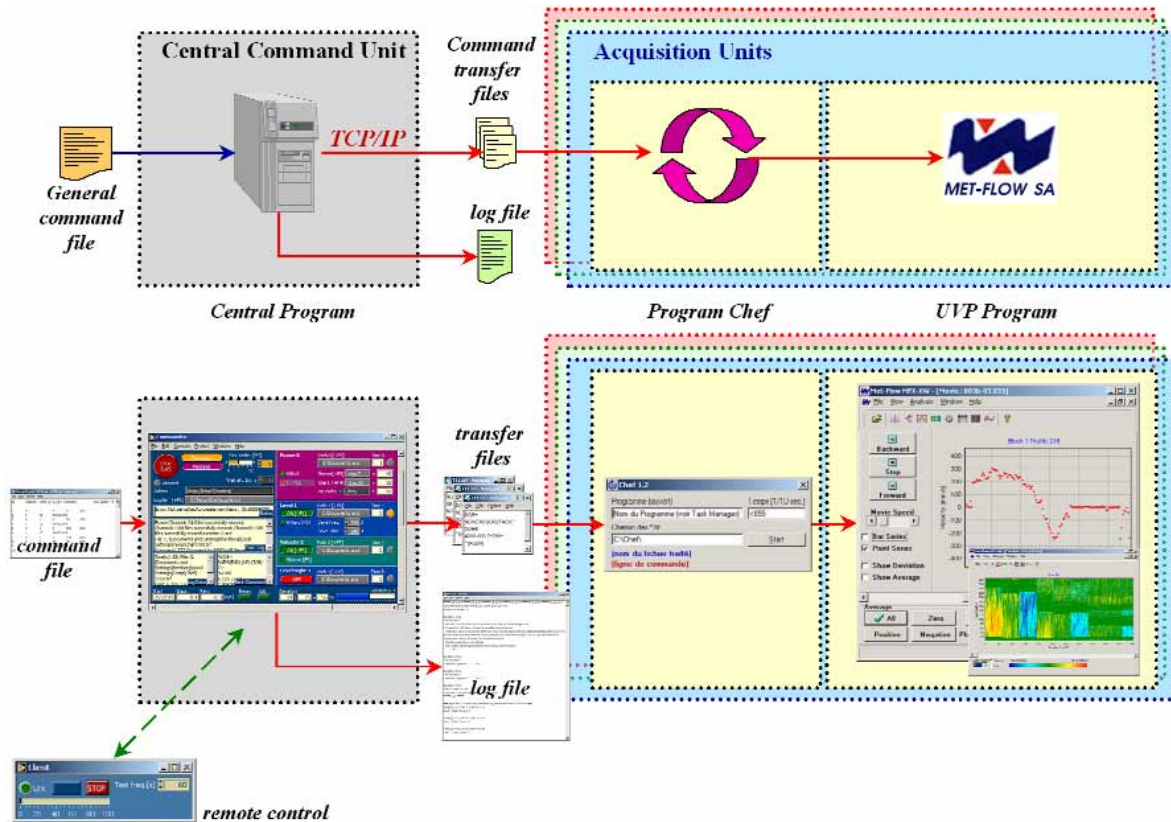
Figure 4.18: Data flux between the central command unit and the data acquisition programs
ON TOP: schematic view; BOTTOM: *illustrated with program interfaces*

4.4.3   The level acquisition unit

The level data (voltage between 0 and 10V), recorded with an ultrasonic gauge, was directly written into an Excel file (Version 7.0a). In order to increase the precision of the measurement, 32 data samples (sampling rate 10 Hz) were averaged at each measurement point. The voltage was transformed into a distance to a reference level located about 50 cm below the ground of the channel. The error of the level measurement is less than 1 mm (average ±0.5 mm). Additional information on the used probes and on the level acquisition can be found in Appendix 2.1.1 and 2.2.2.

4.4.4   The Ultrasonic Doppler Velocity Profiler (UVP)

The velocities were measured with an Ultrasonic Doppler Velocity Profiler (Metflow SA, Model UVP-XW, Version 1.1b, see also Appendix 2.1 and 2.2.3) allowing to obtain instantaneously a 1D-velocity profile over the whole channel depth (METFLOW, 2000). To measure the 3D-flow field, three probes were mounted on a probe support plate (Fig. 4.17 and Fig. 4.21). Since the number of measurement points was very high (about 1500 points over the whole channel), three plates

were mounted on the measurement frame, allowing to record three groups of three 1D profiles (constituting one 3D profiles) simultaneously to accelerate the data acquisition (see also HERS-BERGER, 2002).

The used probes had an emitting frequency of 2 MHz. The frequency of the finally acquired profile depends on the measurement depth; most samples were recorded at 77 Hz (measurement depth of 30 cm). The technical specifications of the velocity profiler and the probes can be found in Appendix 2.1.2. A multiplexer (Fig. 4.17, next to number. 5) allowed switching between the different UVP-probes.

Velocity profiles were recorded for all measurement points on a 9 x 9 cm grid. But due to the big amount of data, only the measurements in one cross-section is given for each frame position (center of the measurement frame) in Appendix . These profiles are exactly perpendicular to the channel axis (Fig. 4.19).
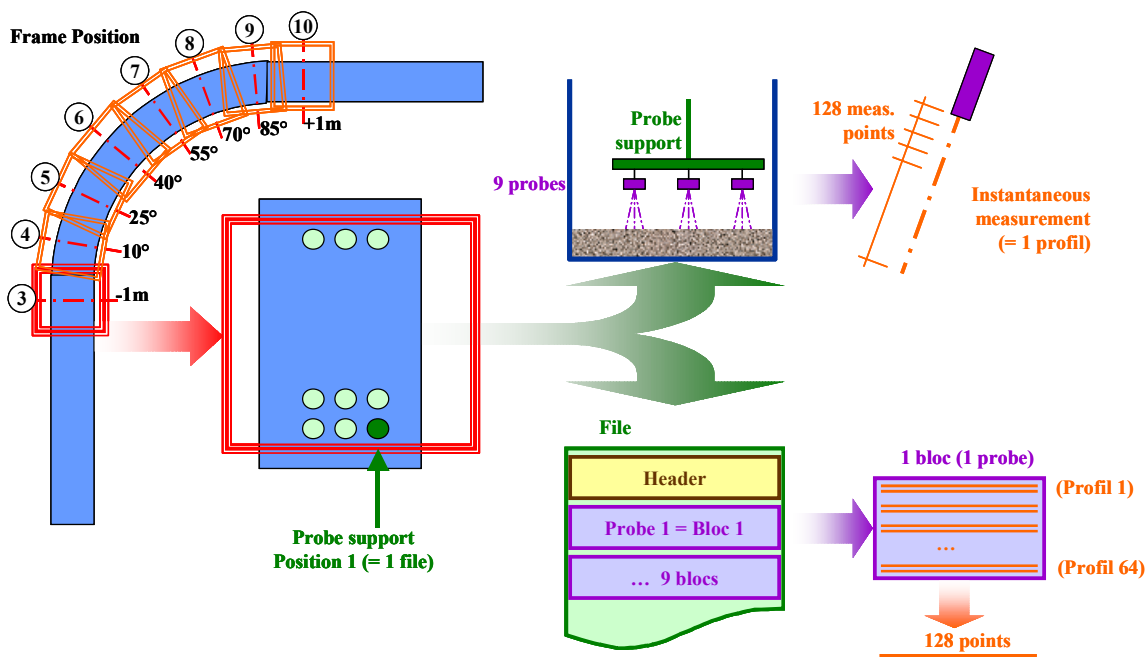
Figure 4.19: Frame positions and file format of the velocity raw data

Several specific problems due to the complexity of the flow field in bends had to be solved:

1. The measured velocities in tangential direction were rather high (up to 1.5 m/s),
2. the radial velocities were an order of magnitude smaller than the velocities in tangential direction and
3. the radial velocities were positive and negative due to the secondary flow.

Therefore, the scale of the measurements had to be fixed to allow good quality records for high as well as for small records with positive and negative sign. Two measures were taken to reduce the value of the measured velocity.

1. The UVP-probes were inclined by 20° allowing a reduction of the highest velocities to 34% (sin 20°) of the unprojected value (Fig. 4.21). The inclination was not increased to higher values because a very small error in the frame geometry would lead to an important measurement error. Furthermore, this inclination still gives a satisfying resolution for low velocities. Despite this inclination, the high velocities were somewhat too big to be measured.

2. Therefore an interesting characteristic of the Doppler measurement device was explored. If the measured velocity is higher than the maximum velocity, the UVP shifts the measured value by minus 2 times the velocity range into the negative domain of the measurement (ROLLAND, 1995). If the sign of the velocity is known, the recorded velocity profile can be corrected, by shifting the negative values again into the positive domain (Fig. 4.20). This was done for the high velocities in tangential direction whose sign was clearly given (see also § 4.6.2). The same procedure applies in analogy for negative velocities.
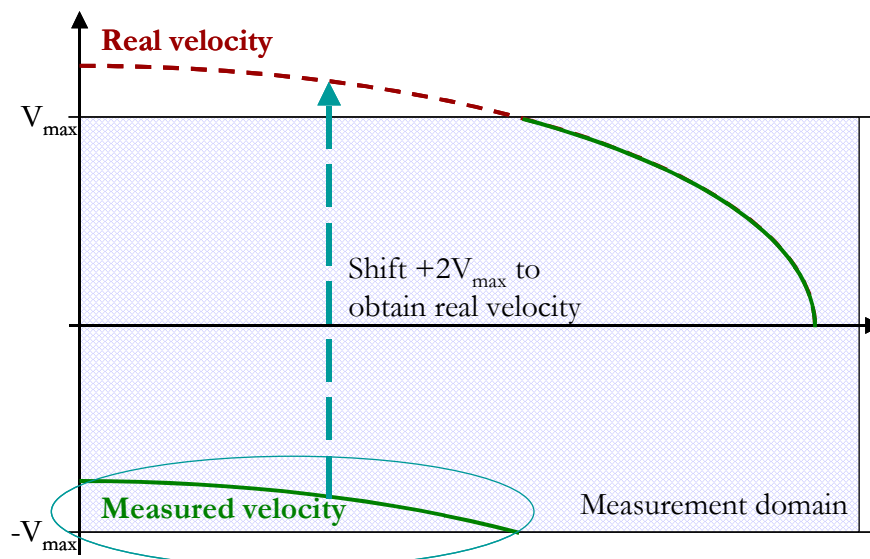
Figure 4.20: Shifting the measured velocity exceeding the measurement domain back to its correct position

Since the UVP-probes could not be placed vertically, the vertical control volume had a diameter of up to 3 to 6 cm, depending on the considered distance to the measurement plate.
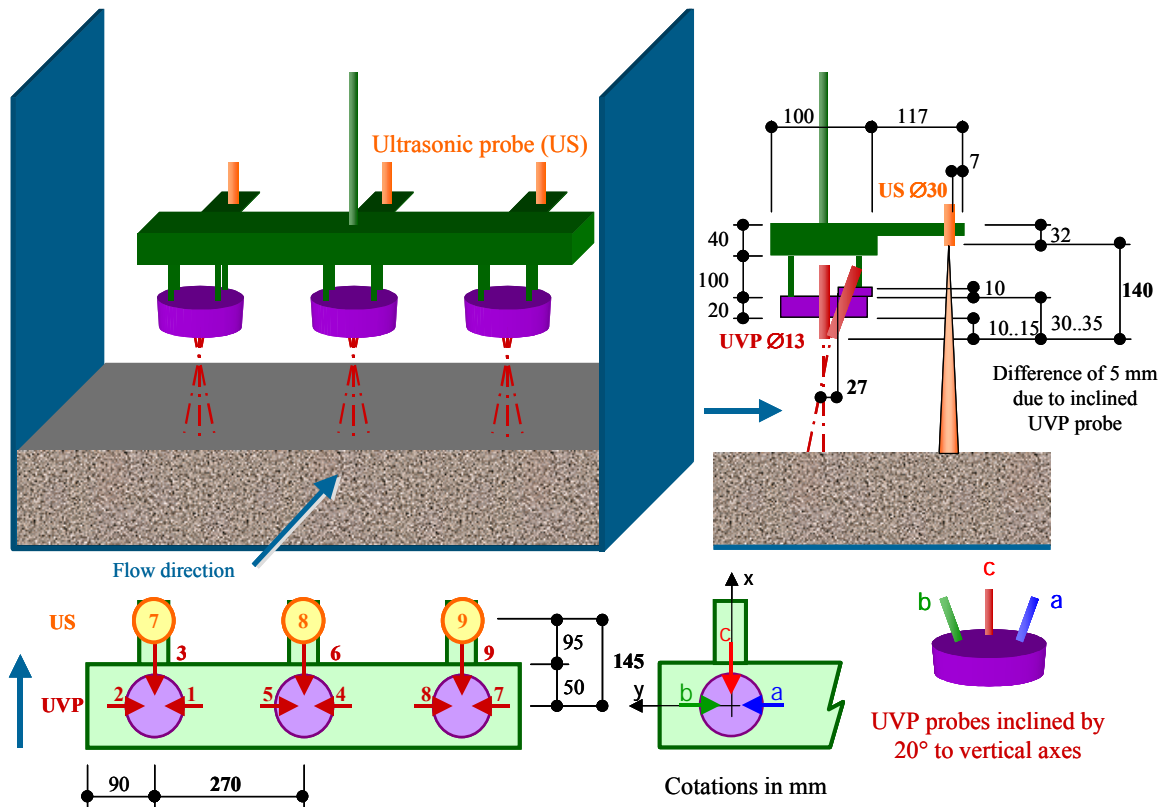
Figure 4.21: Geometry of the probe support

In the present study, the main interest was the average flow field. Therefore a rather short measurement was performed. For each 1D-velocity profile, 64 data points (in time) were recorded with a resolution of 128 points (in space) over the flow depth. The multiplexer switched to the next probe after 64 measured profiles. Consequently the measured flow field is not an instantaneous 3D-field. But for average values, it can be assumed to be constant considering the short record time. The acquisition frequency was of 77 Hz for most tests, which would even allow an analysis of turbulence characteristics for longer samples. Therefore longer recordings were performed with 2048 data points (in time) for some selected cases. A set of nine 1D-profiles performed at a given frame location was stored in a specific binary file for later treatment and analysis (§ 4.6.2).

The velocity measurement is quite short with 64 time averaged data points (about 1 second). Therefore longer recordings (more than 2000 measurements) were analyzed by averaging the measured velocities over different time spans (Fig. 4.22), showing that a sampling time of about 1 second (64 measurements) gives satisfactory results.
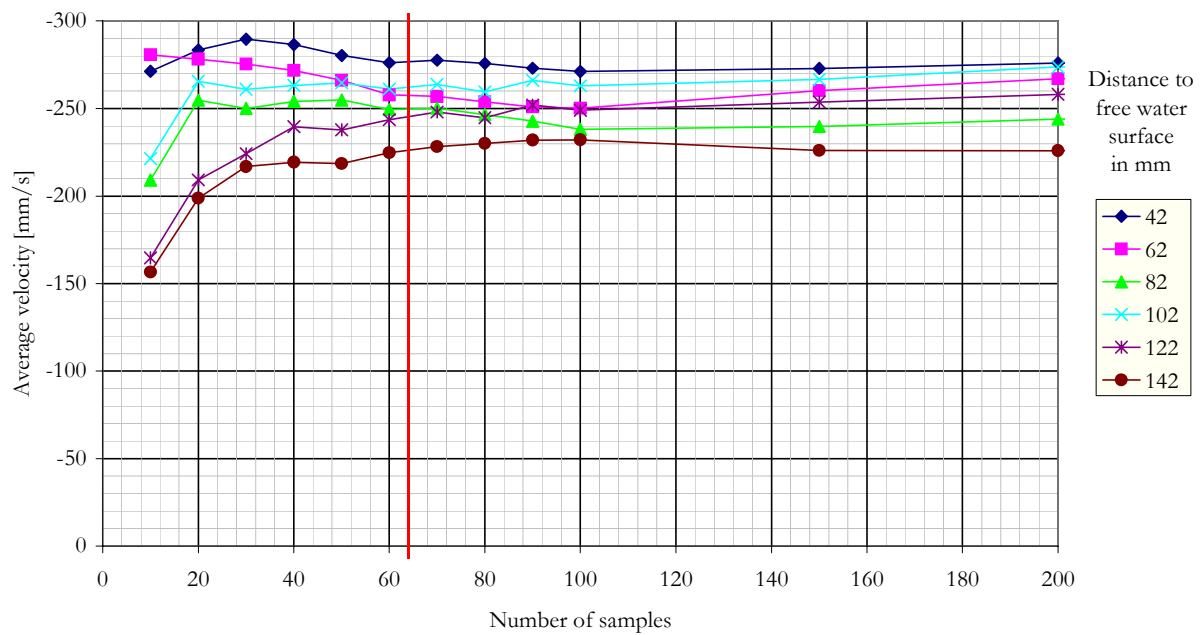
Figure 4.22: Influence of the sampling time on the time-averaged velocity (in the tangential direction). The vertical axis gives the computed average velocity over the number of samples (horizontal axis).

4.4.5   Other automatic recordings

The discharge during the tests was automatically regulated by an electromagnetic flow meter, which is a part of the fixed laboratory equipment. The guaranteed precision of the pumps is of 1 % of the maximum flow scale corresponding to 2.5 l/s. Automatic recordings of the discharge showed that the precision is even higher.

4.4.6   Manual readings

a)   Water and bed-levels on the outer side wall

The water and bed levels on the outer side wall were recorded manually every 30 minutes during the test every 2.5° (= 28 cm) starting at 1°. Towards the end of the test the frequency of readings was reduced due to slower bed level changes. The water level changes were generally less important than the bed level changes. The reading precision is of about 5 mm, which is mainly due to the size of the grains making it rather difficult to determine an exact bed level.

b)   Bed levels in the inlet and outlet reach

The bed level at the inlet (1.5 to 5.5 m) and at the outlet (2.0 to 5.0 m) was measured manually every 1.0 m over the whole cross-section (every 10 cm). Therefore a metallic profile was put on top of the channel. The distance between this profile and the bed surface was measured with a

graduated bar. The bed level was assumed being on top of the stones (and not between the stones).

c) Sediment feeding

The volume of the introduced sediments at the inlet was measured approximately by counting the number of fillings of the sediment feeding machine which could contain a volume of 0.50 m^3 (§ 4.1.2). Different parameters complicated a precise estimation of the introduced volume: the upper surface of the sediment reservoir was quite large (Fig. 4.6), the filling was performed by crane and in the end of the test, the remaining sediment volume in the sediment reservoir was estimated visually. Therefore the error on the quantity of added sediments can be estimated to about 15 to 20 %.

d) Sediment sampling at the outlet

During most tests, the volume of sediments was manually measured at the outlet. A sieve was lowered in the outlet part (§4.1.4, Fig. 4.9) for 1 to 10 minutes, allowing to get a sample of 3 to 10 liters (in general about 8 liters, see also §3.1.1 c) for the minimum size of a sample). One of the last samples of a test was sieved in order to check if the grain size distribution of the transported sediment corresponded to the substrate material. The samples were sieved in an automatic shaker during 20 minutes. The sieve openings were quadratic.

e) Sediment sampling of the armor layer

Once the test finished, four samples of the armoring were taken at the two maximum scour locations in the scour hole (outside) and on the inner bank. Therefore, a zone of 15 x 60 cm was colored with a red spray. The so marked stones were manually taken out and sieved (see also § 3.1.1 b).

f) Photos and videos

During all tests systematic pictures were taken of the water surface from different fixed points. Additional pictures were taken to document special phenomena and observations.

Two tests were documented by video recordings:
- Test C01b without macro-roughness (Q = 150 l/s, J_0 = 0.70%) and
- Test E03b with macro-roughness (Q = 150 l/s, J_0 = 0.50%, e_s = 2°, e_d = 40 mm).

4.5 Test procedure

Before the test was started, the sediments in the channel were levelled to the initial bed slope[1]. During 8 to 12 hours (in general during one night) a low discharge (70 l/s) was run to armor the bed. In general the outer side of the bend was more or less armored, but in the straight inlet and outlet reach no significant armoring was obtained due to lower bed solicitation. In fact, a choice was necessary: it was possible to obtain either an armoring of the straight reaches (which would have needed higher discharges and which would have eroded bed material in the bend) or a partial armoring of the channel in the bend (with only little armoring in the straight parts of the channel). For the present tests, it was preferred to keep a clearly defined initial bed topography (especially the longitudinal bed slope and a horizontal transversal bed) and to perform only a partial armoring, which allowed to eliminate the smallest fractions from the surface. Furthermore, observations showed that the bed in the inlet and outlet reach armored quickly at the beginning of the tests.

Then, the initial bed level was recorded on the dry bed. After a slow filling and a progressive increase of the discharge, the tilting gate was lowered (which is the start time of the main test). During the test, the water levels at the beginning of the inlet (fixed gauge at 2.50 and 3.50 m from the inlet), at the end of the bend (gauge on measurement frame located at 90°) and at the end of the outlet reach (fixed gauge at 4.00 and 5.00 m from the end of the bend) as well as the discharge were automatically recorded at a sampling frequency of 0.1 Hz. Every 30 minutes, the manual readings (§ 4.4.6, water and bed levels on the outer side wall, a sediment sample at the outlet and systematic pictures) were performed. Furthermore the sediment feeding rate, the remaining storage volume of the filtering basket as well as the discharge were checked and adjusted.

In general the channel bed stabilized after about 6 to 10 hours. The decision that the bed was stable enough to perform the water level and velocity measurements was taken based on the recorded water levels and bed levels on the outer side wall, where the changes were in general less than 5 to 10 mm in 2 hours. Furthermore the sediment transport rate at the outlet stabilized to a quite constant value[2].

Once the bed stabilized, the water level and velocity measurements were performed. These measurements needed in general about 8 to 12 hours (25 to 35 minutes for each set of recordings within one frame position). Some velocity measurements had to be repeated at the maximum scour locations since the scour depth exceeded the standard velocity measurement depth[3] of 30 cm. During these recordings, the water and bed levels on the outer side wall were periodically tracked (every 1 or 2 hours) to make sure that no significant bed changes occurred during the recordings.

---

1. The bed was only levelled before the test with the lowest discharge (Q=150 l/s). For the higher discharges the tests were started with the final bed topography of the previous test.
2. Some fluctuations were observed due to the fact that the sediments are often transported by packages (see Fig. 6.17 on page 132).
3. The measurement depth was maintained as short as possible to reduce the acquisition time, growing linearly with increasing measurement depth.

After these measurements, the tilting gate was slowly lifted (to prevent any bed changes) and the pumps stopped. Once the channel was empty, the bed level was recorded and sediment samples at the two maximum scour locations were taken out next to the outer and inner bank. Systematic pictures were taken to document the final bed topography and the grain size distribution over the whole channel. All performed operations and observations were documented on protocols (see Fig. 4.23 and Appendix 2.3):

- A general protocol (2 pages) giving the overall test procedure and the progress of the work.
- A protocol to track the evolution of the water and bed levels on the outer side wall.
- Protocols related to the sediment sampling at the outlet and the sieving of these samples.
- A protocol indicating the positions from which pictures were taken.
- A protocol to record the final bed topography after each test.
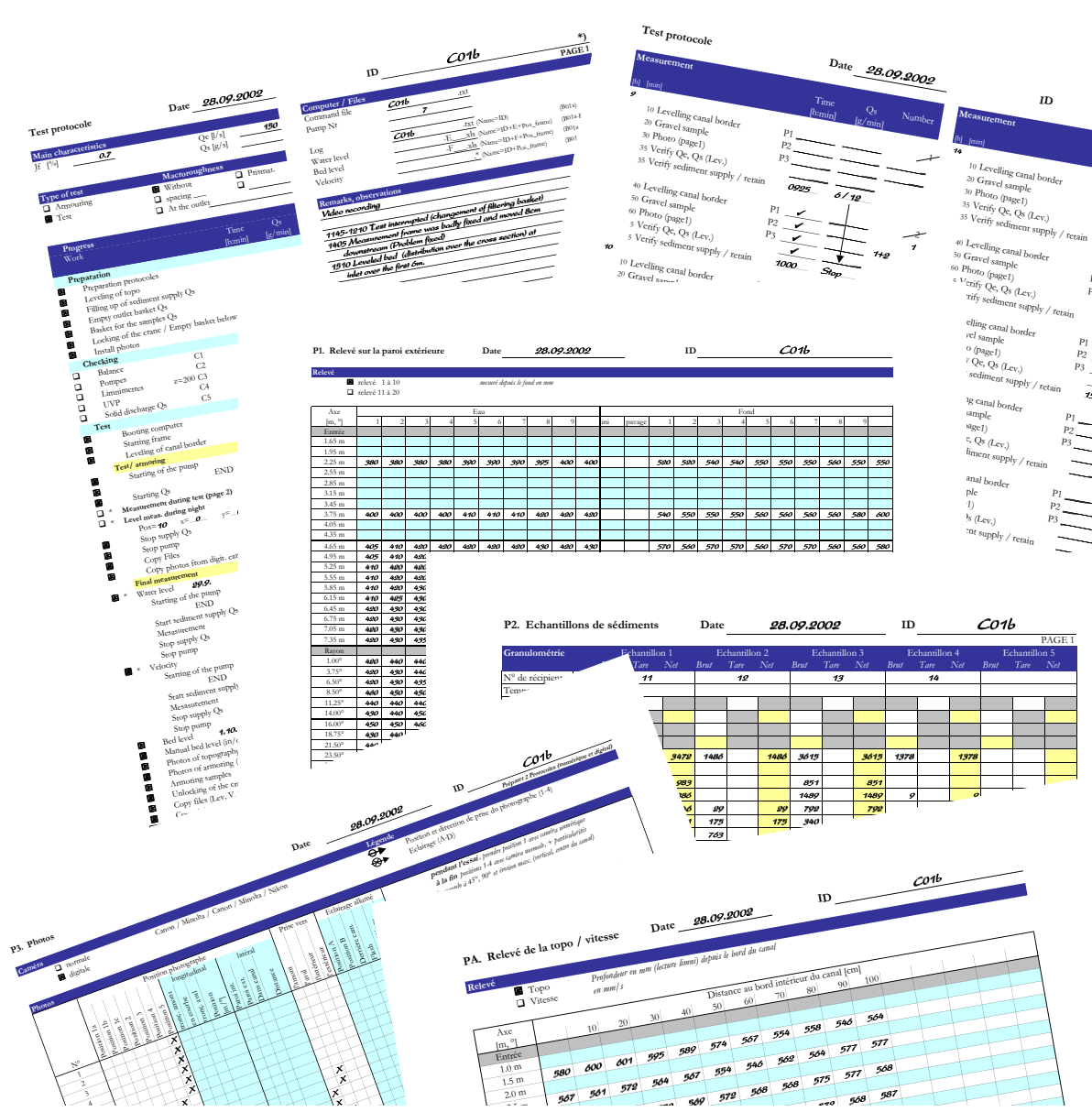
Figure 4.23: Test protocoles (see also Appendix 2.3)

4.6 *Data treatment*

4.6.1 Level treatment
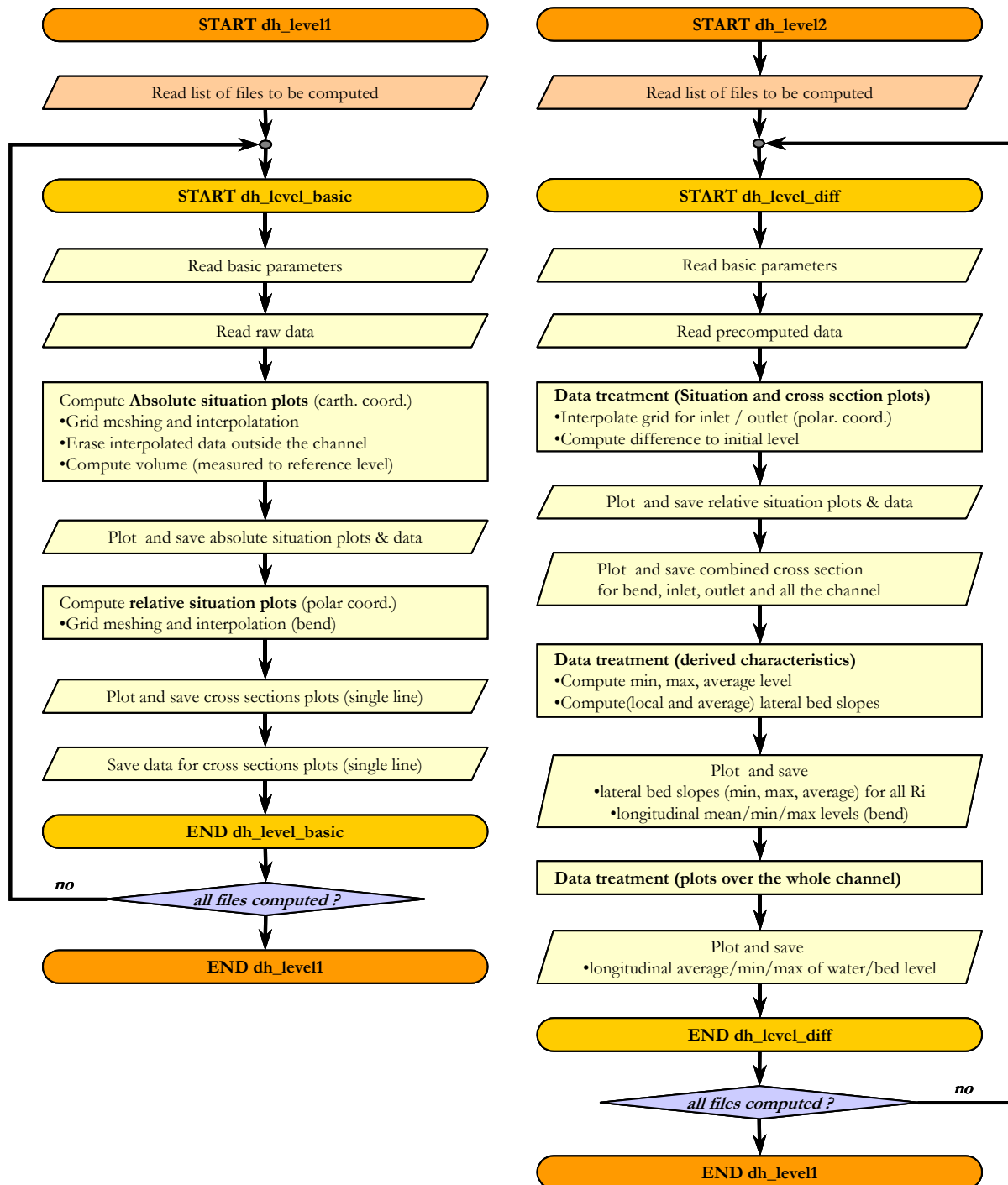
Figure 4.24: Flowchart of the MatLab treatment of the water and bed level data

During the measurements, the (water and bed) levels were recorded in an Excel file. For each measurement point, 32 values were recorded at 5 Hz and stored in a spreadsheet. The average of these 32 values was computed in a further step (Visual Basic Macro) and recorded in a file summarizing all data points over the whole channel. The coordinates were transformed from the local measurement frame coordinates to absolute frame coordinates relative to the bend (Fig. 4.1 and Fig. 4.19). The so obtained Excel spreadsheet was exported to a text file for further treatment with Matlab. A scheme of the performed Matlab treatment[1] is described in the flowchart on Fig. 4.24.

The Matlab treatment combined the automatically acquired levels, the manual readings on the outer side wall and the manually recorded levels in the straight inlet and outlet reaches. The computation was performed in two steps. First, the different input files were combines for each individual test (water respectively bed level). Then first graphics of the obtained raw data were plotted and analyzed to make sure that the data contained no errors (procedure dh_level1 on Fig. 4.24). In a second step the pretreated data sets were combined and compared to each other. At this stage the following plots were computed and printed: water and bed level changes compared to the initial bed level (Appendix 4 and 5), longitudinal plots (Appendix 8) and cross-section plots (Appendix 7) containing measured water and bed levels as well as the initial bed level (procedure (dh_level2 on Fig. 4.24).

4.6.2 Velocity treatment

In order to extract the 3D velocity field in six cross-sections over the whole channel (10°, 25°, 40°, 55°, 70° and 85°), the acquired binary velocity file (see § 4.4.4) needed some treatment.

First, the nine 1D records were extracted from the raw data file (Fig. 4.26) and written to a text file. The high velocities in tangential direction exceeding the measurement domain (negative sign) were then corrected to be located in the positive range (see § 4.4.4). Then the time-averaged measured components (average over 64 velocity profiles) at a given location had to be projected in a cylindrical coordinate system relative to the bend (tangential, radial and vertical velocities). Assuming that the measured velocity components are a, b and c (Fig. 4.21), the velocity components in a point are given with (Fig. 4.25):

$$v_\theta = \frac{a + b - 2 \cdot c}{2 \cdot \sin\alpha}, \; v_r = \frac{-a + b}{2 \cdot \sin\alpha}, \; v_z = \frac{a + b}{2 \cdot \cos\alpha} \tag{4.1}$$

---

1. The developed Matlab treatment needed about 4400 lines of program code.
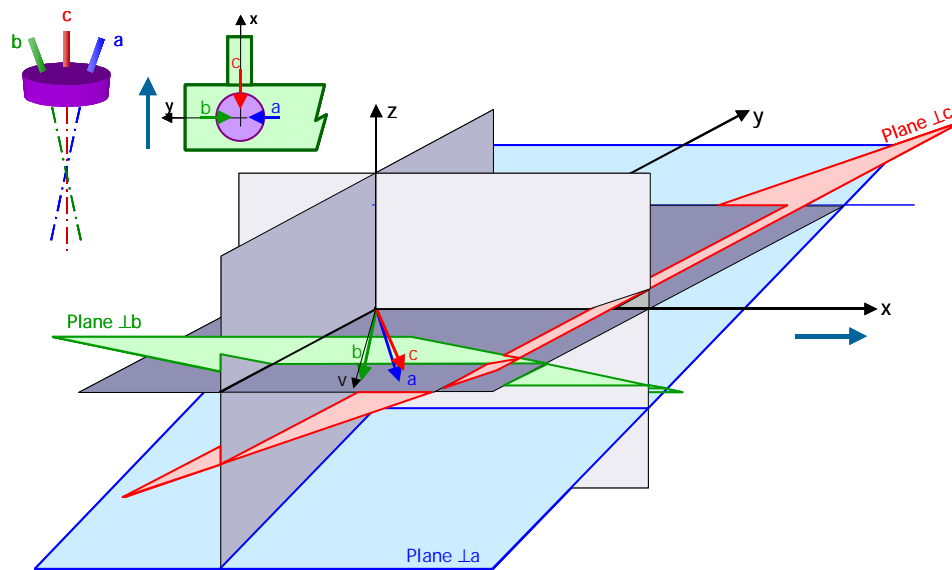
Figure 4.25: Schematic view of the projection of the measured velocity components a, b and c to obtain the final velocity vector v

The so obtained velocity components cover the whole measurement depth. As is can be seen on Figure 4.26, the bottom of the flume is clearly detectable. Due to the high amount of velocity profiles, it would be useful to detect the bottom automatically. In the present study tests were performed to detect the ground[1]. The bottom was fixed at the level for which the velocity as well as the variance were close to zero (absolute value below a given threshold). This method was tested with success.

---

1. There was not enough time to program an automatic velocity profile treatment; therefore the ground was detected manually, based on the described criteria.
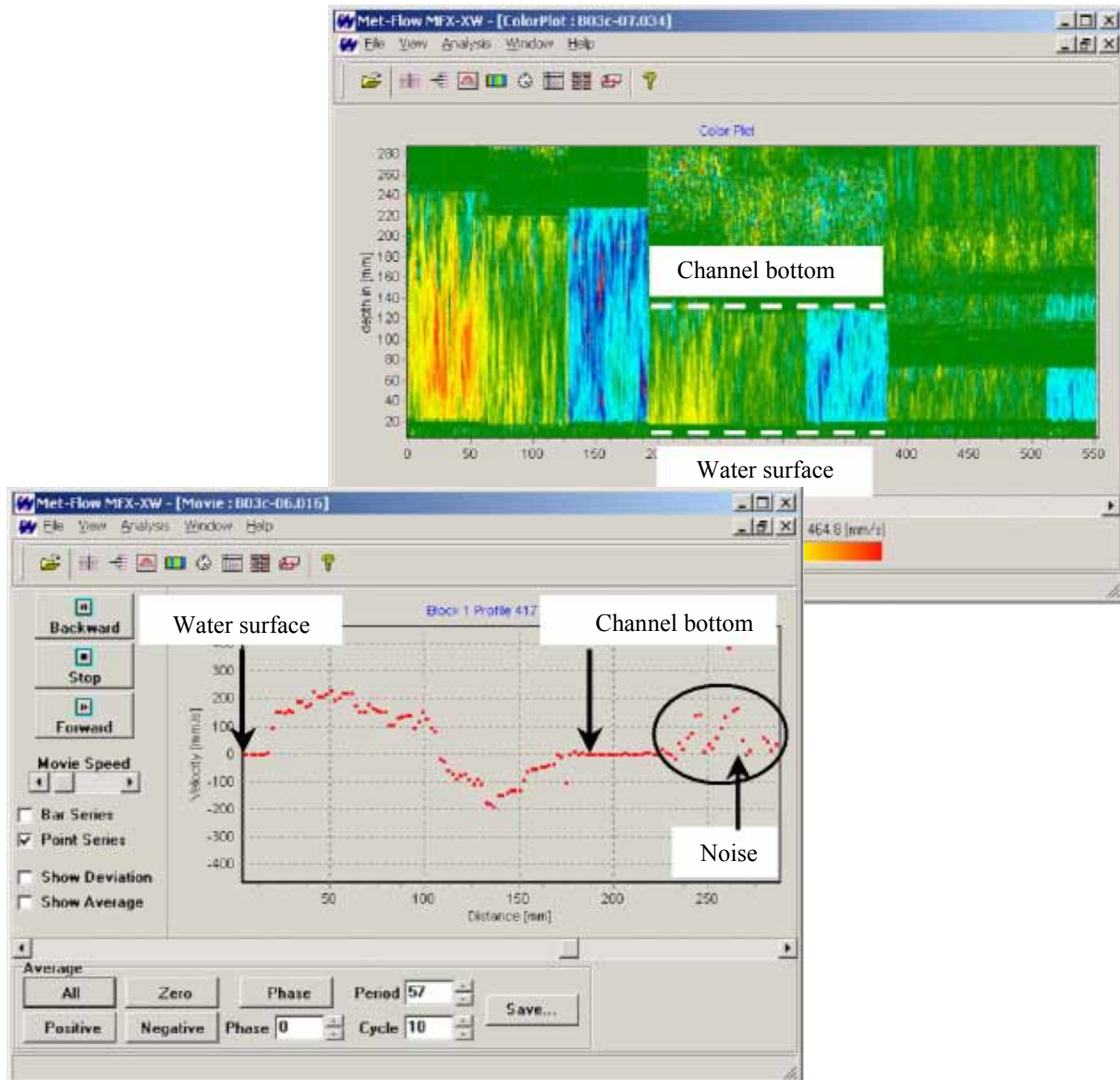
Figure 4.26: Used UVP Software, showing a sample file

After rearrangement of the velocity profiles[1], the data was exported to a text file for further automatic treatment with Matlab.

The Matlab treatment, which is described schematically in the flowchart on Fig. 4.27, served to plot isoline fields of tangential velocities, the flow field in the cross-sections (radial and vertical velocity components) and finally 3D plots of the velocity vectors over the whole channel. Since the density of velocity vectors on the plot was much too high, only every fourth measurement point (in vertical direction) was used for the plots. These plots are given in Appendix 11.

---

1. Three raw data files cover one cross-section of the channel. If the vertical profiles are numbered from outer bank to inner bank from 1 to 9, the first measurement gives positions 3, 6 and 9, the second one 2, 5 and 8 and the third one 1, 4 and 7.
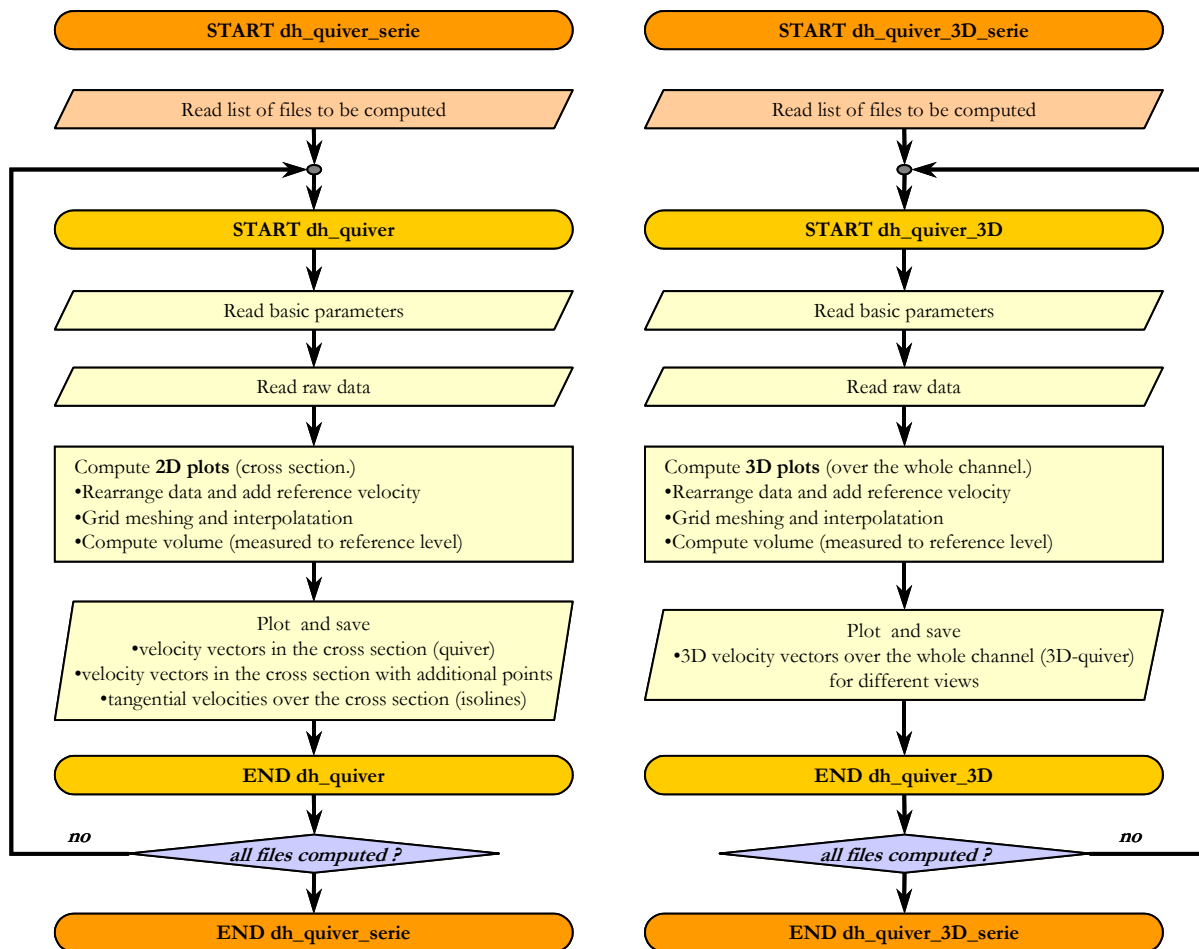
Figure 4.27: Flowchart of the velocity treatment with MatLab

CHAPTER 5

TEST RESULTS

5.1   Introduction

The present section briefly describes the obtained results and special observations that were made during the tests. The first section (§ 5.2) presents the preliminary tests, which served to establish the whole test procedure and to adjust and refine the measurements and the measurement technique. The main tests, described in section 5.3 are made for different bed slopes, discharges and rib-spacings. Finally an additional set of tests was performed to study the influence of the depth of the macro-roughness elements (§ 5.4). A detailed analysis of the tests is performed in chapter 6.

Some limits were fixed for the tests:
- The flow regime is maintained subcritical (Froude < 1).
- The maximum discharge of the pumps was of 210 l/s.
- The discharge had to be big enough in order to obtain any sediment transport.

All these conditions were evaluated in the following table, which shows the sediment transport rate in g/min. The underlayed zones (in the right part of the table) represent Froude numbers higher than 0.8, 0.9 and 1.0. Two lines were added to the plot to indicate the used minimum and maximum discharge. On the horizontal axis, the bed slope is given, and on the vertical one, the flow depth. The domain of the tests is highlighted with bold characters (center of the table). Since the armoring layer is destroyed in the beginning of the tests, the following table gives the sediment transport rates without armoring (with d_{30} = 4.4 mm, d_m = 8.5 mm, d_{90} = 14.8 mm).

hw Qb [g/min]

h_w [m]	So = 0.2%	So = 0.3%	So = 0.35%	So = 0.4%	So = 0.45%	So = 0.5%	So = 0.55%	So = 0.6%	So = 0.65%	So = 0.7%	So = 0.8%	So = 0.9%	
0.05	---	---	---	---	---	---	---	---	---	---	---	---	
0.06	---	---	---	---	---	---	---	---	---	---	---	---	
0.07	---	---	---	---	---	---	---	---	---	---	---	---	
0.08	---	---	---	---	---	---	---	---	---	---	---	1 605	
0.09	---	---	---	---	---	---	---	---	---	---	1 508	4 257	
0.10	---	---	---	---	---	---	---	---	---	927	3 704	7 211	
0.11	---	---	---	---	---	---	---	17	1 232	2 653	6 122	10 440	
0.12	---	---	---	---	---	---	16	1 288	2 794	4 537	8 742	13 922	
0.13	---	---	---	---	---	---	1 121	2 670	4 485	6 568	11 550	17 636	Q=150
0.14	---	---	---	---	---	768	2 314	4 155	6 294	8 734	14 531	21 566	
0.15	---	---	---	---	275	1 770	3 588	5 735	8 213	11 026	17 673	25 697	
0.16	---	---	---	---	1 091	2 836	4 938	7 403	10 234	13 436	20 964	30 015	Q=210
0.17	---	---	---	338	1 956	3 961	6 358	9 153	12 350	15 954	24 396	34 507	
0.18	---	---	---	1 016	2 868	5 142	7 845	10 981	14 556	18 575	27 959	39 163	
0.19	---	---	86	1 729	3 823	6 375	9 393	12 881	16 846	21 292	31 645	43 974	
0.20	---	---	620	2 475	4 819	7 657	10 999	14 849	19 214	24 099	35 448	48 929	
0.21	---	---	1 178	3 253	5 852	8 986	12 660	16 882	21 657	26 992	39 360	54 021	
0.22	---	11	1 759	4 059	6 922	10 357	14 373	18 975	24 170	29 965	43 375	59 242	
0.23	---	421	2 362	4 893	8 026	11 770	16 134	21 125	26 750	33 015	47 488	64 586	
0.24	---	848	2 986	5 754	9 163	13 222	17 942	23 329	29 392	36 136	51 693	70 045	
0.25	---	1 289	3 630	6 639	10 329	14 711	19 793	25 585	32 093	39 326	55 987	75 614	
0.26	---	1 745	4 292	7 548	11 525	16 235	21 686	27 889	34 852	42 580	60 363	81 287	
0.27	---	2 215	4 972	8 479	12 748	17 791	23 619	30 240	37 664	45 897	64 819	87 060	
0.28	---	2 697	5 669	9 431	13 998	19 380	25 589	32 635	40 527	49 272	69 351	92 927	
0.29	---	3 192	6 382	10 404	15 272	20 998	27 595	35 072	43 438	52 702	73 954	98 884	Fr > 1.0
0.30	---	3 698	7 110	11 396	16 570	22 646	29 635	37 549	46 397	56 187	78 626	104 927	
0.31	---	4 215	7 853	12 406	17 890	24 320	31 708	40 064	49 399	59 722	83 364	111 052	
0.32	---	4 743	8 609	13 433	19 233	26 021	33 812	42 616	52 444	63 306	88 164	117 255	
0.33	8	5 282	9 379	14 478	20 596	27 747	35 945	45 202	55 529	66 936	93 024	123 533	
0.34	215	5 830	10 161	15 538	21 978	29 497	38 107	47 822	58 654	70 611	97 941	129 883	

no sediment transport — sediment transport — Fr > 0.8 — Fr > 0.9

Table 5.1:   Computed sediment transport capacity (without armoring) - overview over the test domain Q_b, Fr and h_w

Table 5.2 gives the same information but computed with an armoring layer (computed according to Gessler, 1990, see section 3.3, d_{30} = 5.5 mm, d_m = 11.5 mm, d_{90} = 18.1 mm). This allows

to predict if some erosion is to be expected in the straight inlet and outlet reach and if any sediment transport can be observed or not (breakup of the armoring layer).

hw	Qb [g/min]											
[m]	So = 0.2%	So = 0.3%	**So = 0.35%**	So = 0.4%	So = 0.45%	**So = 0.5%**	So = 0.55%	So = 0.6%	So = 0.65%	**So = 0.7%**	So = 0.8%	So = 0.9%
0.10	- - -	- - -	- - -	- - -	- - -	- - -	- - -	- - -	- - -	- - -	- - -	232
0.11	- - -	- - -	- - -	- - -	- - -	- - -	- - -	- - -	- - -	- - -	- - -	2 933
0.12	- - -	- - -	- - -	- - -	- - -	- - -	- - -	- - -	- - -	- -	1 876	5 893
0.13	- - -	- - -	- - -	- - -	- - -	- - -	- - -	- - -	- - -	451	4 255	9 092	Q=150
0.14	- - -	- - -	- - -	- - -	- - -	- - -	- - -	- - -	432	2 273	6 812	12 511
0.15	- - -	- - -	- - -	- - -	- - -	- - -	- - -	184	**2 048**	**4 225**	9 534	16 135
0.16	- - -	- - -	- - -	- - -	- - -	- - -	- - -	**1 588**	**3 770**	**6 298**	12 410	19 949	Q=210
0.17	- - -	- - -	- - -	- - -	- - -	942	**3 078**	**5 591**	**8 484**	15 429	23 941
0.18	- - -	- - -	- - -	- - -	- - -	165	**2 204**	**4 649**	**7 504**	**10 776**	18 583	28 099
0.19	- - -	- - -	- - -	- - -	- - -	**1 207**	**3 530**	**6 294**	9 505	13 167	21 862	32 414
0.20	- - -	- - -	- - -	- - -	155	**2 301**	4 917	8 011	11 587	15 650	25 261	36 876	Fr > 1.0
0.21	- - -	- - -	- - -	- - -	**1 031**	3 443	6 362	9 794	13 745	18 222	28 770	41 476
0.22	- - -	- - -	- - -	- -	1 945	4 631	7 860	11 639	15 976	20 876	32 385	46 207
0.23	- - -	- - -	- - -	500	2 895	5 861	9 409	13 544	18 275	23 608	36 100	51 062
0.24	- - -	- - -	- - -	1 235	3 879	7 133	11 006	15 506	20 639	26 414	39 909	56 033
0.25	- - -	- - -	- - -	1 995	4 895	8 443	12 648	17 520	23 065	29 290	43 807	61 116

no sediment transport   sediment transport   Fr > 0.8   Fr > 0.9

Table 5.2:   *Computed sediment transport capacity (with armoring) - overview over the test domain Q_b, Fr and h_w*

Table 5.3 gives an overview of the performed tests and measurements. During the preliminary tests, velocities were measured at some positions which allowed to define the velocity range for the measurement device of the main tests. Appendix 1 contains detailed tables of all test parameters.

Test	ID	J_0 [%]	e_s [°]	e_d [mm]	Q [l/s]	MEASUREMENTS			
						Waterlevel	Bedlevel	Velocity	Grain size
Pre-lim.	A1	0.50	---	---	20...210	✓	✓	*	✓
	A2	0.50	2°	20	170...210	✓	✓	---	✓
Main tests	B1	0.50	---	---	70...210	✓	✓	✓	✓
	B2	0.50	4°	20	70...210	✓	✓	✓	✓
	B3	0.50	2°	20	70...210	✓	✓	✓	✓
	B4	0.50	1°	20	70...210	✓	✓	✓	✓
	C1	0.70	---	---	70...210	✓	✓	✓	✓
	C2	0.70	4°	20	70...210	✓	✓	✓	✓
	C3	0.70	2°	20	70...210	✓	✓	✓	✓
	C4	0.70	1°	20	70...210	✓	✓	✓	✓
	D1	0.35	---	---	70...210	✓	✓	✓	✓
	D2	0.35	4°	20	70...210	✓	✓	✓	✓
	D3	0.35	2°	20	70...210	✓	✓	✓	✓
	D4	0.35	1°	20	70...210	✓	✓	✓	✓
Additional	E2	0.50	4°	40	70...210	✓	✓	---	✓
	E3	0.50	2°	40	70...210	✓	✓	---	✓
	E5	0.50	8°	40	70...210	✓	✓	---	✓

Table 5.3:   *Overview of the performed tests and measurements*
        * some sample velocities were taken with a micro-propeller to confirm the estimated velocities

5.2 Preliminary tests

Two series of preliminary tests (A1 and A2) were performed. Both of them had an initial bed slope of 0.5 %. For these preliminary tests, the sediment feeding rate was maintained at a constant value. The order of magnitude of the transport rate was estimated with SMART & JÄGGI's (1983) formula (§ 3.4.2/4) and adjusted at the beginning of each discharge by observing the straight inlet reach (maintain the longitudinal bed slope at the initially built in value). The first series of measurements was taken without macro-roughness (A1), the second one with ribs placed every 2° (about 23 cm).

5.2.1 Tests without macro-roughness

1) Test procedure

The test series was started with a low discharge (20 l/s) and increased progressively by steps of 10 l/s. At discharges between 120 and 140 l/s the bed started eroding. Then the discharge was progressively increased to 170 and 212.5 l/s (maximum possible discharge of the pumps). These two discharges were maintained until the scour hole stabilized. The following table gives an overview of the discharges (Q), the bed load supply (Q_S), the runtimes and whether the bed topography was measured (✔) after the experiment or not (-). The bed topography was manually measured (see 4.4.6 b) at the following positions: in the inlet reach at 2.90 and 5.90 m, in the bend at 10°, 40°, 70° and 90° and in the bend at 4.40 m. The final bed topography after the tests is given in Appendix 3.1.

Q [L/S]	Q_S. [G/MIN]	DURATION [H:MIN]	TOPOGRAPHY MEASURED
Initial topography	-	-	✔
120	-	0:45	✔
130	100	2:00	✔
140	800	2:50	✔
150	1'500	0:50	–
170	4'400	3:30	✔
212.5	5'000	1:40	✔

Table 5.4:   Overview of the preliminary tests without macro-roughness

The Froude numbers ranged between 0.75 (Q = 120 l/s) and 0.76 (Q = 212.5 l/s).

2) Results

a) Location of the scour holes

The first movements of the finest fractions were observed at a discharge of about 100 l/s. But still higher discharges were necessary to initiate the scour process. Appendix 3.1 gives the situation plots of the bed topography after the tests with different discharges. The plots show clearly that the bed topography starts changing at a discharge between 120 and 140 l/s. The formation of a point bar can be observed in the lower part of the bend between 70 and 90°. Parallel to the development of this point bar, the scour process starts at almost the same location. This process can also be seen on Appendix 3.3.1 (difference plots of the transversally averaged / minimum / maximum bed profile) and on Figure 5.1. The longitudinal profiles (Appendix 3.3) show the minimum respectively the maximum bed level of each cross-section, corresponding to the maximum scour and the maximum point bar elevation. These extreme values are very close to the profiles along the outer and inner walls. The average bed level is the arithmetic mean value of the measured points in the cross-section.

These plots further show that the scour starts towards the end of the bend. The first signs of a scour hole become visible in the cross-section at 90° (17 m at Q=120 l/s). With an increasing discharge the hole moves in the upstream direction to 75° (15.5 m, Q=130 l/s) and 65° (14 m, Q=140 l/s) to reach its final position at 35° (11 m) for the discharges of 170 and 212.5 l/s (see arrow on Fig. 5.1 and Appendix 3.3.1).
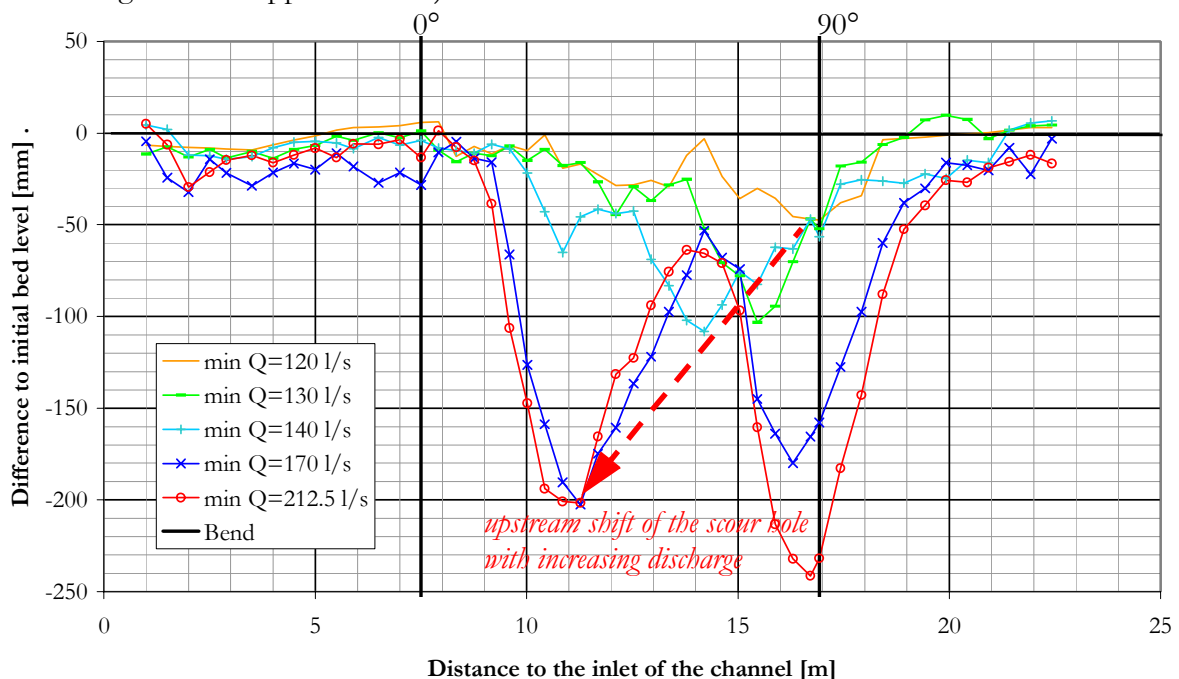
Figure 5.1:   Evolution of the scour (Thalweg) for the preliminary test without macro-roughness (A1)

b) Comparison of the scour holes

A comparison between the final bed topography (after Q=170 and 212.5 l/s) and the initial bed is given in Appendix 3.2. The Appendix further gives a comparison between the bed topography

with and without macro-roughness which will be discussed later (§ 5.2.2). For these two highest discharges, a second scour hole can be observed at the end of the bend.

Fig. 5.1 shows that it is difficult to determine weather the first or second scour will be more important: In the present case, the maximum scour depth appears in the first scour hole for a discharge of 170 l/s and in the second scour hole for the highest discharge (212.5 l/s).

c) Point bars

Appendix 3.1 and 3.2 show that there are important deposition zones at the inner bank at high discharges. The point bar is located almost at the position of maximum scour depth. Since the measured cross-sections for the preliminary tests were not as dense as for the final tests, the point bar seems to appear exactly at the location of the scour holes. But the main tests will show, that the upstream point bar is located downstream the first scour hole and upstream the second scour hole (see § 6.2.1).

d) Grain size distribution

Figure 5.2 shows the channel bed at 45° after the test run with macro-roughness. It can be stated that the coarse grains are accumulated near the outer wall and that the fine sediments are deposed on the point bar at the inner side. The same phenomenon is observed both, with and without macro-roughness.

Figure 5.2:   Grain sorting, view across the outer side wall at 45° (test with macro-roughness - A2)

e) Velocities

Some velocities were measured with a micro propeller during the preliminary tests (with and without macro-roughness). The measured depth-averaged velocities are given in the following table:

TEST	Q [l/s]	LOCATION	INLET 4 m	BEND 0°	15°	30°	45°	60°	75°	90°	OUTLET 3 m
A1	40	inner bank					0.35*				
		center	0.55*				0.5				
		outer bank					0.6				
	90	inner bank	0.85*				0.55*				
		center									
		outer bank					0.8				
	120	inner bank	1.00*			0.55*	0.7**				
		center									
		outer bank				0.95	1.2*				
	140	inner bank		1.20	1.10	0.60	0.55	0.50		0.8	0.8
		center								1.05	
		outer bank	1.25*	0.95	0.95	1.05	1.10	1.10		1.25	1.40
	170	inner bank	1.20**	1.15		0.65	0.70	0.80		0.40	0.90
		center	1.30	1.20		1.20	0.80	1.15		0.80	1.15
		outer bank	1.15	1.00		1.20	1.20	1.25		1.25	1.40
A2	170	inner bank				0.80	0.80	0.80	1.00	1.10	1.00
		center	1.20			1.10	1.00	1.10	1.20	1.30	1.40
		outer bank		0.80		1.10	1.00	1.10	1.10	1.15	1.20
	212	inner bank	1.40**	1.30	1.20	1.05	0.80	0.75	1.00	1.05	1.05
		center	1.50*	1.30	1.25	1.40	1.20	1.20	1.45	1.50	1.50
		outer bank	1.50*	1.35	1.15	1.15	1.35	1.30	1.30	1.30	1.15*

Table 5.5:   Velocities in m/s measured during the preliminary test without macro-roughness
* average value (±0.05 m/s), ** average value (±0.1 m/s)

These measurements were used to scale the range of the velocity measurement with the Ultrasonic Doppler Velocity Profiler (UVP). An interesting observation can be made at 140 l/s. Just after the inlet reach at the beginning of the bend, the highest velocities can be measured at the inner bank. This corresponds to the flow fields observed by researchers working on fixed beds. But this phenomenon is limited to the first part of the bend (up to 20°). For higher discharges, this phenomenon is not that pronounced or even non existent, since the bed topography is modified by the scour and point bar formation, leading therefore to higher velocities (and water depth) along the outer bank.

5.2.2   Tests with macro-roughness

1)   *Test procedure*

The tests with macro-roughness followed the same scheme as the ones without vertical ribs in order to allow a comparison of the results. The different discharges were maintained during the same period of time as for the tests without macro-roughness except the one at 170 l/s. The discharge was maintained longer since the erosion reduced considerably compared to the test without macro-roughness (to make sure that the equilibrium bed topography was reached). Only the results of the discharges 170 and 212.5 l/s are documented since the smaller ones represent transitions in the development towards the maximum scour.

Q [L/S]	Q_S [G/MIN]	DURATION [H:MIN]	TOPOGRAPHY MEASURED
Initial topography	-	-	✓
120	-	0:45	–
140	800	2:00	–
170	4'400	5:35	✓
212.5	5'000	2:15	✓

Table 5.6:   Overview of the preliminary tests with macro-roughness (spacing 2°)

2)   *Results*

a)   *Location of the scour holes*

The scour holes are located farther downstream compared to the previous tests (see Appendix 3.2, 3.3.2 and 3.3.3).

b)   *Comparison of the scour holes*

Appendix 3.2 allows the comparison of the depth of the two scour holes. It can be observed that the important scour holes almost disappear for the tests with macro-roughness (see also Appendix 3.3). For both discharges the scour holes (with macro-roughness) have approximately the same maximum depth. Compared to the tests without macro-roughness, the scour depth is significantly reduced. It is obvious that if the scour depth is reduced due to the vertical ribs (and if the point bars are not higher), the transversal bed slope is diminished.

Some other bed changes due to macro-roughness were observed:
- The scour was reduced almost over the whole bend (Appendix 3.3.3).
- The macro-roughness induced a head loss in the bend. In order to pass the same discharge in the bend, the longitudinal slope had to increase. Therefore, water accumulated upstream the bend, reducing the local velocities and consequently the local transport capacity. The depositions resulting from this process are shown on Appendix 3.3.3.

- Some additional erosion was observed after the bend in the straight outlet reach in the central part of the flume (Appendix 3.2). This is due to increased velocities after the bend.

c) Point Bars

The highest point of the observed point bars shift in the downstream direction. For the preliminary tests, they were somewhat longer compared to the configuration without macro-roughness. The height of the second point bar was slightly reduced (see Appendix 3.2 and 3.3).

d) Grain size distribution

The grain size distribution of the armoring layer and of the samples taken at the outlet (with and without macro-roughness) does not seem to differ much for the preliminary tests. In the first hole, an important accumulation of coarse grain and the formation of an armoring layer were observed. The maximum scour depth in the second hole seems to be rather governed by the equilibrium conditions of the grains than by the influence of an armoring layer.

e) Velocities

The velocities in the channel are more uniform over the whole cross-section in the bend if vertical ribs are placed on the outer bank (Table 5.5 on page 105). Without macro-roughness, a clear gradient of velocities in the cross-section can be observed (e.g. from 30° to 60°): the velocities at the inner bank are at about 55 to 65% of the value of the ones at the outer bank. With macro-roughness this ratio is reduced to 75 to 80%. These observations need to be confirmed by the main tests.

5.3 Main tests

The main tests were performed during one year from February 2000 to February 2001. The tests followed the general test procedure described in section 4.5. For all the tests a complete set of measurements was recorded including the water surface, the bed topography, the velocities, the evolution of the water and bed topography on the outer side wall, the grain size distribution of the armoring layer after the test, the discharge and the bedload transport rate.

5.3.1 Description of the Appendixes

The test results are summarized in the different Appendixes at the end of the present report. Most representations are based on the same structure with 3 rows and 4 columns. In general, the rows are the different discharges (150, 180 and 210 l/s) and the columns represent the different spacings of the macro-roughness (no macro-roughness, rib-spacing every 4°, 2° and 1°). The tests are presented from the lowest (Appendix *.1)[1] to the highest channel bed slope (Appendix *.3) for the ribs of 20 mm depth and finally for a bed slope of 0.50% with deeper ribs (40 mm) (Appendix *.4). Special phenomenon and measurements are usually documented in Appendix *.5.

- Appendix 1 summarizes all test parameters and results including the tests of PETER (1986).
- Appendix 2 gives tables, schemes and informations relative to the data acquisition, the acquisition devices and the data treatment. Furthermore sample protocols and observations made during the test can be found in this section.
- Appendix 3 shows situation plots, longitudinal bed profiles and comparisons between initial and final bed topography for the preliminary tests (see also § 5.2).
- Appendix 4 gives the measured final bed topography compared to the initial one (recorded after the armoring at a discharge of 70 l/s). The isolevels correspond to an elevation difference of 20 mm. The data points for the plots (a grid of 50 x 50 mm with an absolute reference relative to the bend) were interpolated linearly between the measured data points (grid of 90 x 90 mm with a reference relative to the measurement frame). Positive bed elevations correspond to depositions and negative values to erosion.
  The last section (4.5) compares the results of a long term test with a "normal" duration. The final bed topographies after 13 and 27 hours are compared.
- Appendix 5 shows the final water surface compared to a horizontal average surface over the whole channel (average of all data points). The isosurfaces correspond to a distance of 10 mm. The resolution of the data points is the same as for Appendix 4.
- Appendix 6 presents systematic pictures of the water surface in the bend between 10° and 90° taken in the downstream direction.
- Appendix 7 gives the water and bed levels in selected cross-sections every 15° from 1 m upstream the bend to 1 m downstream the bend. The plots further indicate the mean water and bed levels (average over the cross-section) and the initial bed level. The vertical axis of

---

1. * is used as a placeholder for the number of the different Appendixes.

the plots gives the distance to a reference level fixed about 50 cm below the channel bottom (to avoid negative values). The interpolation resolution in radial direction was of 10 mm.

- Appendix 8 shows the longitudinal equilibrium bed and water profiles (after the test). The plots show the average, the minimum and maximum value (over the cross-section) of the water and bed levels. The initial average bed level is also given to facilitate comparisons. The values were computed every 1° in the bend and about every 10 cm (translated to degrees[1]) in the straight inlet and outlet reach. Two vertical lines indicate the beginning and the end of the bend (0° and 90°).

- Appendix 9 presents the grain size distributions of the armoring layer at the two maximum scour locations at the inner and outer bank (surface samples). An additional grain size distribution is given of a volume sample taken at the outlet at the end of the test.

- Appendix 10 gives a selection of pictures taken vertically every 15° between 10° and 85°. They document the evolution of the grain size distribution of the armoring layer after each test.

- Appendix 11 shows the measured velocities. The first part shows the results without macro-roughness (Appendix 11.1 to 11.3) and the second part the ones with vertical ribs (Appendix 11.4 to 11.6). Each part first gives the tangential velocities, then the velocity vectors in the cross-section (radial and vertical velocity components) and finally the 3D-velocity vectors in the bend. For the 3D-plots, the bend is represented as a prismatic block. The velocity profiles are located every 15° at cross-sections from 10° to 85°. All presented velocity measurements were made at an initial bed slope of 0.50%. The influence of the macro-roughness is shown for a discharge of 210 l/s. Due to the big number of measurement points over the depth (128 points), only every 4th point was used for the vector plots to facilitate the reading.

- Appendix 12 gives the results of the genetic programming used to search for a new scour formula.

5.3.2   Observations during the tests

a)   Development of the scour and point bars

For the tests without macro-roughness, the scour process started in general at discharges between 100 and 140 l/s (see § 5.2). At a discharge of 150 l/s, sediment transport was observed over the whole cross-section (except for the flattest bed slope of 0.35%, where a discharge of about 180 l/s was needed to move the sediments). The formation of the first scour hole started almost at the final location of the second scour hole at the downstream end of the channel and moved with increasing discharge in the upstream direction where it started oscillating around its final position between 30° and 45°. For the main test, which were started directly at the final discharge (150, 180

1.Since straight and curved parts of the channel had to be merged on one plot, the same distance unit had to be used for the horizontal axis. Since the main interest is the behavior in the bend, an angular reference was chosen. The distances in the straight parts were converted to angles corresponding to a position on a bend located on the center line of the channel.

and 210 l/s), the first scour started developing at about 60 to 70° and moved quickly upstream towards its final position. This upstream "walk" took less than half an hour. At the same time the scour deepened.

The second scour developed quite rapidly, too, almost proportionally to the development of a point bar at the inner bank. Depositions at the inner bank started at about 60°. The fine sediments fractions moved over the point bar and were deposited at its downstream end until the end of the point bar was finally located close to 90°.

Another interesting observation can be made concerning the location of the point bar, compared to the position of the maximum scour. The end of the upstream point bar was located downstream the first scour whereas the end of the second point bar was located upstream the second scour. This may be an explanation of the growth of the second scour being proportional to the point bar formation (Appendix 4).

The scour seems to be dominated by different phenomena: In the first scour, the armoring probably plays a controlling role, whereas the second scour seems to be governed by another phenomenon.

Both scour holes oscillated around their mean position until they stabilized at their final location. The phenomenon is very sensitive to small changes in the upstream or downstream part of the channel. If the sediment transport rate at the inlet was somewhat too high, causing an increase of the inlet bed slope, the scour process reactivated respectively increased a few minutes later first in the upstream and then in the downstream scour hole. At the opposite, if the outlet conditions in the channel were slightly modified (during some tests the tilting gate at the outlet came up[1], so that the flow depth at the outlet was higher than the critical depth), the second scour started decreasing slowly but almost instantaneously. This influence of the backwater curve on scouring was also observed by REINDL (1994). Due to a continuous control of the bed and water levels, all these fluctuations were stabilzed which allowed to obtain good results.

b) Armoring

The first scour hole and the straight inlet reach armored quickly at the beginning of the test. Afterwards, the sediments were mainly transported over this armoring layer.

The armoring layer in the second scour needed much more time to be formed than the one in the first scour. This was due to the fact that the armoring propagated from upstream to downstream. The second scour started armoring, once the first one was armored.

c) Particular events and phenomena during the tests

During the performed tests, an important number of irregularities occurred related to the different elements of the quite complete experimental setup. In order to track irregularities is the history of the tests, Appendix 2.4 gives the main problems encountered during the tests as well as special

---

1. As soon as this phenomenon was detected, the tilting gate was pushed down again and fixed to the ground. If the gate came up towards the end of the test, the run was continued some more time to make sure that the final test result was not influenced by this event.

observations. All necessary precautions have been taken to limit their impact on the results and to ensure a relyable dataset.

For the tests with macro-roughness, vertical ribs were placed at the outer side wall with a regular spacing. The last meter in the inlet upstream the bend as well as the first two meters in the outlet reach, downstream the bend, were also equipped with ribs. The spacing between ribs increased with increasing distance from the bend with a factor $\sqrt{2}$ compared to the previous spacing (Fig. 5.3). The following table gives the spacings of the ribs for the different tests:

TEST	e_s [°]	INLET [MM] DIST. TO BEND	BEND [°]	OUTLET [MM] DIST. TO BEND
B2, C2, D2, E2	4°	384, 1026*	0.6, 4.6, ..., 88.6	298, 752, 1394
B3, C3, D3, E3	2°	157, 478, 932**	0.6, 2.6, ..., 88.6	71, 298, 525, 752, 979, 1300, 1754
B4, C4, D4	1°	43, 203, 429, 749	0.6, 1.6, ..., 89.6	70, 183, 296, ..., 974, 1134, 1360, 1680
E5	8°	838, 2121	0.6, 8.6, ..., 88.6	752, 1815

Table 5.7:   *Spacing of the macro-roughness*
* 384, 927mm for test B2, ** 157, 379, 693, 1137mm for tests A2 and B3
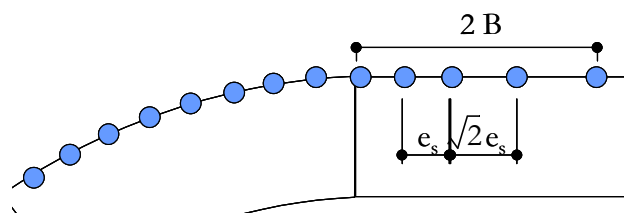
Figure 5.3:   *Macro-roughness arrangement in the straight transition zones in the inlet and outlet reach*

5.4   Additional tests

A series of additional tests was performed during the month of May and June 2001 in the frame set of a diploma work by GÜNTHER (2001). The aim of these tests was to examine the influence of the macro-roughness thickness on the scour depth. Therefore the vertical ribs were modified and a rectangular, 20 mm thick wooden bar was mounted between the side wall and the macro-roughness. Fig. 4.11 in paragraph 4.2.1.d) shows the two type of rib geometries: on the left side, the one for the main tests and on the right side the one for the additional tests.

The tests followed exactly the same procedure like the main tests (§ 4.5), yet without velocity measurements and without sediment sampling at the outlet. The results are presented with the main tests in the different Appendix (usually in section *.4).

5.5 Tests of Peter (1986)

Though the performed tests cover quite a large number of discharges, longitudinal bed slopes and different types of wall roughness, many important parameters were kept constant: the radius and the width of the channel as well as the grain size distribution. To establish a generally applicable scour formula, the acquired data set had to be extended to determine the influence of these parameters. Therefore 32 tests performed by PETER (1986) at the "Versuchsanstalt für Wasserbau, Hydrologie und Glaziologie" (VAW) of the "Eidgenössische Technische Hochschule, Zürich" (ETHZ) were introduced in the database. This allowed an extension of the data set (45 tests) to 77 tests.

The additional tests cover radii to width ratios of 2 and 3.5 compared to 6 in our tests. Peter performed his tests with 5 different sediments from almost uniform grain size to wide sediment mixtures (d_m = $0.45 \div 5.1$ mm, σ = $1.19 \div 3.21$). The Froude numbers ranged from 0.3 to 1.2 (compared to 0.68 to 0.97 in our tests) and the Reynolds numbers from 700 to 4100 (compared to 44'000 to 63'000). Peter performed his tests in a 50 to 80 cm wide channel, with a radius of 1.60 and 1.75 m in a 135° bend (see also § 3.5.2/10) with a rectangular cross-section[1]. The bend was located between a 2.60 m long inlet reach and a 1.50 long outlet reach. The discharges between 2 and 48 l/s were rather small compared to the tests performed in this study. The results of Peters tests are given in Appendix 1.4.

---

1. Peter also performed some tests with a trapezoidal cross-section; but they were not used in the present study.

CHAPTER 6

ANALYSIS OF THE TEST RESULTS

6.1   Introduction

In this section the main tests will be analyzed. The observations and discussions are presented in the following order:

- First the final scour is analyzed (§ 6.2). The bed topography (§ 6.2.1) including the scour depth, the location of the point bars and scour holes, their volumes, the shape of the scour hole and finally the geometrical aspect of the scour hole and of the cross-sections are discussed.
- Then observations regarding the free water surface are presented (§ 6.2.2).
- The next section (§ 6.3) deals with the evolution and formation of the scour.
- Sediment transport related phenomena are documented in section 6.4.
- Afterwards the grain sorting due to a wide grain size distribution and the formation of an armoring layer is presented (§ 6.5).
- Finally the flow field and the velocity distributions are analyzed (§ 6.6).

All the results are summarized and discussed in the last section (§ 6.7).

The following table gives a summary of where the different topics can be found in the report and in the Appendixes.

Topic	Report	Appendixes
Bed topography	§ 6.2.1	A.4, A.7, A.8
Water surface	§ 6.2.2	A.5, A.6, A.7, A.8
Scour process	§ 6.3	A.4, A.7, A.8
Bed load transport	§ 6.4	-
Grain sorting	§ 6.5	A.9, A.10
Velocities	§ 6.6	A.11
Macro-roughness	in all sections	A.4, A.5, A.6, A.7, A.8, A.9, A.10, A.11
Summaries, tables	§ 6.7	A.1

Table 6.1:   Overview of the topics of chapter 6 and Appendixes

6.2 *Analysis of the final scour*

Subsequently, the final bed topography is analyzed. In particular the characteristics of the scour holes and of the point bars are discussed. The influence of the macro-roughness is discussed at the end of each of the following paragraphs.

6.2.1   Analysis of the final bed topography

Parameters related to the bed topography like the scour depth, the location of the scour holes and point bars, the shape of the scour hole and the volume of the scour are studied hereafter.

a) *Depth of the scour holes*

First, the scour depth in the first and second scour was analyzed. The scour depth given in Appendixes 4, 7 and 8 is defined as the distance between free water surface and the final channel bed topography (Fig. 3.6). Some parameters influencing the maximum scour depth are discussed in the present paragraph.

The first characteristic influencing the scour depth is the discharge. With increasing discharge, the erosive power of the flow grows. Figure 6.1 (top) shows this phenomenon. If we have a look at the plot at the bottom, we can make another interesting observation: with increasing discharge, the relative scour depth[1] decreases. A possible explanation is that important discharges induce high mean water depths and that the growth of the absolute scour is less important than Δh_m, which reduces the relative scour. In a formula describing the maximum scour, the discharge frequently enters as a velocity or in dimensionless form as a Froude number or as (average) water depth.

Secondly, the slope of the channel in stream direction influences the scour depth[2]. Despite a poor correlation, Figure 6.2 clearly shows the tendency that the relative scour depth gets bigger with increasing energy slope. This phenomenon is particularly important for the first scour. The second scour hole is probably much more influenced by the flow conditions after the first scour than by the channel slope.

---

1. In this chapter, the ratio h_s/h_m (scour depth to mean water depth) is called relative scour.
2. This parameter is not independent from the discharge but linked by well known laws like the ones of Strickler, Weissbach-Darcy, a.s.o.
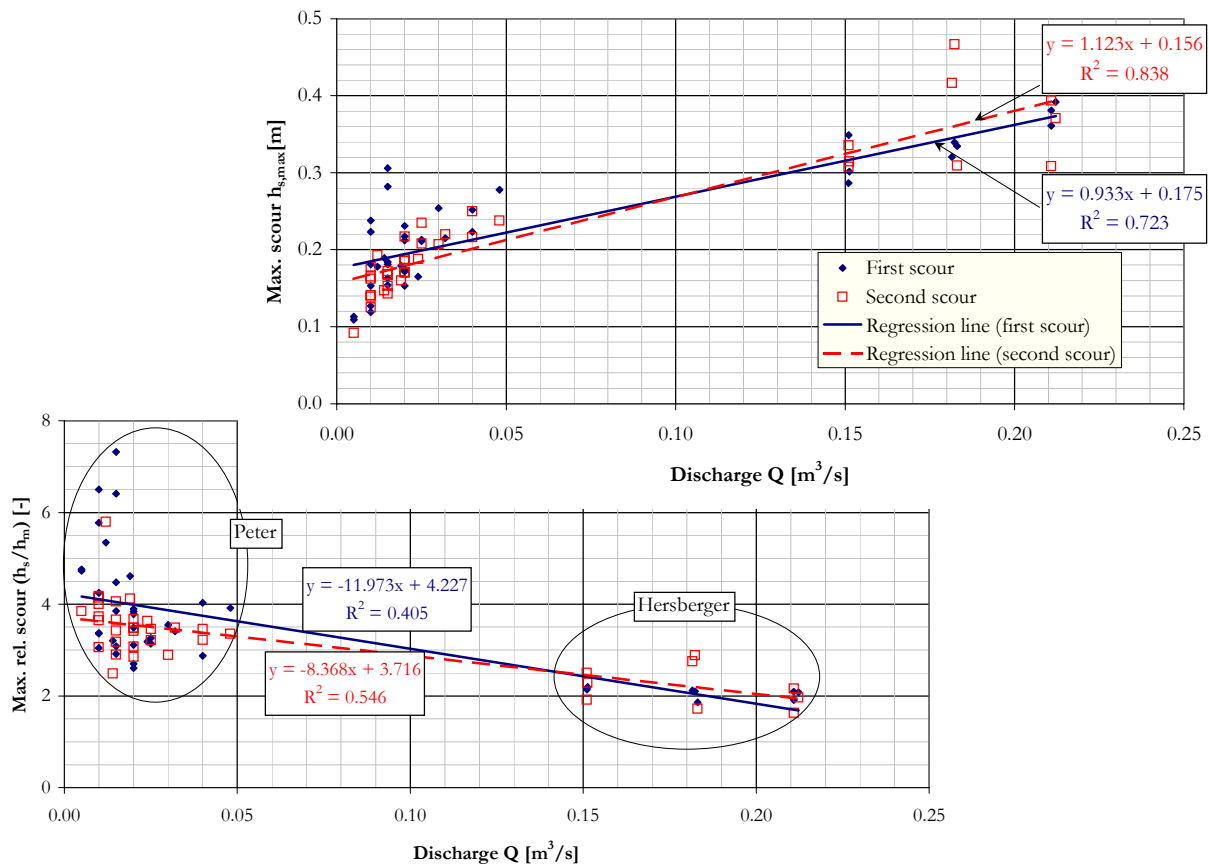
Figure 6.1: *Absolute (on top) and relative scour depth (bottom) as a function of the discharge (without macro-roughness tests, with Peters tests)*
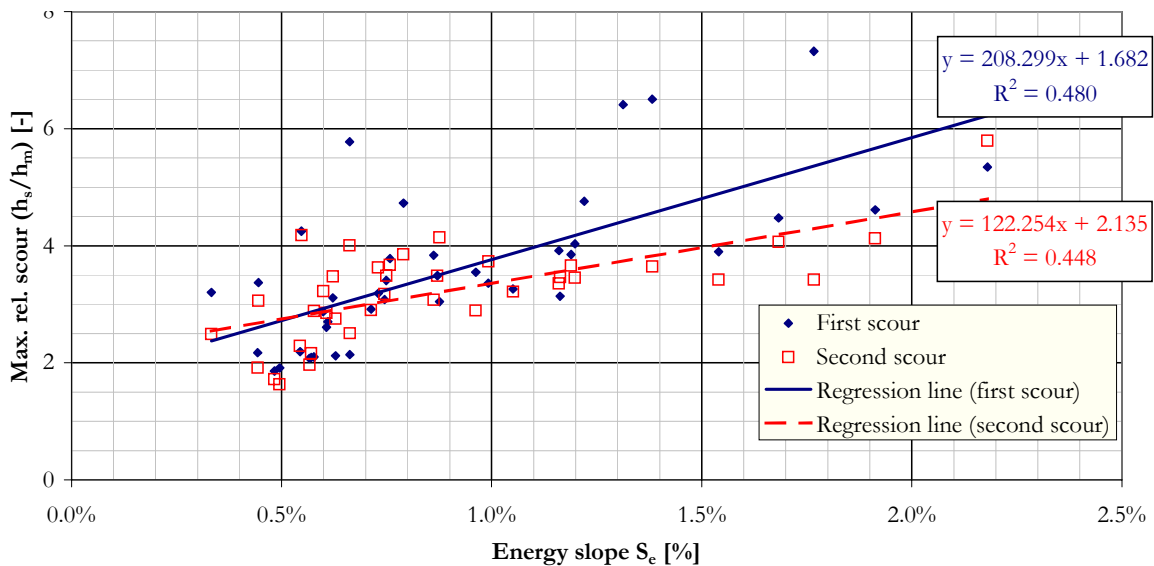
Figure 6.2: *Relative scour depth as a function of the energy slope S_e over the whole channel (without macro-roughness tests, with Peters tests)*
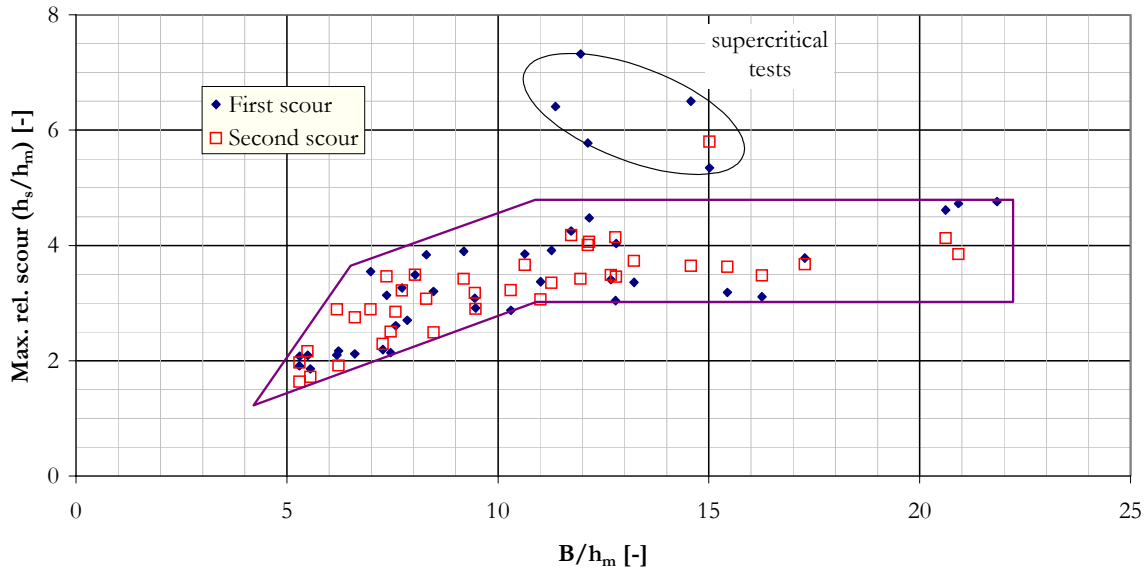
Figure 6.3: *Relative scour depth as a function of the width to depth ratio (without macro-roughness tests, with Peters tests)*

Furthermore, the channel geometry influences the scour. With increasing radius of curvature to width ratio (R_c/B), the relative scour reduces. If the width to flow depth ratio $(B/h_m$, Figure 6.3) is increased, the relative scour also increases. But this tendency does not seem to continue without limit; probably the relative scour stabilizes at a value between 3 and 5 if the width to depth ratio becomes greater than about 10. This can be explained in the following way. If we approach the real cross-section (Figure 6.4) with two straight lines, we see that the radial bed slope $\tan\beta$ in the outer half of the cross-section gets close to the maximum possible bed slope of $\tan\phi$. Lets consider a cross-section with $B/h_m = 10$ and compare the maximum scour depth to the mean water depth. If we simplify and assume that h_m is located on the axis of the channel, we can write: $h/h_m \cong (4/6 \cdot B)/(1/6 \cdot B) = 4$. The bed slope in radial direction can now be determined: $\tan\beta \cong h_m/(B/6)$. Knowing that $h_m/B = 1/10$, finally yields

$$\tan\beta \cong 0.6 \cong \tan\phi .$$

This "demonstration" is very approximative and one can reply that the separation point S does not need to be on the axis of the channel. But the cross-sections in Appendix 7, show that S is located somewhere in the central one third of the channel width. If S shifts towards the inner bank, the cross-section profile becomes s-shaped with an almost horizontal bed slope at the outer bank. In this case the maximum scour as well as the mean water depth increase only little. Therefore the ratio h_s/h_m is not submitted to a big influence due to the radial shift.
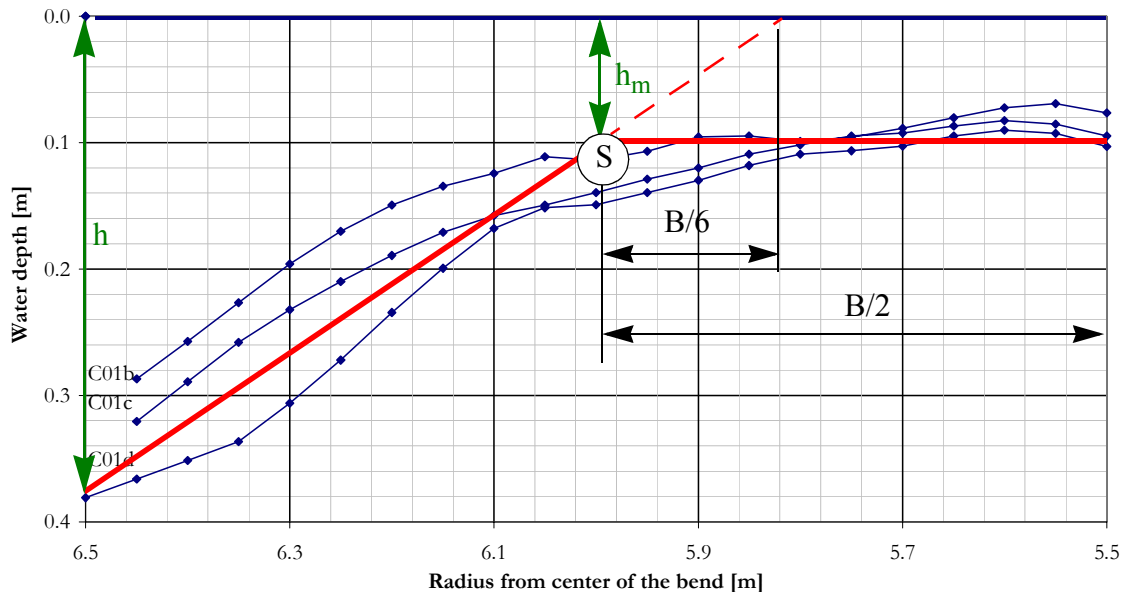
Figure 6.4: *Approximation of the real cross-section profile by a simplified one*

Other parameters having an influence on the scour depth are the grain size and the grain size distribution. These parameters determine the roughness of the bed and the possibility to get an armoring layer. They will be discussed in section 6.5.

Finally, the macro-roughness of the outer bank has a significant influence on the scour depth. If vertical ribs are placed with an appropriate spacing (2° and 4° for the performed tests) on the outer side wall, the following observations can be made:

- The erosion is well distributed over the whole bend and almost no prominent scour holes can be found (Figure 6.8 and Appendix 4).
- The maximum scour depth is significantly reduced, especially for high bed slopes and high discharges (Figure 6.5), where the reduction of the scour depth can reach up to 38%.

But it is important to use an optimum rib-spacing. GAIROLA (1996) (see also § 6.6 c) investigated vertical ribs of different shape in a straight channel. He observed the highest impact on the flow (in terms of head losses) if the ratio of rib-depth to rib-spacing is of about 12. This order of magnitude is confirmed by our tests, but the optimum ratio can also be somewhat bigger $(e_s/e_d = 10 \div 20)$, depending on the tangential bed slope and on the curvature.
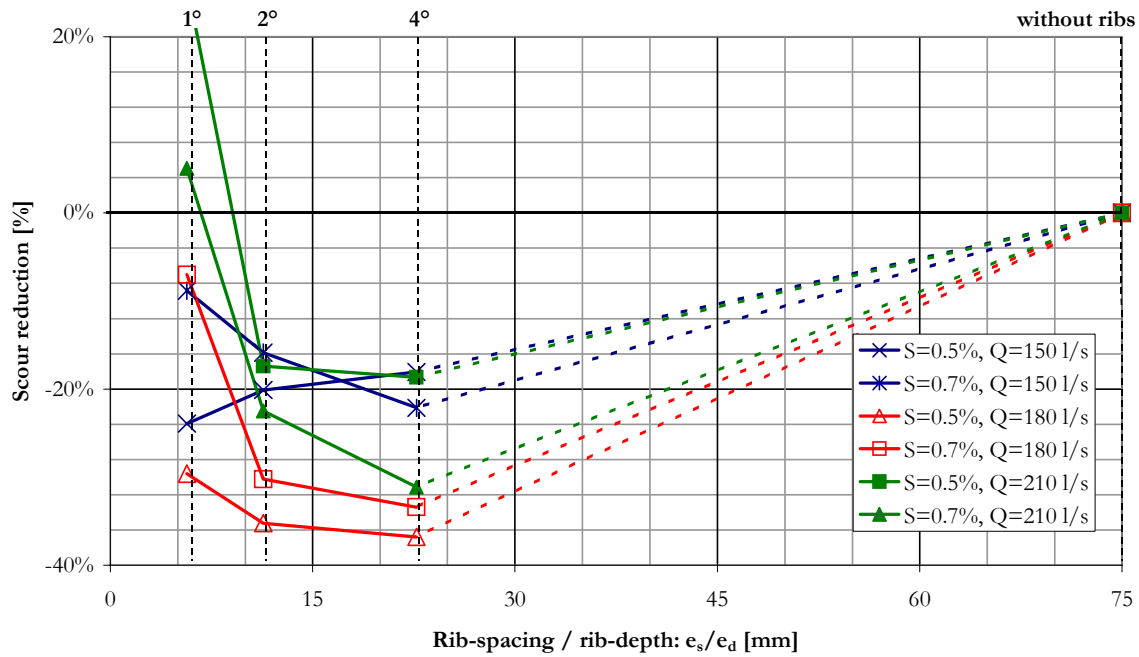
Figure 6.5:   Reduction of the scour depth due to macro-roughness (e_d = 20 mm)

b)   Location of the scour holes

As already observed by other authors (e.g. GARBRECHT, 1953, PETER, 1986), two scour holes occurred systematically in the bend. The deepest point of the upstream hole was located at the beginning of the bend (Table 6.2) at about 30° (no ribs) and at the exit of the bend for the down-stream scour. For higher slopes and increasing discharges, the scour moved slightly downstream.

For the estimation of the location of the scour holes, PETER (1986) proposed the following for-mulae based on the standard deviation σ of the grain size distribution of the substrate:

$$\text{upstream scour: } \alpha_1 \ = \ 26.3 \cdot \sqrt{\sigma} + 11 \, ; \quad \text{downstream scour: } \alpha_2 \ = \ 104 + 5.66 \cdot \sigma \qquad (6.1)$$

For the used sediment mixture (σ = 1.82), the first hole should develop at 46°, the second at 114°, which is too far downstream compared to the observed scour holes. It needs to be mentioned that both equations (6.1) have a rather poor correlation (less than $r^2 \ = \ 0.5$).

Maximum scour location	no mr	$e_s \ = \ 8\,°$	$e_s \ = \ 4\,°$	$e_s \ = \ 2\,°$	$e_s \ = \ 1\,°$
1st scour - erosion start 1st scour - max. depth 1st scour - min. thalweg	10° 30° 50...60°	10...20° 45...50° 60...70°	10° 45...55° 70...80° *	10° 50...60° 70...80°	10° 60...70° 80°
2nd scour - erosion start 2nd scour - max. depth 2nd scour - min. thalweg	70° 90°...1 m 2...(3) m	70° 90° 2 m	70...80° 90°...1 m 2...3 m	70...80° 90°...1 m 2...3 m	90° ** 1...2 m 3...4 m

Table 6.2:   Overview of the observed scour positions
*   Often the thalweg does is not reduced between the two scour holes*
*   ** The second scour is very small*

Analyzing the thalweg over the whole channel (Table 6.2, Figure 6.6 and Appendix 8) it can be observed that without macro-roughness, the erosion of the bed (thalweg) starts at about 10°, reaches its maximum in the first scour hole at approximately 30°[1] and reduces again up to a position between 50° and 60°.

From 70° downwards, the erosion gets deeper again to reach its maximum (second scour) between the end of the bend (90°) and 1 m after the bend. Towards the end of the channel the thalweg comes up again (at about 2 m, sometimes 3 m after the bend). Between the two maximum scour locations, the thalweg remains clearly below the initial bed level.
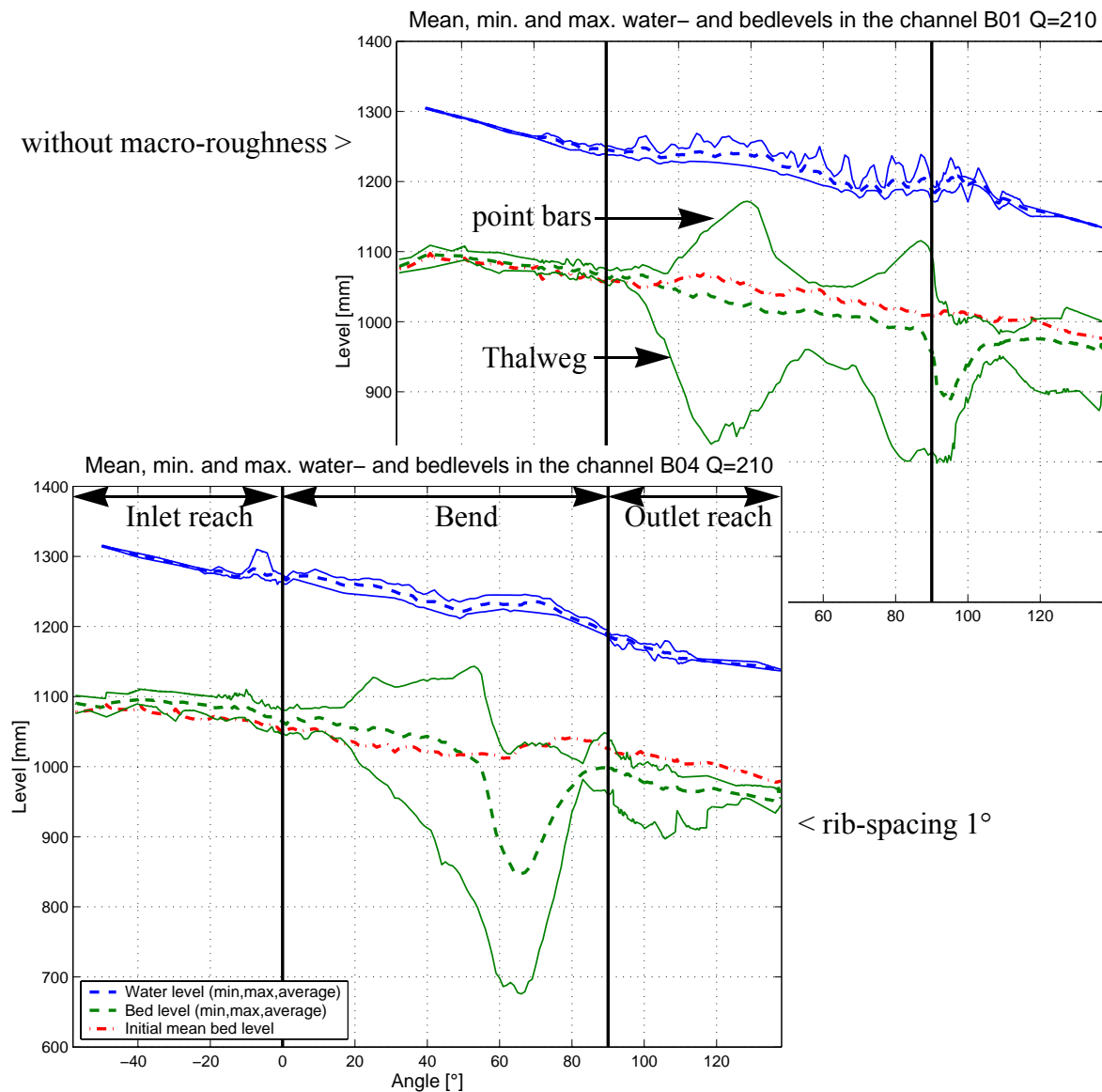
Figure 6.6:   Longitudinal plot over the whole channel; average / min. / max. bed and water levels for S_0=0.50%, Q=210 l/s, without ribs (on top) and with a rib spacing of 1° (bottom)

Adding vertical ribs along the outer side wall (Table 6.2, Appendix 8), the erosion still starts at 10°, but the location of the maximum scour shifts more and more in the downstream direction with an

---

1. Sometimes the maximum scour is extended over the following 20° (between 30 and 50°).

increasing rib density: at 8° the maximum (first) scour is located between 45° and 50°, for 4° between 45 and 55°, for 2° between 50 and 60° and for 1° in general at 60° (sometimes up to 70°). For a rib spacing of 4°, the two scour holes frequently merge to form one continuous hole. If the two scours remain distinct (also for the other rib spacings), the highest point of the thalweg between the two scour holes is located between 70 and 80°. The second scour remains in general at the same position between 90° and 1 m after the bend.

At the highest rib density of 1° (Figure 6.6, Appendix 8) there is only a very small second scour hole in the outlet reach with a maximum depth located between 3 and 4 m after the bend; particularly for high longitudinal bed slopes the second scour does not develop. Furthermore an important lowering of the average bed level in the first scour can be observed.

c) *Location of the point bars*

Let's now consider the evolution of the maximum bed elevation in the channel representing the evolution of the point bars (Figure 6.6, Table 6.3 and Appendix 8). Like for the scour locations, the point bar formation always starts at the same position (at about 20°). Without macro-roughness, the highest point bar elevation is reached at 40° and decreases again towards 60°.

By adding vertical ribs, the maximum elevation is shifted in the downstream direction; but if the rib-spacing becomes too dense, the maximum point bar elevation seems to shift in the upstream direction again (for both, the maximum deposition location and the following highest point of the thalweg).

Maximum point bar	no mr	$e_s = 8°$	$e_s = 4°$	$e_s = 2°$	$e_s = 1°$
1st scour - depos. start	20°	20°	20°	20°	20°
1st scour - max. height	40°	50°	40...60°	50...60°	50°
1st scour - max. thalweg	60°	60°	70...80° *	70...80°	60°
2nd scour - depos. start	70...80°	80°	80° *	80°	
2nd scour - max. height	85°	1m	1m	1m	1m **
2nd scour - max. thalweg	1m	2m	2...3m	3m	

Table 6.3:   *Overview of the observed point bar positions*
         * Diminution of the point bar almost inexistent between the two scour holes.
         ** Almost no second point bar can be observed

The second point bar always starts growing at about the same position, independent from the end of the first point bar (if the two point bars are not completely merged). The same observation is valid for the location of the maximum scour except for the case with a 1° spacing.

d) Volume of the scour and deposition on the point bars

Some interesting observations can be made concerning the volumes of the scour holes and depositions[1] (Figure 6.7):

- The eroded volume shows the tendency to increase with higher discharges (Fig. 6.7, bottom). The influence of the channel slope is not very important (almost constant).
- On one hand the *scour* volume is significantly influenced by the presence of macro-roughness, which can be seen at the wide scatter in vertical direction (Fig. 6.7, bottom).
- On the other hand, the volume of the *depositions* shows less influence due to the presence of macro-roughness at the outer bank. Especially the second point bar has a quasi constant deposited volume. The first point bar shows a slight increase of deposited volume for higher discharges.
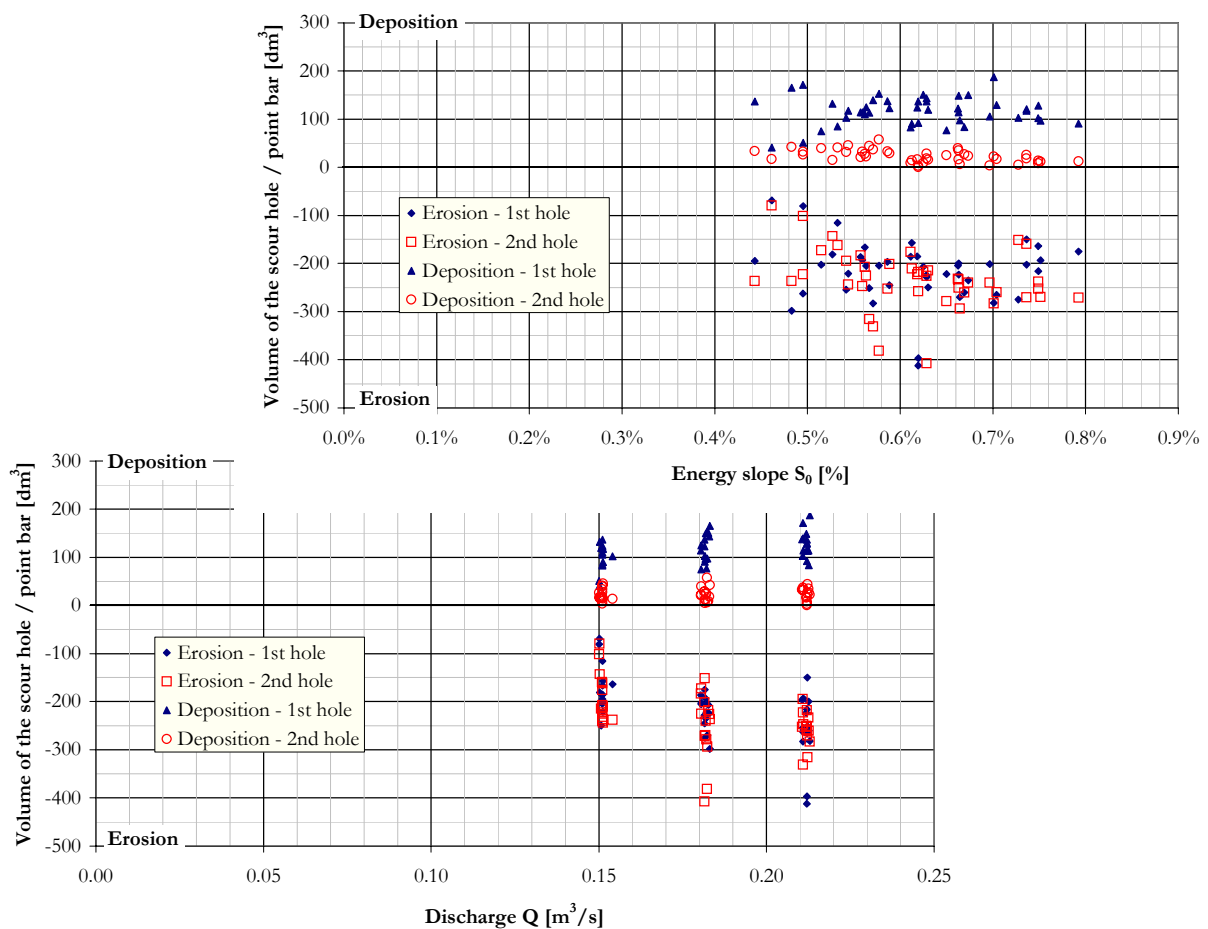
Figure 6.7: *Volume of the scour holes and depositions on the point bars as a function of the discharge (bottom) and the overall energy slope $S_{e,all}$ (top) (including the tests with macro-roughness, without Peters tests)*

---

1. The volumes were measured above / below a regular bed level corresponding a plane with a constant slope over the whole channel fitting the bed surface at the beginning and the end of the channels.

e) *Shape of the scour holes - development of the scour*

Without macro-roughness the two scour holes have a completely different shape (Figure 6.8): the first scour has an elongated elliptic shape with its deepest point at about 10 cm from the outer side wall. This scour hole is located just upstream the maximum elevation of the first point bar.

The second scour looks like a drop, sticking to the outer side wall and "dropping" in downstream direction. Its deepest point is at about the same distance from the side wall, located downstream the highest point of the second point bar.
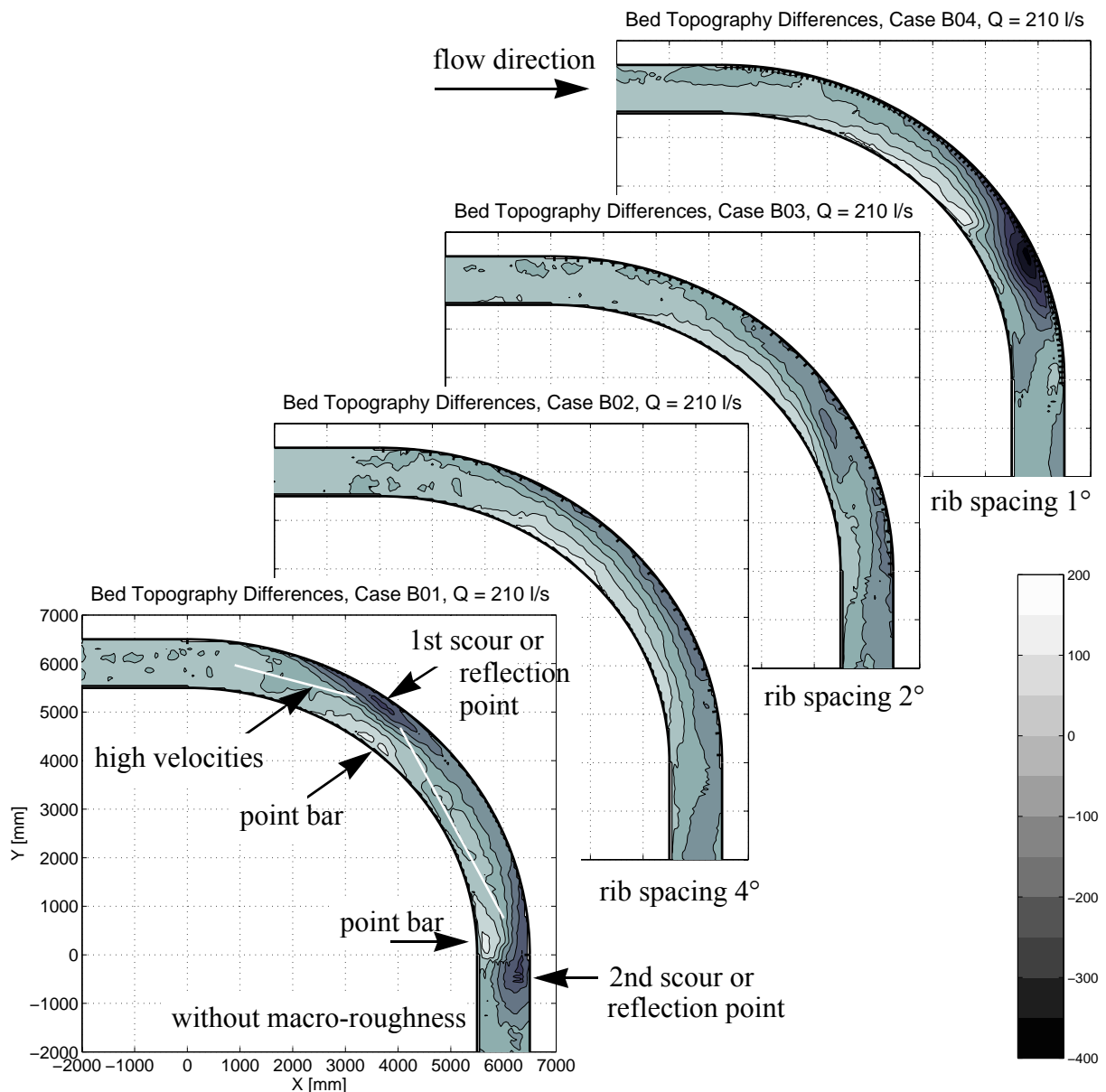
Figure 6.8: Shape of the scour holes and point bars with and without macro-roughness ($S_0 = 0.50\%$, $Q = 210 \, l/s$)

It is interesting to observe that almost no distinct scour holes can be found for a rib spacing of 4° (about 40 cm). Increasing the rib density (2°) induces the creation of a first scour, which is still quite small. This scour has the interesting property that it is located after the first point bar. This becomes even more evident if additional ribs are placed in the channel (1°). This scour is even

more important than the one without ribs. A possible explanation is that this scour behaves like a combination of the first *and* second scour.

Probably the first scour is essentially due to the flow being reflected on the side wall in the bend (causing the flow to head towards the bottom and increasing the secondary current), and the second one is influenced by the point bar (which is itself influenced by the flow), concentrating the flow at the outer side wall in combination with the main stream. For the highest rib density, the location of the first scour is shifted in the downstream direction due to the roughness of the outer wall, but the point bar forms as usual or is even shifted in the upstream direction (see 6.2.1 c). At the point where the scour now occurs, the two phenomena are superposed and an important amplification of the scour depth.

A last observation concerns the erosion after the bend: the presence of macro-roughness causes some additional erosion in the outlet reach. Since the ribs create head losses in the bend, the water is accumulated upstream the bend and accelerated after the bend to pass the same discharge (steepening of the bed slope). Fortunately, this additional erosion is of limited depth and located towards the center of the channel where it does not endanger bank protection structures. If the curve is immediately followed by a bend in the other direction, bank protection measures may be necessary in the following curve.

f) Shape of the cross-sections - line bend

SCHÖBERL (2002) made an interesting observation in the sinuous channel used by REINDL (1994) (see also § 3.5.2/11). In the scour holes, the cross-section presents a point where the lateral slope abruptly changes. At the inner bank the bed is quite flat and towards the outer bank, an important lateral bed slope can be observed. This abrupt change in the bed slope (see Figure 6.4) will be called in this report as "line bend".

Considering the measured cross-sections (Appendix 7), this line bend can be found, too. But it is mainly observed in the part where the scour develops than at the maximum scour location (Figure 6.9).
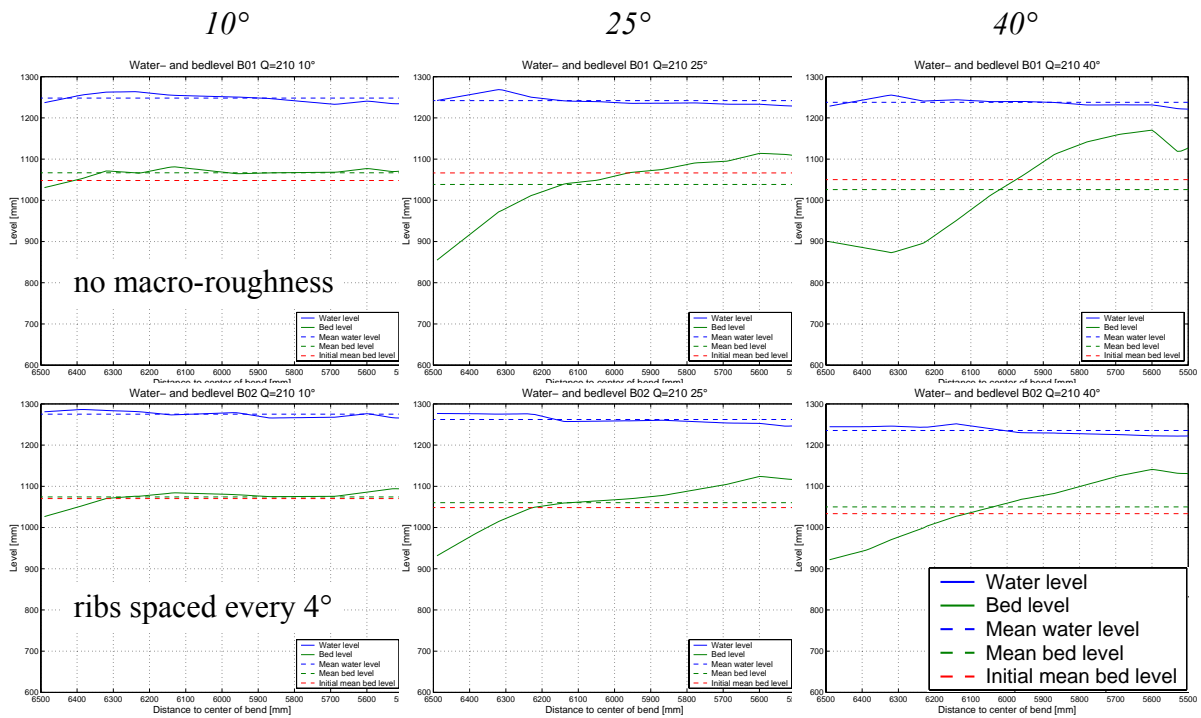
Figure 6.9:   Development of the line bend in the first scour (test B1d on top and B2d at the bottom)

Without macro-roughness, the line bend starts at about 10° at a distance around 20% of the channel width from the outer bank to finally disappear between 50% and 80% from the outer bank. In the maximum scour cross-section, the line bend is attenuated and the profile becomes s-shaped.

The same process can be observed for the second scour. At 55° the bed has flattened again partially (between the two scour holes). Downstream this point (70°), up to the end of the bend, the development of the line bend can be observed a second time.
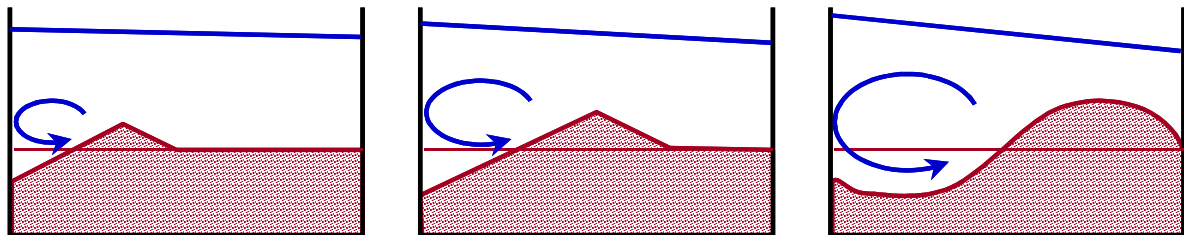
Figure 6.10: Scheme of the development of the line bend

This process can be explained in a schematic way with the development of the secondary current (Figure 6.10). Between 10° and the first maximum scour, the secondary current grows (the inclination of the radial water surface slope also increases slightly which is exaggerated on the schematic view) and leads progressively to a more pronounced scour hole. At the final state, the shape of the scour hole is more s-shaped. This can be explained by the fact that the main secondary current does not "attack" the bed at the outer wall anymore, shifts towards the center, but remaining in the outer half of the channel.

6.2.2   Analysis of the water surface

Without macro-roughness, stationary waves can be observed at the outer side wall (Figure 6.11, Appendix 6 and 8). The amplitude of these surface waves is about 10 cm and their length about 60 cm to 1 m. For the highest channel slope (S_0 = 0.70%), the one or two last waves after the bend showed small surface rollers (Fig. 6.12, left).
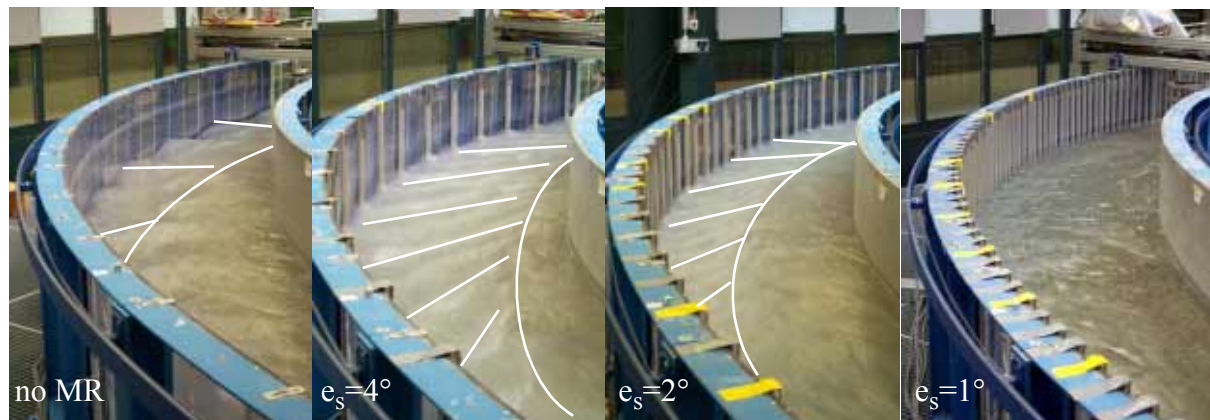
Figure 6.11: Water surface views for tests C1 to C4 at Q = 210 l/s

With vertical ribs, the previously observed stationary waves are replaced by shock waves, resulting from the reflection of the water on the macro-roughness elements. They emerge about 0.5° upstream the ribs (Figure 6.14) and redirect the flow towards the center (with a deviation angle from the channel axis of about 50 to 55° depending on the local Froude number[1]). The waves can be observed over the outer 70% of the channel for a rib spacing of 4° and over the outer half of the channel for 2°-spacing. If even more ribs are added (1°), these shock waves disappear and the ribs no longer work as isolated elements but rather as continuous roughness on the outer wall. The roughness is too important to observe the stationary shock waves that were observed without ribs.

Figure 6.12: Stationary wave at the end of the bend with surface roller (left) and a common one (right). Picture taken across the outer side wall

---

1. The local Froude numbers are of about 1.2 to 1.4, indicating supercritical flow conditions along the outer side wall.

The macro-roughness has the advantage to reduce the oscillations of the free water surface long the outer side wall. The wave amplitude is reduced by 50% from about 10 cm (~50% of h_m) to about 5 cm (~25% of h_m).

At the outer bank, the water surface is normally super elevated by 2 to 4 cm (~10 to 15% of h_m) due to the influence of the curve. With macro-roughness, the superelevation remains the same order of magnitude or gets smaller (Appendix 7 and 8). The superelevation Δh of the free water surface can be calculated as[1]:

$$\Delta h = \frac{B \cdot R_c}{R_i \cdot R_o} \cdot \frac{V_m^2}{2g} \tag{6.2}$$

The measured and the computed water superelevation agree quite well.

Since the ribs introduce a head loss in the bend, the water depth upstream the bend increases. For the performed tests the water depth increased by 10 to 20% depending essentially on the discharge (Appendix 7 and 8). In the bend, the mean water level remains about 10% higher than without ribs.

Combining the different effects of the presence of macro-roughness - the reduction of the oscillations, the increased mean water level and the superelevation due to the curve - the highest water levels in the bend remain about the same as without ribs.

Another interesting phenomenon is the flow separation that can be observed when the depositions are quite important (Figure 6.13). This separation is visible both at the first and the second scour location.

Furthermore the flow at the water surface carries any floating object towards the center of the channel. This is valid for all tested configurations. An object placed anywhere in the cross-section upstream the bend, leaves the bend more or less in the center. The phenomenon remains the same with and without macro-roughness. It can be explained with the velocity field concentrating at the beginning of the bend in the center (attracting objects near the inner wall towards the center). Farther downstream, the stationary waves or shock waves deflect floating objects towards the center.

---

1. This formula applies for the case without macro-roughness. But, since the superelevation of the free water surface in radial direction remains about the same with ribs, the same equation can be used.
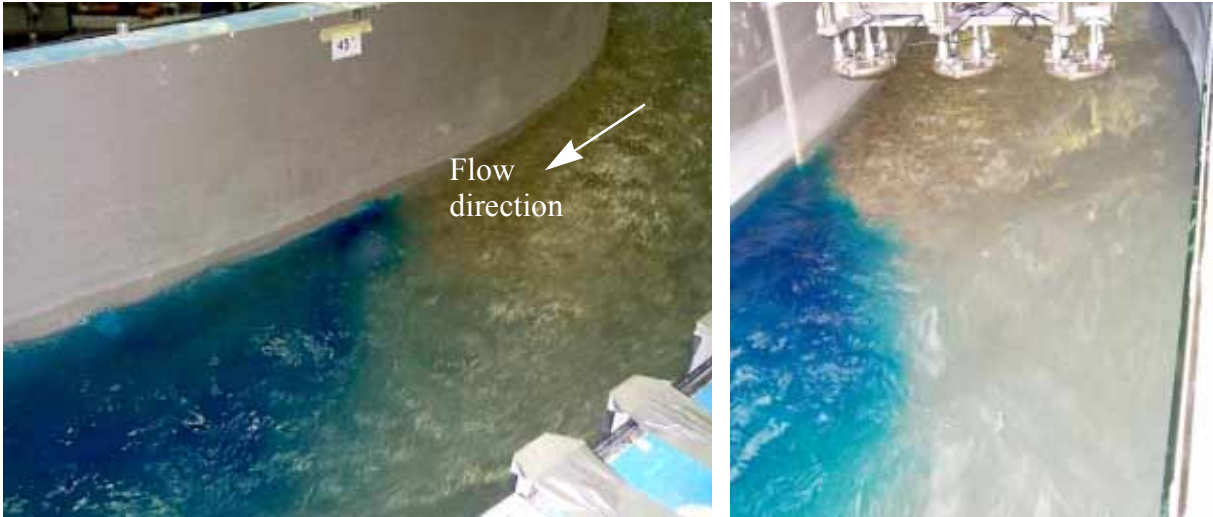
Figure 6.13: Flow separation behind the point bars (LEFT: at 45°, test C4d, RIGHT: at 90°, test C1d)

Figure 6.14: Vertical view on the water surface waves; ribs-spacing 4°, test C2c

6.3 *Analysis of the evolution of the scour*

As mentioned in the discussion of the preliminary tests (§ 5.2.1 2) a), the erosion first starts almost at the end of the bend at a discharge of about 120 l/s (for a bed slope of 0.5%); then it moves quickly in the upstream direction with increasing discharge to stabilize or rather oscillate around its final position at about 30° to 35°.

Considering the evolution of the scour on the outer side wall without ribs (Figure 6.15), it can be seen that the first scour hole armors quickly and gets stable. But the second one needs much more time. The scour deepens and is filled again, until the scour finally stabilizes at the end of the test. This is probably the moment when the armoring layer is well formed in the second scour, too. The phenomenon is the same, independent from the discharge.

Analyzing the same cases but with macro-roughness (Figure 6.16) reveals that the first scour takes some more time to be formed, but without oscillations. The second scour shows some oscillations, but with a significantly reduced amplitude (reduction of about 50%).

The study of these plots (Figures 6.15 and 6.16) rises a question: Is the final scour the maximum scour ? In order to answer this question, we have to remind ourselves that the maximum scour is in general not located directly at the outer side wall but at about 10 to 20 cm from the wall. Some sediments remain just next to the outer bank. The height of these sediments was frequently twice the maximum grain size diameter d_{max}. During the development of the scour, this depositions became sometimes like a steep outer bank that collapsed from time to time. This can in part explain the oscillations along the outer side wall. The amplitude of the oscillations in the second scour is up to 3 times d_{max} (or 50% of h_m) for the tests without macro-roughness and up to 1 times d_{max} (or 15% of h_m) with ribs. With vertical ribs the oscillations can only be observed for the lowest discharge (Q = 150 l/s). At higher discharges, the oscillations seem to disappear.

Turning back to our question, we see that the given final scour depth may be about one maximum grain size diameters too small for the measurements without macro-roughness, but this is a part of the uncertainty: if only one big sediment grain moves, the scour will locally increase by this order of magnitude. For the tests with macro-roughness, it can be assumed that the final scour depth corresponds to the maximum scour, since the deepest scour is not found at the outer bank, and since the oscillations (for the smallest discharge only!) are less that the maximum grain size diameter; for higher discharges they were too small to be measured (if there were any).

The other rib-spacings (4° and 1°) that are not given on Figures 6.15 and 6.16 behave like the mentioned case (2°) with macro-roughness.

In conclusion, it is evident that the macro-roughness contributes to a smoother development of the scour holes, reducing considerably (for small discharges) and even suppressing (for higher discharges) the oscillations of the scour depth, especially in the second scour hole, where the phenomenon is more pronounced.
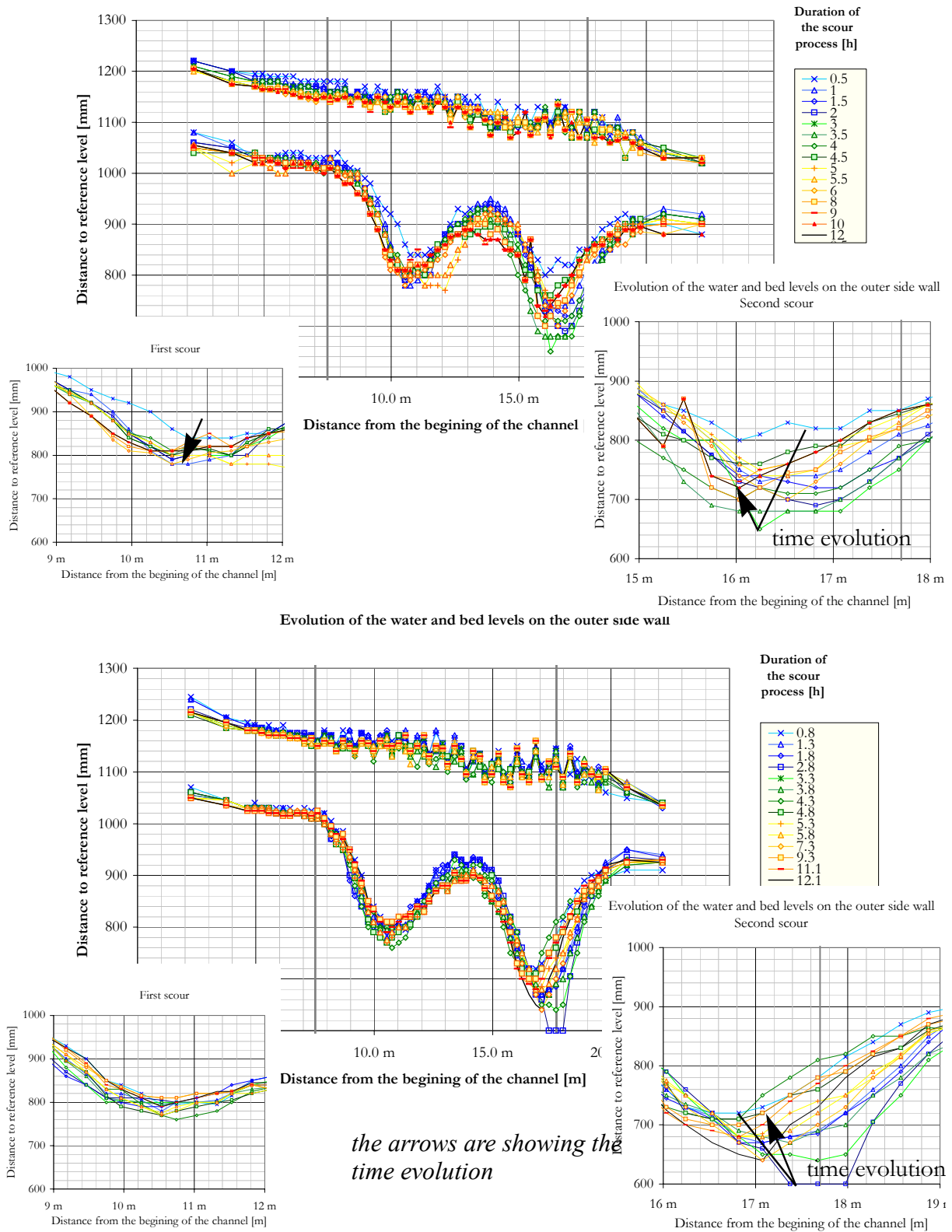
Figure 6.15: Evolution of the water and bed levels along the outer side wall for tests without macro-roughness - $S_0 = 0.70\%$, $Q = 150$ (on top) and 180 l/s (bottom)
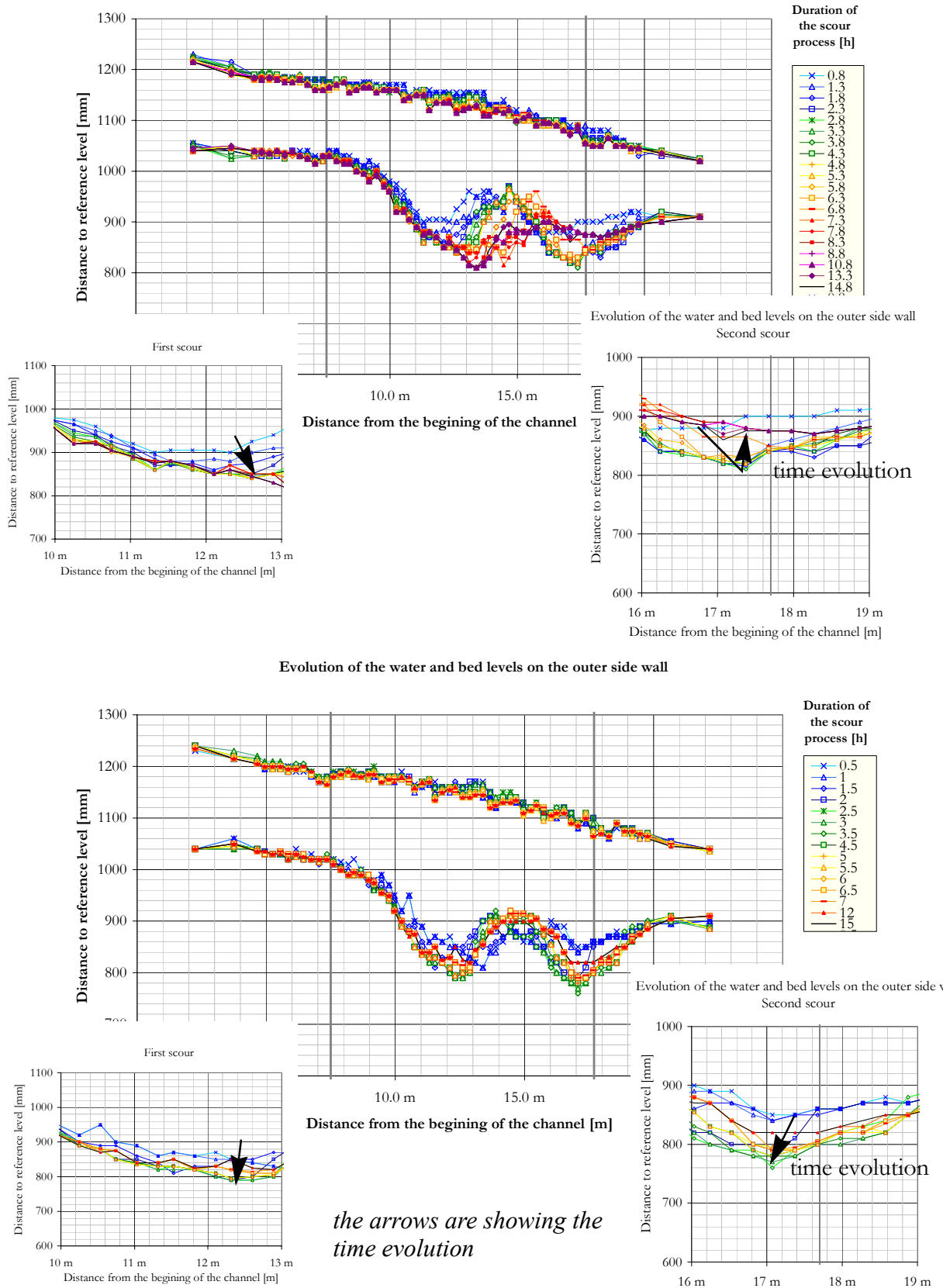
Figure 6.16: Evolution of the water and bed levels along the outer side wall for tests with macro-roughness, spaced every 2° - S_0 = 0.70%, Q = 150 (on top) and 180 l/s (bottom)

6.4   Analysis of the sediment transport

Lets consider the evolution of the sediment transport rates measured at the outlet of the channel during the test (Figure 6.17). The plots for the lowest discharge (on top), show that the sediment transport rate at the outlet decreases approximately with an exponential function[1]. Without ribs, the transport rate stabilizes around an average value after 6 to 8 hours. With ribs, the transport rate stabilizes faster, but on a lower mean value. This indicates, that the transport capacity is significantly reduced by the presence of the macro-roughness (to 35 to 50% for high discharges).
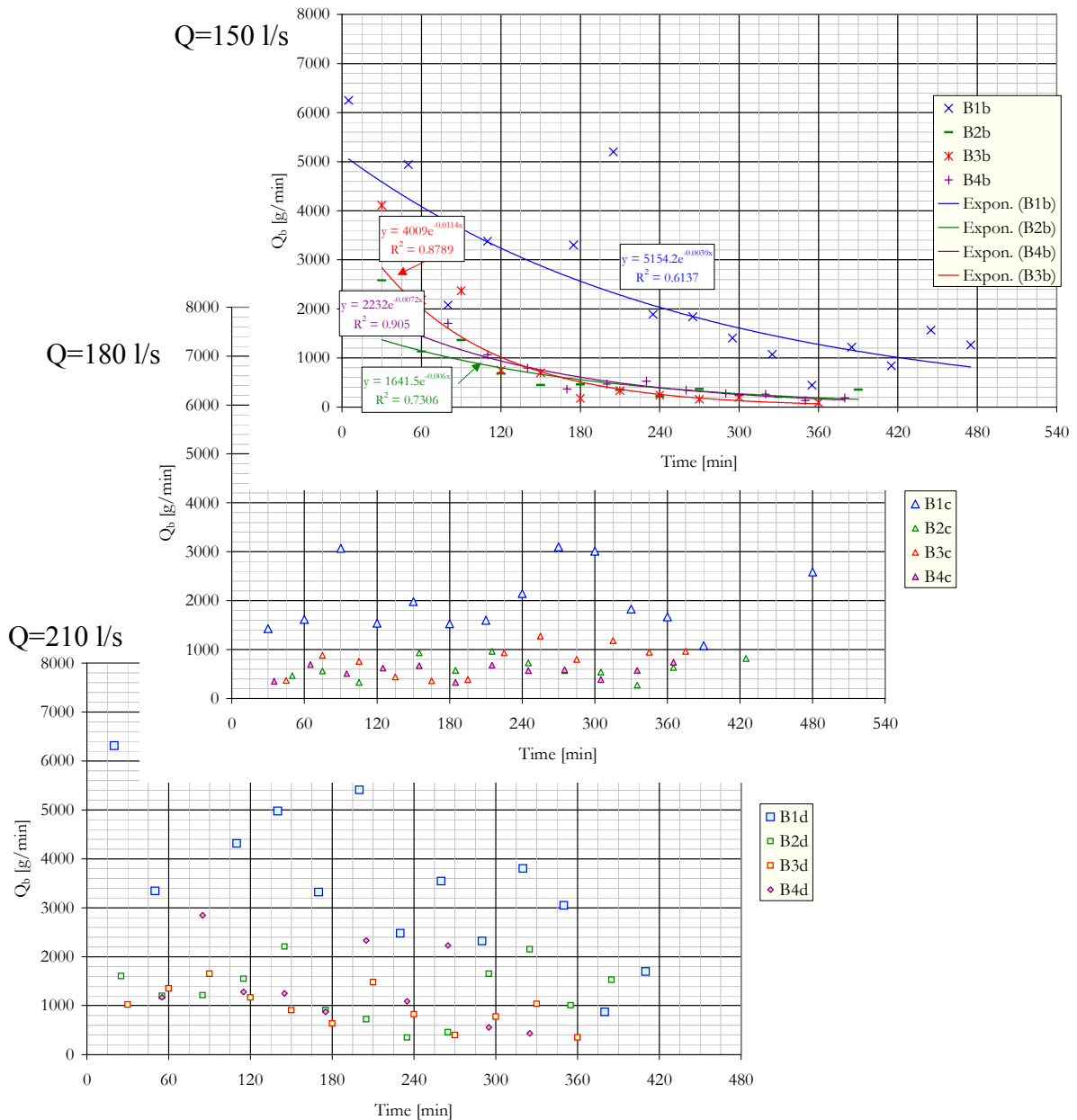
Figure 6.17: Evolution of the sediment transport rate Q_b at $S_0 = 0.5\%$, for 3 measured discharges, without macro-roughness (B1), and with ribs spaced every 4, 2 and 1° (B2 to B4).

---

1. This was at least the best fit obtained with a commonly used function.

The higher discharges (Figure 6.17 center and bottom) show an almost constant transport rate (a slightly decreasing tendency can be figured out for the case without macro-roughness). This is mainly due to the circumstance that the tests were performed as a series with increasing discharge. The bed was only levelled after the first test (Q = 150 l/s). The next tests continued with the bed topography of the previous test. Since the discharges were high enough to provoke bed changes this was no problem, but as far as the sediment transport is concerned, the bed was already armored; therefore the sediments introduced at the inlet were transported over the armoring layer to the outlet.

In the presence of macro-roughness, a natural river, subject to a constant sediment transport rate will compensate the reduced transport capacity in the bend by steepening the slope in the bend: Upstream the bend, the water depth increases locally. Therefore the transport capacity is reduced and sediments accumulate in the inlet reach. The overall channel slope increases, till it is sufficient to pass the bedload across the bend. The increased slope leads to higher velocities in the exit reach, inducing some additional erosion after the curve.

This phenomenon was observed during the preliminary tests, for which the sediment transport rate was kept constant (Figure 6.18 and Appendix 3.3.3). For a discharge of 170 l/s respectively 210 l/s the overall bed slope increased by about 40%, respectively 50% from the initial value (0.50%).

Comparison of the bed levels with and without macro-roughness - Q = 212.5 l/s
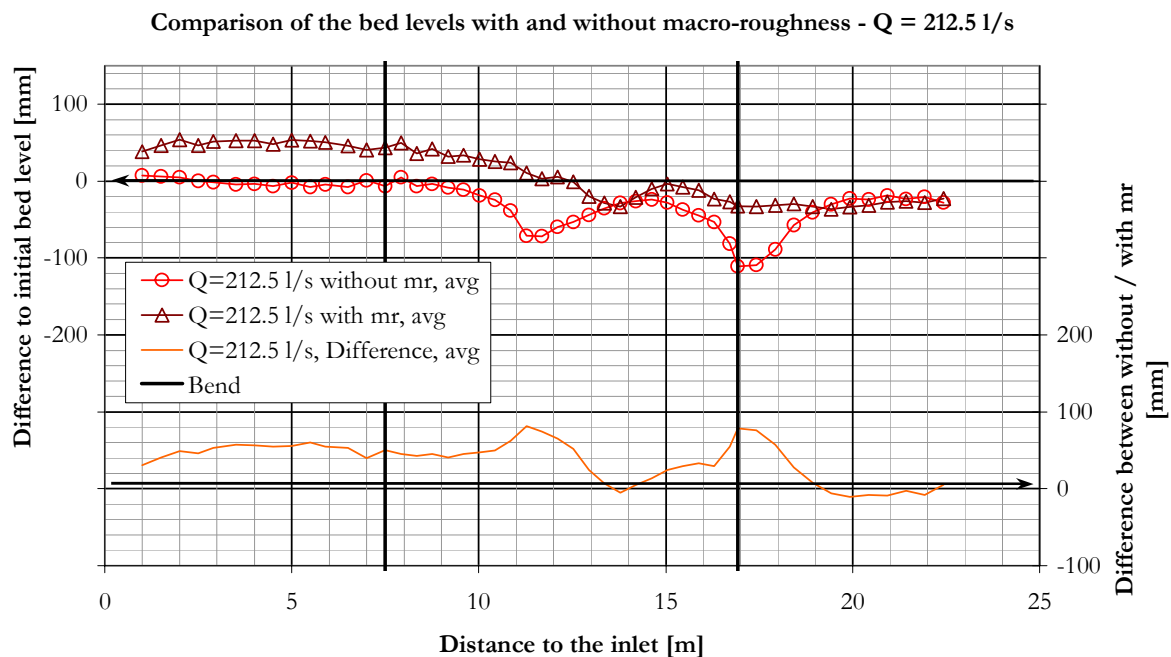
Figure 6.18: Changes of the average bed level for the preliminary tests (with and without ribs) at a constant sediment transport rate

6.5   Analysis of the grain sorting of the armoring layer

As described in paragraph 4.4.6 e), sediment samples were taken at the end of each test at the two scour locations. The grain size distributions of the armoring layer after the tests are given in Appendix 9 (see also Table 6.5). It can easily be seen on Figure 6.20 that by using a wide grain size distribution, as observed in natural rivers, a significant transversal grain sorting process occurs. The coarse grains are left or deposited along the outer wall in the scour hole, whereas the fine sediments are moved towards the inner side forming a point bar. An armoring layer is formed by the coarse grains in the scour holes, which limits their maximum depth (see also SCHLEISS & HERSBERGER, 2001).

Computing the grain size distribution of the armoring layer based on the initial grain size distribution (GESSLER, 1965, 1970, 1990), the following result is obtained (Figure 6.19). It can be seen that the predicted order of magnitude fits quite well with the armoring of the second scour. The conditions in the first scour do not seem to be exactly the same, leading to a more uniform armoring layer. This method allows to get an estimation of the order of magnitude of the mean diameter, but the shape of the grain size distribution of the armoring layer in a bend is not easily predicted. The mean diameter of the predicted armoring layer is of 11.5 mm, which is too fine compared to the measured one (15.6 and 15.8 for the upstream scour and 17.3 for the downstream scour).

Grain size distribution of the armoring layer
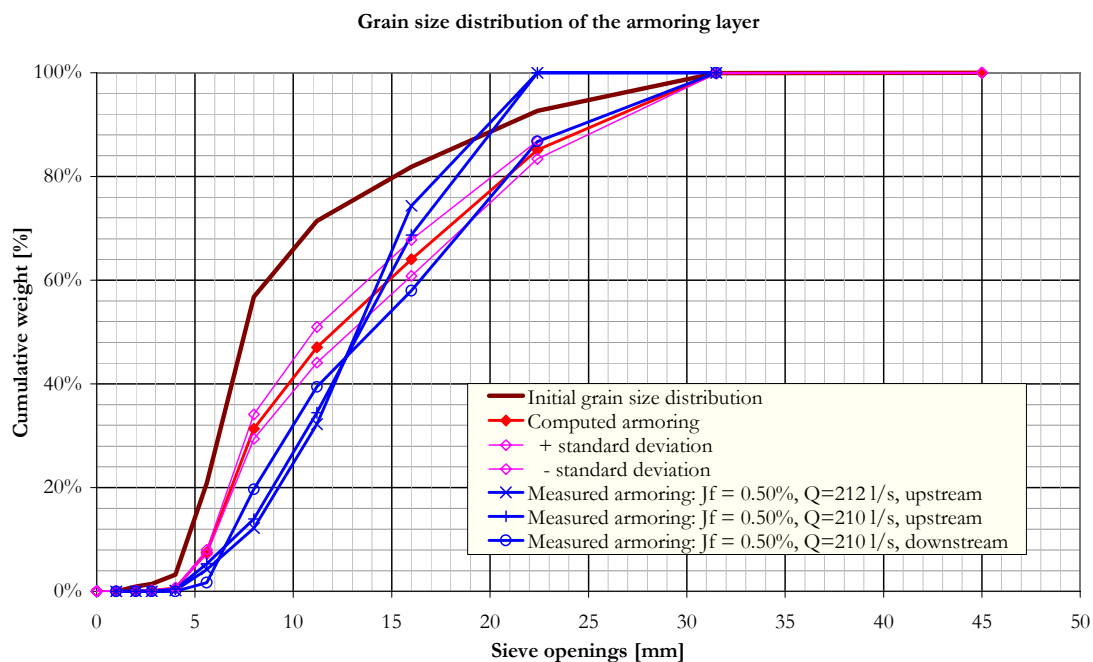
Figure 6.19: Comparison of predicted and computed armoring layer (computed with Gessler, 1965, 1670, 1990)

The width of the grain size distribution σ of the final armoring layer is reduced and we find an almost uniform grain size on the point bar and in the scour hole (see Appendix 9 for the plots). The grain sorting process is somewhat more significant in the region of the first, upstream scour hole, which leads to coarser sediment at the outer bank and finer grains on the depositions (Figure 6.20).
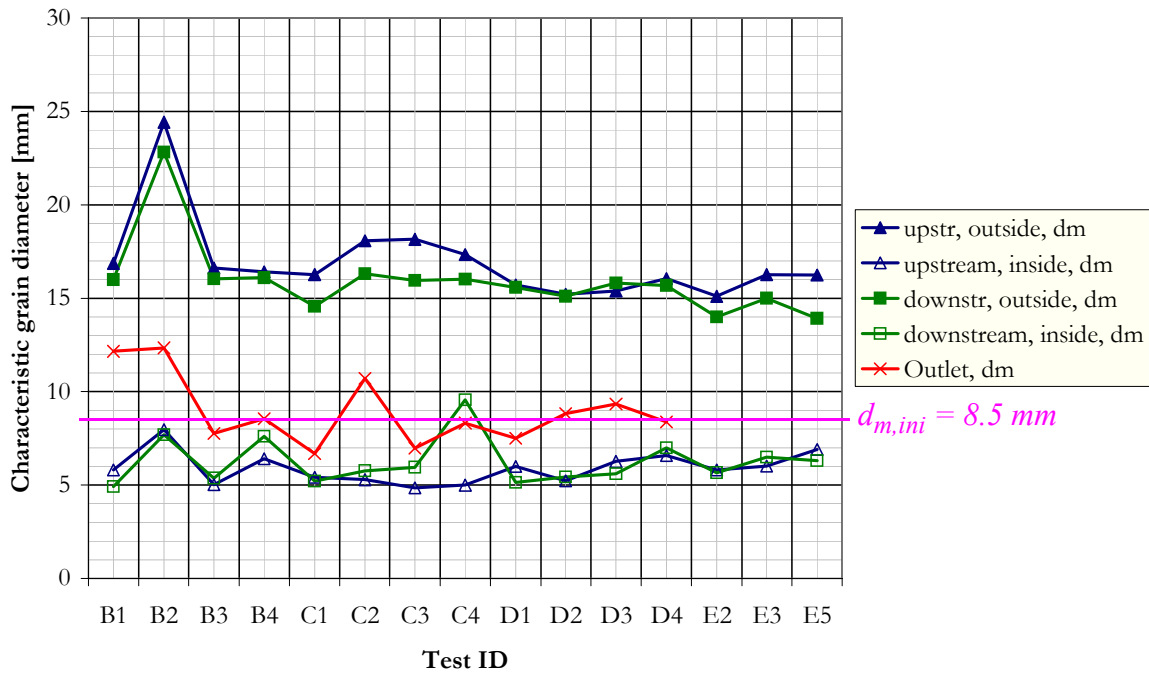
Figure 6.20: Characteristic average grain size diameter for the different test series (average over the 3 discharges)

The presence of macro-roughness does not seem to influence the grain sorting process in a significant way. The finally obtained grain size distributions are of the same order of magnitude as without ribs. A strange phenomenon occurs during test B2. The sediments in both scour holes are much coarser than the ones during all other tests. Since the samples taken at the outlet were also somewhat coarser than the other ones (Figure 6.20), this could be due to an irregularity in the sediment feeding with a too coarse mean diameter.

Once scouring has started, the transversal sorting of grains in the bend is almost independent of the discharge and the initial longitudinal bed slope (Table 6.5). Analyzing all the tests, the following approximate relationship of the sorted mean grain sizes at different locations and the mean grain size of the initial mixture (bed material) d_m can be given (see also SCHLEISS & HERSBERGER, 2001):

	outside (scour)	inside (point bars)
upstream	$d_{ma,\,1o} = 1.93 \cdot d_m$	$d_{ma,\,1i} = 0.68 \cdot d_m$
downstream	$d_{ma,\,2o} = 1.80 \cdot d_m$	$d_{ma,\,2i} = 0.74 \cdot d_m$

Table 6.4:   Formula for the determination of the grain size in the scour holes and on the point bars

Since all tests were performed with the same initial sediment mixture, the influence of the with of the grain size distribution is not found in Table 6.4.

With a somewhat wider grain size distribution ($\sigma = 3.21$), Peter (1986) observed for the deepest scour similar relationships ($d_{ma,\,12,\,o} \approx 2 \cdot d_m$ and $d_{ma,\,12,\,i} \approx 0.8\ldots1 \cdot d_m$).

d in [mm]	UPSTREAM OUTSIDE		UPSTREAM INSIDE		DOWNSTREAM OUTSIDE		DOWNSTREAM INSIDE		SAMPLE TAKEN AT OUTLET	
ID	d_m	d_{90}	d_m	d_{90}	d_m	d_{90}	d_m	d_{90}	d_m	d_{90}
B1b	16.3	20.4	5.0	5.5	14.5	19.0	5.0	5.5	9.1	14.8
B1c	18.5	21.2	5.4	6.3	16.1	20.7	4.9	5.4		
B1d	15.8	20.4	7.0	7.8	17.3	24.6	4.8	5.4	15.2	21.5
B2b	23.4	29.1	9.9	12.9	20.9	27.6	8.5	10.6	12.1	18.8
B2c	24.9	29.2	6.7	7.6	23.4	28.2	8.0	9.7	10.9	15.9
B2d	25.0	29.2	7.3	7.9	24.1	28.7	6.6	7.6	14.0	21.3
B3b	15.2	20.0	5.7	6.6	15.9	20.4	5.7	7.2	7.9	11.6
B3c	17.0	20.5	4.8	5.3	16.3	20.3	5.4	6.2	7.6	11.1
B3d	17.7	20.9	4.6	5.3	16.0	19.8	5.0	5.5	7.8	12.1
B4b	15.6	19.8	7.0	9.3	16.1	20.5	8.4	13.7	8.0	13.2
B4c	17.9	20.9	4.9	5.4	15.9	20.5	6.2	7.6	9.4	13.8
B4d	15.7	19.9	7.4	12.1	16.2	20.3	8.2	13.9	8.3	12.9
C1b	15.9	20.1	5.4	6.4	15.3	19.7	5.1	5.5	7.5	11.4
C1c	16.2	20.3	5.4	6.2	14.8	19.6	5.8	6.9		
C1d	16.7	20.0	5.4	5.8	13.6	18.6	4.7	5.3	5.9	7.6
C2b	18.2	20.9	4.8	5.4	16.1	20.2	6.5	9.4	7.4	10.1
C2c	17.9	20.8	5.4	6.1	16.1	19.5	5.9	7.2	8.0	10.9
C2d	18.2	20.9	5.6	6.6	16.7	20.3	4.9	5.4	16.7	20.3
C3b	17.5	20.7	4.6	5.2	15.0	19.3	7.0	10.3	6.8	9.8
C3c	18.7	21.1	4.6	5.3	16.2	20.2	5.2	6.4	6.5	9.5
C3d	18.2	20.9	5.4	5.9	16.6	20.2	5.6	6.5	7.6	11.2
C4b	17.1	20.8	4.9	5.4	16.4	20.3	11.2	17.2	7.9	12.5
C4c	17.7	20.8	5.3	6.1	16.3	20.2	8.7	15.1	7.5	11.7
C4d	17.2	20.7	4.9	5.4	15.3	19.5	8.9	16.1	9.6	14.3
D1b	14.8	20.0	6.7	8.5	14.9	19.6	5.4	6.6	6.9	10.0
D1c	15.5	19.0	5.1	5.5	15.6	19.5	5.2	5.6	7.3	10.9
D1d	16.8	20.6	6.1	7.5	16.2	19.9	4.8	5.4	8.4	14.1
D2b	13.3	19.1	5.5	6.6	14.3	18.9	6.0	7.5	8.1	12.7
D2c	16.4	20.2	5.2	5.7	15.4	19.3	5.3	6.1	10.4	15.2
D2d	16.0	20.0	5.0	5.4	15.5	19.5	4.9	5.4	8.0	11.9
D3b	13.1	17.6	9.6	13.7	15.6	20.0	6.1	7.7	8.2	13.8
D3c	16.1	20.0	4.5	5.1	16.1	19.9	5.5	6.5	10.7	15.1
D3d	17.0	20.4	4.8	5.3	15.8	19.6	5.2	5.6	9.1	13.9
D4b	13.8	17.8	9.0	13.7	15.5	19.9	8.2	12.8	7.6	11.6
D4c	16.7	20.3	6.1	7.3	16.0	20.2	6.9	9.0	9.1	14.4
D4d	17.7	20.8	4.7	5.3	15.6	19.3	6.0	7.2	-	-

Table 6.5: d_m and d_{90} for the sediment samples of the armoring layer after the tests and at the outlet

d in [mm]	UPSTREAM OUTSIDE		UPSTREAM INSIDE		DOWNSTREAM OUTSIDE		DOWNSTREAM INSIDE		SAMPLE TAKEN AT OUTLET	
ID	d_m	d_{90}	d_m	d_{90}	d_m	d_{90}	d_m	d_{90}	d_m	d_{90}
E2b	13.1	19.2	6.7	9.3	12.6	16.0	5.3	6.1	-	-
E2c	16.4	20.4	5.7	6.9	14.4	18.5	7.9	12.7	-	-
E2d	15.8	19.5	5.1	5.5	15.0	19.4	3.8	4.2	-	-
E3b	15.9	20.0	6.3	7.6	14.3	19.3	5.9	7.6	-	-
E3c	15.9	19.8	6.1	7.7	15.7	19.9	5.8	6.9	-	-
E3d	16.9	20.5	5.7	7.3	15.0	18.6	7.7	10.4	-	-
E5b	16.6	20.8	8.9	10.9	11.8	17.0	7.6	10.3	-	-
E5c	16.3	20.3	6.0	7.2	14.3	18.7	5.6	6.7	-	-
E5d	15.8	19.7	5.8	7.0	15.7	20.1	5.7	6.5	-	-

Table 6.5: d_m *and* d_{90} *for the sediment samples of the armoring layer after the tests and at the outlet*

Another interesting observation concerns the part of the channel being subject to the armoring (Figure 6.21 and Appendix 10). Without macro-roughness, the armoring is limited to the outer quarter of the channel cross-section. Adding vertical ribs, this zone is extended to 50% of the cross-section. It is interesting that the tests without ribs and the one with the smallest rib spacing (1°) behave the same way; the ones with a more optimal spacing of 2 and 4°, too. This phenomenon can be explained by a flatter bed slope in radial direction and especially an almost horizontal bed towards the outer side wall, facilitating the deposition of the coarse sediments.
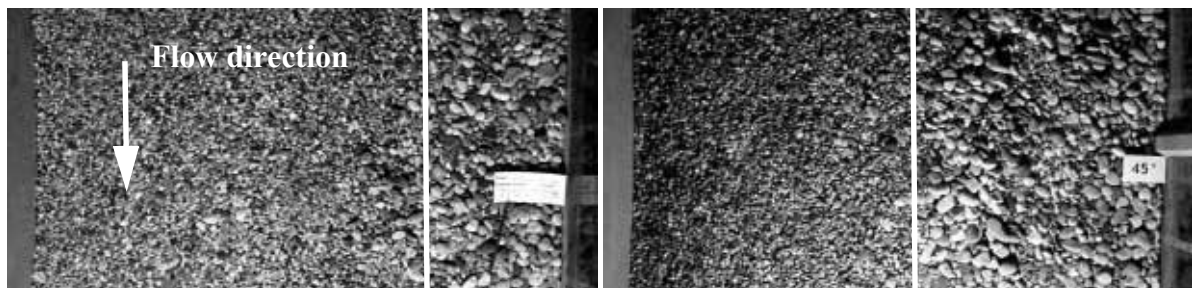
Figure 6.21: Bed surface in the first scour hole (tests B1d and B2d) without (left) and with ribs (right)

6.6   *Analysis of the flow field*

The presence of the macro-roughness influences the scour process by modifying the velocity distribution in the bend. It is well known that the velocity is higher on the outside of the bend and that there is a secondary circulation also. Both factors combine to give a large scour on the outside of the bend. A brief description of the flow field was already given in the paragraph discussing the preliminary tests (§ 5.2.1/2)e). The analysis of the main tests is presented here.

a)   *Tangential velocities*

The velocities in tangential direction (along the channel axis) are somewhat modified in the bend. Instead of a classical "log"-velocity profiles as it can be seen on top of Table 6.6[1] undergoes the following modifications in a curved channel. The maximum velocity is no longer found close to the free water surface but close to the bed surface, particularly in the scour holes; this can be seen very well in cross-section 40° in the second profile from the left. The highest tangential velocities (V_θ) are now found in the outer half of the cross-section.

With macro-roughness, the previously mentioned increase of the water depth in the inlet reach (§ 6.2.2) is well visible. But this has no influence on the shape of the velocity profile in this zone. In the bend and especially in the scour holes, the near bed velocity is reduced and the maximum velocity shifts towards the free water surface (Table 6.6 at 40°, first two profiles at the outer bank).

Appendix 11.1 shows that the highest velocities are located in a straight reach next to the free water surface. In the bend, this zone of maximum velocity first shifts towards the outer side wall and then down the wall towards the channel ground. At the maximum scour location, high (tangential) velocities can be observed near the bottom (Figure 6.22).
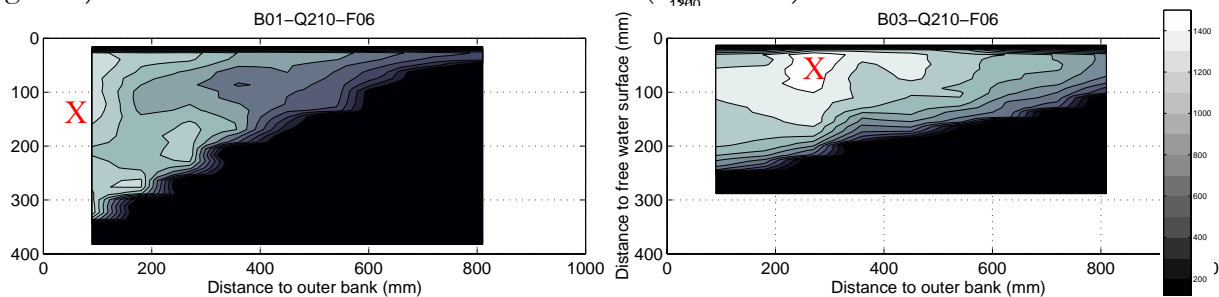
Figure 6.22:   Tangential velocities at 40° without macro-roughness (left) and with ribs spaced every 2° (right); view in the downstream direction (see also Appendix 11.4)
X = max. velocity

With macro-roughness (Appendix 11.4), the zone of maximum velocity remains all over the bend close to the surface for the ribs spaced every 4°. Introducing additional ribs (every 2°) the maximum velocity moves towards the channel ground, but at a significant distance from the outer wall (about 20 cm, that is about the average flow depth). For the smallest rib-spacing, the high-velocity zone gets even closer to the ground, but again at about 20 cm from the outer side wall.

---

1. Table 6.6 gives the raw velocity profiles. It shows that the first 2 cm from the free water surface are strongly influenced by the measurement, since the velocity probe had to touch the fluid.
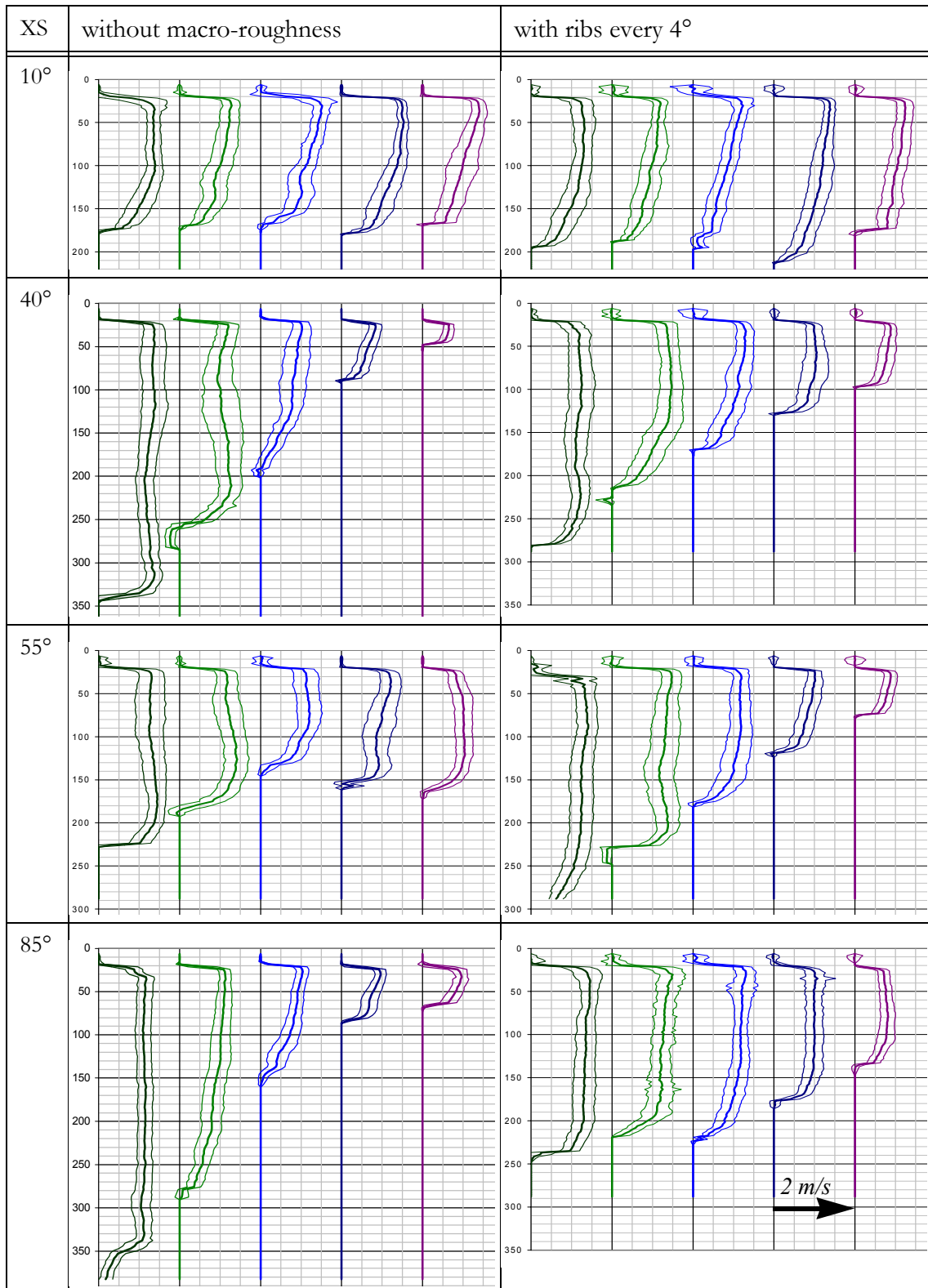
Table 6.6:   *Mean velocity profiles and standard deviation in tangential direction (along the channel axis) View in the downstream direction. Left profile at 90 cm from the outer bank, right profile at the inner bank. Radial distance between two profiles 180 cm (every 2nd measured profile was left out). On the vertical axis the distance to the free water surface is given (in mm).*

b) Velocities in the cross-section - secondary current

The flow field in the cross-section (radial and vertical components combined) shows the evolution of the secondary current (Appendix 11.2 and 11.5). Just after the inlet (10°) the flow field does not show a clear structure. Upstream the first scour, a small secondary current starts developing near the bed. At the maximum scour location (Figure 6.23), a big secondary cell (main cell) has developed in the scour hole. At the inner bank, another secondary cell (with the same rotation direction) emerges and grows if we move downstream. Towards the second scour hole, the main cell gets again more important, but not as important as for the first scour. The near bed radial velocities are of the same order of magnitude over the whole channel (about 10% of the tangential velocity components).
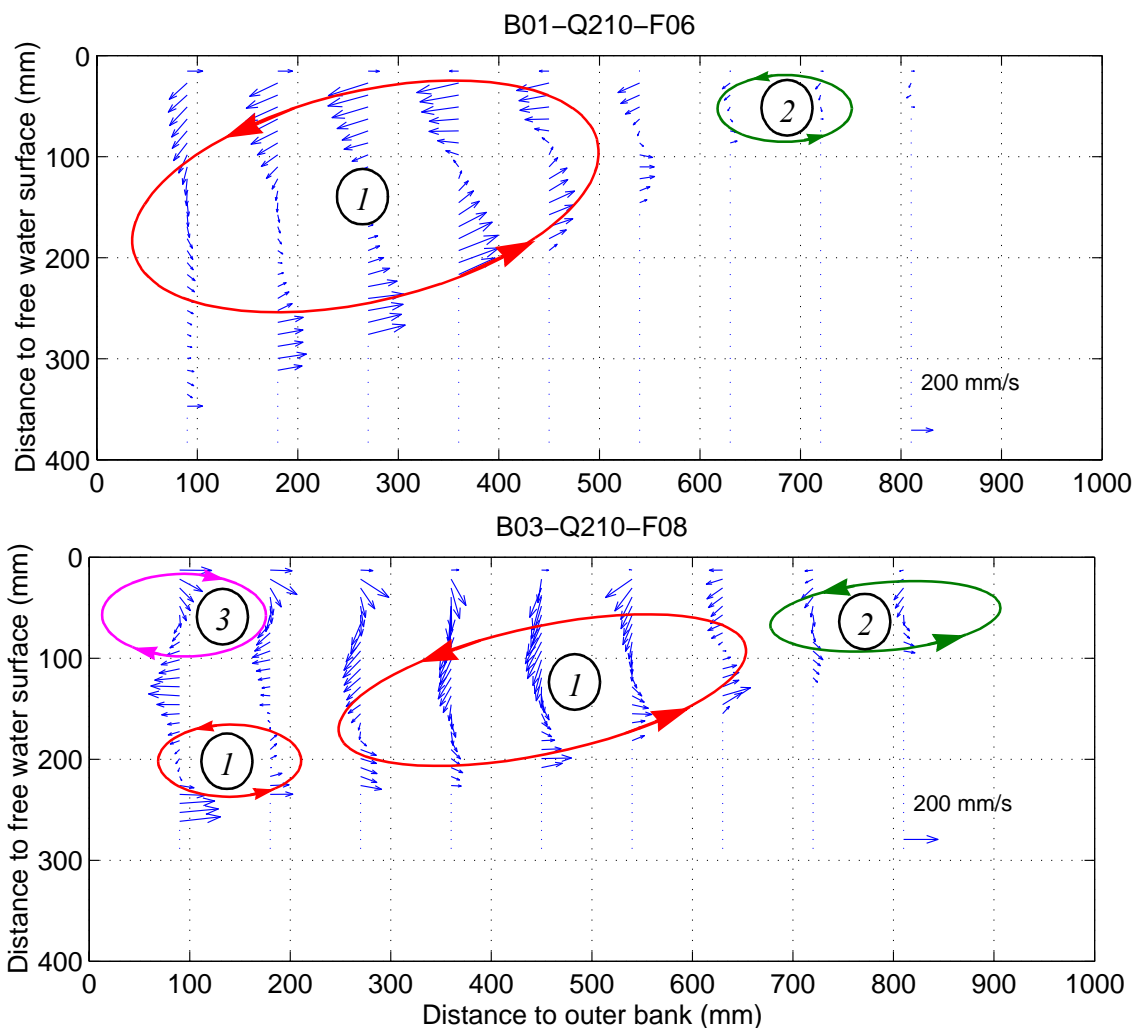
Figure 6.23: Top: *Main (1) and inner bank (2) secondary cells in the first scour hole at 40° (no MR)*
Bootom: *Main (1) and inner bank (2) secondary cells and outer bank secondary cell (3) protecting the wall of the channel (rib spacing 2°) at 70°*

Placing ribs at the outer side wall (every 4°), a secondary current of almost constant intensity over the whole bend is well visible.

At the outer bank at the free water surface a very small secondary cell (outer bank cell) gets visible (Figure 6.23). This cell was described by Blanckaert & Graf (2001). For the performed tests, this cell keeps the same intensity over the whole bend. If more ribs are added (2°), the cell

increases. But if the rib spacing is too dense (1°), it decreases again, but does not disappear (see 55°). BLANCKAERT (2001) observed the highest tangential velocities at the interface between the two cells. If we compare Appendix 11.4 with 11.5 we find high velocities at the interface, but the highest velocities occur inside the main secondary cell either towards the free water surface or near the outer bank.

The intensity of the radial velocity components on the ground is of the same order of magnitude as without macro-roughness for all rib spacings. This leads to the conclusion, that the radial velocity components cannot explain the difference in the scour depth. And if the radial components cannot explain this difference, the secondary current cannot explain it either, even if it contributes to the erosion process. But if we look at the tangential velocities, wee see a significant reduction of the near bed velocities due to the presence of vertical ribs along the outer bank. Furthermore the tangential velocities are about 10 times bigger than the radial ones. Therefore we may conclude that the modification of the tangential flow field seems to be determinant for the reduction of the scour depth due to macro-roughness.

c) *Velocity fluctuations and discussion*

The extent of scour will be governed not only by the magnitude of the mean velocity but also by the velocity fluctuations, since the force (drag or shear) acting on the particles will be a combined effect of both.

Studies on the flow past rectangular obstructions on a flat bed (GAIROLA, 1996) indicate that the flow separation at the obstruction reattaches the wall a certain distance downstream. According to Gairola, the length (L_d) of the so formed separation bubble is a function of the Reynolds number and the ratio length (e_θ) to depth (e_d) of the rib. The ratio L_d/e_θ for e_θ/e_d ratios of the order of 1 is about 12.0, for turbulent flows. In the present case, since the macro roughness is on a curved bank, it can be expected that the length of the separation bubble may be somewhat smaller. However, it is quite clear that a zone of separation exists which will reduce velocities in the neighborhood of the outer bank. Further the turbulence intensities will be higher in the vicinity of the separation zone and decrease as one moves away from this zone. It is therefore expected that the flow will undergo a modification in the following manner (with macro-roughness):

- Mean velocities will reduce near the outer bank due to separation.
- Turbulence intensity will be maximum near the shear layer, where the mean flow velocity is quite low.
- There will be an increase in velocity towards the center of the channel.
- The strength of the secondary circulation may decrease.

The effect of the macro roughness on the scour will be a combined effect of all these factors i.e. the mean velocity, the turbulence intensity and the strength of the secondary circulation. The observations made in the present study generally confirm the expected flow pattern. The strength of the secondary circulation decreases. In addition to this, the main velocity reduces and the turbulence intensity distribution is modified, which results in a reduced scour depth.

6.7   Summary and discussion

6.7.1   Summary of observations without macro-roughness

a) Bed topography

The scour depth depends on the discharge and the overall energy slope of the channel. With increasing values of theses parameters, the scour increases. It is interesting to observe that the relative scour (h_s/h_m) decreases with an increasing discharge. Probably the relative scour is limited to values between 3 and 5 if the width to depth ratio exceeds 10 (§ 6.2.1 a).

In the present study the maximum scour holes are located at about 30° to 35° and between the end of the bend and the following one meter (§ 6.2.1 b). The first point bar ends *after* the first scour and the second one *upstream* the second scour. The second scour hole seems to be influenced by this point bar at its upstream end (§ 6.2.1 c).

The shape of the scour holes changes, too: the first one has an elliptic shape with its deepest point located at about the average water depth from the outer bank, whereas the second one looks like a drop flowing in the downstream direction along the outer side wall (§ 6.2.1 e).

The shape of the cross-section (in radial direction) presents a discontinuity developing between about 10° and the first scour and between 70° and the second scour. The slope in the radial direction towards the inner bank is rather flat. Towards the outer bank a pronounced line bend can be observed and the bed slope steepens. The separation point between the two zones starts at the outer bank and shifts - if we movein the downstream direction - towards the inner bank. A possible explanation is the development of the secondary current starting at the outer bank and growing in the bend. In the final scour, the cross-section is generally s-shaped (§ 6.2.1 f).

b) Water surface

Characteristic stationary waves can be observed in the bend[1]. Their amplitude can reach up to 50% (!) of the mean water depth. The wave length is between 3 and 5 times the mean water depth. It is well known that the free water surface is inclined due to the centrifugal force. In the present case, the water surface was super elevated by 10 to 15% of the mean water depth h_m (§ 6.2.2).

Behind the point bars, return currents were observed. They were very weak and did not produce systematically. In general they appeared if the height of the point bars was quite important.

Another interesting observation concerns floating objects introduced into the channel upstream the bend. Independent of their radial position, they quit the channel more or less in the center (§ 6.2.2).

---

1. The local Froude numers along the outer side wall range up to 1.2 ... 1.4.

c) Evolution of the scour

The scour process starts in the downstream part of the bend and moves quickly in the upstream direction. At the same time, the scour deepens. The first scour armors rather quickly and gets stable after a few hours. The second one needs much more time to get armored and stabilized. The formation of the scour, especially the second one, goes along with important fluctuations in the maximum scour depth. These oscillations have an amplitude up to 50% of the mean water depth (§ 6.3).

d) Sediment transport

The sediment transport rate during the test decreases with an exponential function. For the higher discharges, this decreasing function was not observed, but this is due to the fact that the test at 180 and 210 l/s were performed without initial bed levelling but continued with the bed topography of the previous test (§ 6.4).

e) Grain sorting

Due to a wide grain size distribution - as it can be found in natural mountain rivers - a significant grain sorting process can be observed over the cross-section. At the outer bank coarse sediments form an armoring layer and at the inner bank, fine sediments are deposited. The mean grain size diameter of the sediments along the outer bank is about twice as big as the mean diameter of the substrate d_m; at the inner bank it is about two third of d_m (Table 6.4 and § 6.5).

f) The flow field

In the bend, the flow field undergoes some modifications. Instead of the typical log-velocity profile of a straight channel flow, the observed profile has its maximum value shifted from the free surface towards the ground.

An analysis of the evolution of the tangential velocities (in direction of the channel axis) reveals that the maximum velocity is located close to the free surface at the inlet. In the bend, the velocity first shifts toward the outer side wall and then plunges down towards the bed surface. At the maximum scour location, high velocities are found next to the ground (§ 6.6 a).

The velocity plots in the cross-sections show the secondary currents. At the beginning of the curve a secondary cell starts developing, growing up to the first scour. At the first scour location, another secondary cell forms at the inner bank. Since this new cell has the same rotation direction, it hinders the primary cell to grow. The primary cell is first reduced in the downstream direction and then growing again towards the second scour. The secondary current is less important in the second scour than in the first one (§ 6.6 b).

6.7.2   Influence of the macro-roughness on the scour process

a) Bed topography

By placing verical ribs on outer side walls with an appropriate spacing, the scour depth can be reduced up to 38% (Figure 6.5), especially for high discharges and steep slopes (§ 6.2.1 a).

The first scour location shifts in the downstream direction in the presence of macro-roughness by 15 to 40° (Table 6.2). It is interesting that the second scour remains more or less at the same place (§ 6.2.1 b). The first point bar moves in the downstream direction (by up to 20°), too. But as for the second scour, the downstream point bar remains at about the same position (§ 6.2.1 c).

For an optimum rib spacing the shape of the two scour holes remains the same as without macro-roughness. The difference concerns essentially the length of the first scour covering a larger segment of the bend and being of reduced depth. The second scour (if there is one) has about the same extend (surface) as without ribs (§ 6.2.1 e).

Concerning the shape of the cross-section (in radial direction), the same line bend can be observed; there is no significant difference (§ 6.2.1 f).

b) Water surface

The stationary waves on the free water surface (without ribs) are replaced by shock waves emerging at the outer bank and spreading out over more than half of the channel. The maximum amplitude of these waves is significantly smaller than the one of the stationary waves. It is reduced by 50% to 0.25% of the mean water depth h_m. The inclination of the free surface shows no significant modification due to the presence of macro-roughness (§ 6.2.2).

An important influence of the ribs is the head loss they create in the bend, which induces an increased water level in the inlet reach[1] just upstream the bend.

Return currents behind the point bars were also observed with macro-roughness if important point bars formed. Since the first point bar was in general much smoother, the cross-section was better used for the flow and the return currents were less frequent.

Alike the case without macro-roughness, floating objects introduced upstream the bend quit the channel at the center not depending on the radial point of introduction (§ 6.2.2).

c) Evolution of the scour

An important effect of the ribs is the smoothing of the scour process. Instead of having important oscillations (especially in the second scour) during the development of the scour, the scour develops more regularly. The oscillations are reduced by 50% to 0.25% of the mean flow depth for small discharges and they even disappear for higher discharges (180 and 210 l/s) (§ 6.3).

---

1. The increase is of about 10% of h_m. For constant sediment feeding rates, an additional increase needs to be considered (§ 6.4).

d) Sediment transport

The sediment transport rate during the test decreases with an exponential function, too. The behavior is like the one without ribs, except that the transport capacity is considerably reduced. For the performed tests the reduction of the transport capacity was up to 50 to 65%. In a natural river, the upstream reach will continue bringing sediments to the bend. But since the transport capacity in the bend is insufficient, the sediment will deposit in a first stage upstream the bend and increase in this way the overall bed slope. With an increased slope, the transport capacity is increased again, and the entire bedload transits through the bend. The observed necessary increase of the overall bed slope was the same order of magnitude as the reduction of the transport capacity. Since the observations on the steepening of the slope are based on one test series (the preliminary tests), these results should be confirmed by additional research (§ 6.4).

e) Grain sorting

The macro-roughness has no significant influence on the grain sorting process, beside the fact that the zone in the scour holes where a coarse armoring layer can be observed is extended to about 50% of the channel instead of 25% without ribs. But this is rather due to a flatter transversal bed slope than to a modified behavior concerning grain sorting (§ 6.5).

f) The flow field

Ribs on the outer wall influence the tangential velocity field considerably. If the ribs density is 4°, the maximum velocities remain close to the free surface all over the bend. With additional ribs, the maximum velocity shifts towards the bottom but at a distance of about the average flow depth h_m of the outer wall (§ 6.6 a).

In the presence of macro-roughness the secondary current does not seem to undergo an important modification. Only in at the first scour location a slight decrease in the intensity can be observed. But the near bed velocities in radial direction remain about the same as without ribs.

An interesting phenomenon which was not yet visible for the case without macro-roughness[1] is the small secondary cell on top of the outer wall (Figure 6.22). This cell is of about constant intensity all over the bend. If the rib spacing becomes very small (1°), the intensity of this cell decreases again (§ 6.6 b).

g) The special case of the smallest rib spacing of 1°

In the special case of the smallest rib spacing of 1°, as the ribs are very close to each other, the isolated effect of each roughness is lost to the profit of a continuous roughness along the outer wall. The first scour location shift even farther downstream and the scour depth increases again. This indicates that the ribs loose their efficiency. It is obvious that if the separation zone cannot reattach at the outer wall before hitting the next vertical rib, the energy dissipation will not be optimal.

But this does not yet explain why the scour gets deeper than without macro-roughness. It could be mentioned that the channel width is reduced due to the ribs. But the decrease by 2% of the chan-

---

1. ...since the phenomenon was too weak and the measurements too far away from the outer wall.

nel width cannot explain such an important increase in scour depth. Based on the shape of the scour hole (like a drop with an elliptic center) and on the location of the scour compared to the point bar (downstream the first point bar), the hypothesis that the scour hole corresponds to a combination of the first and second scour seems to be confirmed. Furthermore the flow field shows many secondary cells indicating a highly perturbed flow field (Figure 6.24). Behind the point bar, the inner bank cell is considerably amplified. The big amount of secondary cells indicates that the velocity fluctuations are quite important in this cross-section.
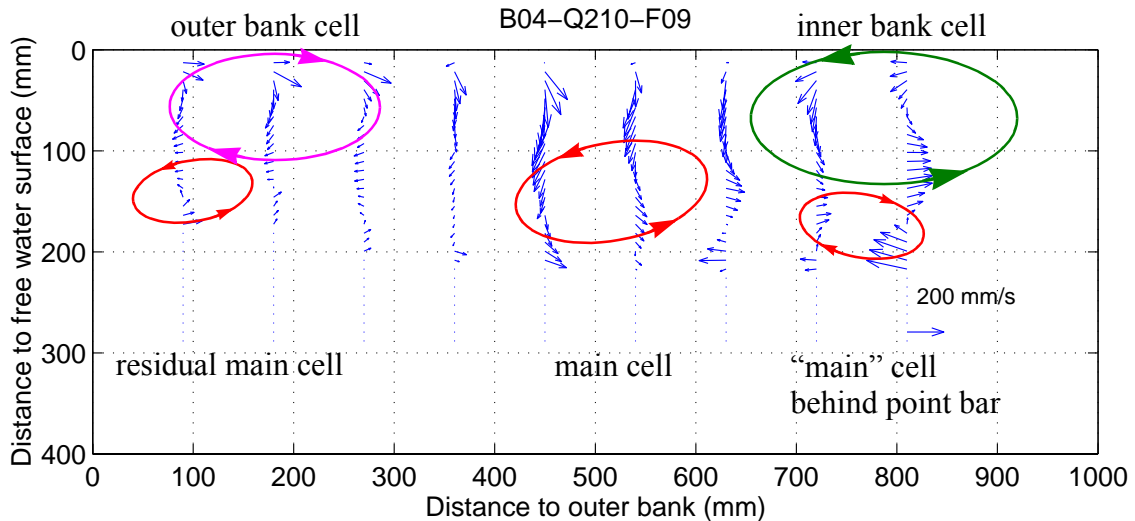
Figure 6.24: Flow field after the first point bar for a rib spacing of 1° (at 85°)

And since the scour depth depends on

- the tangential velocities - being comparable or reduced compared to the other cases,
- the secondary currents - which are not more important than for the other cases, and finally
- the velocity fluctuations (turbulence)

the last ones have to be the key element for the heavily increased scour depth for this rib configuration. Since these fluctuations seem to be provoked by the discontinuity after the point bar, we see that the scour hole is submitted to an influence of the point bar as it is usually only the case for the second scour hole.

6.7.3 Discussion

a) Scour mechanism

It has been shown in this section that the scour formation and development depend on many factors acting in a combined way:

- the tangential velocity components play a major role in the scour process,
- the secondary currents are important; but they explain only in part the modification of the flow field due to the presence of macro-roughness,
- the velocity fluctuations contribute to the scour process, too.

The first scour formed between 30° and about 40° in the tests. At the beginning of the bend, the secondary current starts and grows towards this first maximum scour at the outer bank. Since the point bar towards the inner channel wall is located after the maximum scour location, the flow is not particularly perturbated and the velocity fluctuation can be assumed to be less important than in the second scour. But the highest tangential velocities are located close to the bed surface inducing an important solicitation of the bed.

Already at the first scour location, an additional secondary cell (inner bank cell) emerges. This cell hinders the main cell to grow, since it has the same direction.

Finally the main secondary cell grows again towards the second scour. But the intensity of the circulation is weaker than in the first scour. This second scour is located after the second point bar. Therefore the flow field is perturbed and the velocity fluctuations are getting important for the scour process. The main (tangential) velocities are of about the same intensity close to the bed surface.

Comparing the two scour holes, it can be concluded that the first one is dominated by the flow field and especially by the secondary currents developing their strongest intensity in the first maximum scour. The second scour, is most likely dominated by the velocity fluctuations induced by the discontinuity created behind the second point bar.

Both scour holes stabilize, once the bed surface armored. It takes a few hours to armor the first scour hole, but about twice as long for the second one. This armoring layer formed of coarse sediments (about twice the mean diameter of the substrate) can be observed in the outer part of the bend, whereas the point bars are formed of fine sediments (about two third of the mean diameter).

b) Influence of the macro-roughness

Vertical ribs placed with an optimal spacing on the outer side wall have the following influences on the scour:

- The maximum scour depth is considerably reduced (up to 38% for the highest discharges and slopes).
- The first scour location shifts in the downstream direction (by 15 to 40°), but the second scour remains about at the same place.
- As for the scour, the first point bar moves in the downstream direction; but for the second one it remains at the same position.

- The prominent local scour holes disappear and make place to an elongated scour hole. Sometimes, the first and second scour cannot be distinguished.
- Important oscillation of the scour depth, observed especially in the second hole, are significantly reduced by the presence of macro-roughness. They even disappear for high discharges.
- The maximum water levels in the bend is not subject to important changes since the increase of the average water level goes along with the reduction of the surface wave amplitude.
- At the upstream end of the bend, the water level is increased by about 10% due to the head losses in the bend[1].
- The transport capacity is considerably reduced by the macro-roughness (to 35 to 50%). In natural rivers, this reduction is compensated by a steepening of the channel slope (mainly realized by depositions in the upstream reach). The channel slope was increased by about 40 to 50% of the initial bed slope for the perliminary tests performed at constant sediment feeding rate.
- The grain sorting process is not significantly influenced by the ribs, beside the fact that about 50% of the channel width are armored compared to 25% without ribs.
- The flow field is considerably modified by the macro-roughness. The highest tangential velocities remain closer to the free surface than without ribs. If they shift towards the bottom, they remain at about the mean flow depth from the outer wall.

c) Optimum rib spacing

GAIROLA (1996) indicated the length of the separation zone behind the ribs to be 12 times the rib depth e_d for a straight reach. In a bend, we can expect this separation zone to become shorter since the flow in the bend "squeezes" the zone to the side wall (especially in the upper part of the bend). Since it is this separation zone which is responsible for the head losses in the bend, the rib spacing optimum rib spacing corresponds quite well to the length of this separation bubble.

Adapting Gairolas observations to our tests, this would indicate an optimum rib spacing between 2° and 3° (corresponding to e_s/e_d ratios between 10 and 12). In the present chapter it was observed that the reduction of the scour depth was the most effective for spacings between 2° and 4° (Figure 6.5). Since the spacing of 4° gives better results especially for high velocities, the optimum spacing is probably comparable to the one in a straight reach. Therefore a spacing of about 12 times the rib-depth can be proposed for constructions projects.

---

1. It needs to be mentioned that this was observed during the tests for which the bed slope of the inlet reach was maintained constant, by adjusting the sediment transport feeding. For a constant sediment transport rate, the bed level will rise upstream the bend, leading to higher water elevation, too.

CHAPTER 7

ESTABLISHING AN EMPIRICAL FORMULA

7.1   Introduction

This chapter presents the search for an empirical formula allowing the determination of the maximum scour depth. Based on the analysis of existing scour formulae and the parameters used by the different authors, several approaches were explored.

- In a first step a dimensional analysis was performed (§ 7.2) indicating the essential parameters influencing the scour process.
- In a second stage a large number of different approaches were explored to establish a new scour formula. They include the optimization of existing scour formulae, new approaches, based on the s-shaped cross-section profile, the pi-theorem as well as an approach with a dimensionally aware genetic algorithm.
- Finally the influence of the macro-roughness on the scour process is discussed and a formula determined to estimate the scour depth with vertical ribs on the outer side wall.

In this study, the square of the Pearson product moment correlation coefficient R was used defined as:

$$R = \frac{n \cdot \Sigma XY - \Sigma X \cdot \Sigma Y}{\sqrt{(n \cdot \Sigma X^2 - (\Sigma X)^2) \cdot (n \cdot \Sigma Y^2 - (\Sigma Y)^2)}} \tag{7.1}$$

R^2 ranges from 0 to 1 and reflects the extent of a linear relationship between two data sets.

NB: The square of Pearson's correlation factor R^2 quantifies the extent of a linear relationship between two data sets and not the error between measured and computed data!

7.2 *Main parameters for an empirical formula*

In a first step, the different existing scour formulae, mentioned in section 3.5 were used to determine a set of parameters influencing the scour process (see table 7.1).

FORMULA	MAIN PARAMETERS
Fargue (1868)	R_c/B, bed roughness, V
van Bendegom (1947) Engelund (1974) Bridge (1976)	Fr_d $7 \cdot \tan\phi = cst$ $11 \cdot \tan\phi = cst$
Kikkawa et al. (1976) Reindl (1994)	Fr_d, $V*/V$, n Fr_d, $V*/V$, n, G_S
Zimmermann (1978) Falcon & Kennedy (1983) Odgaard (1986)	Fr_d^2, n Fr_d, n, θ, p Fr_d, n, θ
Bazilevich (1982)	h_m/h_{max}
Peter (1986)	R_c/B, σ, h_m/B, Fr

Table 7.1:   List of parameters used in existing scour formulae

The following parameters were correlated with the maximum scour depth in the first and second hole, with the maximum scour over the bend[1] as with the relative scour h_s/h_m (computed in the inlet reach) and with the maximum transversal bed slope $\tan(\beta_{max})$:
R_c/B, Fr_d, V, $V*/V$, θ, $\tan\phi$.

The sediment saturation G_S, used by Reindl was not used because an estimation of this parameter is difficult or almost impossible in engineering practice. Mannings friction factor n and the porosity p are not correlated since they were constant for the tests (p) or not independent of the other parameters (n).

Additional parameters were added to obtain a wide range of characteristics , which could have an influence on the scour process. The test parameters as well as the obtained correlations are given in the following table (Table 7.2). All the correlations are given for the data set without macroroughness, including Peter's tests.

---

1. The maximum scour h_{12} was sometimes located in the upstream and sometimes in the downstream scour.

	$h_{s,max}$			$h_{s,max}/h_m$			$\tan(\beta_{max})$		
	1	2	12	1	2	12	1	2	12
V^*/V	0.043	0.058	0.055	0.207	0.087	0.210	0.296	0.078	0.153
Fr^*	0.061	0.019	0.050	0.060	0.035	0.050	0.031	0.042	0.040
Fr_d	0.263	0.152	0.230	0.006	0.031	0.010	0.001	0.262	0.137
Fr	0.013	0.000	0.016	0.210	0.044	0.231	0.089	0.016	0.036
$Sigma$	0.130	0.020	0.079	0.087	0.009	0.056	0.086	0.036	0.005
d/h_m	0.028	0.055	0.028	0.251	0.053	0.275	0.205	0.026	0.064
Re^*	**0.775**	**0.734**	**0.822**	0.348	0.140	0.338	0.153	0.163	0.165
Re	**0.798**	**0.759**	**0.832**	0.477	0.201	0.475	0.232	0.188	0.204
$V^*R_h/sqrt(g^*B^3)$	**0.812**	**0.751**	**0.839**	0.475	0.210	0.477	0.229	0.204	0.217
$V^*R_h/sqrt(g^*h_m^3)$	**0.814**	**0.785**	**0.863**	0.452	0.175	0.445	0.212	0.151	0.168
$S_{e,in}$	0.031	0.475	0.251	0.169	**0.571**	0.464	0.001	0.404	0.175
$S_{e,mr}$	0.057	**0.553**	0.301	0.128	**0.673**	**0.564**	0.002	0.303	0.125
$S_{e,all}$	0.079	0.161	0.099	**0.512**	0.170	**0.518**	0.366	0.109	0.186
$S_{e,bend}$	0.004	0.027	0.005	0.268	0.071	0.285	0.186	0.012	0.041
Rc/B	**0.529**	0.442	**0.564**	0.279	0.227	0.277	0.253	0.473	0.470
h_m/B	**0.662**	**0.532**	**0.628**	0.486	0.262	**0.521**	0.228	0.297	0.295
r/B	**0.502**	0.416	**0.535**	0.263	0.218	0.262	0.240	0.460	0.455
$V^2/g/r$	0.040	0.011	0.026	0.019	0.026	0.016	0.054	0.148	0.153
$R_c^*h_m/B^2$	**0.699**	**0.586**	**0.696**	0.441	0.261	0.458	0.256	0.376	0.377
$(R_c+h_m)/B$	**0.537**	0.448	**0.571**	0.287	0.230	0.285	0.255	0.472	0.469
V *	**0.807**	**0.735**	**0.855**	0.329	0.130	0.321	0.150	0.119	0.126
V^*R_h *	**0.798**	**0.759**	**0.832**	0.477	0.201	0.475	0.232	0.188	0.204

Table 7.2:   *Table of correlations R^2 for the tests without macro-roughness*
Re^*: computed with d_{90}, $S_{e,in}$ and $S_{e,mr}$ are computed without Peter's data.
1: first scour hole, 2: second scour hole, 12: maximum of the two scour holes
Correlations over 0.5 are in bold characters, correlations below 0.4 on a grey background.
* parameter with a dimension

It can easily be seen that the frequently used parameters V^*/V, Fr_d have almost no influence on the scour process. The particle Froude number seems to have a little influence on the absolute scour depth h_{max} and it may be useful to introduce it in combination with other parameters in a scour formula.

The Reynolds number seems to be an important parameter; but since there is no plausible reason to consider the influence of the viscosity in the scour process, this phenomenon is an expression of the correlation between the velocity and the scour depth. This fact is confirmed if we consider the correlations between the velocity V, the product of the velocity with the hydraulic radius $V \cdot R_h$ with the absolute and relative maximum scour depth. To replace the Reynolds number, a new dimensionless ratio $V \cdot R_h / \sqrt{g \cdot B^3}$ is proposed. It has about the same correlation as the Reynolds number. Replacing B by h_m in this ratio would reduce the correlation.

The energy slope has a significant correlation with the scour depth. If we consider the maximum scour depth in the deepest of the two scour holes h_{12}, the overall energy slope $S_{e,\,all}$ and the energy slope over the domain equipped with macro-roughness elements $S_{e,\,mr}$ play a major role.

Furthermore the geometric ratios R_c/B, h_m/B seem to be important to explain the maximum scour. Since the local radius r is almost constant compared to the channel width B, the ratio r/B gives quite good correlations, too. But since the radius is already by R_c/B, r/B will not be considered as optimization parameter.

The influence of the super elevation of the water surface $V^2/(g \cdot r)$ is already included in the term R_c/B.

Table 7.3 shows the correlations between the chosen parameters and all available tests including the ones with macro-roughness and Peter's data.

The parameters influencing the scour process without macro-roughness still play an important role except the energy slope over the domain equipped with macro-roughness. This is quite normal: because of the head losses being more important than without vertical ribs, the energy slope has to increase. Despite the increased energy slope (over the domain with macro-roughness), the scour depth is reduced. Therefore the overall energy slope will be used in the optimization process.

The influence of the macro-roughness on the maximum scour seems to be dominated by the ratio of rib-spacing to average water depth e_s/h_m. This ratio is more important than the rib spacing compared to the channel width e_s/B. The depth of the macro-roughness appears to play a subordinate role. This seems to be contradictory to the statement that the ratio of rib-depth to rib-spacing (e_d/e_s) plays a predominant role (§ 6.2.1). If we consider that the mean water depth is highly correlated with the relative scour depth, the good correlation for the ratio e_s/h_m gets quite obvious. Therefore the ratio rib-spacing to channel width (e_s/B) can also be considered as a good parameter to quantify the influence of the ribs on the relative scour. Despite a somewhat smaller correlation for the rib-depth to rib-spacing ratio (e_d/e_s) an influence on the relative scour can be made out.

As far as the transversal bed slope β_{max} is concerned, the same parameters play an important role. In addition to them, the sediment Froude number has a significant correlation.

If we summarize the obtained results, we see that the following parameters need to be considered in the scour process:

- general parameters: V or $V \cdot R_h$ represented by $V \cdot R_h/\sqrt{g \cdot B^3}$, $S_{e,\,all}$, R_c/B, h_m/B, (as well as combinations of these parameters)
- macro-roughness related parameters: e_s/h_m, e_d/h_m, and eventually the same ratios relative to the channel width B.

	$h_{s,max}$			$h_{s,max}/h_m$			$\tan(\beta_{max})$		
	1	2	12	1	2	12	1	2	12
V*/V	0.009	0.003	0.002	0.000	0.002	0.000	0.000	0.000	0.000
Fr*	0.109	0.082	0.100	0.002	0.002	0.001	0.002	0.016	0.011
Fr_d	0.292	0.149	0.219	0.255	0.309	0.292	0.263	**0.525**	0.456
Fr	0.014	0.027	0.005	0.288	0.139	0.298	0.199	0.077	0.142
Sigma	0.123	0.028	0.081	0.007	0.003	0.001	0.000	0.053	0.031
d/h_m	0.095	0.115	0.084	0.281	0.111	0.285	0.188	0.056	0.111
$1/h_m$ *	**0.601**	**0.509**	**0.544**	**0.746**	0.408	**0.755**	0.462	0.375	0.395
h_m *	**0.678**	**0.532**	**0.600**	**0.717**	**0.513**	**0.736**	**0.527**	0.455	**0.507**
Re*	**0.652**	**0.504**	**0.592**	**0.613**	0.456	**0.627**	0.457	0.465	0.472
Re	**0.706**	**0.567**	**0.649**	**0.677**	0.482	**0.686**	0.483	0.448	0.480
V*R$_h$/sqrt(g*B^3)	**0.718**	**0.571**	**0.659**	**0.670**	0.481	**0.681**	0.474	0.448	0.479
V*R$_h$/sqrt(g*h$_m$^3)	**0.703**	**0.566**	**0.657**	**0.658**	0.458	**0.664**	0.455	0.434	0.450
$S_{e,in}$	0.001	0.016	0.014	0.080	0.065	0.094	0.042	0.042	0.114
$S_{e,mr}$	0.002	0.004	0.001	0.002	0.009	0.000	0.000	0.019	0.001
$S_{e,all}$	0.123	0.163	0.120	**0.536**	0.281	**0.524**	0.356	0.209	0.285
$S_{e,bend}$	0.000	0.007	0.000	0.120	0.035	0.115	0.056	0.004	0.018
R_c/B	**0.511**	0.346	0.456	**0.579**	**0.535**	**0.597**	**0.528**	**0.681**	**0.677**
h_m/B	**0.644**	0.481	**0.560**	**0.658**	0.494	**0.683**	0.476	0.449	**0.504**
r/B	0.488	0.330	0.435	**0.552**	**0.513**	**0.569**	**0.504**	**0.655**	**0.651**
V^2/g/r	0.000	0.000	0.001	0.113	0.123	0.115	0.160	0.236	0.243
R_c*h$_m$/B^2	**0.642**	0.472	**0.563**	**0.669**	**0.535**	**0.692**	**0.531**	**0.551**	**0.595**
(R$_c$+h$_m$)/B	**0.518**	0.353	0.462	**0.585**	**0.538**	**0.604**	**0.530**	**0.678**	**0.676**
V *	**0.693**	**0.545**	**0.660**	**0.538**	0.381	**0.541**	0.361	0.374	0.370
V*R$_h$ *	**0.706**	**0.567**	**0.649**	**0.677**	0.482	**0.686**	0.483	0.448	0.480
e_s *	0.219	0.088	0.138	0.473	0.470	**0.526**	**0.549**	**0.551**	**0.543**
e_d *	0.169	0.098	0.117	0.378	0.347	0.413	0.457	0.370	0.401
e_s/B	0.383	0.258	0.302	**0.642**	0.478	**0.677**	**0.557**	0.467	0.479
e_d/B	0.169	0.098	0.117	0.378	0.347	0.413	0.457	0.370	0.401
e_s/h_m	**0.539**	0.404	0.459	**0.766**	0.487	**0.792**	**0.553**	0.493	0.497
e_d/h_m	0.139	0.068	0.091	0.361	0.345	0.398	0.437	0.396	0.400
e_d/e_s	0.204	0.083	0.144	0.270	0.271	0.298	0.279	0.303	0.281
e_d*e$_s$/B^2	0.048	0.042	0.038	0.165	0.139	0.175	0.213	0.134	0.175
(e$_d$+e$_s$)/B	0.384	0.258	0.302	**0.642**	0.478	**0.677**	**0.557**	0.466	0.479
(e$_d$+e$_s$)/h$_m$	**0.539**	0.404	0.459	**0.766**	0.487	**0.792**	**0.553**	0.493	0.496

Table 7.3:   *Table of correlations R^2 including the tests with macro-roughness*
The second part of the table gives ratios related to the macro-roughness characteristics
* parameter with a dimension

7.3 Establishment of the scour formula

7.3.1 Introduction

The following possibilities were explored to establish a new formula:
- Enhance existing scour formulae,
- Approach based on the geometry of the cross-section profile,
- Approach based on the Pi-theorem,
- Genetic algorithm.

In order to compare the measured to the computed results, different criteria can be applied. The most important one for engineering concerns is the maximum scour depth. A second one can be of interest: the fit to the bed topography in the cross section at the maximum scour locations (radial direction). In the present section, both criteria were used to establish new formulae.

7.3.2 Enhancement of existing scour formulae

a) Kikkawa, Ikeda & Kitagawa (1976)

Since the formula of KIKKAWA ET AL. (1976) is quite frequently used, a first optimization had the aim to increase the prediction capability of this formula by adjusting its parameters. If Kikkawa's equation is used in its originally published form (see § 3.5.2/5), the correlation between measured and computed max. scour is only $R^2 = 0.35$. To increase the prediction quality of this formula, equations 3.91 and 3.93 were parametrized in the following way:

$$\frac{h_s}{h_m} = \exp\!\left(\frac{A}{2} \cdot \left(\frac{r^2}{R_c^2} - 1\right)\right) \tag{7.2}$$

where
$$A = c_1 \cdot \left(1.8955 - 3.0023 \cdot \frac{V^*}{V}\right) \cdot Fr_d \tag{7.3}$$

The difficulty mainly consists in the fact that either the maximum scour or the bed topography in radial direction can be fitted to the measured data.
- If the above equation is adjusted to the max. scour depth, correlations of $R^2 = 0.60$ (for the maximum scour depth over both holes) can be obtained by using a coefficient $c_1 = 0.689$. The problem is that the obtained equation gives a much too flat cross-section profile, since the maximum bed slope is located at the outer side wall. The correlation between measured and computed maximum transversal bed slope is only 0.25.
- If the data is adjusted to fit the transversal bed topgraphy, the correlation with the bed slope can be increased to 0.36, which is by far not satisfying. But, the maximum scour prediction becomes completely useless ($R^2 = 0.04$).

Even if a factor c_2 is added to the first term in the parenthesis in equation 7.3, the scour depth correlation is not modified in a significant manner.

As next and final step the parenthesis of the constant A is replaced by the sum of the most important parameters combined with a factor to weight each one of them:

$$A = c_1 \cdot \left(c_2 + c_3 \cdot \frac{V \cdot R_h}{\sqrt{g \cdot B^3}} + c_4 \cdot S_{e,\,all} + c_5 \cdot \frac{R_c}{B} + c_6 \cdot \frac{h_m}{B} + \frac{V^*}{V} \right) \cdot Fr_d \qquad (7.4)$$

Introducing the new parameters one by one does not bring an important increase of prediction capability or only with "strange" equations containing factors at the order of magnitude of 10^3 and more and similar aberrations. Finally the following relation for A was found:

$$A = \left(-1.7 + \frac{V \cdot R_h}{\sqrt{g \cdot B^3}} + 1.23 \cdot \frac{R_c}{B} - 16.5 \cdot \frac{h_m}{B} + 18 \cdot \frac{V^*}{V} \right) \cdot Fr_d, \quad R^2 = 0.795 \qquad (7.5)$$
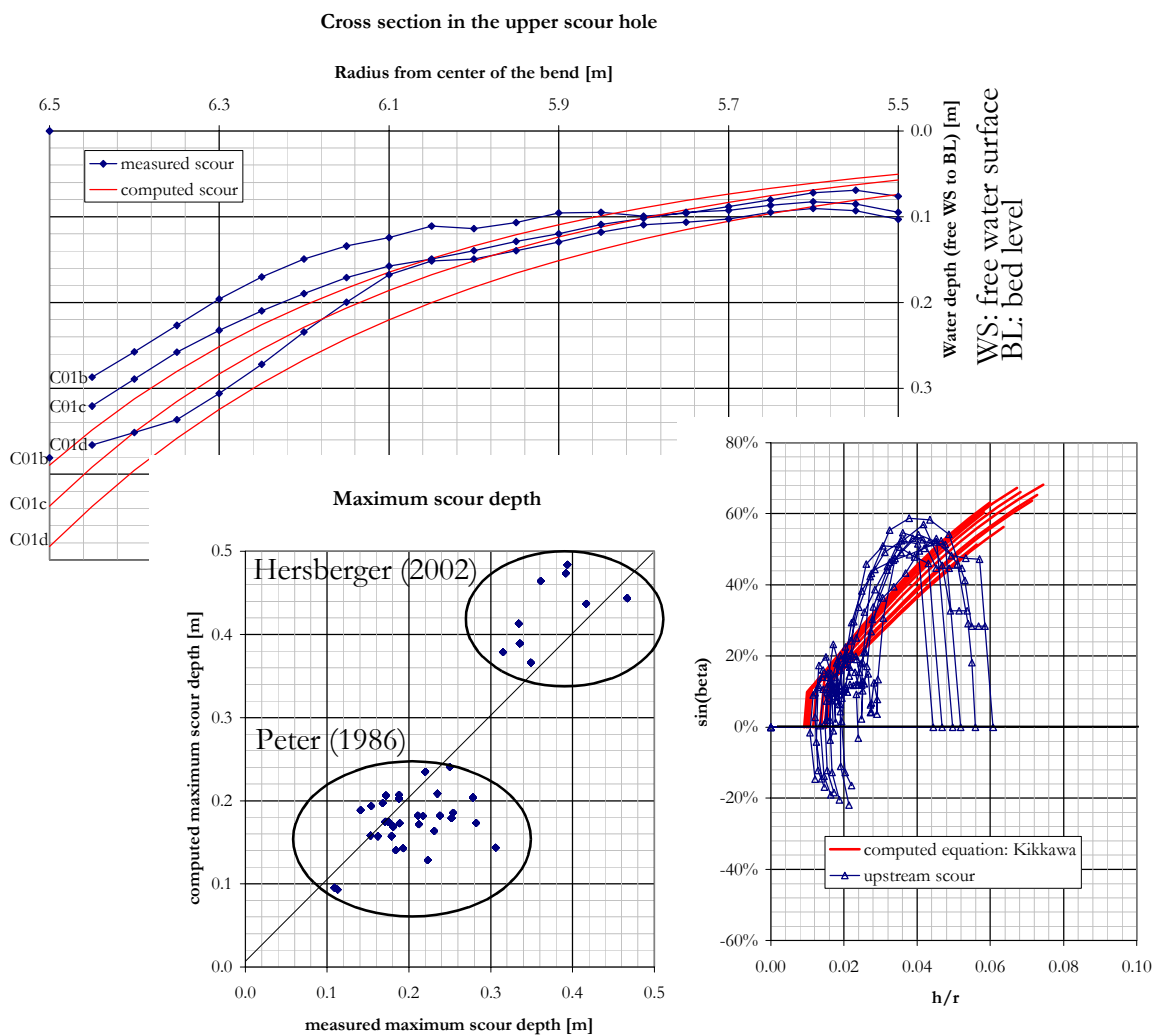
Figure 7.1: *Results of the enhanced equation (eq. 7.5) of Kikkawa (see also* Fig. *7.3 for explanations)*
ON TOP: cross section in the upper scour hole for test C01 (S_0=0.70%);
BOTTOM LEFT: maximum scour depth; RIGHT: transversal bed slope (without Peter's data)

If we compute the scour depth with equation 7.5, a correlation of 0.795 can be obtained. With extensive testing, this result could eventually be refined. A cross-section in the upstream scour for

test C1d ($S_0 = 0.70$ %) is given as an example as well as a comparison between the measured and computed maximum scour depth (Fig. 7.1).

The correlation with the complete dataset (including Peter's tests) seems quite ok. But the predicted scour depth for the tests performed in the present study is systematically overestimated.

b) *Bridge (1976)*

In paragraph 3.5.4 we have seen that the formula of BRIDGE (1976) predicts the scour depth quite well without any correction, but with a big scatter. In the present paragraph, a simple extension of Bridges formula with a better correlation than the one of the original formula ($R^2 = 0.29$) will be presented.

By adding a correction factor depending on the radius to width ratio of the channel, the correlation of Bridge's formula can be significantly increased:

$$\sin\beta = 2.86 \cdot \frac{R_c}{B} \cdot \tan\phi \cdot \frac{h_s}{r}, \quad R^2 = 0.796 \tag{7.6}$$

Most additional factors have almost no influence on the correlation. The highest correlation was found by adding the flow depth to channel width ratio.

$$\sin\beta = 0.394 \cdot \left(11-23 \cdot \frac{h_m}{B}\right) \cdot \frac{R_c}{B} \cdot \tan\phi \cdot \frac{h_s}{r}, \quad R^2 = 0.817 \tag{7.7}$$

Tests to add more parameters did not lead to satisfying results. As for Kikkawa's formula, the predicted scour depth is systematically overestimated for the tests of this study.
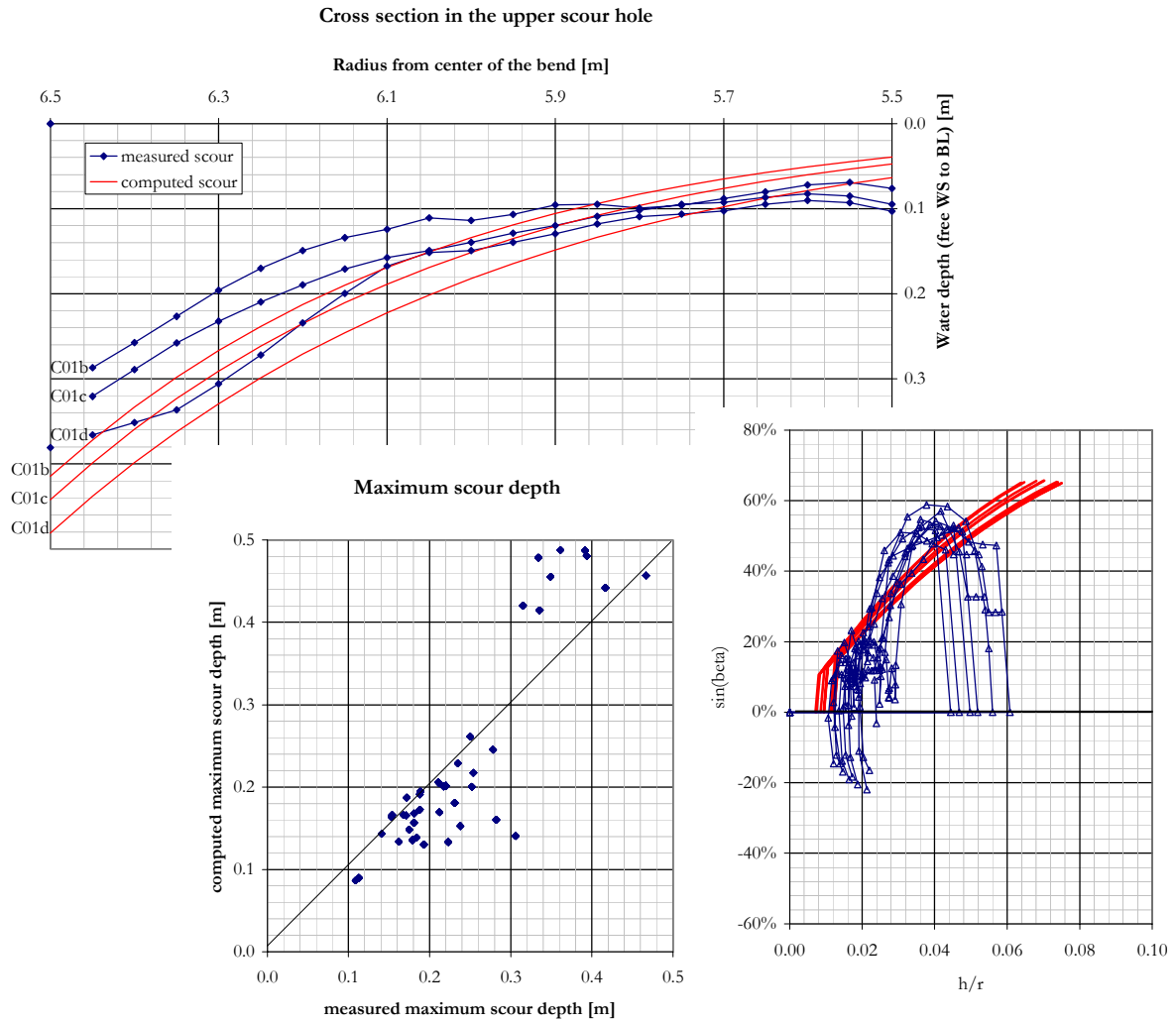
Figure 7.2:   Results of the enhanced equation (eq. 7.6) of Bridge (see Fig. 7.1 and 7.3 for explanations)

c)   Problematic of existing scour formulae

All existing scour formulae have one major problem in common: they give the maximum transversal bed slope at the location of maximum scour. This is due to the used parabolic approximation of the bed surface in radial direction. Figures 7.1 and 7.2 show that the bed topography in radial direction is rather s-shaped than parabolic especially for high discharges. Furthermore the plot of $\sin\beta$ as a function of h/r (Fig. 7.3) demonstrates that the assumption of a constant K is not correct. Most formulae assume that K is more or less constant, since the used parameters are submitted to very small variations over the cross-section. In fact, the measurements are adjusted almost on a ellipse.

Therefore a new approach based on the shape of the radial cross-section profile is described in the following paragraph.

7.3.3   Approach based on the bed shape of the cross-section

In a typical cross-section profile, the following three important points can be found (Fig. 7.3):

1. In general, the maximum scour depth can be found at the outer side wall. For some tests, especially the ones with thick vertical ribs (test series E), the maximum scour was sometimes located close to the outer side wall but not at the wall[1]. For practical reasons, these eventual depositions (or less scour) were not considered.

2. Somewhere in the outer half of the cross-section, the maximum lateral bed slope can be found. Since $\sin\beta$ is an approximation of the lateral bed slope, the highest point on the vertical axis corresponds to this maximum transversal bed slope (Fig. 7.3).

3. Close to the inner side wall, the highest point in the cross-section can be found (location with maximum depositions).

The idea explored in this paragraph is to fit a function to the cross-section, passing through the above mentioned characteristic points. The boundary conditions are given in the following way:

- At the inflection point (steepest transversal bed slope), the first derivative is equal to the friction slope. The following assumptions are made: (1) the angle of repose of coarse gravel is the same with dry material as with wet sediments, (2) the maximum transversal bed slope reaches its maximum possible value ϕ^* and (3) this maximal possible value is equal to the fraction angle multiplied with a factor depending on the main parameters.

- For some functions, the inflection point is assumed being at the center of the channel, for other ones it is assumed being at a distance $\xi \cdot B$ from the channel axis.

- Other functions fix the transversal bed slope either at the inner or outer bank equal to zero (translated by a first derivative of the function being equal to zero).

Looking at the right part of Figure 7.3, the elliptic shape of the curve is obvious. Therefore, functions fitting that kind of curve were searched. Possible functions are a semi-ellipse, the cosines hyperbolical (cosh) function or a quadratic polynomial function.

Elliptic and the cosh functions have a solution for $y = \text{fct}(h_s/r)$, but they cannot be integrated. Therefore polynomial functions were chosen. The following paragraphs summarize the investigated functions. Out of a large number of tested parameters, only the best solutions are documented for each case.

---

1. This can be explained by some coarse sediments remaining next to the outer wall. In addition, the secondary current may be less important in the "corner" between the vertical side wall and the channel bed, leaving coarse sediments in this zone.

Cross section in the upper scour hole

Radius from center of the bend [m]
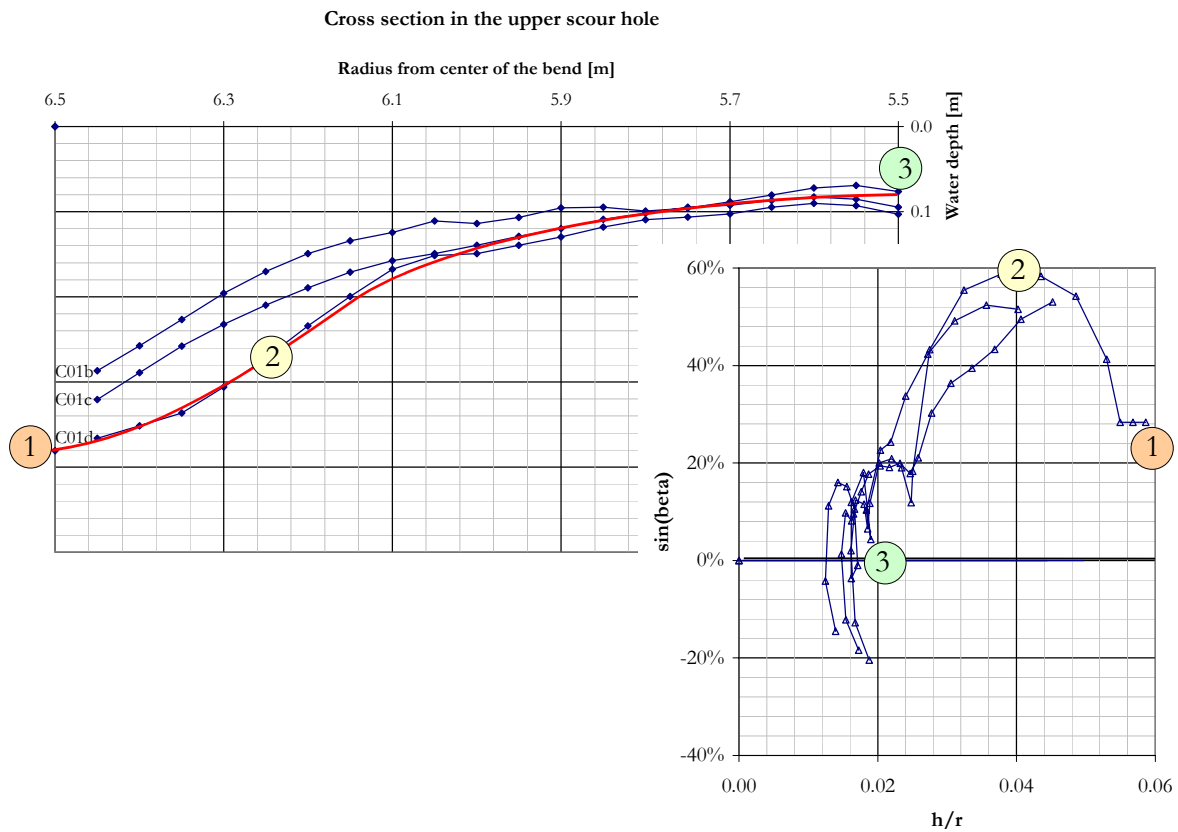
Figure 7.3: Characteristic points in a cross-section profile at the (upstream) maximum scour location
on top: cross-section in the upper scour; bottom right: transversal bed slope as a function of h/r

a) Polynomial function of the 3rd degree - centered

First a centered polynomial function is analyzed:

$$h_s = h_s(r) = \frac{c_1}{3} \cdot (r - c_2)^3 + c_3(r - c_2) + c_4 \tag{7.8}$$

$$\frac{dh_s}{dr} = c_1 \cdot (r - c_2)^2 + c_3 \tag{7.9}$$

The boundary conditions are:

1. $dh_s(R_c)/dr = \tan\phi^*$: the maximum bed slope is $\tan\phi^*$, located on the channel axis.
2. $h_s(R_c) = h_m$: the water depth in the center of the channel is equal to the mean water depth in the cross-section.
3. $dh_s(r_i)/dr = dh_s(r_o)/dr = 0$: the transversal bed slope is equal to zero at the outer and inner side wall.

After introducing these boundary conditions in the above equations, the following result is obtained:

$$h_s = h_m + \tan\phi^* \cdot \left[-\frac{4}{3 \cdot B^2} \cdot (r - R_c)^3 + (r - R_c) \right] \tag{7.10}$$

$$\frac{dh_s}{dr} = \tan\beta = \tan\phi^* \cdot \left[-\frac{4}{B^2} \cdot (r - R_c)^2 + 1 \right] \tag{7.11}$$

Without any correction factor ($\tan\phi^* = \tan\phi$), a correlation of $R^2 = 0.70$ is obtained between measured and computed maximum scour depth (see Fig. 7.4). The introduction if a correction factor $\tan\phi^* = 3.2 \cdot V \cdot R_h / \sqrt{g \cdot B^3} \cdot \tan\phi$ does not bring a significant increase of the correlation ($R^2 = 0.72$).
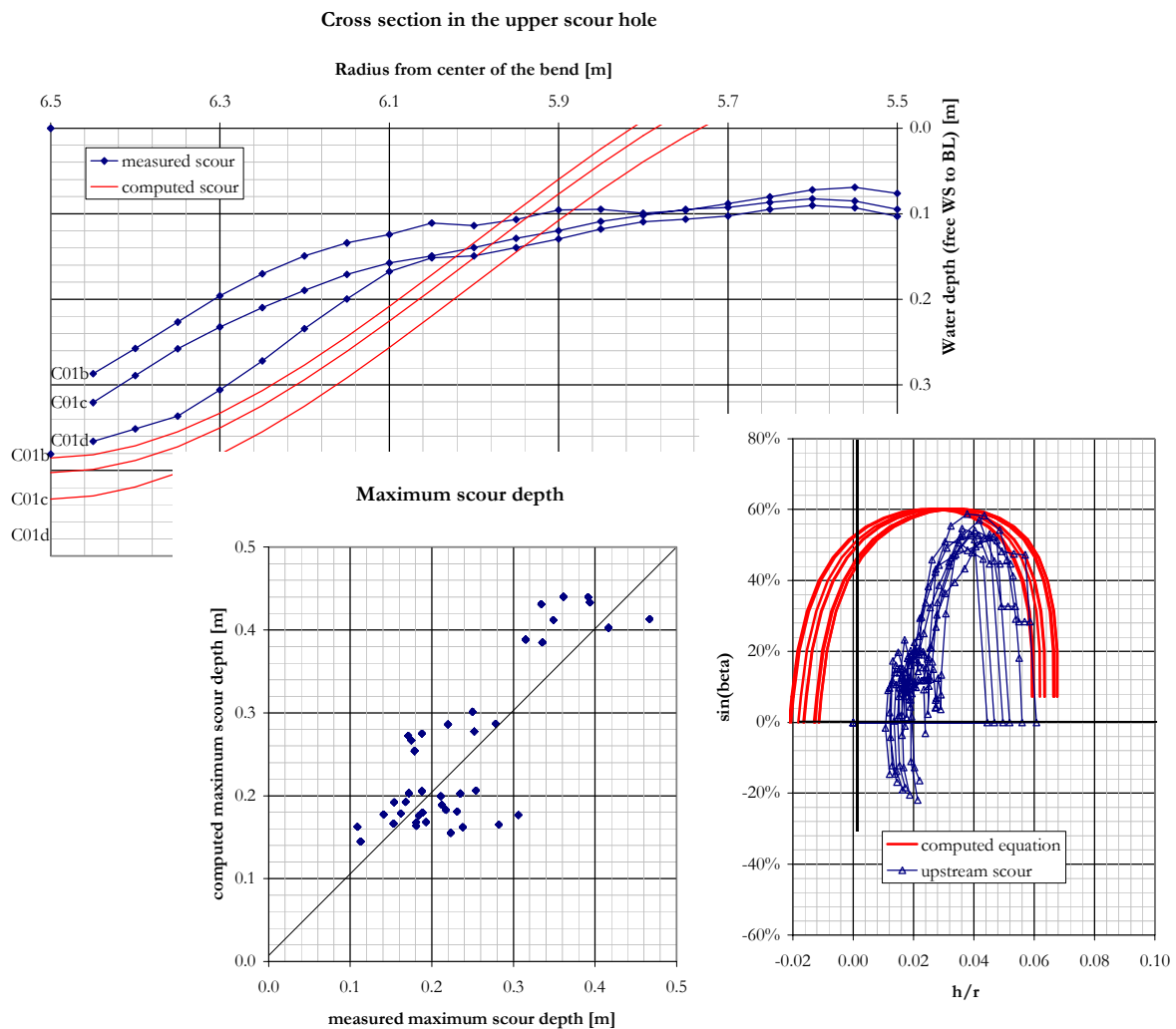
Figure 7.4: *Results of the centered polynomial equation (3rd degree) without correction factor (eq. 7.10, $\tan\phi^* = \tan\phi$) (see Fig. 7.1 and 7.3 for explanations)*

Looking at the cross-section profile, it is obvious that a polynomial equation centered on the axis of the channel cannot be the best solution. Therefore the next approach consisted in shifting the inflection point of the function towards the outer bank.

b) Polynomial function of the 3rd degree - uncentered

To shift the inflection point towards the outer bank, the coefficient $c_2 = R_c$ is replaced in equations 7.8 and 7.9 by $c_2 = R_c + \xi \cdot B$:

The boundary conditions become:
1. $dh_s(R_c + \xi \cdot B)/dr = \tan\phi^*$ (maximum bed slope).
2. $h_s(R_c + \xi \cdot B) = h_m$: the water depth at the inflection point is equal to the mean water depth in the cross-section.
3. $dh_s(r_o)/dr = 0$: the transversal bed slope is equal to zero at the outer side wall.

Equations 7.8 and 7.9 give the following equations after introduction of these boundary conditions:

$$h_s = h_m + \tan\phi^* \cdot \left[-\frac{4}{3 \cdot B^2 \cdot (1 - 2\xi)^2} \cdot (r - R_c - \xi B)^3 + (r - R_c - \xi B) \right] \qquad (7.12)$$

$$\frac{dh_s}{dr} = \tan\phi^* \cdot \left[-\frac{4}{B^2 \cdot (1 - 2\xi)^2} \cdot (r - R_c - \xi B)^2 + 1 \right] \qquad (7.13)$$

Without any correction factor $(\tan\phi^* = \tan\phi)$ and putting $\xi = 8\%$, a correlation of $R^2 = 0.71$ is obtained between measured and computed maximum scour depth (see Fig. 7.5). Introducing the following correction factor c and putting $\xi = 10\%$, increases the correlation to $R^2 = 0.82$ (compared to the maximum scour over the bend $h_{12, \, max}$):

$$\tan\phi^* = c \cdot \tan\phi = 20 \cdot \left(195 \cdot S_{e, \, all} + 1.1 \cdot \frac{h_m}{B} \right) \cdot \frac{V \cdot R_h}{\sqrt{g \cdot B^3}} \cdot \tan\phi \qquad (7.14)$$

It is obvious (Fig. 7.5) that the obtained equation does not fit well to the observed cross-section. Especially the inner bank elevation is much too high. There are two reasons for this:
- The fact that the bed slope at the outer wall is fixed to zero avoids a flatter bed slope.
- The fixed water depth (h_m) at the inflection point makes it impossible to get a vertical adjustment of the equation.

Therefore tests with the same equation and the same boundary conditions were carried out, but with a horizontal bed slope at the inner side wall. The coefficient $(1 - 2\xi)^2$ in equations 7.12 and 7.13 becomes $(1 + 2\xi)^2$. Putting $\xi = 16\%$ without any other correction factor gives a correlation of $R^2 = 0.74$. If the correction factor $c = 6.8 \cdot h_m/B - 4.5 \cdot V \cdot R_h/\sqrt{g \cdot B^3}$ is used with $\xi = 5\%$, the correlation can be increased to 0.78, which still is not very satisfying.

Cross section in the upper scour hole

Radius from center of the bend [m]

Maximum scour depth

Figure 7.5 contains three plots: a cross-section plot (measured scour vs computed scour), a maximum scour depth scatter plot, and a sin(beta) vs h/r plot with computed equation and upstream scour.
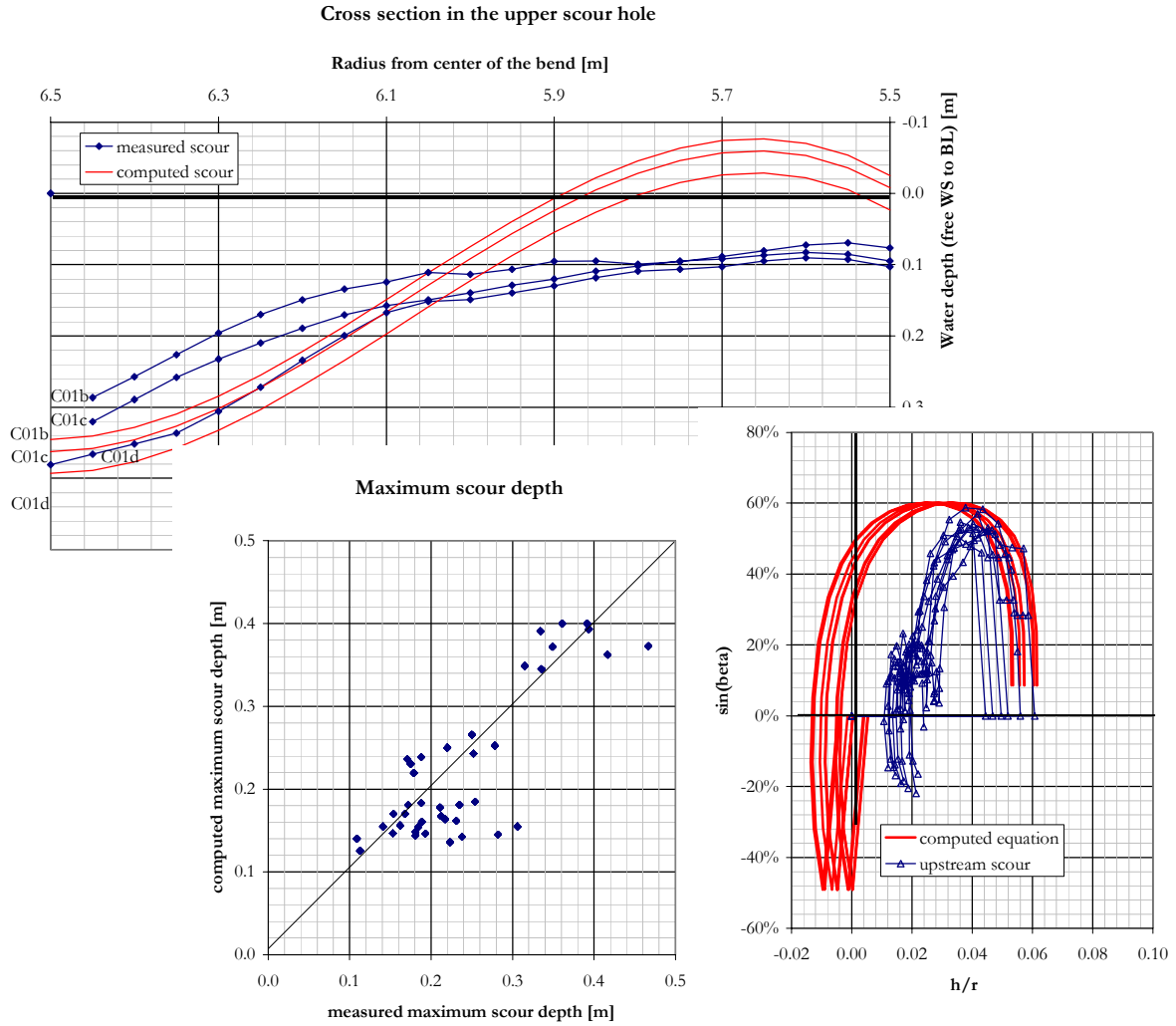
Figure 7.5: *Results of the uncentered polynomial equation (3rd degree) without correction factor (eq. 7.12,* $\tan\phi^* = \tan\phi$ *) (see Fig. 7.1 and 7.3 for explanations)*

c) *Polynomial function of the 3rd degree - uncentered with vertical adjustment*

In order to allow a vertical adjustment in the cross-section, the second boundary condition (average water depth at the inflection point) is replaced by the condition that the average water depth over the whole cross-section (integration) is equal to h_m.

The new boundary conditions are:

1. $dh_s(R_c + \xi B)/dr = \tan\phi^*$ (maximum bed slope).
2. The average water depth over the cross-section is equal to h_m

$$\int_{(R_c - B/2)}^{(R_c + B/2)} h_s(r)dh_s = B \cdot h_m$$

3. $dh_s(r_o)/dr = 0$ or $dh_s(r_i)/dr = 0$ the transversal bed slope is equal to zero at the outer or inner side wall.

Introducing these boundary conditions in equations 7.8 and 7.9 yields:

$$h_s = h_{corr} + \tan\phi^* \cdot \left[-\frac{4}{3 \cdot B^2 \cdot (1 + sig \cdot 2\xi)^2} \cdot (r - R_c - \xi B)^3 + (r - R_c - \xi B) \right] \quad (7.15)$$

$$\frac{dh_s}{dr} = \tan\phi^* \cdot \left[-\frac{4}{B^2 \cdot (1 - 2B)^2} \cdot (r - R_c - \xi B)^2 + 1 \right] \quad (7.16)$$

where

$$h_{corr} = h_m + \xi B \cdot \tan\phi^* \cdot \left[1 - \frac{1 + 4\xi^2}{3 \cdot (1 + sig \cdot 2\xi)^2} \right] \quad (7.17)$$

The sign sig is positive if the horizontal bed slope is assumed to be at the inner bank and negative at the outer bank. Looking at the results assuming a horizontal bed slope at the outer bank ($sig = -1$) and putting $\xi = 13\%$, without any correction the correlation is of $R^2 = 0.71$. It is interesting to see (Fig. 7.6) that the cross-section fits already much better to the measured data than without vertical correction. But the height of the bank is still overestimated whereas the maximum scour depth is quite well reproduced.
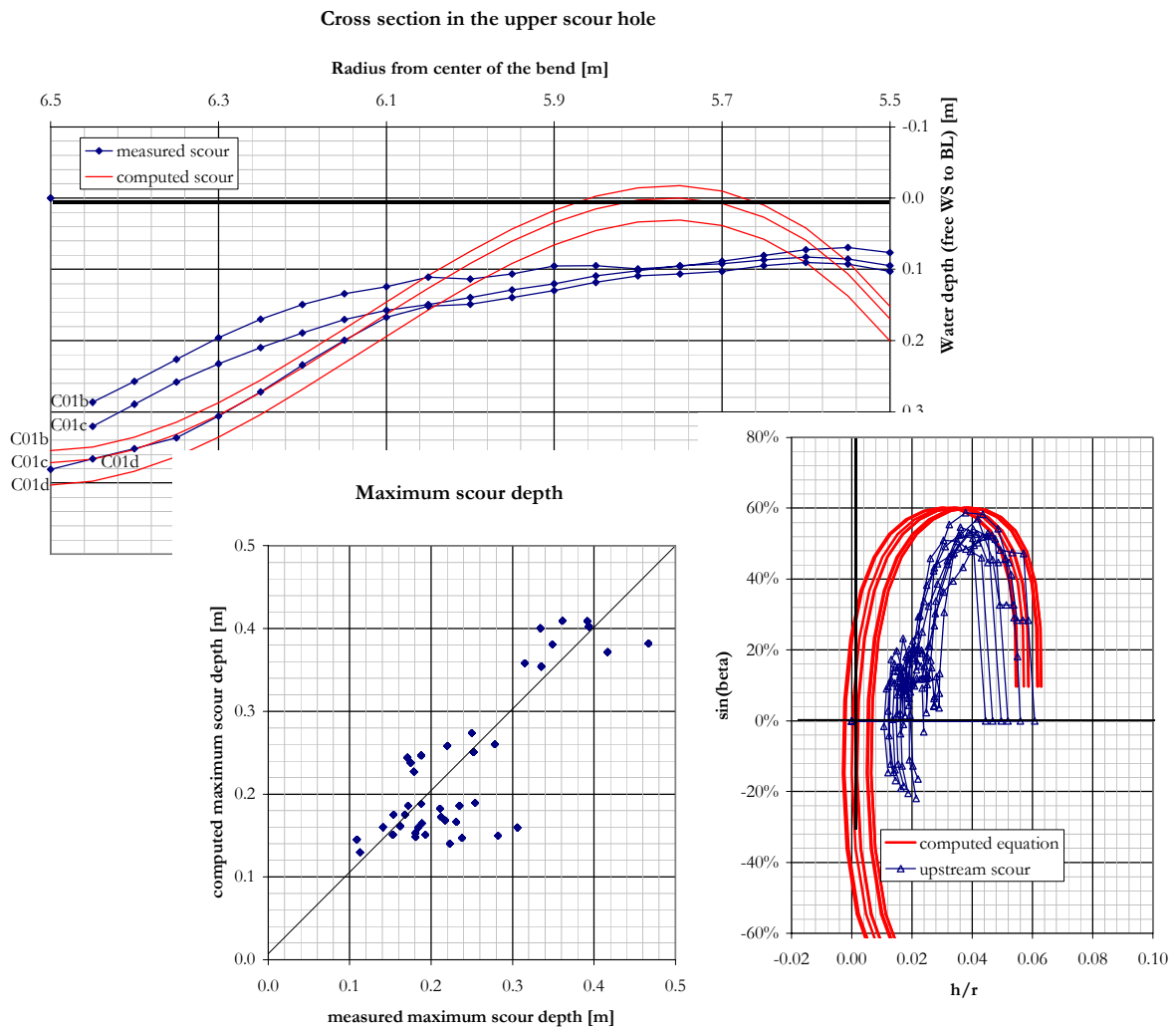
Figure 7.6: Results of the uncentered polynomial equation (3rd degree) with vertical correction and horizontal bed slope at the outer bank, without correction factor (eq. 7.15) (see Fig. 7.1 and 7.3 for explanations)

Adding the following correction factor c and choosing $\xi = 13\%$, allows to obtain a correlation of 0.82 (compared to $h_{12,\,max}$).

$$c = 79 \cdot \left(-0.074 \cdot \frac{R_c}{B} - 1.44 \cdot \frac{h_m}{B} + 1\right) \cdot \frac{V \cdot R_h}{\sqrt{g \cdot B^3}} \qquad (7.18)$$

If as boundary condition the bed slope at the inner bank is put to zero ($sig = 1$), a correlation of $R^2 = 0.70$ can be obtained without any corrections (for $\xi = -1\%$). Different equations allow to get a better correlation:

$$\xi = 87\%, \quad c = 420 \cdot \left(0.133 - 0.007 \cdot \frac{R_c}{B} - 0.235 \cdot \frac{h_m}{B}\right) \cdot \frac{V \cdot R_h}{\sqrt{g \cdot B^3}}, \quad R^2 = 0.844 \quad (7.19)$$

$$\xi = 880\%, \quad c = 290 \cdot \left(1 - 3.2 \cdot \frac{h_m}{B}\right) \cdot \frac{V \cdot R_h}{\sqrt{g \cdot B^3}}, \quad R^2 = 0.856 \qquad (7.20)$$
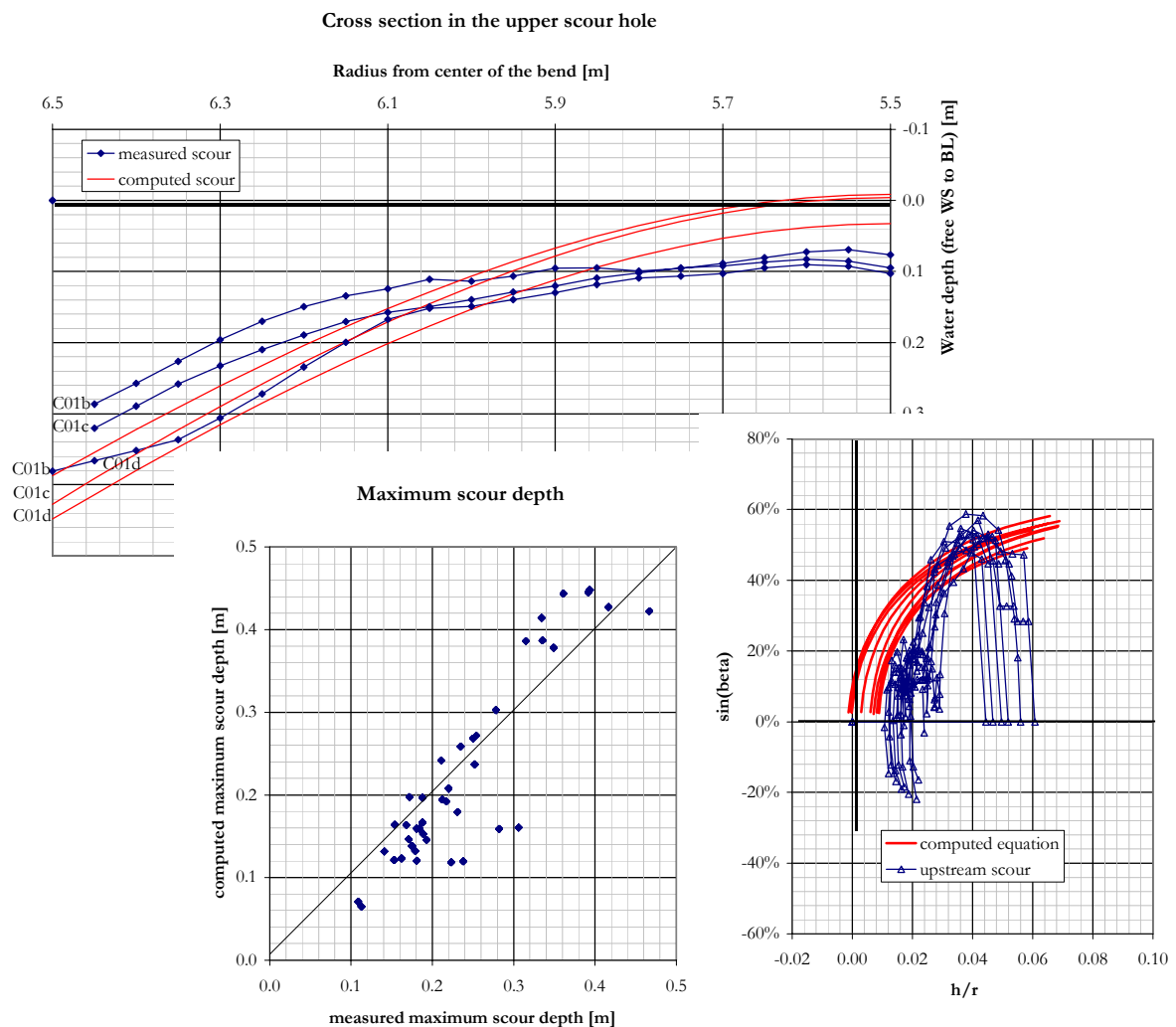
Figure 7.7:   Results of the uncentered polynomial equation (3rd degree) with vertical correction and horizontal bed slope at the inner bank, with correction factor (eq. 7.20) (see Fig. 7.1 and 7.3 for explanations)

The shape of the last equation gets quite close to the parabolic form of many traditional equations. To allow an appreciation of the quality of the obtained relation, an equation with corrections (eq. 7.20) is given on Fig. 7.7.

The so obtained correlation for the maximum scour depth can be compared to the empirical formula of PETER (1986), who obtains a correlation of 0.87 compared to the complete data set.

Hoping to obtain even higher correlations with other functions, the following two type of functions were explored: a polynomial function of the 3rd degree, but with additional terms ($y = x^3 + x^2 + x$) and a polynomial function of the 5th degree.

d) Polynomial function of the 3rd degree with additional terms - uncentered with vertical adjustment

The following function was used with the boundary conditions mentioned in paragraph c).

$$h_s = \frac{c_1}{3} \cdot (r - c_2)^3 + \frac{c_3}{2}(r - c_2)^2 + c_4 \cdot (r - c_2) + c_5 \tag{7.21}$$

Solving for the different constants, leads to:

$$h_s = h_m + \tan\phi^* \cdot \left[\frac{4}{3B^2} \cdot \frac{1}{4\xi^2 - 1} \cdot (r - R_c - \xi B)^3 + \frac{4}{B} \cdot \frac{\xi}{4\xi^2 - 1} \cdot (r - R_c - \xi B)^2 \right. \tag{7.22}$$
$$\left. + (r - R_c - \xi B) + \frac{B}{3} \cdot \frac{4\xi^3 - 3\xi}{4\xi^2 - 1} \right]$$

$$\frac{dh_s}{dr} = \tan\phi^* \cdot \left[\frac{4}{B^2} \cdot \frac{1}{4\xi^2 - 1} \cdot (r - R_c - \xi B)^2 + \frac{8}{B} \cdot \frac{\xi}{4\xi^2 - 1} \cdot (r - R_c - \xi B) + 1 \right] \tag{7.23}$$

The final solution has quite a strange behavior as far as the choice of ξ is concerned. At $\pm 50\%$ the curvature (second derivative) has a discontinuity. Therefore this value had to be avoided.

Without any correction factor the correlation is very low (below 0.50) and the order of magnitude of the predicted scour does not fit at all. The correlation (maximum scour) can be increased up to 0.81 by introducing a correction factor $c = 4.45 \cdot (690 \cdot S_{e, all} + 5.8 \cdot R_c / B - 79 \cdot h_m / B)$, but the shape of the predicted bed does not fit well to the measured one (Fig. 7.8). With other correction factors, the bed shape fits better, but with lower correlations up to 0.75.

Rendering the function more complicated does not bring the desired effect of a better prediction of the maximum scour nor a better fit to the transversal bed topography.

Cross section in the upper scour hole

Maximum scour depth
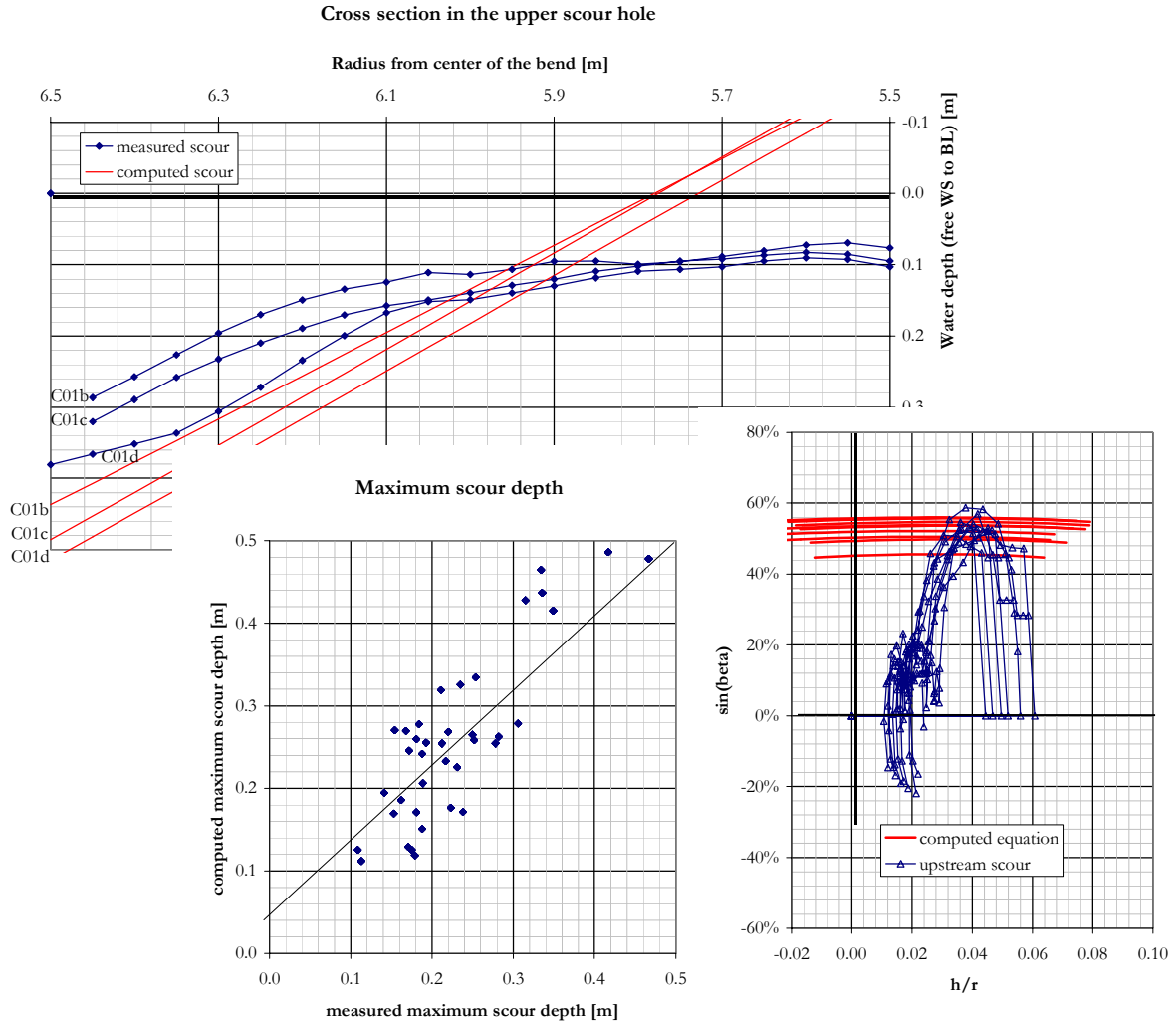
Figure 7.8: *Results of the uncentered polynomial equation (3rd degree with additional terms) with vertical correction, with correction factor (eq. 7.22) (see Fig. 7.1 and 7.3 for explanations)*

e) Polynomial function of the 5th degree - uncentered with vertical adjustment

The following function was used with the boundary conditions mentioned in paragraph c).

$$h_s = \frac{c_1}{5} \cdot (r - c_2)^5 + c_3 \cdot (r - c_2) + c_4 \tag{7.24}$$

Solving for the different constants, finally gives:

$$h_s = h_m + \tan\phi^* \cdot \left[\frac{-16}{5B^4} \cdot \frac{1}{(2\xi \pm 1)^4} \cdot (r - R_c - \xi B)^5 + (r - R_c - \xi B) \right. \tag{7.25}$$

$$\left. - \frac{B}{(2\xi \pm 1)^4} \cdot \left\{ -\frac{16}{5} \cdot \xi^5 - \frac{8}{3} \cdot \xi^3 - \frac{1}{5} \cdot \xi \right\} + \xi B \right]$$

$$\frac{dh_s}{dr} = \tan\phi^* \cdot \left[\frac{-16}{B^2} \cdot \frac{1}{(2\xi \pm 1)^4} \cdot (r - R_c - \xi B)^4 + 1 \right] \tag{7.26}$$

The expression $2\xi \pm 1$ uses the $+$ if the boundary condition of a horizontal slope is placed at the inner sidewall and $-$ if placed outside.

Without any correction factor, the following correlations can be obtained:
- $R^2 = 0.67$ for $\xi = 5\%$ for a horizontal slope at the outer bank
- $R^2 = 0.70$ for $\xi = -4\%$ for a horizontal slope at the inner bank

Adding a correction factor (defined by $\tan\phi^* = c \cdot \tan\phi$) the following results are obtained:
- for a horizontal transversal bed slope at the outer bank:

$$\xi = 8\%, \quad c = 20 \cdot \left(1 + 58 \cdot S_{e,\,all} - 2.35 \cdot \frac{h_m}{B}\right) \cdot \frac{V \cdot R_h}{\sqrt{g \cdot B^3}}, \quad R^2 = 0.850 \qquad (7.27)$$

- for a horizontal transversal bed slope at the inner bank:

$$\xi = 8\%, \quad c = 25 \cdot \left(1 + 47 \cdot S_{e,\,all} - 3.33 \cdot \frac{h_m}{B}\right) \cdot \frac{V \cdot R_h}{\sqrt{g \cdot B^3}}, \quad R^2 = 0.856 \qquad (7.28)$$
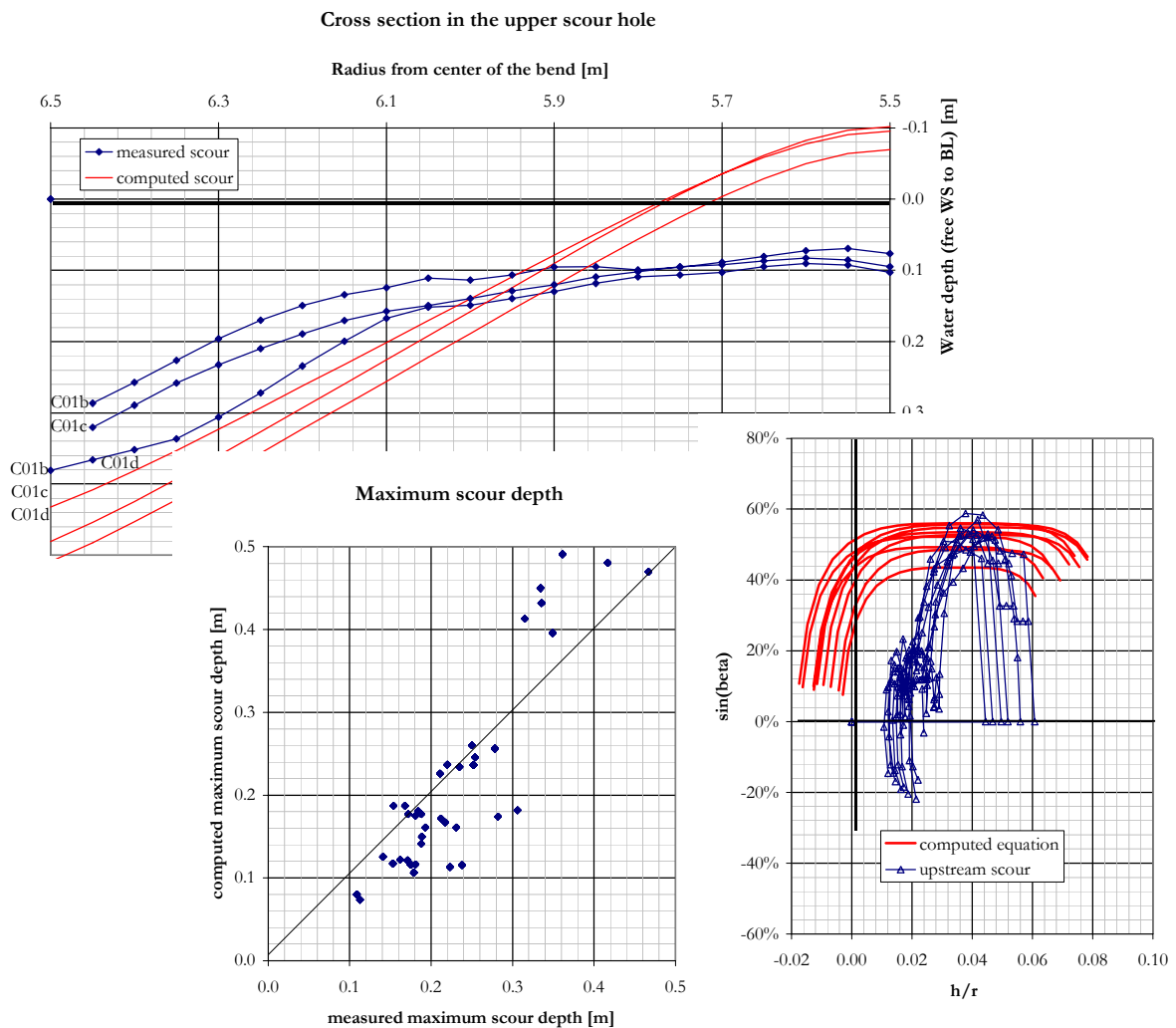
Figure 7.9: *Results of the uncentered polynomial equation (5th degree), horizontal bed slope at the inner bank, with correction factor (eq. 7.27) (see Fig. 7.1 and 7.3 for explanations)*

Cross section in the upper scour hole

Radius from center of the bend [m]

Maximum scour depth
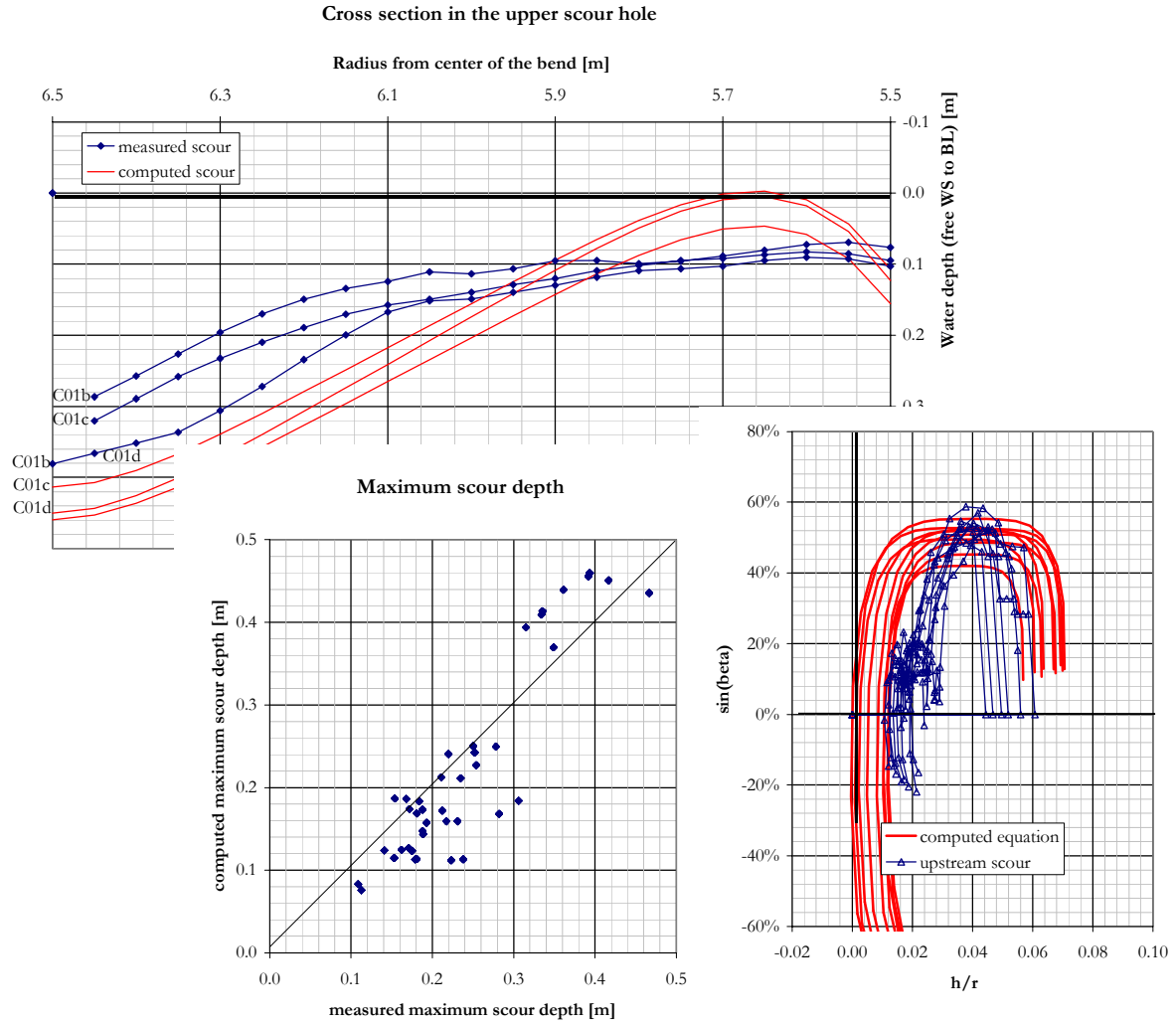
Figure 7.10: Results of the uncentered polynomial equation (5th degree), horizontal bed slope at the outer bank, with correction factor (eq. 7.28) (see Fig. 7.1 and 7.3 for explanations)

f) Polynomial function of the 3rd degree without restricted bed slope at the banks

A last equation based on the shape of the cross-section in radial direction was tested: a polynomial function of the 3rd degree like the one used in paragraph a) but without fixing the boundary condition of a horizontal bed slope at the outer or inner bank. The cross-section was adjusted in vertical direction (average flow depth over the cross-section corresponds to the average water depth).

The constants of equations 7.8 and 7.9 become $c_1 = c_c/B^2$ (to respect the units), $c_2 = R_c + \xi B$, $c_3 = \tan\phi^* = c \cdot \tan\phi$ and $c_4 = h_m + c_1/12 \cdot B^3 \cdot (\xi + 4\xi^3) + \xi B \tan\phi$. This leads to the following equations.

$$h_s = h_m + \frac{c_c}{12 \cdot B^2} \cdot [4 \cdot (r - R_c - \xi B)^3 + (\xi + 4\xi^3) \cdot B^3] + \tan\phi^*(r - R_c) \qquad (7.29)$$

$$\frac{dh_s}{dr} = \frac{c_c}{B^2} \cdot (r - R_b - \xi B)^2 + \tan\phi^* \qquad (7.30)$$

There are finally three parameters which need to be fixed: c_c, c (in $\tan\phi^*$) and ξ. The best found combination of the different parameters is: $\xi = 8.6\,\%$, $c = 0.843 - 0.272 \cdot V \cdot R_h / \sqrt{g \cdot B^3}$ and $c_c = 28 \cdot V \cdot R_h / \sqrt{g \cdot B^3} - 9 \cdot h_m / B - 10$. But the correlation for the maximum scour depth is only 0.76. For all tested combinations of parameters, the shape of the cross-section fitted badly to the measured bed level.

g) Conclusions

By using polynomial functions to fit an equation to the cross section shape quite decent correlations can be obtained. The maximum scour depth can be predicted with good precision, but it is rather difficult to obtain a good fit to the shape of the cross section. Polynomial functions of the third degree give the best results. But a radial and vertical adjustment is necessary to obtain a satisfying scour formula.

Introducing additional terms (e.g. $x^3 + x^2 + x$ instead of $x^3 + x$) does not lead to a better prediction capability but to an important increase of the complexity of the formula. The same observation applies for polynomes of a higher degree (the fifth degree was analyzed). They only result in more complicated equations without improving the prediction of the maximum scour depth, nor the fit to the cross section shape.

The best results were obtained with equation 7.15 and the constant given by equation 7.20. Combining the two equations and performing some simplifications results in:

$$h_s = h_m + \tan\phi \cdot c \cdot \left[6.23 \cdot B - \frac{(r - R_c - 8.8B)^3}{260 \cdot B^2} + (r - R_c - 8.8B)\right] \tag{7.31}$$

$$h_{s,\,max} = h_m + \tan\phi \cdot c \cdot [0.129 \cdot B] \tag{7.32}$$

where
$$c = 290 \cdot \left(1 - 3.2 \cdot \frac{h_m}{B}\right) \cdot \frac{V \cdot R_h}{\sqrt{g \cdot B^3}} \tag{7.33}$$

The local scour depth depends on the ratio water depth to channel width and the dimensionless parameter $V \cdot R_h / \sqrt{gB^3}$. The maximum lateral bed slope is given at the inflection point of the polynomial function with a value of $\tan\phi^* = c \cdot \tan\phi$. It is important to note that the equation for the maximum scour depth does not consider the radius of curvature R_c.

7.3.4 Approach based on the similitude and approximation theory

The analysis performed in the present paragraph served to determine parameters having an important influence on the scour phenomenon. The similitude and approximation theory of KLINE (1965) is based of a dimensional analysis[1]. Kline calls the dimensionless parameters (usually formed by ratios of primary and secondary parameters with units[2]) pi's.

The pi-theorem makes the following statements:

Given a relation among m parameters of the form

$$f_1(q_1, q_2, ..., q_m) = 0 \qquad (7.34)$$

an equivalent relation expressed in terms of n non dimensional parameters can be found of the form

$$f_2(\pi_1, \pi_2, ..., \pi_n) \qquad (7.35)$$

where the number n is given by the relation

$$n = m - k$$

where m is the number of q's in equation 7.34, and k is the large number of parameters contained in the original list of parameters $q_1, q_2, ..., q_m$ that will not combine in any non dimensional form. Generally k is equal to the minimum number of independent dimensions needed to construct the dimensions of all parameters q_i.

The parameters q should be independent. If they are not, additional conditions needs to be introduced to compensate for the redundancy. The compensation is normally compensated in the following manner. For each redundant dimension either a physical constant with the same dimensions needs to be introduced, or the number of dimensions has to be decreased by one $(k - 1)$.

HUNTLEY (1953) extended the pi-theorem by restricting the combination to parameters acting in the same direction.

The method of similitude is based on the following basic steps:

1. The forces that are supposed to be important in a given problem are enumerated, including the dependent and all the independent forces. Each of these forces is then expressed in terms of the parameters of the problem by physical or dimensional arguments.
2. The pertinent non dimensional groups (pi's) are constructed by forming ratios of these forces and including enough length ratios to ensure geometric similarity.

The number of pi's constructed from force ratios are equal to the number of independent forces. For convenience it is useful to introduce the dependent force only into one ratio in order to provide an explicit rather than an implicit solution to the problem.

---

1. also known as Pi-theorem, Buckingham's method or Bridgman's method.
2. An example for a primary parameter is the length, for a secondary parameter the velocity since it is derived from a length and a time span.

Based on the hypothesis that complete similarity will be contained in a flow field if geometric, kinematic and dynamic similarity are all achieved and that these three types of similarities will occur if the geometry is similar and all the forces are similar. Or expressed in a more general way: If two systems obey the same set of governing equations and conditions and if the values of all parameters in these equations and conditions are made the same, then the two systems must show similar behavior provided only that a unique solution to the set of equations and conditions exists.

In stream direction, the considered forces[1] acting on a control volume of water over the whole channel width are (Fig. 7.11):

- Drag force D with the dimension of $\rho \cdot V^2 \cdot L^2$
- Bed shear stress / friction force F_S with the dimension of $\rho \cdot V^2 \cdot L^2$
- Gravity force G with the dimension of $\rho \cdot g \cdot L^3$

where ρ is the density, L the length, V the velocity and g the local acceleration of gravity.
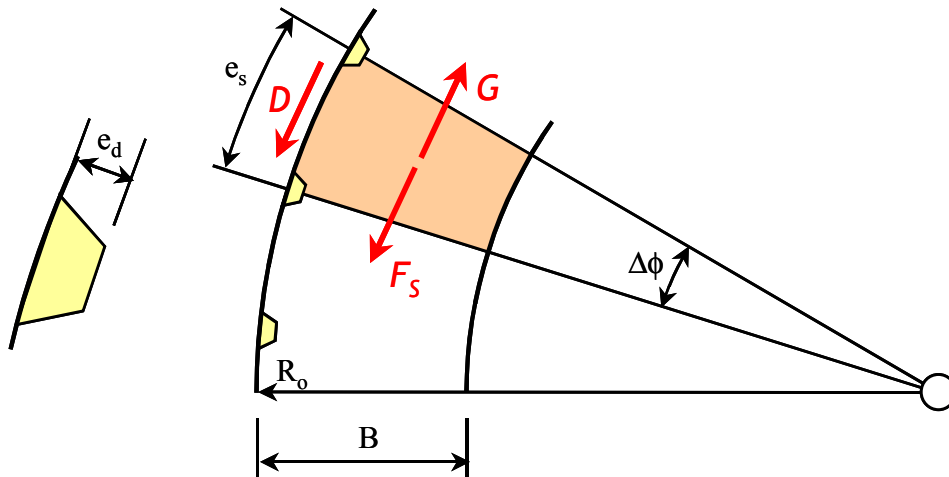
Figure 7.11: Tangential forces acting on a control volume

The comparison of the tangential forces assumes that the flow is uniform in the control volume and that the difference in momentum over the control volume is zero. On the following pages the situation with macro-roughness is analyzed first. The so obtained equation is then generalized to the case without macro-roughness.

1)   *With macro-roughness*

Considering the macro-roughness on the side wall, the drag force D is proportional to the mass density of the water, to the square of the velocity (for practical reasons we take the mean velocity), the rib surface opposed to the flow (depth of the ribs e_d x scour depth h).

$$D \propto \rho_w \cdot V_m^2 \cdot e_d \cdot h \tag{7.36}$$

---

1. The drag at the inner wall was neglected, since the velocities are much weaker than the ones along the outer wall.

The bed friction force is proportional to the bed friction $\tau_0 = \rho_w \cdot g \cdot R_h \cdot S_e = \rho_w \cdot V^{*2}$ and the surface of the considered control volume $S = \Delta\phi \cdot R_o^2 - \Delta\phi \cdot R_i^2$. Replacing R_o and R_i by $R_c \pm B/2$, we finally obtain $S = 2 \cdot \Delta\phi \cdot B \cdot R_c$ and:

$$F_S \propto \tau_0 \cdot \Delta\phi \cdot B \cdot R_c = \rho_w \cdot V^{*2} \cdot \Delta\phi \cdot B \cdot R_c \tag{7.37}$$

The gravity force is proportional to the volume of the water in the control volume $h_m \cdot \Delta\phi \cdot B \cdot R_o$ and the water density.

$$G \propto \gamma_w \cdot h_m \cdot \Delta\phi \cdot B \cdot R_c \cdot S_e \tag{7.38}$$

The dependant parameter, the scour depth is contained in the drag force D. The equilibrium of the forces writes:

$$G = D + F_S \tag{7.39}$$

Dividing this equation by G yields:

$$1 = \frac{D}{G} + \frac{F_S}{G} \tag{7.40}$$

Introducing the proportionalities 7.36, 7.37 and 7.38 in equation 7.40 results in:

$$1 = \frac{\rho_w \cdot V_m^2 \cdot e_d \cdot h_s}{\rho_w \cdot g \cdot h_m \cdot \Delta\phi \cdot B \cdot R_c \cdot S_e} + \frac{\rho_w \cdot V^{*2} \cdot \Delta\phi \cdot B \cdot R_c}{\rho_w \cdot g \cdot h_m \cdot \Delta\phi \cdot B \cdot R_c \cdot S_e} \tag{7.41}$$

Since $\Delta\phi \cdot R_c$ is the spacing of the ribs e_s equation 7.41 becomes:

$$1 = \frac{\rho_w \cdot V_m^2 \cdot e_d \cdot h_s}{\rho_w \cdot g \cdot h_m \cdot e_s \cdot B \cdot S_e} + \frac{\rho_w \cdot V^{*2} \cdot e_s \cdot B}{\rho_w \cdot g \cdot h_m \cdot e_s \cdot B \cdot S_e} \tag{7.42}$$

Considering the shields parameter (eq. 3.42) $\theta = V^{*2}/((s-1) \cdot g \cdot d)$, V^{*2} can be replaced in the above equation by $\theta \cdot (s-1) \cdot g \cdot d_{90}$.

$$\frac{h_s}{B} = \frac{e_s}{e_d} \cdot \frac{g \cdot h_m}{V_m^2} \cdot S_e \cdot \left(1 - \theta \cdot (s-1) \cdot \frac{d_{90}}{h_m} \cdot \frac{1}{S_e}\right) = \frac{e_s}{e_d} \cdot \left(\frac{S_e}{Fr^2} - \frac{\theta}{Fr_d^2}\right) \tag{7.43}$$

In this equation, most parameters which had a high correlation with the maximum scour can be found: ratios containing the velocity appear as Froude number ($V_m/\sqrt{g \cdot h_m}$ and Fr_d), the overall bed slope S_e, the rib spacing e_s and additional parameters like the ratio of the sediment to the water density s, the characteristic grain size d_{90} and the Shields parameter θ. The geometry of the channel, especially the radius of the bend is missing. Another point of interest is the observation that equation 7.43 (right part) contains three terms: one to characterize the macro-roughness, a second one to give the flow conditions and the last one to describe the bedload and sediment related characteristics.

But there is a problem in the first term: the ratio e_s/e_d leads to a division by zero for a rib-depth $e_d = 0$ without macro-roughness. Therefore it is useful to replace the rib depth by another length (moreover the analysis of the parameters has shown that this parameter does not show an important correlation with the tests). If the mean water depth is used, h_m in the Froude number is "neutralized". Since the geometry of the channel is not represented, it might be interesting to replace e_d by the radius of curvature or the channel width or even a combination of both

$(\sqrt{B \cdot h_m})$. The ratios e_s/B, e_s/R_c and $e_s^2/B \cdot R_c$ shows correlations of $R^2 = 0.677$, 0.707 and 0.728 compared to the maximum scour depth. With this modification, equation 7.43 can be written as:

$$\frac{h_s}{B} = \frac{e_s^2}{B \cdot R_c} \cdot \left(\frac{S_e}{Fr^2} - \frac{\theta}{Fr_d^2} \right) \tag{7.44}$$

Unfortunately it is impossible to get satisfying predictions with this equations or slightly modified ones, namely by testing other ratios for the macro-roughness term, by introducing adjustment constants for the whole equation and for one of the terms in brackets. The highest obtained correlation remains remained below 0.5.

2) *Without macro-roughness*

Without macro-roughness, the drag force D acting on the ribs is replaced with a friction force acting on the surface of the outer side wall $(\Delta\phi \cdot R_o \cdot h)$. The friction along the inner side wall is neglected since the water depth is small on the inner bank and the influence on the scour depth can be neglected. A dimensionless friction coefficient C_F is introduced.

$$D \propto \rho_w \cdot V_m^2 \cdot C_F \cdot \Delta\phi \cdot R_o \cdot h \tag{7.45}$$

Forming the ratios in equation 7.40 by introducing the proportionalities 7.37, 7.38 and 7.45 yields:

$$1 = \frac{\rho_w \cdot V_m^2 \cdot C_F \cdot \Delta\phi \cdot R_o \cdot h_s}{\rho_w \cdot g \cdot h_m \cdot \Delta\phi \cdot B \cdot R_c \cdot S_e} + \frac{\rho_w \cdot V^{*2} \cdot \Delta\phi \cdot B \cdot R_c}{\rho_w \cdot g \cdot h_m \cdot \Delta\phi \cdot B \cdot R_c \cdot S_e} \tag{7.46}$$

After some simplifications (like for the case with macro-roughness), we obtain:

$$1 = \frac{V_m^2 \cdot C_F \cdot R_o \cdot h_s}{g \cdot h_m \cdot B \cdot R_c \cdot S_e} + \frac{V^{*2}}{g \cdot h_m \cdot S_e} \tag{7.47}$$

And finally the following equation for the maximum scour depth is found:

$$\frac{h_s}{B} = \frac{1}{C_F} \cdot \frac{R_c}{R_o} \cdot \frac{g \cdot h_m}{V_m^2} \cdot S_e \cdot \left(1 - \theta \cdot (s-1) \cdot \frac{d_{90}}{h_m} \cdot \frac{1}{S_e} \right) = \frac{R_c}{C_F \cdot R_o} \cdot \left(\frac{S_e}{Fr^2} - \frac{\theta}{Fr_d^2} \right) \tag{7.48}$$

This equation has the same layout as the one taking into account the scour reduction due to the vertical ribs on the outer bank. Furthermore the radius of curvature appears as a parameter in this equation. The radius to channel width ratio is hidden in the ratio R_c/R_o ($R_o = R_c + B/2$).

The last parenthesis in equations 7.43 and 7.48 can also be written as:

$$\frac{S_e}{Fr^2} - \frac{\theta}{Fr_d^2} = \frac{S_e}{Fr^2} - \left(\frac{V^*}{V} \right)^2 \tag{7.49}$$

since $\theta = Fr^{*2} = (Fr_d \cdot V^*/V)^2$.

If we compare the computed maximum scour depth (equation 7.48) to the measured values, it is difficult to obtain satisfying correlations. The best fit was obtained with:

$$\frac{h_s}{B} = \frac{R_c}{0.189 \cdot R_o} \cdot \left(\frac{S_e}{Fr^2} + 6.3 \cdot \frac{\theta}{Fr_d^2} \right), \quad R^2 = 0.724 \tag{7.50}$$

7.3.5   Genetic algorithm

With the evolution of informatics, new techniques for data treatment were developed. One of these techniques are genetic algorithms allowing to search for functions fitting to a given data set. It is important to use genetic algorithms not like a magic black box, but knowing the important parameters for the process to obtain a result which has a physically correct form. To analyze the data in this research study, a genetic program called GPKernel (Genetic Programming Kernel) developed by Maarten Keijzer and Vladan Babovic at the Danish Hydraulic Institute (DHI) was used.

The program looks for mathematical relations based on a set of input parameters, constants, operations, genetic parameters and on user-defined target(s)[1]. The genetic parameters like for example the size of the population, the number of generations to produce or time of run, different probabilities of mutations and genetic operations can be modified. A big advantage of the program is the possibility to perform a dimensionally aware genetic programming (KEIJZER & BABOVIC, 1999). Additional information on GPKernel can be found in the Users Manual (RODRIGUEZ AGUILERA, 2000).

The following tables (Appendix 12.1 and 12.2) give a small subset (< 0.1%) of obtained results. It can be seen that most of the previously identified main parameters appear in the equations. The following characteristics are found in the maximum scour equation: Re, Fr, Fr^*, V^*/V, S_e and h_m/B. In the relation giving the first and second scour locations, some other characteristics are dominant: σ (Peter found this parameter, too), Fr_d, R_c/B, h_m/B and d_{90}/h_m.

The plots in Tables 7.4 and 7.5 compare the computed and the measured relative maximum scour, and the two scour locations. All available data are included in the plots (with the tests of PETER, 1986).

a)   Tests without macro-roughness

For the equations obtained with the genetic algorithm it is sometimes difficult to get a plausible physical explanation of the phenomena. If we analyze the first equation for the maximum scour depth (Appendix 12.1, ID 1), we obtain after regroupment of the terms and omission of terms without significant influence:

$$\frac{h_{s,\,max}}{h_m} = \left[2.4 \cdot \sigma + 1.2 \cdot Fr \cdot Fr_d \cdot \frac{R_c}{B} \cdot \left(\frac{1}{\sigma^3} + \frac{1}{\sigma^4}\right)\right] \cdot \left(\frac{d_{90}}{h_m} + Fr^* - \frac{2 \cdot h_m}{B} + \theta\right) + 1.85 \qquad (7.51)$$

This equation has a correlation of $R^2 = 0.832$ which is quite high, but less that what was obtained previously (equation 7.20). Looking for a physical explanation of this equation, some parameters show the right tendency: the relative scour increases with increasing Froude numbers, Shields parameter and increasing mean flow depth to width ratio. But a smaller radius of curvature should lead to an increase of the scour depth and the equation gives an opposite tendency. Therefore this formula will not be considered for the final evaluation.

---

1. The program also allows multi target searches.
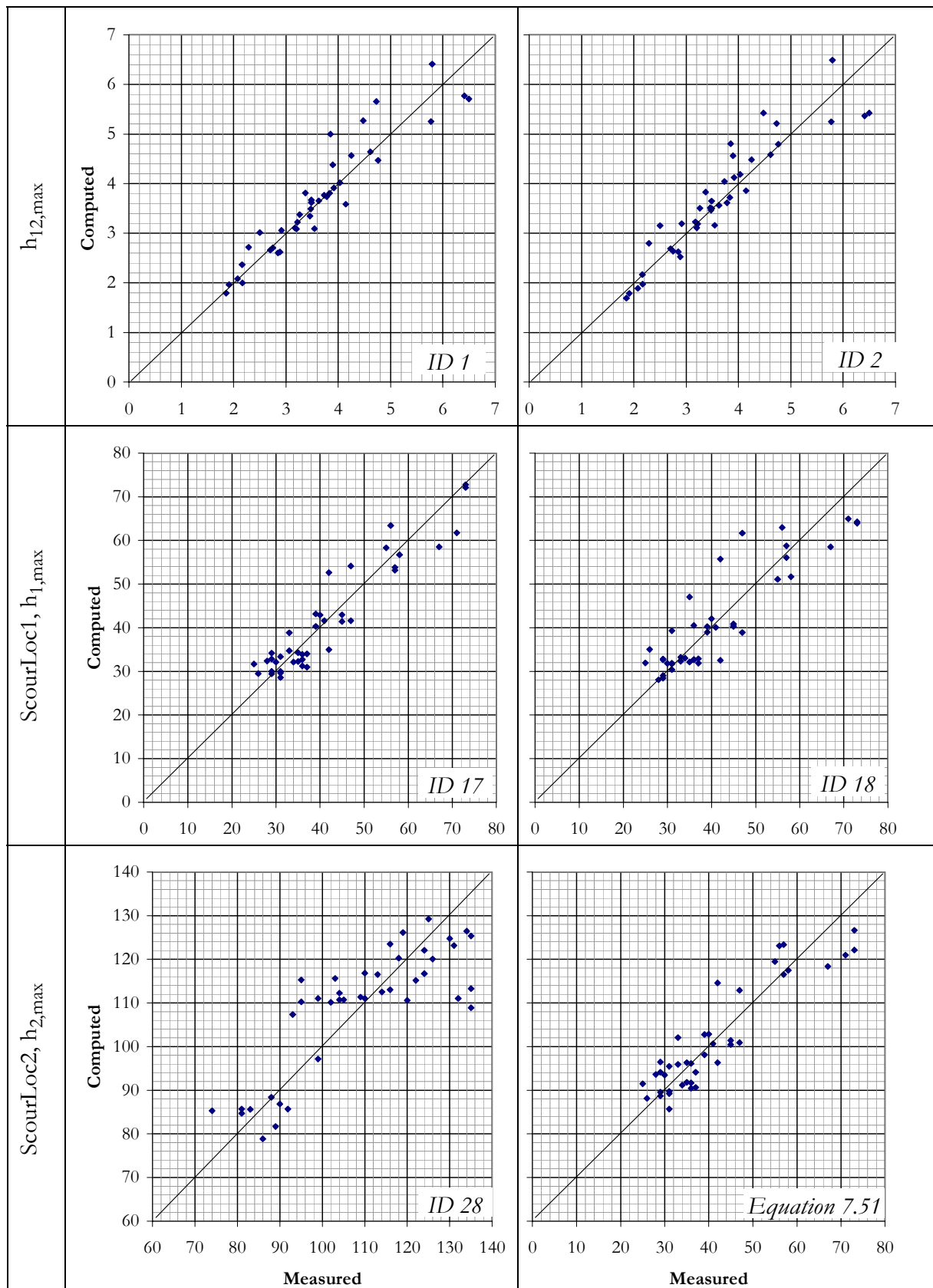
Table 7.4:   Plots of the maximum relative scour depth obtained with GPKernel - without macro-roughness
See also Appendix 12.1 (ID 1 corresponds to eq. 7.28, ID 17 to eq. 7.30 and ID 28 to eq. 7.35)

Considering the second equation (Appendix 12.1, ID 2), a correlation of $R^2 = 0.825$ was obtained, after some simplifications:

$$\frac{h_{s,max}}{h_m} = 1.63 \cdot \frac{\frac{d_{90}}{h_m} \cdot Fr_d \cdot \left(\frac{V^*}{V} + \frac{\theta}{\sigma^2}\right) + \frac{\theta^2}{\sigma^2} + 2 \cdot \frac{V^*}{V} \cdot \frac{B}{R_c}}{\left(\frac{h_m}{B}\right)^2 - \theta^2 + \frac{V^*}{V} \cdot \frac{B}{R_c}} \tag{7.52}$$

All contained ratio have a physical meaning: d_{90}/h_m is the relative roughness, V^*/V the influence of the velocity distribution, θ/σ^2 gives the influence of the non-uniformity of the sediments on the Shields stress and B/R_c can be interpreted as the influence of the curvature.

But since the correlation is not exceptional, no further analysis of this equation will be performed.

Lets analyze the formulae proposed for the computation of the location of the first scour. After simplifications, the following equation is obtained (Appendix 12.1, ID 17):

$$\alpha_1 = 0.94 \cdot \left[\frac{\sigma\left(\tan\phi - \frac{d_{90}}{h_m}\right)}{\frac{h_m}{B} \cdot \left(Fr + \frac{V^*}{V}\right)} + \frac{\sigma \cdot S_e \cdot Fr_d \cdot \left(\sigma - \frac{R_c}{B} + 3.75\right)}{\sigma - Fr_d} \cdot \frac{\frac{R_c}{B}(Fr_d - \sigma)}{\frac{R_c}{B} - \sigma} + \frac{Fr_d}{\frac{V^*}{V}}\right] + 2.5 \tag{7.53}$$

with a correlation of $R^2 = 0.885$. The task of searching a physical signification of the formula is a big challenge. Some influences like the width of the grain size distribution σ, the densimetric Froude number are correctly represented. Performing some important simplifications and omissions, results in the following equation:

$$\alpha_1 = \sigma \cdot \left(0.58 \cdot \frac{B}{h_m} + 12.7 \cdot \frac{S_e}{\sigma - Fr_d}\right) + 1.4 \cdot Fr_d \cdot \frac{V}{V^*} - 6.6, \quad R^2 = 0.829 \tag{7.54}$$

For this equation it is much easier to explain the physical phenomena. Like for the previous equation, the scour shifts downstream with increasing σ. This tendency was also observed by Peter (1986, see equation 3.119 on page 55). With higher velocities (and consequently higher Froude numbers), steeper slopes and higher width to depth ratio, the first scour slightly shifts in the downstream direction. This equation can be recommended for the determination of the first scour location.

Examining the results for the second scour location (Appendix 12.1, ID 28), results in the following "simplified" equation depending on only two parameters, the density Froude number and the ratio radius of curvature to channel width:

$$\alpha_2 = \left(9.36 + Fr_d - \frac{R_c}{B}\right) \cdot \left(9.73 + \frac{R_c}{B}\right) - \frac{0.5 \cdot \frac{R_c}{B} + 0.15 \cdot Fr_d \cdot \frac{B}{R_c}}{Fr_d - \frac{0.75}{Fr_d} - 1.468 \cdot \frac{R_c}{B}}, \quad R^2 = 0.676 \tag{7.55}$$

After rearrangement, increasing the clarity of the equation, a slightly better correlation can be found for:

$$\alpha_2 = 12.6 \cdot Fr_d - 0.9 \cdot \left(\frac{R_c}{B}\right)^2 - \frac{0.8}{Fr_d^2 - 1.5 \cdot Fr_d \cdot R_c/B - 0.5} \cdot \frac{R_c}{B} \cdot Fr_d + 86.5, \; R^2 = 0.678 \quad (7.56)$$

If the third term[1] is omitted, we obtain the following equation, having still quite a good prediction capability, but with a considerably simplified formula:

$$\alpha_2 = 12.6 \cdot Fr_d - 0.9 \cdot \left(\frac{R_c}{B}\right)^2 + 91.6, \; R^2 = 0.602 \quad (7.57)$$

For practical applications, the use of this last equation is recommended since the numerically sensitive term found in equation 7.56 is eliminated. The correlation is still much better than the one proposed by other authors (the best relation proposed by Peter, 1986 had a correlation of less than $R^2 = 0.2$).

---

1. The third term is quite sensitive to the choice of the constants in the denominator (1.5 and -0.5).

b) With macro-roughness

By analyzing the first equation for the maximum scour depth with macro-roughness (Appendix 12.2, ID 101), it can be seen (after some regroupments and simplifications) that the first term e_d/e_s can be left away without significant changes in the precision of the result. The relation:

$$\frac{h_{s,\,max}}{h_m} = \left[\frac{0.85 \cdot S_e \cdot Fr_d}{3 \cdot \dfrac{e_d}{e_s} + \tan^2\phi \cdot Fr^* - 2 \cdot \tan\phi \cdot Fr^{*2}} + Fr^* + \tan\phi \cdot \frac{V^*}{V}\right] \cdot \frac{1}{\dfrac{h_m}{B} + \dfrac{V^*}{V}} + 0.5 \quad (7.58)$$

has a correlation of $R^2 = 0.893$. A plausibility check of the different parameters shows that the observed tendencies are confirmed by this equation: the relative scour increases with increasing bed slope, with increasing Froude numbers ($Fr_d \approx 10 \cdot Fr^*$), with decreasing roughness depth to spacing ratio (up to an optimum spacing, afterwards it should decrease again). It was observed that with increasing mean water depth to width ratio, the scour decreased (Figure 6.3 on page 121). But the equation is quite complex.

The analysis of another maximum scour formula that obtained a good correlation (Appendix 12.2, ID 112) results in the following simplified relation:

$$\frac{h_{s,\,max}}{h_m} = 0.862\left(\frac{1}{1.4}\left(\frac{V^*}{V} + \theta\right)\theta \cdot Fr\frac{e_s}{R_h} + \sigma\left(Fr^* - 2\frac{h_m}{B}\right) - \left(\theta \cdot Fr - \frac{h_m}{B}\right)Fr^2 + Fr\right) + 1.33 \quad (7.59)$$

Since the third and the fourth term have almost no influence on the correlation they are removed.

$$\frac{h_{s,\,max}}{h_m} \propto \frac{1}{1.4} \cdot \left(\frac{V^*}{V} + \theta\right) \cdot \theta \cdot Fr \cdot \frac{e_s}{R_h} + \sigma \cdot \left(Fr^* - 2 \cdot \frac{h_m}{B}\right) + 1.2, \quad R^2 = 0.894 \quad (7.60)$$

If we continue to remove terms with a small influence we get:

$$\frac{h_{s,\,max}}{h_m} = 0.95 \cdot \frac{e_s}{R_h} \cdot \left(\frac{V^*}{V} + \theta\right) \cdot \theta \cdot Fr + 1.83, \quad R^2 = 0.886 \quad (7.61)$$

This equation is now rather simple. With an increasing ratio rib-spacing to hydraulic radius, the scour increases. This tendency is due to the fact that a big rib-spacing was associated to the tests without ribs ($e_s = 100°$)[1]; knowing this, the equation reflects quite well the observations. If the mean water depth in the channel increases (for the same width), the hydraulic radius increases, too, but more slowly. Therefore the absolute scour will increase with increasing water depth,

---

1. This allows the computation of the maximum scour depth of the configuration without ribs with the same equation by replacing e_s with $100/360 \cdot 2R_o\pi = 2\pi/3.6 \cdot R_o$

which is correct. The ratio friction velocity to mean velocity has no significant influence on the scour but is almost constant at about 0.1.
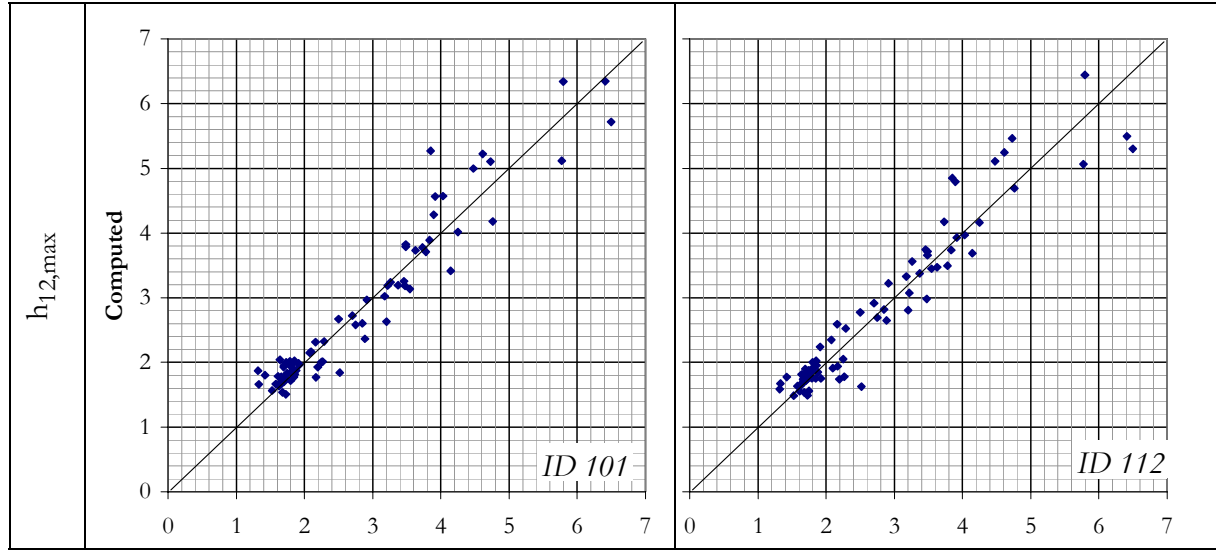
Table 7.5: *Plots of the maximum relative scour depth obtained with GPKernel with macro-roughness (ID 101 corresponds to eq. 7.58, ID 112 to eq. 7.59, ID 124)*

Replacing V^*/V by a constant of 0.2, leads to almost the same correlation ($R^2 = 0.885$). If we regroup the two terms θ to form $Cst + \theta^2$, and adjust the constant, the correlation is even increased to $R^2 = 0.887$. The constant has a value of 0.002. Since the square of $\theta_{cr} = 0.047$ gives exactly the same result, it is tempting to write:

$$\frac{h_{s,\,max}}{h_m} = 0.95 \cdot \frac{e_s}{R_h} \cdot (\theta_{cr}^2 + \theta^2) \cdot Fr + 1.83, \quad R^2 = 0.887 \tag{7.62}$$

The problem is that $\theta_{cr}^2 + \theta^2$ has not directly a physical signification. But if we write $(\theta - \theta_{cr})^2 = \theta^2 - 2 \cdot \theta \cdot \theta_{cr} + \theta_{cr}^2$, we find a physical explanation (unfortunately with a worse correlation). Some additional simplifications and optimizations result in:

$$\frac{h_{s,\,max}}{h_m} = 7.7 \cdot \frac{e_s}{R_h} \cdot Fr \cdot (0.001 + (\theta - \theta_{cr})^2) + 1.7, \quad R^2 = 0.876 \tag{7.63}$$

If we check this equation with the data set without macro-roughness, (admitting $e_s = 11.3$ m for the tests without ribs), we find $R^2 = 0.766$. Considering only the data set with macro-roughness, the correlation is rather poor ($R^2 = 0.537$) (see Figure 7.12) but still much better compared to directly computed scour depth (see § 7.4). This poor correlation is due to the fact that the tests performed with ribs cover only a limited range of the hydraulic parameters. In average, the prediction capability is quite well (see Figure 7.12).

All parameters in equation 7.63 have a physical meaning. The scour depth grows with increasing rib spacing, Froude number and Shields parameter. A possible explanation for the constant 0.001 is that the Shields parameter θ is computed in the inlet reach; but in the bend, the erosive power is more important, which is translated by the constant 0.001.
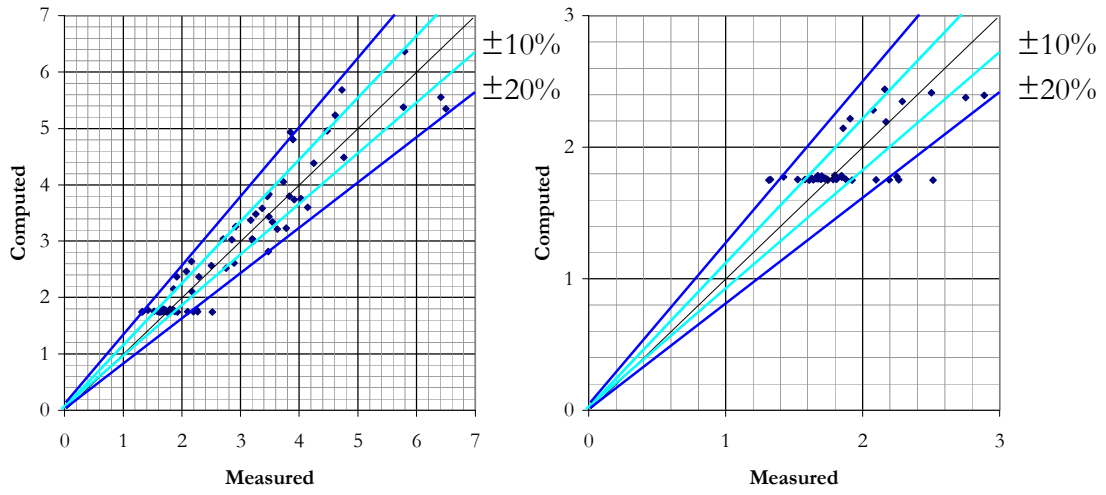
Figure 7.12: Comparison of maximum relative scour depth computed with equation 7.63 with the complete dataset ($R^2 = 0.876$) (left) and the one without Peter's tests (right).

7.4 Reduction of scour due to macro-roughness

In a first step the parameters that were identified having a major influence on the scour process are analyzed. On Figure 7.13 and Figure 6.5 on page 119 the only detectable tendencies are shown. No significant correlation can be made out (R^2 is always smaller than 0.1!). A small trend towards an reduction of the scour can be observed for low rib densities (e_s/R_h, and $e_s^2/B/R_c$), low depth to width ratio (h_m/B) and low velocities ($V \cdot R_h/\sqrt{gB^3}$). The other parameters (see Tables 7.1 and 7.2) are either about constant for the different scour reductions or present such an important scatter that no tendency can be determined.
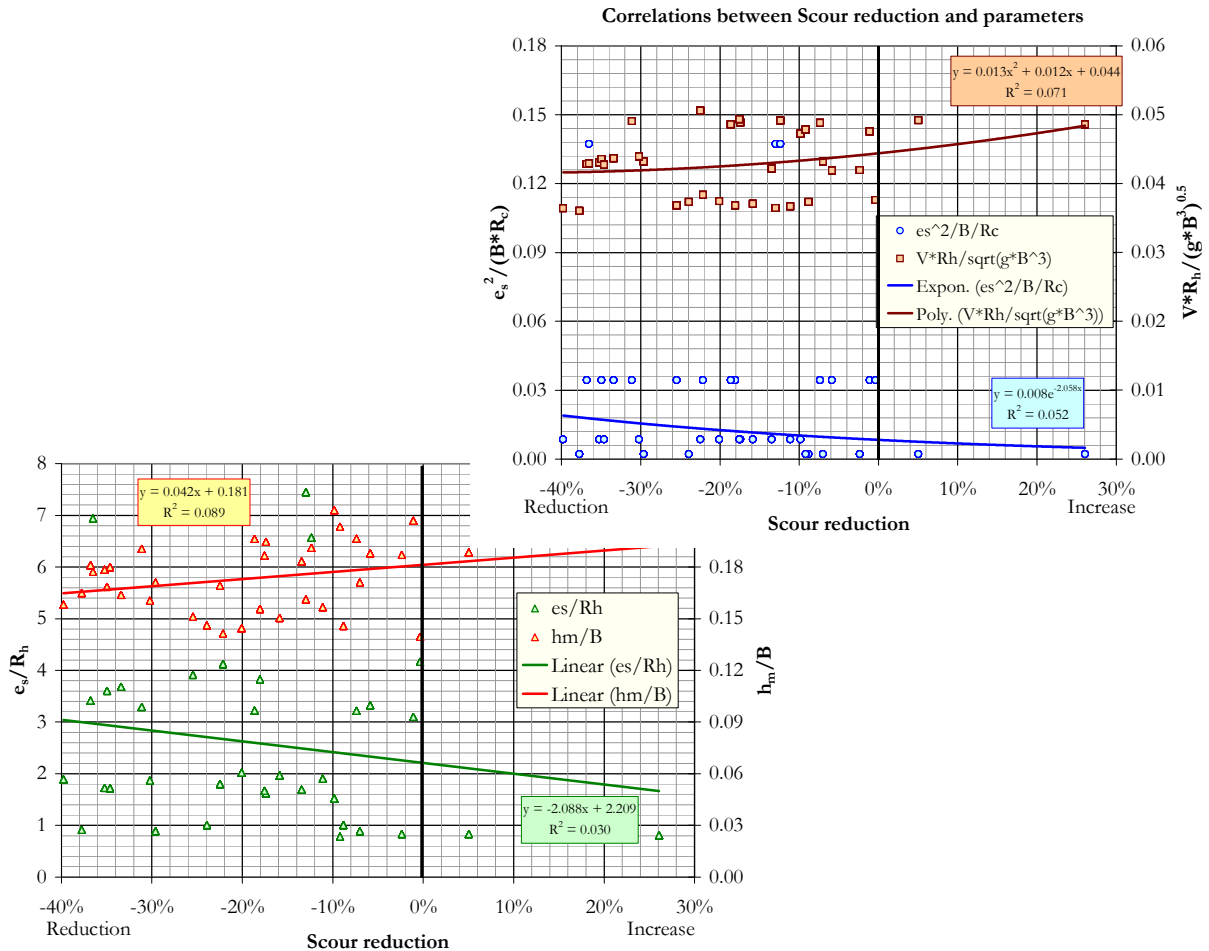
Figure 7.13: Analysis of parameters influencing the reduction of the maximum scour depth (see also Fig. 6.5!)

A big number of tests were carried out to determine an equation giving the scour reduction as a function of main parameters, but without success. The best correlations were obtained by means of the genetic algorithm, but they remained below 0.4 (Appendix 12.3). Therefore it is proposed to compute the scour depth in the presence of vertical ribs on the outer side wall directly by means of equation 7.63.

7.5 Comparison with scale model tests and field data

7.5.1 Scale model tests (Gurtnellen)

In August 1987, a flood on the Reuss River caused important damages on infrastructures in Gurtnellen/Wiler, Switzerland. In order to protect the village from future floods, scale model tests were performed at the "Versuchsanstalt für Wasserbau, Hydrologie und Glaziologie" (VAW) at the Swiss Federal Institute of Zurich (ETHZ) (KUSTER, JÄGGI & BEZZOLA, 1992). As scour reducing measure, vertical ribs were placed along the outer side walls. Since these tests were scaled on the flood event data[1], the test results will be used hereafter to test the applicability of equation 7.63 to field data.

The situation of the analyzed bend and the measured water levels and bed topography are given on Figures 7.14 and 7.16.
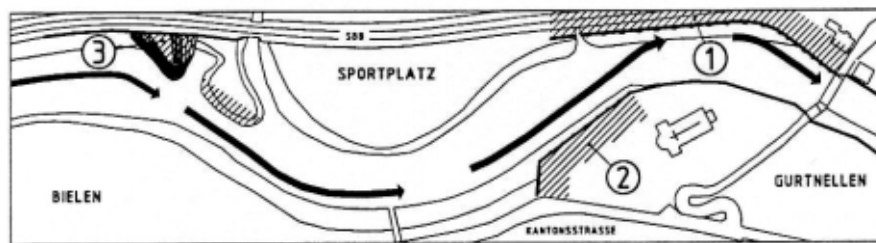
Figure 7.14: Schematic view of the bank protection elements upstream the Wilerbrücke (right end of the scheme). Element 1 is the vertical side wall equiped with ribs [Kuster et al, 1992, Fig. 22]
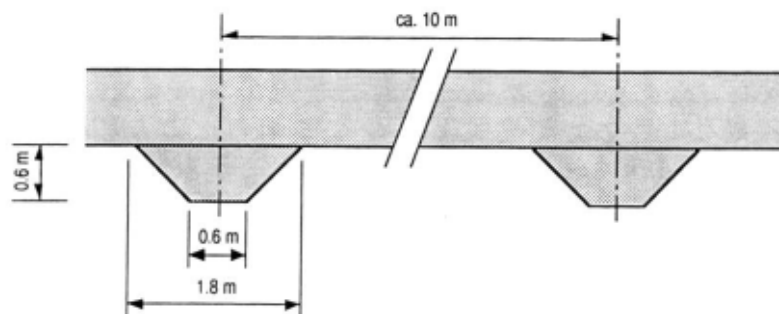
Bild 27 Grundrissanordnung der Rauhigkeitsrippen.

Figure 7.15: Configuration of the vertical ribs along the outer side wall (Schutzelement 1) [Kuster et al, 1992, Bild 27]

---

1. Based on the caused damages, the scour depth was determined.
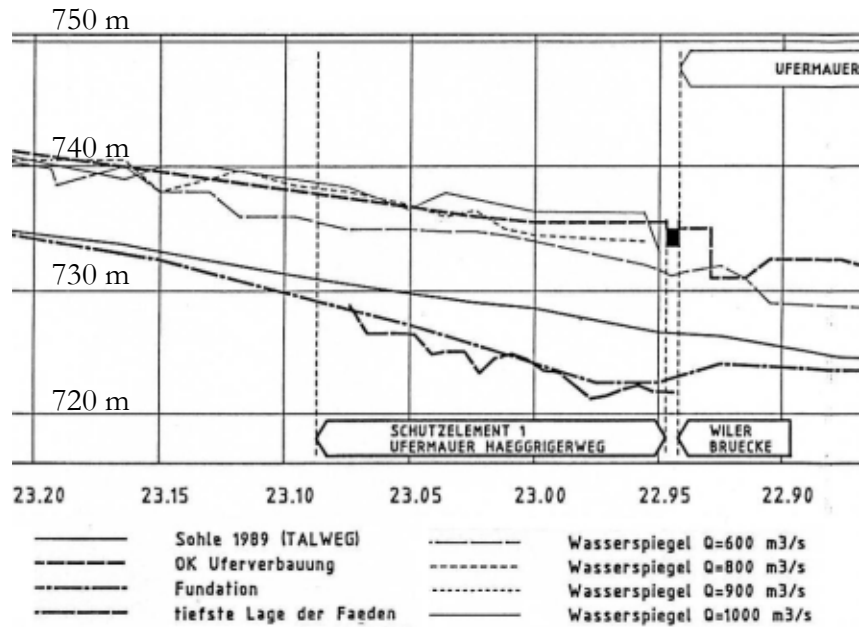
Figure 7.16: Measured water and bed elevation (scale model) along the left bank (wall) upstream the bridge (Wilerbrücke); Schutzelement 1 is the vertical side wall equiped with trapezoidal ribs [Kuster et al, 1992, Appendix G, Plan 30]
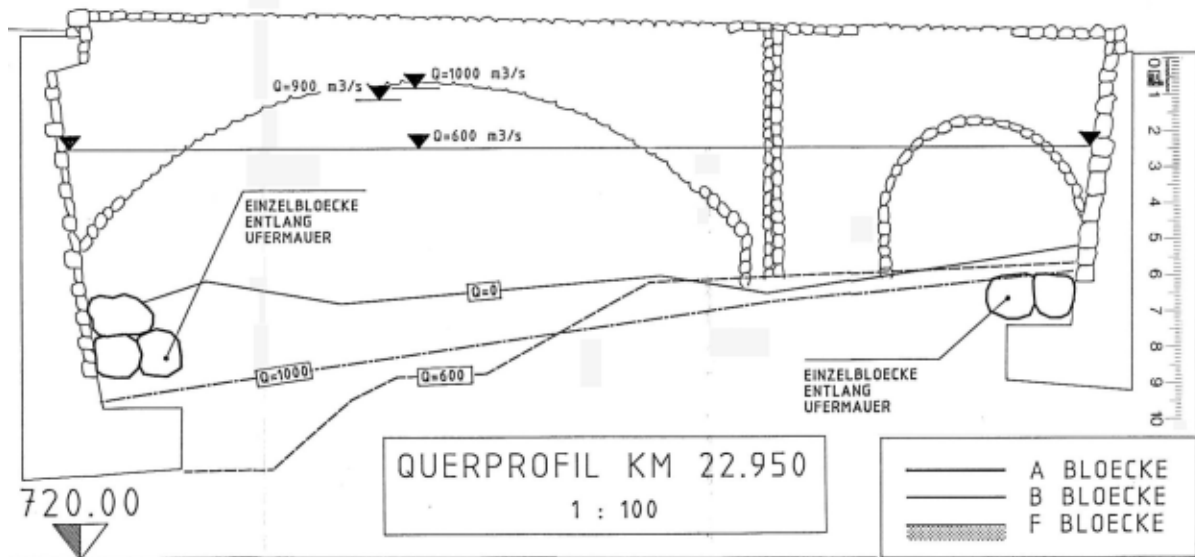
Figure 7.17: Cross section in the scour hole, upstream the bridge[Kuster et al., 1992, Appendix F, Plan 22]

The following characteristics of the reach were used for the computations: $R_c = 110$ m, $B = 30$ m, $A \cong 150$ m^2, $S_0 = 2.6\%$, $d_{90} = 0.60$ m, $\sigma = 10$, $\phi = 38°$, $V \cong 4$ m/s, $Fr = 0.7$, $\theta = 0.110$ and $\theta_{cr} = 0.047$.

The mean water depth upstream the bend equiped with macro-roughness is obtained taking into account the influence of the wall roughness (see section 3.3 on page 31) is of 3.8 m. Taking also into account the backwater curve in the Reuss River (Fig. 7.17), a water depth of $h_m \cong 5$ m is found. The hydraulic radius is of $R_h = 4.3$ m. The (experimentally scour depth is of $h_{s, max} = 10.9$ m.

The macro-rougness related characteristics are the rib-spacing $e_s = 10$ m, the rib-depth $e_d = 0.6$ m, the rib-length $e_\theta = 1.8$ m

The scour depth is computed based on equation 3.55:

$$h_s = h_m \cdot \left(1 + \frac{B}{2 \cdot R_c}\right)^K \tag{7.64}$$

Different scour formulae lead to a set of scour depth for these characteristics:

- The *modified formula of Bridge* (eq. 7.7) gives the exponent K and the maximum scour depth $h_{s,\,max}$ with:

$$K = 0.394 \cdot \left(11 - 23 \cdot \frac{5}{30}\right) \cdot \frac{110}{30} \cdot \tan 38 = 8.1 \, , \quad h_{s,\,max} = 14.1 \text{ m}.$$

- *Peter's equation for rectangular cross sections* (eq. 3.117) results in:

$$K = 5.23 - 13 \cdot \frac{5}{30} - 0.379 \cdot 10 + 68.4 \cdot 0.026 = 1.05 \, , \quad h_{s,\,max} = 5.7 \text{ m}$$

which occurs to be a significant underestimation.

His equation *for trapezoidal cross sections* (eq. 3.118) gives:

$$K = 4.2 \, , \quad h_{s,\,max} = 8.6 \text{ m}.$$

- The *formula fitted to the cross-section shape* (eq. 7.31 and 7.32) leads to:

$$c = 290\left(1 - 3.2 \cdot \frac{5}{30}\right)\frac{4 \cdot 4.3}{\sqrt{9.81 \cdot 30^3}} = 4.5 \, , \quad h_{s,\,max} = 18.7 \text{ m}$$

- Equation 7.63 (*GPKernel*), *taking into account the influence of the macro-roughness* results in a maximum scour depth of:

$$h_{s,\,max} = 5 \cdot \left(7.7 \cdot \frac{10}{4.3} \cdot 0.7 \cdot (0.001 + (0.110 - 0.047)^2) + 1.7\right) = 8.8 \text{ m}$$

Comparing the obtained results, it can be seen that the computed scour depths show a big scatter. **Without macro-roughness**, the formulae of Peter for rectangular and for trapezoidal cross sections (3.117 and 3.118) underestimate the scour depth. The formula established in the present work, fitted to the cross-section profile (7.31) may lead to a somewhat overestimated scour depth. The best results are obtained with the modified equation of Bridge (7.7) with a computed scour depth which is about 30% bigger than the scour depth measured with ribs[1].

Compared to a measured scour depth (with vertical ribs) of 10.9 m, the computed water depth taking into account the **macro-roughness** of the banks is underestimated. But if we take into account the insecurity of the formula (Fig. 7.12 on page 181), the computed results are within the interval of ±20 %. Furthermore, the scale model tests rather overestimated the scour depth.

---

1. Since the scour depth without ribs was not determined for the same configuration without ribs, it is assumed that the reduction of the scour depth is of the same order of magnitude as observed in this study.

7.5.2 Field data from the Sacramento River

It is quite difficult to obtain relyable field data of the bed topography in scour holes. To the authors knowledge, no field data of alpine river bends is available. For this reason, the field measurements on the Sacramento River of ODGAARD & KENNEDY (1982) and ODGAARD (1984b) are used in the present study to check the prediction capability of the developed formulae:

- The first dataset (1982) contains measurements in a test reach between miles 188 and 189 (Fig. 7.18). The grain size of the bed material is quite fine compared to the one of alpine rivers. The median diameter d_{50} ranges between 6 and 21 mm for high flow conditions (discharge of Q = 700 to 800 m^3/s).

- The second dataset (1984) was recorded in selected cross sections between miles 144 and 189 (about 100 miles north of San Francisco) in Colusa, Princeton, Larkin, Jacinto, Old Ferry and at the Road 29. The bed material is very fine (d_{50} = 0.4 mm).
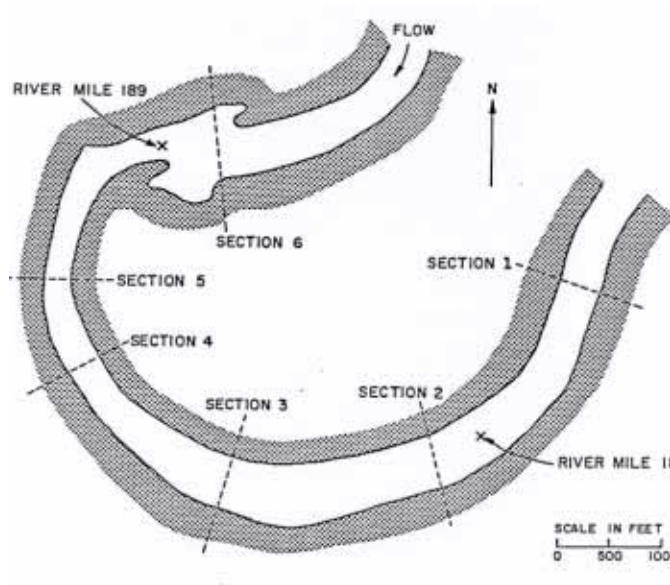
Figure 4 - Schematic Plan View of Sacramento River Study Bend
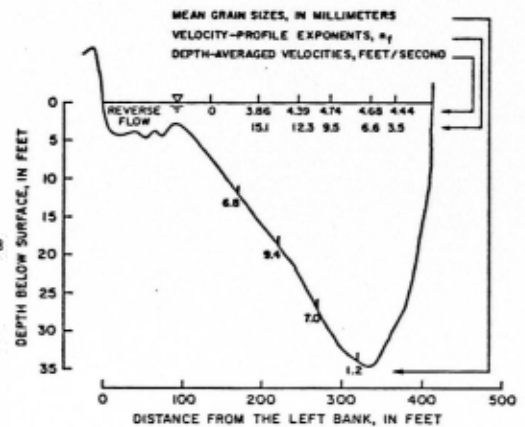
Figure 12 - Cross Section No. 4 at High Flow, 24,900 Cubic Feet Per Second
24'900 ft^3/s = 700 m^3/s

Figure 7.18: Sacramento River: location of the field data set [Odgaard and Kennedy , 1982, Fig.4 + 12]
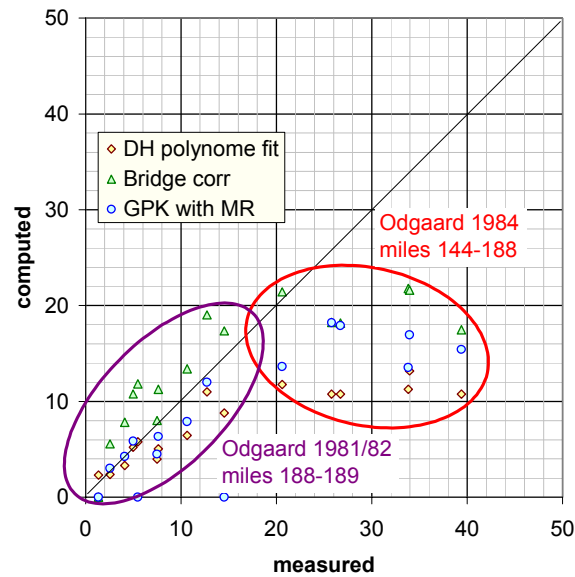
Figure 7.19: Comparison between measured field data and computed maximum scour depth (Sacramento River)

The comparison of the field data with the computed results (equations 7.31: polynome fit, 7.63: GPKernel and 7.7: modified Bridge) shows in general an acceptable agreement for Odgaard & Kennedy's (1982) data set. The modified equation of Bridge shows a systematic overestimation of the scour, whereas the polynomial function, developed in the present study underestimates the scour in the test reach. This might be due to the much finer grain size distribution of the bed material. Compared to the modified scour formula of Bridge, the computed scour depth is reduced by 25 to 35% which is the same order of magnitude as observed in the laboratory tests performed in this study.

7.6 Summary and conclusions

7.6.1 Summary

A dimensional analysis (§ 7.2) allowed for the identification of the main parameters influencing the scour process. These are the overall energy slope $S_{e, all}$, the water depth to channel width ratio h_m/B, the ratios $V \cdot R_h/\sqrt{g \cdot B^3}$ (replacing the Reynolds number that showed an important correlation) and $R_c \cdot h_m/B^2$. The frequently used ratio V^*/V and Fr_d do not seem to play a determinant role. An additional parameter was found to characterize the macro-roughness: the spacing of the ribs e_s. To make this ratio dimensionless it can be divided either by the channel width B, the mean water depth h_m or the radius of curvature R_c.

In a first step, existing scour formulae were enhanced (§ 7.3.2). Table 7.6 gives a summary of the obtained results. Since the formula of KIKKAWA ET AL. (1976) is quite frequently used in practice, an effort was made to enhance its prediction capability for mountain rivers with a coarse bed by adding additional parameters. The result is quite good but it is possible to get a better prediction with other equations. BRIDGE (1976) gives the smallest error on the predicted average scour depth. Therefore, this formula was enhanced too. By introducing two additional parameters, related to the channel geometry, the correlation for the maximum scour depth can be increased to 0.82 and the predicted cross-section shape fits quite well to the measured one. The predicted values fit well to the results obtained with scale model tests (Gurtnellen) and field data (Sacramento River) (§ 7.5).

Since the observed cross-section is rather s-shaped than an exponential function (which is an assumption of most existing formulae), an attempt was made to establish a scour formula based on the shape of the cross-section (§ 7.3.3). It was assumed that the maximum bed slope in a radial direction is limited to a maximum value corresponding to the friction angle of the bed material. Different polynomial functions (Table 7.6) of the third and fifth degree were tested. A large set of boundary conditions was analyzed, by fixing the cross-section slope at the outer and / or inner bank and by admitting or omitting a symmetry point on the channel axis. The results range from poor to good. The best result was obtained with a polynomial function of the third degree (equation 7.20) obtaining a correlation of $R^2 = 0.856$ and fitting well to the measured cross-section. Unfortunately this equation shows some lacking (underestimation of the scour depth) when applied to additional laboratory and field data (§ 7.5 and Fig. 7.19).

Hoping to increase the precision of the predicted scour depth, an approach based on the similitude and approximation theory of KLINE (1965) was explored (§ 7.3.4). Based on the most important forces acting on a control volume in the cross-section, dimensionless ratios between the different characteristics were derived. The advantage of this method is that the parameters obtained in this way are based on the physical process. Unfortunately the result is not very satisfying. The highest obtained correlations are of 0.72 and for the case with macro-roughness $R^2 < 0.5$.

Finally a genetic algorithm written by KEIJZER & BABOVIC (1999) was used to search for a function fitting well with the measured data (§ 7.3.5). Without ribs, the best obtained formula had a correlation of 0.83 which is less than for the approach based on the cross-section shape. Therefore none of the equations were retained.

The search for an equation predicting the scour locations was more successful. Formulae with a correlation of 0.83 respectively 0.60 are proposed to compute the first and second scour location.

Finally a formula was established (eq. 7.63), allowing for the computation of the maximum scour depth in the presence of macro-roughness. The prediction capability is very satisfying ($R^2 = 0.876$).

FORMULA	EQ.	COM-PUTES	PARAMETERS	R^2	FIT TO CROSS-SECTION
modified Kikkawa	7.5	h_s	R_c/B , h_m/B , $V \cdot R_h/\sqrt{gB^3}$	0.795	quite well
modified Bridge	7.6	h_s	R_c/B	0.796	quite well
	7.7	h_s	R_c/B , h_m/B	0.817	quite well
Polynomial functions of					
3rd degree, centered	7.11	h_s	$\tan\phi$, $V \cdot R_h/\sqrt{gB^3}$	0.72	poor
3rd degree, non-centered (nc)	7.14	h_s	$\tan\phi$, $S_{e,\,all}$, h_m/B , $V \cdot R_h/\sqrt{gB^3}$	0.82	less poor
3rd degree, nc, vertical adjust. (va)	7.18	h_s	$\tan\phi$, R_c/B , h_m/B , $V \cdot R_h/\sqrt{gB^3}$	0.82	better
same but $dh_s/dr = 0$ inside	7.20	h_s	$\tan\phi$, h_m/B , $V \cdot R_h/\sqrt{gB^3}$	0.856	good
3rd degree, nc, va, add. terms	7.22	h_s	$\tan\phi$, $S_{e,\,all}$, R_c/B , h_m/B	0.81	very poor
3rd degree, nc, va, no	7.29	h_s	$\tan\phi$, h_m/B , $V \cdot R_h/\sqrt{gB^3}$	0.76	very poor
restr.bound.	7.27	h_s	$\tan\phi$, $S_{e,\,all}$, h_m/B , $V \cdot R_h/\sqrt{gB^3}$	0.850	poor
5th degree, $dh_s/dr = 0$ outside	7.28	h_s	$\tan\phi$, $S_{e,\,all}$, h_m/B , $V \cdot R_h/\sqrt{gB^3}$	0.856	poor
5th degree, $dh_s/dr = 0$ inside					
Similitude & approx. theory					-
with macro-roughness	7.43	$h_{s,\,max}$	e_s/e_d , S_e , θ , Fr^2 , Fr_d^2 [1]	---	
	7.44	$h_{s,\,max}$	$e_s^2/B/R_c$, S_e , θ , Fr^2 , Fr_d^2 [1]	< 0.5	
without macro-roughness	7.48	$h_{s,\,max}$	$R_c/(C_F \cdot R_o)$, S_e , θ , Fr^2 , Fr_d^2 [1]	0.724	
Genetic algorithm		$h_{s,\,max}$	most of the previously mentioned parameters		-
with adjustments	7.63	$h_{s,\,max}$	$\theta - \theta_{cr}$, Fr , e_s/R_h	0.876	

Table 7.6: Summary of the tested type of formulae for establishing a new scour formula

1. θ/Fr_d^2 can be replaced by $V*/V$

7.6.2   Conclusions

Without macro-roughness, the best correlation was obtained by an approach based on the shape of the cross-section in the scour holes. A polynomial function of the third degree combines an excellent correlation ($R^2 = 0.86$) with a good fit over the cross-section[1].

$$h_s = h_m + \tan\phi \cdot c \cdot \left[6.23 \cdot B - \frac{(r - R_c - 8.8B)^3}{260 \cdot B^2} + (r - R_c - 8.8B) \right] \qquad (7.31)$$

$$h_{s,\,max} = h_m + \tan\phi \cdot c \cdot [0.129 \cdot B] \qquad (7.32)$$

where

$$c = 290 \cdot \left(1 - 3.2 \cdot \frac{h_m}{B} \right) \cdot \frac{V \cdot R_h}{\sqrt{g \cdot B^3}} \qquad (7.33)$$

Unfortunately, the application to results of scale model tests and field data shows that the predicted scour depth is too small compared to the measured one. Therefore the *modified formula of Bridge* (eq. 7.7) is proposed for the computation of the maximum scour depth without macro-roughness. Despite a slightly lower correlation, this formula gives a much better prediction if applied to field data. It further takes into account the bend geometry (R_c, B) the flow conditions (h_m) and the bed characteristics ($\tan\phi$)

$$\sin\beta = 0.394 \cdot \left(11 - 23 \cdot \frac{h_m}{B} \right) \cdot \frac{R_c}{B} \cdot \tan\phi \cdot \frac{h_s}{r}, \quad R^2 = 0.817 \qquad (7.7)$$

In the presence of vertical ribs, equation 7.63 is recommended for the computation of the maximum scour depth ($R^2 = 0.876$ compared to the whole dataset, with Peter's tests):

$$\frac{h_{s,\,max}}{h_m} = 7.7 \cdot \frac{e_s}{R_h} \cdot Fr \cdot (0.001 + (\theta - \theta_{cr})^2) + 1.7 \qquad ^{2)} \qquad (7.63)$$

This formula is very simple, depending only on the Froude number and the difference between the Shields stress and the critical Shields stress. The ratio rib spacing to hydraulic radius accounts for the influence of the ribs. It is important to use an optimum rib spacing to compute the maximum scour depth since the scour depth decreases linearly with the reduction of the rib spacing. If the rib spacing is reduced sufficiently (below an optimum spacing), the scour depth can become even more important than the scour depth obtained without the presence of ribs. This tendency cannot be found in equation 7.63. Figure 6.5 on page 119 gives some indications on the reduction of the scour depth as a function of the rib spacing. Furthermore it needs to be mentioned that the result $h_{s,\,max}/h_m$ is close to 1.7 and that the different parameters in equation 7.63 have only a reduced impact on the result.

---

1. The main parameters in this equation are the friction slope , a ration combining a flow characteristic (velocity) with the channel geometry (R_h and B) and the flow depth to width ratio. These ratios determine the scour depth compared to the mean bed level. The expression in the brackets "fits" the 3rd-degree polynome on the cross-section with a steepest slope of $\tan\phi \cdot c$. The term $r - R_c - 8.8B$ stands for the radius corrected by the radial shift of the inflection point of the cross section (point for which the radial bed slope is maximum).
2. for $\theta > \theta_{cr}$

The location of the scour holes (without macro-roughness) can be computed with the following equations:

$$\alpha_1 = \sigma \cdot \left(0.58 \cdot \frac{B}{h_m} + 12.7 \cdot \frac{S_e}{\sigma - Fr_d} \right) + 1.4 \cdot Fr_d \cdot \frac{V}{V^*} - 6.6, \quad R^2 = 0.829 \quad (7.54)$$

$$\alpha_2 = 12.6 \cdot Fr_d - 0.9 \cdot \left(\frac{R_c}{B} \right)^2 + 91.6, \quad R^2 = 0.602 \quad (7.57)$$

For the second scour, a slightly better correlation can be obtained, but with a much more complicated equation (7.56) which is quite sensitive to the choice of the used parameters.

The equations for the two scour locations illustrate that the two scour holes do not depend on the same parameters. The first scour depends e.g. on σ, but not the second one.

CHAPTER 8

SUMMARY, CONCLUSIONS AND RECOMMENDATIONS

8.1 Summary and conclusions

Analysis of existing scour assessment approaches

An extensive literature review (§ 2) showed that little work has been done on the effect of macro-roughness of the side walls on the flow and scouring in curved channels. The little known research that was done was limited to general bank roughness, macro-roughness in straight reaches (numerical studies) or isolated "roughness-elements" like bridge abutments. The only known work on macro-roughness in bends compared different types of wall roughness with each other. There is no known work which systematically studied the influence of macro-roughness placed as vertical ribs on scouring and flow in river bends.

Performing a detailed study of existing scour formulae (§ 3) revealed that most known equations considerably underestimate the scour in mountain rivers with a coarse gravel bed. The scour formulae of PETER (1986), ZIMMERMANN (1978), VAN BENDEGOM (1947), FALCON & KENNEDY (1983) and ODGAARD (1986) obtained fairly good correlations ($R^2 > 0.70$)[1]. But the predicted mean value is substantially underestimated. The maximum scour depth computed with the above equations needs to be multiplied by a correction factor between 1.8 and 2.4 to get an accurate prediction (see Table 3.7 on page 64), except PETER's formula (1986), which overestimates the scour by 15%.

The best prediction of the average scour depth was obtained by BRIDGE's formula (1976) (needing no correction factor), but with a poor correlation ($R^2 = 0.3$) due to a wide scatter around the average value. This shows that essential parameters are neglected in this formula.

Laboratory tests

Laboratory tests (§ 4 and 5) were performed in a 23 m long and 1 m wide channel with a 90° bend, 6 m radius bend on a mobile bed composed of coarse gravel with a wide grain size distribution as found in natural mountain rivers. The bed topography, the water surface, the 3D-velocity field, as well as the sediment transport rate and the grain size distribution of the armoring layer, were measured. The tests covered a wide range of different parameters: discharges between 150 and 210 l/s, bed slopes from 0.44% to 0.79% and Froude numbers between 0.68 and 0.97. The macro-roughness was analyzed for rib spacings of 8°, 4°, 2° and 1° (about 80, 40 20 and 10 cm) and rib depths of 20 and 40 mm. The longitudinal bed slope was maintained constant in the inlet reach during the tests, by adjusting the sediment transport rate.

Flow and sediment transport in bends

The tests showed that the scour process is principally influenced by the combined action of the main flow (tangential velocity), the secondary flow and the velocity fluctuations. Two scour holes can be observed in the bend; a first one between 30° and 40° and a second one at the end of the bend. The first scour is located upstream of the point bar formed towards the inner wall of the channel by the deposition of fine sediment, and the second one downstream of the second point

---

1. The square of Pearson's correlation factor r^2 quantifies the extent of a linear relationship between two data sets and not the error between measured and computed data!

bar. The upstream scour is essentially influenced by the action of the main velocity (along the channel axis) on the outer bank and the induced secondary flow. Downstream, the scour is governed by another phenomenon. The point bar upstream of the scour induces important velocity fluctuations which are at the source of this scour.

The flow field in the channel undergoes important changes over the whole bend. At the inlet, the maximum main velocity is located close to the free water surface in the center of the channel. Over the bend, this maximum velocity zone shifts towards the outer bank and finally plunges down along the outer wall to reach the bed surface at the first scour location. The secondary current develops from the beginning of the bend at about 10° to increase up to the first scour. In the upstream scour hole, another secondary cell appears at the inner bank, hindering the growth of the main secondary cell. In the downstream direction, the secondary current reduces and then increases again towards the second scour. The intensity of the secondary cell is less important at the second scour location than in the first one.

During the development of the scour, an important oscillation of the scour depth can be observed, especially in the second one. The scour depth along the outer wall shows fluctuations of about 50% of the average water depth. On the free water surface, stationary waves are observed. Their amplitude is of about the same order of magnitude as the oscillations of the scour depth.

A considerable grain sorting, due to the wide grain size distribution, can be observed over the cross-section. At the outer bank, coarse sediments are found in the scour holes and, on the inner banks, fine material is deposited.

Influence of the macro-roughness on the outer side wall

The presence of vertical ribs on the outer side wall placed with appropriate spacing, has a major impact on the scour process and the flow field. The maximum scour depth is significantly reduced, specially for high bed slopes and discharges (Figure 6.5 on page 119). The reduction of the scour depth can be of up to 40%. With increasing wall roughness, the first scour is shifted in a downstream direction, but the second one remains at about the same position. The prominent scour holes disappear and frequently, the two scour holes cannot be distinguished from one another.

Important oscillations of the scour depth observed during the formation of the second scour hole are reduced by half for small discharges. They even disappear completely for the highest discharges. The maximum level of the water surface is not significantly influenced. The ribs create a head loss in the bend inducing an increased mean water depth; but at the same time, the ribs avoid the important stationary surface waves by inducing smaller shock waves. Superposing the two phenomena results in the same maximum water level as observed without macro-roughness. Furthermore, it is interesting to observe that the amplitude of the water surface oscillations is of the same order of magnitude for the tests, both with and without macro-roughness.

By deflecting the flow away from the outer wall and inducing additional wall roughness, the ribs modify the velocity field in the bend. The highest velocities remain longer next to the free water surface. Once they shift bottom-wards, the highest velocities occur at a distance of about the mean water depth from the outer wall. In this way, the impact of the high tangential velocities is directed away from the outer wall foundations.

On the water surface at the outer wall, an outer bank secondary cell can be observed. This cell has been identified as contributing to bank protection. For an optimum spacing, this cell shows the greatest degree of extension.

Due to the increase of the water level in the bend, and the reduction of the near bed main velocities, the sediment transport capacity is significantly reduced (about 40 to 50%). In a natural river, the bed slope steepens by the same order of magnitude (40 to 50%) as a result of depositions upstream of the bend, if the bedload is maintained at the same rate.

An influence of the ribs on the grain sorting process is not found, except with respect to the size of the zone where the coarse sediments are found in the scour holes. A marked armoring layer is found over approximately the outer half of the cross-section, compared to a quarter without ribs. But this is rather due to a smoother radial bed slope than to a modified pattern in the grain sorting process.

At the extremities of the bend, the macro-roughness induces some modifications: in the upstream reach, the water surface is increased by about 10% due to the head losses in the bend[1]. In the outlet reach, some additional erosion can be found due to the increased velocities in the end of the curve. This erosion is not found next to the outer bank, but towards the center of the channel, where usually no important civil engineering structures are located.

Optimum rib dimensions

Based on the numerical investigation of GAIROLA (1996) and the performed tests, an optimum rib spacing can be recommended. To obtain the most important energy dissipation along the outer wall, the separation bubble behind the roughness element needs to reattach itself to the wall before meeting the next rib. The length of this bubble is about 12 times the depth of the roughness element in a straight reach. The tests showed that the optimum length is of the same order of magnitude in a bend. Therefore, the optimum rib spacing can be indicated with 10 to 15 times the rib depth.

The depth of the ribs was chosen about 2.5 to 5 times the mean diameter of the initially build-in bed material (substrate). Almost no local scour was observed at the bottom of the ribs having a depth of 2.5 times the mean diameter, whereas for the deeper ribs, some local scour was observed. Therefore a rib depth of about 2.5 times the mean diameter (or about one time d_{90}) can be recommended for engineering applications.

Empirical scour assessment formulae

By means of a dimensional analysis (§ 7.2) the main parameters influencing the scour process were identified ($S_{e, all}$, h_m/B, $V \cdot R_h / \sqrt{g \cdot B^3}$, $R_c \cdot h_m / B^2$). The influence of the macro-roughness on the scour process seems to be essentially determined by the spacing of the ribs e_s.

In a first step, existing scour formulae were enhanced (§ 7.3.2 and Table 7.6). To the formula of KIKKAWA ET AL. (1976) frequently used in practice, additional parameters were introduced with quite good results. BRIDGE's (1976) formula, giving the smallest error on the predicted average

---

1. In addition to this, the steepening of the bed slope due to the reduced sediment transport capacity in the bend needs to be considered.

scour, was also enhanced. The correlation for the maximum scour depth can be increased to 0.82 and the predicted cross-section shape fits quite well to the measured one (without macro-roughness).

A new way was explored to establish a formula based on the shape of the cross-section (§ 7.3.3). Assuming that the maximum bed slope in a radial direction is limited to a maximum value corresponding to the friction angle of the bed material, different polynomial functions (Table 7.6) of the third and fifth degree were tested. The best correlation ($R^2 = 0.856$) was obtained with a polynome of the third degree (equation 7.31), fitting well to the measured cross-section. But the application to results of scale model tests and field measurements showed a significant underestimation of the maximum scour depth. Therefore the modified formula of Bridge (eq. 7.7) is proposed for the scour depth computation for the configuration without macro-roughness. This equation showed a good agreement with field data (§ 7.5)

$$\sin\beta = 0.394 \cdot \left(11 - 23 \cdot \frac{h_m}{B}\right) \cdot \frac{R_c}{B} \cdot \tan\phi \cdot \frac{h_s}{r}, \quad R^2 = 0.817 \tag{7.7}$$

Another approach, inspired by the similitude and approximation theory of KLINE (1965) was investigated (§ 7.3.4), resulting in physically based dimensionless parameters. Unfortunately the resulting correlations are quite low.

Finally a genetic algorithm written by KEIJZER & BABOVIC (1999) was used to search for a function fitting well to the measured data (§ 7.3.5). Without ribs, the previously obtained results could not be enhanced. The search for an equation predicting the scour locations was more successful, resulting in two formulae with good correlations.

Finally a formula was established, allowing for the prediction of the maximum scour depth in the presence of macro-roughness with an excellent result ($R^2 = 0.876$):

$$\frac{h_{max}}{h_m} = 7.7 \cdot \frac{e_s}{R_h} \cdot Fr \cdot (0.001 + (\theta - \theta_{cr})^2) + 1.7 \tag{7.63}$$

Enhancing the results obtained with the genetic algorithm, the following equations were established for the determination of the location of the scour holes without macro-roughness:

$$\alpha_1 = \sigma \cdot \left(0.58 \cdot \frac{B}{h_m} + 12.7 \cdot \frac{S_e}{\sigma - Fr_d}\right) + 1.4 \cdot Fr_d \cdot \frac{V}{V^*} - 6.6, \quad R^2 = 0.829 \tag{7.54}$$

$$\alpha_2 = 12.6 \cdot Fr_d - 0.9 \cdot \left(\frac{R_c}{B}\right)^2 + 91.6, \quad R^2 = 0.602 \tag{7.57}$$

For the second scour, a slightly better correlation can be obtained with equation (7.56) but which is much more complicated and quite sensitive to the choice of the used parameters.

8.2   Outlook and further research

One of the main problems with which researchers are confronted when developing numerical models, is their validation. Only a small number of physical tests are available for that kind of work, especially for 3D problems like flow and sediment transport in river bends. The present study furnishes a very precious data set including the free water surface, the bed topography, the average 3D velocity field as well as grain size distributions of the armoring layer and sediment transport rates. About 1500 datapoints were measured for each test. Such detailed data is needed for the verification and testing of numerical 3D-models.

Further treatment of the data, especially concerning the measured velocities, could be done. Due to the large amount of records, the velocities were only analyzed in eight selected cross-sections over the bend for about 10% of the available test configurations. But the velocities were recorded in 3 directions on a 9 x 9 cm grid over the whole channel with 128 data points over the measurement depth. By treating and analyzing this available raw data, additional insight into the scour process and the effect of macro-roughness on erosion in bends can be obtained.

All the tests with macro-roughness were performed with ribs applied to vertical outer walls. The influence of the shape, as well as the type of macro-roughness were not examined in this research study. Therefore, other rib shapes and types of roughness e.g. rock-dumps, need further testing. It would be interesting to study the influence of bank protections realized by a rip-rap, designed for natural rivers.

At this stage, the influence of inclined outer walls is not well known. The action of macro-roughness on the scour process, for example applied in trapezoidal cross sections could be further investigated.

With additional research, these gaps can be closed in order to provide a better understanding of the flow in bends in general and especially of the scour process in natural rivers with banks equipped with macro-roughness.

8.3 Recommendations for practical engineers

a) Advantages and inconveniences of macro-roughness on outer walls

Vertical ribs placed on the outer side wall with an optimum spacing have the following advantages:
- The maximum scour depth is significantly reduced (20 to 40% for an optimum rib-spacing).
- Prominent scour holes almost disappear.
- Important oscillations of the bed level during development of the scour are considerably reduced or even suppressed for high discharges.
- The amplitude of the stationary surface waves is diminished by half. But at the same time, the mean water level increases, resulting in about the same maximum water levels in the curve as without ribs.
- High main velocities are shifted from the outer wall to a distance of about an average water depth from the outer bank.
- The armoring layer zone next to the outer wall due to grain sorting is doubled, now covering about half of the channel.

But the macro-roughness on the outer wall has also some negative effects, such as:
- A significantly reduced transport capacity in the bend. This reduction is compensated in natural rivers by a steepening of the bed slope obtained by depositions upstream of the curve (see also preliminary tests).
- Some additional erosion can be found after the bend in the center of the channel. But with the possible exception of bridge piers, no civil engineering structures are endangered by this limited local erosion.

b) Estimation of the maximum scour depth, transversal bed slope and scour locations

If existing scour formulae are applied to mountain rivers, attention needs to be paid to the fact that most of them underestimate the maximum scour depth by a factor of up to 2.4. In order to adjust the maximum scour obtained using existing equations, the result can be multiplied with a correction factor given in Table 3.7 on page 64 (in general $R^2 < 0.8$, except for Peter's formula with a higher correlation).

Without macro-roughness, equation 7.7 can be used to compute the maximum scour depth and the transversal bed slope. This formula combines both, a good prediction of the maximum scour depth and a good fit with the cross-section at the maximum scour locations.

It is difficult to compute the reduction of the scour depth directly. Therefore formula 7.63 is proposed to compute the scour depth in the presence of vertical ribs.

The location of the two scour holes can also be predicted by two relations (equations 7.54 and 7.57). The prediction of the first scour gives quite good results ($R^2 = 0.83$), but the forecast of the second one is more difficult ($R^2 = 0.60$).

During the development of the scour holes, important bed fluctuations were observed for the tests without macro-roughness. They can reach amplitudes of up to 50% of the mean water depth

in the second scour hole. These oscillations are reduced by half by the presence of vertical ribs on the outer wall for low discharges and they even disappear for high discharges.

All the proposed formulae should be used within the domain for which they were established. The tests were performed at rather high Froude numbers (> 0.3) but at subcritical flow regimes. The radius of curvature to width ratio (R_c/B) ranged between 2 and 6 and the flow depth to mean diameter of the substrate (h_m/d_m) was between 6.5 and 39. The study of the influence of the macro-roughness was performed at R_c/B ratios of 6 and h_m/d_m ratios between 18 and 24, but the positive influence of the macro-roughness on scour and flow in bends can certainly be observed in a much wider range of parameters.

c) *The optimum rib spacing*

A rib spacing to rib depth ratio of 10 to 15 is recommended. The depth of the ribs was chosen in the present research study at about 2.5 to 5 times the mean diameter of the initially built-in bed material (substrate). Almost no local scour was observed at the bottom of the ribs having a depth of 2.5 times the mean diameter, whereas for the deeper ribs, some local scour was observed. Therefore a rib depth of about 2.5 times the mean diameter (or about one time d_{90}) can be recommended for engineering applications.

It is important to choose an appropriate rib spacing, since the scour can be even amplified by a too small a rib spacing.

In order to obtain a smooth transition with the upstream and downstream reaches next to the bend, additional ribs should be placed in a transition zone towards the bend. The laboratory tests were carried out with a transition zone having a length of about 10 times the mean flow depth. The ribs were placed with increasing spacing (factor $\sqrt{2}$ compared to the previous spacing, Fig. 5.3 on page 111) for an increasing distance from the bend with good results.

Notations

Generalities

Upper case characters: average or global values (applied to the whole channel)

Lower case characters: local values

Variables and constants

A	$[m^2]$	cross-section area of the channel
B	$[m]$	width of the channel
C	$[m^{1/2}/s]$	CHEZY coefficient
c	$[-]$	correction factor defined as $\tan\phi^* = c \cdot \tan\phi$
c_x	$[-]$	coefficient for the optimization of existing scour formulae
C_L	$[-]$	lift coefficient
C_D	$[-]$	drag coefficient
d	$[m]$	characteristic grain size diameter, if not mentioned, the characteristic diameter is related to the substrate
d*	$[-]$	dimensionless grain size diameter $d^* = (\gamma_s - \gamma_w) \cdot d / \tau_0$ $d^* = ((s-1) \cdot d)/(h \cdot S_e)$
D	$[N^1]$	dynamic drag force
e_d	$[° \text{ or } m]$	depth of the macro-roughness (dimension in radial direction)
e_s	$[° \text{ or } m]$	spacing between the macro-roughness (from axis to axis)
f	$[-]$	friction coefficient of DARCY-WEISSBACH
Fr	$[-]$	FROUDE number $Fr = V/(\sqrt{g \cdot h})$
Fr_d	$[-]$	densimetric FROUDE number $Fr_d = V/(\sqrt{(s-1) \cdot g \cdot d})$
Fr*	$[-]$	particle FROUDE number $Fr^* = V^*/(\sqrt{(s-1) \cdot g \cdot d})$, $Fr^* = \sqrt{\tau_0}/\sqrt{\gamma_s - \gamma_w \cdot d}$, $Fr^* = \sqrt{\tau^*} = \sqrt{\theta}$
F_S	$[N]$	Force due to the bed shear stress
g	$[m/s^2]$	gravitational acceleration (9.81)
G'	$[N]$	gravity force (vertical resulting force)
h	$[m]$	flow depth
h_s	$[m]$	scour depth (water surface to ground)
K	$[-]$	constant

---

1. $N = kg \cdot m/s^2$

Notations

K_S	$[m^{1/3}/s]$	roughness coefficient of STRICKLER
k_x	[-]	coefficient of proportionality
L	[N]	dynamic lift force
m	[-]	bank slope
n	$[s/m^{1/3}]$	friction coefficient of MANNING $1/n = K_S$
n	[-]	friction factor used by Zimmermann $n = 1.13/\sqrt{f}$
p	[-]	porosity
P	[m]	wetted perimeter
p_i	[-]	part (weight) of the sediment fraction i of a sediment sample
Q	$[m3/s]$	discharge
q_i	[-]	probability that the fraction i of a sediment sample will stay in place (no movement)
r	[m]	radius of curvature
R	[-]	Pearson product moment correlation coefficient
R_c	[m]	radius of curvature at the centerline
Re	[-]	Reynolds number $Re = V \cdot 4R_h/\nu$
Re*	[-]	Grain or shear Reynolds number $Re* = V* \cdot d/\nu$
R_h	[-]	Hydraulic radius
s	[-]	sediment density coefficient $s = \rho_s/\rho_w = 2.635$
sig	[-]	sign ±1 depending on the boundary condition; used for the establishment of a new scour formula
S	[-]	longitudinal slope
V, v	[m/s]	average respectively local velocity
Vol	$[m^3]$	volume
V_*	[m/s]	friction velocity $V* = \sqrt{\tau_0/\rho_w} = \sqrt{g \cdot R_h \cdot S_e}$
X, x	[m]	carthesian coordinates in stream direction (inlet reach)
Y, y	[m]	carthesian coordinates in lateral/radial direction
Z, z	[m]	carthesian coordinates - elevation
α_1, α_2	[°]	location of the first / second scour hole (opening angle between beginning of the bend and the scour hole)

α	[-]	projected area of a grain normalized by d^2 (by the projected area of a sphere for Zimmermann)
β	[°]	lateral bed slope
γ	[N/m^3]	weight
δ	[°]	opening angle between D et D_θ
ε	[m]	size of the characteristic roughness element
Φ	[-]	dimensionless sediment transport rate
φ	[°]	static friction coefficient / shear angle (see 3.1.1/g)
ϕ	[°]	dynamic (bedload) friction coefficient / shear angle, which is in most cases of the same order as the static friction coefficient / shear angle (Bagnold, 1973) *in the formula of Odgaard:* opening angle of channel (0° = beginning of bend)
θ	[-]	SHIELDS parameter or dimensionless shear stress (also noted τ^*) $\theta = V^{*2}/((s-1) \cdot g \cdot d)$, $\theta = \tau_0/((\gamma_s - \gamma_w) \cdot d)$, $\theta = R_h \cdot S_0/((s-1) \cdot d)$
κ	[-]	VON KARMAN constant ($\kappa \approx 0.4$)
λ_0	[-]	Sheltering coefficient of Kikkawa et al. $\lambda_0 = 0.592$
η	[m]	scour depth (initial or average over cross-section to bed level)
$\mu = \tan\phi$	[-]	friction coefficient
ρ_s	[kg/m^3]	density of the sediments (= 2'635)
ρ_w	[kg/m^3]	density of the fluid (water)
σ	[-]	scatter / width of the grain size distribution $\sigma = \sqrt{d_{84}/d_{16}}$
τ	[N/m^2]	shear stress $\tau_0 = \rho_w \cdot g \cdot R_h \cdot S_e$, $\tau_0 = \rho_w \cdot V^{*2}$
τ^*	[-]	see θ
ν	[m^2/s]	cinematic viscosity of the water
ξ	[%]	distance of the maximum transversal bed slope location from the channel axis in % of the channel width.

Subscripts and exponents

0	bed
1, 2	first and second scour hole
12	maximum of minimum and maximum scour hole
A, arm	armoring (layer)

Notations

bed	bed
b	bedload
bf	bedforms
c	center or computed
cr	critical
d	deposition (deposited volume)
e	energy / erosion (eroded volume)
g	grain
w	fluid (water) or wall / bank
o	outside
out	outlet reach
i	inside
in	inlet reach
m, $\bar{x}$	mean / average or measured
max, min	maximum, minimum
md, $\bar{x}_d$	mean / average over the depth
mw, $\bar{x}_w$	mean / average over the width of the channel
ms, $\bar{x}_s;\bar{x}_x$	mean / average over the cross-section
r	radial direction / component
s	sediment
S	substrate
ug	uniform grain
w	wall (influence) or acting on the wall
$\perp$	perpendicular / projection
θ	tangential / stream direction / component
*	grain

References

Ackers, P & White, W.R. (1973). *Sediment transport: New approach and analysis*, Journal of the Hydraulics Division, 99(11), 2041-2060

Ahmad, M. (1953). *Experiments on design and behaviour of spur dikes*. Proceedings IAHR conference, Minnesota, USA, 145-159

Allen, J.R.L (1970a). *A quantitative model of grain size and sedimentary structures in lateral deposits*, Geological Journal 7, 129-146

Allen, J.R.L. (1970b). *Studies in fluviatile sedimentations: A comparison of fining upwards cyclotherms, with special reference to coarse-member composition and interpretation*, Journal of sedimentary petrology, 40, 298-323

Ashida, K. & Michiue, M. (1971). *An investigation of river bed degradation downstream of a dam*. 14th IAHR Congress Paris, Vol.3

Atsuyuki, D. (1992). *Control of local scour in bend channel by roughness on embankment*, 5th International Symposium on River Sedimentation, Karlsruhe, Germany, 61-70

Babovic, V., Keijzer, M., Rodriguez Aguilera, D., Harrington, J. (2001). *An evolutionary approach to knowledge induction: genetic programming in hydraulic engineering*. Proceedings of the World Water & Environmental Resources Congress, ASCE, May 21-24, 2001, Orlando, Fl. USA.

Bagnold, R.A. (1954). *Experiments on a gravity-free dispersion of large solid spheres in a Newtonian fluid under shear*, Proceedings of the Royal Society of London, A.225, 49-63

Bagnold, R.A. (1956). *The flow of cohesionless grains in fluids*, Proceedings of the Royal Society of London A.249, 235-297

Bagnold, R.A (1966). *An approach to the sediment transport problem from general physics*, U.S. Geological Survey Professional Paper 422-I, 37 pp.

Bagnold, R-A. (1973). *The nature of saltation and of 'bed-load' transport in water*, Proceedings of the Royal Society of London, A.340, 473-504

Bagnold, R.A. (1974). *Fluid forces on a body in shear flow; experimental use of 'stationary flow'*, Proceedings of the Royal Society of London, A.340, 147-171

Bathurst, J.C., Thorne C.R. & Hey, R.D. (1979). *Secondary flow and shear stress at river bends*, Journal of the Hydraulics Division, ASCE 105(10), 1277-1295, October 1979

Bazilevich, V.-A. (1982). *Calculation of a local scour depression near a concave bank of a gravel-pebble channel*, Gidrotechniceskoe Stroitelstvo 10, 19-22, October 1982, Translated 1983 by Plenum Publishing Corp.

Billi, P., Hey, R.D., Thorne, C.R. & Tacconi, P. (1992). *Dynamics of gravel bed rivers*, John Wiley and Sons, New York, 673 pp.

Bishop, A.A, Simons, D.B. & Richardson, E.V. (1965). *Total bed material transport*. Proceedings ASCE, Journal opf the Hydraulics Division 91(2), 175-191

Blanckaert, K. & Graf, W.H. (2001). Mean flow and turbulence in open-channel bend. Journal of Hydraulic Engineering, ASCE 127(10), 835-847

Bluck, B.J. (1971). *Sedimentation in the meandering river Endrick*, Scottish Journal of Geology, 7(2) 93-138

Breusers, H.N.C. & Raudkivi, A.J. (1991). *Scouring*, IAHR Hydraulic Structures Design Manual 2, A.A. Balkema, Rotterdam, Brookfield, The Netherlands, 142 pp.

Bridge, J.S. (1976). *Bed topography and grain size in open channel bends*, Sedimentology, Int. Association of Sedimentologists, 23, 407-414

Brown, C.B. (1950). *Sediment transportation in Engineering Hydraulics*. H. Rouse, Editor, Wiley & Sons, New York

Chepil, W.S. (1958). *The use of evenly spaced hemispheres to evaluate aerodynamic forces on a soil surface*, Transactions of the American Geophysical Union, Vol. 39, 397-403, June 1958

Childs, S.J. (2001). *Incipient motion criteria for a rigid sediment grain on a rigid surface*, Journal of Engineering Mechanics, ASCE, 127(5), 524-529, May 2001

Choi, K-S. (2000). *Drag reduction research at the University of Nottingham*, European Research Community on Flow, Turbulence and Combustion (ERCOFTAC) Bulletin 22, 15-21

Costet, J & Sanglerat, G. (1981). *Cours pratique de mécanique des sols, Tomme 1: Plasticité et calcul des tassements*, 3rd Edition, Dunod, Paris (1st & 2nd Edition: 1969, 1975)

Crickmore, M.J. (1967). *Measurement of sand transport in rivers with special reference to tracer methods*, Sedimentology, 8, 175-228

Crickmore, M.J. (1970). *Effects of flume width on bed-form characteristics*, Journal of the Hydraulics Division, 96(2), 473-496, Proceeding Paper 7077, February 1970

de Vriend, H.J. (1976). *A mathematical model of steady flow in curved shallow channels*. Journal of Hydraulic Research, IAHR, 15(1), 37-54

References

de Vriend H.J. (1981). *Steady Flow in Shallow Channel Bends*, Communications on Hydraulics, Report no. 81-3, Department of Civil Engineering, Delft University of Technology.

Donat, J. (1929). *Über Sohlangriff und Geschiebetrieb.* Die Wasserwirtschaft 26,27

du Boys, P. (1879). *Etudes du régime du Rhône et l'action exercée par les eaux sur un lit à fond de graviers indéfiniment affouillable*; Annales des ponts et chaussées, 5(18) 141-195

Dubois, J. (1998). *Comportement hydraulique et modélisation des écoulements de surface*; Ph.D. work Nr. 1890, Swiss Federal Institute of Technology (EPFL) Lausanne, Switzerland, also published as Communication 8 du Laboratoire de Constructions Hydrauliques (LCH) de l'EPFL, 1998

Dysli, M. (1993). *Compléments aux cours polycopiés de technologie et de mécanique des sols*, 3rd Edition, Laboratoire de Méchanique des Sols, Ecole Polytechnique Fédérale (EPFL), Lausanne, Switzerland, September 1993

Egiazaroff, I.V. (1965). *Calculation of nonuniform sediment concentrations.* Journal of the Hydraulics Division, ASCE, 91(4)

Einstein, H.A. (1934). *Der hydraulische oder Profilradius*, Schweizerische Bauzeitung, 103(8), 147-150

Einstein, H.A. (1950). *The bed-load function for sediment transportation in open channel flows*; Technical Bulletin 1026, U.S. Department of Agriculture, Soil Conservation Service, September 1950; 70 pp.

Einstein, H.A. & Chien, N. (1953). *Transport of sediment mixtures with large range of grain sizes*; MRD Series 2; Institute of Engineering Research; University of California, Berkeley, 1953

Einstein, H.A. & El Samni, S.A. (1949). *Hydrodynamic forces on a rough wall,* in Review of modern physics 21, McGraw Hill, London, 491 pp.

Engelund, F. (1974). *Flow and bed topography in channel bends*, Journal of the Hydraulics Division, ASCE, 100(11), 1631-1648, November 1974

Engelund, F. (1976). *Errata to "Flow and bed topography in channel bends"*, Journal of the Hydraulics Division, ASCE, 102(3), 416-418, March 1976

Engelund, F. & Hansen, E. (1967). *A monograph on sediment transport in alluvial streams*, Teknish Forlag, Technical Press, Copenhagen, Denmark, 62 pp.

Falcon, A.M. (1979). *Analysis of flow in alluvial channel bends*, Ph.D. thesis, University of Iowa, Iowa City

Falcon, A.M. & Kennedy, J.F. (1983). *Flow in alluvial-river curves*; Journal of Fluid Mechanics 133, 1-16

Fargue (1868). *Etude sur la corrélation entre la configuration du lit et la profondeur d'eau dans les rivières à fond mobile*, Annales des ponts et chaussées, 1868

Fehr, R. (1987). *Geschiebeanalysen in Gebirgsflüssen*, Mitteilung 92 der Versuchsanstalt für Wasserbau, Hydrologie und Glaziologie (VAW), ETHZ, Zürich, Switzerland, 1987, 139 pp.

Gairola, A. (1996). *Finite element solutions of fluid flow with heat transfer past obstructions*, Ph.D. thesis Nr. 247-667, Department of Civil Engineering, University of Roorkee, India, September 1996, 212 pp.

Garbrecht, G. (1953) *Wasserabfluss in gekrümmten Gerinnen*, Die Wasserwirtschaft 44(2+3), 29-35, 66-71

Gaudio, R., Marion, A. & Bovolin, V. (2000). Morphological effects of bed sills in degrading rivers, Journal of Hydraulic Research, IAHR, 38(2)

Gessler, J. (1965). *Der Geschiebetriebbeginn bei Mischungen untersucht an natürlichen Abpflästerungerscheinungen in Kanälen*; Ph.D. work No. 3711, Eidgenössische Technische Hochschule (ETHZ), Zürich, Switzerland; also published as: Mitteilung 69 der Versuchsanstalt für Wasserbau, Hydrologie und Glaziologie (VAW), ETHZ, Zürich, Switzerland, 1966, 67 pp.
translated by E.A. Prych: *The beginning of bedload movement of mixtures investigated as natural armoring in channels*; Keck Laboratory of Hydraulics and Water Resources. Pasadena: California Institute of Technology; October 1968, 89 pp.

Gessler, J. (1970). *Self-stabilizing tendencies of alluvial channels*, Journal of the Waterways, harbors and coastal engineering Division, ASCE, 96(2), 235-249

Gessler, J. (1990). Friction factor of armored river beds, Journal of Hydraulic Engineering, ASCE, 116(4), 531-543

Graf, W.H. (1971). *Hydraulics of sediment transport*, McGraw Hill, London, 513 pp.

Graf, W.H. (1984). *Hydraulics of sediment transport*, Water Research Publications, LLC (reprinted)

Graf, W.H. & Altinakar, M. (1998). *Fluvial hydraulics*, Book, John Wiley and Sons, 682 pp.

Günter A. (1971). *Die kritische mittlere Sohlenschubspannung bei Geschiebemischungen unter Berücksichtigung der Deckschichtbildung und der turbulenzbedingten Sohlenschubspannungsschwankungen*, Mitteilung. 3 der Versuchsanstalt für Wasserbau Hydrologie und Glaziologie (VAW) der Eidgenössische Technische Hochschule (ETHZ), Zürich, Switzerland

Günther, O. (2001). *Investigation of the influence of macro-roughness elements on the erosion process in a curved open channel*, Diploma work at the Laboratoire de Constructions Hydrauliques (LCH), Ecole Polytechnique Fédérale de Lausanne (EPFL), Switzerland, July 2001, 63 pp.

Habib A.M. (1986). *Turbulent structure in a river bend*, Journal of Hydraulic Engineering, ASCE 112(8), 657-669, August 1986

Harrison, A.S. (1950). *Report on a special investigation of bed sediment segregation in a degrading bed*, 33(1), University of California, Berkeley, USA (cited in Hunziker 1995)

Heckel H. (1978). *Spiral und Sedimentbewegung in Fluss- und Kanalkrümmungen*, Die Wasserwirtschaft 68(10), 287-294

Hersberger, D.S. (2002). *Measurement of 3D flow field in a 90° bend with ultrasonic Doppler velocity profiler*, Third International Symposium on Ultrasonic Doppler Methods for Fluid Mechanics and Fluid Engineering, EPFL, Lausanne, Switzerland, September 9 - 11, 2002, pp. 59-66

Hersberger, D.S. & Schleiss, A.J. (2002). *Scour formulae and their applicability to coarse gravel alpine rivers*, River Flow 2002, Int. Conference on Fluvial Hydraulics, Louvain-la-Neuve, Belgium, Sept. 4-6, Vol. 2, p. 1031-1039

Hjulström, F. (1935). *Studies of the morphological activity of rivers as illustrated by the River Fyris*, Bulletin of the Geological Institution, University of Upsala

Hoffmans, G.J.C.M. & Verheij, H.J. (1997). *Scour manual.* A.A. Balkema, Rotterdam, 205 pp.

Hook, R.L. (1974). *Shear-stress and sediment distribution in a meander bend*, Ungi Report 30, University of Upsala, Sweden, 1974 (cited in Engelund 1974)

Huntley, H.E. (1953). *Dimensional analysis*, McDonald and Company, London

Hunziker, R.P. (1995). *Fraktionsweiser Geschiebetransport* / Fractionwise sediment transport; Mitteilung 138 der Versuchsanstalt für Wasserbau, Hydrologie und Glaziologie (VAW); Eidgenössische Technische Hochschule (ETHZ); Zürich, Switzerland, 209 pp.

Inglis, C.C. (1949). *The behaviour and control of rivers and canals*, Research publication 13, C.W.I.N.R.S Poona

Ikeda, S. (1971). *Some studies on the mechanics of bed load transport*, Proceedings of the Japan Society of Civil Engineers (JSCE), 185, 56-57

Iwagaki, Y. (1956). *Hydrodynamic study on the tractive force*; Transactions of the Japan Society of Civil Engineers (JSCE), 41, 36 pp.

Jäggi, M. (1985,1995,1999). *Flussbau*, Lecture notes, First edition 1985, Reviewed 1995, 1999, Versuchsanstalt für Wasserbau, Hydrologie und Glaziologie (VAW), Swiss Federal Institute of Technology (ETHZ), Zürich, Switzerland, 347 pp. (3rd Ed.)

Jäggi, M., Bezzola, G.R. & Kuster, P. (1996). *Hydraulische Modellversuche für das Hochwasserschutzprojekt Gurtnellen*, Wasser, Energie, Luft, 88(5/6)

Karim, M.F. (1981). *Computer-based prediction for sediment discharge and friction factor of alluvial streams*, Ph. D. thesis, Department of Mechanics and Hydraulic, University of Iowa (cited in Falcon & Kennedy, 1983)

Keijzer, M. & Babovic., V. (1999). *Dimensionally Aware Genetic Programming.* GECCO-99: Proceedings of the Genetic and Evolutionary Computation Conference. July 13-17, 1999, Orlando, Florida

Keulegan, G.H. (1938). *Laws of turbulent flow in open channels*; Journal of Research of the National Bureau of Standards, US Department of Commerce, 21(6), 707-741, December 1938

Kikkawa, H., Ikeda, S. & Kitagawa, A (1976). *Flow and bed topography in curved open channels*, Journal of the Hydraulics Division, ASCE, 102(9), 1372-1342, September 1976

Kline, S.J. (1965). *Similitude and approximation theory*, McGraw-Hill, New York

Kramer, H. (1935). Sand mixtures and sand movement in fluvial models, Transactions ASCE, 100, 798-838

Kuhnle, R.A., Alonso, C.V. & Shields, F.D. (1999) *Geometry of scour holes associated with 90° spur dikes*, Journal of Hydraulic Engineering, ASCE, 125(9), 972-933.

Kuster P., Jäggi, M. & Bezzola, G.R. (1992). *Gurtnellen - Bericht über die Modellversuche für das Hochwasserschutzprojekt Gurtnellen-Wiler, Band 1 & 2 (Anhang)*, Report 3977, Versuchsanstalt für Wasserbau, Hydrologie und Glaziologie (VAW), Eidgenössische Technische Hochschule (ETHZ), Zürich, October 1992

Lang, H-J., Huder, J. & Amann, P. (1986). *Bodenmechanik und Grundbau: das Verhalten von Böden und Fels und die wichtigsten grundbaulichen Konzepte*; 6th Edition, Springer Verlag, Berlin, Heidelberg, New York (1st Edition: 1982)

Lemmin, U, & Rolland, T. (1997). *Acoustic velocity profiler for laboratory and field studies.* Journal of Hydraulic Engineering, ASCE, 123(12), 1089-1098

Liu, H.K., Chang, F.M. & Skinner, M.M. (1961). *Effect of bridge construction on scour and backwater*, Report CER60-HKL22, Department of Civil Engineering, Colorado State University,

Luque, R.F, & van Beek, R. (1976). Erosion and transport of bedload sediment. Journal of Hydraulic Research, ASCE, 15(2)

Masson, S. & Martinez, J. (2001) *Micromechanical analysis of the shear behavior of a granular material*, Journal of Engineering Mechanics, ASCE, 127(10), 1007-1016, October 2001

Mavis, F.T. & Laushey, L.M. (1948). *A reappraisal of the beginning of bed movement-competent velocity*, Report on the Second meeting, IAHSR (today IAHR), Stockholm, Sweden, 7-9 June 1948

McEwan, I.K., Jefcoate, B.J., Willetts, B.B. (1999) *The grain-fluid interaction as a self stabilizing mechanism in fluvial bed load transport,* Sedimentology, Blackwell Publishing, 46(3), 407-416

Melville, B.W. & Coleman, S.E. (1999). *Bridge scour*, Water Resources Publications, Littleton, Colorado

Melville, B. & Raudkivi, A.J. (1984). *Local scour at bridge abutments*, National Roads Board, New Zealand, RRU Seminar on bridge design and research, Auckland

Metflow (2000). *UVP Monitor Model UVP-XW - Users guide.* March 2000, Metflow SA, Lausanne, Switzerland

References

Meyer-Peter, E., Favre, H. & Einstein, A. (1934). *Neuere Versuchsresultate über den Geschiebetrieb*, Schweizerische Bauzeitung 103 (8), 147-150

Meyer-Peter, E. & Müller, R. (1948). *Formulas of bed-load transport*, Report on the second meeting of the IAHSR (today IAHR), Stockholm, Sweden, 7-9 June 1948, 39-64

Milhous, R.T. (1973). *Sediment transport in gravel-bottomed stream*. Ph.D. thesis, Department of Civil Engineering, Oregon State University, USA

Misri, R.L., Garde, R.J. & Ranga Raju, K.G. (1984). *Bed load transport of coarse nonuniform sediment*, Journal of Hydraulic Engineering, ASCE, 110(3), 312-328, March 1984

Molinas, A., Kheireldin, K. & Wu, B. (1998). *Shear stress around vertical wall abutments*, Journal of Hydraulic Engineering, ASCE, 124(8), 822-830.

Molinas, A. & Wu, B. (1998). *Effect of size gradation on transport of sediment mixtures*, Journal of Hydraulic Engineering, ASCE, 124(8), 786-793.

Molinas, A. & Wu, B. (2001). *Transport of sediment in large sand-bed rivers*; Journal of Hydraulic Research; IAHR, A.A. Balkema, Rotterdam, Brookfield, 39(2) 135-146, April 2001

Nikuradse, J. (1933). *Strömungsgesetze in rauhen Röhren*; Beilage zu Forschung auf dem Gebiete des Ingenieurwesens; Ausgabe B, Band 4, Juli/August; VDI-Verlag GmbH; Berlin NW7.

Nunner, W. (1956) *Wärmeübergang und Druckabfall in rauhen Rohren*, VDI-Forschungsheft 455, Serie B, Band 2

Odgaard, A.J. (1981). *Transverse bed slope in alluvial channel bends*; Journal of the Hydraulics Division, ASCE, 107(12), 1677-1694

Odgaard, A.J. (1982). *Bed characteristics in alluvial channel bends*; Journal of the Hydraulics Division, ASCE, 108(11) 1268-1281

Odgaard, A.J. (1984). *Flow and bed topography in alluvial channel bend*, Journal of Hydraulic Engineering, ASCE, 110(4), 521-536

Odgaard, A.J. (1984b). *Bank erosion contribution to stream sediment load*, Report No. 280, Iowa Institute of Hydraulic Research, University of Iowa, August 1984, 92 pp.

Odgaard, A. J. (1986). *Meander flow model I: Development*, Journal of Hydraulic Engineering, ASCE, 112(12), 1117-1136

Odgaard, A.J. & Kennedy, J.F. (1982). *Analysis of Sacramento River bends flow and development of a new method for bank protection*, Report 241, Iowa Institute of Hydraulic Research, University of Iowa, May 1982, 85 pp.

Odgaard, A.J. & Kennedy, J.F. (1983). *River-bend bank protection by submerged vanes*, Journal of Hydraulic Engineering, ASCE, 109(8), 1161-1173

Odgaard, A.J. & Lee, H-Y.E. (1984). *Submerged vanes for flow control and bank protection in streams*, Report 279, Iowa Institute of Hydraulic Research, University of Iowa, July 1984, 92 pp.

Odgaard, A.J. & Mosconi, C.E. (1987). *Streambank protection by Iowa Vanes*, Report 306, Iowa Institute of Hydraulic Research, University of Iowa, January 1987, 34 pp.

Onishi, Y., Subhash, C.J. & Kennedy, J.F. (1976). *Effects of meandering in alluvial streams*, Journal of the Hydraulics Division, ASCE 102(7), 899-917, July 1976

Orlandi, O. & Leonardi, S. (2000). *DNS of bounded flows with manipulated walls*, European Research Community on Flow, Turbulence and Combustion (ERCOFTAC) Bulletin 44, 22-29

Papanicolau, A.N., Diplas, P., Dancey, C.L., Balakrishnan, M. (2001). *Surface roughness effects in near-bed turbulence: Implications to sediment entrainment,* Journal of Engineering Mechanics, ASCE, 127(3), 211-218

Parker, G., Klingeman, P.C. & McLean, D.G. (1982). Bedload and size distribution in paved gravel-bed streams. Journal of the Hydraulics Division, ASCE, 108(4)

Parker, G. (1990). *Surface-based bedload transport relation for gravel rivers*. Journal of Hydraulic Research, IAHR, 28(4), 417-436

Peter, W. (1986). *Kurvenkolk- Untersuchungen über Sohlenausbildung in Flusskrümmungen*, Mitteilung 85 der Versuchsanstalt für Wasserbau, Hydrologie und Glaziologie (VAW), Eidgenössische Technische Hochschule (ETHZ), Zürich, Switzerland, 165 pp.

Prantl, L. (1926). *Über die ausgebildete Turbulenz*, Proceedings of the 2nd International congress of applied mechanics, Zürich, 62-74

Przedwojski, B., Blazejewski, R. & Pilarczyk, K.W. (1995). *River training techniques: Fundamentals, design and applications*, A.A. Balkema, Rotterdam

Raudkivi, A.J. (1967, 1976, 1990). *Loose Boundary Hydraulics*. Pergamon Press, Oxford, New York

Reindl, R. (1994). *Sohl- und Strömungsausbildung in einer Bodenfolge mit und ohne Rückstaueinfluss*, Ph.D thesis, Institut für Wasserbau, Leopold-Franzens-Universität, Innsbruck, 174 pp.

Rhodes, D. & Senior, A.K. (2000). *Numerical study of resistance with rib roughness of various scales*, Journal of Hydraulic Engineering, ASCE, 126(7), 541-546

Ribberink, J.S. (1987). *Mathematical modelling of one-dimensional morphological changes in rivers with non-uniform sediment*, Ph.D. thesis, Delft University of Technology; also published as Communication 87-2 on Hydraulic and Geotechnical Engineering, TU Delft, 200 pp.

Rodriguez Aguilera, D. (2000). *Genetic programming with GPKernel* - Software developed by V. Babovic and M. Keijzer, Users Manual, Version November 2000, Danish Hydraulic Institute (DHI), 65 pp.

Rolland, T. (1995). *Développement d'une instrumentation Doppler ultrasonore: Application aux écoulements turbulents*, Ph.D. thesis 1281, Laboratoire de Recherches Hydrauliques (LRH) (today: Laboratoire d'Hydraulique Environnementale, LHE), Ecole Polytechnique Fédérale (EPFL), Lausanne, Switzerland, 159 pp.

Rolland, T. & Lemmin, U. (1997). A two-component acoustic velocity profiler for use in turbulent open channel flow. Journal of Hydraulic Research, IAHR, 35(4)

Rozovskii, I.L. (1957). *Flow of water in bends of open channels*, Institute of Hydrology and Hydraulic Engineering, Academy of Sciences of the Ukrainian SSR, Kiew, Translated 1961 by Y. Prushansky, Israel Program for Scientific Translation, Jerusalem, National Science Foundation, Cat. No 363, 23 pp.

Rubey, W.W. (1933). *Settling velocities of gravel, sand, and silt particles*; American Journal of Science, 25(148), 325-338

Scherl, G. (1996). *Der Einfluss der Wandrauhigkeit auf den Bodenkolk*, Diploma work, Institut für Wasserbau Innsbruck, Leopold-Franzens-Universität Innsbruck, 95 pp.

Scheuerlein, H. & Schöberl, F. (2001). *Integrated conception of hydraulic structures - Intake structures*, Lecture notes of the Sub module 3.2 of the Postgraduate Studies in Hydraulic Structures, Laboratoire de Constructions Hydrauliques (LCH), Ecole Polytechnique Fédérale (EPFL), Lausanne, Switzerland

Schleiss, A. (2000). *Uferschutz an Gebirgsflüssen*, Wasser, Energie, Luft, Baden, Switzerland, 92. Jahrgang, 9/10, 271-280

Schleiss, A. & Hersberger, D. (2001). *Grain sorting process and scour in a curved channel with coarse gravel bed*, Proceedings of the 29th IAHR Congress, September 16-21, 2001, Beijing, China, Theme D, Volume 2, 140-145

Schöberl, F. (2002). *Personal communication.* Institut für Wasserbau, Universität Innsbruck, April 2002

Schoklitsch, A. (1934). *Geschiebetrieb und die Geschiebefracht.* Wasserkr. Wasserwirtschaft, 39(4)

Shields, A. (1936). *Anwendungen der Ähnlichkeitsmechanik und der Turbulenzforschung auf die Geschiebebewegungen*, Mitteilungen der Preussischen Versuchsanstalt für Wasserbau und Schiffbau, Heft 26, Berlin, Deutschland; [*Application of similarity principles and turbulence research to bed-load movement*, English translation: W.M. Keck Laboratory of Hydraulics and Water Resources, California Institute of Technology, Report 167, 43 p.]

Shukry, A. (1950). *Flow around bends in an open flume*, Transactions ASCE, 115, 751-779.

Sibanda, E., McEwan, I. & Marion, A. (2000). *Measuring the structure of mixed-grain-size sediment beds.* Journal of Hydraulic Engineering, ASCE, 126(5), 347-353

Sinniger, R.O. & Hager, W.H. (1989). *Constructions Hydrauliques*, Traité de Génie Civil 15, Presses Polytechniques Romandes, Lausanne, Switzerland, 439 pp.

Sleath, J.F.A. (1984). *Sea bed mechanics.* John Wiley & Sons, New York, 335 pp.

Smart, G.M. (1999). *Turbulent velocity profiles and boundary shear in gravel bed rivers.* Journal of Hydraulic Engineering, ASCE, 125(2), 106-116

Smart, G.M. & Jäggi, M.N.R. (1983). *Sedimenttransport in steilen Gerinnen / Sediment transport on steep slopes*: Mitteilung 64 der Versuchsanstalt für Wasserbau, Hydrologie und Glaziologie (VAW), Eidgenössische Technische Hochschule (ETHZ), Zürich, Switzerland, 191 pp.

Strickler A. (1923). *Beiträge zur Frage der Geschwindigkeitsformel und der Rauhigkeitszahlen für Ströme, Kanäle und geschlossene Leitungen*; Mitteilung 16 des Eidgenössischen Amtes für Wasserwirtschaft, Bern, Switzerland

Talmaza, V.F. & Kroshkin, A.N. (1968). *Hydromorphometric characteristics of mountain rivers* [in Russian], Kyrgyzstan, Frunze (cited in Bazilevich, 1982)

Ting, F.C.K, Briaud, J-L. & Chen, H.C. (2001). *Flume tests for scour in clay at circular piers*, Journal of Hydraulic Engineering, ASCE, 127(11), 969-978

Uijttewaal, W.S.J., Lehmann, D. & van Mazijk, A. (2001). *Exchange processes between a river and its groyne fields: model experiments,* Journal of Hydraulic Engineering, ASCE 127(11), 928-936

van Bendegom, L. (1947). *Eenige beschouwingen over riviermorphologie en rivierverbetering*, De Ingenieur, 59(4), 1-11

Vanoni, V. (1975). *Sedimentation Engineering*, ASCE Manual No. 54

Velikanov, M.A. (1954). *Gravitational theory for sediment transport*; Journal of Science of the Soviet Union, Geophysics, 4 (in Russian), cited in Molinas & Wu (2001)

von Karman, Th. (1921). *Über laminare und turbulente Reibung*; Zeitschrift für angewandte Mathematik und Mechanik, Verlag des Vereines Deutscher Ingenieure 1 (4), 233-252

Wallbridge, S., Voulgaris, G., Tomlinson, B.N., Collins, M.B. (1999). *Initial motion and pivoting characteristics of sand particles in uniform and heterogenous beds: experiments and modelling,* Sedimentology, 46(1), 17-32, Blackwell Publishing, Williston VT, USA and Abingdon, Oxon, UK

Wang, Z-Y. (1999). *Experimental study on scour rate and river bed inertia.* Journal of Hydraulic Research, IAHR, 37(1), 17-37

References

Williams, R. (1899). *Flussbefestigungen erläutert an einer Flussstrecke der weissen Elster sowie Beispiele zur Nachprüfung der Fargue'schen Gesetze mit Hilfe der Stossflächen*, Verlag Wilhelm Engelmann, Leipzig, 66 pp.

Yang C.T. (1973). *Incipient motion and sediment transport*, Journal of the Hydraulics Division; ASCE 99(10), 1679-1704

Yang C.T. & Molinas, A. (1982). *Sediment transport and unit stream power function*, Journal of the Hydraulics Division; ASCE, 108(6), 774-793

Yankielun, N. & Zabilansky, L. (2000). *Laboratory experiments with an FM-CW reflectometry system proposed for detecting and monitoring bridge scour in real time*, Canadian Journal of Civil Engineering, NRC, 27(1), 27-32

Yalin M.S. (1977). *Mechanics of sediment transport*, 2nd edition, Pergamon Press, Oxford

Yalin, M.S. & Scheuerlein, H. (1988). *Friction factors in alluvial rivers*, Report 59; Instituts für Wasserbau und Wassermengenwirtschaft, Oskar von Miller-Institut, Obernach, Technische Universität München, 1988

Yalin, M.S. & da Silva, A.M. (2001). *Fluvial processes.* IAHR Monograph, Delft, The Netherlands, 197 pp.

Yen, C. (1970). *Bed topography effect on flow in a meander*, Journal of the Hydraulics Division, ASCE 96(1), 57-73.

Zanke, U. (1982). *Grundlagen der Sedimentbewegung*; Springer Verlag, Heidelberg, Germany

Zarn, B. (1997). *Einfluss der Flussbreite auf die Wechselwirkung zwischen Abfluss, Morphologie und Geschiebetransportkapazität*, Mitteilung 154 der Versuchsanstalt für Wasserbau, Hydrologie und Glaziologie (VAW), Eidgenössische Technische Hochschule (ETHZ), Zürich, Switzerland, 240 pp.

Zimmermann, C. (1974). *Sohlausbildung, Reibungsfaktoren und Sedimenttransport in gleichförmig gekrümmten und geraden Gerinnen.* Ph.D. thesis, Universität Karlsruhe, June 1974

Zimmermann, C. (1983). *Einfluss der Sekundärströmung auf Sohlausbildung und Transportvorgänge in offenen Gerinnen*, Wasserwirtschaft, 73(11) 447-452

Zimmermann, C. & Kennedy, J.F. (1978). *Transverse bed slopes in curved alluvial streams*, Journal of the Hydraulics Division, ASCE, 105(1), 33-48

Zimmermann, C. & Naudascher, E. (1979). *Sohlausbildung und Sedimentbewegung in Krümmungen alluvialer Gerinne*, Wasserwirtschaft, 69(4) 110-117

References by chapter

Chapter 1 - Introduction
Jäggi, Bezzola, Kuster (1996)
Kuster, Jäggi, Bezzola (1992)
Schleiss (2000)

Chapter 2.1 - Flow in bends
Bathurst, Thorne & Hey (1979)
Blanckaert & Graf (2001)
de Vriend (1976, 1981)
Garbrecht (1953)
Habib (1986)
Heckel (1978)
Onishi, Subhash & Kennedy (1976)
Rozovskii, I.L. (1957)
Shukry, A. (1950)
Yen, C. (1970)

Chapter 2.2 - Sediment transport
Ackers & White (1973)
Bagnold (1966)
Billi, Hey, Thorne & Tacconi (1992)
Bishop et al. (1965)
Brown (1950)
Childs (2001)
Donat (1929)
du Boys (1879)
Egiazaroff (1965)
Einstein (1950)
Engelund & Hansen (1967)
Graf (1971, 1984)
Graf & Altinakar (1998)
Günter (1971)
Hunziker (1995)
Jäggi (1995)
Luque & van Beek (1976)
Masson & Martinez (2001)
McEwan, Jefcoate & Willetts (1999)
Meyer-Peter & Müller (1948)
Milhous (1973)
Misri et al. (1984)
Molinas & Wu (1998)
Papanicolau et al. (2001)
Parker et al. (1982)
Parker (1990)
Ribberink (1987)
Rubey (1933)
Schoklitsch (1934)
Shields (1936)
Sleath (1984)
Smart & Jäggi (1987)
Velikanov (1954)
Wallbridge et al.(1999)
Wang (1999)
Yalin & da Silva (2001)

Yang (1973)
Yang & Molinas (1982)
Zarn (1997)

Chapter 2.3 - Scouring
Ackers & White (1973)
Ahmad (1953)
Breusers & Raudkivi (1991)
Bridge (1976)
du Boys (1879)
Engelund (1974)
Engelund & Hansen (1967)
Falcon & Kennedy (1982)
Fargue (1868)
Gaudio, Marion & Bovolin (2000)
Hoffmans & Verheij (1997)
Inglis (1949)
Kikkawa et al. (1976)
Kuhnle, Alonso & Shields (1999)
Liu, Chang & Skinner (1961)
Melville & Coleman (1999)
Melville & Raudkivi (1984)
Molinas, Kheireldin & Wu (1998)
Molinas & Wu (1998)
Odgaard (1981)
Odgaard & Kennedy (1982, 1983)
Odgaard & Lee (1984)
Odgaard & Mosconi (1987)
Peter (1986)
Przedwojski, Blazejewski & Pilarczyk (1995)
Raudkivi (1967)
Reindl (1994)
Scherl (1994)
Ting, Briaud & Chen (2001)
Uijttewaal, Lehmann & van Mazijk (2001)
van Bendegom (1947)
Wang (1999)
Williams (1899)
Yang (1973)
Zarn (1997)
Zimmermann (1979)

Chapter 2.4 - Macro-roughness of banks
Atsuyuki (1992)
Choi (2000)
Gairola (1996)
Kikkawa et al. (1976)
Orlandi & Leonardi (2000)
Reindl (1994)
Rhodes & Senior (2000)
Scherl (1996)

Chapter 2.5 - Grain sorting
Gessler (1965)
Günter (1971)
Harrison (1950)
Hunziker (1995)

References by chapter

Keulegan (1938)

Chapter 2.6 - Measurement technique
Babovic et al. (2001)
Keijzer & Babovic (1999)
Kline (1965)
Lemmin & Rolland (1997)
Metflow (2000)
Rodriguez Aguilera (2000)
Rolland (1995)
Rolland & Lemmin (1997)
Smart (1999)
Yankielun & Zabilansky (2000)

Chapter 3.1 - Theory - Introduction
Costet & Sanglerat (1981)
Dysli (1993)
Fehr (1987)
Jäggi (1999)
Lang, Huder & Amann (1986)

Chapter 3.2 - Runoff and flow resistance
Dubois (1998)
Einstein (1950)
Hunziker (1995)
Jäggi (1999)
Keulegan (1938)
Nikuradse (1933)
Prantl (1926)
Sinniger & Hager (1989)
Strickler (1923)
Vanoni (1975)
von Karman (1921)
Zarn (1997)

Chapter 3.3 - Wall influence and armoring
Einstein (1934)
Einstein & El Samni (1949)
Gessler (1965, 1970, 1990)
Günter (1971)
Harrison (1950)
Hunziker (1995)
Keulegan (1938)

Chapter 3.4 - Sediment transport capacity
Ackers & White (1973)
Ashida & Michiue (1971)
Bagnold (1966)
Crickmore (1967, 1970)
du Boys (1879)
Egiazaroff (1965)
Einstein (1950)
Einstein & Chien (1953)
Graf (1971, 1984)
Graf & Altinakar (1998)

Hunziker (1995)
Iwagaki (1956)
Jäggi (1985,1995,1999)
Kramer (1935)
Meyer-Peter, Favre & Einstein (1934)
Meyer-Peter & Müller (1948)
Misri, Garde & Ranga Raju (1984)
Molinas & Wu (2001)
Ribberink (1987)
Rubey (1933)
Scheuerlein & Schöberl (2001)
Shields (1936)
Smart & Jäggi (1983)
Velikanov (1954)
Yang (1973)
Yang & Molinas (1982)
Yalin & Scheuerlein (1988)
Yalin (1977)
Zanke (1982)
Zarn (1997)

Chapter 3.5 - Bed topography (scouring)
Allen (1970a+b)
Bagnold (1954, 1956, 1966, 1973, 1974)
Bazilevich (1982)
Bluck (1971)
Bridge (1976)
Chepil.(1958)
Engelund (1974, 1976)
Fargue (1868)
Falcon (1979)
Falcon & Kennedy (1983)
Hersberger & Schleiss (2002)
Hjulström(1935)
Hook (1974)
Ikeda (1971)
Karim (1981)
Kikkawa, Ikeda & Kitagawa (1976)
Mavis & Laushey (1948)
Nunner (1956)
Odgaard (1981, 1982, 1984, 1986)
Peter (1986)
Reindl (1994)
Rozovskii (1957)
Schleiss & Hersberger (2001)
Talmaza & Kroshkin (1968)
Williams (1899)
Yang (1973)
Zanke (1982)
Zimmermann (1983)
Zimmermann & Kennedy (1978)
Zimmermann & Naudascher (1979)

Chapter 4.4 - Measurement technique
Hersberger (2002)
Metflow (2000)

Chapter 5.3 - Main tests
Reindl (1994)

Chapter 5.4 - Additional tests
Günther (2001)

Chapter 5.5 - Tests of Peter
Peter (1986)

Chapter 6.2 - Analysis of final scour
Gairola (1996)
Garbrecht (1953)
Peter (1986)

Chapter 6.5 - Analysis of the grain sorting
Gessler (1965, 1970, 1990)

Chapter 6.5 - Analysis of the flow field
Blanckaert & Graf (2001)
Gairola (1996)

Chapter 7.2 - Parameters for new formula
Bazilevich (1982)
Bridge (1976)
Engelund(1974)
Falcon & Kennedy (1983)
Fargue (1868)

Kikkawa et al. (1976)
Odgaard (1986)
Peter (1986)
Reindl (1994)
van Bendegom (1947)
Zimmermann (1978)

Chapter 7.3 - Establishing a new formula
Bridge (1976)
Huntley (1953)
Keijzer & Babovic (1999)
Kikkawa et al. (1976)
Kline (1965)
Peter (1986)
Rodriguez Aguilera (2000)

Chapter 7.5 - Validation with field data
Kuster, Jäggi & Bezzola (1992)
Odgaard & Kennedy (1982)
Odgaard (1984b)

Chapter 8.1 - Summary and conclusions
Bridge (1976)
Gairola (1996)
Keijzer & Babovic (1999)
Kikkawa et al. (1976)
Kline (1965)

References by chapter

Index of Authors

Index of Figures

5. Test results 99

6. Analysis of the test results 113

7. Establishing an empirical formula 149

8.   Summary, conclusions and recommendations 193

Index of Tables

8. Summary, conclusions and recommendations 193

Index of Keywords

Acknowledgments

Special tanks to Prof. Dr. A. Schleiss, initiator of this research project, who gave me the opportunity to carry out this interesting project.

Acknowledgments

Appendix - Table of contents

Appendix - Table of contents

APPENDIX 1

OVERVIEW OF THE TESTS

This Appendix contains tables summarizing the tests performed in the present study as well as the tests of Peter (1986).

The used variables are explained in the chapter *Notations*. If not especially mentioned, the characteristics were computed in the upstream reach (this applies e.g. for $h_{m, in, c}$, R_h, V_m, V^*, τ, θ, the different Froude and Reynolds numbers).

$S_{0, ini}$ is the initially built in bed slope (in tangential direction, along the axis of the channel).

h_1, h_2, h_{max} are the scour depth in the first, second scour hole and the maximum of them.

$\tan\beta_1$, $\tan\beta_2$, $\tan\beta_{max}$ are the maximum bed slopes in radial direction for the first and second scour and the maximum value.

ScLoc is the location of the scour.

The energy slope is given over three different areas: over the whole channel from the inlet to the outlet (from 4 m before to 4.6 m after the bend, $S_{e, all}$), over the domain equipped with macro-roughness (from 2 m before to 2 m after the bend, $S_{e, mr}$) and over the bend only (0° to 90°, $S_{e, bend}$).

The different characteristics were computed with d_{90} (at the final stage the bed surface was armored).

1.1 Table of basic test parameters

ID	$S_{0,ini}$ [%]	e_s [°]	e_d [mm]	Q_w [l/s]	Q_s [g/min]	Duration of test [h:min]	Measurements Water L.	Measurements Bed T.	Measurements Velocity	Sediment sampling Armor.	Sediment sampling outlet
A1a	0.50%	none	-	120	-	0:45	-	X	(X)	-	X
A1b				130	100	2:00	-	X	-	-	X
A1c				140	800	2:50	-	X	(X)	-	X
A1d				150	1 500	0:50	-	-	-	-	X
A1e				170	4 400	3:30	-	X	(X)	-	X
A1f				212.5	5 000	1:40	-	X	-	-	X
A2a	0.50%	2°	20	140	800	2:00	-	X	-	-	X
A2b				170	4 400	5:35	-	X	(X)	-	X
A2c				212.5	5 000	2:15	-	X	(X)	-	X
B1b	0.50%	none	-	151	1 579	15:10	X	X	X	X	X
B1c				182	2 385	17:50	X	X	X	X	X
B1d				212	4 819	18:55	X	X	X	X	X
B2b	0.50%	4°	20	151	255	17:05	X	X	X	X	X
B2c				183	577	16:10	X	X	X	X	X
B2d				212	1 566	14:20	X	X	X	X	X
B3b	0.50%	2°	20	151	830	14:40	X	X	X	X	X
B3c				183	873	16:20	X	X	X	X	X
B3d				213	1 744	17:20	X	X	X	X	X
B4b	0.50%	1°	20	151	435	15:05	X	X	X	X	X
B4c				182	408	15:40	X	X	X	X	X
B4d				212	1 806	13:00	X	X	X	X	X
C1b	0.70%	none	-	151	3 831	12:50	X	X	X	X	X
C1c				182	6 077	12:00	X	X	X	X	X
C1d				211	7 975	16:15	X	X	X	X	X
C2b	0.70%	4°	20	154	2 336	13:10	X	X	X	X	X
C2c				182	2 355	14:00	X	X	X	X	X
C2d				212	4 388	15:40	X	X	X	X	X

Table 1.1:   Basic test parameters (B = 1.00 m, R_c = 6.00 m, d_m = 8.5 mm, d_{90} = 14.8 mm, σ = 1.82, $\tan\phi$ = 0.754)

ID	$S_{0,ini}$ [%]	e_s [°]	e_d [mm]	Q_w [l/s]	Q_s [g/min]	Duration of test [h:min]	Measurements			Sediment sampling	
							Water L.	Bed T.	Velocity	Armor.	outlet
C3b	0.70%	2°	20	151	1 719	15:25	X	X	X	X	X
C3c				182	2 500	14:55	X	X	X	X	X
C3d				212	3 464	14:10	X	X	X	X	X
C4b	0.70%	1°	20	151	2 244	11:50	X	X	X	X	X
C4c				182	2 321	12:50	X	X	X	X	X
C4d				212	3 865	18:50	X	X	X	X	X
D1b	0.35%	none	-	151	693	16:10	X	X	X	X	X
D1c				183	875	24:15	X	X	X	X	X
D1d				211	1 309	18:30	X	X	X	X	X
D2b	0.35%	4°	20	150	303	14:20	X	X	X	X	X
D2c				181	767	17:15	X	X	X	X	X
D2d				211	1 236	17:55	X	X	X	X	X
D3b	0.35%	2°	20	150	298	14:45	X	X	X	X	X
D3c				180	184	17:25	X	X	X	X	X
D3d				211	647	17:50	X	X	X	X	X
D4b	0.35%	1°	20	150	385	15:20	X	X	X	X	X
D4c				181	159	18:25	X	X	X	X	X
D4d				211	1 295[1]	17:40	X	X	X	X	-
E2b	0.50%	4°	40	151	1 174	12:15	X	X	-	X	-
E2c				182	655	11:55	X	X	-	X	-
E2d				213	1 040	12:25	X	X	-	X	-
E3b	0.50%	2°	40	151	611	12:10	X	X	-	X	-
E3c				182	973	11:35	X	X	-	X	-
E3d				212	1 368	12:00	X	X	-	X	-
E5b	0.50%	8°	40	151	630	12:10	X	X	-	X	-
E5c				182	731	11:55	X	X	-	X	-
E5d				213	1 873	26:05	X	X	-	X	-

Table 1.1: Basic test parameters ($B = 1.00\ m$, $R_c = 6.00\ m$, $d_m = 8.5\ mm$, $d_{90} = 14.8\ mm$, $\sigma = 1.82$, $tan\phi = 0.754$)

1. Computed with added sediments (at the inlet), since the outlet volume was not measured for this test.

1.2 Table 1 of measured and computed parameters

ID	$h_{m,in,c}$ [m]	R_h [m]	h_1 [m]	h_2 [m]	h_{max} [m]	$\tan\beta_1$ [-]	$\tan\beta_2$ [-]	$\tan\beta_{max}$ [-]	$ScLoc_1$ [°]	$ScLoc_2$ [°]	$S_{e,all}$ [%]	$S_{e,mr}$ [%]	$S_{e,bend}$ [%]
B1b	0.138	0.108	0.302	0.315	0.315	0.592	0.573	0.592	29	81	0.54%	0.70%	0.83%
B1c	0.162	0.122	0.339	0.467	0.467	0.654	1.100	1.100	31	92	0.58%	0.78%	0.74%
B1d	0.189	0.137	0.392	0.371	0.392	0.644	0.536	0.644	29	83	0.57%	0.73%	0.71%
B2b	0.156	0.119	0.258	0.251	0.258	0.401	0.292	0.401	44	90	0.61%	0.80%	0.77%
B2c	0.181	0.133	0.295	0.229	0.295	0.329	0.255	0.329	49	90	0.62%	0.89%	0.88%
B2d	0.196	0.141	0.319	0.316	0.319	0.594	0.378	0.594	30	71	0.66%	0.93%	0.96%
B3b	0.145	0.112	0.251	0.252	0.252	0.399	0.381	0.399	70	71	0.56%	0.79%	0.74%
B3c	0.178	0.131	0.303	0.281	0.303	0.456	0.466	0.466	60	89	0.63%	0.86%	0.84%
B3d	0.195	0.140	0.324	0.315	0.324	0.451	0.538	0.538	55	80	0.66%	0.91%	0.81%
B4b	0.146	0.113	0.240	0.217	0.240	0.249	0.238	0.249	64	87	0.53%	0.76%	0.69%
B4c	0.171	0.127	0.329	0.268	0.329	0.656	0.469	0.656	54	83	0.59%	0.85%	0.75%
B4d	0.196	0.141	0.425	0.494	0.494	0.631	0.655	0.655	55	71	0.62%	0.83%	0.77%
C1b	0.134	0.106	0.287	0.336	0.336	0.615	0.641	0.641	28	81	0.66%	0.80%	0.93%
C1c	0.151	0.116	0.321	0.417	0.417	0.625	0.694	0.694	29	88	0.63%	0.84%	0.89%
C1d	0.182	0.134	0.381	0.394	0.394	0.726	0.765	0.765	31	90	0.57%	0.77%	0.68%
C2b	0.141	0.110	0.261	0.219	0.261	0.362	0.216	0.362	41	89	0.75%	0.80%	1.01%
C2c	0.164	0.123	0.277	0.252	0.277	0.291	0.316	0.316	44	89	0.79%	0.84%	1.13%
C2d	0.190	0.138	0.271	0.267	0.271	0.312	0.409	0.409	41	71	0.74%	0.77%	1.05%
C3b	0.150	0.116	0.282	0.213	0.282	0.550	0.244	0.550	56	73	0.70%	1.00%	0.93%
C3c	0.160	0.121	0.291	0.240	0.291	0.576	0.306	0.576	41	90	0.75%	1.06%	1.03%
C3d	0.169	0.126	0.305	0.242	0.305	0.404	0.270	0.404	54	90	0.75%	1.01%	0.96%
C4b	0.146	0.113	0.306	0.194	0.306	0.691	0.247	0.691	53	99	0.74%	1.01%	0.88%
C4c	0.171	0.127	0.387	0.221	0.387	0.676	0.320	0.676	53	100	0.73%	0.97%	0.85%
C4d	0.189	0.137	0.414	0.368	0.414	0.703	0.477	0.703	54	71	0.62%	0.95%	0.81%
D1b	0.161	0.122	0.349	0.308	0.349	0.694	0.609	0.694	31	86	0.44%	0.61%	0.62%
D1c	0.180	0.132	0.335	0.310	0.335	0.628	0.427	0.628	26	89	0.48%	0.64%	0.64%
D1d	0.189	0.137	0.361	0.309	0.361	0.615	0.508	0.615	29	74	0.50%	0.66%	0.66%

Table 1.2:   Table 1 of measured and computed parameters

ID	$h_{m,in,c}$ [m]	R_h [m]	h_1 [m]	h_2 [m]	h_{max} [m]	$\tan\beta_1$ [-]	$\tan\beta_2$ [-]	$\tan\beta_{max}$ [-]	$ScLoc_1$ [°]	$ScLoc_2$ [°]	$S_{e,all}$ [%]	$S_{e,mr}$ [%]	$S_{e,bend}$ [%]
D2b	0.151	0.116	0.260	0.219	0.260	0.518	0.237	0.518	44	89	0.53%	0.69%	0.58%
D2c	0.188	0.137	0.315	0.257	0.315	0.348	0.320	0.348	44	90	0.56%	0.79%	0.82%
D2d	0.207	0.146	0.357	0.285	0.357	0.422	0.311	0.422	44	74	0.59%	0.81%	0.89%
D3b	0.158	0.120	0.210	0.188	0.210	0.154	0.301	0.301	60	118	0.46%	0.57%	0.46%
D3c	0.183	0.134	0.290	0.259	0.290	0.435	0.442	0.442	54	90	0.56%	0.72%	0.65%
D3d	0.213	0.149	0.325	0.316	0.325	0.327	0.588	0.588	44	90	0.56%	0.79%	0.75%
D4b	0.165	0.124	0.217	0.199	0.217	0.269	0.164	0.269	53	100	0.50%	0.62%	0.54%
D4c	0.187	0.136	0.327	0.286	0.327	0.368	0.404	0.404	44	92	0.51%	0.71%	0.63%
D4d	0.203	0.145	0.328	0.284	0.328	0.421	0.477	0.477	29	86	0.54%	0.76%	0.69%
E2b	0.139	0.109	0.314	0.219	0.314	0.657	0.233	0.657	46	90	0.63%	0.89%	0.74%
E2c	0.168	0.126	0.304	0.289	0.304	0.458	0.542	0.542	36	74	0.66%	0.91%	0.94%
E2d	0.197	0.141	0.343	0.363	0.363	0.428	0.577	0.577	44	91	0.70%	0.92%	0.94%
E3b	0.157	0.119	0.267	0.280	0.280	0.361	0.454	0.454	44	94	0.62%	0.85%	0.83%
E3c	0.180	0.132	0.304	0.305	0.305	0.368	0.498	0.498	46	89	0.67%	0.95%	0.88%
E3d	0.187	0.136	0.309	0.323	0.323	0.353	0.588	0.588	44	94	0.70%	1.02%	0.92%
E5b	0.161	0.122	0.274	0.227	0.274	0.362	0.409	0.409	44	89	0.61%	0.78%	0.72%
E5c	0.177	0.131	0.296	0.289	0.296	0.393	0.423	0.423	44	89	0.65%	0.90%	0.91%
E5d	0.191	0.138	0.291	0.343	0.343	0.445	0.620	0.620	41	89	0.67%	1.00%	0.92%

Table 1.2:   Table 1 of measured and computed parameters

1.3 Table 2 of measured and computed parameters

ID	V_m [m/s]	V^* [m/s]	$Vol_{e,1}$ [m³]	$Vol_{e,2}$ [m³]	$Vol_{d,1}$ [m³]	$Vol_{d,2}$ [m³]	τ [kN/m²]	θ [-]	Fr [-]	Fr_d [-]	Fr^* [-]	Re [-]	Re^* [-]
B1b	1.099	0.105	0.237	0.244	0.132	0.046	11.1	0.047	0.946	2.256	0.217	8 648	1 186
B1c	1.127	0.123	0.221	0.381	0.169	0.058	15.2	0.064	0.895	2.313	0.253	11 450	1 387
B1d	1.125	0.124	0.264	0.316	0.125	0.044	15.3	0.064	0.827	2.308	0.254	12 860	1 389
B2b	0.972	0.119	0.176	0.211	0.107	0.014	14.1	0.060	0.787	1.995	0.244	10 722	1 338
B2c	1.009	0.111	0.223	0.218	0.167	0.009	12.3	0.052	0.758	2.072	0.228	11 201	1 248
B2d	1.080	0.120	0.235	0.251	0.161	0.017	14.4	0.061	0.778	2.217	0.246	12 849	1 350
B3b	1.045	0.100	0.186	0.207	0.129	0.028	10.1	0.043	0.878	2.145	0.206	8 561	1 130
B3c	1.026	0.122	0.246	0.226	0.164	0.018	14.9	0.063	0.775	2.105	0.250	12 187	1 372
B3d	1.092	0.137	0.217	0.233	0.130	0.035	18.9	0.080	0.791	2.242	0.282	14 626	1 545
B4b	1.034	0.092	0.127	0.162	0.096	0.041	8.4	0.035	0.864	2.123	0.188	7 862	1 029
B4c	1.062	0.112	0.263	0.202	0.139	0.029	12.5	0.053	0.820	2.179	0.230	10 842	1 259
B4d	1.079	0.117	0.432	0.218	0.156	0.003	13.7	0.058	0.777	2.215	0.240	12 556	1 317
C1b	1.127	0.113	0.219	0.232	0.137	0.040	12.8	0.054	0.982	2.312	0.232	9 080	1 271
C1c	1.200	0.116	0.239	0.407	0.147	0.028	13.4	0.056	0.985	2.462	0.238	10 217	1 302
C1d	1.157	0.130	0.303	0.331	0.161	0.037	16.8	0.071	0.866	2.376	0.266	13150	1 458
C2b	1.091	0.117	0.182	0.238	0.119	0.014	13.8	0.058	0.927	2.239	0.241	9 829	1 321
C2c	1.109	0.121	0.201	0.271	0.115	0.012	14.6	0.062	0.876	2.277	0.248	11 340	1 361
C2d	1.114	0.132	0.180	0.271	0.145	0.026	17.4	0.073	0.815	2.286	0.271	13 840	1 485
C3b	1.004	0.115	0.212	0.240	0.116	0.004	13.2	0.056	0.827	2.062	0.236	10 104	1 294
C3c	1.133	0.119	0.212	0.270	0.114	0.012	14.1	0.059	0.903	2.326	0.243	10 943	1 333
C3d	1.254	0.124	0.242	0.252	0.153	0.008	15.3	0.064	0.973	2.573	0.254	11 883	1 391
C4b	1.036	0.117	0.217	0.159	0.135	0.018	13.6	0.057	0.866	2.126	0.240	10 006	1 312
C4c	1.062	0.120	0.292	0.152	0.120	0.005	14.4	0.061	0.820	2.179	0.246	11 629	1 350
C4d	1.125	0.122	0.409	0.258	0.104	0.000	15.0	0.063	0.827	2.309	0.251	12 734	1 377
D1b	0.940	0.097	0.211	0.236	0.152	0.034	9.3	0.039	0.748	1.929	0.198	8 934	1 087
D1c	1.017	0.103	0.319	0.237	0.188	0.043	10.7	0.045	0.765	2.087	0.212	10 410	1 164
D1d	1.116	0.119	0.275	0.223	0.184	0.032	14.1	0.059	0.820	2.291	0.243	12 350	1 333

Table 1.3:   Table 2 of measured and computed parameters

ID	V_m [m/s]	V^* [m/s]	$Vol_{e,1}$ [m³]	$Vol_{e,2}$ [m³]	$Vol_{d,1}$ [m³]	$Vol_{d,2}$ [m³]	τ [kN/m²]	θ [-]	Fr [-]	Fr_d [-]	Fr^* [-]	Re [-]	Re^* [-]
D2b	0.995	0.110	0.228	0.143	0.175	0.015	12.1	0.051	0.817	2.042	0.226	9 703	1 238
D2c	0.961	0.108	0.219	0.225	0.139	0.022	11.6	0.049	0.708	1.973	0.221	11 179	1 212
D2d	1.018	0.111	0.216	0.252	0.158	0.033	12.4	0.052	0.714	2.089	0.228	12 361	1 250
D3b	0.950	0.099	0.087	0.080	0.058	0.017	9.7	0.041	0.762	1.949	0.203	9 009	1 110
D3c	0.985	0.121	0.208	0.183	0.134	0.021	14.6	0.061	0.734	2.021	0.248	12 297	1 357
D3d	0.991	0.127	0.205	0.247	0.125	0.032	16.1	0.068	0.685	2.033	0.260	14 379	1 425
D4b	0.910	0.100	0.093	0.101	0.063	0.026	9.9	0.042	0.715	1.867	0.204	9 389	1 120
D4c	0.965	0.114	0.215	0.173	0.087	0.040	12.9	0.054	0.713	1.981	0.233	11 758	1 278
D4d	1.037	0.119	0.272	0.195	0.121	0.032	14.2	0.060	0.734	2.127	0.244	13 076	1 338
E2b	1.081	0.123	0.288	0.215	0.155	0.016	15.2	0.064	0.924	2.218	0.253	10 202	1 385
E2c	1.083	0.127	0.307	0.294	0.132	0.007	16.2	0.068	0.843	2.224	0.261	12 191	1 433
E2d	1.083	0.142	0.312	0.283	0.216	0.022	20.2	0.085	0.780	2.223	0.291	15 221	1 597
E3b	0.964	0.114	0.208	0.223	0.146	0.016	13.0	0.055	0.777	1.978	0.234	10 331	1 282
E3c	1.011	0.129	0.258	0.240	0.172	0.024	16.6	0.070	0.761	2.075	0.264	12 953	1 449
E3d	1.136	0.134	0.297	0.260	0.160	0.017	18.0	0.076	0.840	2.332	0.276	13 869	1 510
E5b	0.938	0.114	0.220	0.176	0.115	0.009	13.0	0.055	0.746	1.925	0.234	10 559	1 283
E5c	1.028	0.119	0.254	0.278	0.107	0.025	14.3	0.060	0.779	2.109	0.245	11 874	1 343
E5d	1.113	0.123	0.276	0.261	0.099	0.027	15.1	0.064	0.813	2.284	0.252	12 901	1 381

Table 1.3:   Table 2 of measured and computed parameters

1.4   Tests of Peter (1986)

ID	Q_w [l/s]	Q_s [g/min]	B [m]	R_c [m]	d_m [mm]	d_{90} [mm]	σ [-]	tanφ [-]
P01	10	90	0.50	1.75	1.7	2.0	1.19	0.727
P02	10	300	0.50	1.75	1.7	2.0	1.19	0.727
P03	14	90	0.50	1.75	1.7	2.0	1.19	0.727
P06	5	180	0.50	1.75	1.7	2.0	1.19	0.727
P07	10	180	0.50	1.75	1.7	2.0	1.19	0.727
P10	20	90	0.50	1.75	3.9	5.0	1.25	0.727
P11	10	90	0.50	1.75	3.9	5.0	1.25	0.727
P13	15	90	0.50	1.75	3.9	5.0	1.25	0.727
P14	20	270	0.50	1.75	3.9	5.0	1.25	0.727
P15	15	360	0.50	1.75	3.9	5.0	1.25	0.727
P23	15	180	0.50	1.75	2.0	4.6	3.21	0.839
P24	20	360	0.50	1.75	2.0	4.6	3.21	0.839
P25	15	360	0.50	1.75	2.0	4.6	3.21	0.839
P26	10	90	0.50	1.75	2.0	4.6	3.21	0.839
P27	10	270	0.50	1.75	2.0	4.6	3.21	0.839
P28	5	90	0.50	1.75	2.0	4.6	3.21	0.839
P30	20	180	0.50	1.75	2.0	4.6	3.21	0.839
P32	15	90	0.50	1.75	5.1	7.7	1.43	0.810
P33	20	180	0.50	1.75	5.1	7.7	1.43	0.810
P34	15	360	0.50	1.75	5.1	7.7	1.43	0.810
P35	12	180	0.50	1.75	5.1	7.7	1.43	0.810
P36	25	270	0.50	1.75	5.1	7.7	1.43	0.810
P37	25	90	0.50	1.75	5.1	7.7	1.43	0.810
P38	30	180	0.50	1.75	5.1	7.7	1.43	0.810
P39	19	288	0.80	1.60	5.1	7.7	1.43	0.810
P40	48	288	0.80	1.60	5.1	7.7	1.43	0.810
P41	40	144	0.80	1.60	5.1	7.7	1.43	0.810
P42	24	288	0.80	1.60	2.0	4.6	3.21	0.839
P43	32	288	0.80	1.60	2.0	4.6	3.21	0.839
P44	40	288	0.80	1.60	2.0	4.6	3.21	0.839
P45	20	0	0.80	1.60	2.0	4.6	3.21	0.839
P46	20	90	0.80	1.60	2.0	4.6	3.21	0.839

Table 1.4:   Basic test parameters - Tests of Peter (1986)

ID	$h_{m, in, c}$ [m]	R_h [m]	h_1 [m]	h_2 [m]	$\tan\beta_1$ [-]	$\tan\beta_2$ [-]	$ScLoc_1$ [°]	$ScLoc_2$ [°]	$S_{e, all}$ [%]	$S_{e, bend}$ [%]
P01	0.045	0.038	0.153	0.139	0.850	0.800	39	114	0.45%	0.36%
P02	0.041	0.035	0.238	0.165	0.800	0.750	45	124	0.66%	0.61%
P03	0.059	0.048	0.189	0.147	0.900	0.950	40	103	0.33%	0.32%
P06	0.024	0.022	0.113	0.092	0.750	0.900	45	120	0.79%	0.80%
P07	0.043	0.036	0.181	0.178	0.750	0.800	41	122	0.55%	0.50%
P10	0.062	0.050	0.217	0.217	0.800	0.800	34	99	0.87%	0.66%
P11	0.034	0.030	0.223	0.125	1.000	0.700	25	93	1.38%	0.94%
P13	0.047	0.040	0.181	0.172	1.000	0.900	35	105	1.19%	1.07%
P14	0.060	0.049	0.231	0.185	1.100	0.750	37	104	0.86%	0.81%
P15	0.044	0.037	0.282	-	0.950	-	33	-	1.31%	1.05%
P23	0.053	0.044	0.163	0.168	0.600	0.700	58	126	0.75%	0.74%
P24	0.064	0.051	0.172	-	0.600	-	67	-	0.61%	0.51%
P25	0.053	0.044	0.154	0.153	0.700	0.750	55	118	0.71%	0.69%
P26	0.038	0.033	0.127	0.141	0.500	0.800	57	110	0.99%	0.89%
P27	0.039	0.034	0.119	0.162	0.500	0.800	42	95	0.88%	0.96%
P28	0.023	0.021	0.109	-	1.100	-	57	-	1.22%	1.22%
P30	0.066	0.052	0.172	0.188	0.600	0.550	47	116	0.61%	0.55%
P32	0.041	0.035	0.184	0.167	1.050	1.200	31	104	1.68%	1.47%
P33	0.054	0.045	0.212	0.186	0.750	1.000	37	110	1.54%	1.46%
P34	0.042	0.036	0.306	0.143	1.100	0.700	30	102	1.77%	1.66%
P35	0.033	0.029	0.178	0.193	0.800	0.900	36	95	2.18%	1.77%
P36	0.065	0.051	0.211	0.208	0.800	1.050	42	116	1.05%	0.95%
P37	0.068	0.053	0.213	0.235	0.950	0.650	36	132	1.16%	0.90%
P38	0.072	0.056	0.254	0.207	1.000	0.950	33	113	0.96%	0.87%
P39	0.039	0.035	0.179	0.160	1.300	1.400	36	109	1.91%	1.61%
P40	0.071	0.060	0.278	0.238	0.800	1.000	39	134	1.16%	0.98%
P41	0.063	0.054	0.252	0.216	0.850	1.450	47	124	1.20%	1.02%
P42	0.052	0.046	0.165	0.188	0.850	1.200	35	99	0.73%	0.60%
P43	0.063	0.055	0.215	0.220	0.650	1.400	56	130	0.75%	0.48%
P44	0.078	0.065	0.223	0.250	1.000	1.600	71	119	0.60%	0.41%
P45	0.049	0.044	0.153	0.171	0.700	0.900	73	131	0.62%	0.53%
P46	0.046	0.041	0.175	0.170	0.900	0.850	73	125	0.76%	0.60%

Table 1.5:   Table 1 of measured and computed parameters - Tests of Peter (1986)

ID	V_m [m/s]	V^* [m/s]	θ [-]	Fr [-]	Fr_d [-]	Fr^* [-]	Re [-]	Re^* [-]
P01	0.441	0.045	0.062	0.66	2.66	0.247	1 299	67.6
P02	0.486	0.052	0.083	0.76	2.93	0.287	1 390	78.6
P03	0.475	0.044	0.061	0.62	2.86	0.246	1 603	67.2
P06	0.419	0.043	0.058	0.87	2.53	0.239	713	65.3
P07	0.470	0.048	0.071	0.73	2.83	0.266	1 322	72.6
P10	0.643	0.073	0.066	0.82	2.56	0.256	2 759	277.0
P11	0.590	0.068	0.058	1.01	2.32	0.240	1 563	259.1
P13	0.639	0.074	0.068	0.94	2.54	0.260	2 225	281.2
P14	0.664	0.071	0.064	0.86	2.64	0.251	2 632	271.3
P15	0.681	0.075	0.071	1.04	2.71	0.265	2 141	286.1
P23	0.568	0.062	0.052	0.79	3.15	0.228	2 060	217.1
P24	0.630	0.062	0.052	0.80	3.49	0.226	2 380	215.7
P25	0.570	0.061	0.050	0.79	3.16	0.223	2 014	212.5
P26	0.531	0.061	0.050	0.87	2.94	0.222	1 512	211.8
P27	0.518	0.058	0.046	0.82	2.84	0.213	1 490	202.7
P28	0.436	0.052	0.037	0.92	2.42	0.192	835	183.2
P30	0.607	0.063	0.053	0.75	3.37	0.230	2 488	219.2
P32	0.730	0.082	0.055	1.15	2.54	0.233	2 210	482.1
P33	0.735	0.091	0.067	1.01	2.56	0.257	3 079	530.7
P34	0.723	0.085	0.059	1.12	2.50	0.241	2 316	497.9
P35	0.721	0.084	0.058	1.26	2.51	0.239	1 885	493.8
P36	0.773	0.082	0.054	0.97	2.69	0.231	3 191	478.0
P37	0.741	0.088	0.063	0.90	2.56	0.249	3 571	514.9
P38	0.841	0.082	0.055	1.00	2.92	0.233	3 477	481.0
P39	0.613	0.085	0.059	0.99	2.13	0.242	2 293	499.1
P40	0.857	0.090	0.065	1.01	2.94	0.255	4 119	526.0
P41	0.800	0.086	0.060	1.02	2.78	0.243	3 528	502.6
P42	0.580	0.061	0.050	0.81	3.22	0.223	2 122	212.9
P43	0.635	0.068	0.063	0.81	3.52	0.250	2 820	238.0
P44	0.644	0.068	0.062	0.74	3.58	0.247	3 334	235.9
P45	0.511	0.055	0.041	0.73	2.83	0.201	1 824	191.6
P46	0.542	0.059	0.047	0.80	3.00	0.215	1 851	205.2

Table 1.6:   Table 2 of measured and computed parameters - Tests of Peter (1986)

APPENDIX 2

DATA ACQUISITION, DATA TREATMENT AND PROTOCOLS

This Appendix gives informations on
- the measurement devices,
- the principle of the data acquisition system,
- the main steps of the data treatment,
- the used protocols,
- observed special phenomena and events during the tests.

2.1 Technical data of the acquisition devices

2.1.1 Ultrasonic gauge

The used ultrasonic gauge (UNAM 30I9001) had the following technical specifications:

PRODUCER	BAUMER ELECTRIC, FRAUENFELD, SWITZERLAND
Measurement domain - distance	100...700 mm
Opening angle	10°
Frequency of sound	230 kHz
Resolution	< 0.3 mm
Temperature - drift	< 2% of distance to object
Working temperature	0...60°C

Table 2.1:   Technical specifications ultrasonic gauge

2.1.2 Ultrasonic velocity profiler (UVP)

Transducers TN2-10-13 ()

Producer	Metflow SA, Lausanne, Switzerland
Transducer (length; diameter)	60; 13 mm
Active diameter	10 mm
Measurement domain - distance	5...1500 mm, (* 300 mm)
Near field length in water, c=1480 m/s	22 mm
Far field divergence	2.7
Opening angle	4.4° (2 x 2.2°)
Emission frequency	2 MHz
Sampling (= recording) frequency	35...230 Hz (* 77 Hz)
Resolution (in beam direction)	0.7...10 mm/s depending on the depth of the measurement domain * 3.6 mm/s in beam direction 14.0 mm/s in flow direction

Table 2.2:   Technical specifications of the used UVP-transducers
*   * designates the most frequently used values; meas. depth = 30 cm*

see also Metflow: Users Monitor UVP-XW - Users Guide, Release 2, November 1st, 2000

List of used transducers

TRANSDUCER NUMBER (2 MHZ)	NUMBER ON EXPERIMENTAL SETUP
0981.0141	2
0981.0142	4
0981.0148	5
0981.0149	8
0981.0150	7
0981.0151	1
0981.0152	3
0981.0153	9
0981.0154	6

Table 2.3:   List of used transducers

Velocity Monitor

Producer	Metflow SA, Lausanne, Switzerland
Monitor Version	UVP XW 3-PSi with external multiplexer
Program Version	UVP-XW 1.1b
Emitting frequency	1, 2, 4 MHz
Emitting voltage on transducer	30, 60, 90, 150 V (at 50Ω)
Emitting cycles per pulse	2 to 32
Pulse repetition frequency	990 to 7400 Hz
Number of channels	128
Receiving amplification	exponential
Space resolution (longitudinal)	~0.5 μs
Channel distance	variable, lowest possible: 0.37 mm
Velocity resolution	1/256 of maximum velocity
Repetition rate (emissions per profile)	8 to 240
Acquisition time per profile	minimum 4ms
Time delay between profiles	0 to 65'000 ms

Table 2.4:   Technical specifications of the Ultrasonic Velocity Profiler Monitor

2.2   Data acquisition
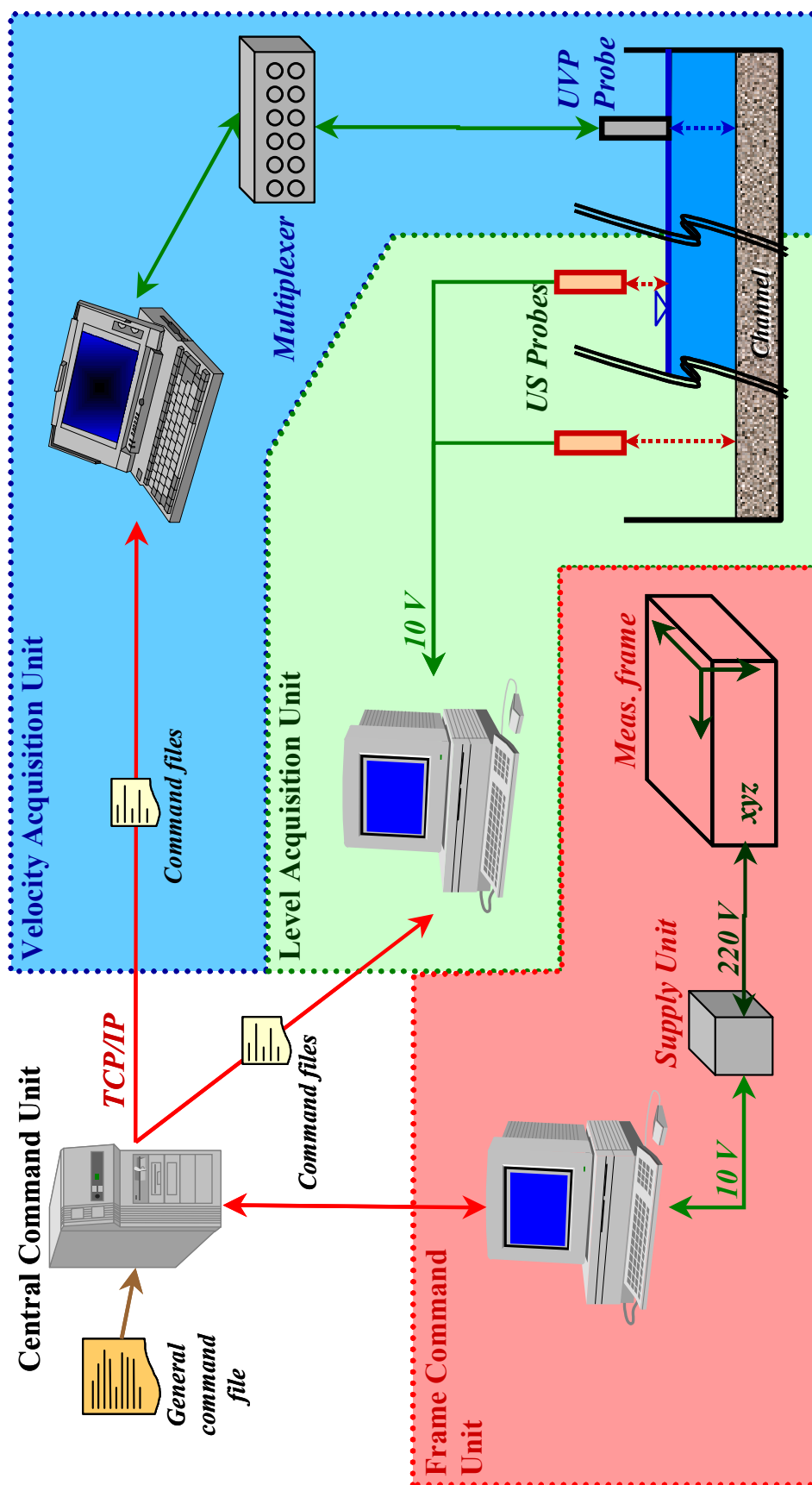
Figure 2.1:   Overview of the data acquisition devices

2.2.1 Frame command unit
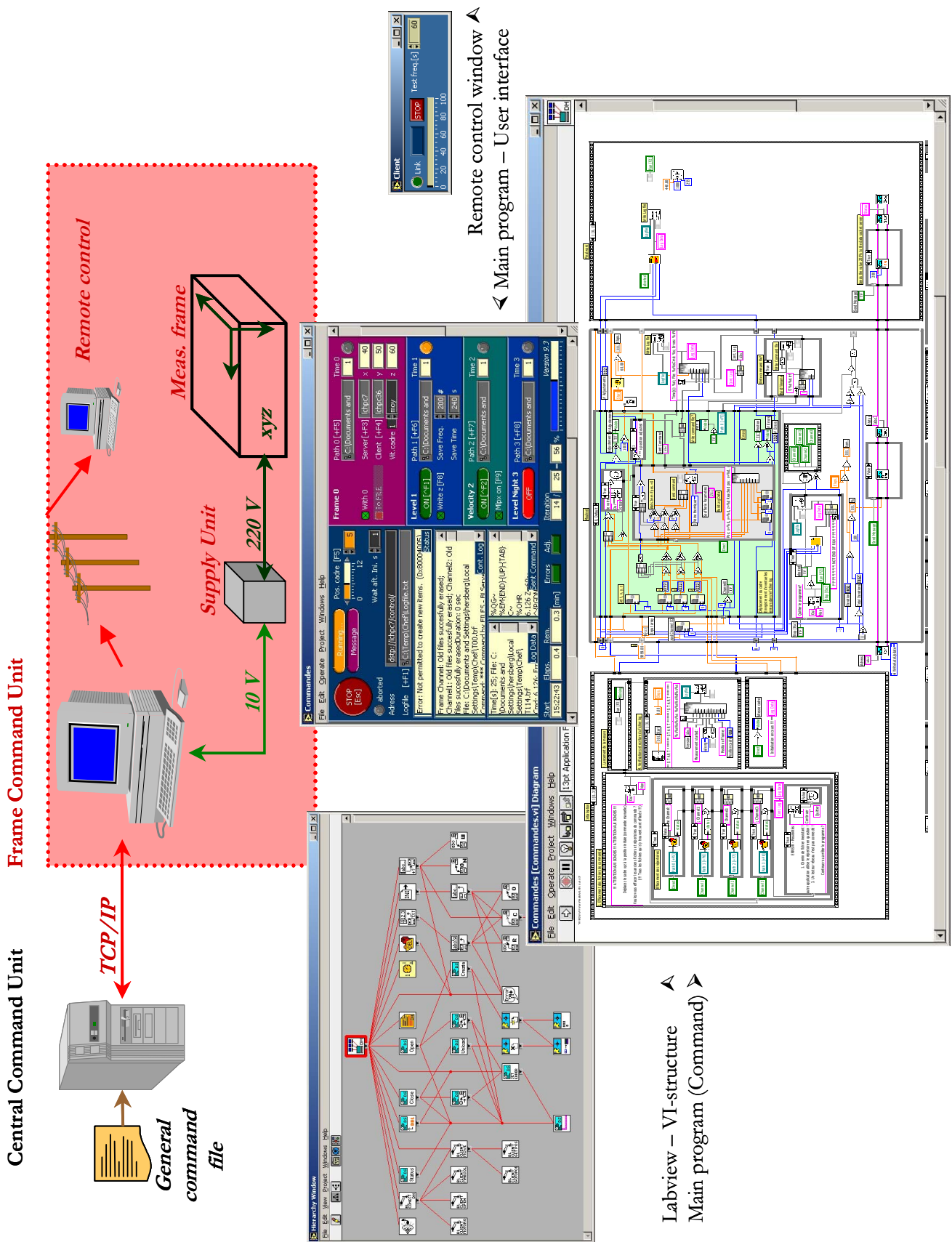
2.2.2   Water and bed levelling unit
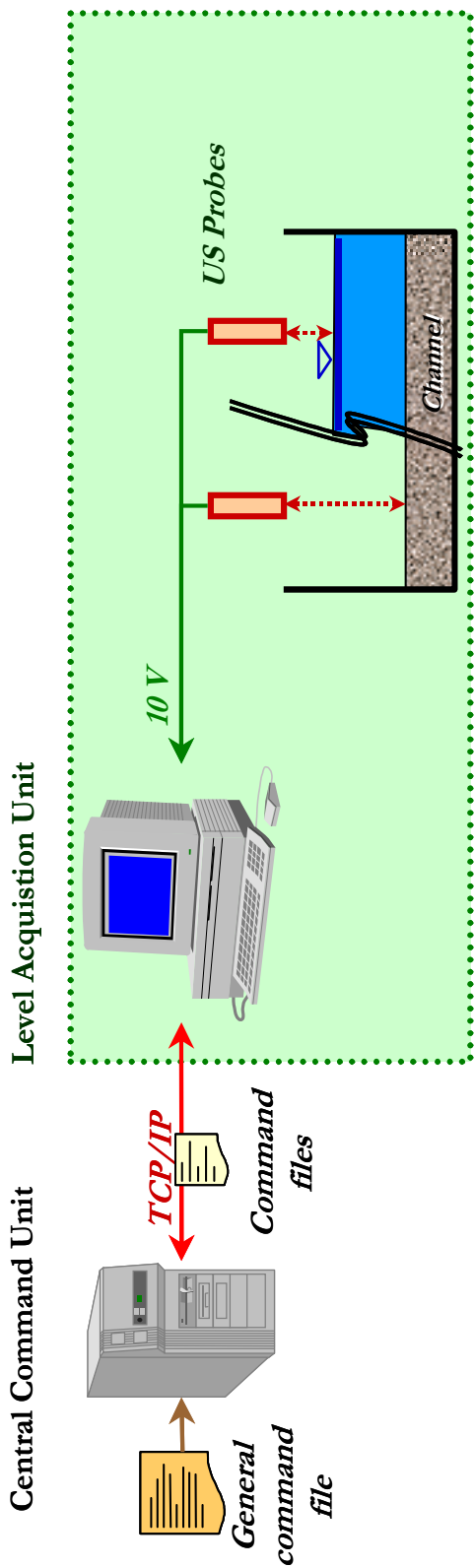
Ultrasonic measurement probe

Acquistion window

2.2.3   Velocity measurement unit

Appendix 2

2.3   Sample protocols

Test protocole	Date _____		ID _____ *)

PAGE 1

Main characteristics

Jf [%] _____   Qe [l/s] _____
                        Qs [g/s] _____

Type of test / **Macroroughness**

- ☐ Armouring ☐ Without ☐ Prismat.
- ☐ Test ☐ spacing ____ ☐ _____
- ☐ At the outlet _____

Computer / Files

Command water level _____ .txt
Command bed level _____ .txt
Command velocity _____ .txt
Log _____ .txt (Name=ID) (B01a)
Water level _____ -E___.xls (Name=ID+E+Pos_frame) (B01a-E04)
Bed level _____ -F___.xls (Name=ID+F+Pos_frame) (B01a-F04)
Velocity _____ .* (Name=ID+Pos_frame) (B01a-04)

Progress

Work	Time [h:min]	Qs [g/min]

Preparation
- ☐ Preparation protocoles
- ☐ Leveling of topo
- ☐ Filling up of sediment supply Qs
- ☐ Empty outlet basket Qs
- ☐ Basket for the samples Qs
- ☐ Locking of the crane / Empty basket below belts
- ☐ Install photos

Checking
- ☐ Balance C1
- ☐ Pompes C2
- ☐ Limnimetres z=200 C3 File:_____.xls
- ☐ UVP C4
- ☐ Solid discharge Qs C5 _____

Test
- ☐ Booting computer _____
- ☐ Starting frame _____
- ☐ Leveling of canal border _____

Test/ armoring
- ☐ Starting of the pump _____
- ☐ END _____
- ☐ Starting Qs _____ _____
- ☐ * **Measurement during test (page 2)** _____
- ☐ * **Level meas. during night**
  - Pos=_____ x=_____ y=_____ z=_____
- ☐ Stop supply Qs _____
- ☐ Stop pump _____
- ☐ Copy Files
- ☐ Copy photos from digit. camera

Final measurement times see log file
- ☐ * Water level
  - Starting of the pump _____
  -   END _____
  - Start sediment supply Qs _____ _____
  - Mesasurement Pos___ _____ _____
  - Stop supply Qs _____ _____
  - Stop pump _____ _____
- ☐ * Velocity
  - Starting of the pump _____
  -   END _____
  - Start sediment supply Qs _____ _____
  - Mesasurement Pos___ _____ _____
  - Stop supply Qs _____ _____
  - Stop pump _____ _____
- ☐ Bed level _____
- ☐ Manual bed level (in/outlet) _____
- ☐ Photos of topography _____
- ☐ Photos of armoring (every 15°) _____
- ☐ Armoring samples _____
- ☐ Unlocking of the crane _____
- ☐ Copy files (Lev, V, Log) PC2 _____
- ☐ Copy / develop photos (PC2) _____

Alimentation			Restitution		
Heure hh:mm	Bacs #	Masse [kg] kg	Heure hh:mm	M brut kg	Tare kg
	filled				
resting:					
resting:					

Remarks, observations

Figure 2.2:   General protocol

A-18

Test protocole Date _____ ID _____ *

PAGE 2

Measurement		Time [h:min]	Qs [g/min]	Number
[h] [min]				
10 Levelling canal border	P1 ____ ____			1
20 Gravel sample	P2 ____ ____ ____			
30 Photo (page1)	P3 ____ ____ ____			
35 Verify Qe, Qs (Lev.)	____ ____			
35 Verify sediment supply / retain	____ ____			
40 Levelling canal border	P1 ____ ____			2
50 Gravel sample	P2 ____ ____ ____			
60 Photo (page1)	P3 ____ ____ ____			
5 Verify Qe, Qs (Lev.)	____ ____			
5 Verify sediment supply / retain	____ ____			
10 Levelling canal border	P1 ____ ____			3
20 Gravel sample	P2 ____ ____ ____			
30 Photo (page1)	P3 ____ ____ ____			
35 Verify Qe, Qs (Lev.)	____ ____			
35 Verify sediment supply / retain	____ ____			
40 Levelling canal border	P1 ____ ____			4
50 Gravel sample	P2 ____ ____ ____			
60 Photo (page1)	P3 ____ ____ ____			
5 Verify Qe, Qs (Lev.)	____ ____			
5 Verify sediment supply / retain	____ ____			
10 Levelling canal border	P1 ____ ____			5
20 Gravel sample	P2 ____ ____ ____			
30 Photo (page1)	P3 ____ ____ ____			
35 Verify Qe, Qs (Lev.)	____ ____			
35 Verify sediment supply / retain	____ ____			
40 Levelling canal border	P1 ____ ____			6
50 Gravel sample	P2 ____ ____ ____			
60 Photo (page1)	P3 ____ ____ ____			
5 Verify Qe, Qs (Lev.)	____ ____			
5 Verify sediment supply / retain	____ ____			
10 Levelling canal border	P1 ____ ____			7
20 Gravel sample	P2 ____ ____ ____			
30 Photo (page1)	P3 ____ ____ ____			
35 Verify Qe, Qs (Lev.)	____ ____			
35 Verify sediment supply / retain	____ ____			
40 Levelling canal border	P1 ____ ____			8
50 Gravel sample	P2 ____ ____ ____			
60 Photo (page1)	P3 ____ ____ ____			
5 Verify Qe, Qs (Lev.)	____ ____			
5 Verify sediment supply / retain	____ ____			
10 Levelling canal border	P1 ____ ____			9
20 Gravel sample	P2 ____ ____ ____			
30 Photo (page1)	P3 ____ ____ ____			
35 Verify Qe, Qs (Lev.)	____ ____			
35 Verify sediment supply / retain	____ ____			
40 Levelling canal border	P1 ____ ____			10
50 Gravel sample	P2 ____ ____ ____			
60 Photo (page1)	P3 ____ ____ ____			
5 Verify Qe, Qs (Lev.)	____ ____			
5 Verify sediment supply / retain	____ ____			

Measurement		Time [h:min]	Qs [g/min]	Number
[h] [min]				
10 Levelling canal border	P1 ____ ____			11
20 Gravel sample	P2 ____ ____ ____			
30 Photo (page1)	P3 ____ ____ ____			
35 Verify Qe, Qs (Lev.)	____ ____			
35 Verify sediment supply / retain	____ ____			
40 Levelling canal border	P1 ____ ____			12
50 Gravel sample	P2 ____ ____ ____			
60 Photo (page1)	P3 ____ ____ ____			
5 Verify Qe, Qs (Lev.)	____ ____			
5 Verify sediment supply / retain	____ ____			
10 Levelling canal border	P1 ____ ____			13
20 Gravel sample	P2 ____ ____ ____			
30 Photo (page1)	P3 ____ ____ ____			
35 Verify Qe, Qs (Lev.)	____ ____			
35 Verify sediment supply / retain	____ ____			
40 Levelling canal border	P1 ____ ____			14
50 Gravel sample	P2 ____ ____ ____			
60 Photo (page1)	P3 ____ ____ ____			
5 Verify Qe, Qs (Lev.)	____ ____			
5 Verify sediment supply / retain	____ ____			
10 Levelling canal border	P1 ____ ____			15
20 Gravel sample	P2 ____ ____			
30 Photo (page1)	P3 ____ ____			
35 Verify Qe, Qs (Lev.)	____ ____			
35 Verify sediment supply / retain	____ ____			
40 Levelling canal border	P1 ____ ____			16
50 Gravel sample	P2 ____ ____ ____			
60 Photo (page1)	P3 ____ ____ ____			
5 Verify Qe, Qs (Lev.)	____ ____			
5 Verify sediment supply / retain	____ ____			
10 Levelling canal border	P1 ____ ____			17
20 Gravel sample	P2 ____ ____ ____			
30 Photo (page1)	P3 ____ ____ ____			
35 Verify Qe, Qs (Lev.)	____ ____			
35 Verify sediment supply / retain	____ ____			
40 Levelling canal border	P1 ____ ____			18
50 Gravel sample	P2 ____ ____ ____			
60 Photo (page1)	P3 ____ ____ ____			
5 Verify Qe, Qs (Lev.)	____ ____			
5 Verify sediment supply / retain	____ ____			
10 Levelling canal border	P1 ____ ____			19
20 Gravel sample	P2 ____ ____ ____			
30 Photo (page1)	P3 ____ ____ ____			
35 Verify Qe, Qs (Lev.)	____ ____			
35 Verify sediment supply / retain	____ ____			
40 Levelling canal border	P1 ____ ____			20
50 Gravel sample	P2 ____ ____ * ____			
60 Photo (page1)	P3 ____ ____ ____			
5 Verify Qe, Qs (Lev.)	____ ____			
5 Verify sediment supply / retain	____ ____			

* **Big sample used for sieving analysis (others only weighting)**

Figure 2.3:   General protocol - page 2

P1. Relevé sur la paroi extérieure   **Date** _____   **ID** _____

Relevé
☐ relevé 1 à 10   *mesuré depuis le fond en mm*
☐ relevé 11 à 20

Axe	Eau									Fond										
[m, °]	1	2	3	4	5	6	7	8	9	ini	pavage	1	2	3	4	5	6	7	8	9
Entrée																				
1.65 m																				
1.95 m																				
2.25 m																				
2.55 m																				
2.85 m																				
3.15 m																				
3.45 m																				
3.75 m																				
4.05 m																				
4.35 m																				
4.65 m																				
4.95 m																				
5.25 m																				
5.55 m																				
5.85 m																				
6.15 m																				
6.45 m																				
6.75 m																				
7.05 m																				
7.35 m																				
Rayon																				
1.00°																				
3.75°																				
6.50°																				
8.50°																				
11.25°																				
14.00°																				
16.00°																				
18.75°																				
21.50°																				
23.50°																				
26.25°																				
29.00°																				
31.00°																				
33.75°																				
36.50°																				
38.50°																				
41.25°																				
44.00°																				
46.00°																				
48.75°																				
51.50°																				
53.50°																				
56.25°																				
59.00°																				
61.00°																				
63.75°																				
66.50°																				
68.50°																				
71.25°																				
74.00°																				
76.00°																				
78.75°																				
81.50°																				
83.50°																				
86.25°																				
89.00°																				
Sortie																				
0.15 m																				
0.45 m																				
0.75 m																				
1.05 m																				
1.35 m																				
1.65 m																				
1.95 m																				
2.25 m																				
2.55 m																				
2.85 m																				
3.15 m																				
3.45 m																				
3.75 m																				
4.05 m																				
4.35 m																				
4.65 m																				
4.95 m																				
5.25 m																				
5.55 m																				
5.85 m																				

Figure 2.4:   Protocol for the manual (water and bed level) recordings on the outer side wall

P2. Echantillons de sédiments   **Date** _____   **ID** _____

Granulométrie		Echantillon 1			Echantillon 2			Echantillon 3			Echantillon 4			Echantillon 5		
		Brut	*Tare*	*Net*	*Brut*	*Tare*	*Net*	*Brut*	*Tare*	*Net*	*Brut*	*Tare*	*Net*	*Brut*	*Tare*	*Net*
N° de récipient	*Nr*															
Temps prise	*h:min*															
Tare halle	*g*															
Poids halle	*g*															
Temps	*min*															
Débit solide	*g/min*															
Poids brut avant	*g*															
31.5	*g*															
22.4	*g*															
16.0	*g*															
11.2	*g*															
8.0	*g*															
5.6	*g*															
4.0	*g*															
2.8	*g*															
2.0	*g*															
Reste	*g*															
Poids après																
Remarques																

Granulométrie		Echantillon 6			Echantillon 7			Echantillon 8			Echantillon 9			Echantillon 10		
		Brut	*Tare*	*Net*	*Brut*	*Tare*	*Net*	*Brut*	*Tare*	*Net*	*Brut*	*Tare*	*Net*	*Brut*	*Tare*	*Net*
N° de récipient	*Nr*															
Temps prise	*h:min*															
Tare halle	*g*															
Poids halle	*g*															
Temps	*min*															
Débit solide	*g/min*															
Poids avant	*g*															
31.5	*g*															
22.4	*g*															
16.0	*g*															
11.2	*g*															
8.0	*g*															
5.6	*g*															
4.0	*g*															
2.8	*g*															
2.0	*g*															
Reste	*g*															
Poids après																
Remarques																

Granulométrie		Echantillon 11			Echantillon 12			Echantillon 13			Echantillon 14			Echantillon 15		
		Brut	*Tare*	*Net*	*Brut*	*Tare*	*Net*	*Brut*	*Tare*	*Net*	*Brut*	*Tare*	*Net*	*Brut*	*Tare*	*Net*
N° de récipient	*Nr*															
Temps prise	*h:min*															
Tare halle	*g*															
Poids halle	*g*															
Temps	*min*															
Débit solide	*g/min*															
Poids brut avant	*g*															
31.5	*g*															
22.4	*g*															
16.0	*g*															
11.2	*g*															
8.0	*g*															
5.6	*g*															
4.0	*g*															
2.8	*g*															
2.0	*g*															
Reste	*g*															
Poids brut après																
Remarques																

Figure 2.5:   Protocols for the sieving / grain size distribution

P2^{LT}. Echantillons de sédiments   **Date** _____   **ID** _____

Granulométrie		Sample 1	Sample 2	Sample 3	Sample 4	Sample 5
Basket Nr	*Nr*					
Time	*h:min*					
Empty	*g*					
Total Weight	*g*					
Sediment weight	*min*					
Duration	*min*					
Remarks						

Granulométrie		Sample 6	Sample 7	Sample 8	Sample 9	Sample 10
Basket Nr	*Nr*					
Time	*h:min*					
Empty	*g*					
Total Weight	*g*					
Sediment weight	*min*					
Duration	*min*					
Remarks						

Granulométrie		Sample 11	Sample 12	Sample 13	Sample 14	Sample 15
Basket Nr	*Nr*					
Time	*h:min*					
Empty	*g*					
Total Weight	*g*					
Sediment weight	*min*					
Duration	*min*					
Remarks						

Granulométrie		Sample 16	Sample 17	Sample 18	Sample 19	Sample 20
Basket Nr	*Nr*					
Time	*h:min*					
Empty	*g*					
Total Weight	*g*					
Sediment weight	*min*					
Duration	*min*					
Remarks		*upstream*	*upstream*	*downstream*	*downstream*	
		outside	*inside*	*outside*	*inside*	

Granulométrie		Sample 22	Sample 22	Sample 23	Sample 24	Sample 25
Basket Nr	*Nr*					
Time	*h:min*					
Empty	*g*					
Total Weight	*g*					
Sediment weight	*min*					
Duration	*min*					
Remarks						

Granulométrie		Sample 26	Sample 27	Sample 28	Sample 29	Sample 30
Basket Nr	*Nr*					
Time	*h:min*					
Empty	*g*					
Total Weight	*g*					
Sediment weight	*min*					
Duration	*min*					
Remarks						

Figure 2.6:   Protocol for sediment sampling at the outlet

P2b. Echantillons pesage   **Date:** _____   **ID** _____   *A-23*

Balance   ❑ LCH   ❑ LRH
Remarques   _____

Température de l'eau	θ_e	17.5 °C	Il faut soit	- vide plus séd sec
Densité de l'eau	ρ_e	0.999 t/m3		- eau plus eau+séd
Densité des sédiments	ρ_s	2.635 t/m3		

Mesure	vide	+eau	+eau+séd	+séd sec	Masse séd mes. à séc	mes. hum.
	g	g	g	g	g	g
Echantillon 1						
Echantillon 2						
Echantillon 3						
Echantillon 4						
Echantillon 5						
Echantillon 6						
Echantillon 7						
Echantillon 8						
Echantillon 9						
Echantillon 10						
Echantillon 11						
Echantillon 12						
Echantillon 13						
Echantillon 14						
Echantillon 15						
Echantillon 16						
Echantillon 17						
Echantillon 18						
Echantillon 19						
Echantillon 20						
Echantillon 21						
Echantillon 22						
Echantillon 23						
Echantillon 24						
Echantillon 25						
Echantillon 26						
Echantillon 27						
Echantillon 28						
Echantillon 29						
Echantillon 30						
SOMME						
MOYENNE	#DIV/0!	#DIV/0!	#DIV/0!	#DIV/0!		

Mesure cumulée

+eau   valeur préc.   Cumul

Figure 2.7:   Protocol to record weighting results of the sediment samples taken at the outlet

P3. Photos Date _____ ID _____

Préparer 2 Protocoles (numérique et digital)

Caméra		Légende	
❑ normale	Canon / Minolta / Canon / Minolta / Nikon	⊖▶	Position et direction de prise du photographe (1-4)
❑ digitale		⊗▶	Eclairage (A-D)

Photos

pendant l'essai, prendre position 1 avec caméra numérique à la fin positions 1-4 avec caméra normale, + particularités + granulo à 45°, 90° et érosion max. (vertical, centre du canal)

Table columns (Position photographe):
- Position 1a, Position 1b, Position 1c, Position 2, Position 3, Position 4, Position 5
- longitudinal: tronç. amont, en courbe, tronç. aval, Position [m/°]
- latéral: Paroi int., Paroi ext., Dans canal, Distance
- Prise vers: l'amont, l'aval, l'intérieur, l'extérieur
- Eclairage allumé: Position A, Position B, Derrière cam., Flash, Halle-Néons, Halle-Spots
- Caméra digitale, Remarques

N° 1–60 (empty rows)

Bottom legend row:
Position: 1a, 1b, 1c, 2, 3, 4, 5
longitudinal: Amont, Courbe, Aval, Pos [m/°]
latéral: Int, Ext, Canal, Dist. [m]
Direction: Amont, Aval, Int, Ext
Lumière: A, B, Derrière, Flash, Halle-Né, Halle-Sp

Remarques:
Positions 1a-c: grands spots de la halle + néons allumés
Autres positions: spot derrière l'observateur (env. 40 cm sur sol)

Figure 2.8:   Protocol of taken pictures

The scheme of the platform gives the positions from which the systematic pictures were taken.

PA. Relevé de la topo / vitesse   **Date** _____   **ID** _____

Relevé

❑ Topo   *Profondeur en mm (lecture limni) depuis le bord du canal*
❑ Vitesse   *en mm/s*

Axe [m, °]	Distance au bord intérieur du canal [cm]														
	10	20	30	40	50	60	70	80	90	100					
Entrée															
1.0 m															
1.5 m															
2.0 m															
2.5 m															
3.0 m															
3.5 m															
4.0 m															
4.5 m															
5.0 m															
5.5 m															
6.0 m															
6.5 m															
7.0 m															
7.5 m															
Rayon															
4°															
8°															
12°															
16°															
20°															
24°															
28°															
32°															
36°															
40°															
44°															
48°															
52°															
56°															
60°															
64°															
68°															
72°															
76°															
80°															
84°															
88°															
90°															
Sortie															
0.5 m															
1.0 m															
1.5 m															
2.0 m															
2.5 m															
3.0 m															
3.5 m															
4.0 m															
4.5 m															
5.0 m															
5.5 m															
6.0 m															
	10	20	30	40	50	60	70	80	90	100					

Figure 2.9:   Protocol to manually record the bed topography at the inlet and outlet reach

2.4 Summary of particular events and phenomena during the tests

2.4.1 Events during the tests - sorted by category

During the performed tests, an important number of irregularities occurred related to the different elements of the quite complete experimental setup. All the possible precautions have been taken to limit an impact on the results. Nevertheless it cannot be excluded that some of the events could have an influence on the final results. For this reasons the following few lines give an overview of the main problems during the tests. All indicated times (in brackets) are counted from the beginning of the test.

a) *Infrastructure - the sediment feeder*

- C3d (1h) the sediment feeder was blocked by a plastic sheet. The sediment feeder was emptied by introducing the sediments "manually" into the channel (by opening the gate 7 on Fig. 4.6 and 4.7).

b) *Infrastructure - the tilting gate at the outlet*

During the tests, the tilting gate at the outlet, lowered during the tests, started floating. This happened during the following tests:
- B3d (2h) tilting gate came up.
- B4d (1h and 3h) tilting gate came up.
- C2d (towards end of velocity measurements at frame pos. 8) tilting gate came up.
- C4d (0.5h, before first sediment sample at outlet was taken) tilting gate came up.
- D4d (6.5h) tilting gate came up.

c) *Infrastructure - the sediment sampling device at the outlet*

The sediment sampling device at the outlet lead to some problems. The L-shaped filter was lowered and lifted by a crank lever. During the sampling, several times individual stones were squeezed in between the lateral walls of the channel and the mobile L (despite a special element closing the gap between the side wall and the L). This crank lever broke several times.
- C3d (4h) the sediment sampling device was not completely lowered (it needed to be pushed down). Therefore the taken sediment samples could be too small.
- D3c (2h) the crank lever broke. It was repaired during the tests.
- D3d (2h) the sediment sampling device was blocked by a stone. One sample was left out and the tests were continued without interruption.
- D4c (2h) the fine grid of the sediment sampling device was replaced during the tests (without interruption of the tests, but some samples are missing).
- D4c (4.5h) the crank lever broke and was not repaired anymore.

d) Infrastructure - the pumps

Several times the used pump was accidentally cut. This had the undesired effect that the channel was emptied without lifted tilting gate. Observations and comparisons between the bed before and after an accidental cut of the pump showed that almost no erosion occurred (maybe locally one or two stones moved, but without influence on the bed topography):

- B2c (3h) the automatic regulation cut pump 7 due to pressure fluctuations.
- C2b (at test start) pump 7 cut six times. The tests were continued with pump 6 over a bypass pipe. The discharge indicator was exchanged, which solved the problem for the next tests.
- C3c (9h) the pump cut twice at a 5 minutes interval.
- C4c (2h) the pump cut.
- C4d (12h) somebody switched off the pump.
- D4d (during startup) somebody cut the pump.

e) Measurements - the frame

Another type of problem was related to the measurements. The frame had to be positioned manually at eight different locations where it was fixed as indicated on Fig. 4.17. A few times this fixation was badly fixed and the frame slightly moved.

- B3d and C1b the frame moved a few centimeters and the measurements were repeated.
- C2d (11h) the measurement frame hit the inner side wall. The frame geometry needed to be readjusted. After a check of the geometry as well of the different probes, the tests were resumed.
- C4c velocity measurements at positions 7 and 8 were recorded at a z-level of -5 mm.
- D2d (end of the test) the probe support dropped down. A check of the geometry and the probes showed that there was no damage.
- D3d water level measurements at position 8: the frame was not fixed, but it did not move.

f) Measurements - informatics

- B3a (7h) Excel (recording of the water levels and discharges) crashed.
- B3b (7h) network connection to UVP computer lost. The test was interrupted to reestablish the connection for the velocity measurements.
- B3d (6.5, 7 and 7.5h) Excel crashed. The number of cells considered for averaging the levels was reduced. 2 hours later, Excel crashed again (o great!)
- B4c (5h) the second half of the test recordings (not the final measurement) failed due to an informatics error during saving the level file.
- B4d due to an Excel problem, the water level recordings are incomplete at frame position 9.
- C4c (2.3h) the power supply of the whole measurement equipment was cut accidentally. After a general startup procedure, the test was resumed.
- D4c (4h) the hard disk of the level acquisition device crashed. Due to a frequent backup, only the automatic level and discharge recordings of the first 4 hours were lost. After replacement of the computer, reinstallation of the data acquisition cards and programs, the

calibration of the ultrasonic gauges was checked. The tests were resumed about 10 days later.

- D4c (11h) the network connection to the UVP device could not be found. A reboot of the machine solved the problem.

g) Others

Other important modifications are given hereafter:
- All tests at high transport rates had to be interrupted periodically to replace the filtering basket at the outlet by an empty one. This was without influence on the scour process since the tilting gate was lifted to avoid any modification of the bed topography.
- B4b (1h) the last 3 vertical ribs at the outlet were introduced.
- C1a before test started the water of the general laboratory circuit was replaced. The temperature (end of september) went from about 20° to 10°.
- C1a before the test started a 3mm thick plastic plate fixed on the inner side wall was removed over the first 1 to 1.5 m at the inlet reach, because the conveyor belt had dropped sediments behind the plate. This was the only way to remove them. The influence on the further tests is not significant (there are still more than 6 m to the beginning of the bend).
- C3 all tests: some ribs did not stick well to the wall during the tests. The gap between the ribs and the wall opened up to a maximum of 10 mm (in general much less). The following ribs sticked well to the side wall: 6°, 8°, 22°, 30°, 50°, 52°, 58°, 60°, 82° and all ribs in the outlet.
- C3d (6h) just after a short break, the top 10 cm of the sill between the inlet reach and the inlet tank lifted up. The test was cut for 10 minutes to fix the problem.
- D3b the ultrasonic level gauge number 2 (at the inlet) had the fixation detached (fixed).

2.4.2   Events during the tests - sorted by test

All tests
- At high transport rates had to be interrupted periodically to replace the filtering basket at the outlet by an empty one. This was without influence on the scour process since the tilting gate was lifted to avoid any modification of the bed topography.

B1
- B1b (10h). Electric shortcut on the measurement frame (axis x). Repaired

B2
- B2c (3h) the automatic regulation cut pump 7 due to pressure fluctuations.

B3
- B3a (7h) Excel (recording of the water levels and discharges) crashed.
- B3b (7h) network connection to UVP computer lost. The test was interrupted to reestablish the connection for the velocity measurements.
- B3d (2h) tilting gate came up.
- B3d the frame moved a few centimeters and the measurements were repeated.

- B3d (6.5, 7 and 7.5h) Excel crashed. The number of cells considered for averaging the levels was reduced. 2 hours later, Excel crashed again (o great!)

B4

- B4**b** (1h) the last 3 vertical ribs at the outlet were introduced.
- B4**c** (5h) the second half of the test recordings (not the final measurement) failed due to an informatics error during saving the level file.
- B4**d** (1h and 3h) tilting gate came up.
- B4d due to an Excel problem, the water level recordings are incomplete at frame position 9.

C1

- C1**a** before test started the water of the general laboratory circuit was replaced. The temperature (end of september) went from about 20° to 10°.
- C1a before the test started a 3mm thick plastic plate fixed on the inner side wall was removed over the first 1 to 1.5 m at the inlet reach, because the conveyor belt had dropped sediments behind the plate. This was the only way to remove them. The influence on the further tests is not significant (there are still more than 6 m to the beginning of the bend).
- C1**b** the frame moved a few centimeters and the measurements were repeated.

C2

- C2**b** (at test start) pump 7 cut six times. The tests were continued with pump 6 (bypass). The discharge indicator was exchanged, which solved the problem for the following tests.
- C2**d** (11h) the measurement frame hit the inner side wall. The frame geometry needed to be readjusted. After a check of the geometry as well of the different probes, the tests were resumed.
- C2d (towards end of velocity measurements at frame pos. 8) tilting gate came up.

C3

- **C3** all tests: some ribs did not stick well to the wall during the tests. The gap between the ribs and the wall opened up to a maximum of 10 mm (in general much less). The following ribs sticked well to the side wall: 6°, 8°, 22°, 30°, 50°, 52°, 58°, 60°, 82° and all ribs in the outlet.
- C3**c** (9h) the pump cut twice at a 5 minutes interval.
- C3**d** (1h) the sediment feeder was blocked by a plastic sheet. The sediment feeder was emptied by introducing the sediments "manually" into the channel (by opening the gate 7 on Fig. 4.6 and 4.7).
- C3d (4h) the sediment sampling device was not completely lowered (it needed to be pushed down). Therefore the taken sediment samples could be too small.
- C3d (6h) just after a short break, the top 10 cm of the sill between the inlet reach and the inlet tank lifted up. The test was cut for 10 minutes to fix the problem.

C4

- C4**c** (2h) the pump cut.
- C4c (2.3h) the power supply of the whole measurement equipment was cut accidentally. After a general startup procedure, the test was resumed.
- C4c velocity measurements at positions 7 and 8 were recorded at a z-level of -5 mm.
- C4**d** (0.5h, before first sediment sample at outlet was taken) tilting gate came up.

- C4d (12h) somebody switched off the pump.

D2

- D2**d** (end of the test) the probe support dropped down. A check of the geometry and the probes showed that there was no damage.

D3

- D3**b** the ultrasonic level gauge number 2 (at the inlet) had the fixation detached (fixed).
- D3**c** (2h) the crank lever broke. It was repaired during the tests.
- D3**d** (2h) the sediment sampling device was blocked by a stone. One sample was left out and the tests were continued without interruption.
- D3d water level measurements at position 8: the frame was not fixed, but it did not move.

D4

- D4**c** (2h) the fine grid of the sediment sampling device was replaced during the tests (without interruption of the tests, but some samples are missing).
- D4c (4h) the hard disk of the level acquisition device crashed. Due to a frequent backup, only the automatic level and discharge recordings of the first 4 hours were lost. After replacement of the computer, reinstallation of the data acquisition cards and programs, the calibration of the ultrasonic gauges was checked. The tests were resumed about 10 days later.
- D4c (4.5h) the crank lever broke and was not repaired anymore.
- D4c (11h) the network connection to the UVP device could not be found. A reboot of the machine solved the problem.
- D4**d** (during startup) somebody cut the pump.
- D4d (6.5h) tilting gate came up.

2.4.3   Observations

- B4b erosion started at the downstream end of the bend at 15 to 20 cm from the outer wall.
- B4b coarse sediments accumulated at the inlet reach due to insufficient transport capacity.
- B4b (5h) the first scour was about 10 cm deeper at 15 cm from the outer wall compared to the value recorded on the side wall.
- B4c bed changes are smoother with a mr-spacing at 1° (compared to 2° and 4°).
- B4c recirculating current observed behind the bank at 60°.
- C1d white water on the first wave in the outlet reach (see pictures 21, 22, 28 and 29).
- C1d (4.5h) there seem to be temporarily 3 scour holes.
- C3b the sediment transport rate at the outlet is very regular.
- C4a some erosion (not very important) occurred in the outlet reach.
- D1c during the tests, the 2nd scour was temporarily about 10 to 15 cm deeper than the final scour. This could be due to a higher bed slope.
- D2b the sediment transport rate (feeding) was probably too high since an accumulation of the sediments in the inlet reach was observed.

APPENDIX 3

PRELIMINARY TESTS

3.1 Bed topography above reference level

The bed levels are given before the tests, after 120, 130, 140, 170 and 212.5 l/s (top to bottom)

TEST WITHOUT MACRO-ROUGHNESS
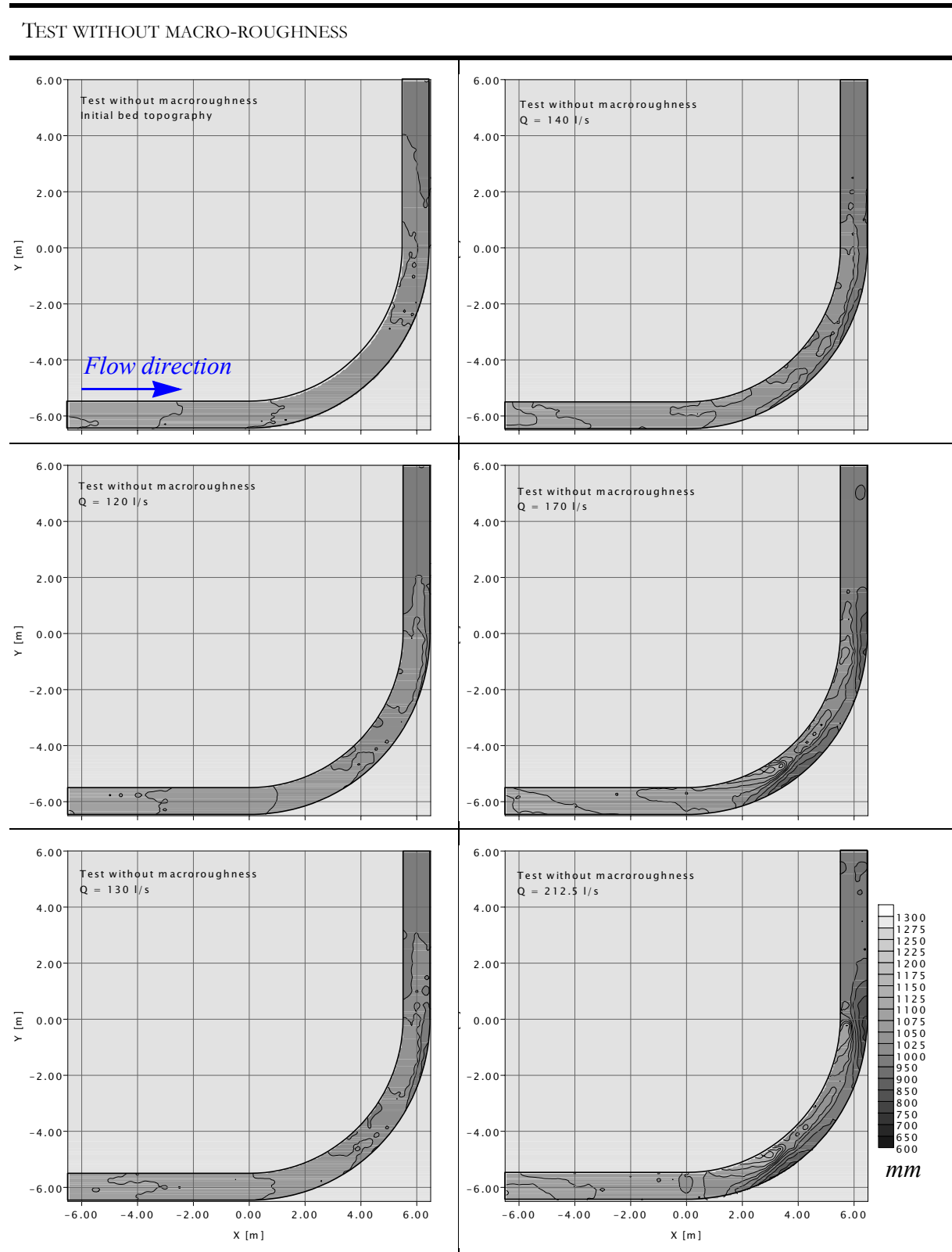
Table 3.1:   *Bed topography above reference level - preliminary test without mr, $J_f = 0.5\%$*

3.2 Bed topography compared to initial bed

The last two plots compare the bed topography with and without mr (scour red. = values > 0).

Q	170 L/S	212.5 L/S

Flow direction

Test with macroroughness
Comparison with initial bed topography
Q = 170 l/s

Test with macroroughness
Comparison with initial bed topography
Q = 212.5 l/s

Comparison of bed topography with / without mr
Q = 170 l/s

Q=170 l/s

Comparison of bed topography with / without mr
Q = 212.5 l/s

Q=212.5 l/s
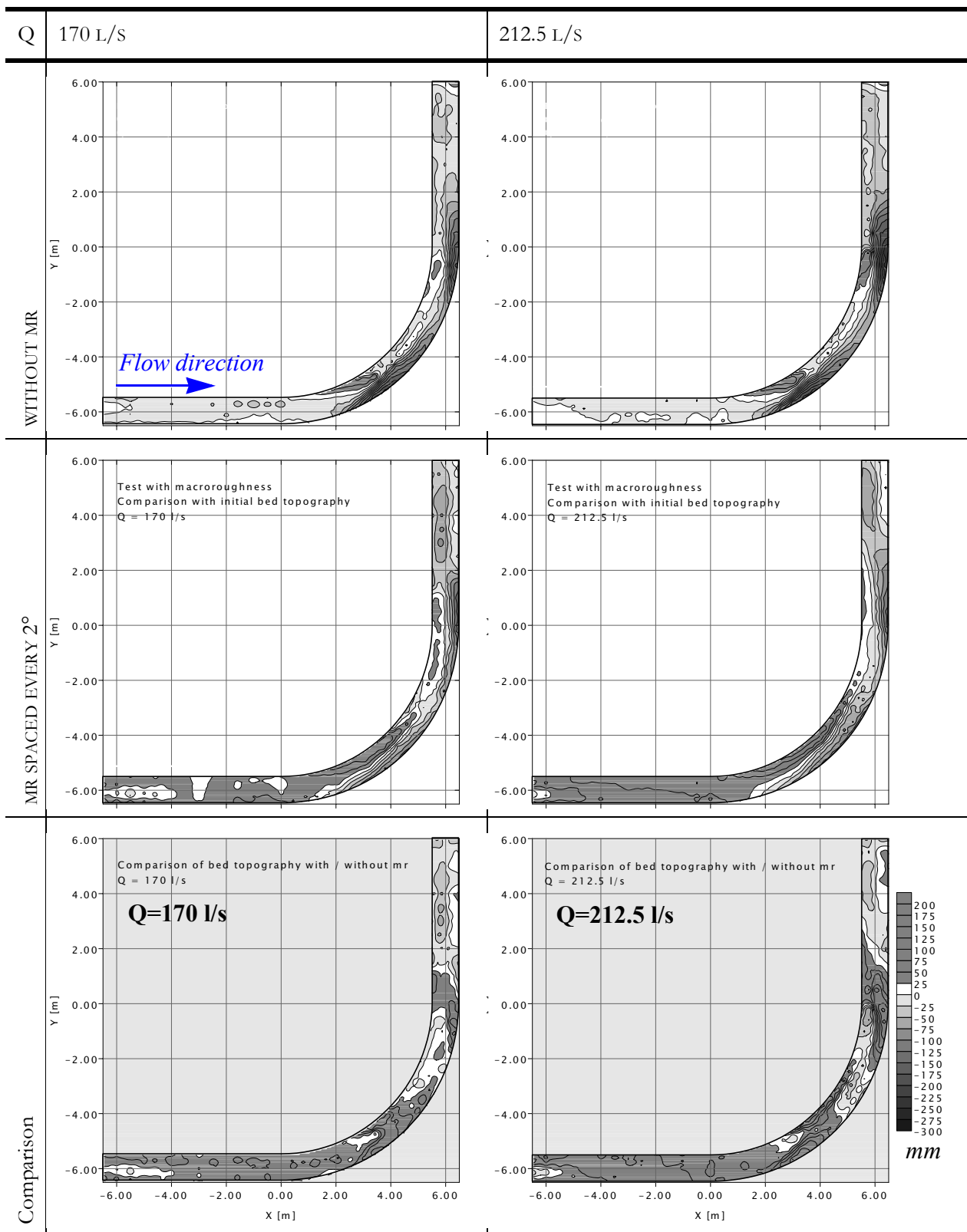
Table 3.2:   Comparison of final topography with initial bed; comparison with/without mr

3.3   *Longitudinal profile of the channel bed*

3.3.1   **Without macro-roughness**
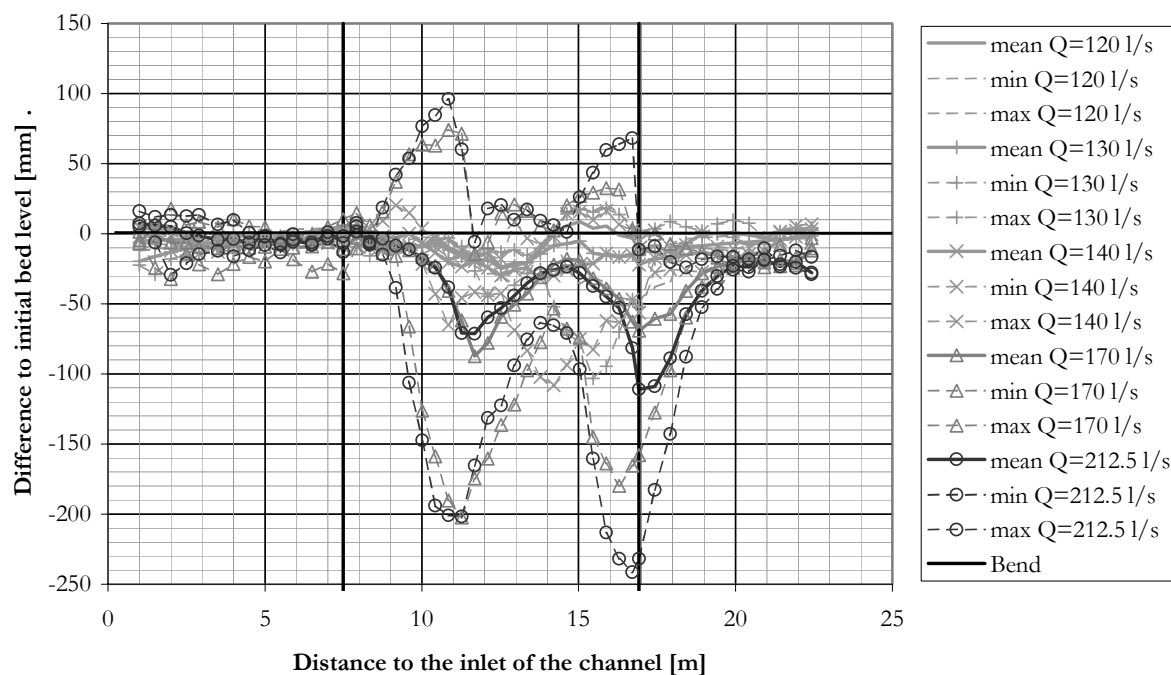
Figure 3.1:   Evolution of the channel bed (average, min. and max. bed levels compared to initial bed) without macro-roughness (Test A01)
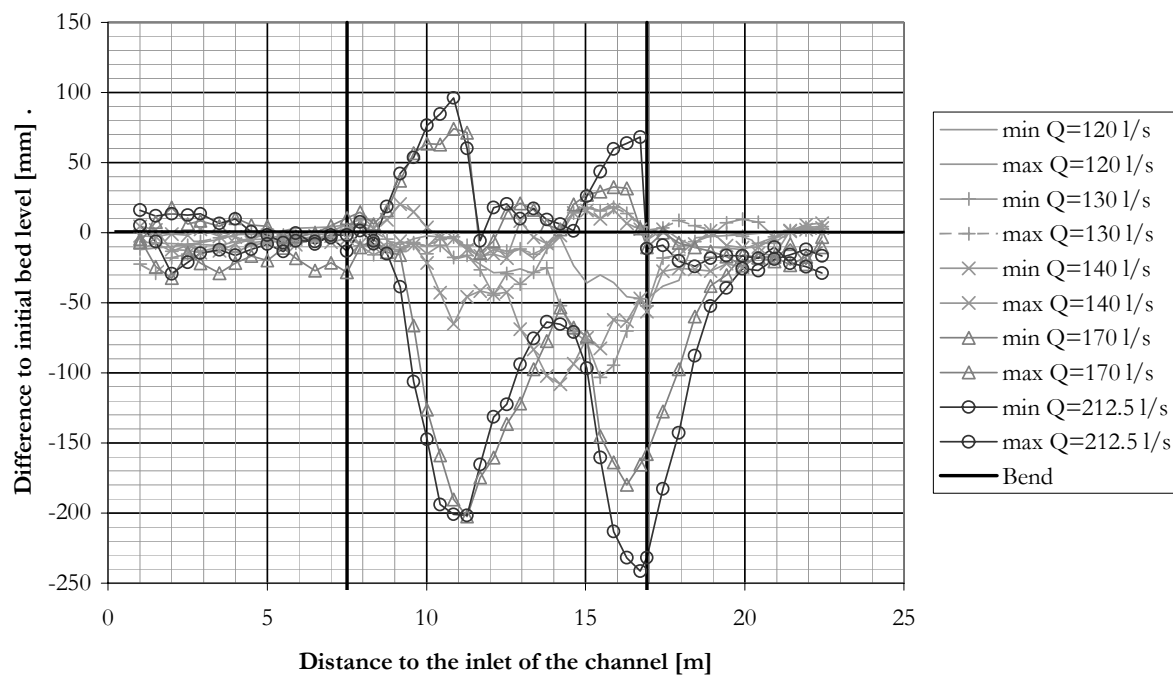
Figure 3.2:   Evolution of the max. scour (min. level) and max. depositions (compared to initial bed) without macro-roughness (Test A01)
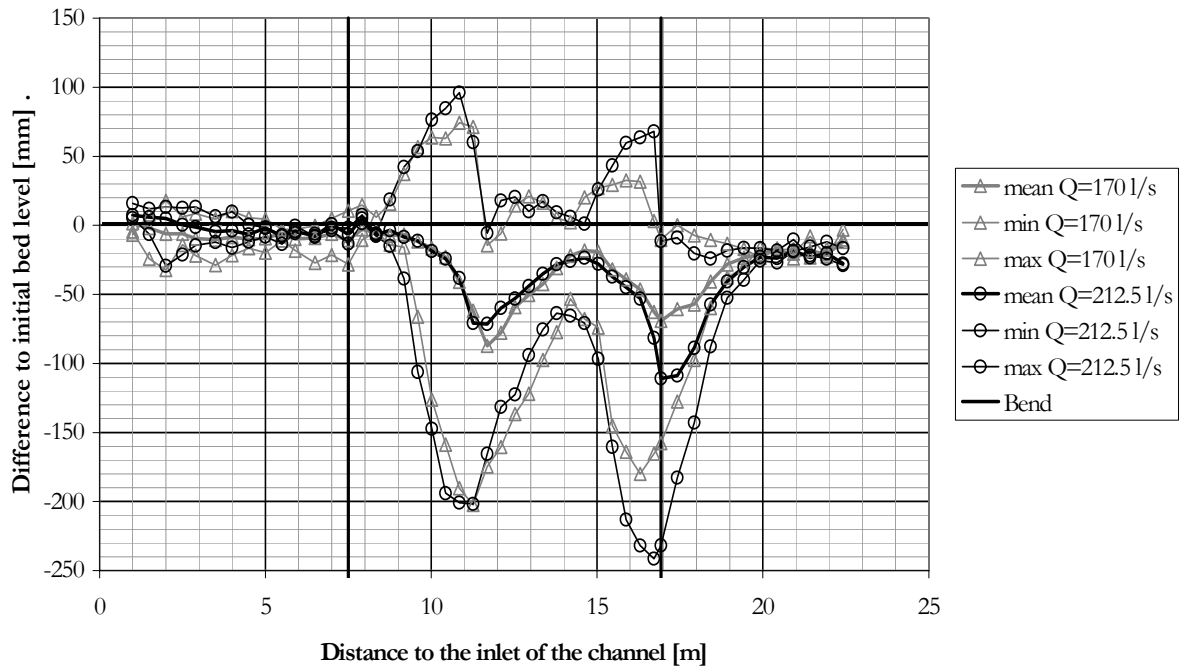
Figure 3.3: *Evolution of the channel bed (compared to initial bed) for Q=170 and 212.5 l/s without macro-roughness (A01)*

3.3.2 With macro-roughness (spaced every 2°)
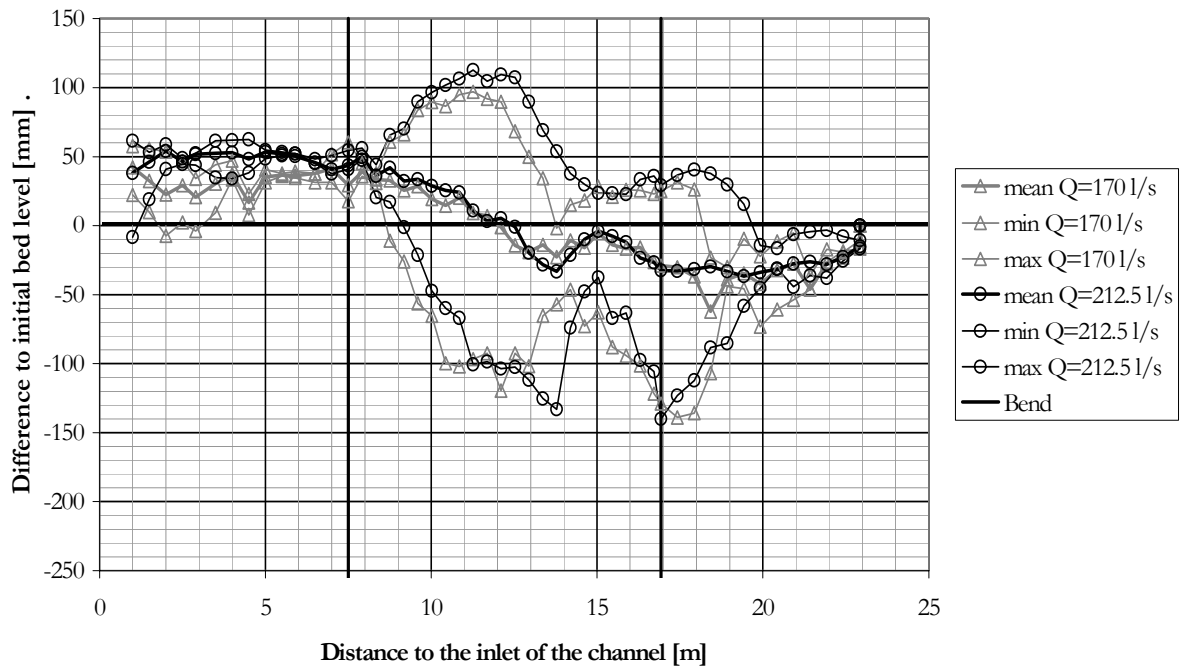
Figure 3.4: *Evolution of the channel bed (compared to initial bed) for Q=170 and 212.5 l/s with macro-roughness every 2° (A02)*

3.3.3   Comparison

Comparison of the bed levels with and without macro-roughness
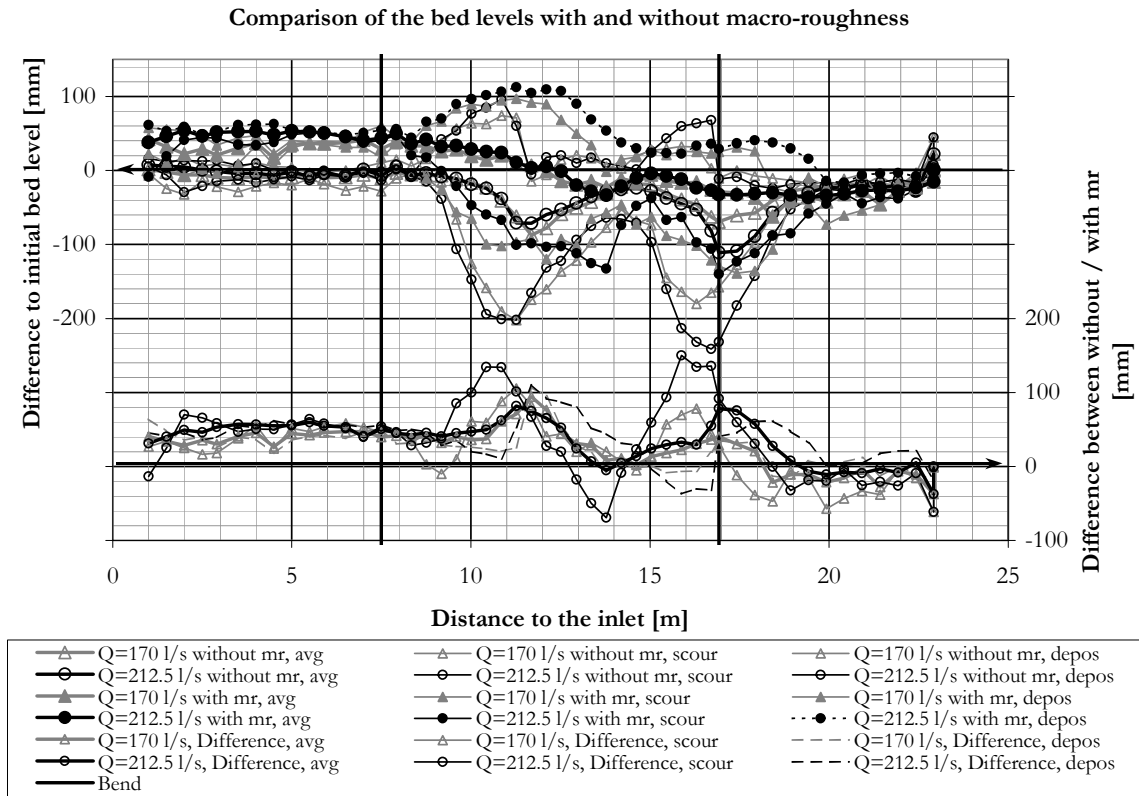
*Figure 3.5:   Comparison of the evolution of the channel bed
Difference with / without macro-roughness for Q=170 and 212.5 l/s*

The lower parts of Fig. 3.5, 3.6 and 3.7 give the difference between the bed topography without ribs and the one with macro-roughness spaced every 2°. Figure 3.5 gives the two highest discharges on the same plot to allow a comparison of the influence of the discharge. The following figures present one discharge at the time.
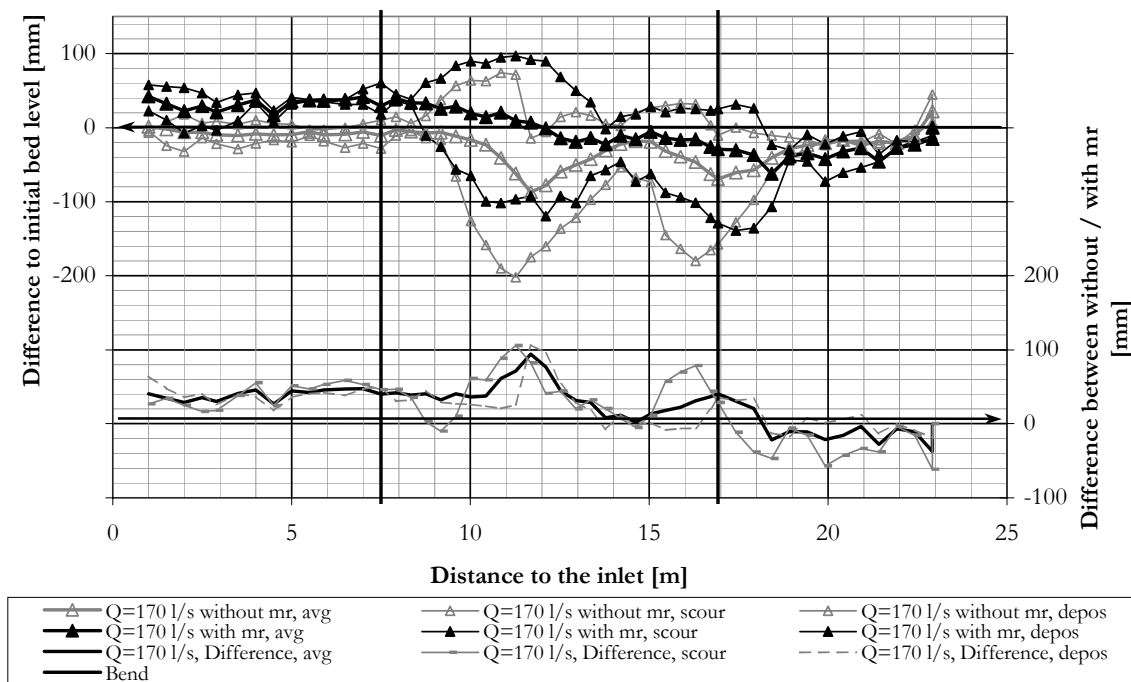
Figure 3.6: *Comparison of the evolution of the channel bed*
Difference with / without macro-roughness for Q=170 l/s
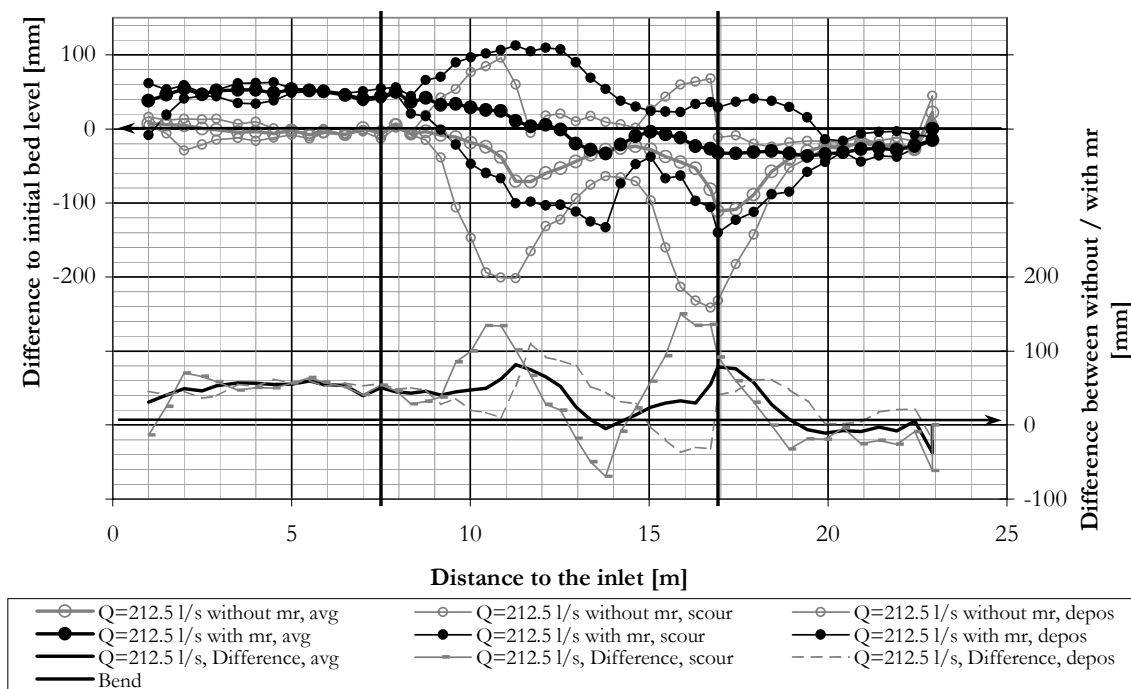
Figure 3.7: *Comparison of the evolution of the channel bed*
Difference with / without macro-roughness for Q=212.5 l/s

Appendix 3

A-38

APPENDIX 4

BED TOPOGRAPHY COMPARED TO INITIAL BED LEVEL

This Appendix gives the measured final bed topography compared to the initial bed topography (recorded after the armoring at a discharge of 70 l/s).
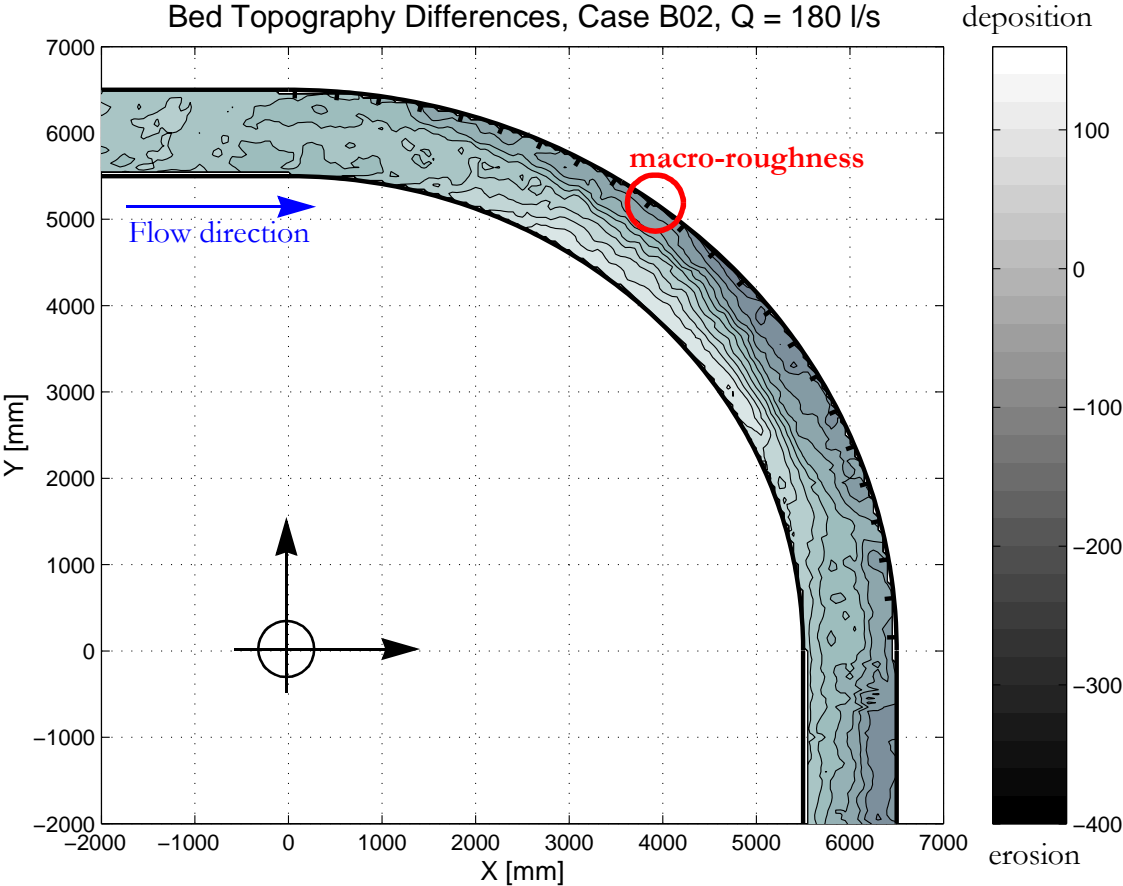
Additional information can be found in the report in Chapter 5.3.1 and 6.2.1.

4.1 *Channel slope S_0 = 0.35% - mr depth = 20 mm*
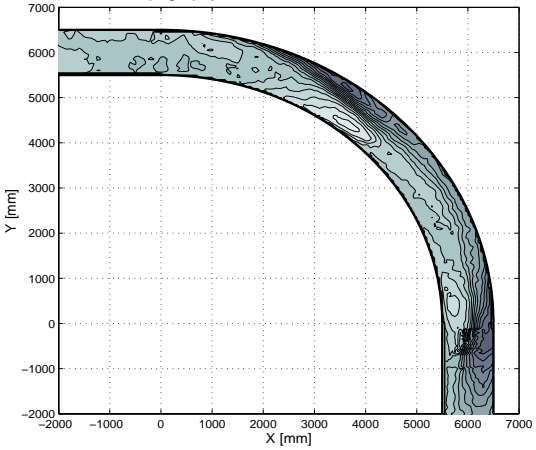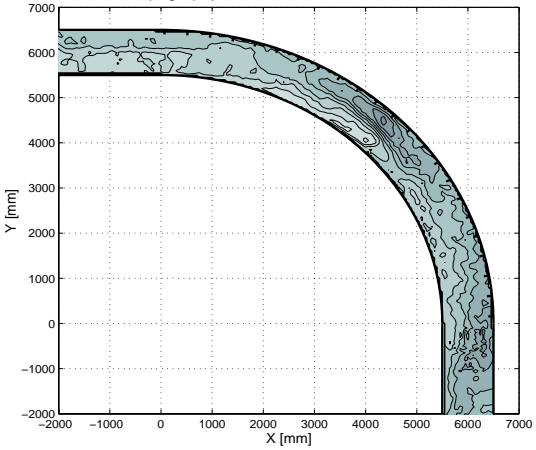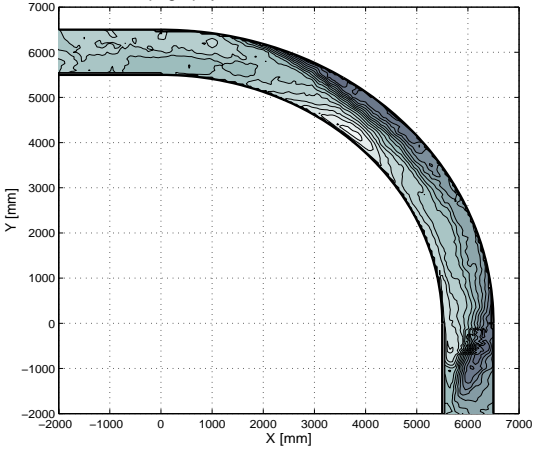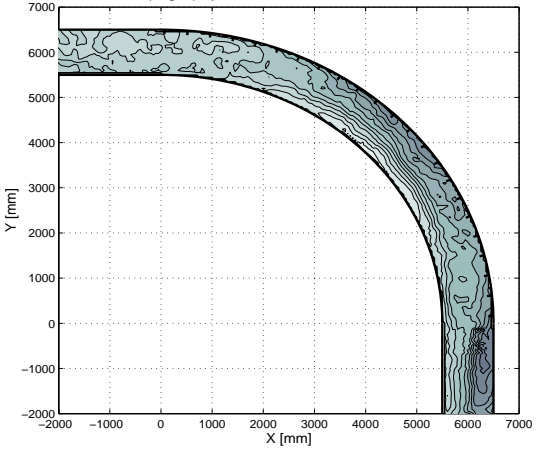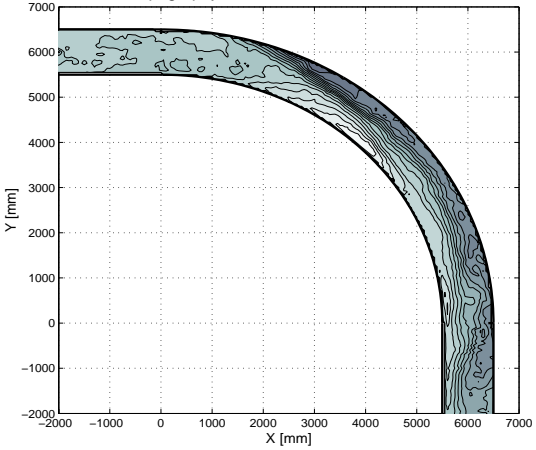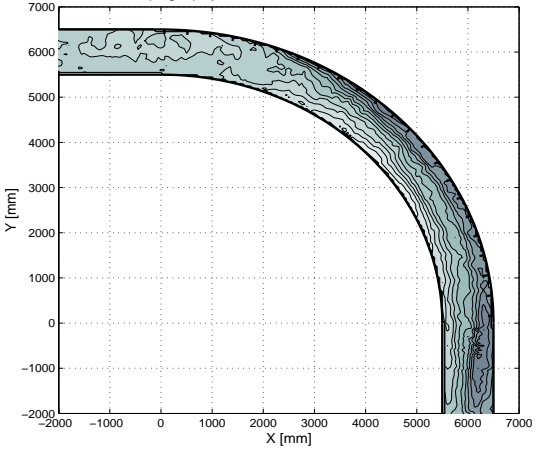
Q [L/S]	WITHOUT MR	WITH MR SPACING 4°
150	Bed Topography Differences, Case D01, Q = 150 l/s	Bed Topography Differences, Case D02, Q = 150 l/s
180	Bed Topography Differences, Case D01, Q = 180 l/s	Bed Topography Differences, Case D02, Q = 180 l/s
210	Bed Topography Differences, Case D01, Q = 210 l/s	Bed Topography Differences, Case D02, Q = 210 l/s

Table 4.1:   Bed topography compared to initial bed level - S_0 = 0.35%

WITH MR SPACING 2°	WITH MR SPACING 1°
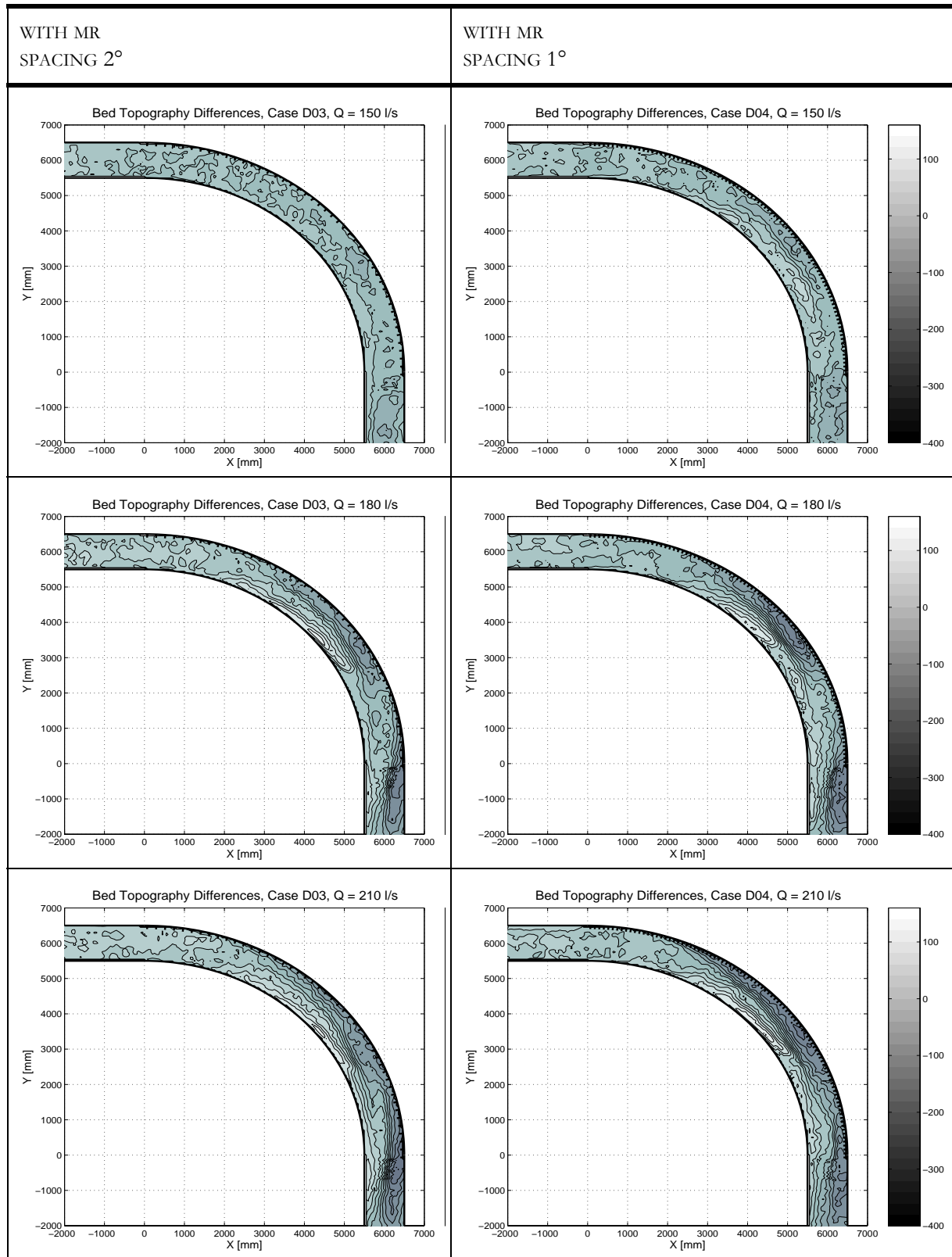
Distances in mm; Equidistance: 20 mm; Linear interpolation

4.2   *Channel slope $S_0 = 0.50\%$ - mr depth = 20 mm*
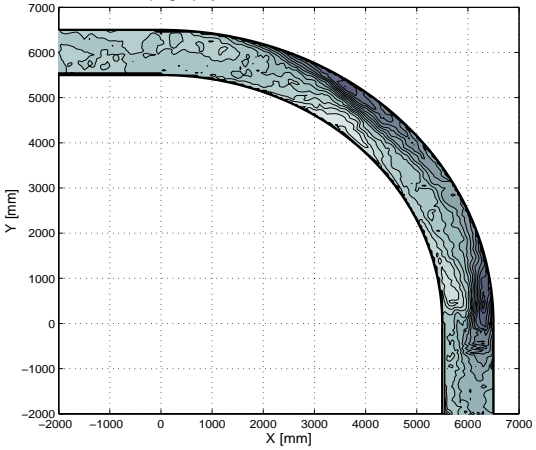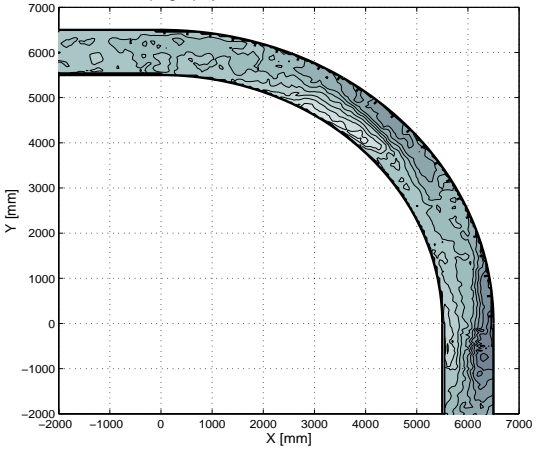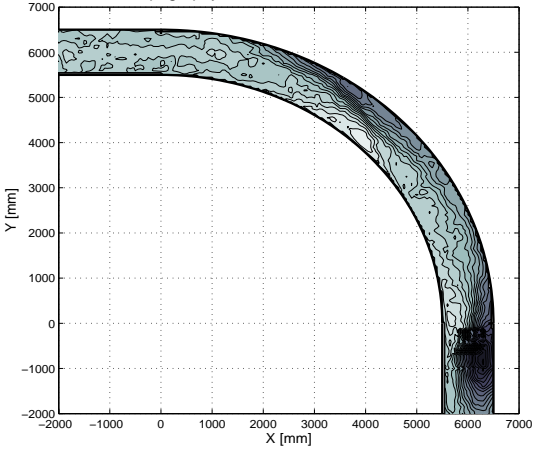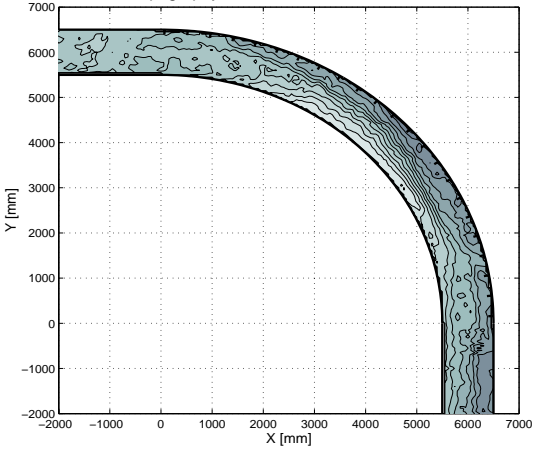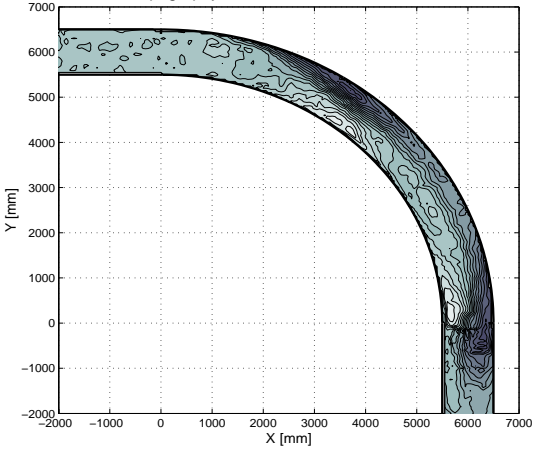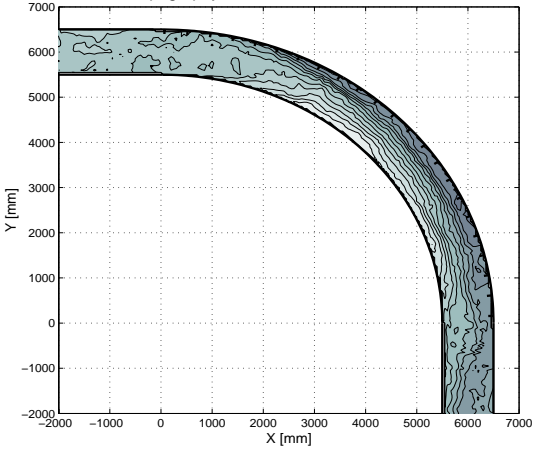
Q [L/S]	WITHOUT MR	WITH MR SPACING 4°
150	Bed Topography Differences, Case B01, Q = 150 l/s	Bed Topography Differences, Case B02, Q = 150 l/s
180	Bed Topography Differences, Case B01, Q = 180 l/s	Bed Topography Differences, Case B02, Q = 180 l/s
210	Bed Topography Differences, Case B01, Q = 210 l/s	Bed Topography Differences, Case B02, Q = 210 l/s

Table 4.2:   Bed topography compared to initial bed level - $S_0 = 0.50\%$

WITH MR SPACING 2°	WITH MR SPACING 1°
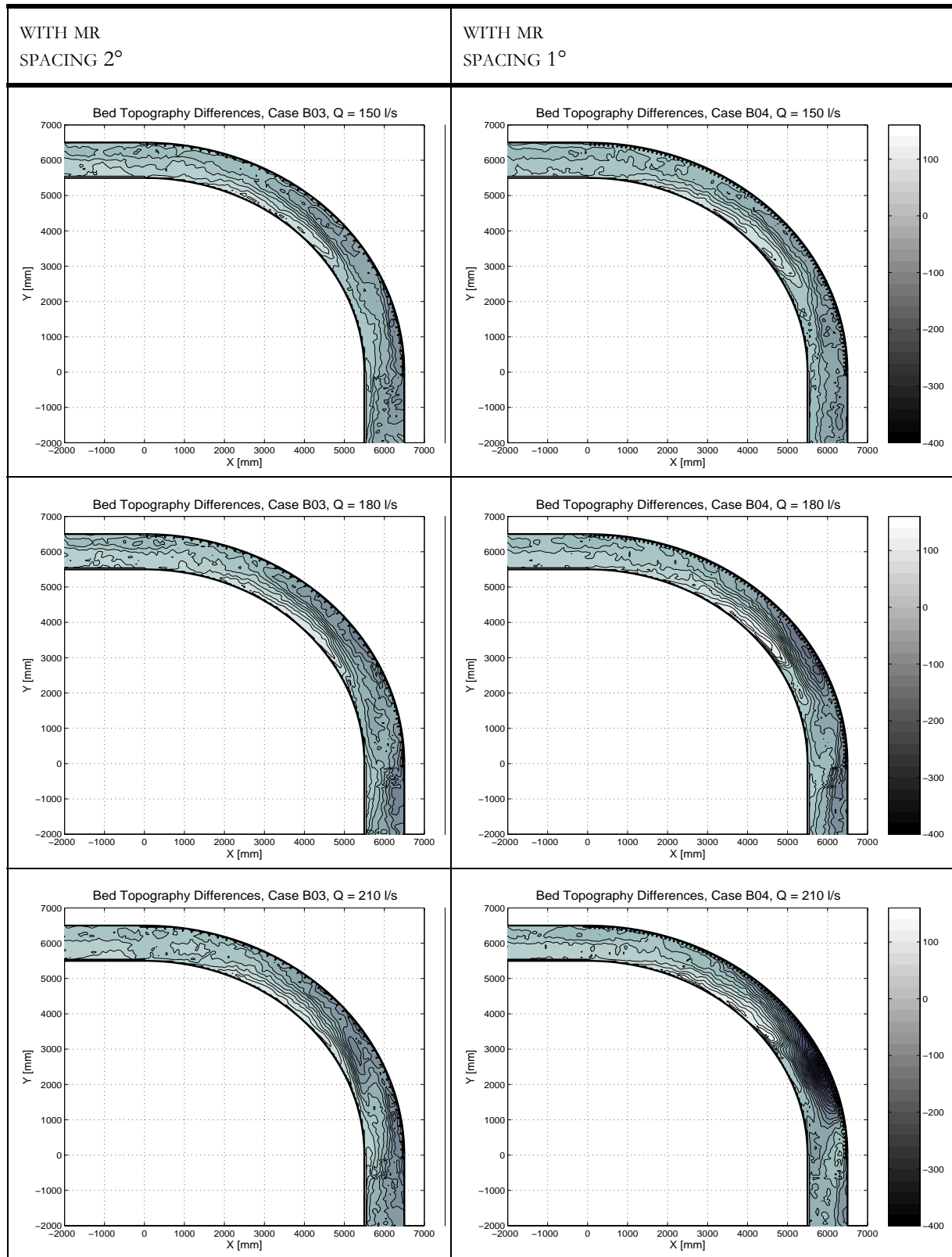
Distances in mm; Equidistance: 20 mm; Linear interpolation

4.3 *Channel slope S_0 = 0.70% - mr depth = 20 mm*
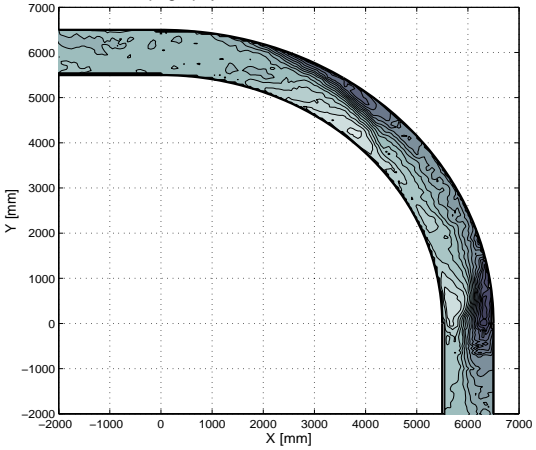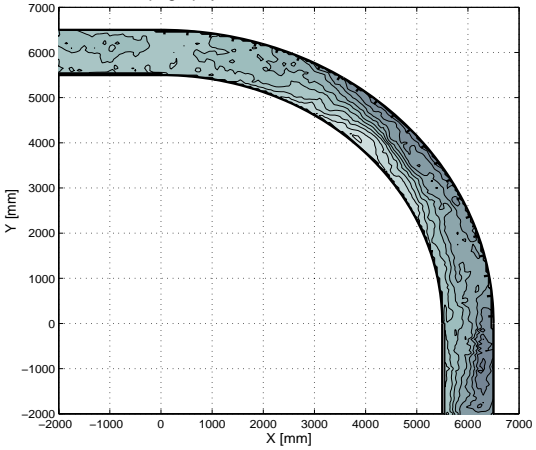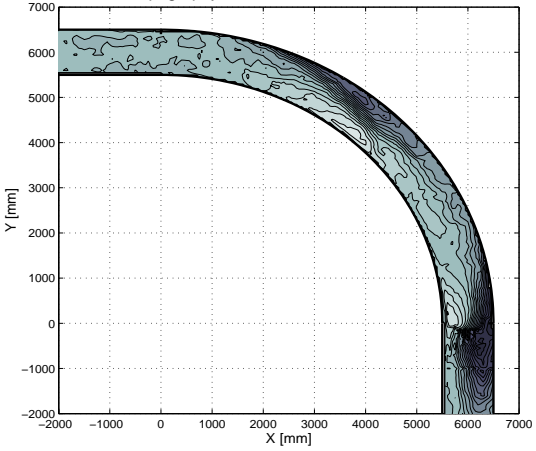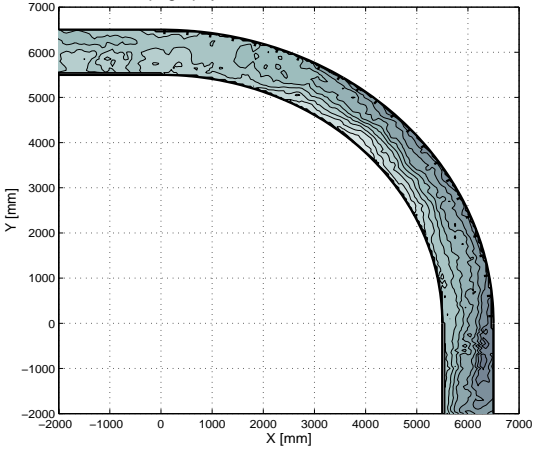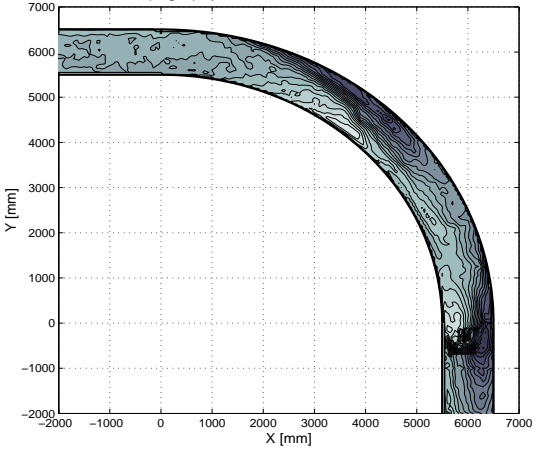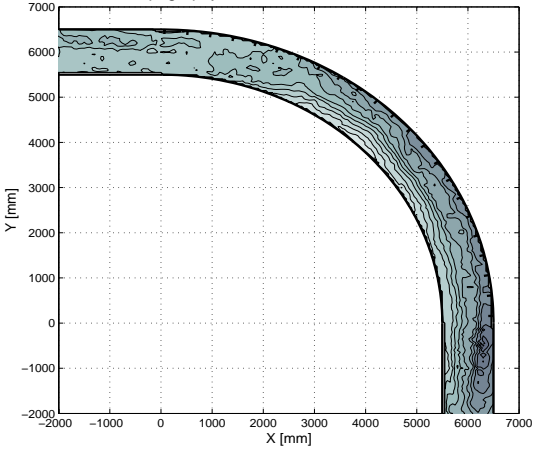
Q [L/S]	WITHOUT MR	WITH MR SPACING 4°
150	Bed Topography Differences, Case C01, Q = 150 l/s	Bed Topography Differences, Case C02, Q = 150 l/s
180	Bed Topography Differences, Case C01, Q = 180 l/s	Bed Topography Differences, Case C02, Q = 180 l/s
210	Bed Topography Differences, Case C01, Q = 210 l/s	Bed Topography Differences, Case C02, Q = 210 l/s

Table 4.3:   Bed topography compared to initial bed level - S_0 = 0.70%
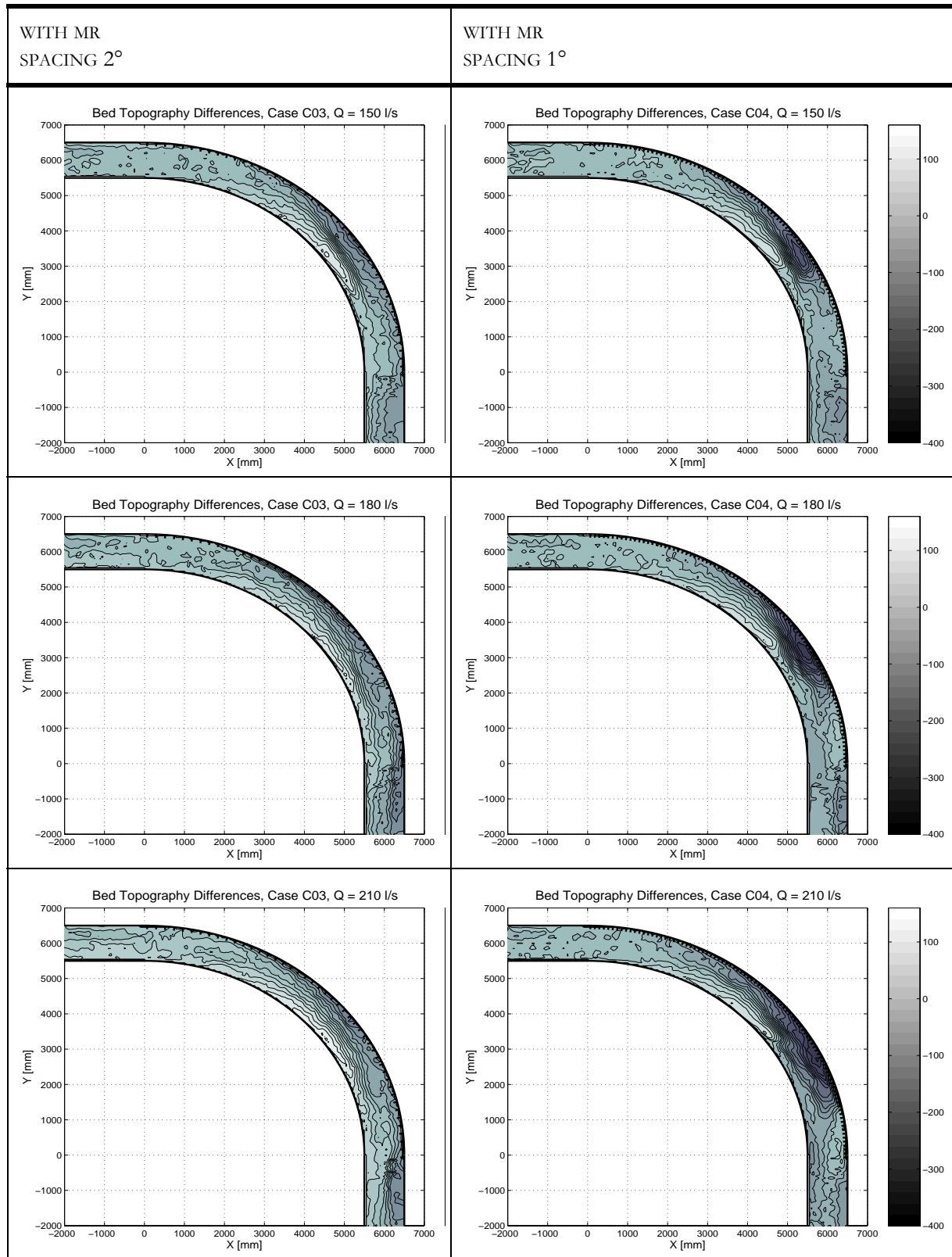
Distances in mm; Equidistance: 20 mm; Linear interpolation

4.4 *Channel slope S_0 = 0.50% - mr depth = 40 mm*
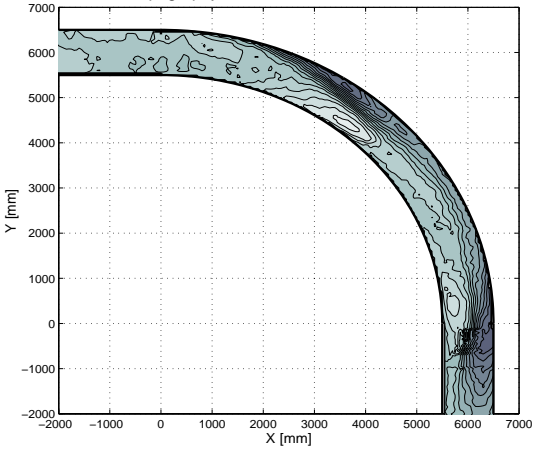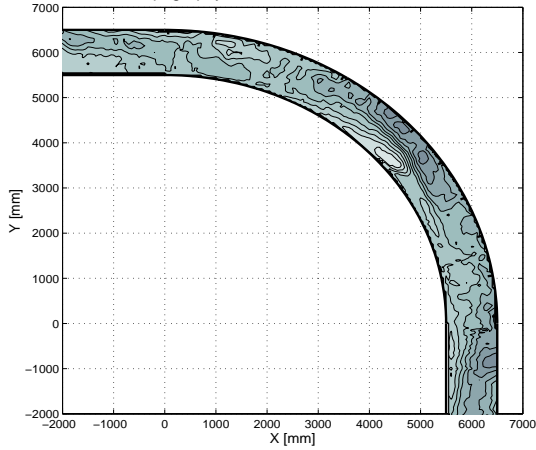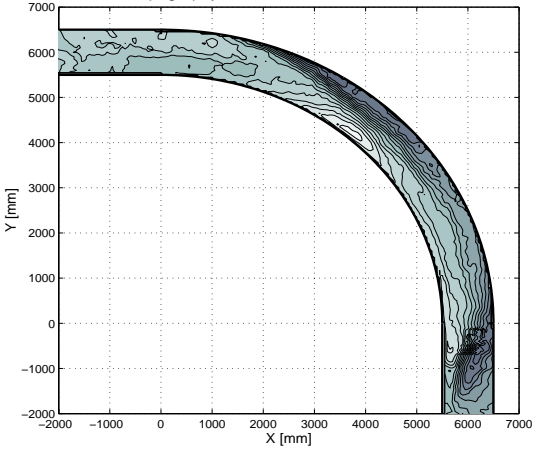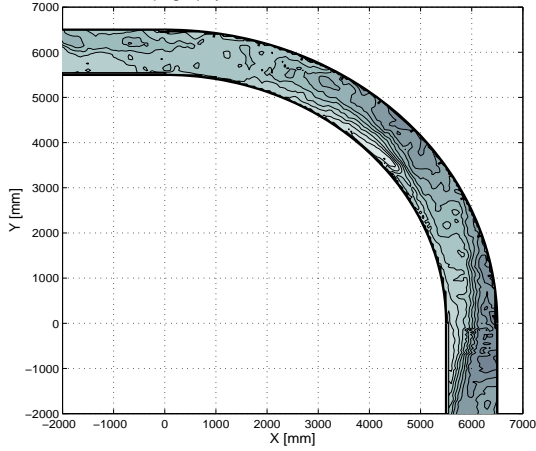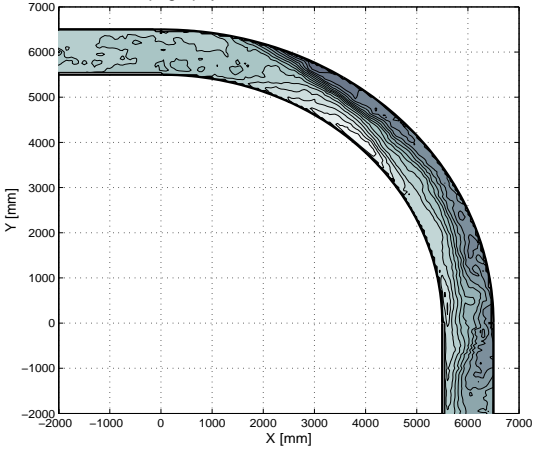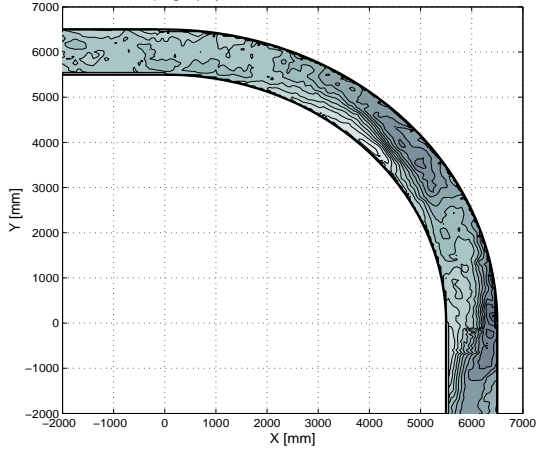
Q [L/S]	WITHOUT MR COPY OF A.4.2	WITH MR SPACING 8°
150	Bed Topography Differences, Case D01, Q = 150 l/s	Bed Topography Differences, Case E05, Q = 150 l/s
180	Bed Topography Differences, Case D01, Q = 180 l/s	Bed Topography Differences, Case E05, Q = 180 l/s
210	Bed Topography Differences, Case D01, Q = 210 l/s	Bed Topography Differences, Case E05, Q = 210 l/s

Table 4.4:   Bed topography compared to initial bed level - S_0 = 0.50% (thick mr)

| WITH MR | WITH MR |
| SPACING **4°** | SPACING **2°** |
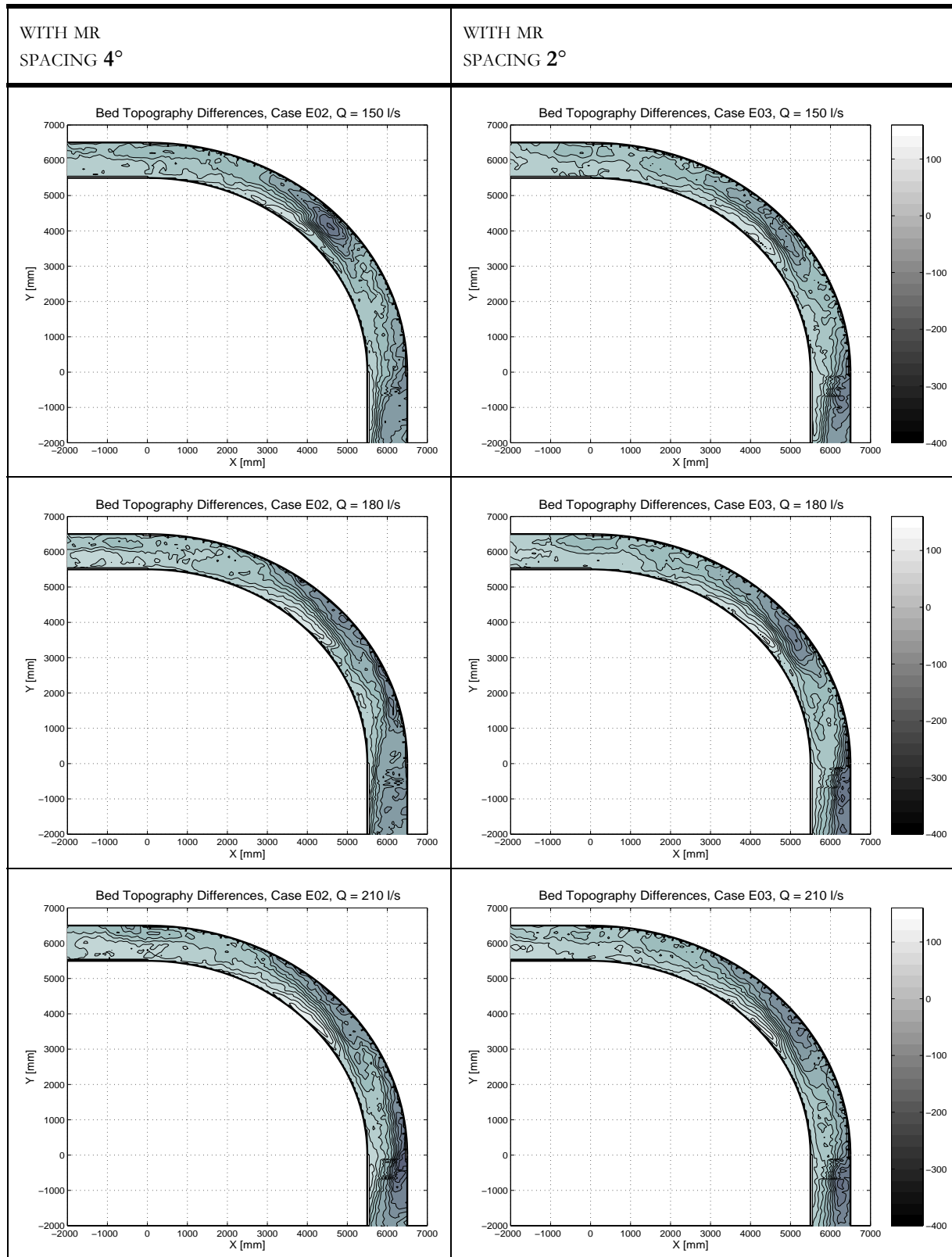
Distances in mm; Equidistance: 20 mm; Linear interpolation

4.5   Long term experience - $S_0 = 0.50\%$, $e_d = 40$ mm
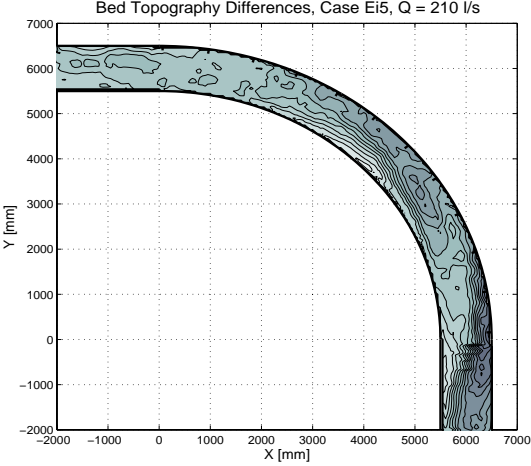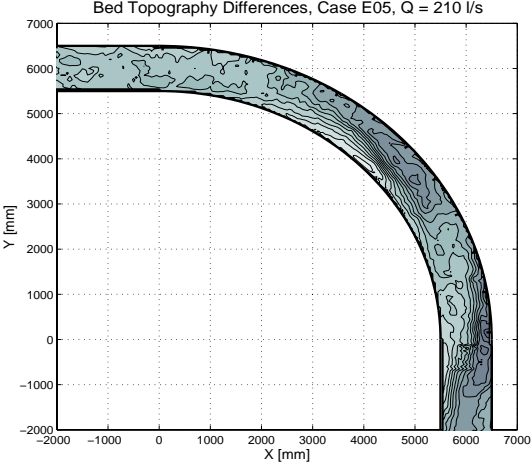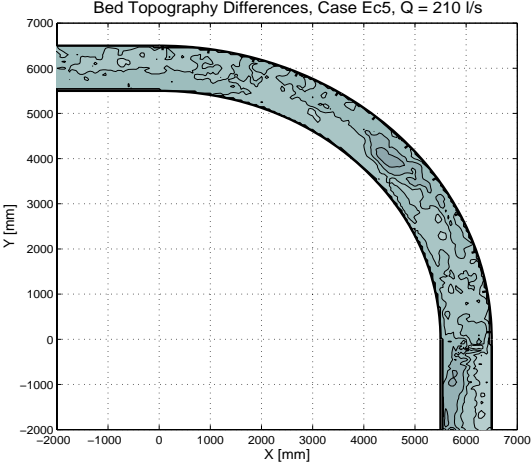
Q [L/S]	INTERMEDIATE MEASUREMENT AFTER ~13 HOURS	FINAL MEASUREMENT AFTER ~27 HOURS
210	Bed Topography Differences, Case Ei5, Q = 210 l/s	Bed Topography Differences, Case E05, Q = 210 l/s
210	comparison between intermediate and final measurement →	Bed Topography Differences, Case Ec5, Q = 210 l/s

Table 4.5:   Bed topography compared to initial bed level - Long term experience
$S_0 = 0.50\%$ (thick mr) - mr-spacing = 8° - Q = 210 l/s
Distances in mm; Equidistance: 20 mm; Linear interpolation

APPENDIX 5

WATER SURFACE COMPARED TO MEAN WATER LEVEL

This Appendix gives the final water surface compared to a horizontal average surface over the whole channel (average of all data points).

Waterlevel Differences, Case B02, Q = 180 l/s
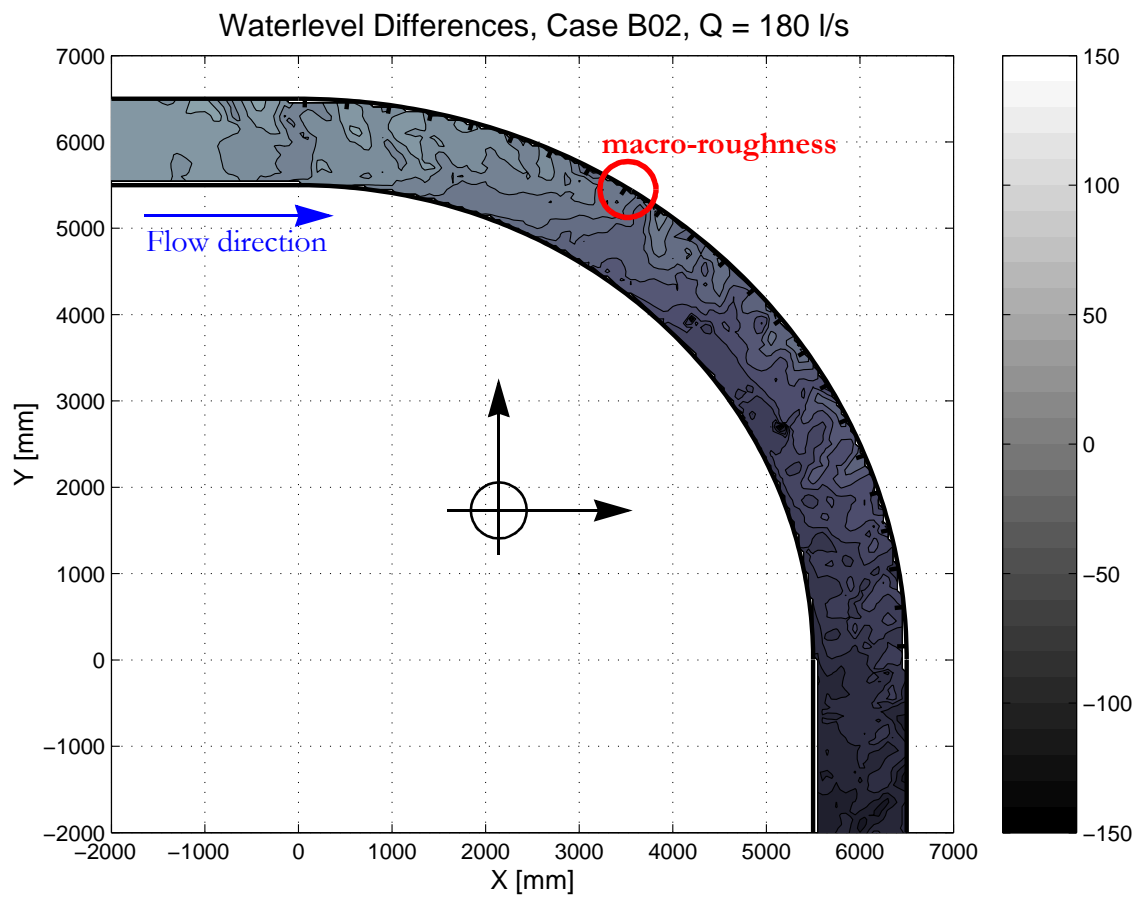
Additional information can be found in the report in Chapter 5.3.1 and 6.2.2.

5.1 *Channel slope S$_0$ = 0.35% - mr depth = 20 mm*

Q [L/S]	WITHOUT MR	WITH MR SPACING 4°
150		
180		
210		

Table 5.1: *Water surface compared to mean water level - S$_0$ = 0.35%*

WITH MR	WITH MR
SPACING 2°	SPACING 1°
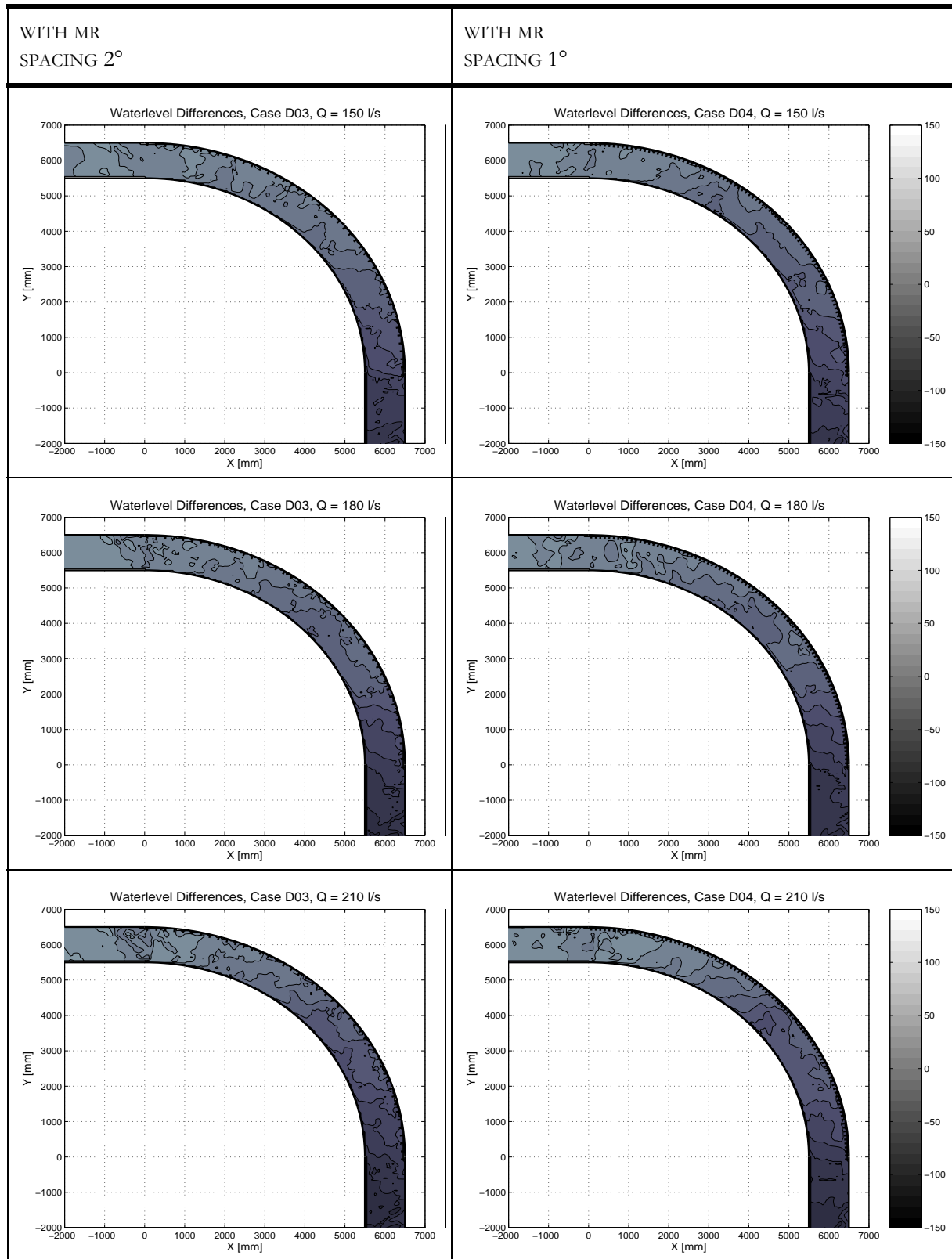
Distances in mm; Equidistance: 10 mm; Linear interpolation

5.2   *Channel slope S_0 = 0.50% - mr depth = 20 mm*

Q [L/S]	WITHOUT MR	WITH MR SPACING 4°
150		
180		
210		

Table 5.2:   Water surface compared to mean water level - S_0 = 0.50%

WITH MR	WITH MR
SPACING 2°	SPACING 1°

Waterlevel Differences, Case B03, Q = 150 l/s

Waterlevel Differences, Case B04, Q = 150 l/s

Waterlevel Differences, Case B03, Q = 180 l/s

Waterlevel Differences, Case B04, Q = 180 l/s

Waterlevel Differences, Case B03, Q = 210 l/s

Waterlevel Differences, Case B04, Q = 210 l/s
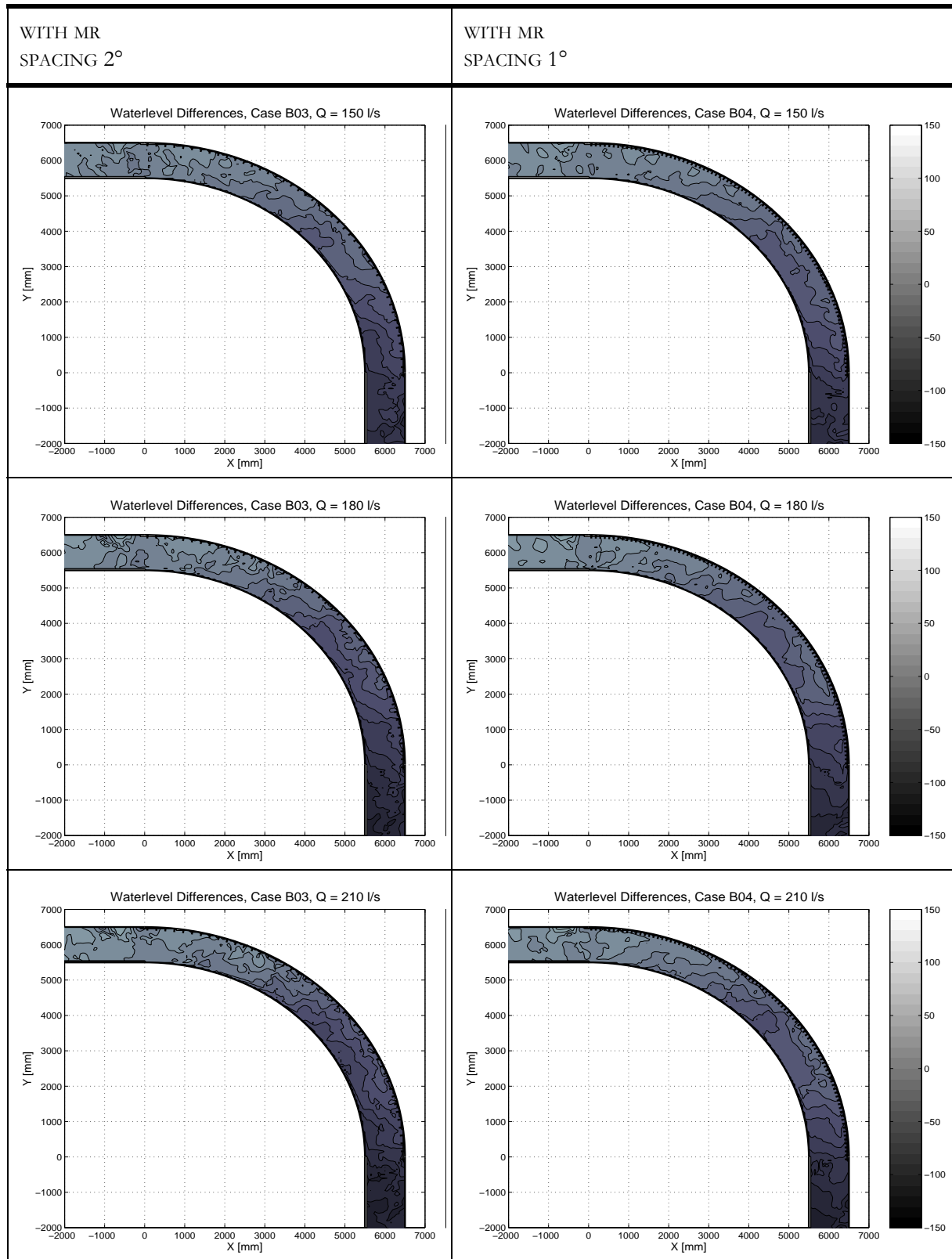
Distances in mm; Equidistance: 10 mm; Linear interpolation

5.3   *Channel slope S_0 = 0.70% - mr depth = 20 mm*

Q [L/S]	WITHOUT MR	WITH MR SPACING 4°
150	Waterlevel Differences, Case C01, Q = 150 l/s	Waterlevel Differences, Case C02, Q = 150 l/s
180	Waterlevel Differences, Case C01, Q = 180 l/s	Waterlevel Differences, Case C02, Q = 180 l/s
210	Waterlevel Differences, Case C01, Q = 210 l/s	Waterlevel Differences, Case C02, Q = 210 l/s

Table 5.3:   Water surface compared to mean water level - S_0 = 0.70%

WITH MR	WITH MR
SPACING 2°	SPACING 1°

Distances in mm; Equidistance: 10 mm; Linear interpolation

5.4 *Channel slope S_0 = 0.50% - mr depth = 40 mm*

Q [L/S]	WITHOUT MR COPY OF A.5.2	WITH MR SPACING **8°**
150		
180		
210		

Table 5.4: *Water surface compared to mean water level - S_0 = 0.50% (thick mr)*

WITH MR SPACING **4°**	WITH MR SPACING **2°**

Distances in mm; Equidistance: 10 mm; Linear interpolation

Appendix 5

A-58
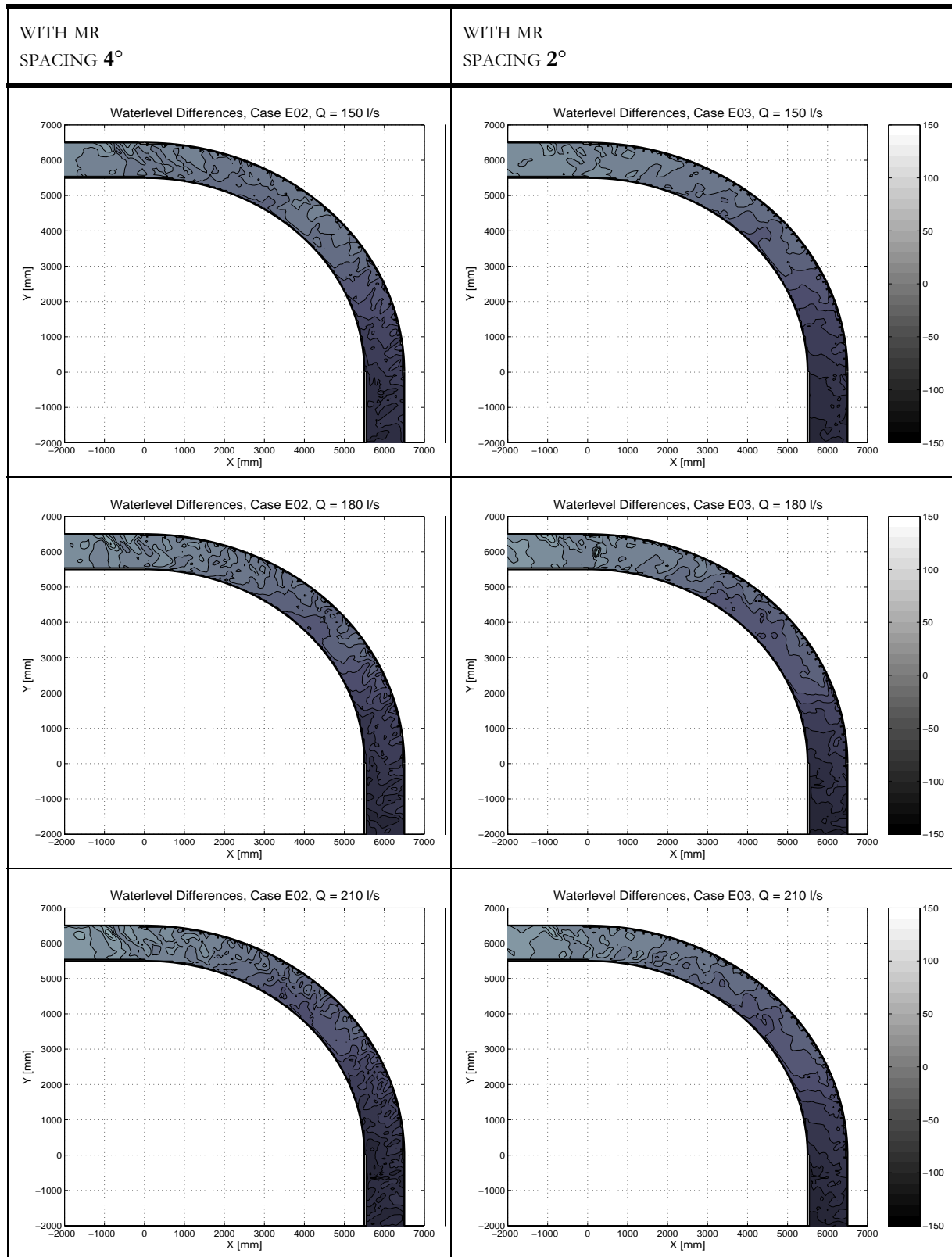
APPENDIX 6

WATER SURFACE VIEWS

This Appendix presents systematic pictures of the water surface in the bend.
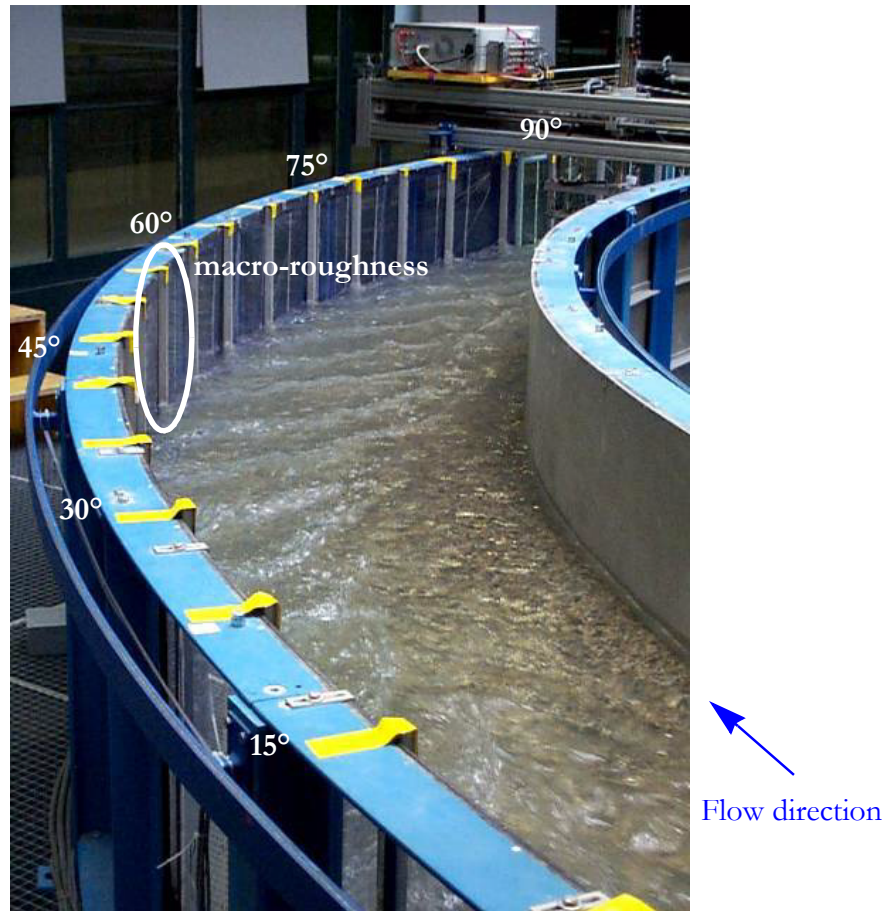
Additional information can be found in the report in Chapter 5.3.1 and 6.2.2.

6.1   *Channel slope S_0 = 0.35% - mr depth = 20 mm*
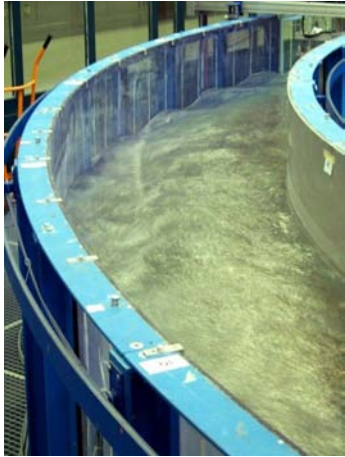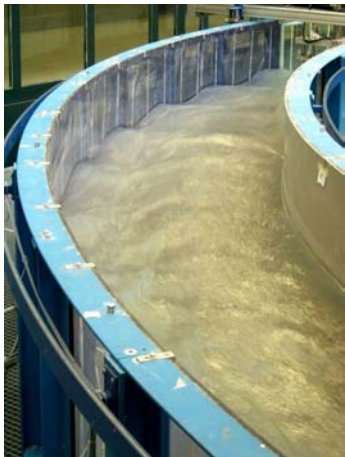
Q [L/S]	WITHOUT MR	WITH MR SPACING 4°
150		
180		
210		

Table 6.1:   Water surface views, S_0 = 0.35%, e_d = 20 mm

WITH MR SPACING 2°	WITH MR SPACING 1°

6.2   *Channel slope S_0 = 0.50% - mr depth = 20 mm*
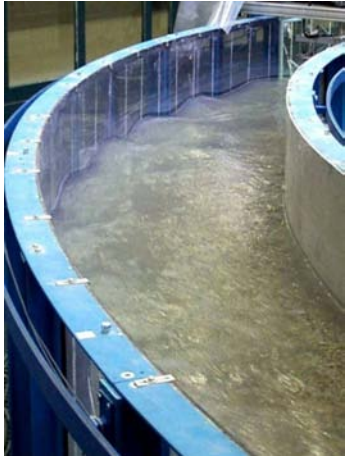
Q [L/S]	WITHOUT MR	WITH MR SPACING 4°
150		
180		
210		

Table 6.2:   Water surface views, S_0 = 0.50%, e_d = 20 mm

WITH MR SPACING 2°	WITH MR SPACING 1°
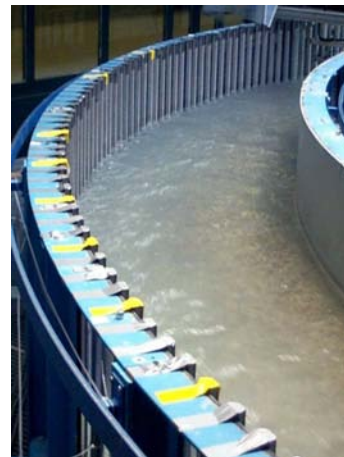
6.3   Channel slope $S_0 = 0.70\%$ - mr depth = 20 mm
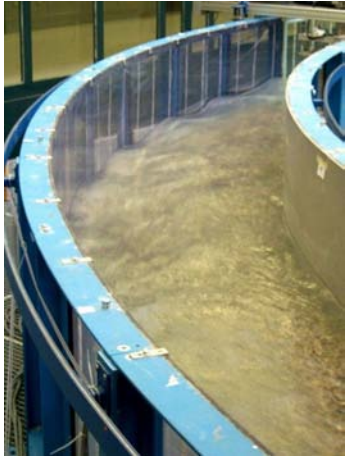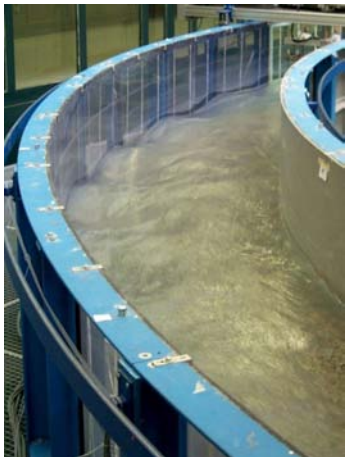
Q [L/S]	WITHOUT MR	WITH MR SPACING 4°
150		
180		
210		

Table 6.3:   Water surface views, $S_0 = 0.70\%$, $e_d = 20$ mm

WITH MR SPACING 2°	WITH MR SPACING 1°

6.4 Channel slope S_0 = 0.50% - mr depth = 40 mm
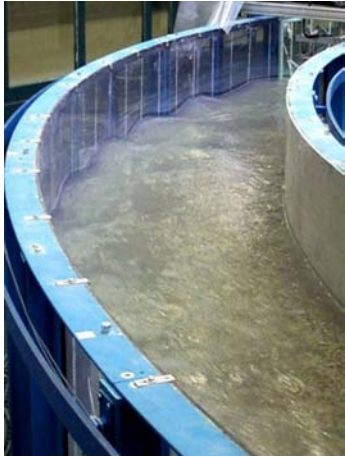
Q [L/S]	WITHOUT MR COPY FROM A.6.2	WITH MR SPACING 8°
150		
180		
210		

Table 6.4:   Water surface views, S_0 = 0.50%, e_d = 40 mm

WITH MR SPACING **4°**	WITH MR SPACING **2°**

APPENDIX 7

EQUILIBRIUM BED AND WATER LEVELS IN SELECTED CROSS SECTIONS

This Appendix gives the final water and bed levels in different cross sections. -1 m indicates the cross section 1 m upstream the bend in the inlet reach.
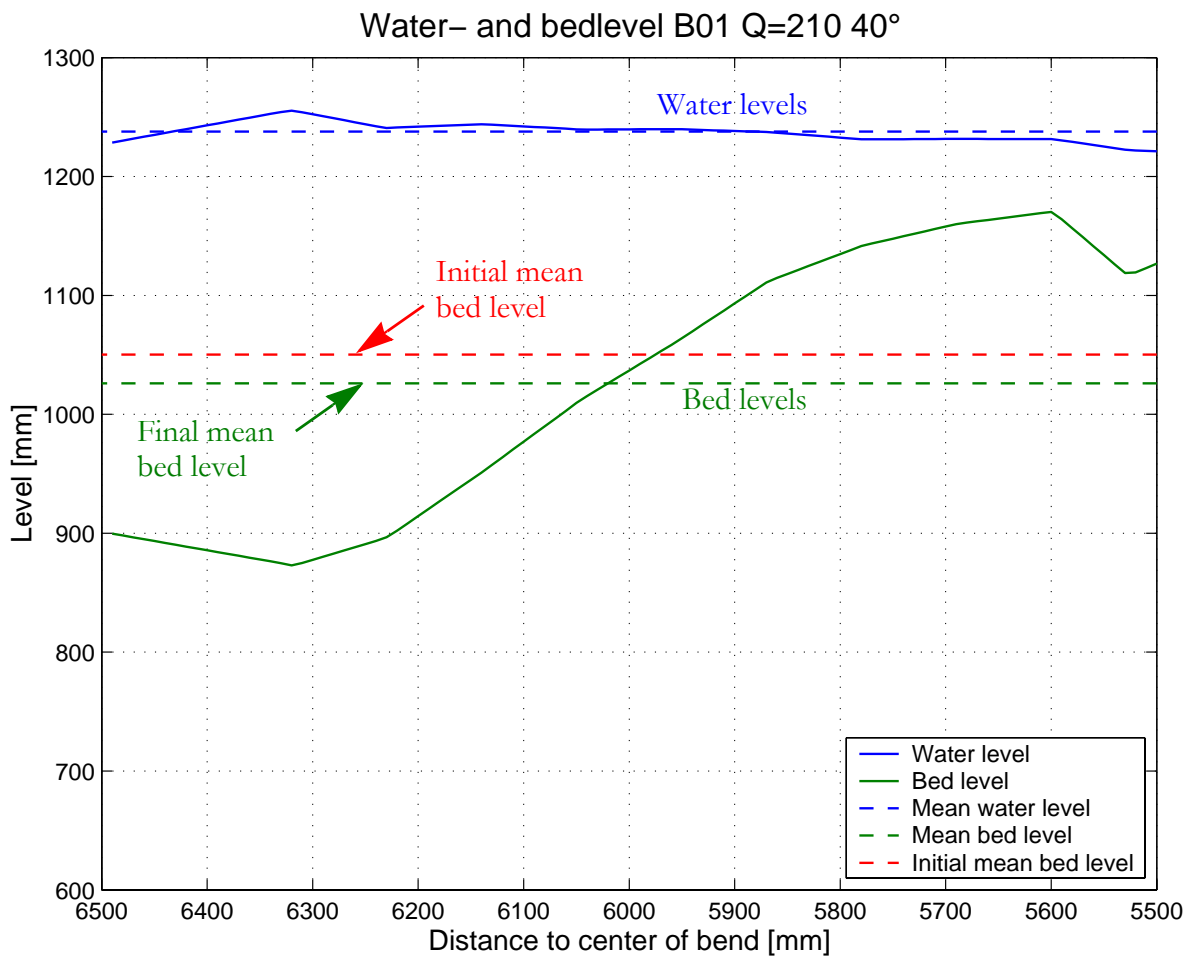
Additional information can be found in the report in Chapter 5.3.1 and 6.2.

7.1 Cross sections at S_0=0.35%, Q=150 l/s, e_d=20mm

Table 7.1: Cross sections, $S_0 = 0.35\%$, $Q = 150$ l/s, mr-depth = 20 mm
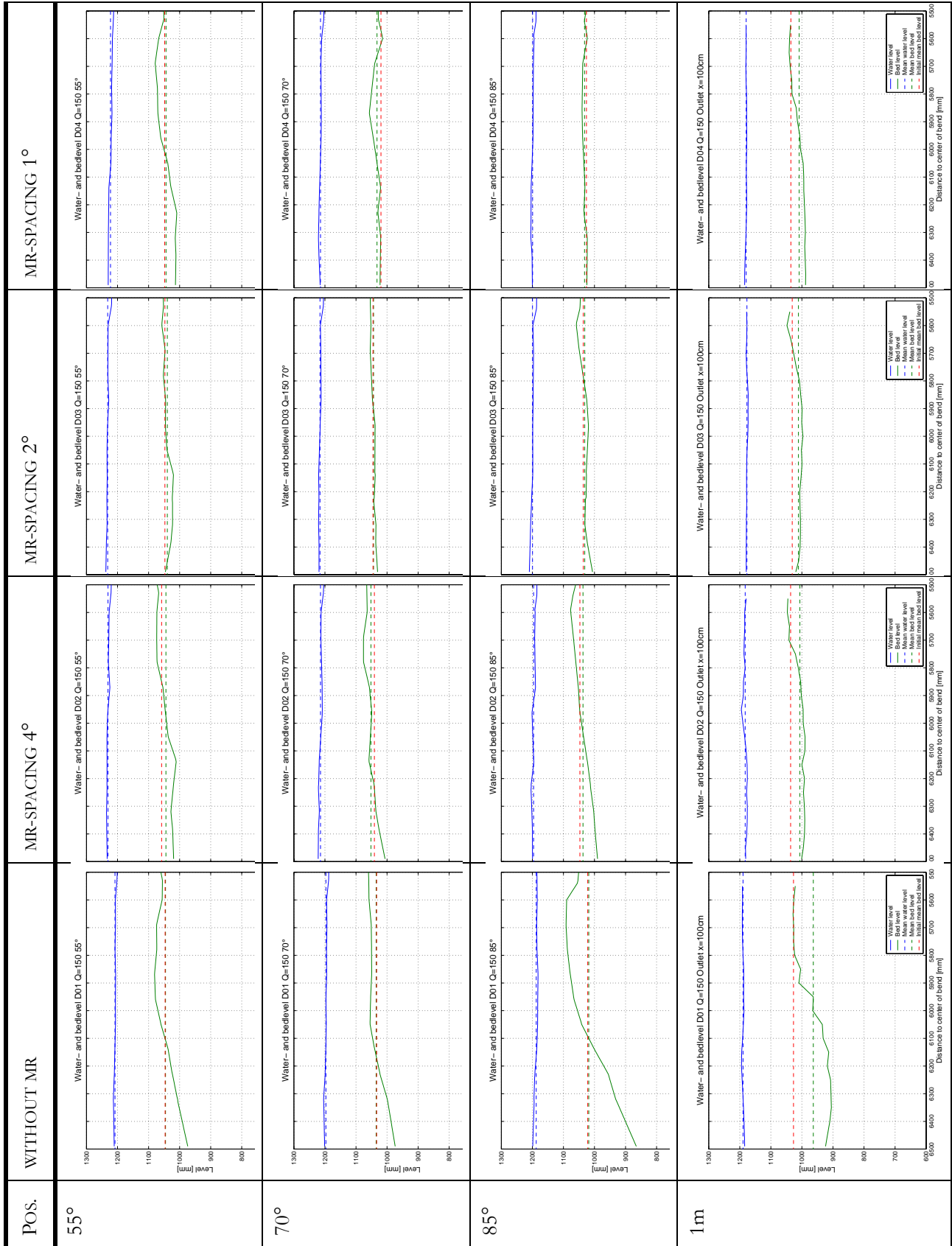
Table 7.1:   Cross sections, $S_0 = 0.35\%$, $Q=150$ l/s, mr-depth $= 20$ mm

7.2   *Cross sections at S_0=0.35%, Q=180 l/s, e_d=20mm*

Table 7.2:   Cross sections, $S_0 = 0.35\%$, $Q=180$ l/s, mr-depth = 20 mm

Table 7.2: *Cross sections, $S_0 = 0.35\%$, $Q=180$ l/s, mr-depth $= 20$ mm*

7.3 *Cross sections at S_0=0.35%, Q=210 l/s, e_d=20mm*
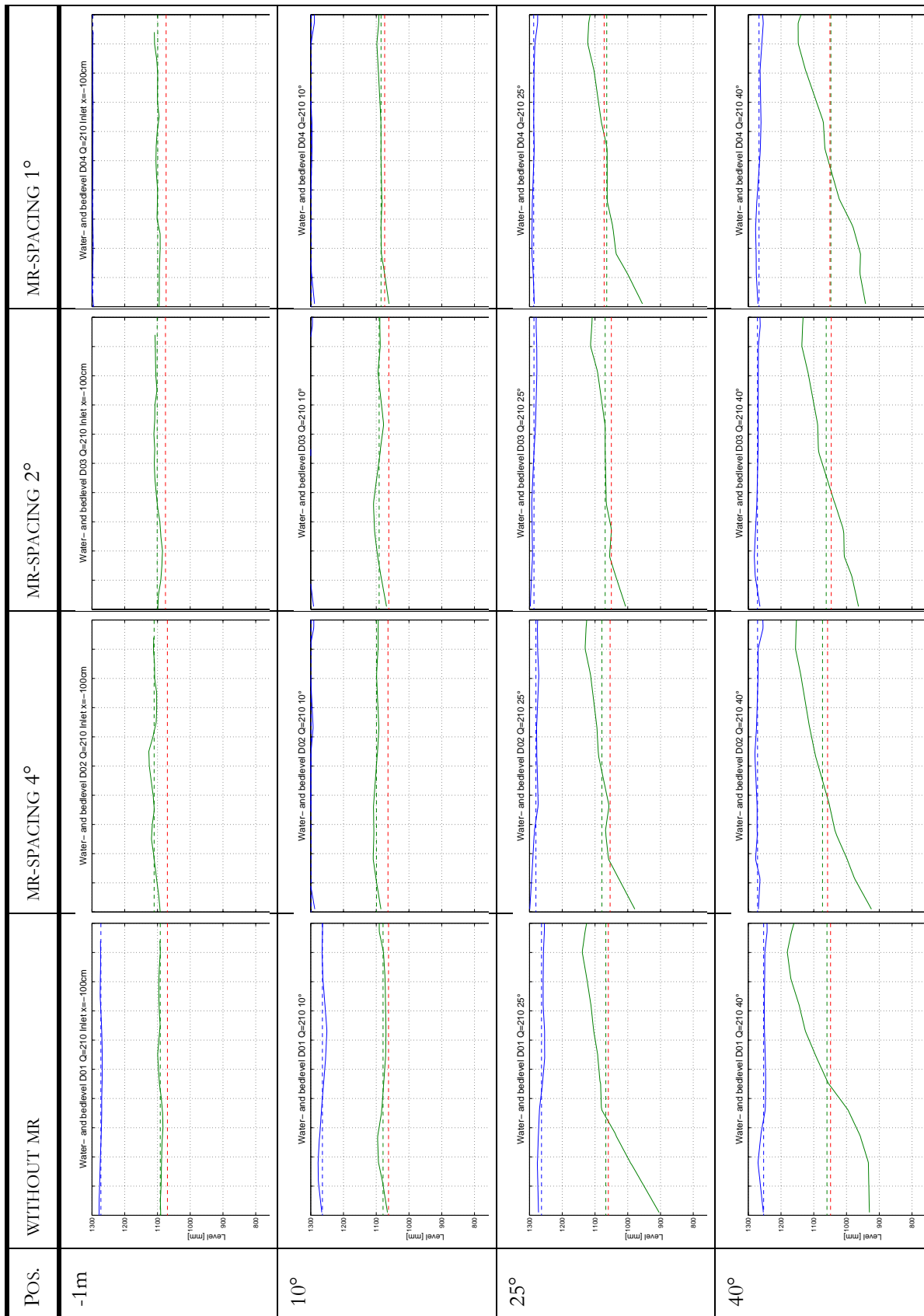
Table 7.3: *Cross sections, $S_0 = 0.35\%$, $Q=210$ l/s, mr-depth = 20 mm*
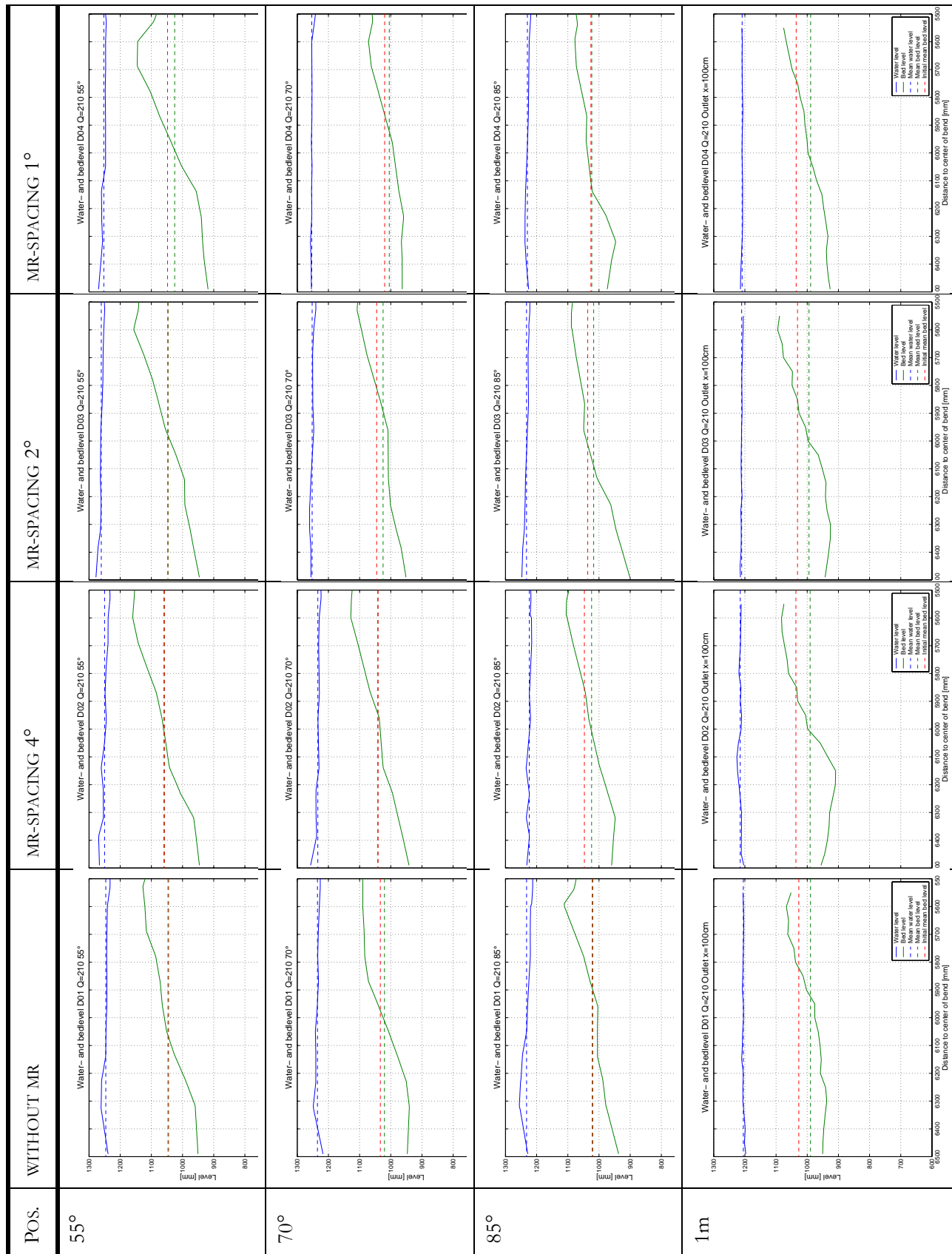
Table 7.3:   *Cross sections, $S_0 = 0.35\%$, $Q=210$ l/s, mr-depth = 20 mm*

7.4   *Cross sections at S_0=0.50%, Q=150 l⁄s, e_d=20mm*
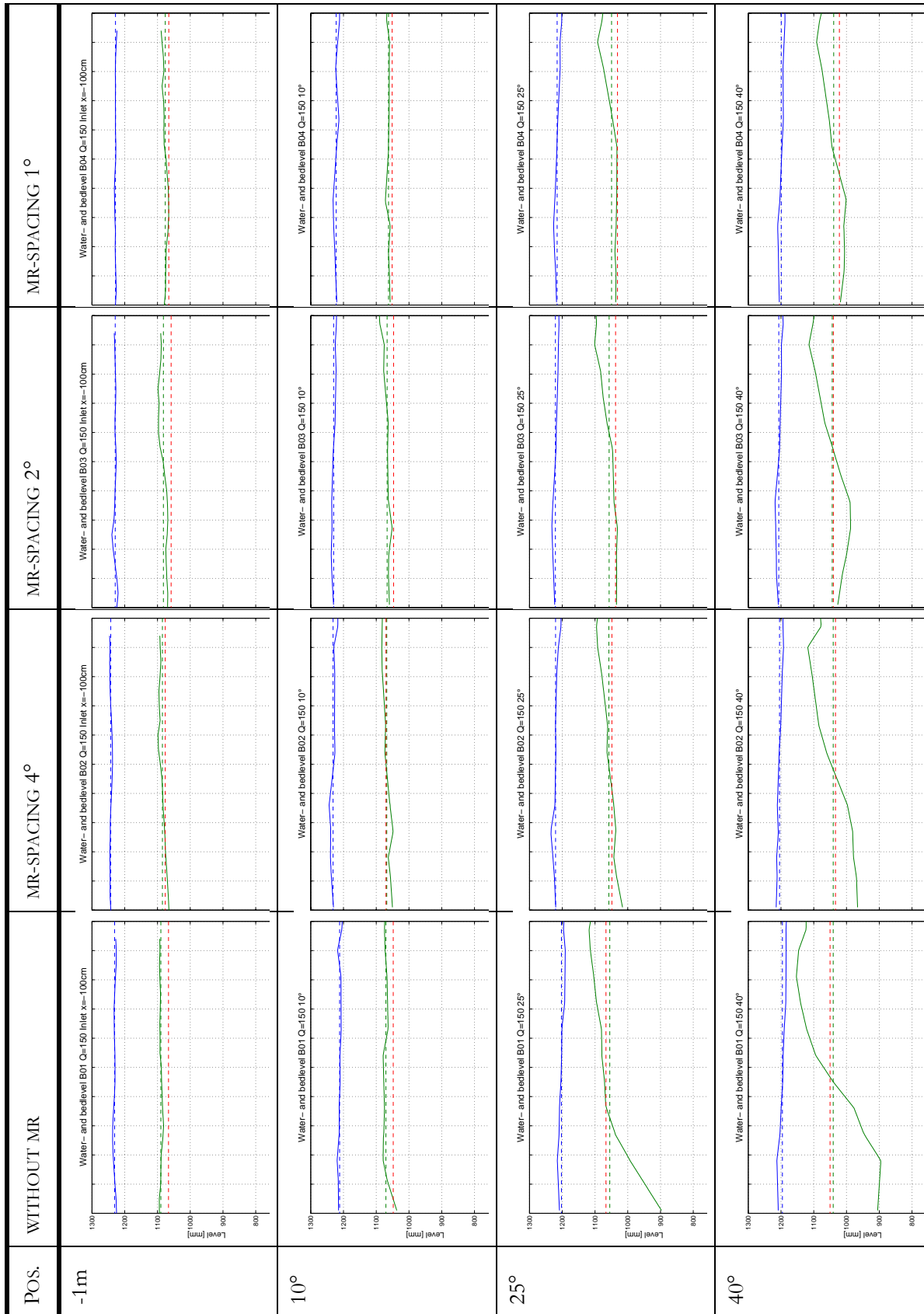
Table 7.4:   *Cross sections, S_0 = 0.50%, Q=150 l/s, mr-depth = 20 mm*
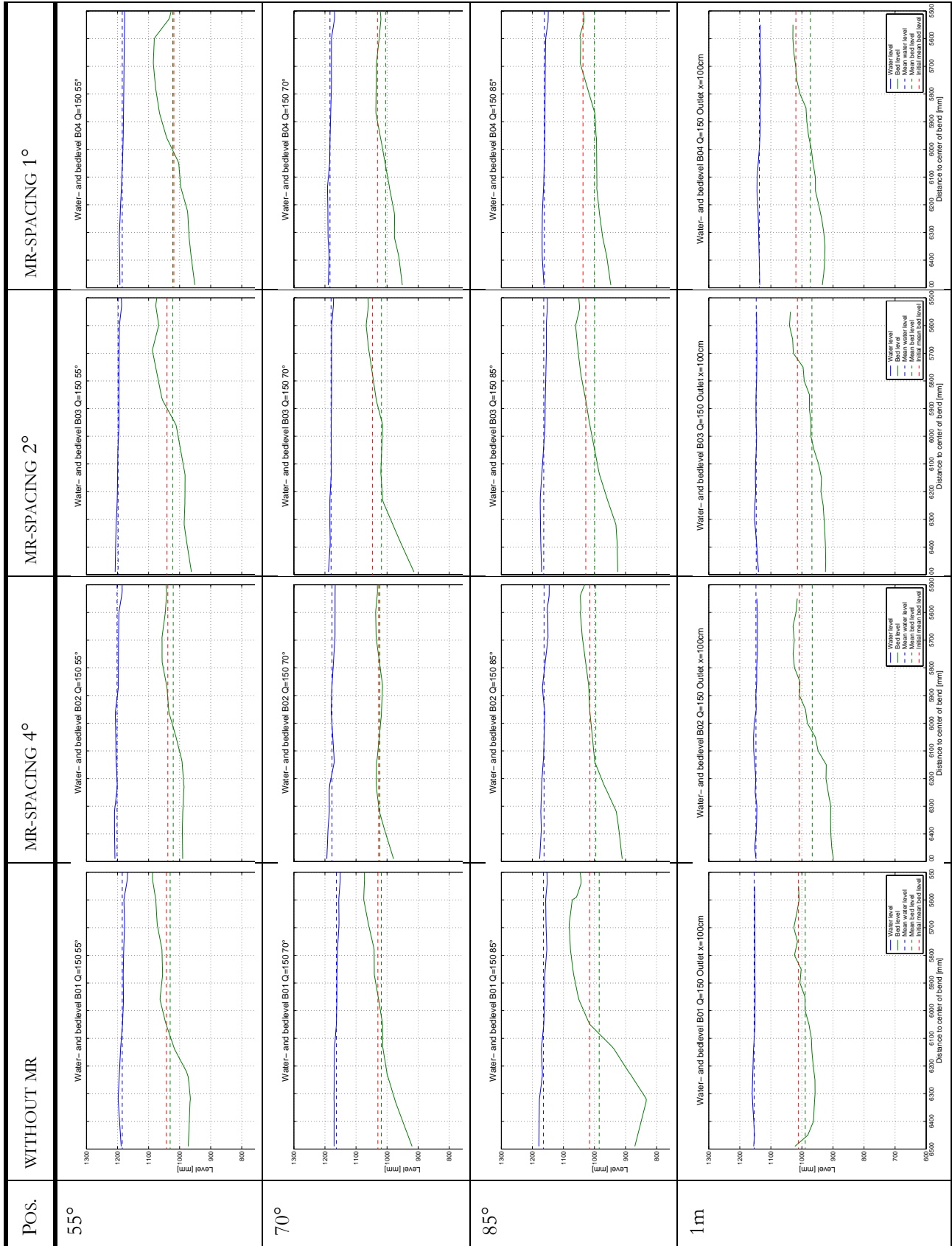
Table 7.4: Cross sections, $S_0 = 0.50\%$, $Q=150$ l/s, mr-depth $= 20$ mm

7.5   *Cross sections at S_0=0.50%, Q=180 l/s, e_d=20mm*
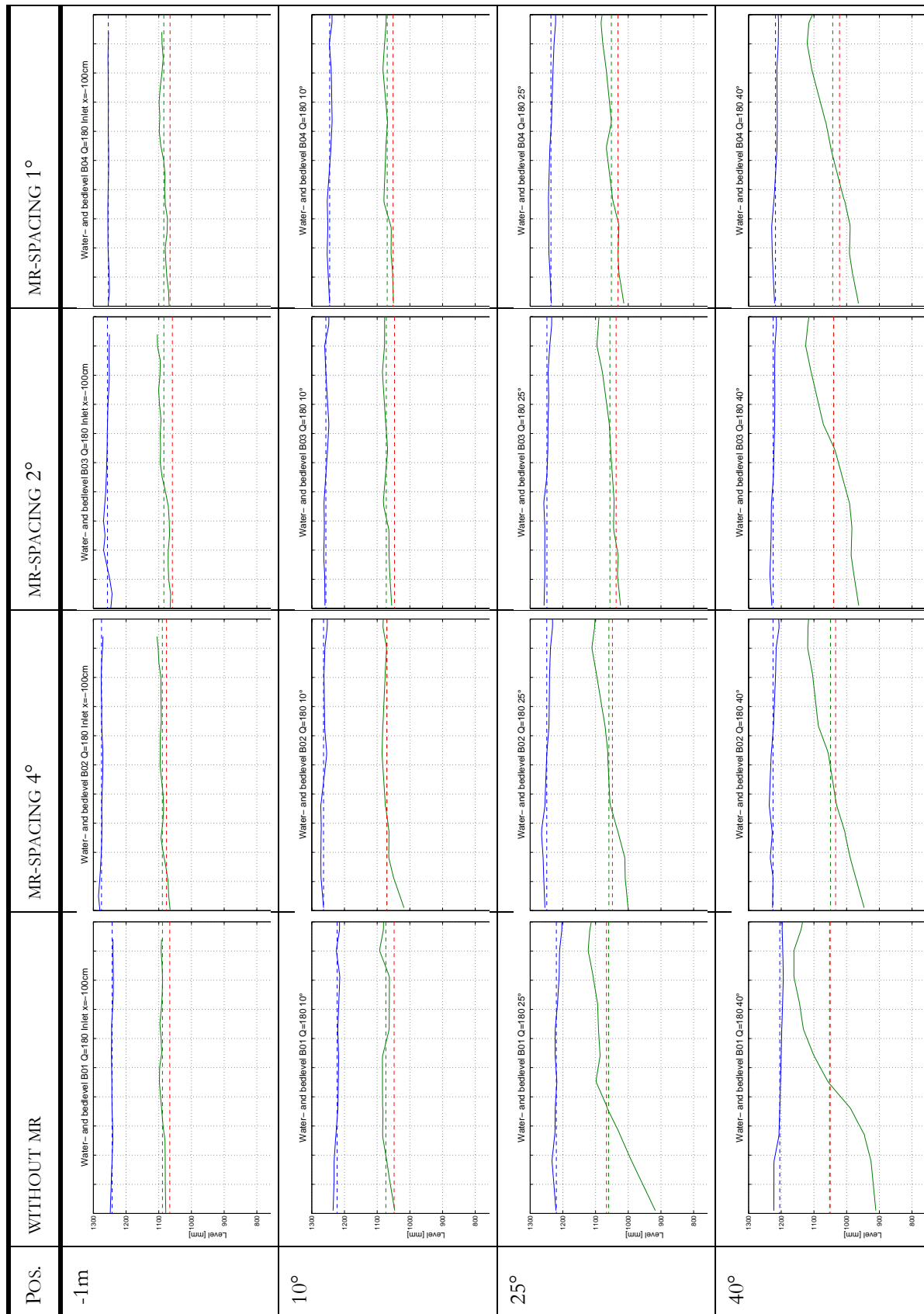
Table 7.5:   Cross sections, $S_0 = 0.50\%$, $Q=180\ l/s$, mr-depth = 20 mm
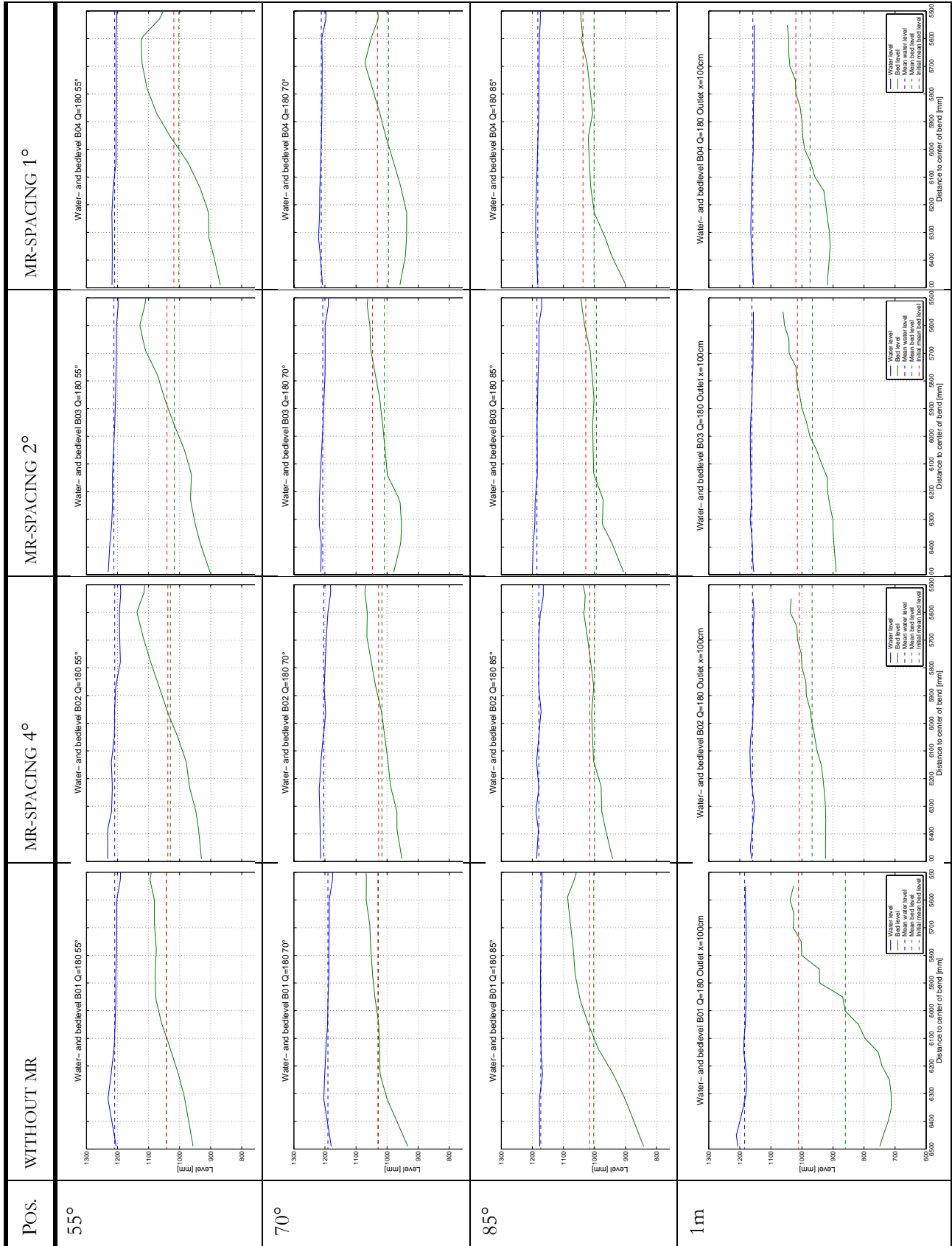
Table 7.5: *Cross sections, $S_0 = 0.50\%$, $Q=180$ l/s, $mr\text{-}depth = 20$ mm*

7.6 *Cross sections at S_0=0.50%, Q=210 l/s, e_d=20mm*
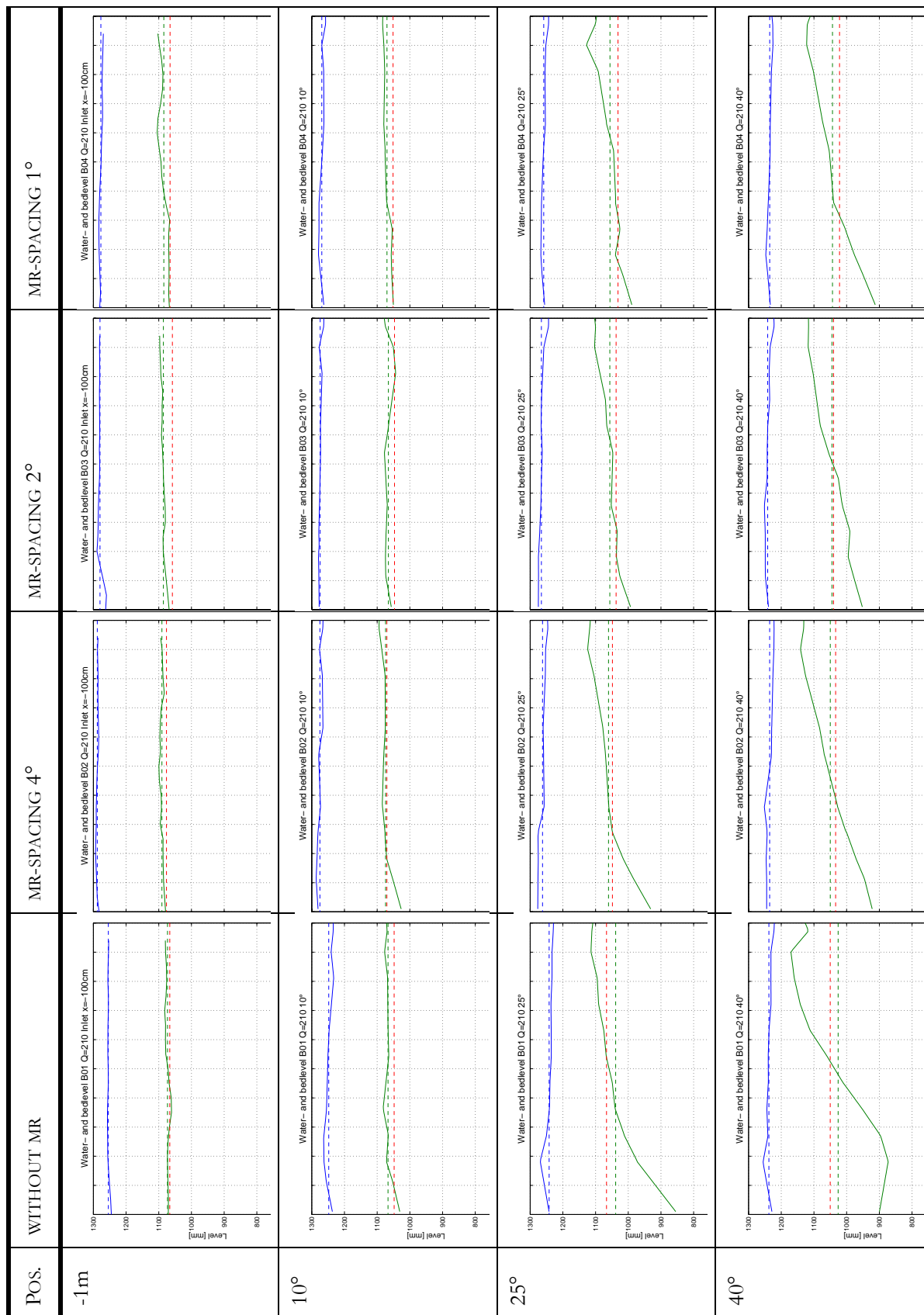
Table 7.6:   Cross sections, $S_0 = 0.50\%$, $Q = 210$ l/s, mr-depth = 20 mm
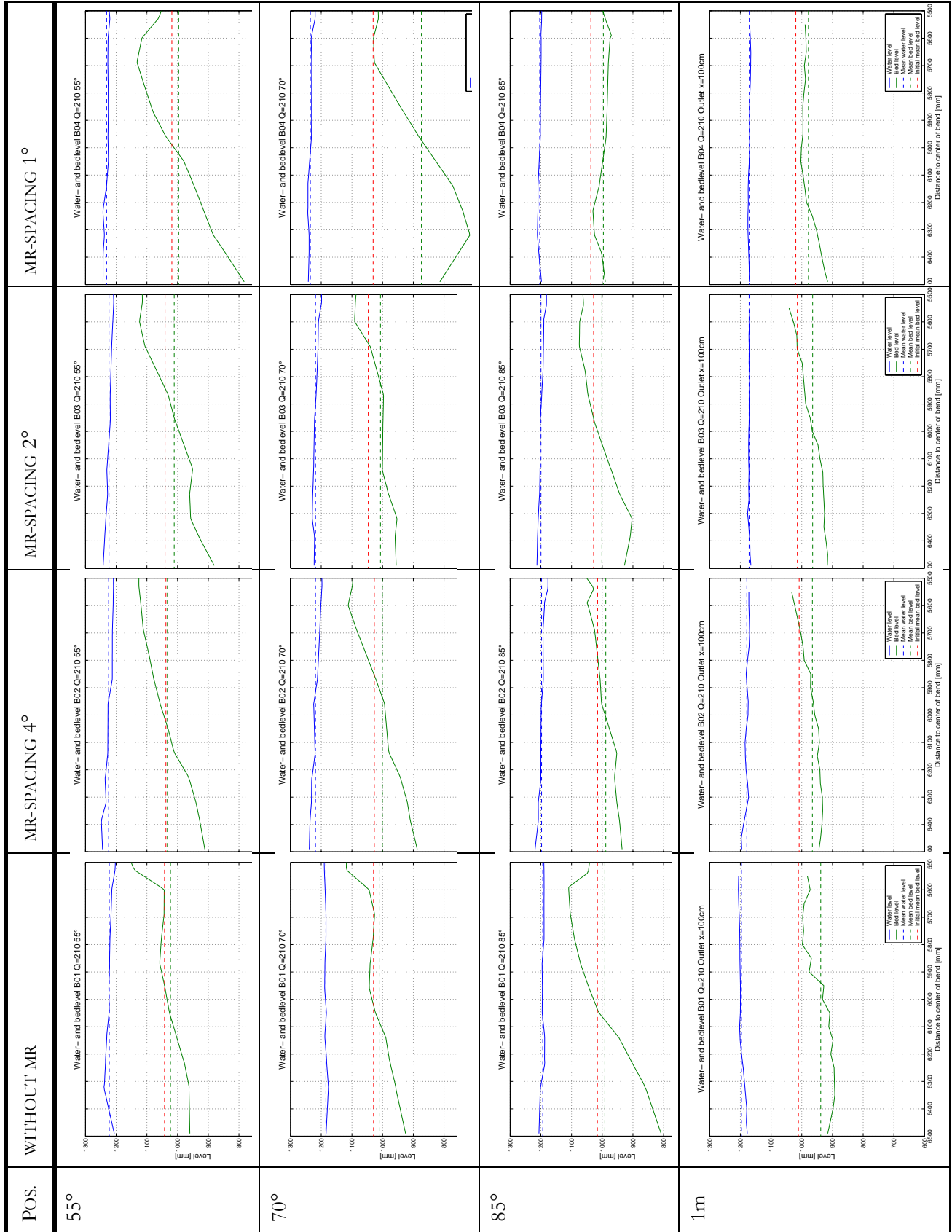
Table 7.6: Cross sections, $S_0 = 0.50\%$, $Q = 210$ l/s, mr-depth = 20 mm

7.7 *Cross sections at S_0=0.70%, Q=150 l/s, e_d=20mm*
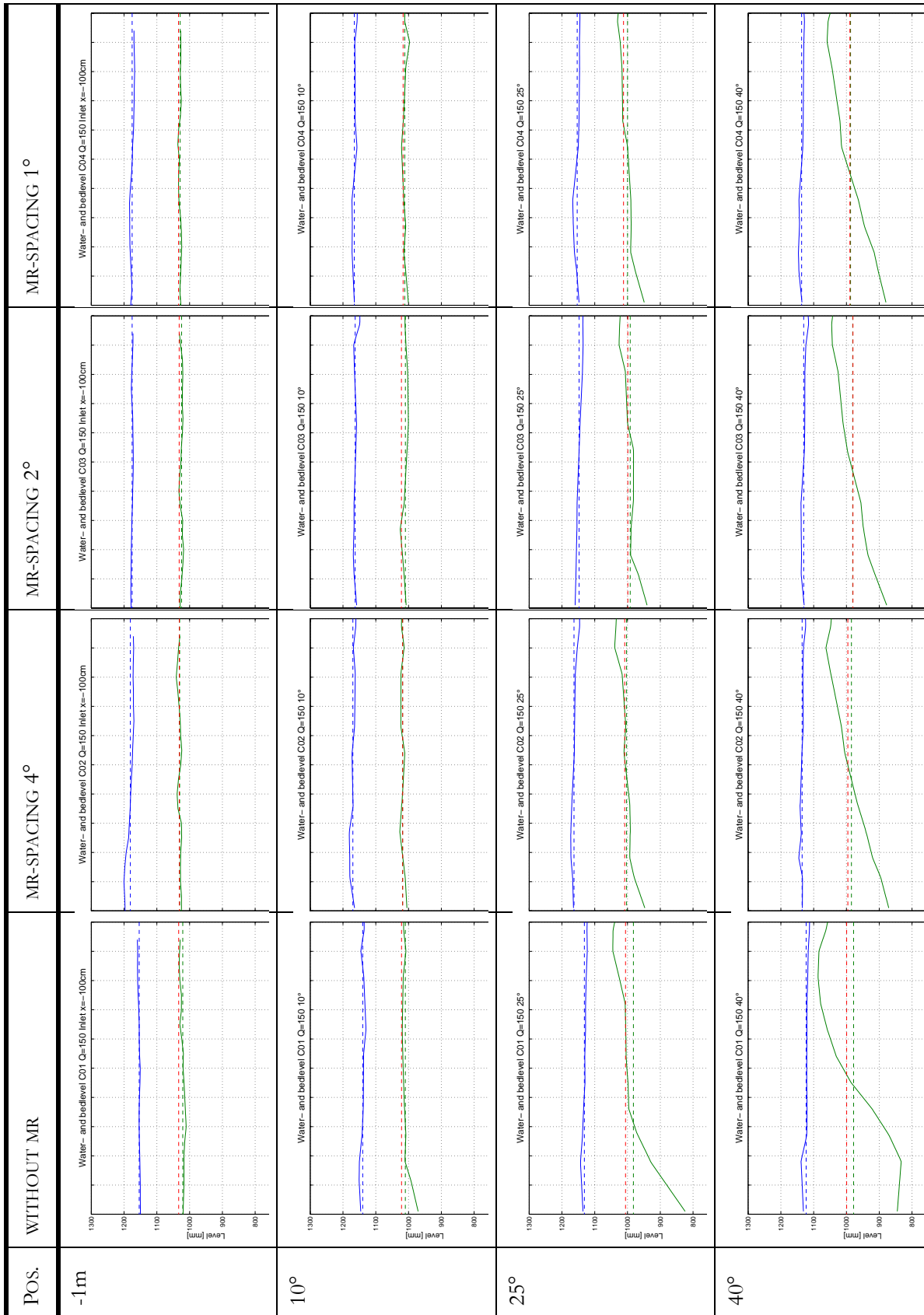
Table 7.7: *Cross sections, S_0 = 0.70%, Q=150 l/s, mr-depth = 20 mm*
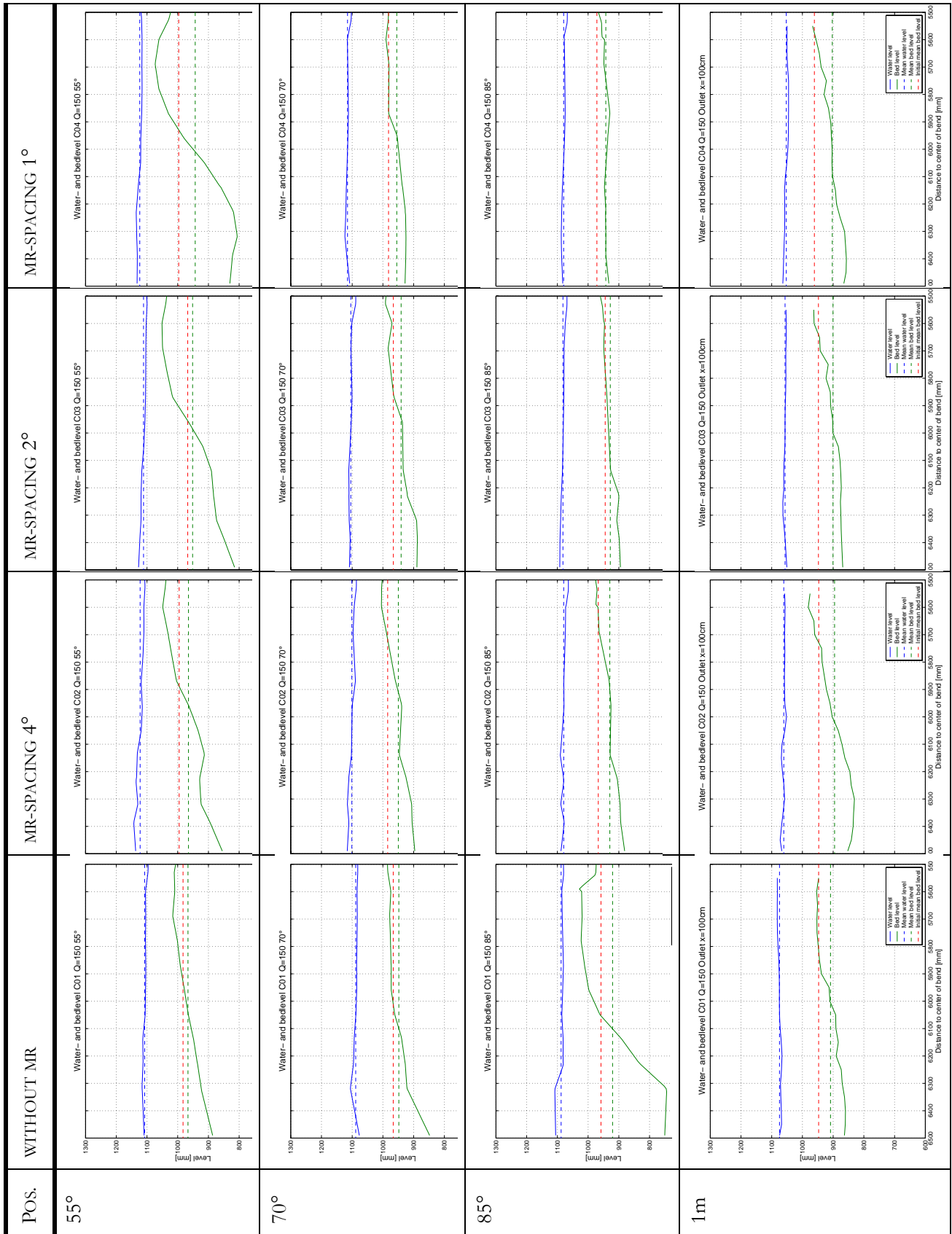
Table 7.7:   Cross sections, $S_0 = 0.70\%$, $Q = 150\ l/s$, mr-depth $= 20\ mm$

7.8 *Cross sections at S_0=0.70%, Q=180 l/s, e_d=20mm*
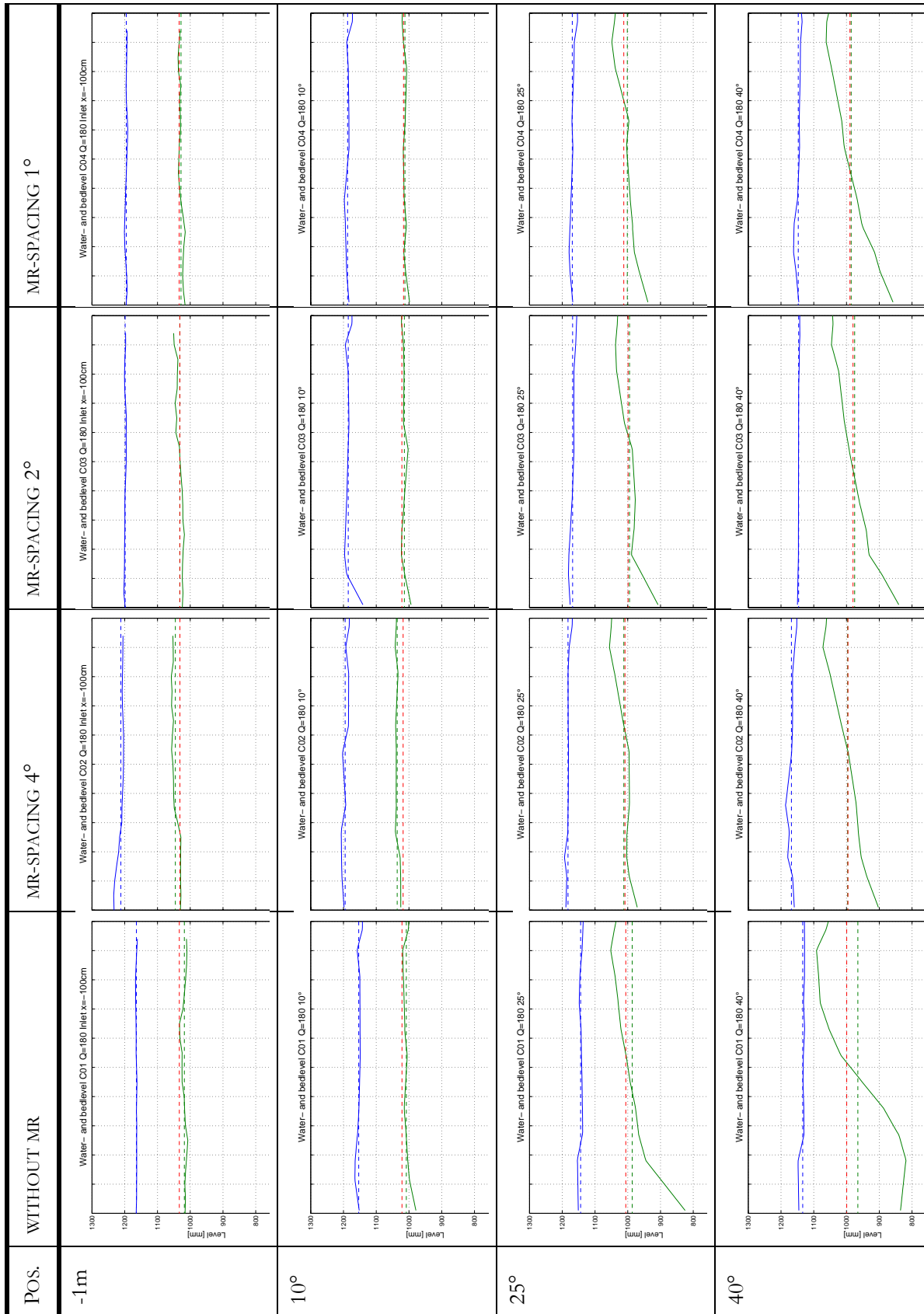
Table 7.8:   *Cross sections, $S_0 = 0.70\%$, $Q=180$ l/s, mr-depth = 20 mm*
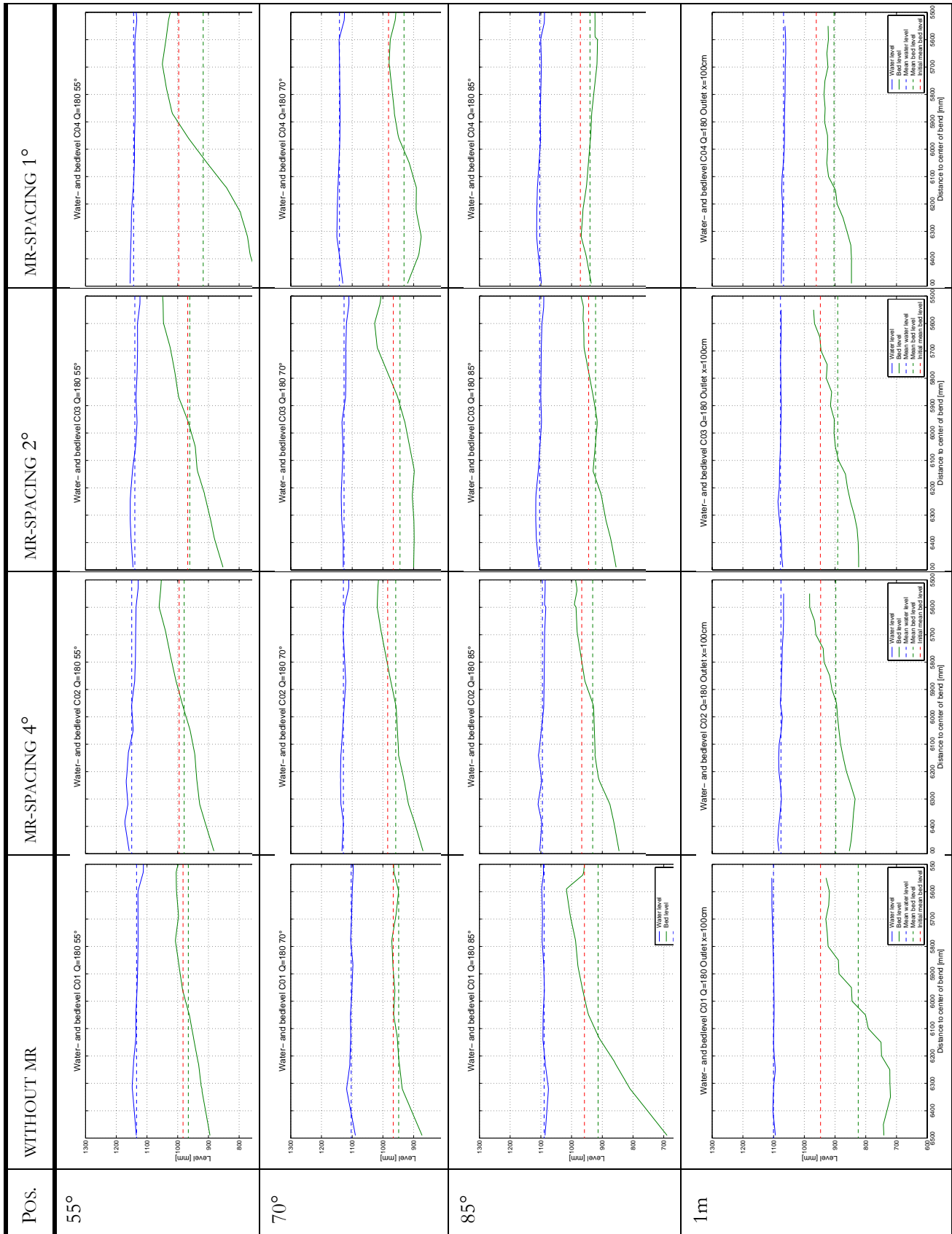
Table 7.8:   *Cross sections, $S_0 = 0.70\%$, $Q=180$ l/s, mr-depth = 20 mm*

7.9 *Cross sections at S_0=0.70%, Q=210 l/s, e_d=20mm*

Table 7.9: *Cross sections, $S_0 = 0.70\%$, $Q=210\ l/s$, mr-depth = 20 mm*

Table 7.9:   Cross sections, $S_0 = 0.70\%$, $Q=210$ l/s, mr-depth = 20 mm

7.10 Cross sections at S_0=0.50%, Q=150 l/s, e_d=40mm
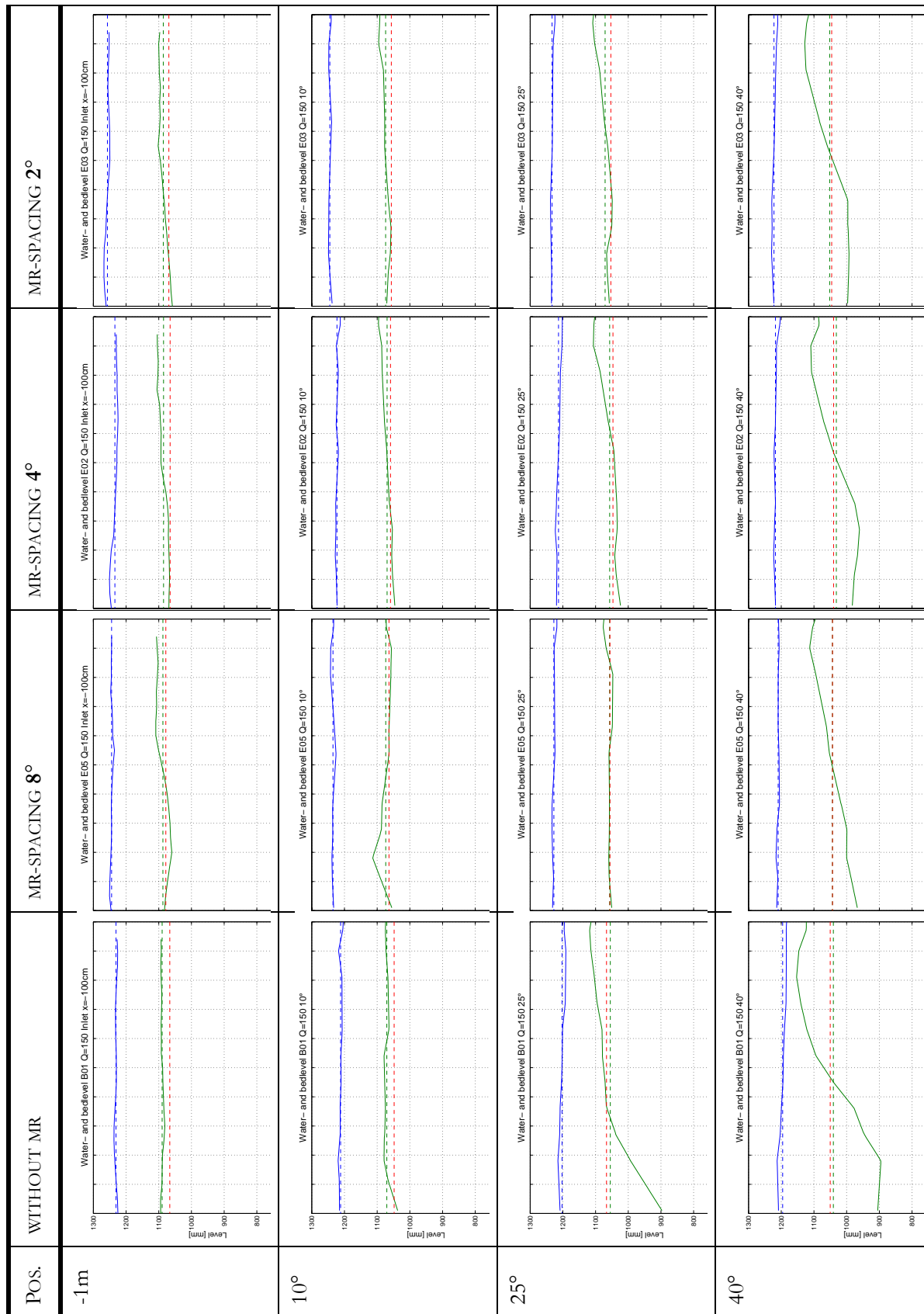
Table 7.10: Cross sections, $S_0 = 0.50\%$, $Q=150$ l/s, mr-depth = 40 mm
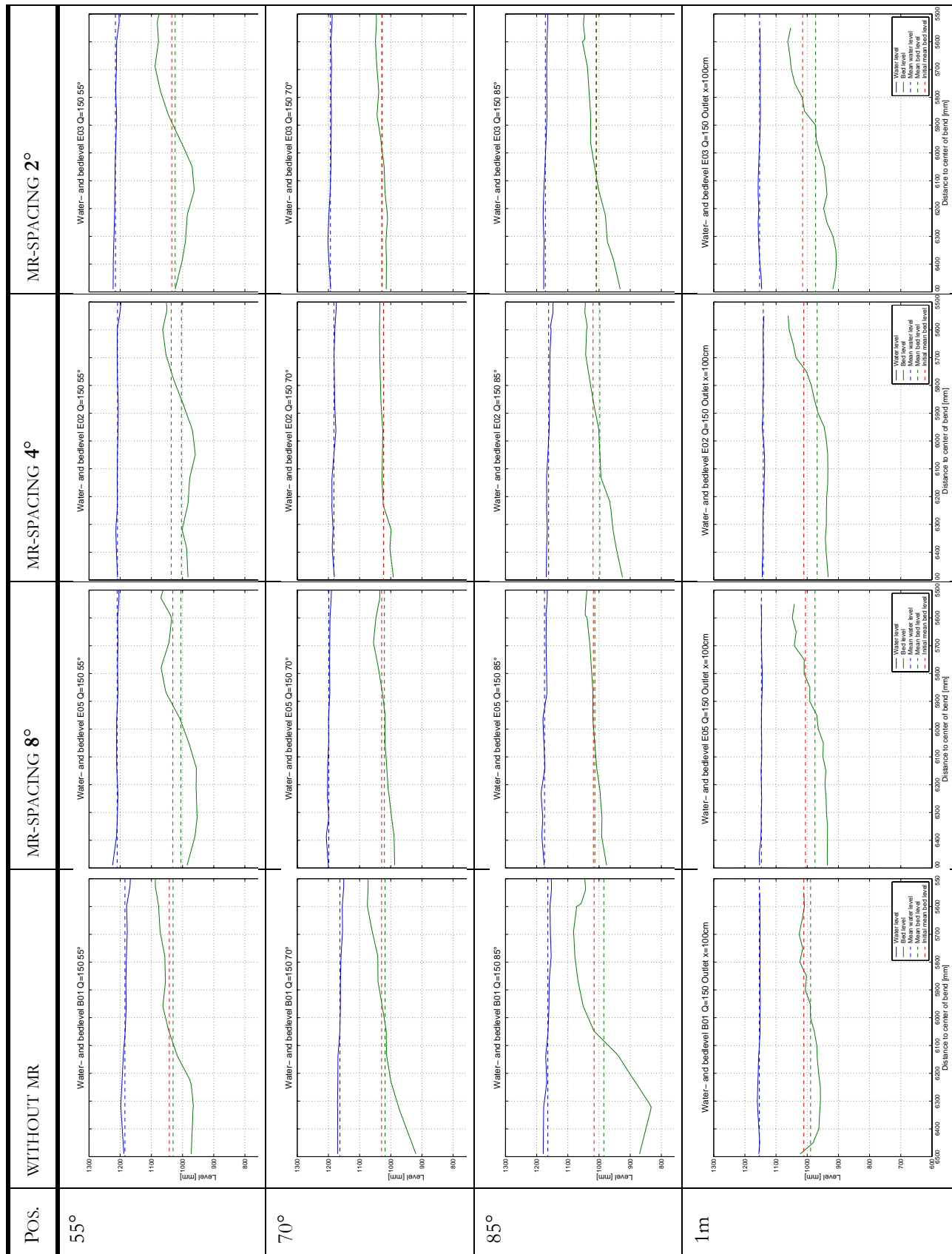
Table 7.10:   Cross sections, $S_0 = 0.50\%$, $Q=150$ l/s, mr-depth = 40 mm

7.11   Cross sections at S_0=0.50%, Q=180 l/s, e_d=40mm
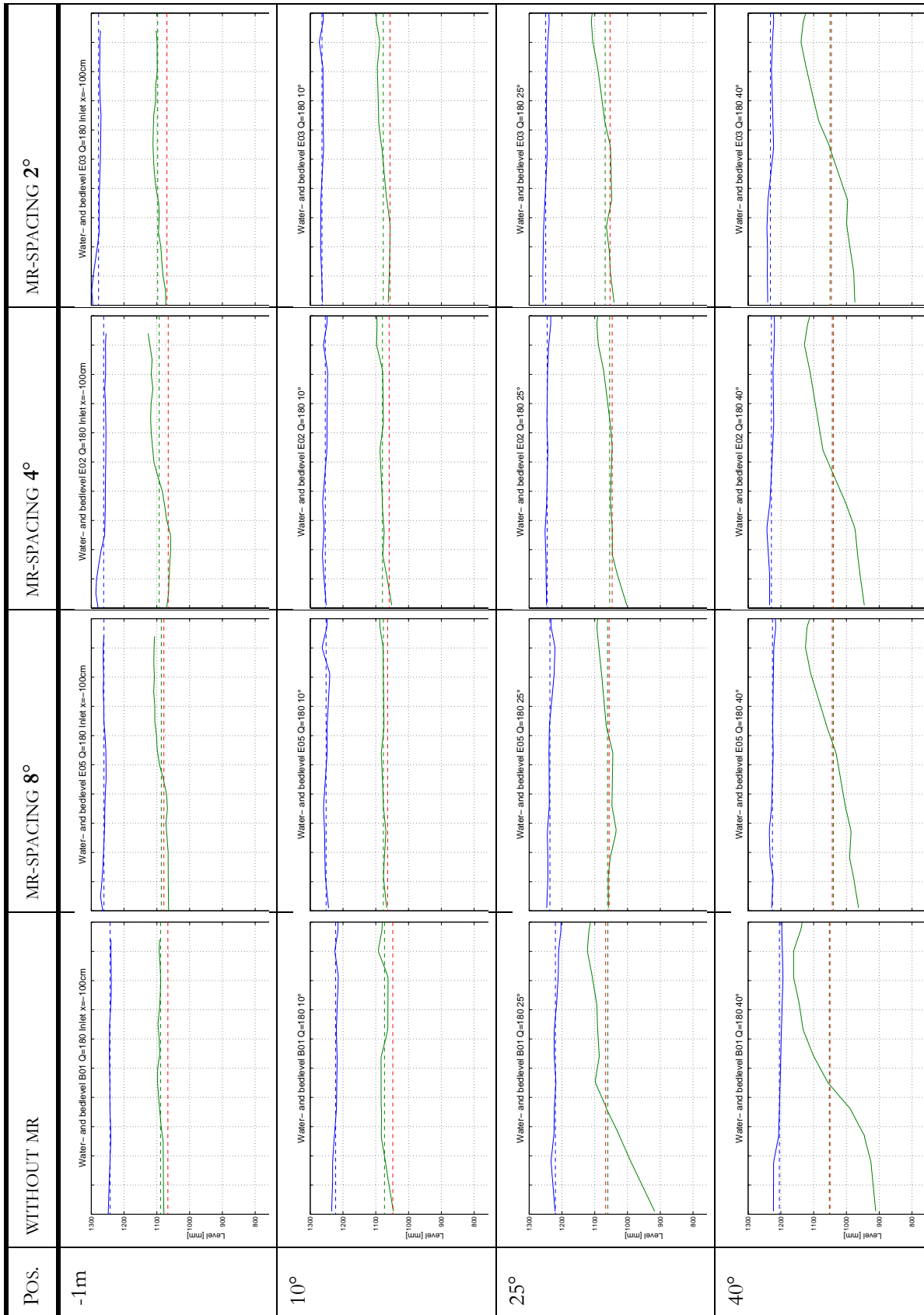
Table 7.11:   Cross sections, $S_0 = 0.50\%$, Q=180 l/s, mr-depth = 40 mm
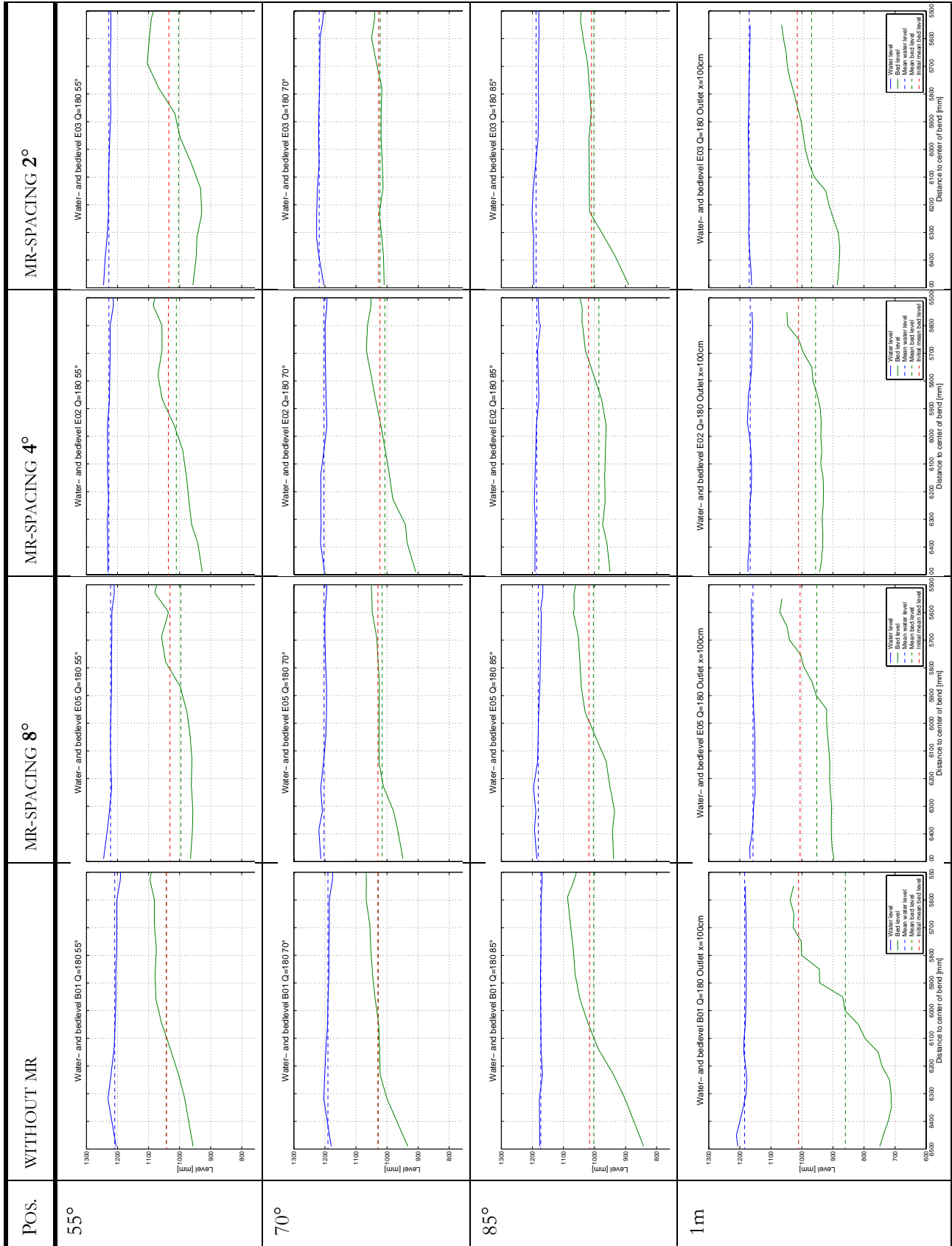
Table 7.11: Cross sections, $S_0 = 0.50\%$, $Q=180$ l/s, mr-depth = 40 mm

7.12   Cross sections at S_0=0.50%, Q=210 l/s, e_d=40mm
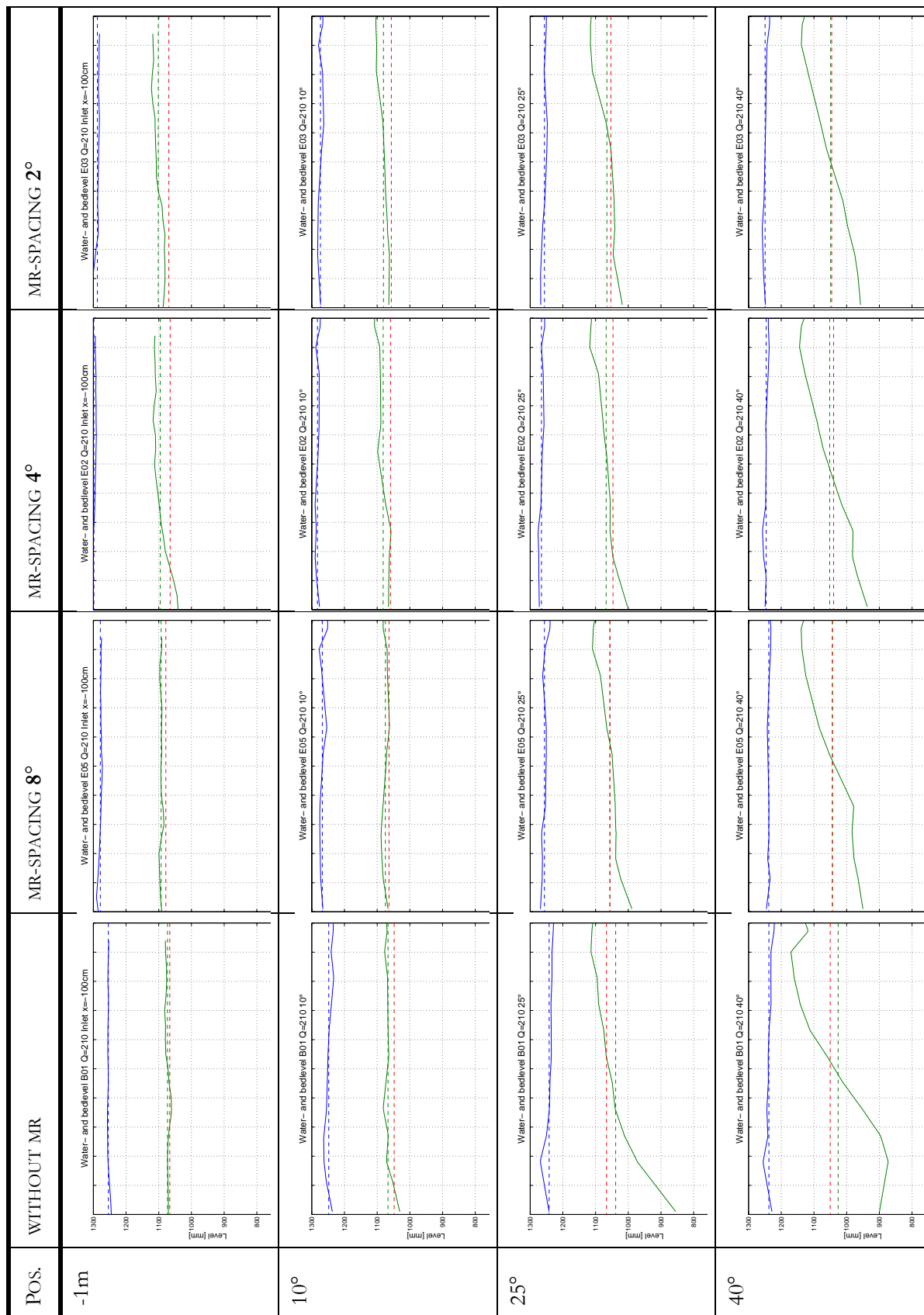
Table 7.12:   Cross sections, $S_0 = 0.50\%$, $Q=210$ l/s, mr-depth = 40 mm
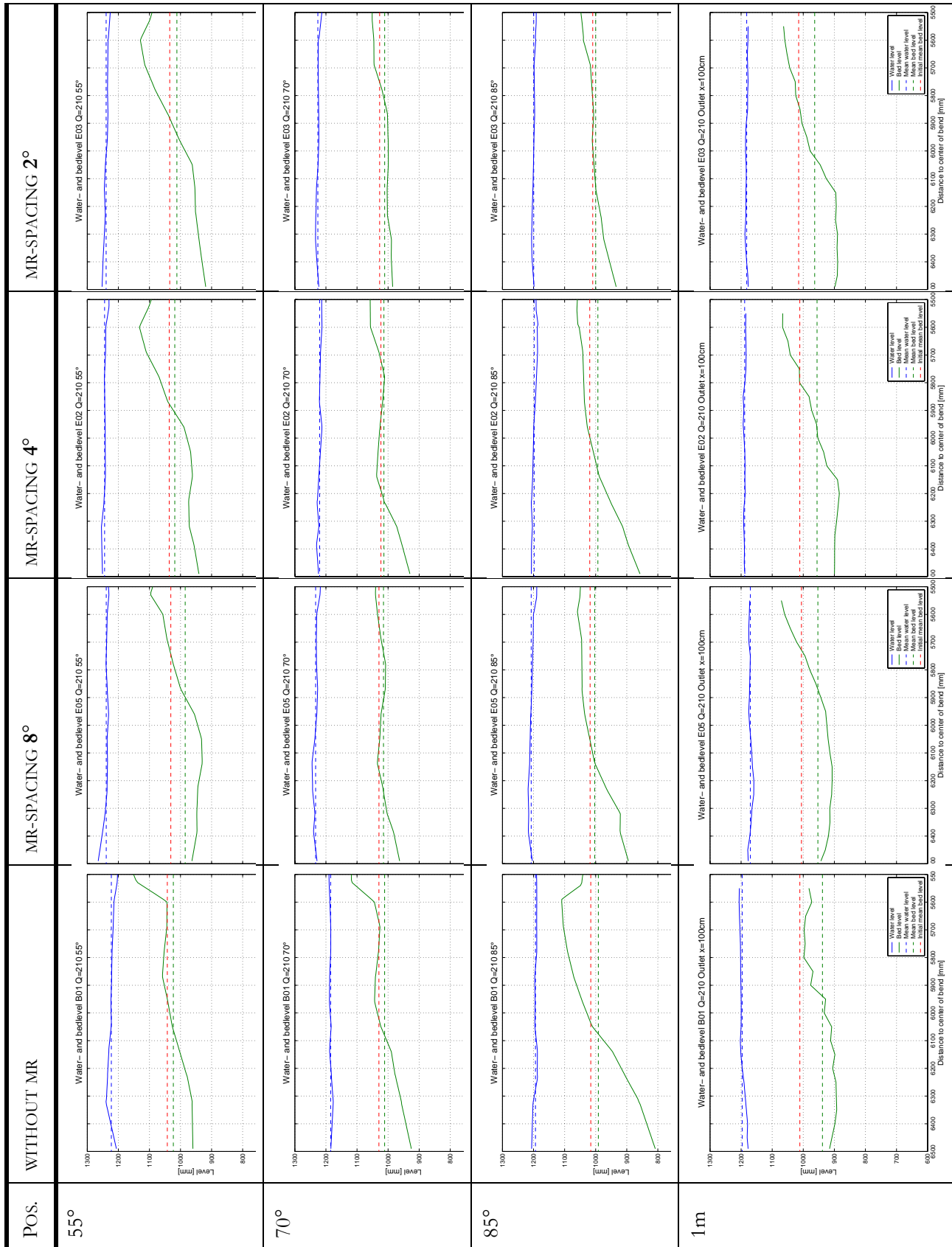
Table 7.12: Cross sections, $S_0 = 0.50\%$, $Q=210$ l/s, mr-depth = 40 mm

Appendix 7

A-94

APPENDIX 8

LONGITUDINAL EQUILIBRIUM AVERAGE / MIN. AND MAX. BED AND WATER PROFILES

This Appendix gives the final water surface compared to a horizontal average surface over the whole channel (average of all data points). The vertical axis is stretched compared to the horizontal one.

Mean, min. and max. water– and bedlevels in the channel B02 Q=180
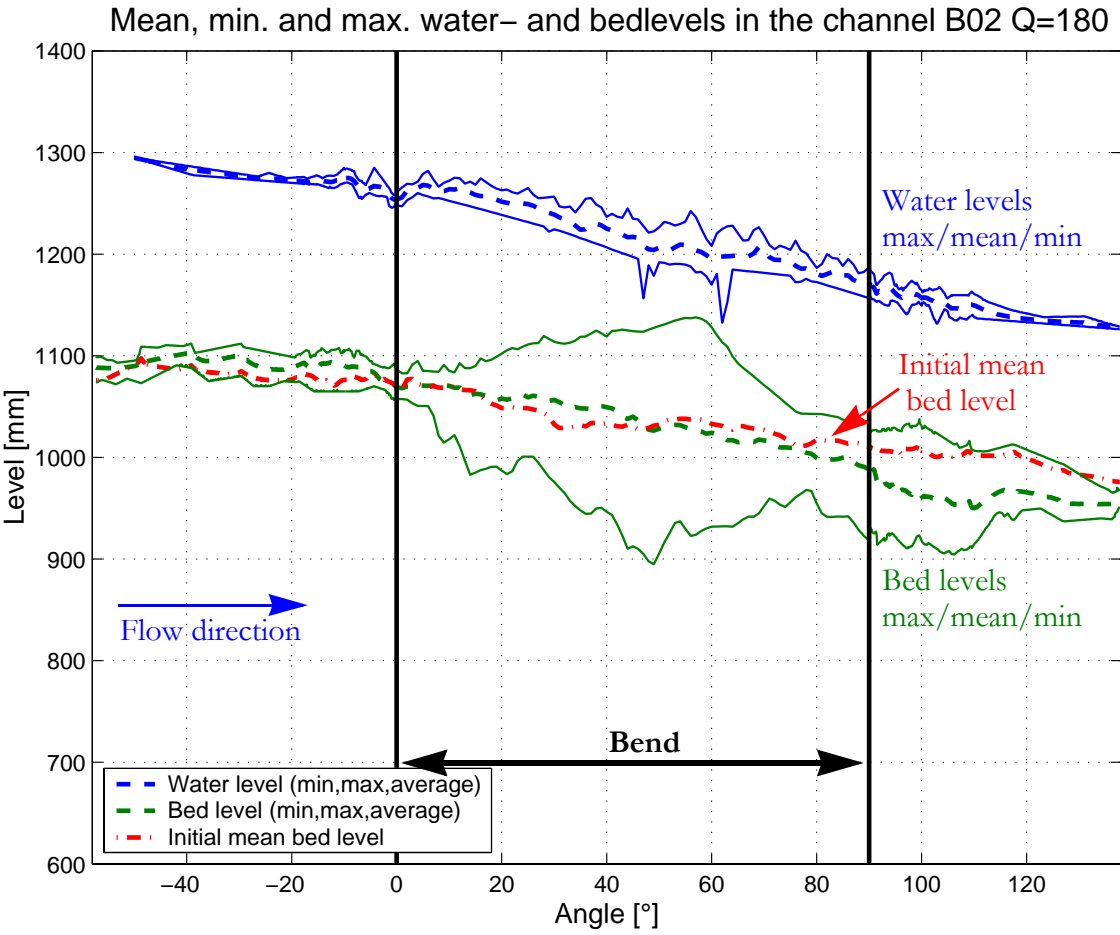
Additional information can be found in the report in Chapter 5.3.1 and 6.2.

8.1   *Channel slope J$_f$ = 0.35% - mr thickness = 20 mm*

Q [L/S]	WITHOUT MR	WITH MR SPACING 4°
150		
180		
210		
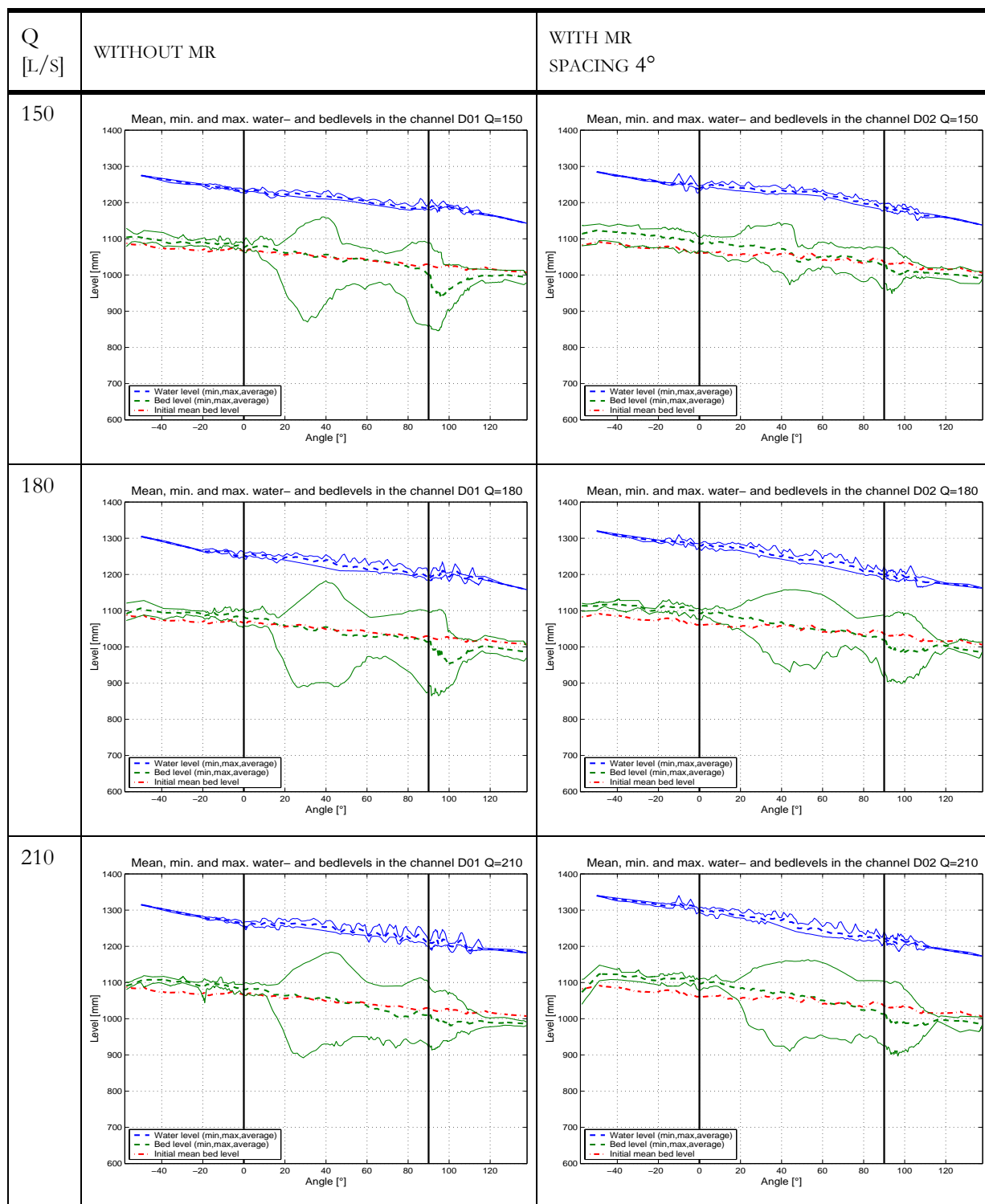
Table 8.1:   Longitudinal equilibrium average / min. and max. bed and water profiles

WITH MR
SPACING 2°
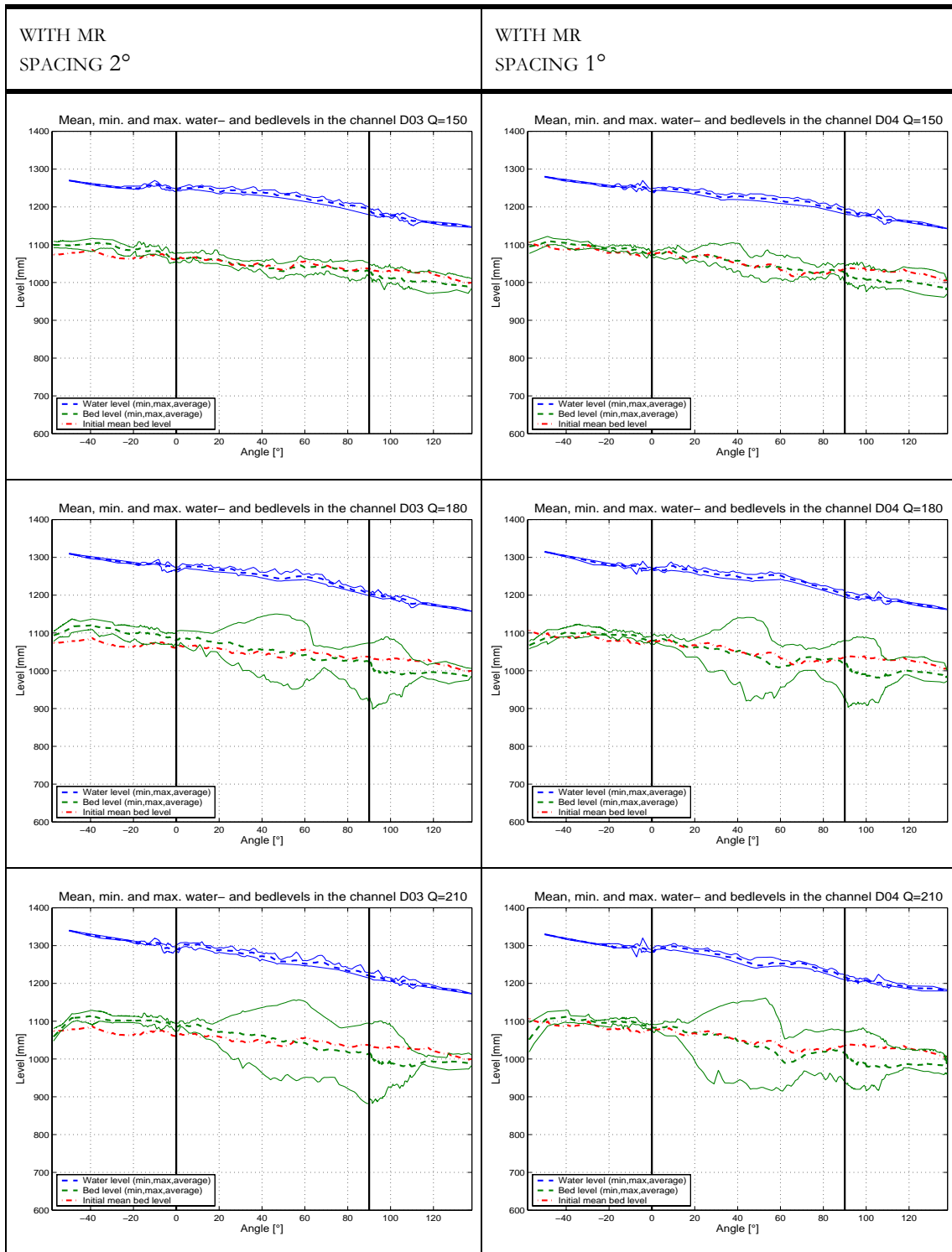
WITH MR
SPACING 1°

$J_f = 0.35\%$ - *mr thickness = 20 mm*

8.2   *Channel slope J$_f$ = 0.50% - mr thickness = 20 mm*

Q [L/S]	WITHOUT MR	WITH MR SPACING 4°
150		
180		
210		
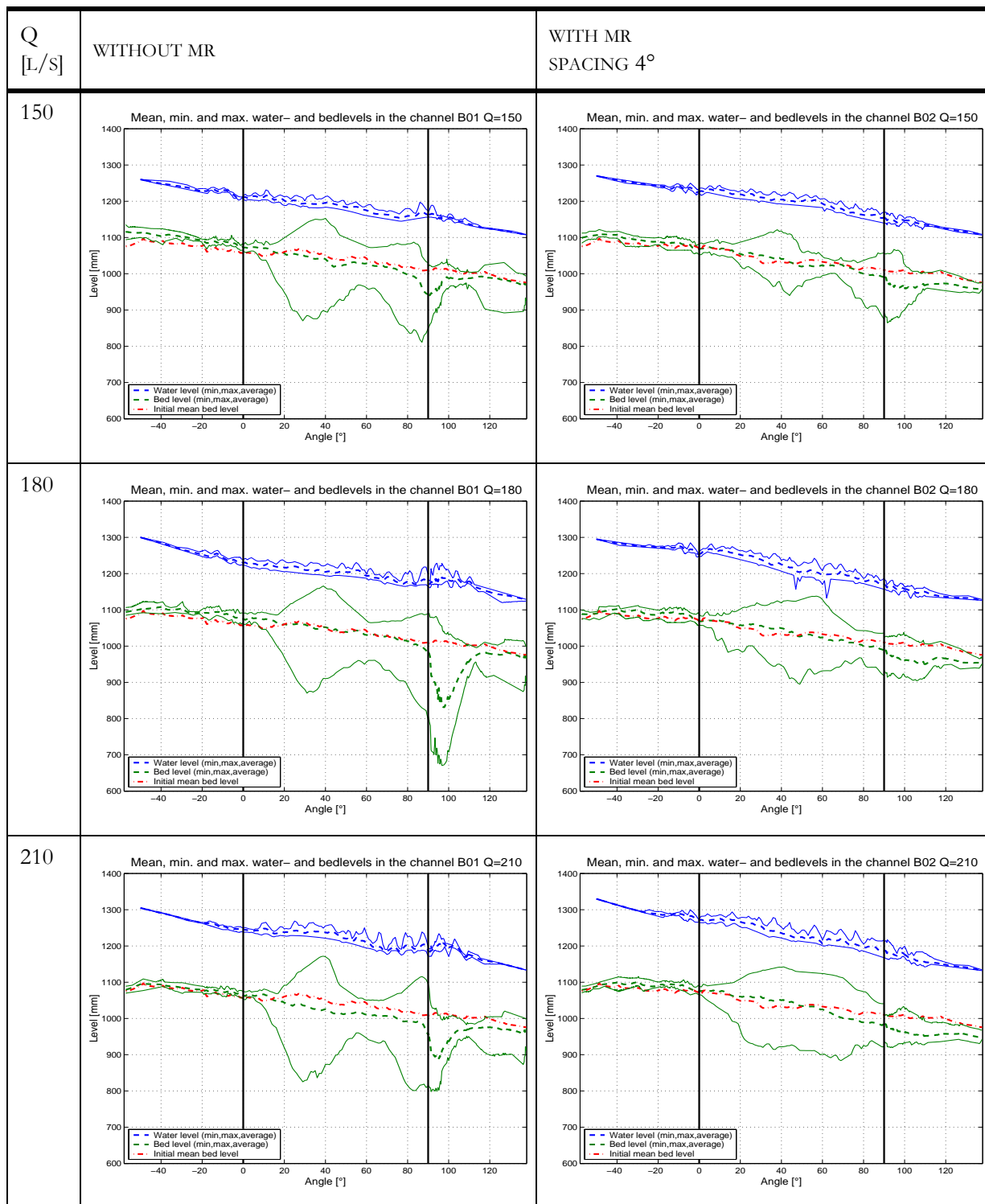
Table 8.2:   Longitudinal equilibrium average / min. and max. bed and water profiles

WITH MR	WITH MR
SPACING 2°	SPACING 1°
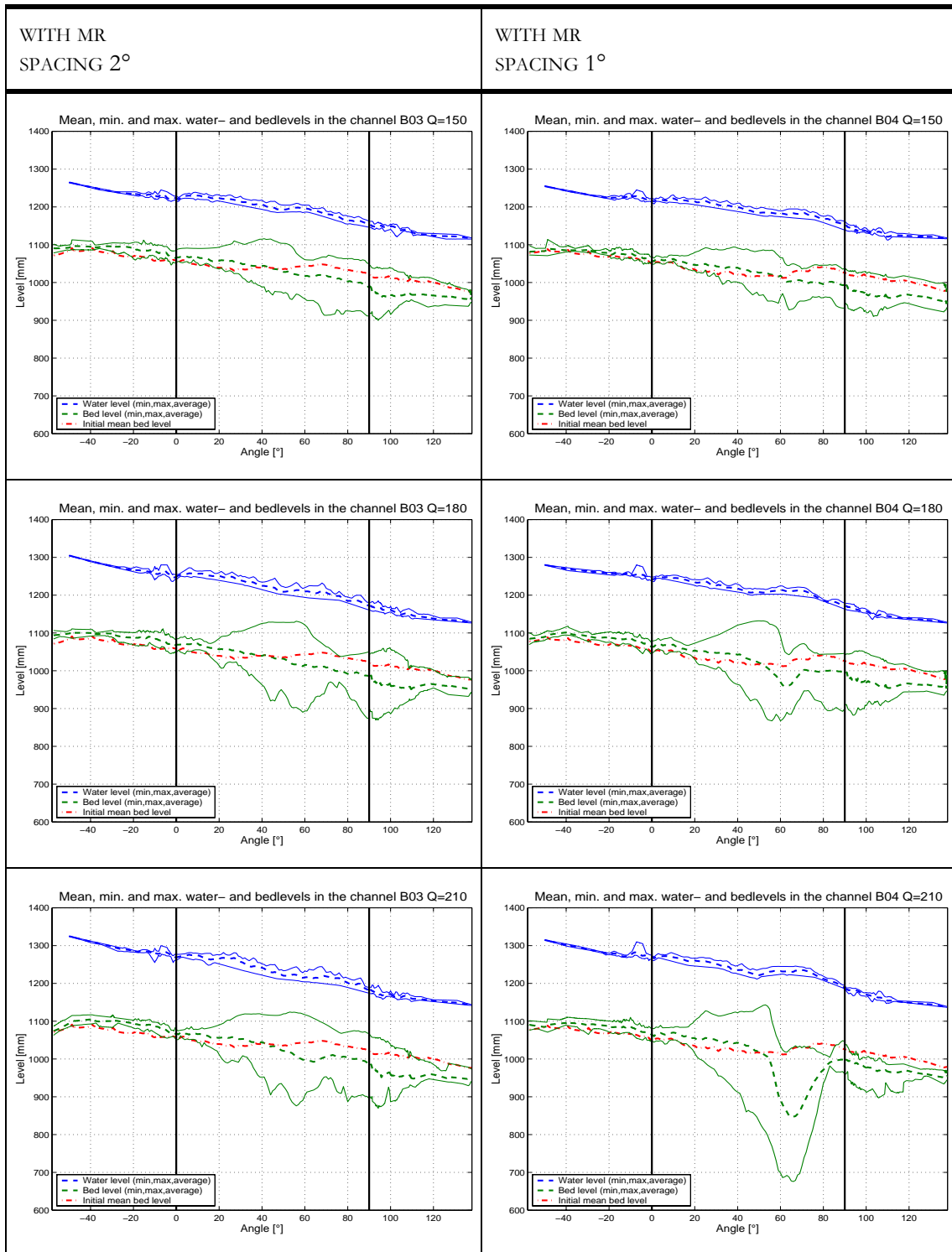
$\mathrm{J_f} = 0.50\%$ - *mr thickness = 20 mm*

8.3 *Channel slope J_f = 0.70% - mr thickness = 20 mm*

Q [L/S]	WITHOUT MR	WITH MR SPACING 4°
150	Mean, min. and max. water– and bedlevels in the channel C01 Q=150	Mean, min. and max. water– and bedlevels in the channel C02 Q=150
180	Mean, min. and max. water– and bedlevels in the channel C01 Q=180	Mean, min. and max. water– and bedlevels in the channel C02 Q=180
210	Mean, min. and max. water– and bedlevels in the channel C01 Q=210	Mean, min. and max. water– and bedlevels in the channel C02 Q=210

Table 8.3:   Longitudinal equilibrium average / min. and max. bed and water profiles

WITH MR	WITH MR
SPACING 2°	SPACING 1°
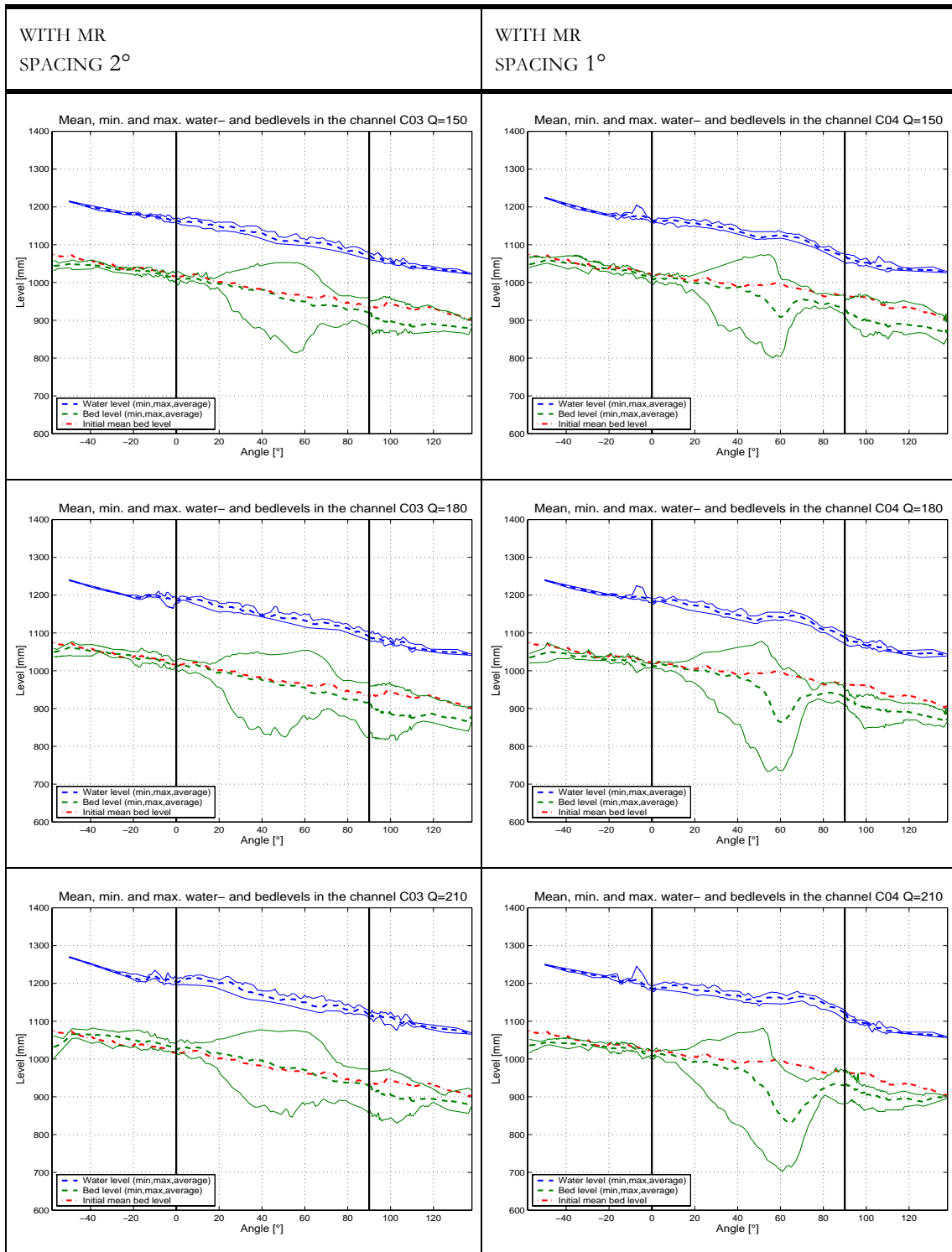
$J_f = 0.70\%$ - *mr thickness = 20 mm*

8.4   *Channel slope J_f = 0.50% - mr thickness = 40 mm*

Q [L/S]	WITHOUT MR COPY FROM A.8.2	WITH MR SPACING **8°**
150		
180		
210		

Table 8.4:   Longitudinal equilibrium average / min. and max. bed and water profiles

WITH MR	WITH MR
SPACING **4°**	SPACING **2°**
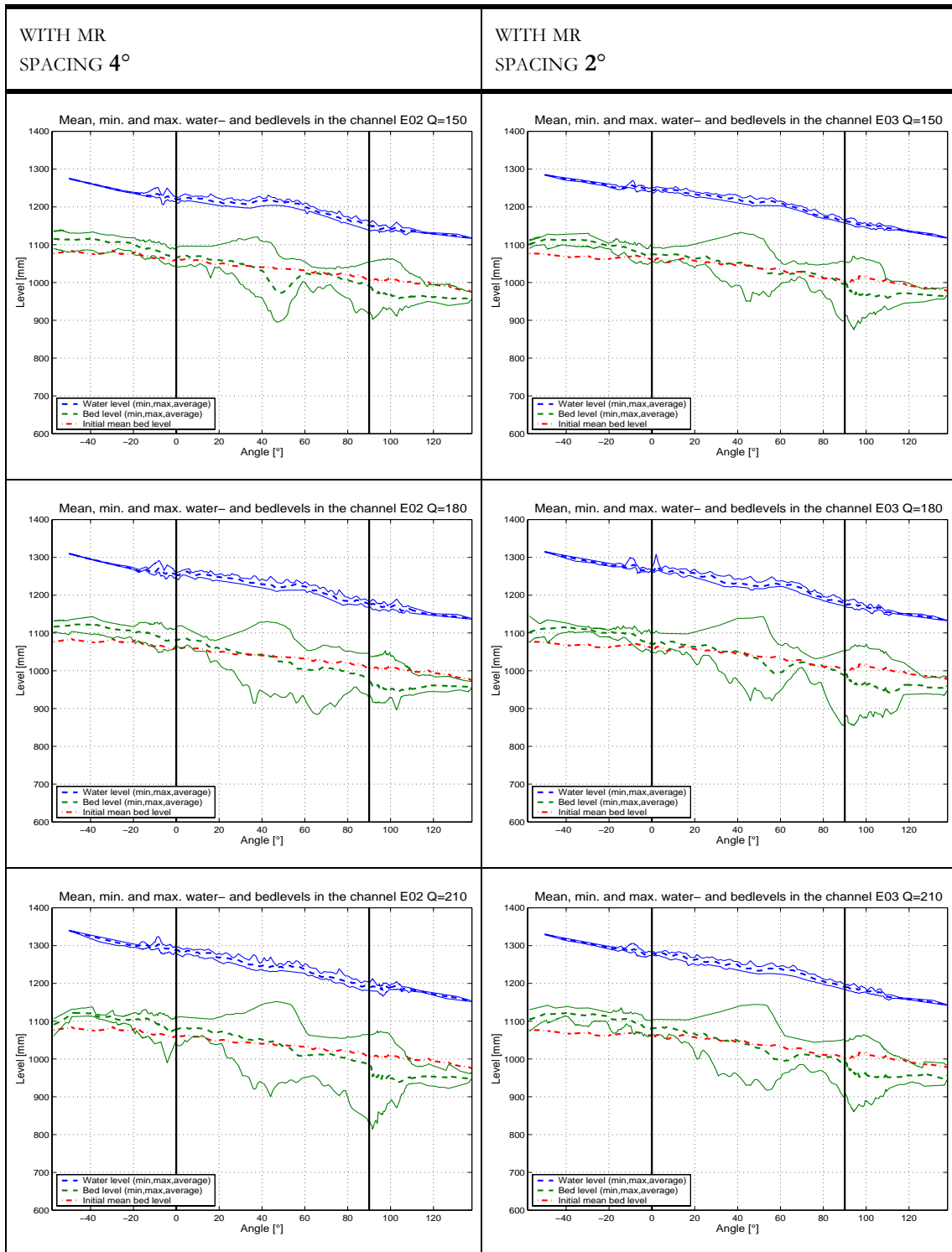
$$\mathrm{J_f} = 0.50\% - \textit{mr thickness} = 40 \; \textit{mm}$$

Appendix 8

A-104

APPENDIX 9

GRAIN SIZE DISTRIBUTIONS

This Appendix gives the grain size distributions of the armoring layer after the tests in the first and second scour holes on the outer side of the bend (in the scour) as well as on the inner bank. Furthermore the grain size distribution of one of the last samples taken at the outlet is given for each performed test (except the complementary tests E).

Additional information can be found in the report in Chapter 5.3.1 and 6.5.

9.1 Grain size distribution in the first scour
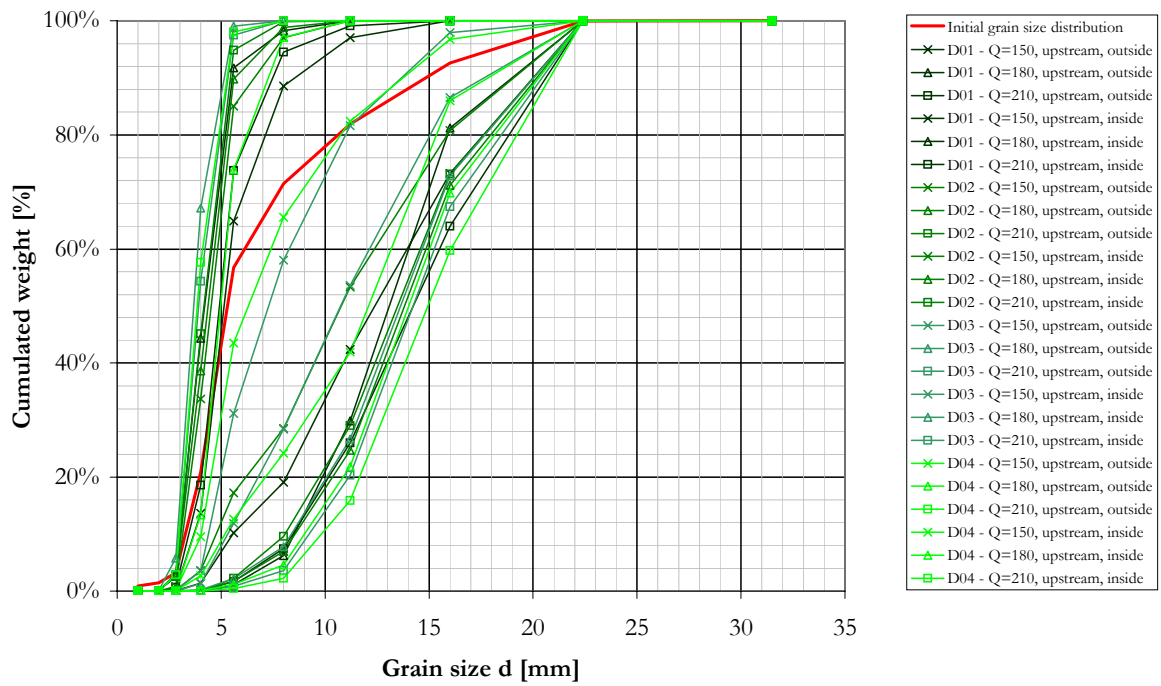
Figure 9.1: Grain size distribution - first scour, $S_0 = 0.35\%$, without mr (x01) and with ribs every 4, 2, 1° (x02...x04), $e_d = 20mm$
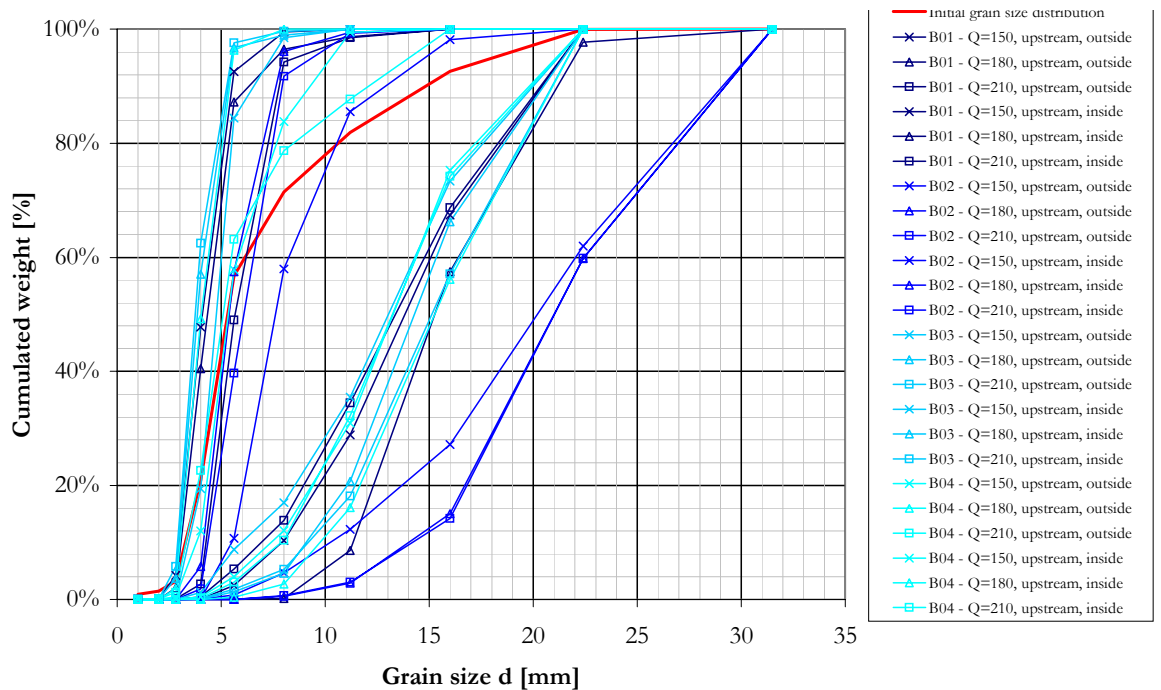
Figure 9.2: Grain size distribution - first scour, $S_0 = 0.50\%$, without mr (x01) and with ribs every 4, 2, 1° (x02...x04), $e_d = 20mm$
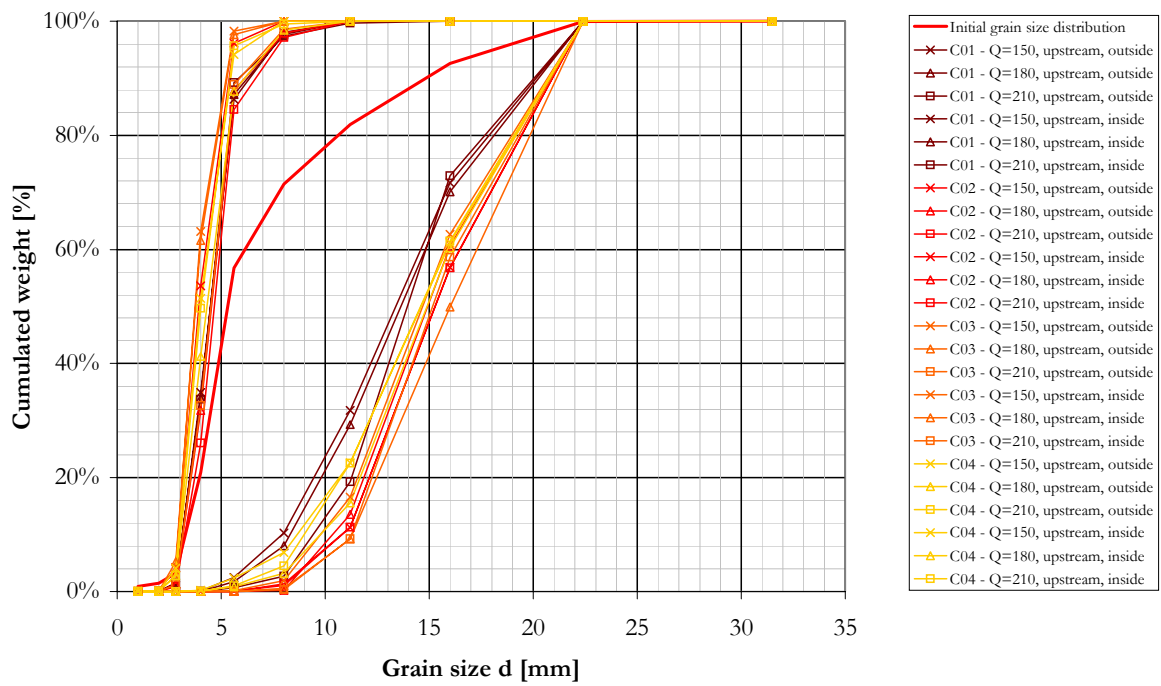
Figure 9.3: *Grain size distribution - first scour, $S_0 = 0.70\%$, without mr (x01) and with ribs every 4, 2, 1° (x02...x04), $e_d = 20mm$*
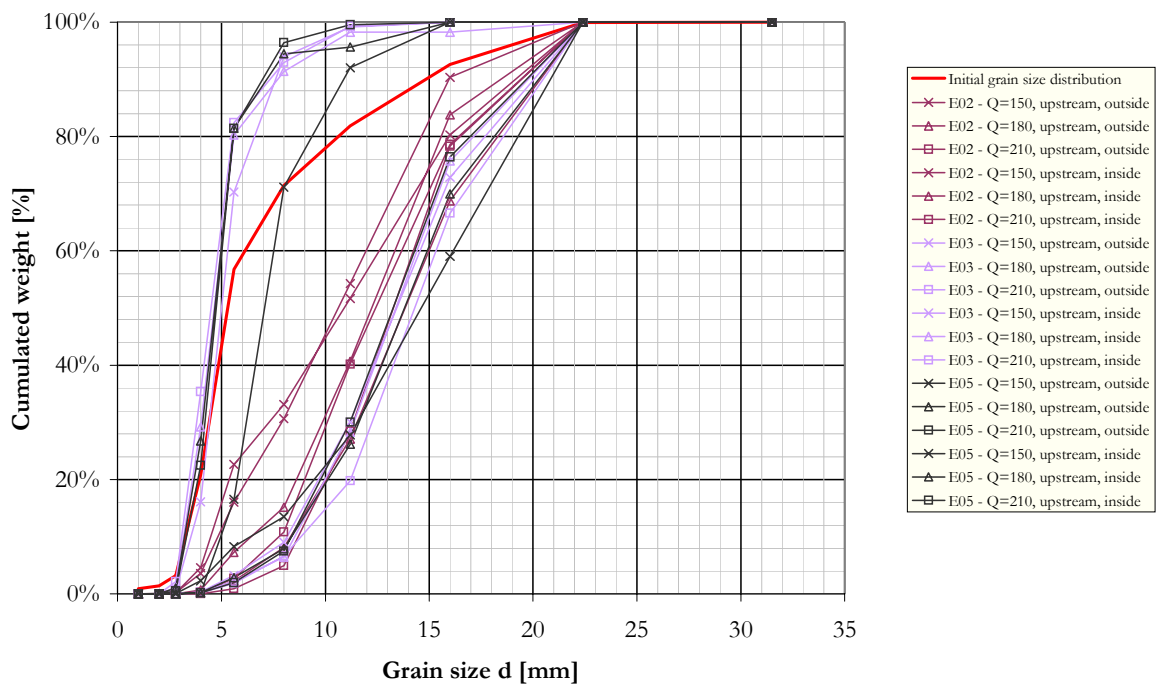
Figure 9.4: *Grain size distribution - first scour, $S_0 = 0.50\%$, without mr (x01) and with ribs every 4, 2, 8° (x02, x03, x05), $e_d = 40mm$*

9.2   *Grain size distribution in the second scour*
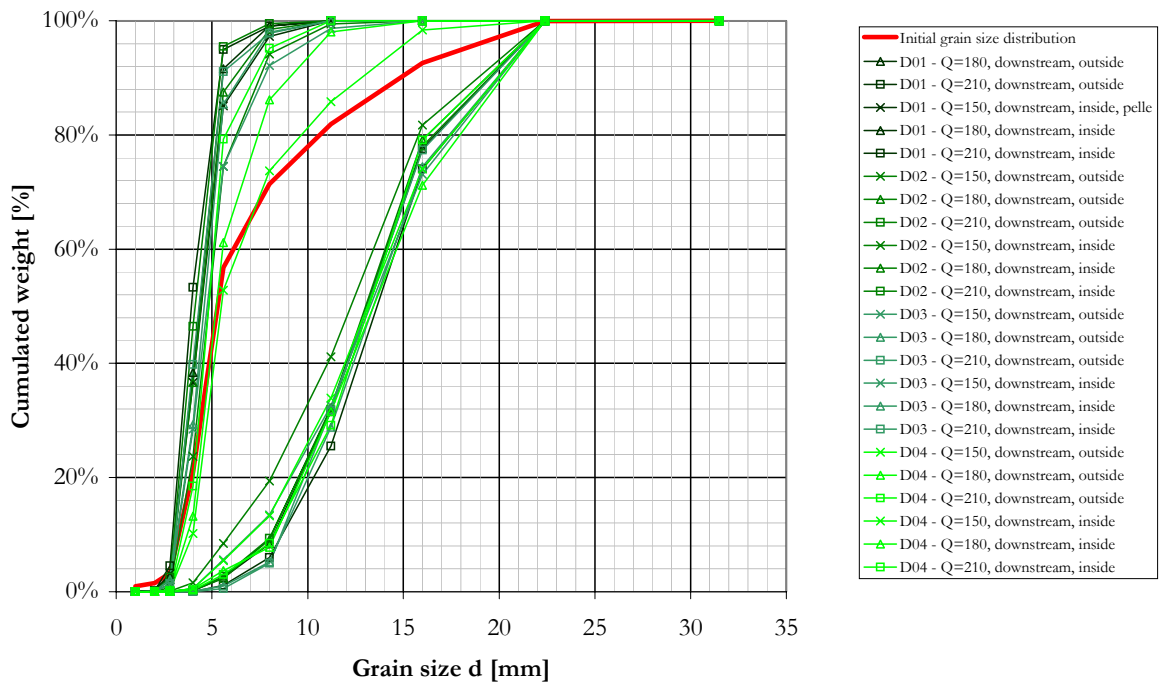
*Figure 9.5:   Grain size distribution - second scour, $S_0 = 0.35\%$, without mr (x01) and with ribs every 4, 2, 1°
(x02...x04), $e_d = 20mm$*
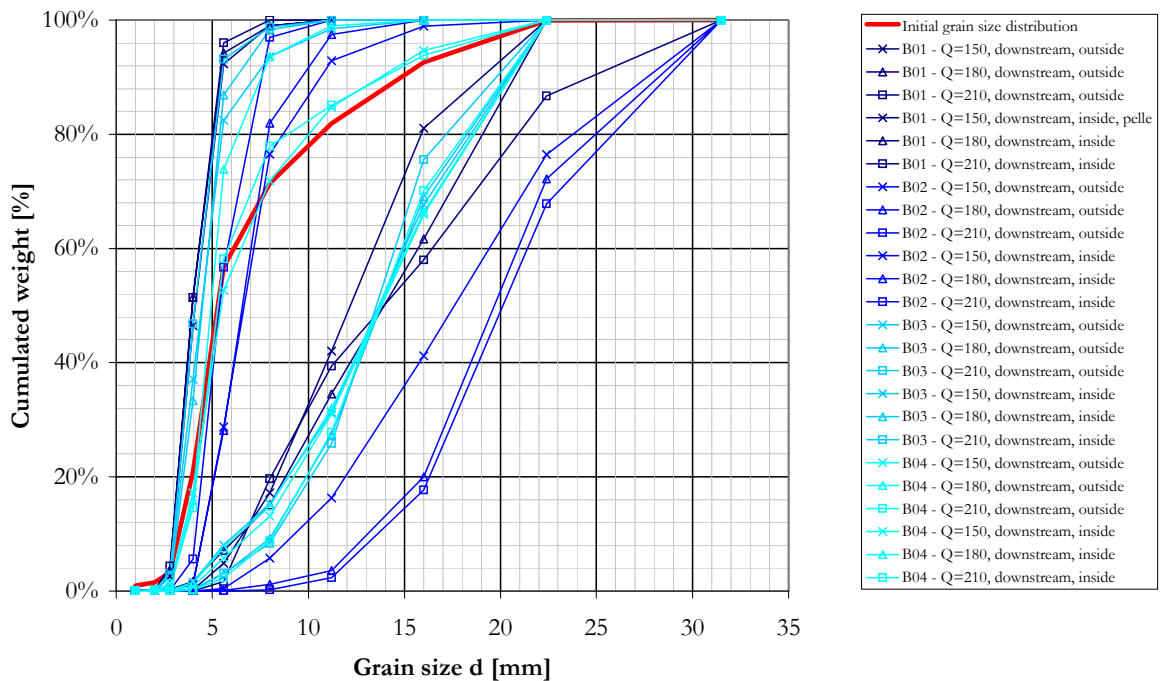
*Figure 9.6:   Grain size distribution - second scour, $S_0 = 0.50\%$, without mr (x01) and with ribs every 4, 2, 1°
(x02...x04), $e_d = 20mm$*
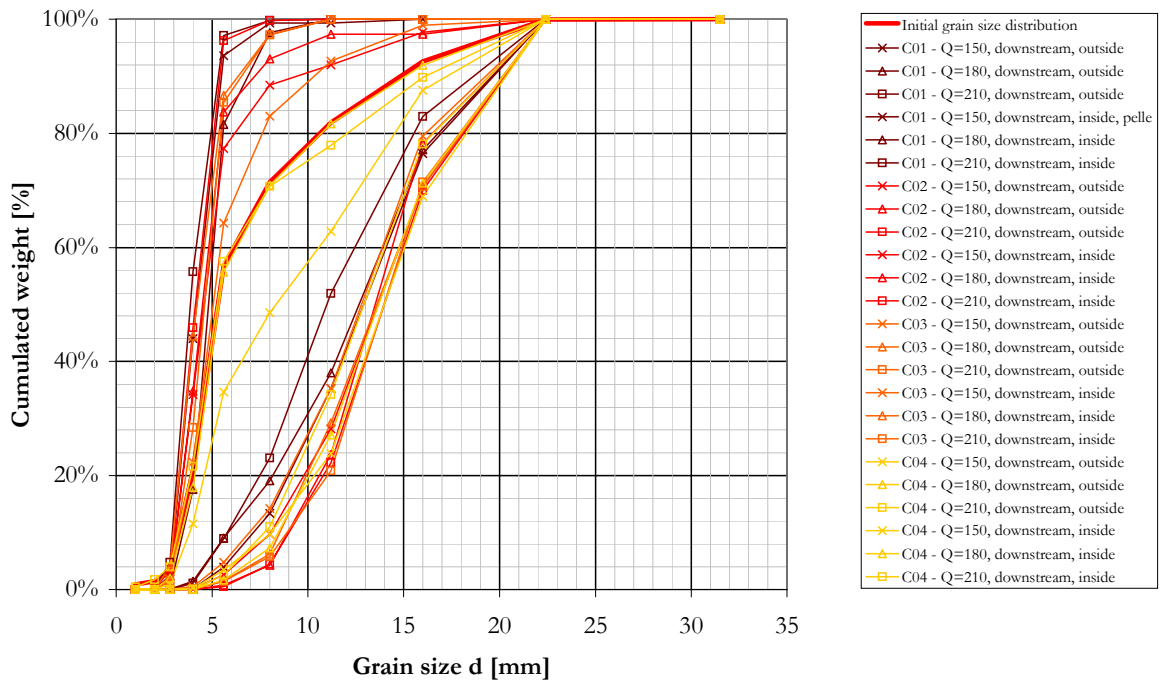
Figure 9.7: *Grain size distribution - second scour, $S_0 = 0.70\%$, without mr (x01) and with ribs every 4, 2, 1° (x02...x04), $e_d = 20mm$*
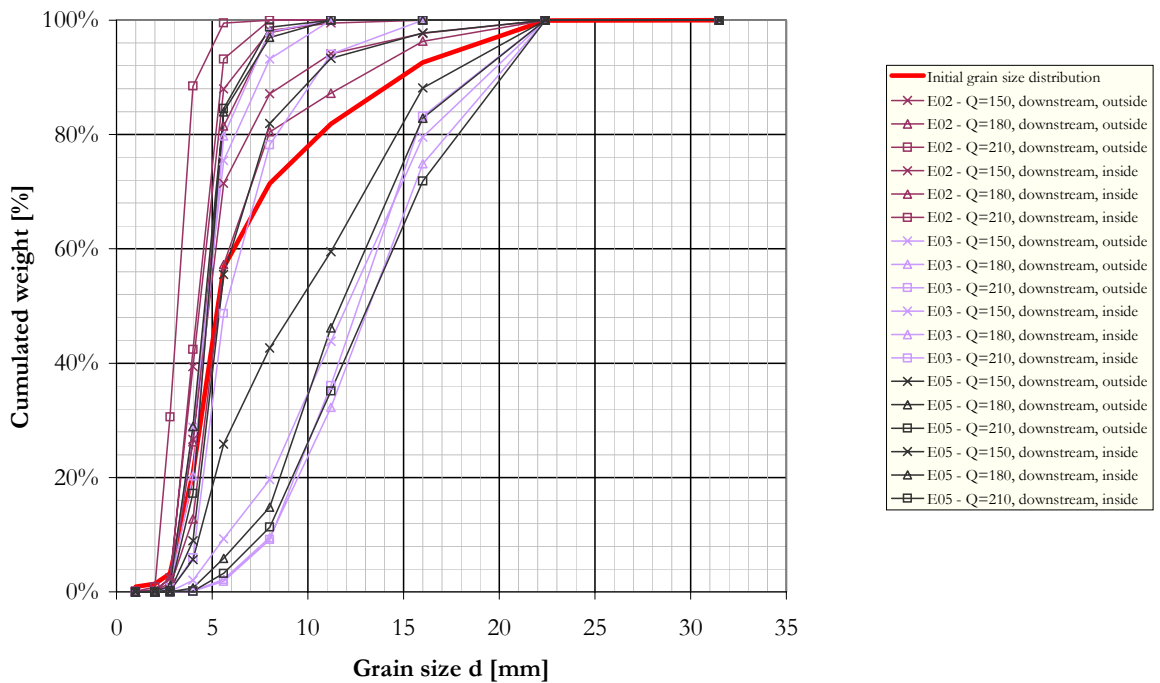
Figure 9.8: *Grain size distribution - second scour, $S_0 = 0.50\%$, without mr (x01) and with ribs every 4, 2, 8° (x02, x03, x05), $e_d = 40mm$*

9.3 *Grain size distribution of the samples at the outlet*
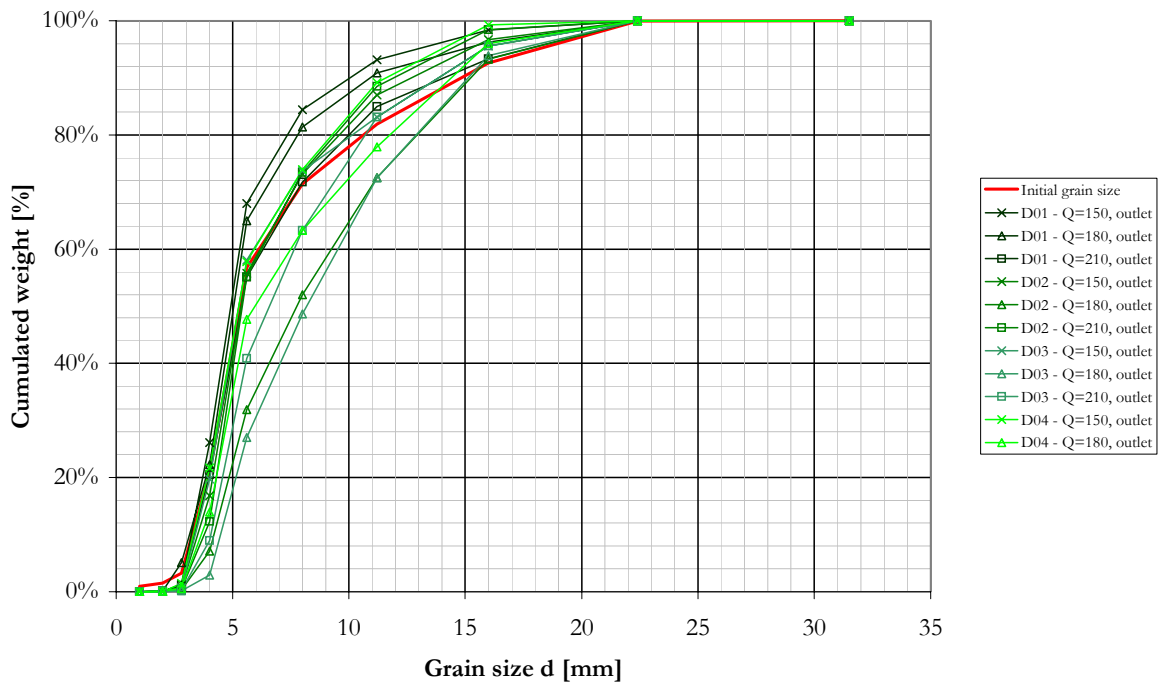
Figure 9.9:   Grain size distribution - samples at the outlet, $S_0 = 0.35\%$, without mr (x01) and with ribs every 4, 2, 1° (x02...x04), $e_d = 20mm$
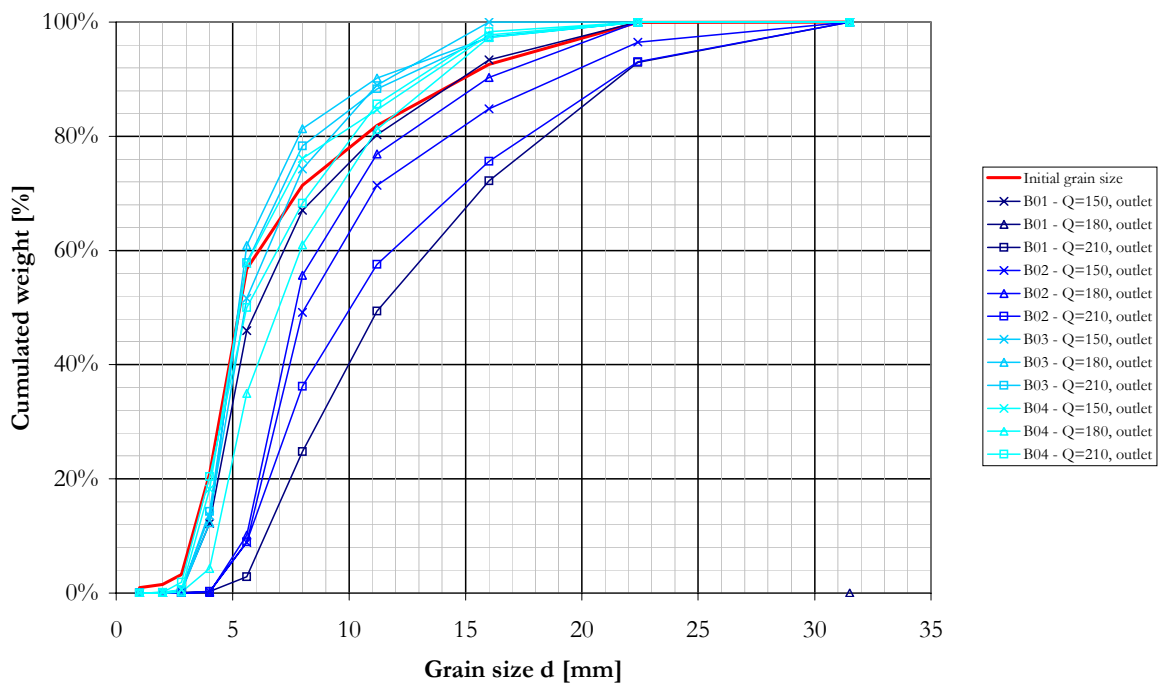
Figure 9.10: Grain size distribution - samples at the outlet, $S_0 = 0.50\%$, without mr (x01) and with ribs every 4, 2, 1° (x02...x04), $e_d = 20mm$
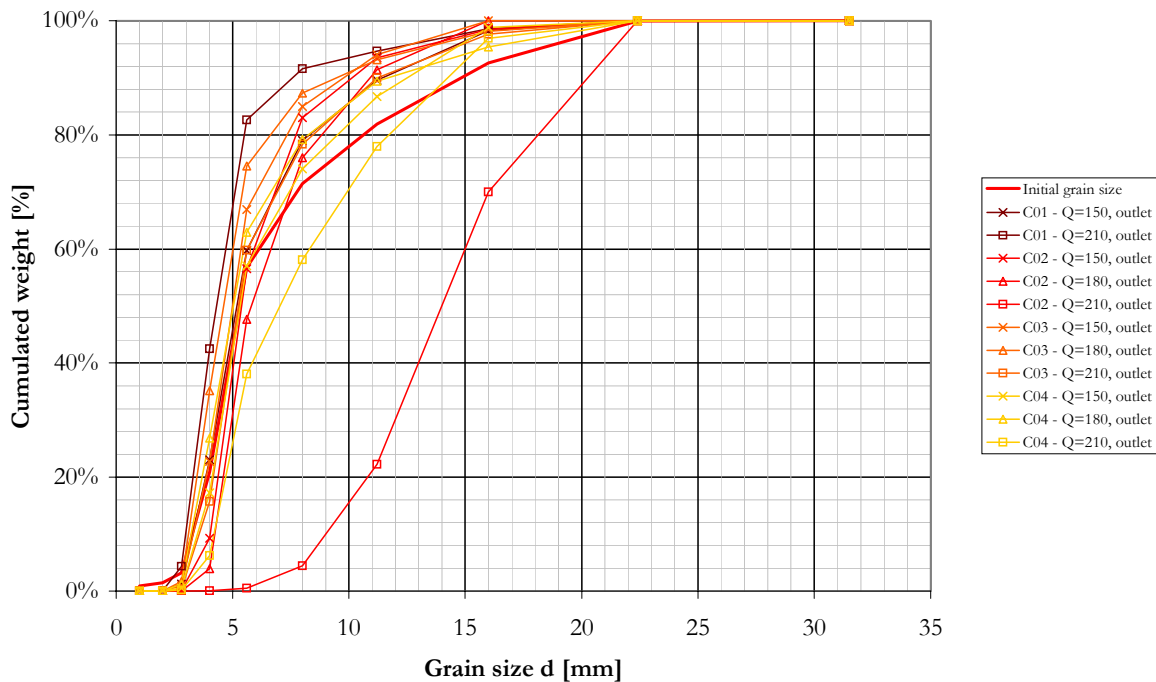
Figure 9.11: Grain size distribution - samples at the outlet, $S_0 = 0.70\%$, without mr (x01) and with ribs every 4, 2, 1° (x02...x04), $e_d = 20mm$

9.4   *Grain size distributions sorted by discharge*

9.4.1   Q= 150 l/s
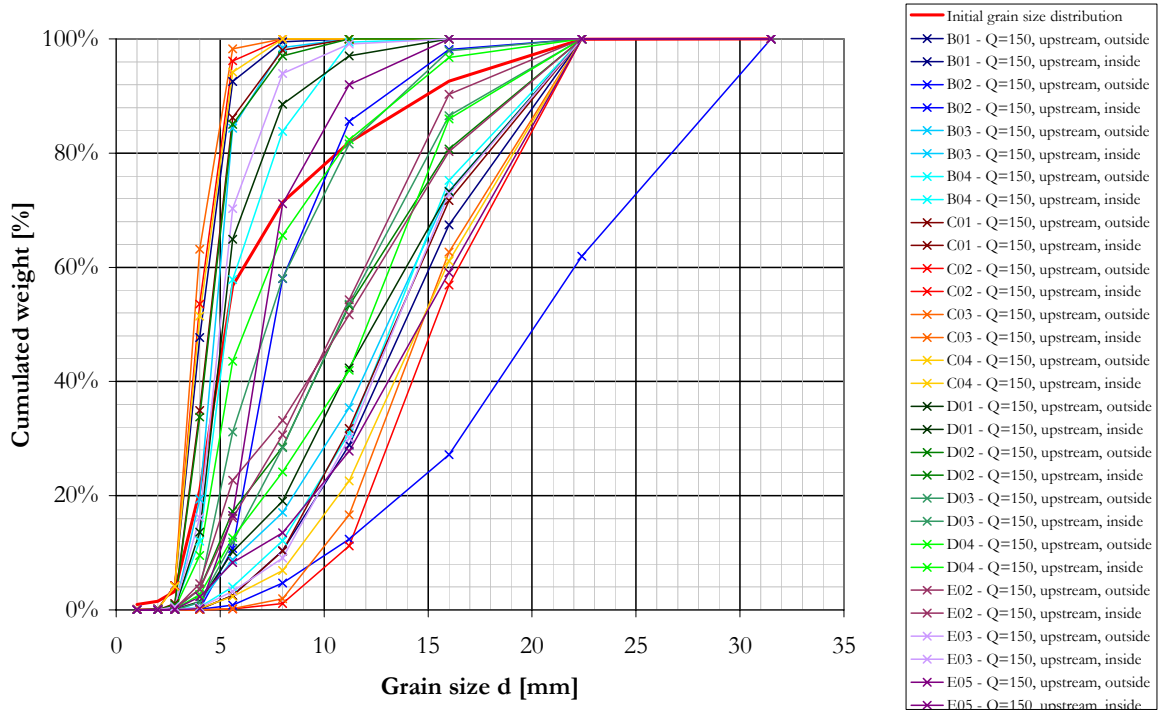
Figure 9.12: Grain size distribution - first scour, Q = 150 l/s, without mr (x01) and with ribs every 4, 2, 1, 8° (x02...x05), e_d = 20mm (cases B-D) and 40mm (E)
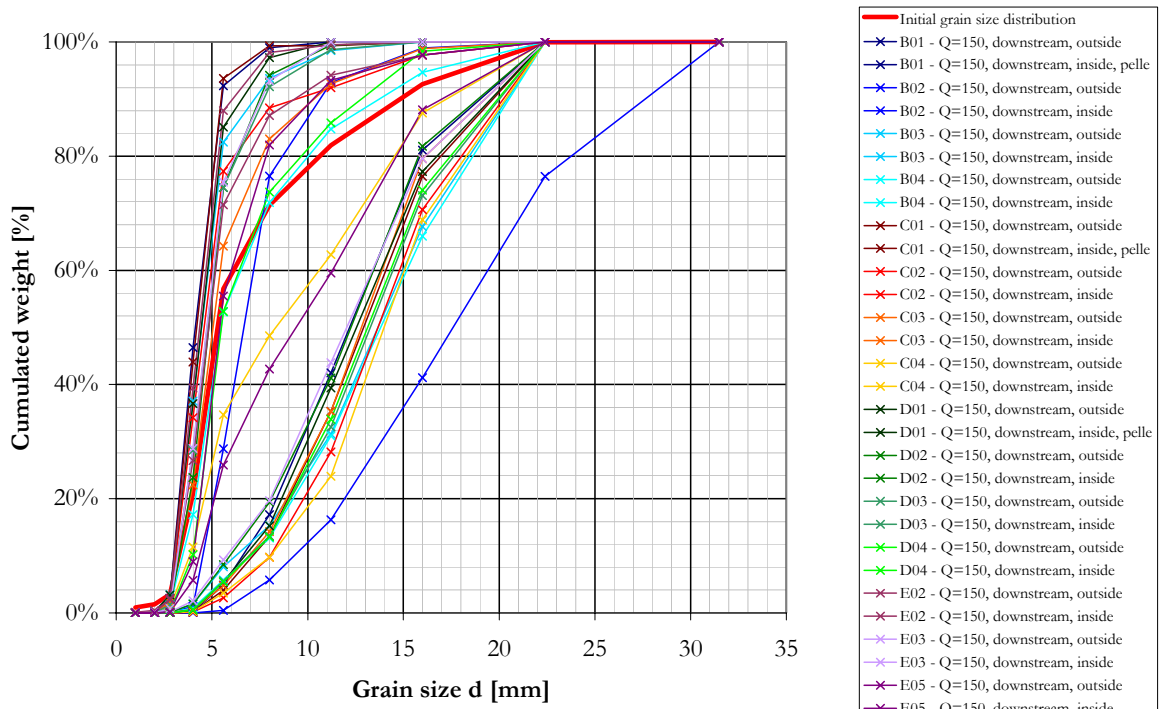
Figure 9.13: Grain size distribution - second scour, Q = 150 l/s, without mr (x01) and with ribs every 4, 2, 1, 8° (x02...x05), e_d = 20mm (cases B-D) and 40mm (E)
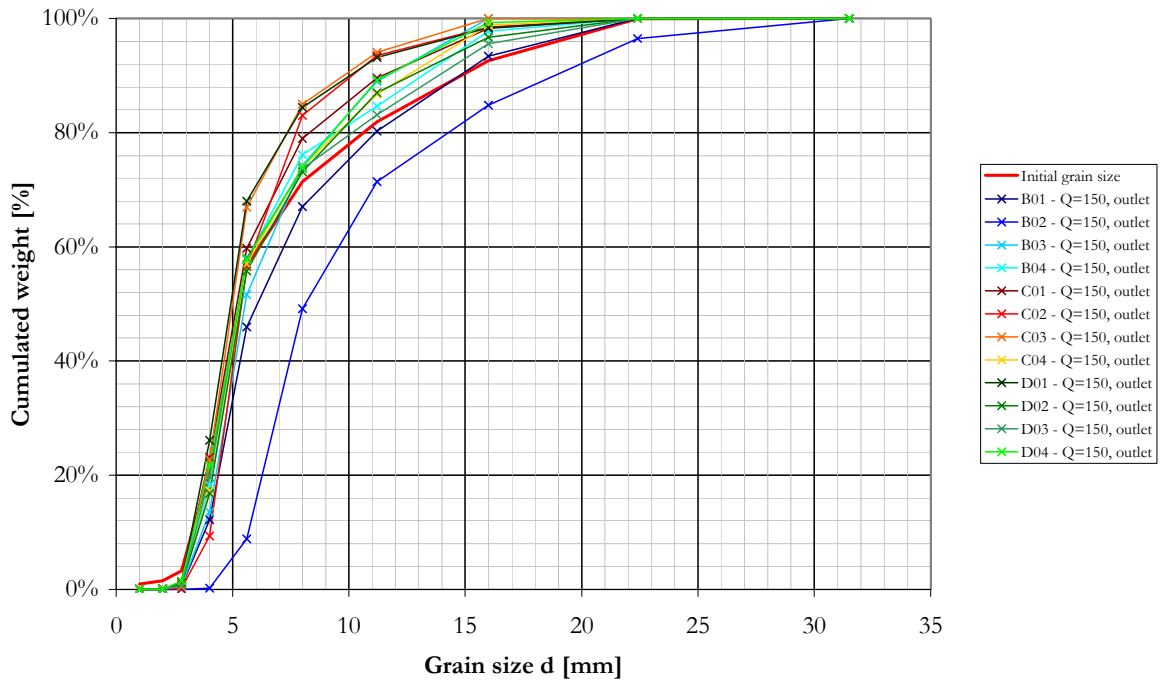
Figure 9.14: Grain size distribution - samples at the outlet, Q = 150 l/ s, without mr (x01) and with ribs every 4, 2, 1, 8° (x02...x05), e_d = 20mm (cases B-D) and 40mm (E)

9.4.2   Q = 180 l/s
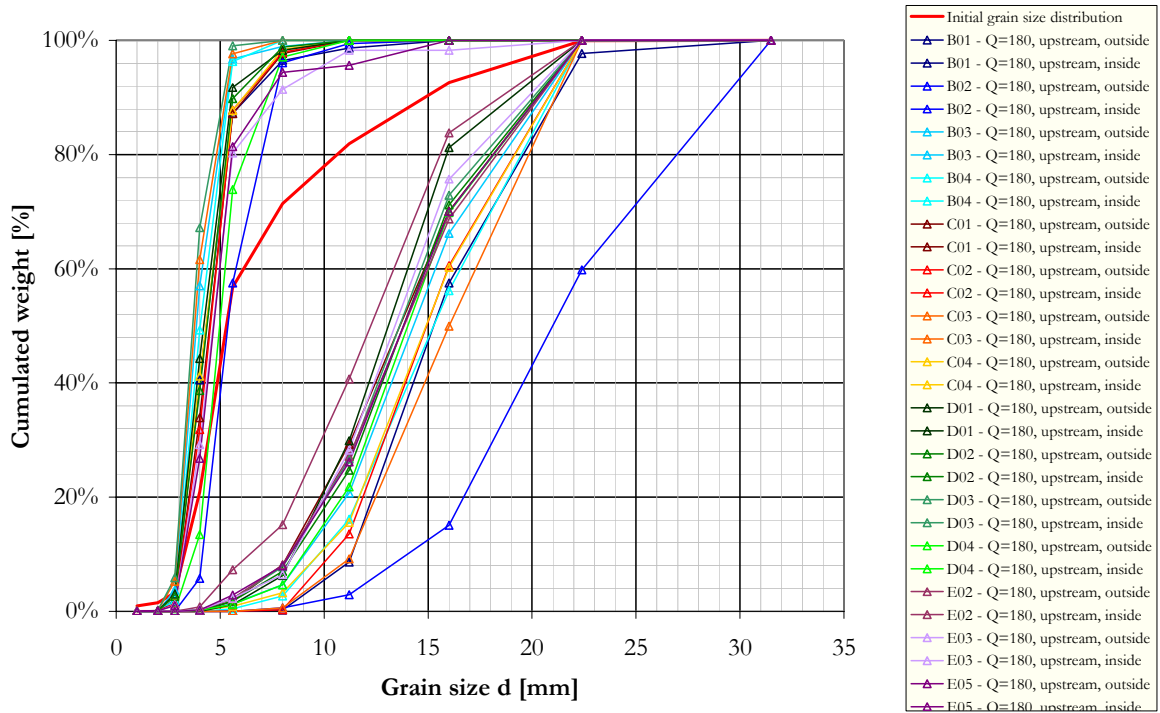
Figure 9.15: Grain size distribution - first scour, Q = 180 l/ s, without mr (x01) and with ribs every 4, 2, 1, 8° (x02...x05), e_d = 20mm (cases B-D) and 40mm (E)
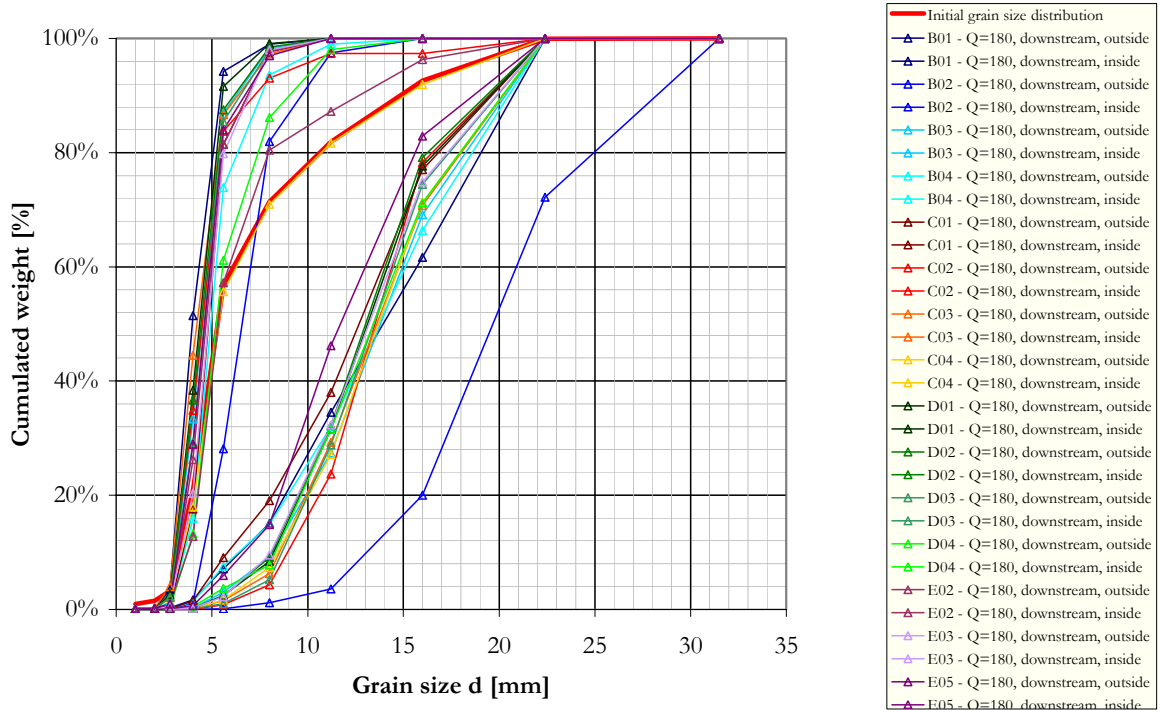
Figure 9.16: Grain size distribution - second scour, Q = 180 l/s, without mr (x01) and with ribs every 4, 2, 1, 8° (x02...x05), e_d = 20mm (cases B-D) and 40mm (E)
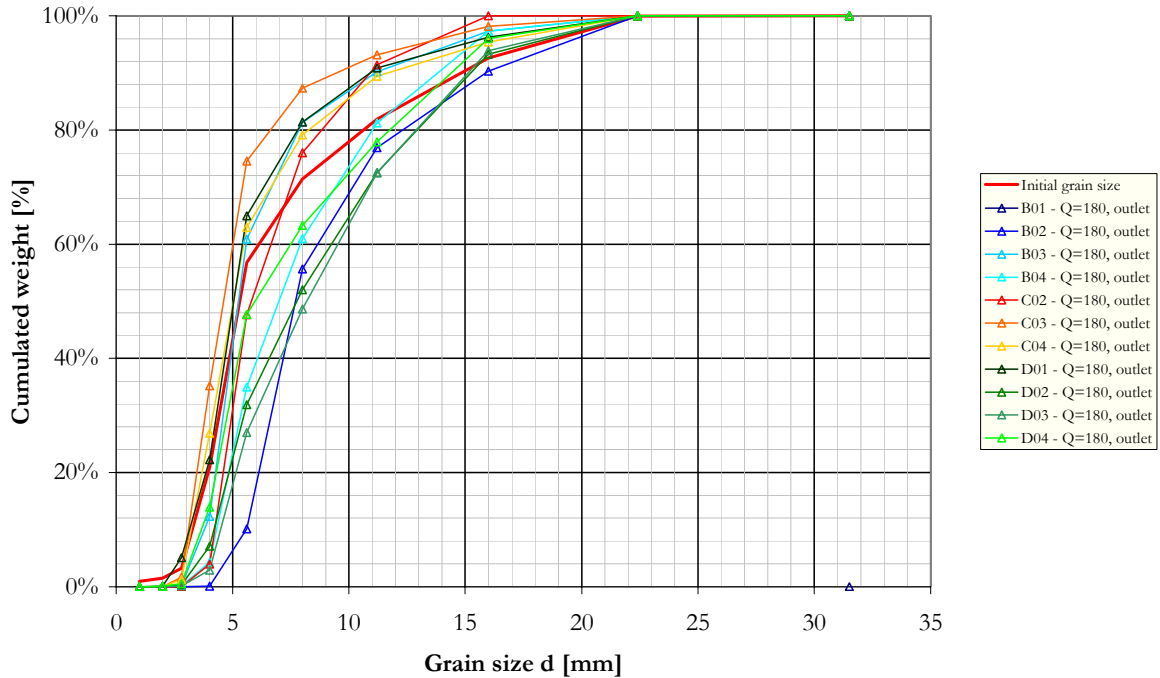
Figure 9.17: Grain size distribution - samples at the outlet, Q = 180 l/s, without mr (x01) and with ribs every 4, 2, 1, 8° (x02...x05), e_d = 20mm (cases B-D) and 40mm (E)

9.4.3 Q = 210 l/s
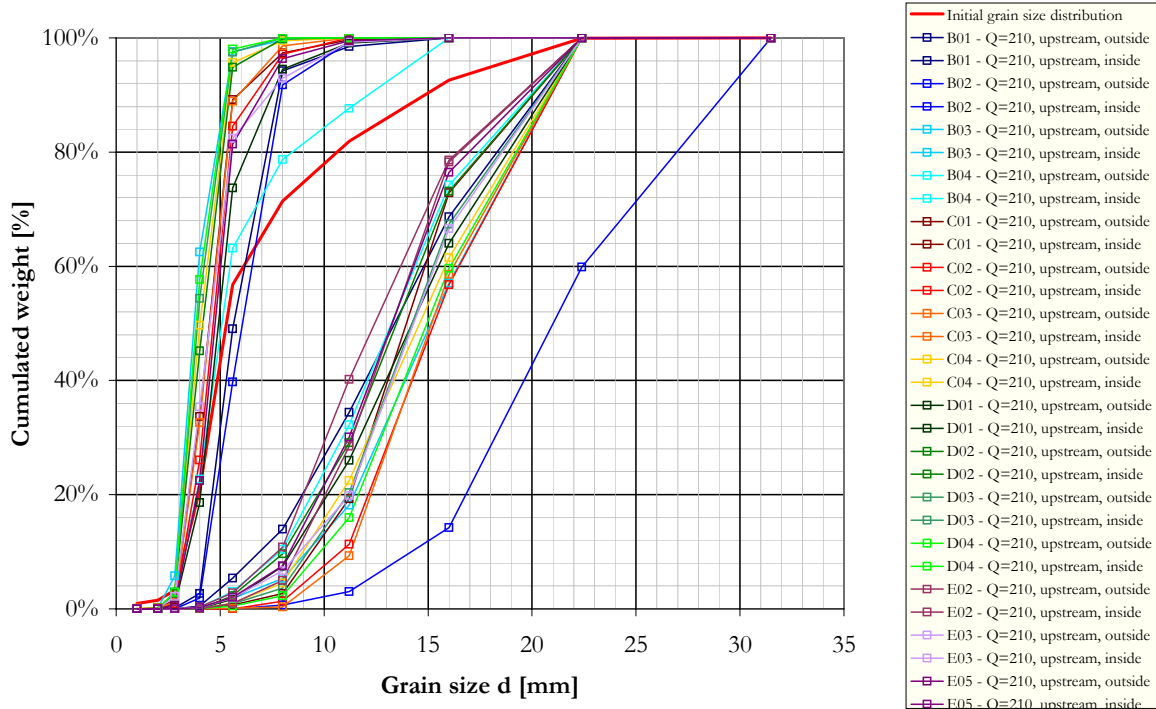
Figure 9.18: Grain size distribution - first scour, Q = 210 l/s, without mr (x01) and with ribs every 4, 2, 1, 8° (x02...x05), e_d = 20mm (cases B-D) and 40mm (E)
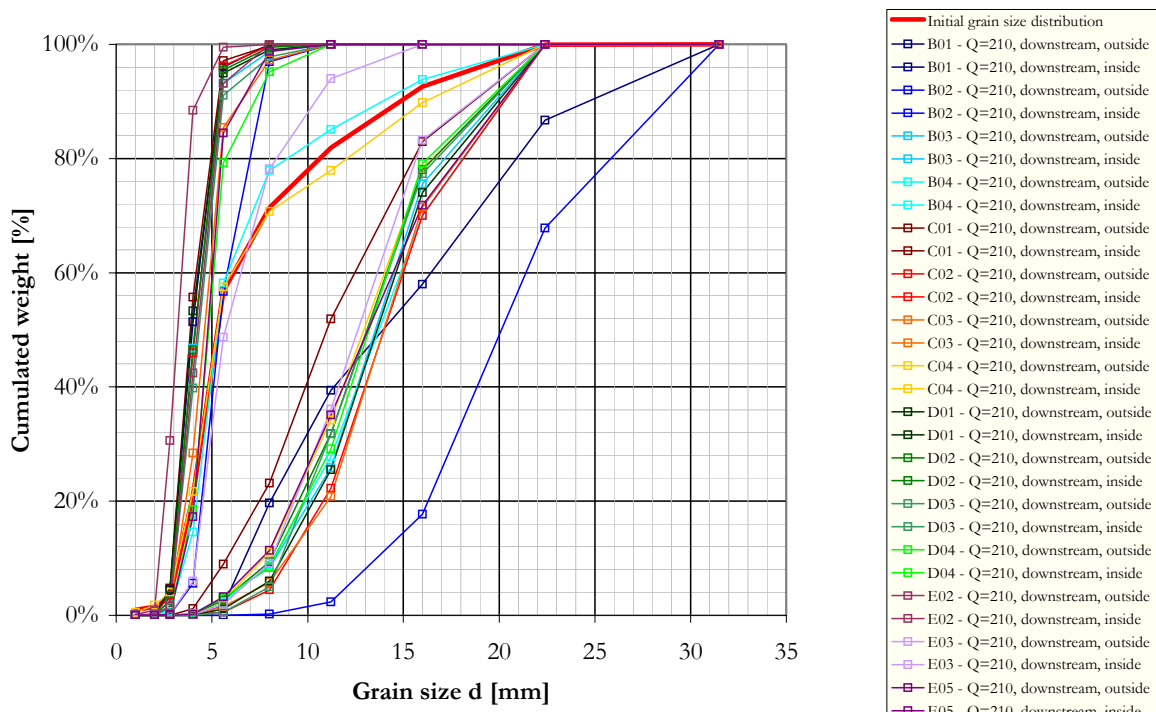
Figure 9.19: Grain size distribution - second scour, Q = 210 l/s, without mr (x01) and with ribs every 4, 2, 1, 8° (x02...x05), e_d = 20mm (cases B-D) and 40mm (E)
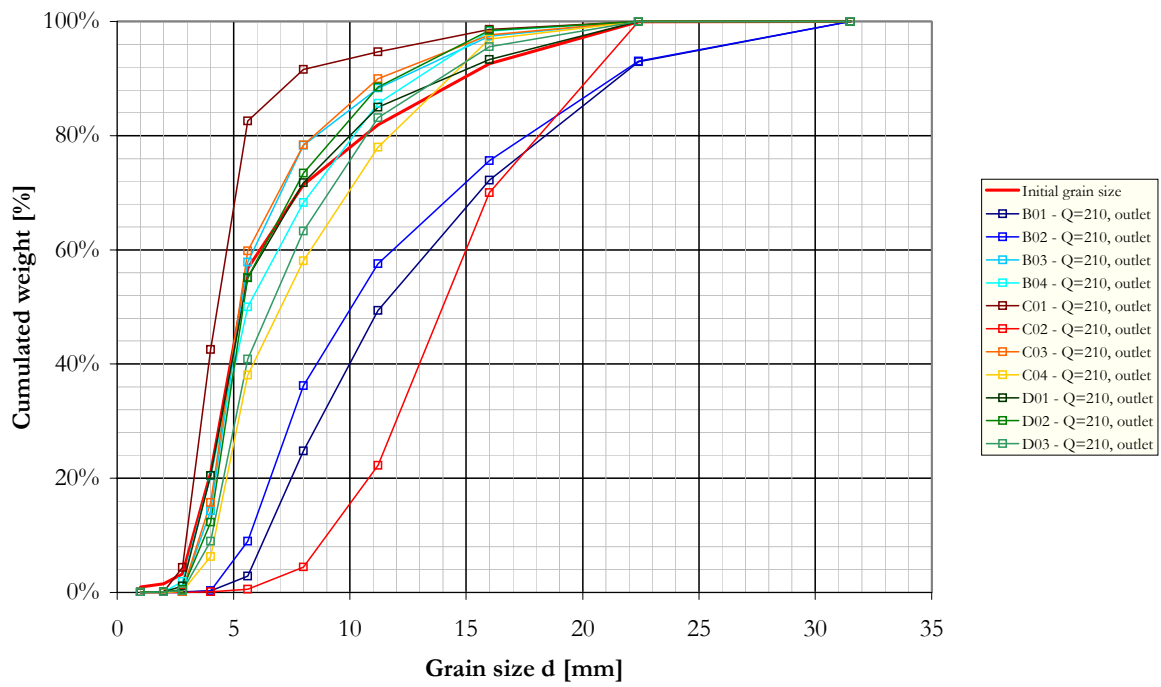
Figure 9.20: Grain size distribution - samples at the outlet, Q = 210 l/s, without mr (x01) and with ribs every 4, 2, 1, 8° (x02...x05), e_d = 20mm (cases B-D) and 40mm (E)

APPENDIX 10

GRAIN SIZE DISTRIBUTION - PICTURES OF THE BED

This Appendix gives the final water surface compared to a horizontal average surface over the whole channel (average of all data points).
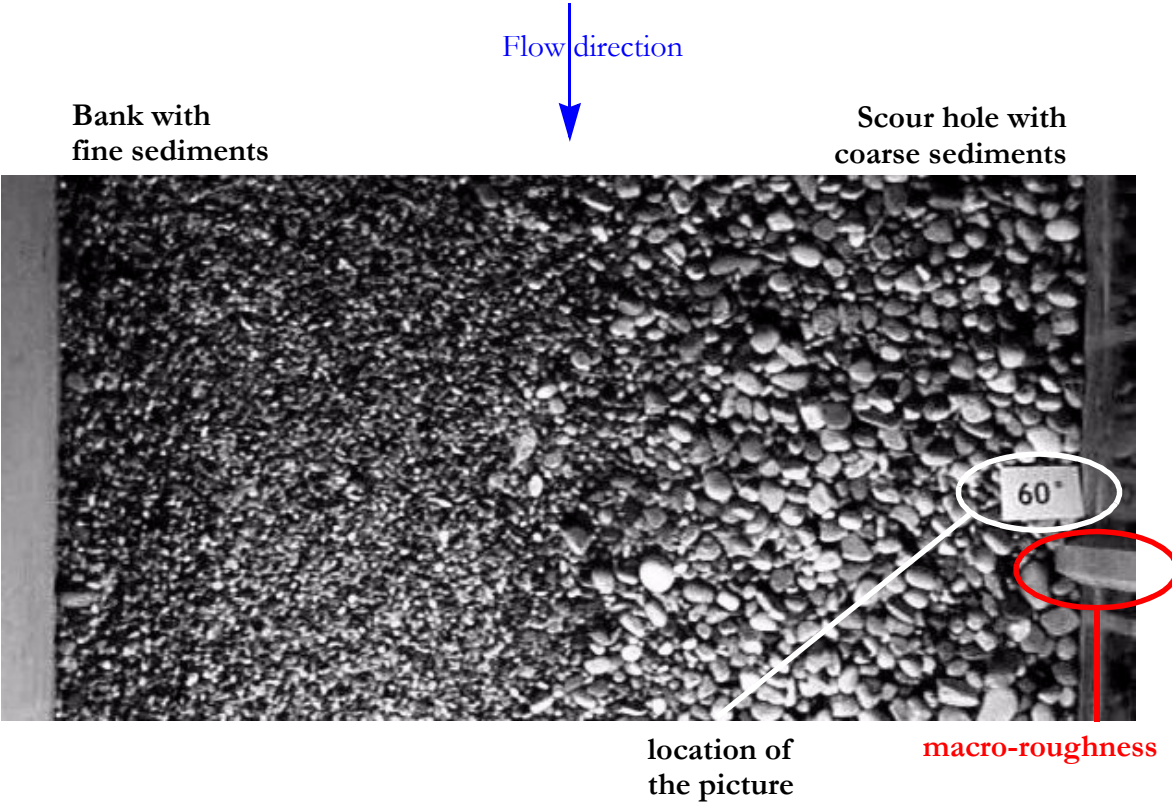
Additional information can be found in the report in Chapter 5.3.1 and 6.5.
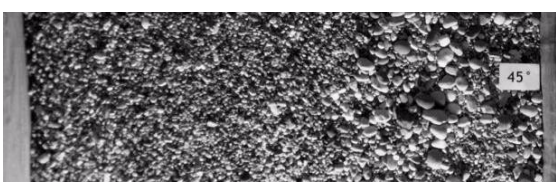
10.1 Channel slope S_0 = 0.35%, Q = 150 l/s, e_d = 20 mm
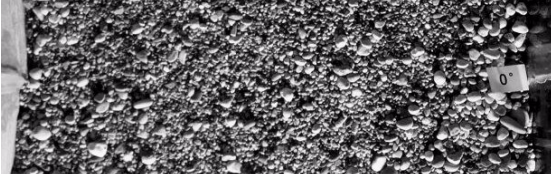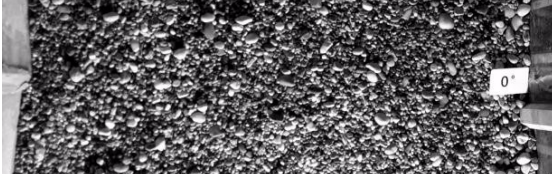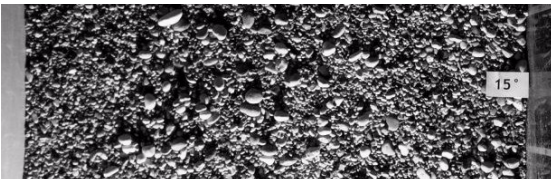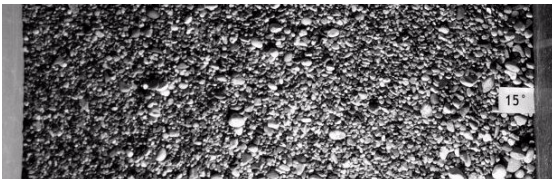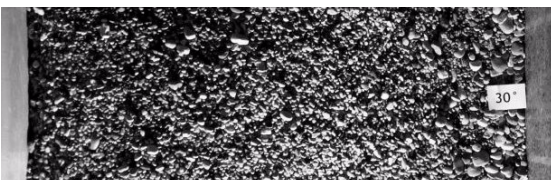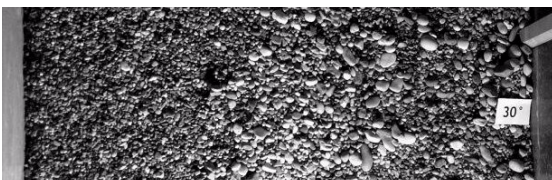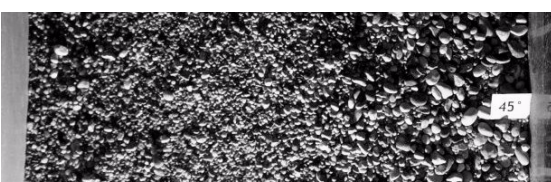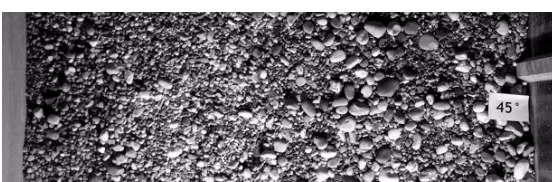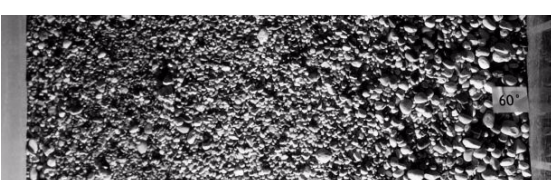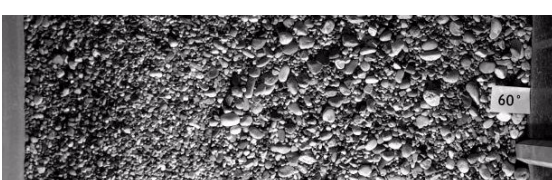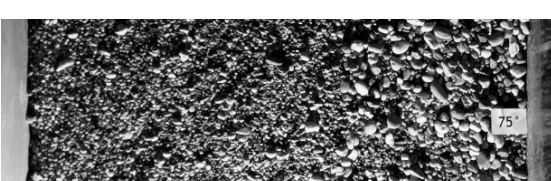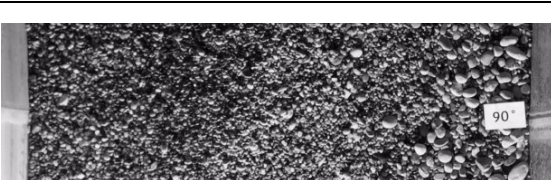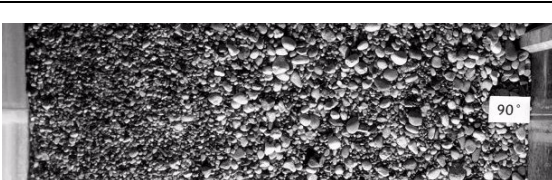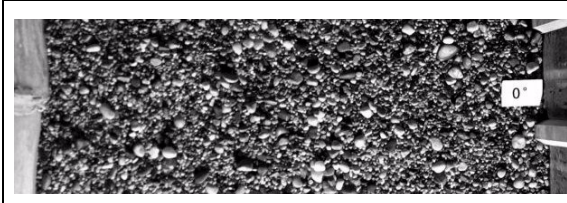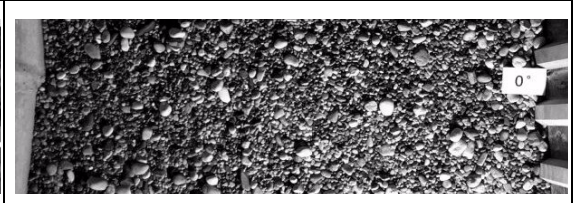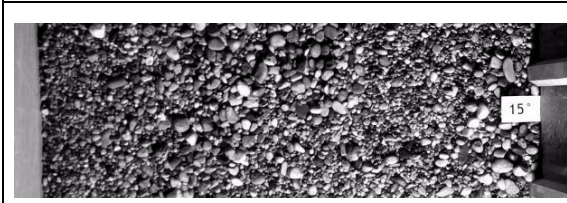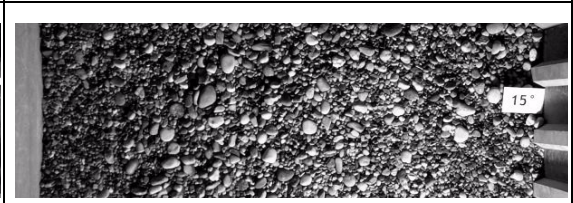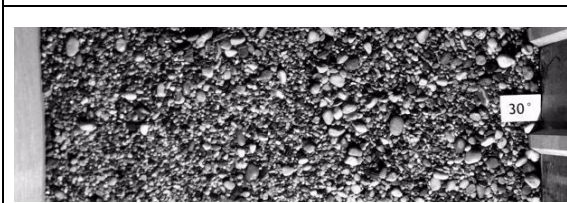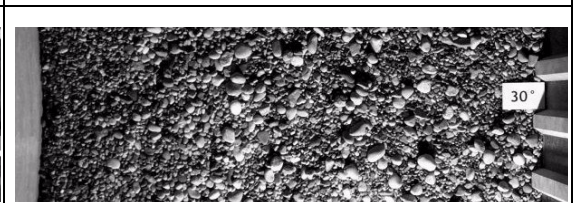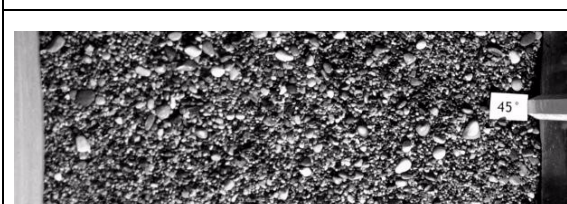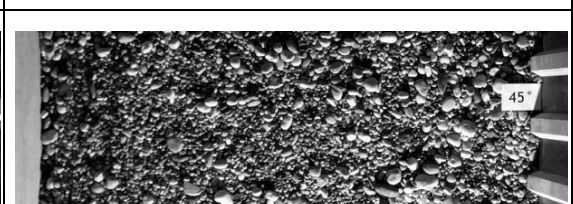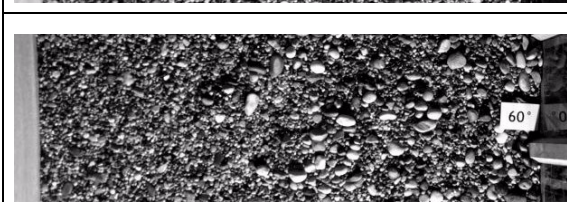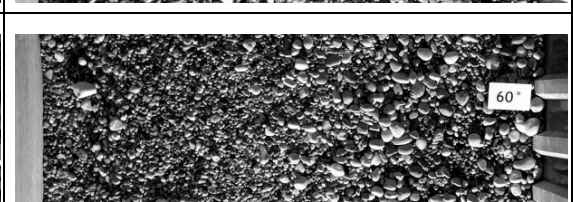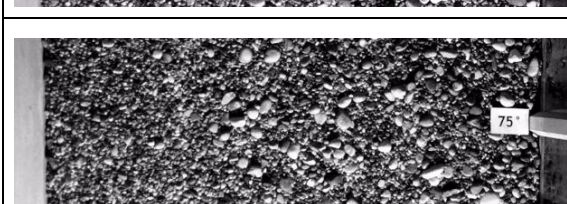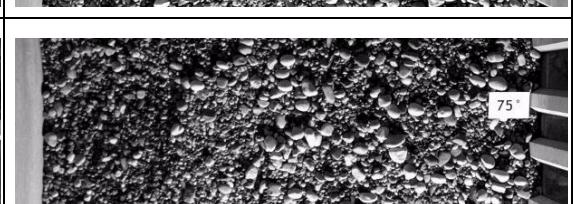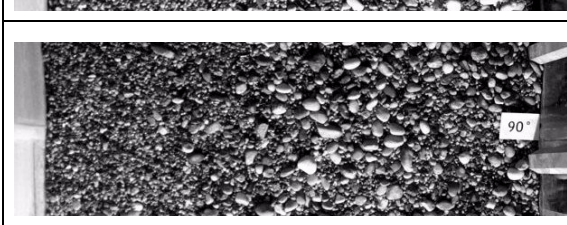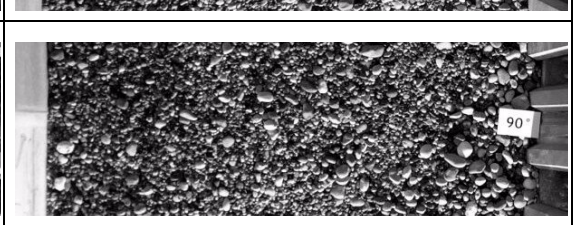
POS. [°]	WITHOUT MR	WITH MR SPACING 4°
0°		
15°		
30°		
45°		
60°		
75°		
90°		

Table 10.1:   Pictures of the grain size distribution - S_0 = 0.35%; Q = 150 l/s; e_d = 20 mm

WITH MR SPACING 2°	WITH MR SPACING 1°
0°	0°
15°	15°
30°	30°
45°	45°
60°	60°
75°	75°
90°	90°

10.2 Channel slope $S_0 = 0.35\%$, $Q = 180$ l/s, $e_d = 20$ mm
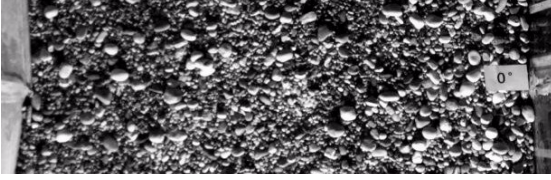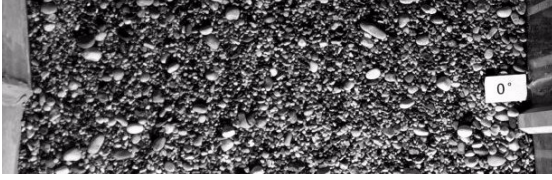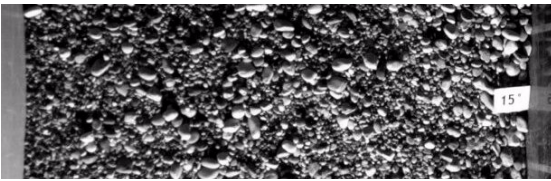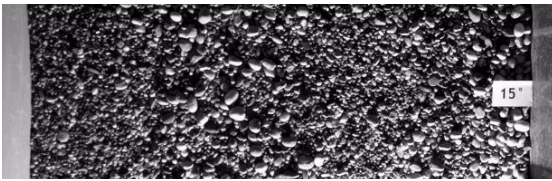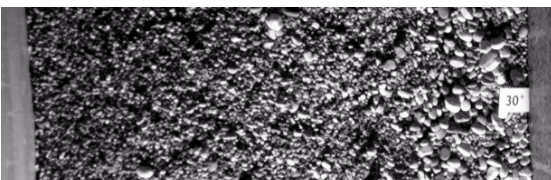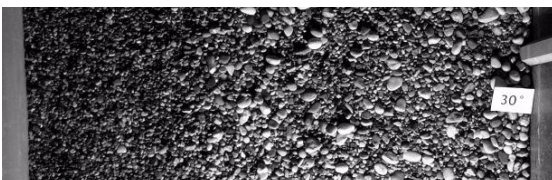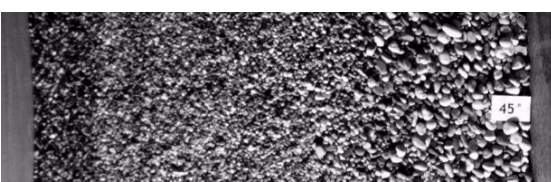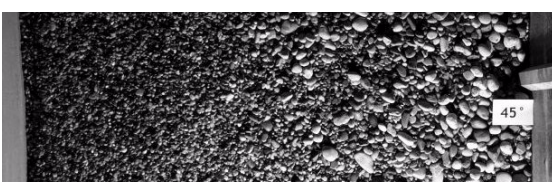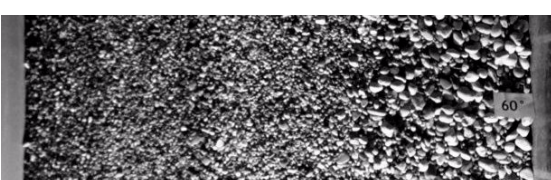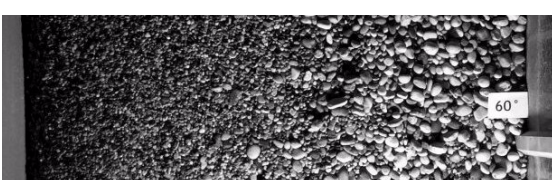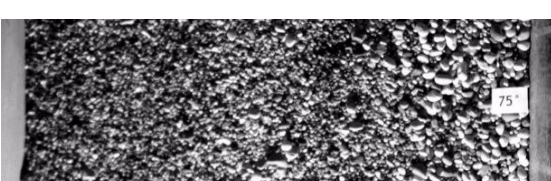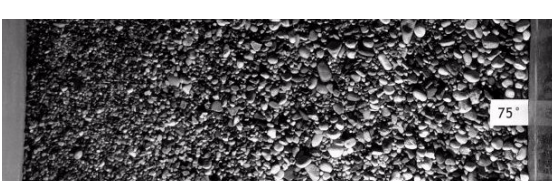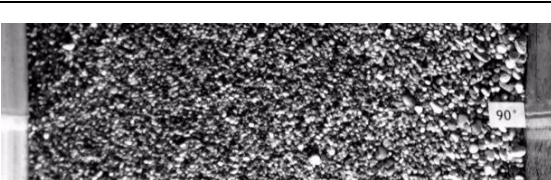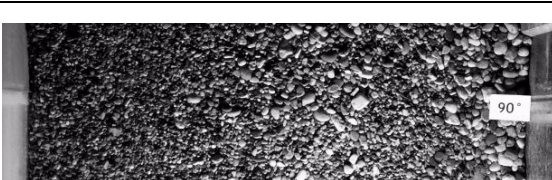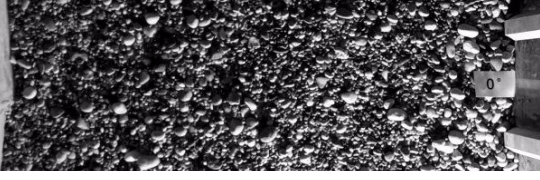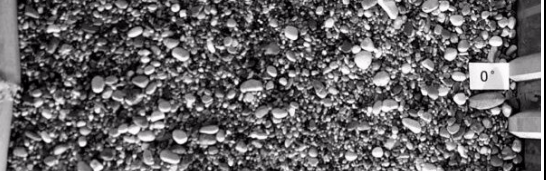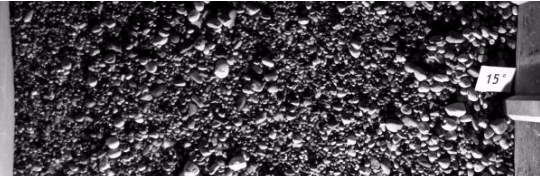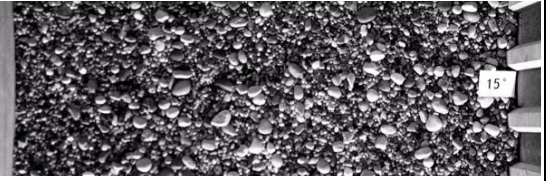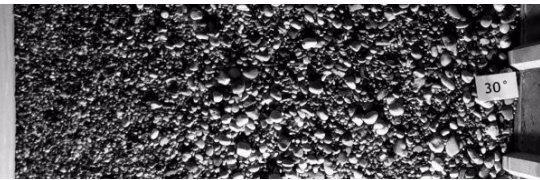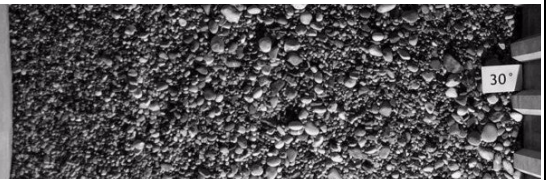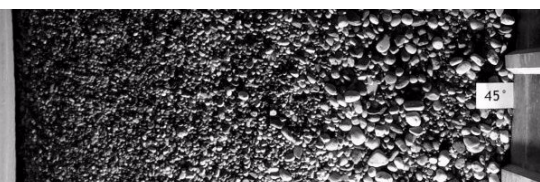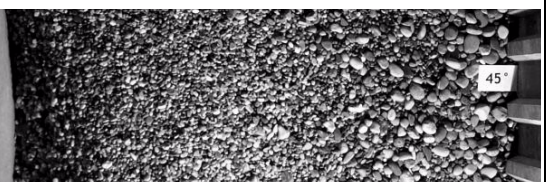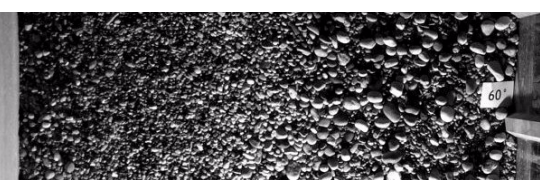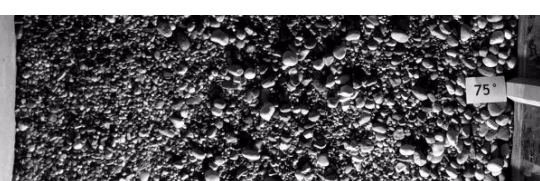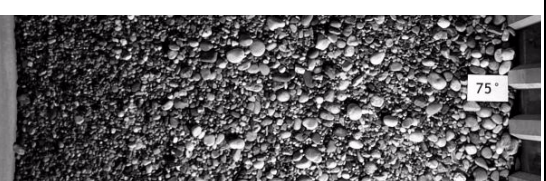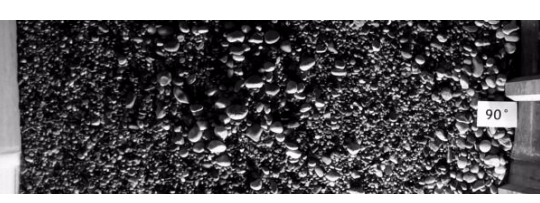
Pos. [°]	WITHOUT MR	WITH MR SPACING 4°
0°		
15°		
30°		
45°		
60°		
75°		
90°		

Table 10.2:   Pictures of the grain size distribution - $S_0 = 0.35\%$; $Q = 180$ l/s; $e_d = 20$ mm

WITH MR SPACING 2°	WITH MR SPACING 1°

10.3 Channel slope $S_0 = 0.35\%$, $Q = 210$ $l\!/s$, $e_d = 20$ mm
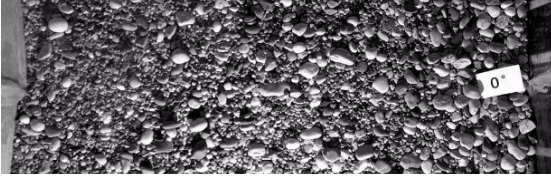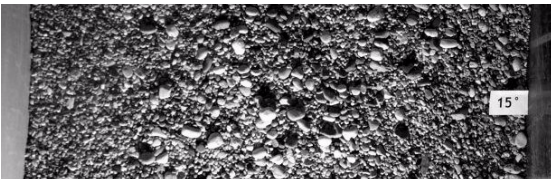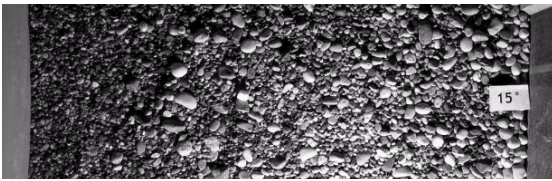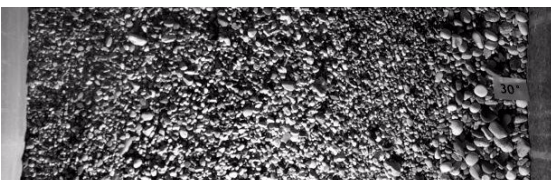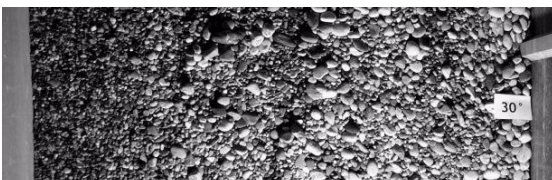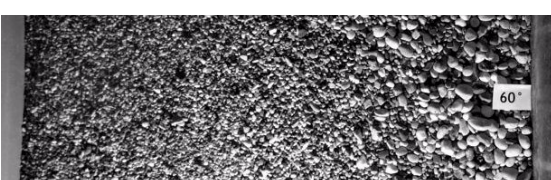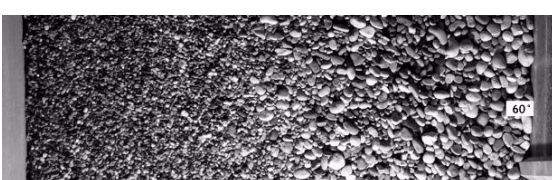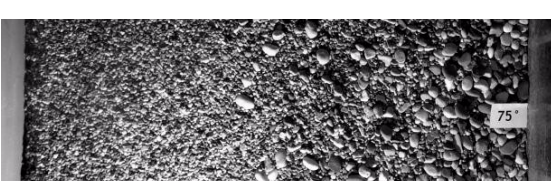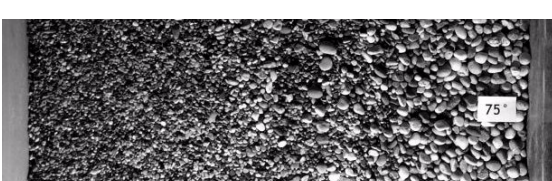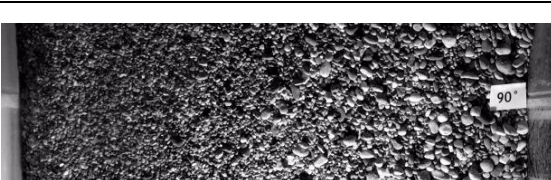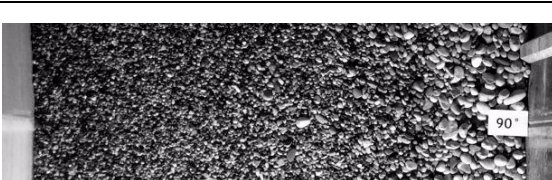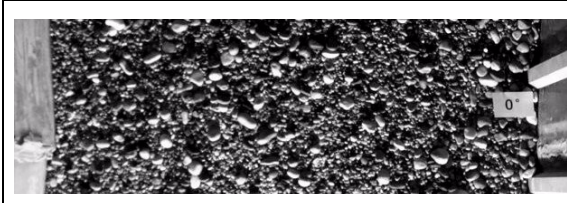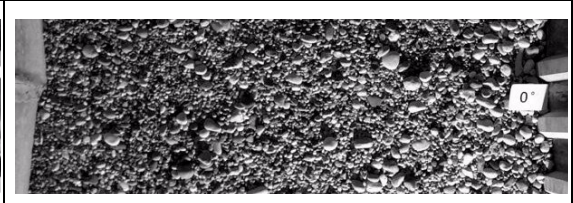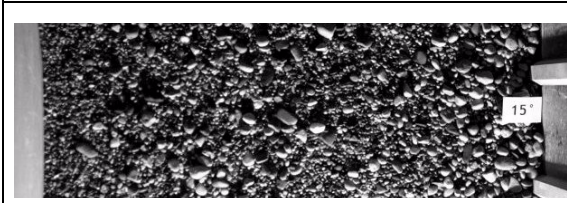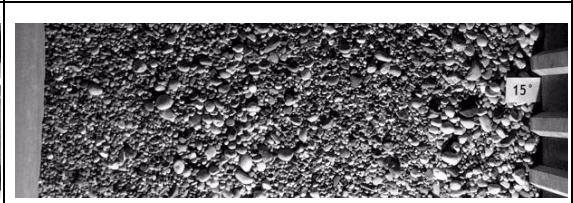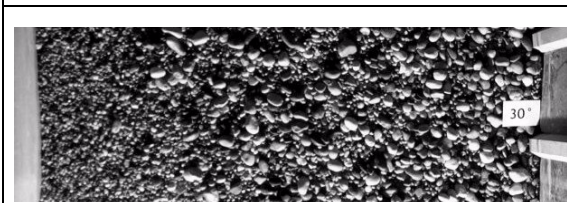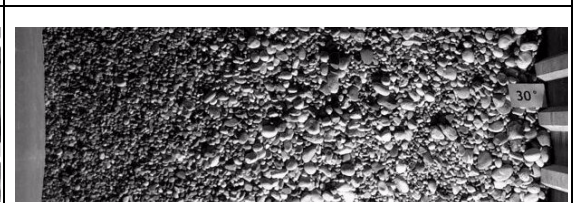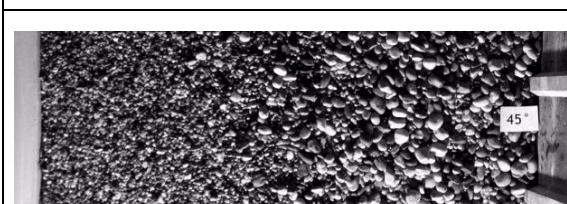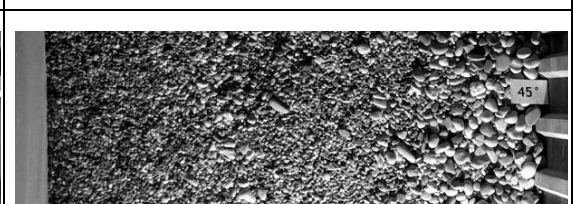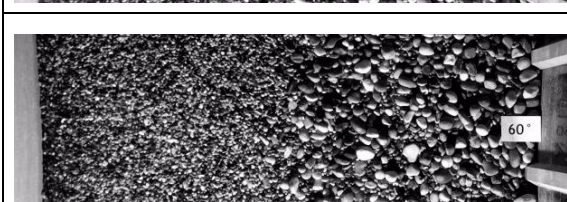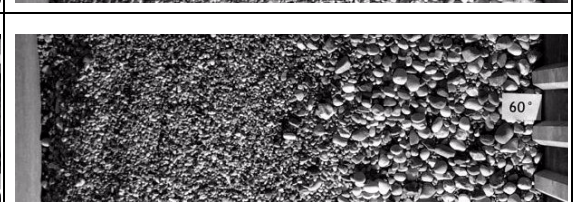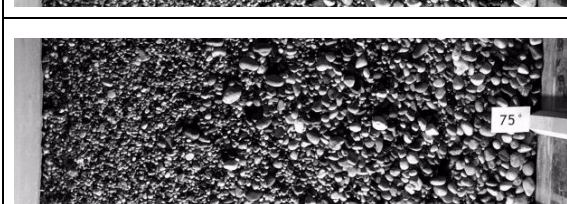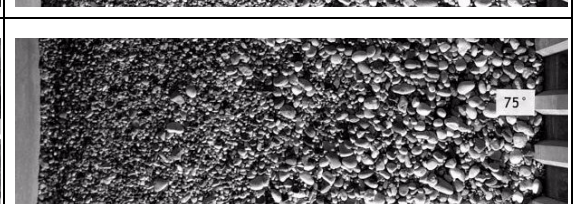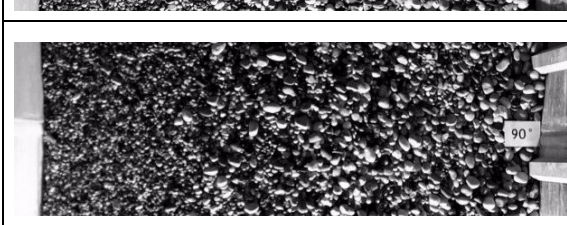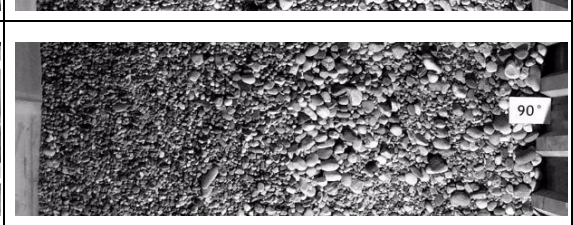
Pos. [°]	WITHOUT MR	WITH MR SPACING 4°
0°		
15°		
30°		
45°		
60°		
75°		
90°		

Table 10.3: Pictures of the grain size distribution - $S_0 = 0.35\%$; $Q = 210$ $l\!/s$; $e_d = 20$ mm

WITH MR SPACING 2°	WITH MR SPACING 1°

10.4 Channel slope $S_0 = 0.50\%$, $Q = 150$ l/s, $e_d = 20$ mm
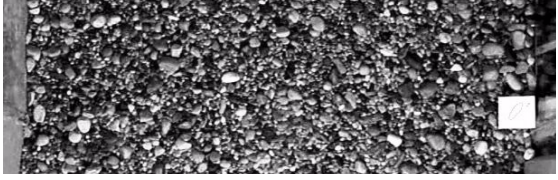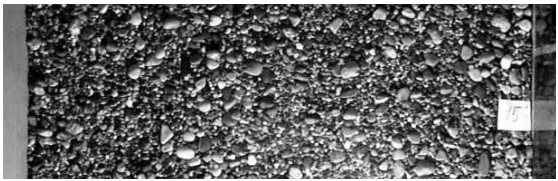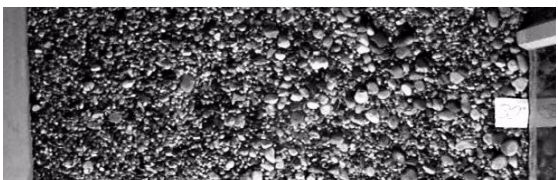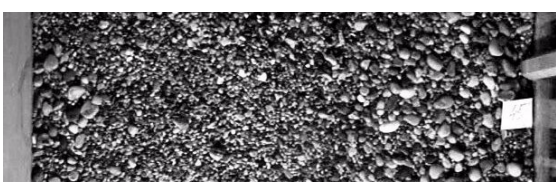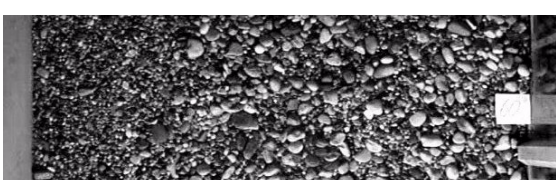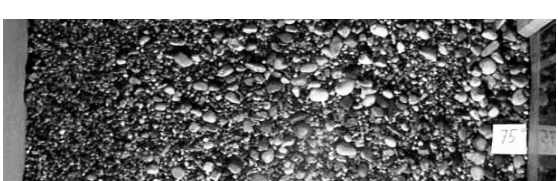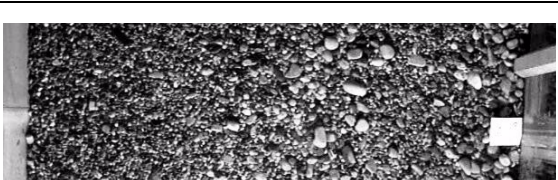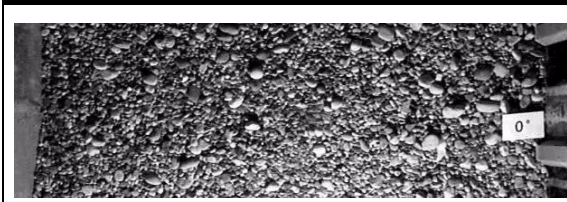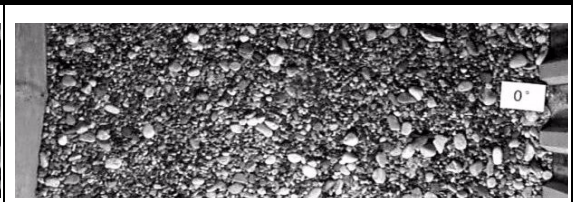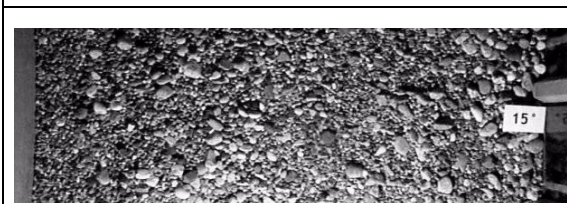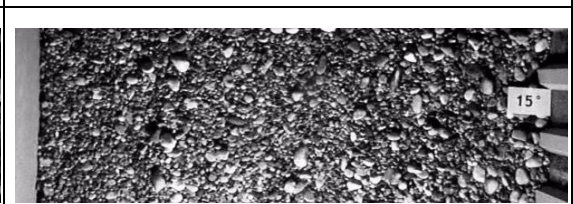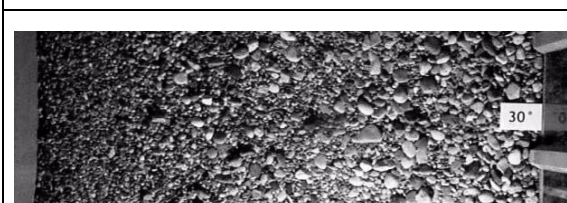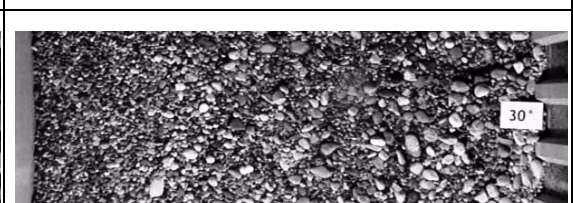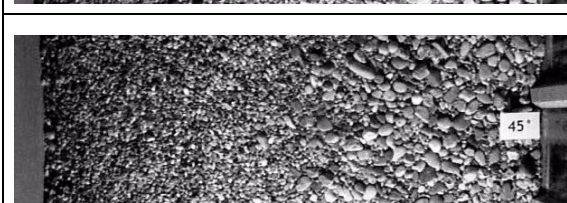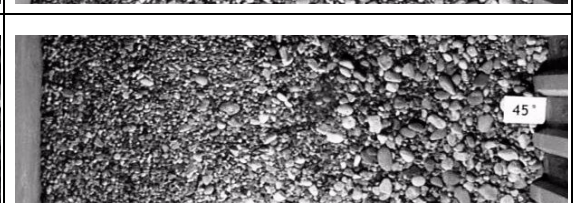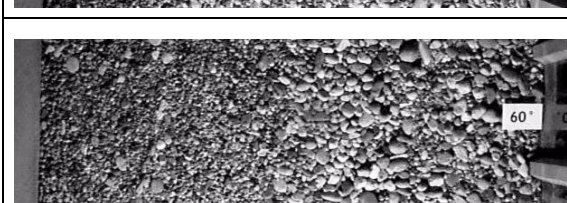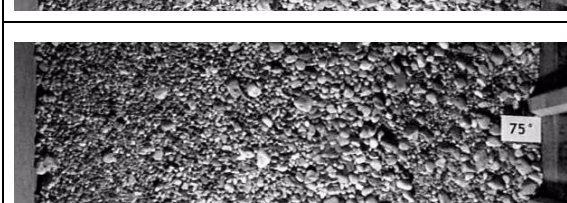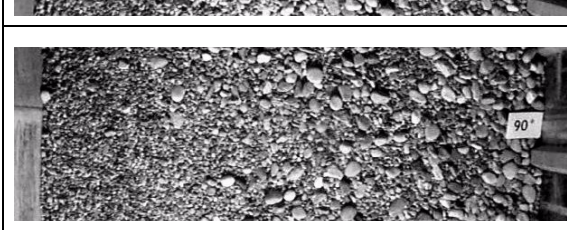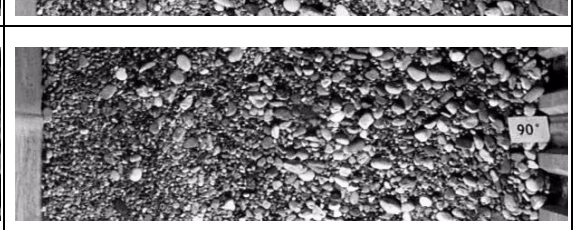
Pos. [°]	WITHOUT MR	WITH MR SPACING 4°
0°		
15°		
30°		
45°		
60°		
75°		
90°		

Table 10.4: Pictures of the grain size distribution - $S_0 = 0.50\%$; $Q = 150$ l/s; $e_d = 20$ mm

WITH MR SPACING 2°	WITH MR SPACING 1°
0°	0°
15°	15°
30°	30°
45°	45°
60°	60°
75°	75°
90°	90°

10.5 Channel slope $S_0 = 0.50\%$, $Q = 180$ l/s, $e_d = 20$ mm
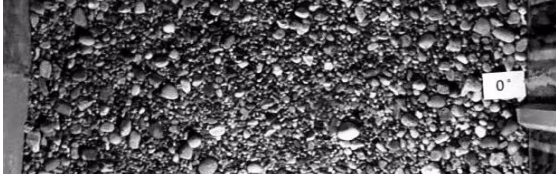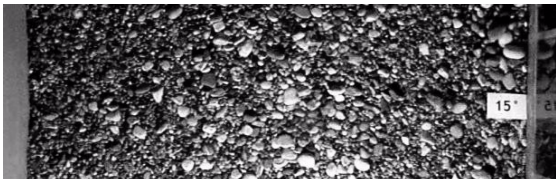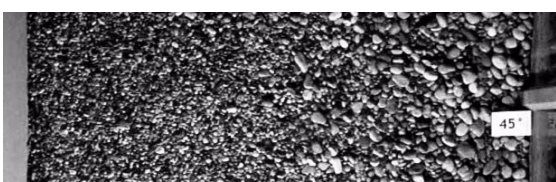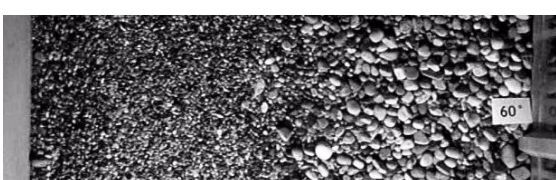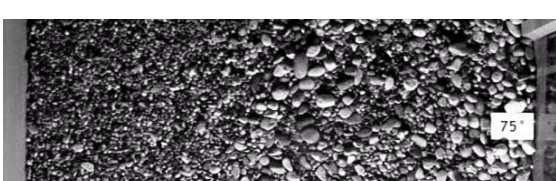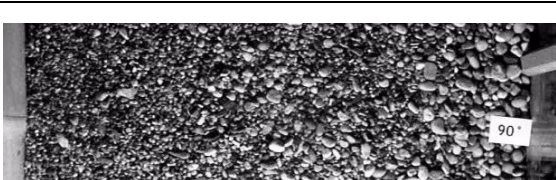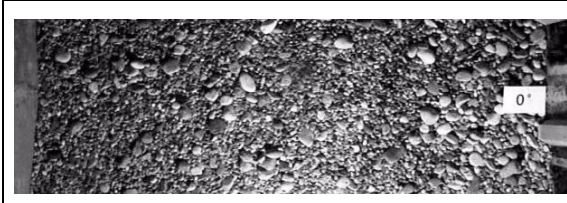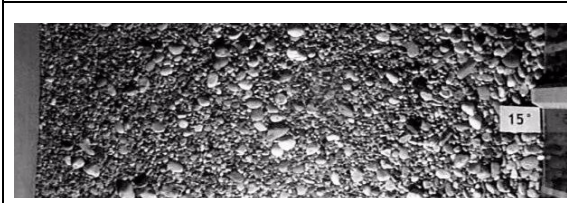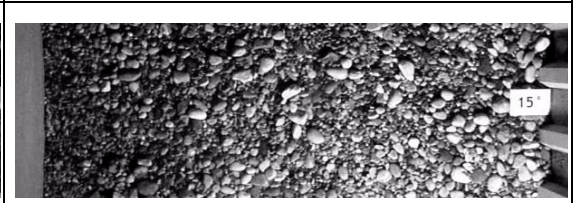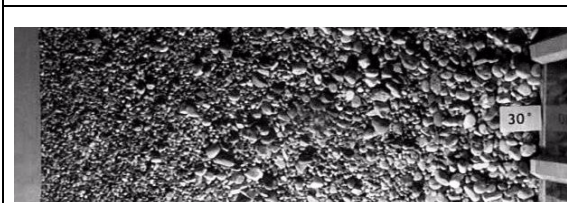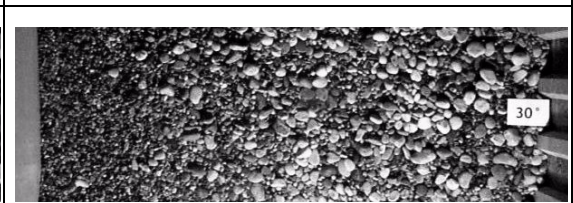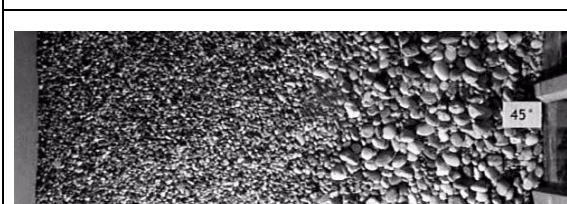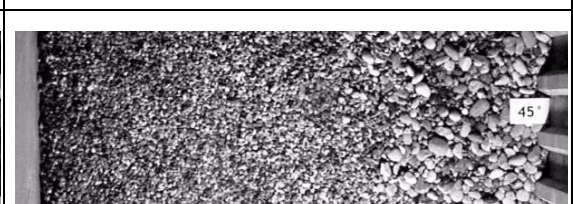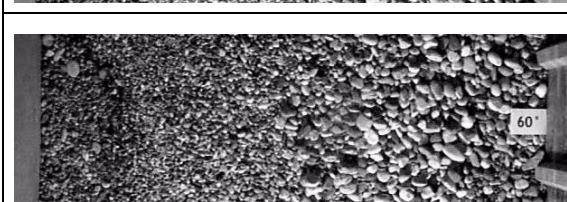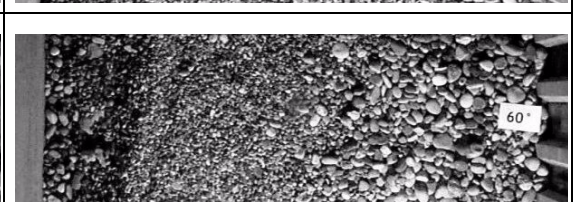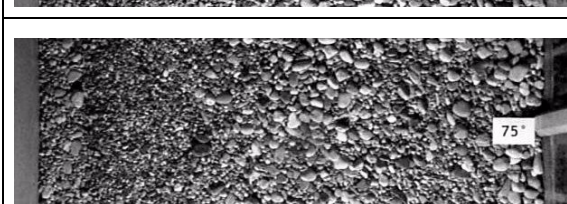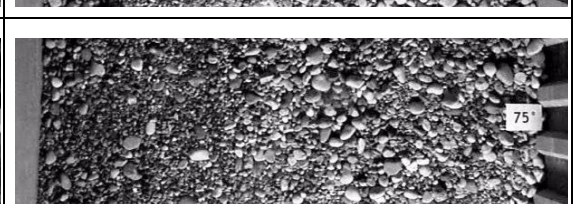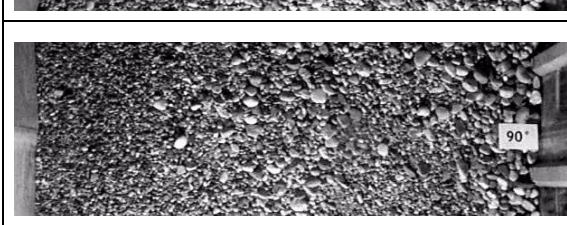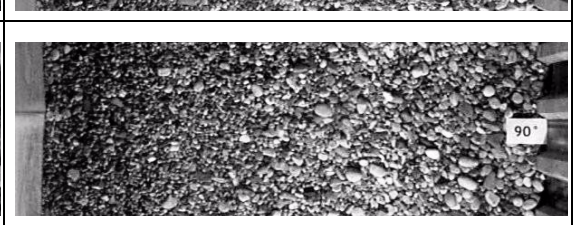
Pos. [°]	WITHOUT MR	WITH MR SPACING 4°
0°		
15°		
30°		
45°		
60°		
75°		
90°		

Table 10.5: Pictures of the grain size distribution - $S_0 = 0.50\%$; $Q = 180$ l/s; $e_d = 20$ mm

WITH MR SPACING 2°	WITH MR SPACING 1°

10.6 Channel slope $S_0 = 0.50\%$, $Q = 210$ l/s, $e_d = 20$ mm
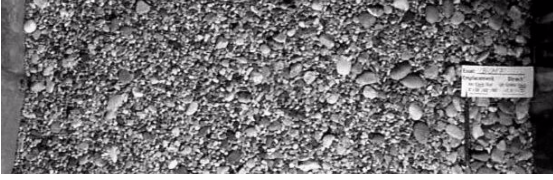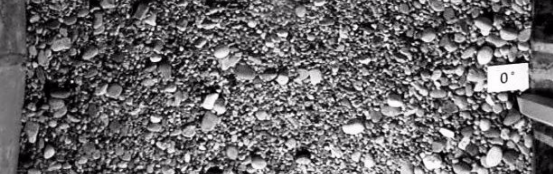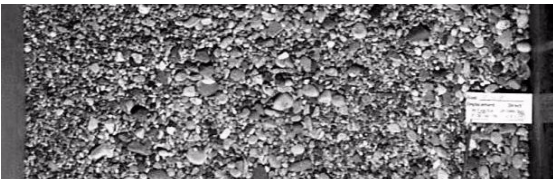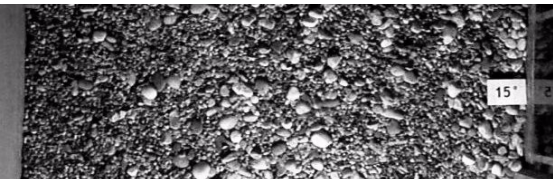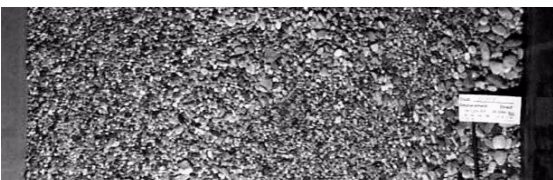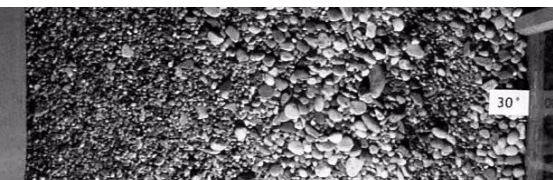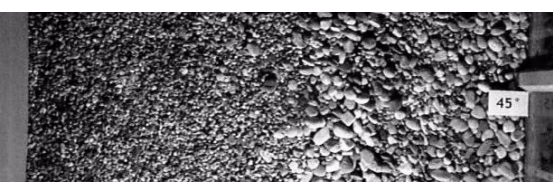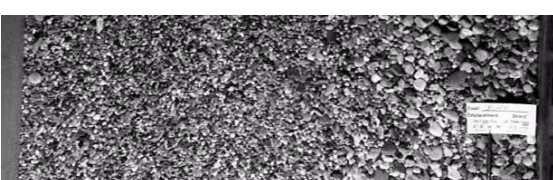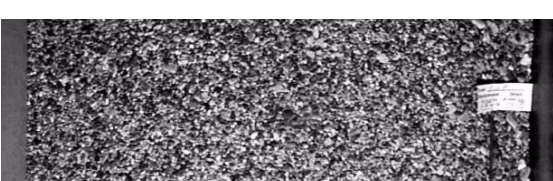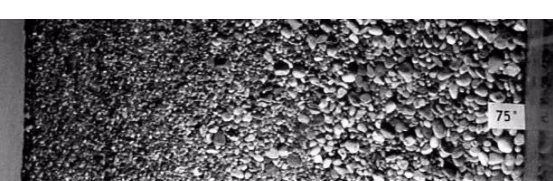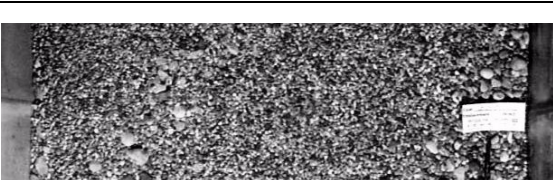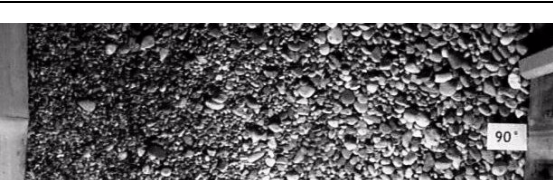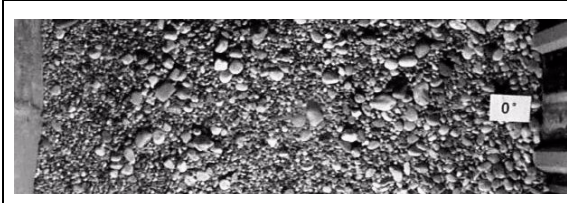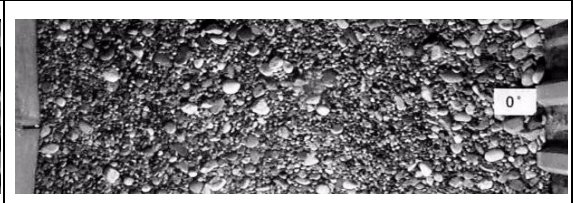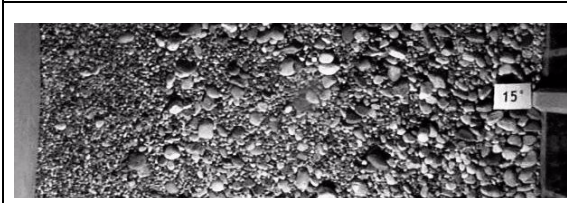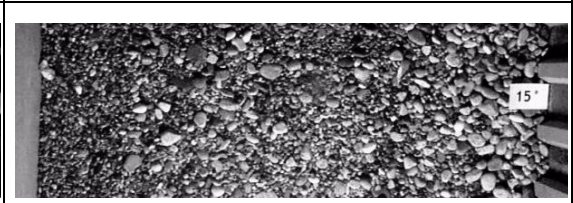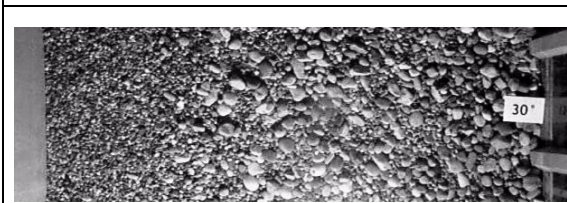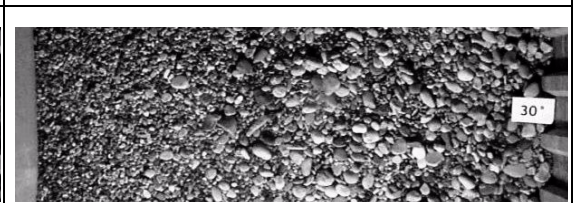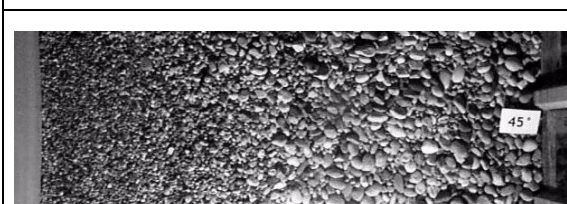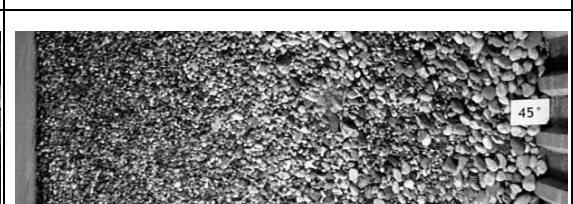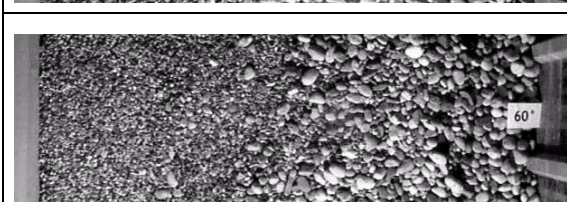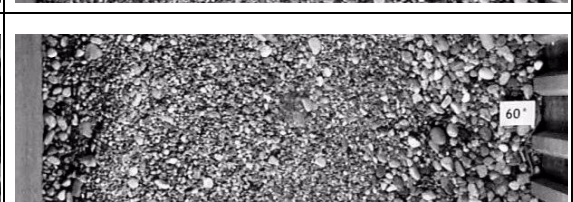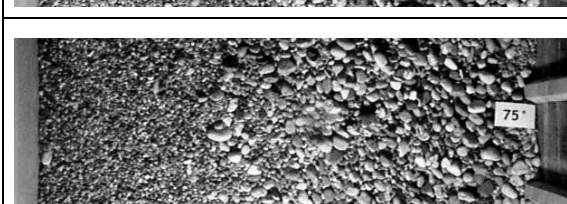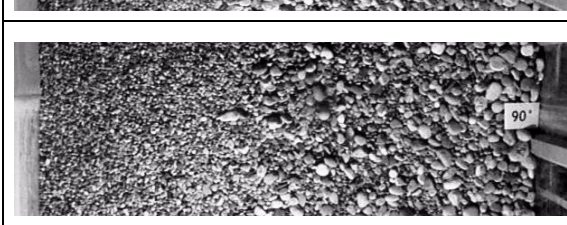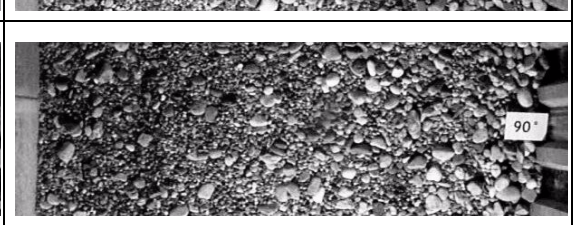
Pos. [°]	WITHOUT MR	WITH MR SPACING 4°
0°		
15°		
30°		
45°		
60°		
75°		
90°		

Table 10.6:   Pictures of the grain size distribution - $S_0 = 0.50\%$; $Q = 210$ l/s; $e_d = 20$ mm

WITH MR SPACING 2°	WITH MR SPACING 1°
0°	0°
15°	15°
30°	30°
45°	45°
60°	60°
75°	75°
90°	90°

10.7   Channel slope $S_0 = 0.75\%$, $Q = 150$ ⅃/s, $e_d = 20$ mm
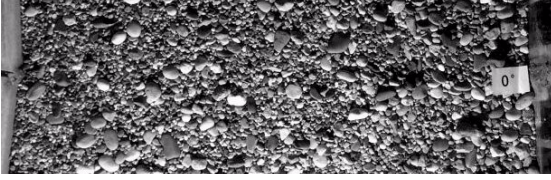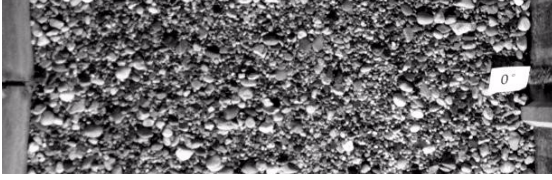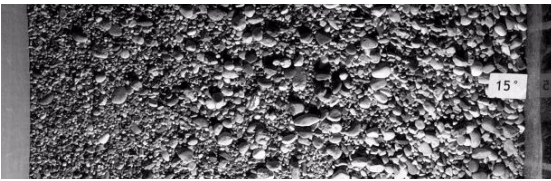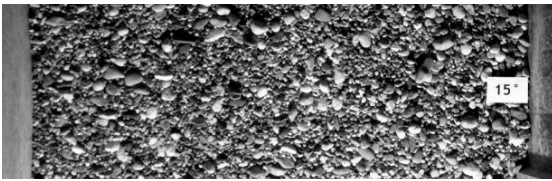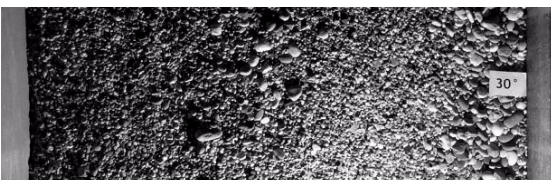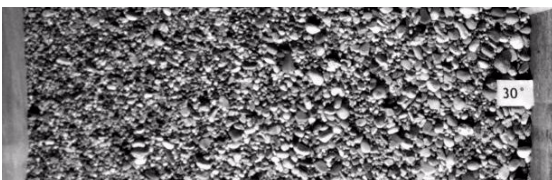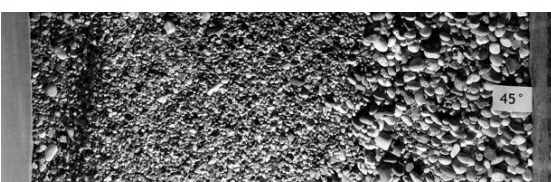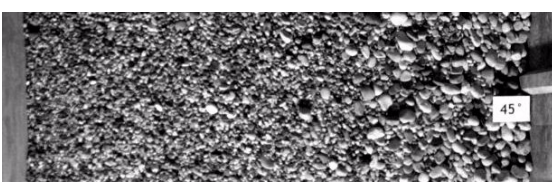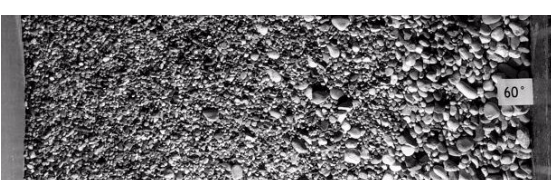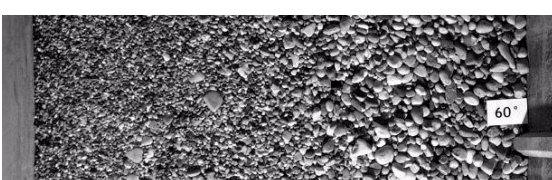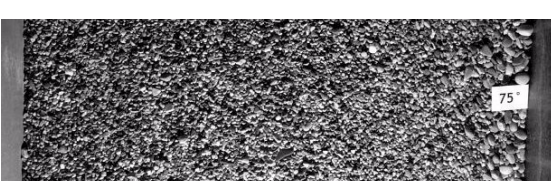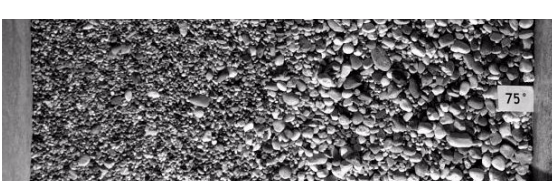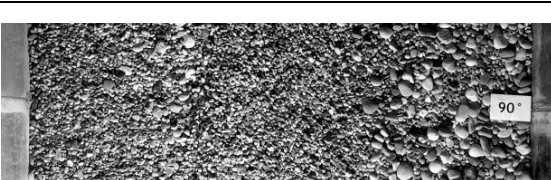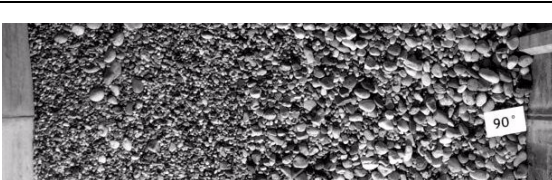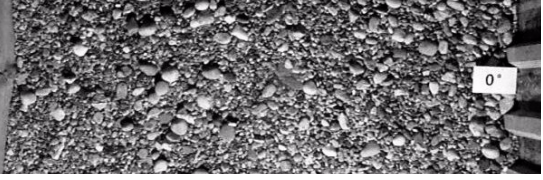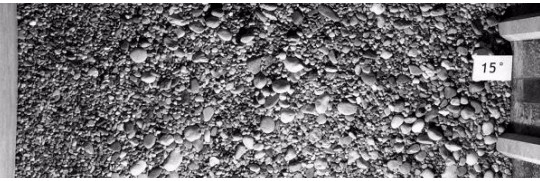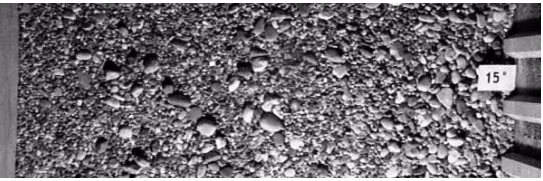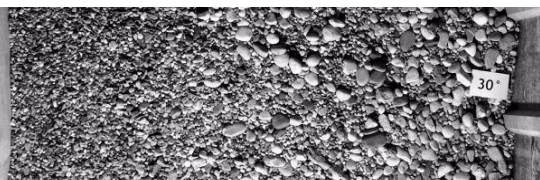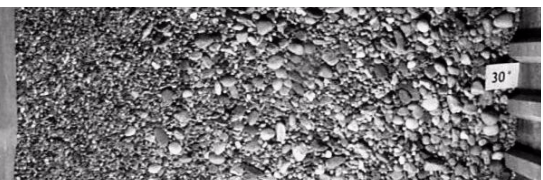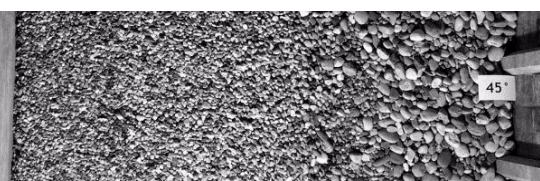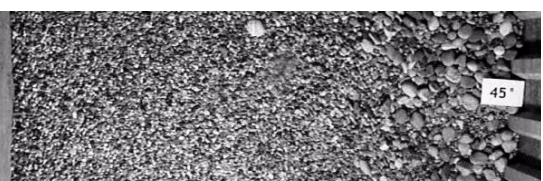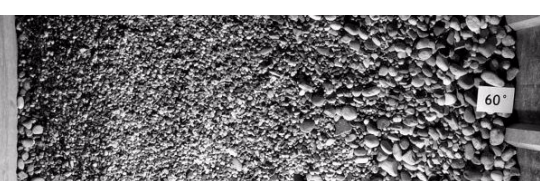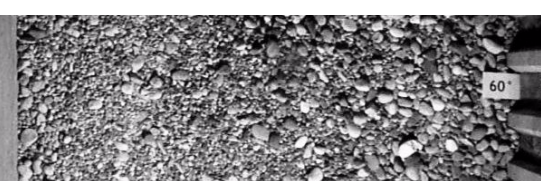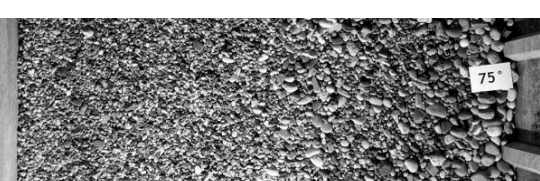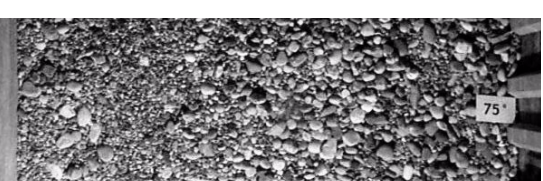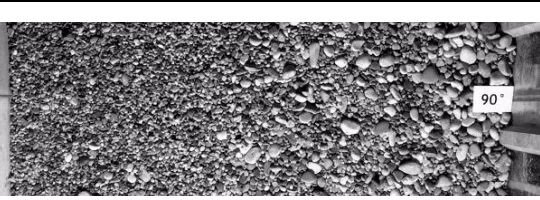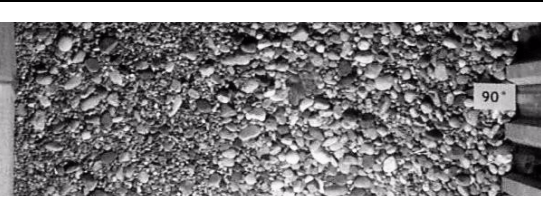
Pos. [°]	WITHOUT MR	WITH MR SPACING 4°
0°		
15°		
30°		
45°		
60°		
75°		
90°		

Table 10.7:   Pictures of the grain size distribution - $S_0 = 0.75\%$; $Q = 150$ l/s; $e_d = 20$ mm

WITH MR SPACING 2°	WITH MR SPACING 1°
0°	0°
15°	15°
30°	30°
45°	45°
60°	60°
75°	75°
90°	90°

10.8 Channel slope $S_0 = 0.75\%$, $Q = 180$ l/s, $e_d = 20$ mm
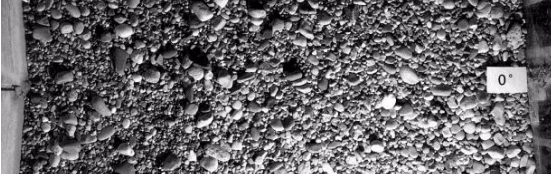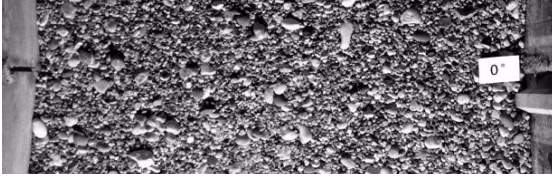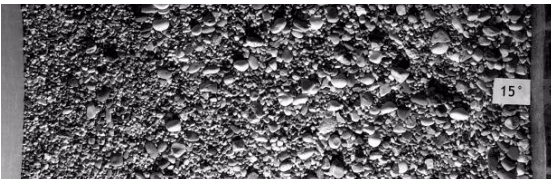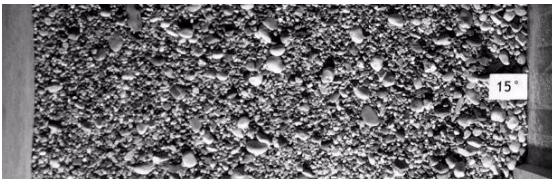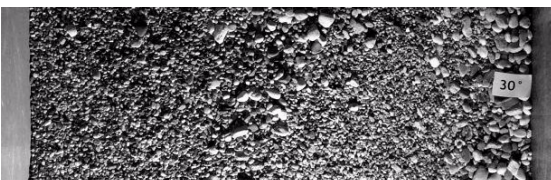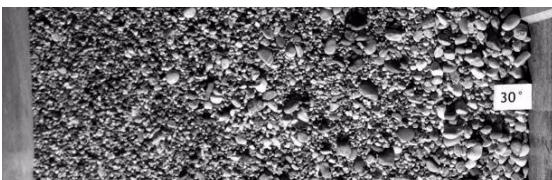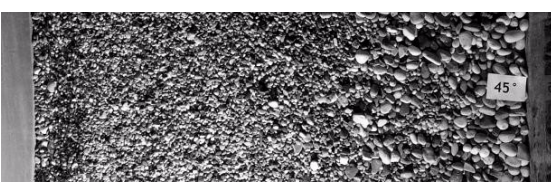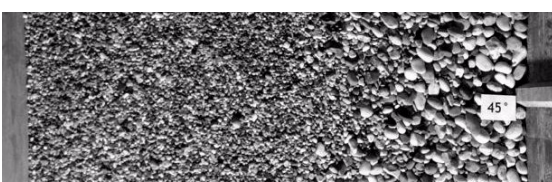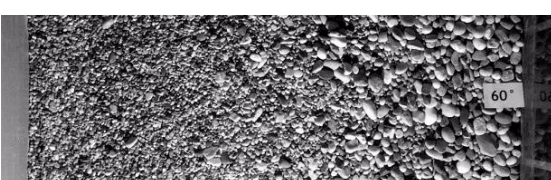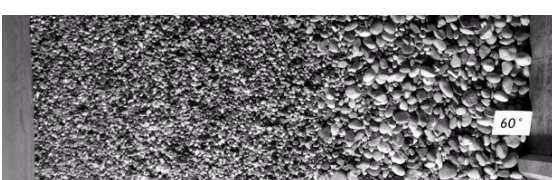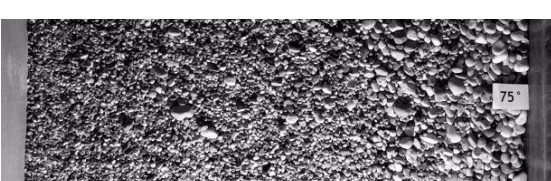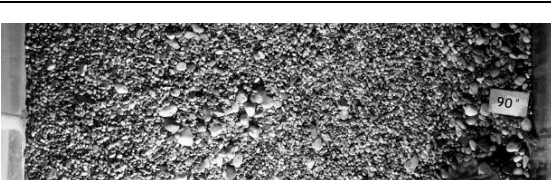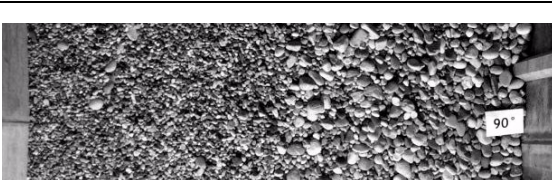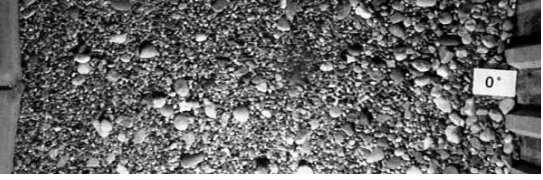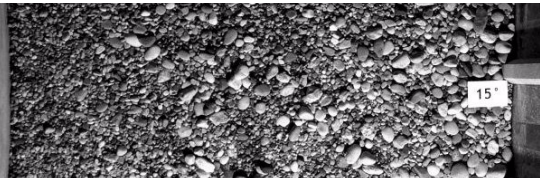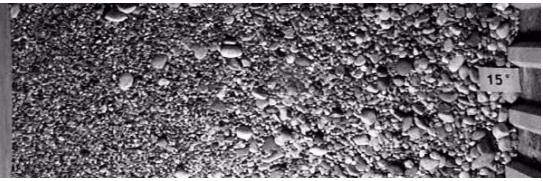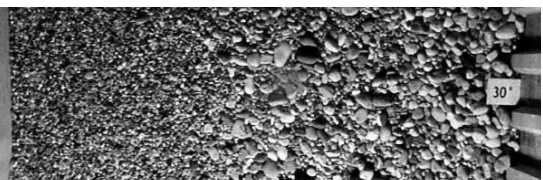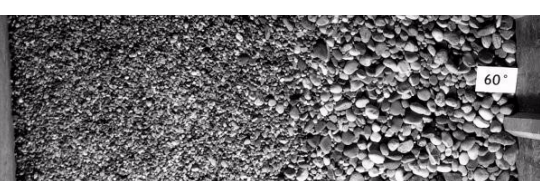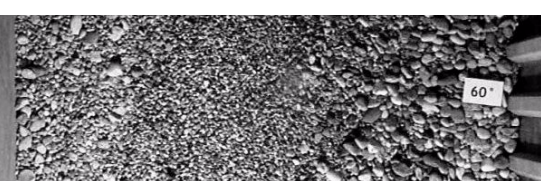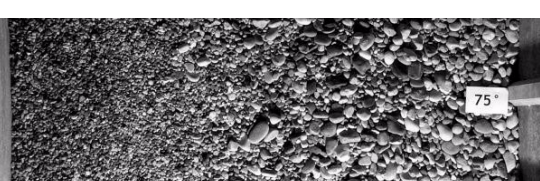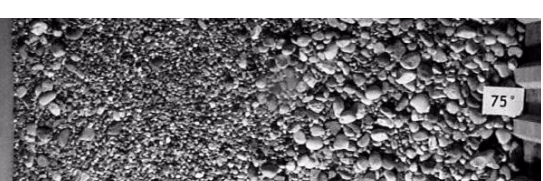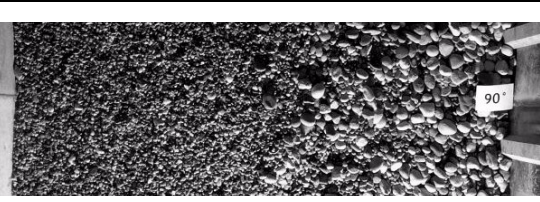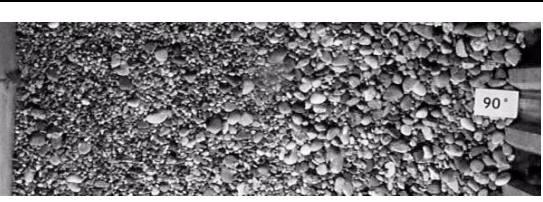
Pos. [°]	WITHOUT MR	WITH MR SPACING 4°
0°		
15°		
30°		
45°		
60°		
75°		
90°		

Table 10.8: Pictures of the grain size distribution - $S_0 = 0.75\%$; $Q = 180$ l/s; $e_d = 20$ mm

WITH MR SPACING 2°	WITH MR SPACING 1°
0°	0°
15°	15°
30°	30°
45°	45°
60°	60°
75°	75°
90°	90°

10.9 Channel slope $S_0 = 0.75\%$, $Q = 210$ l/s, $e_d = 20$ mm
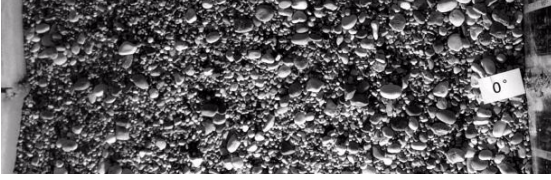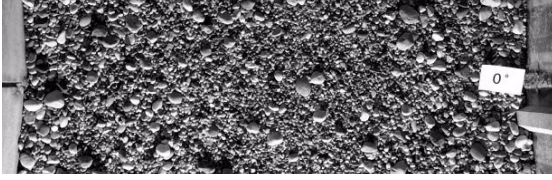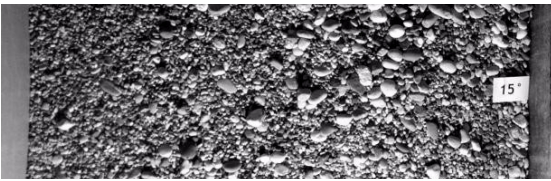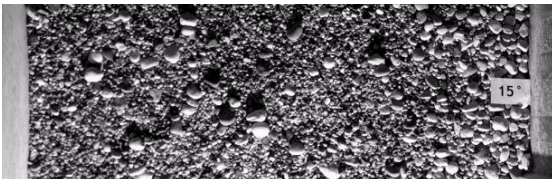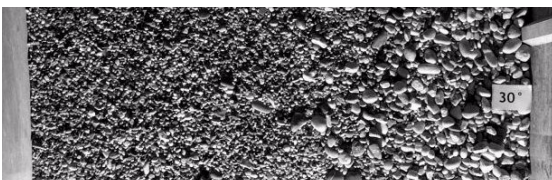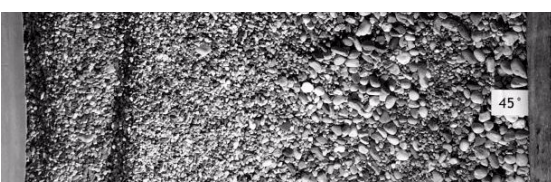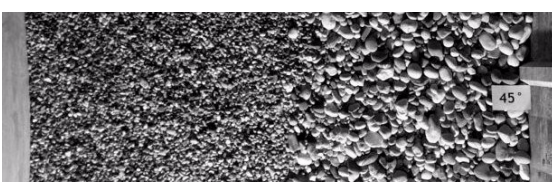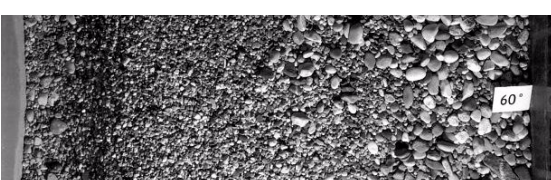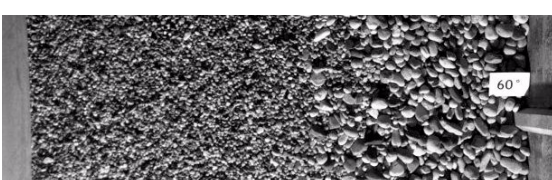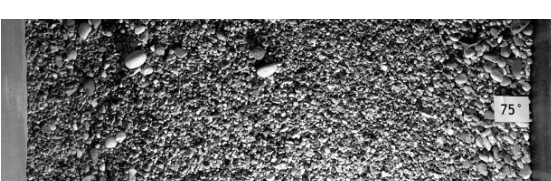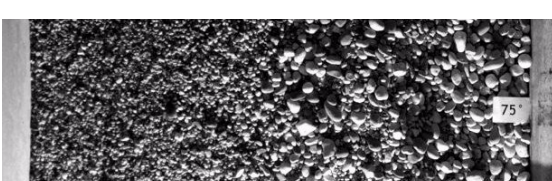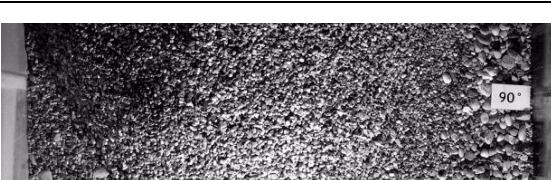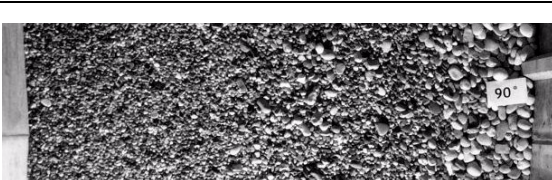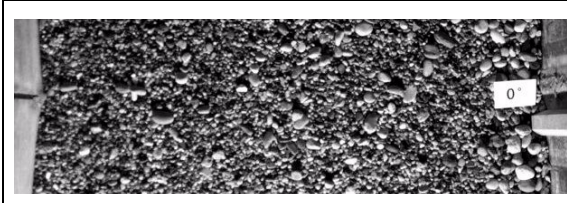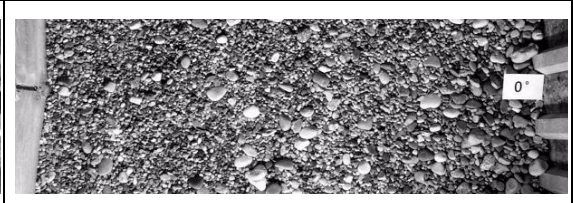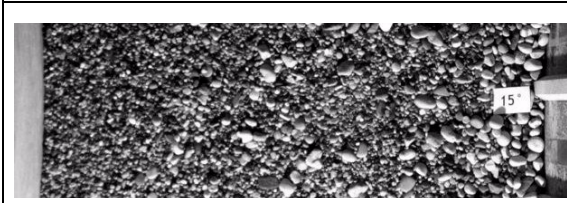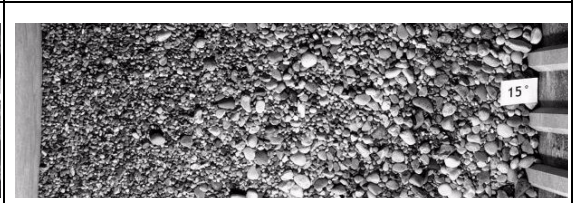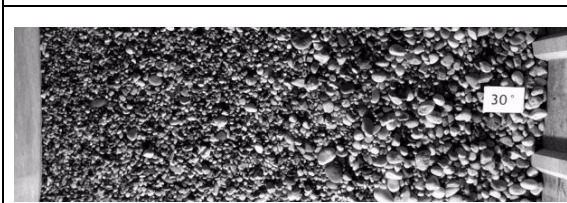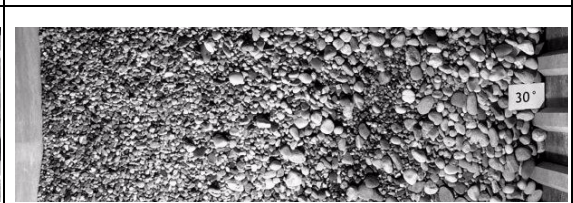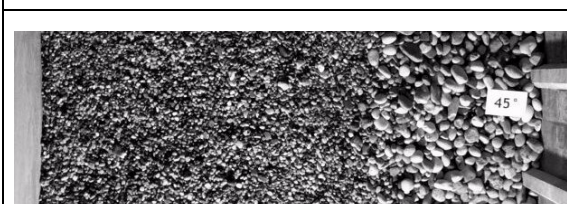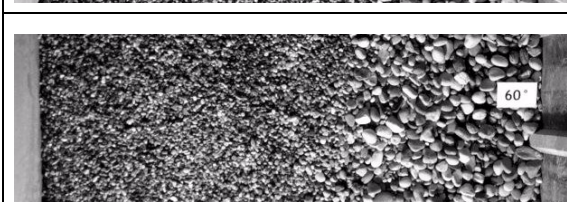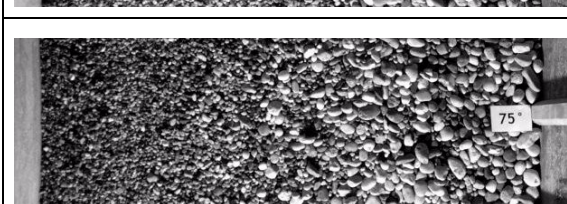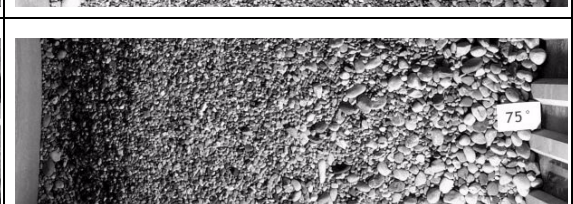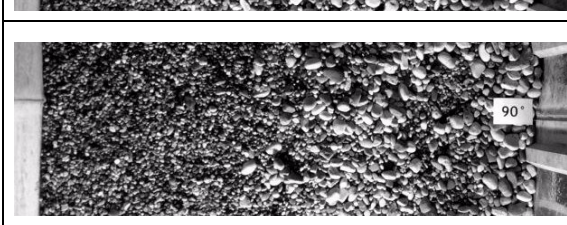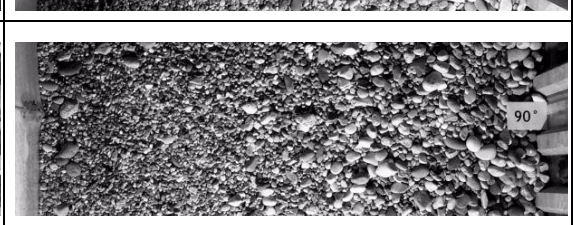
Pos. [°]	WITHOUT MR	WITH MR SPACING 4°
0°		
15°		
30°		
45°		
60°		
75°		
90°		

Table 10.9:   Pictures of the grain size distribution - $S_0 = 0.75\%$; $Q = 210$ l/s; $e_d = 20$ mm

WITH MR SPACING 2°	WITH MR SPACING 1°
0°	0°
15°	15°
30°	30°
45°	45°
60°	60°
75°	75°
90°	90°

10.10 Channel slope $S_0 = 0.50\%$, $Q = 150$ l/s, $e_d = 40$ mm
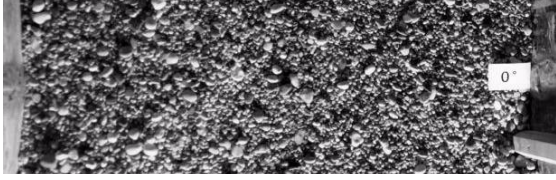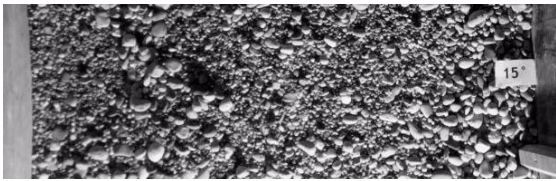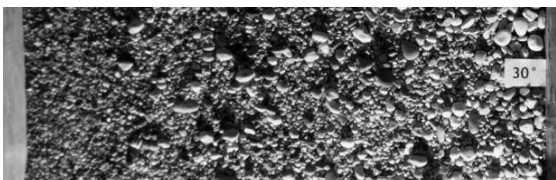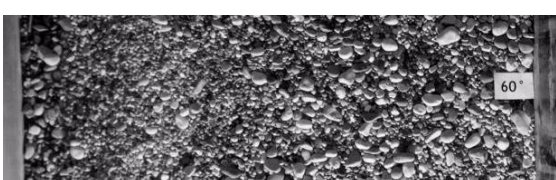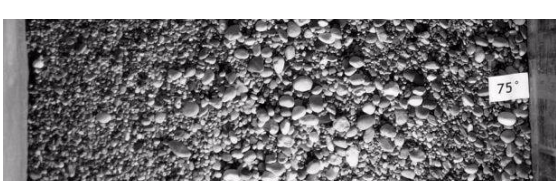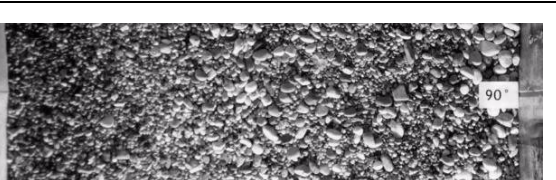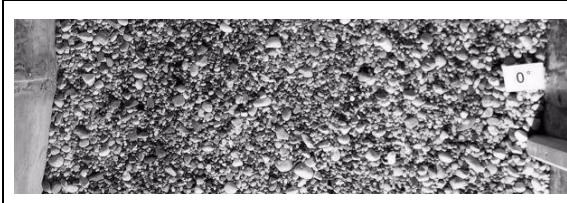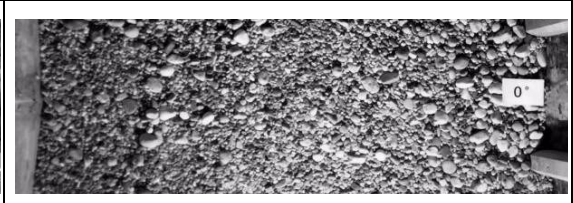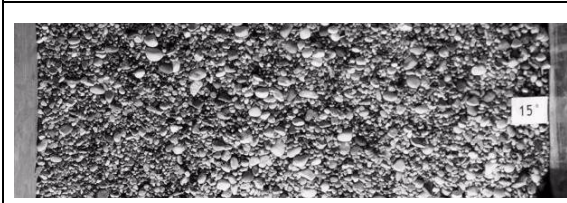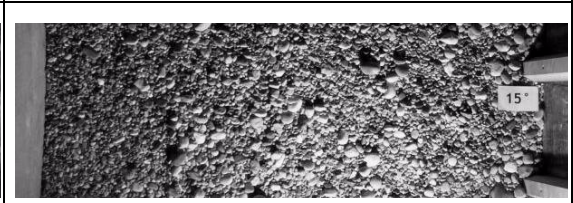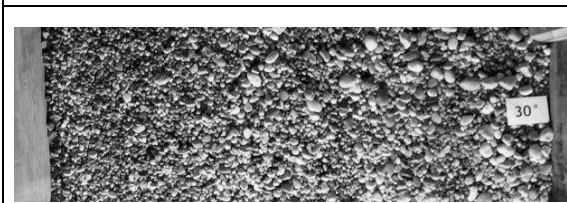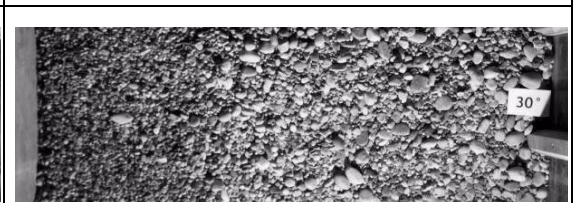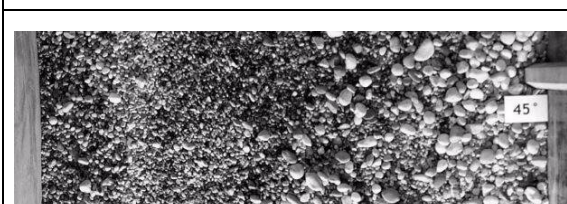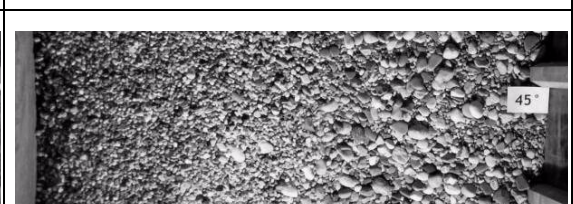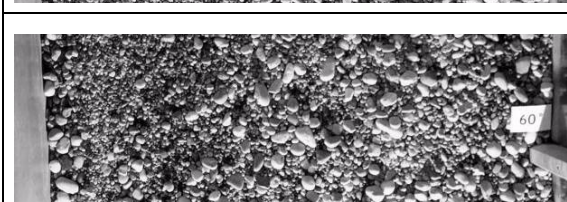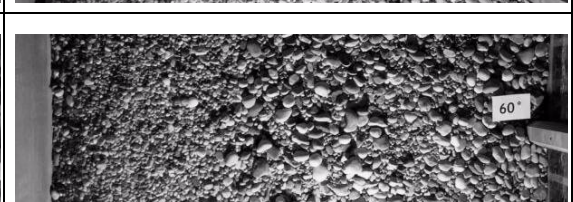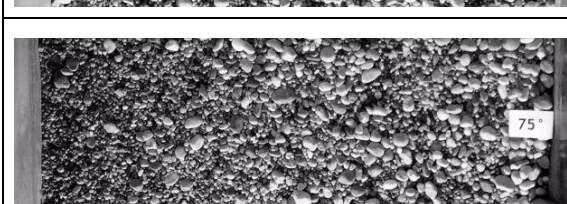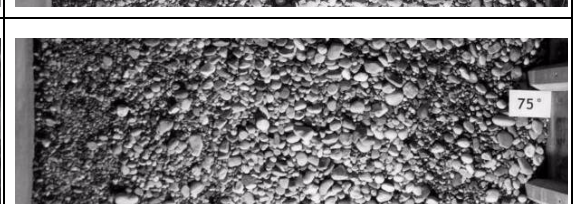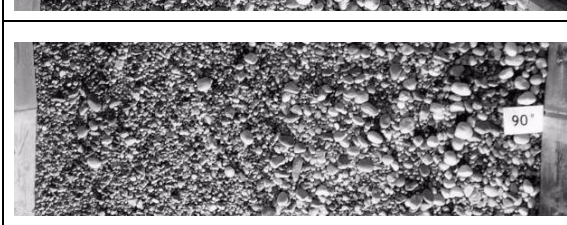
POS. [°]	WITHOUT MR	WITH MR SPACING **8°**
0°		
15°		
30°		
45°		
60°		
75°		
90°		

Table 10.10: Pictures of the grain size distribution - $S_0 = 0.50\%$; $Q = 150$ l/s; $e_d = 40$ mm

WITH MR SPACING **4°**	WITH MR SPACING **2°**
0°	0°
15°	15°
30°	30°
45°	45°
60°	60°
75°	75°
90°	90°

10.11 Channel slope $S_0 = 0.50\%$, $Q = 180$ l/s, $e_d = 40$ mm
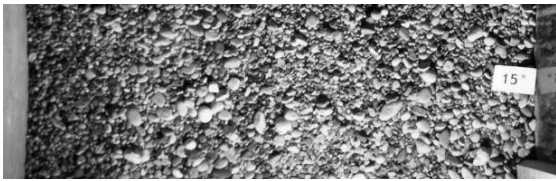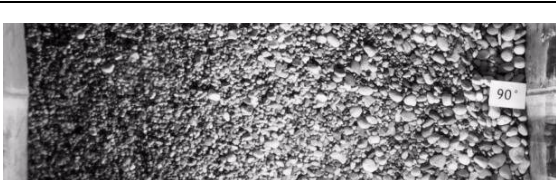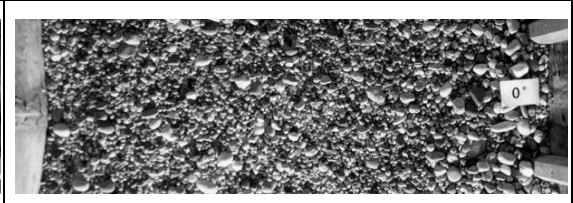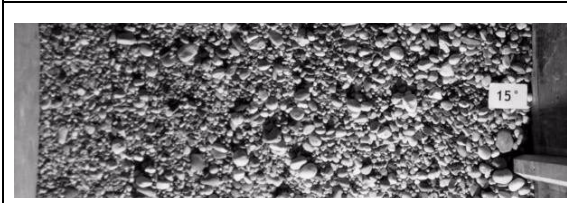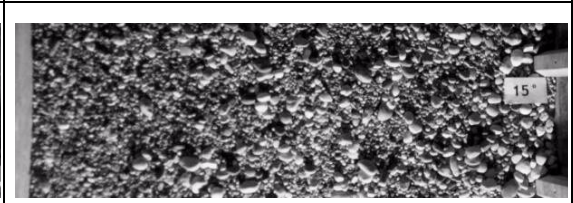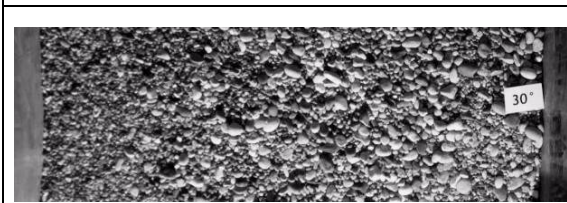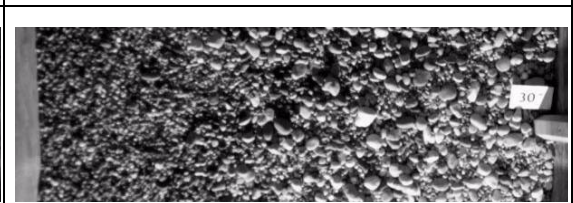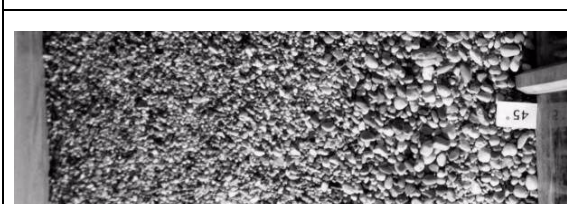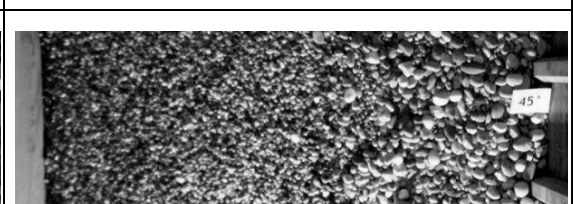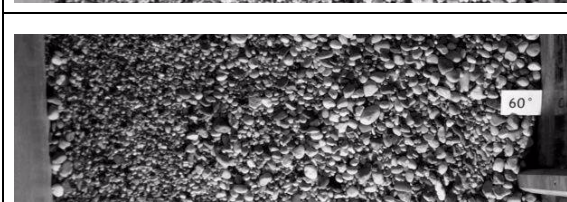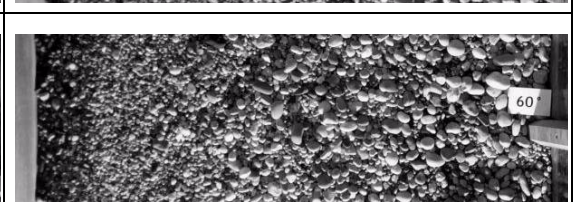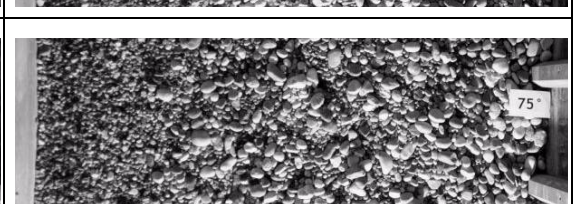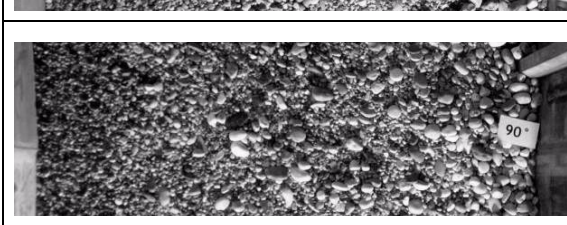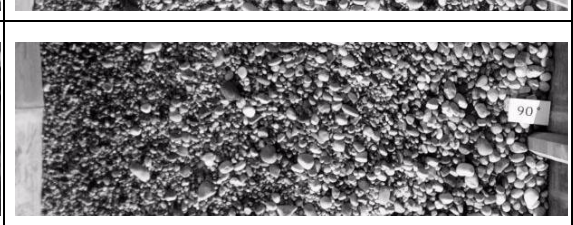
POS. [°]	WITHOUT MR	WITH MR SPACING **8°**
0°		
15°		
30°		
45°		
60°		
75°		
90°		

Table 10.11: Pictures of the grain size distribution - $S_0 = 0.50\%$; $Q = 180$ l/s; $e_d = 40$ mm

WITH MR SPACING **4°**	WITH MR SPACING **2°**
0°	0°
15°	15°
30°	30°
45°	45°
60°	60°
75°	75°
90°	90°

10.12 Channel slope $S_0 = 0.50\%$, $Q = 210$ l/s, $e_d = 40$ mm
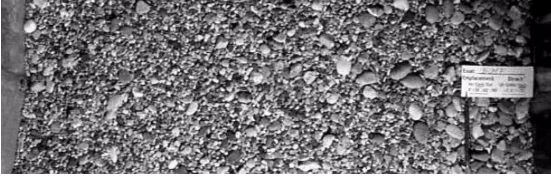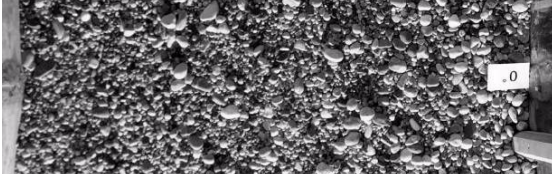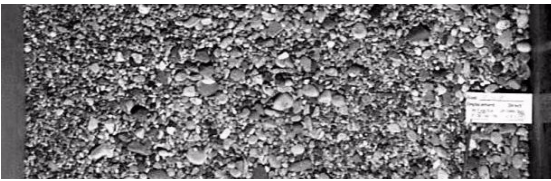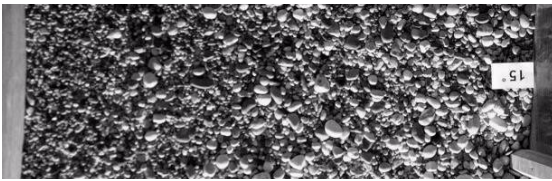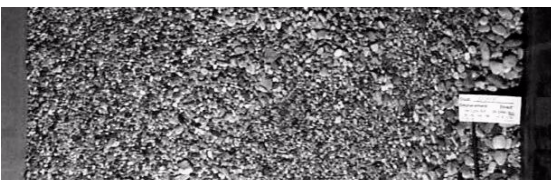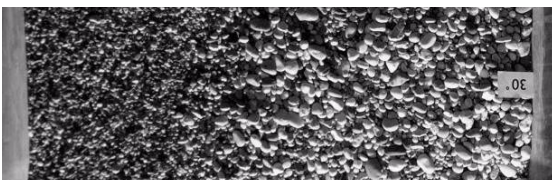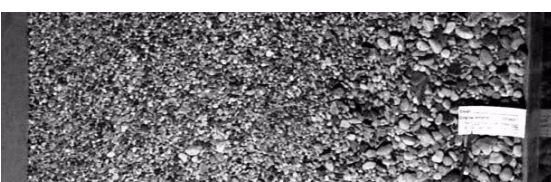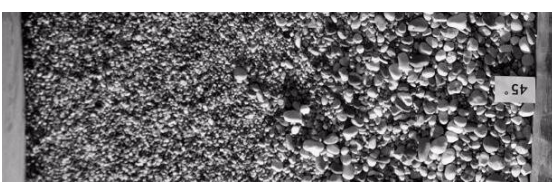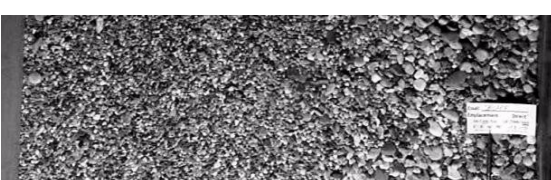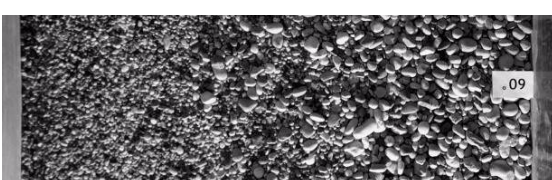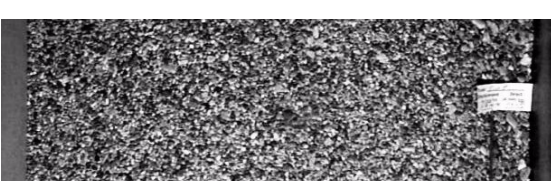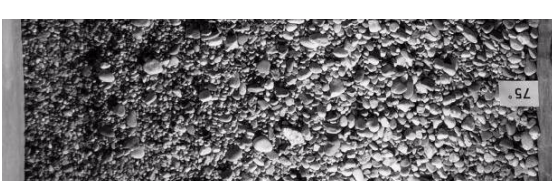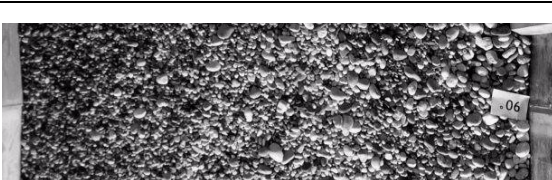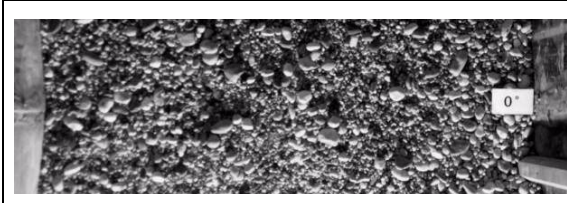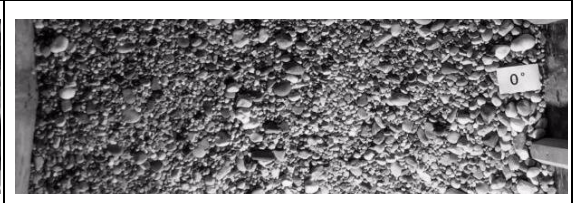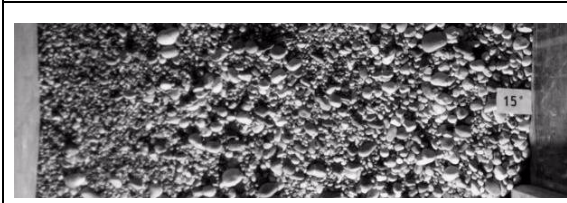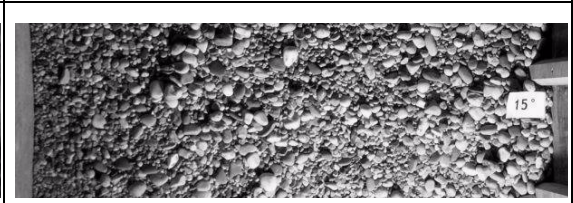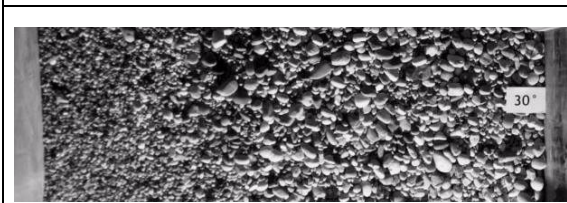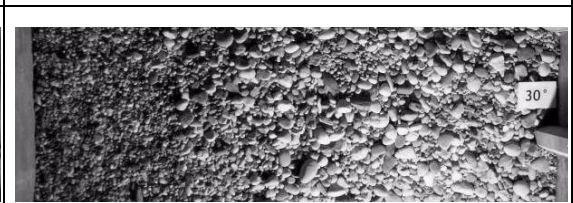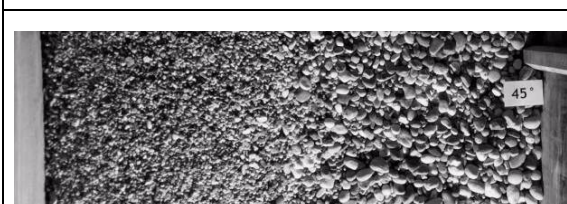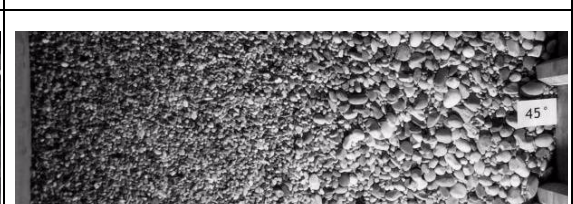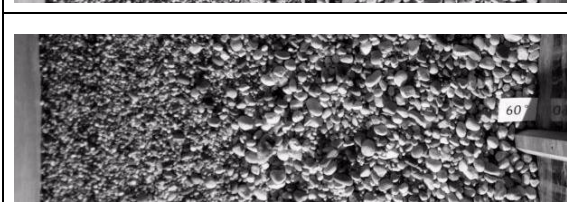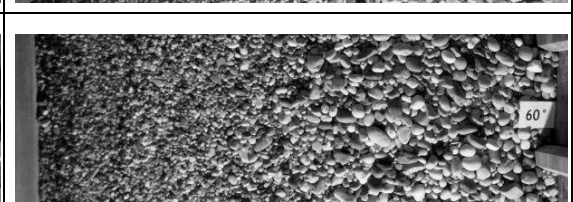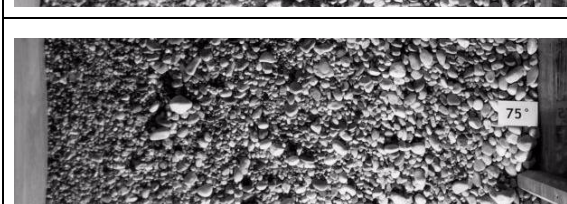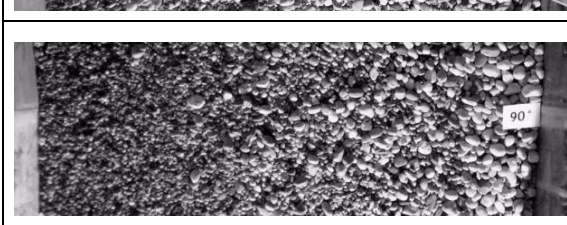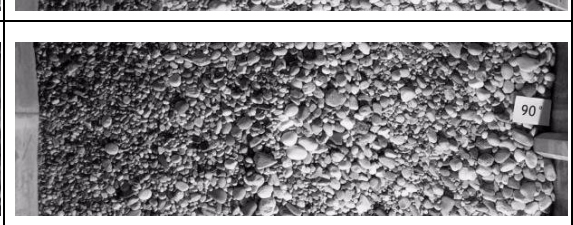
Pos. [°]	WITHOUT MR COPY OF A.	WITH MR SPACING **8°**
0°		
15°		
30°		
45°		
60°		
75°		
90°		

Table 10.12: Pictures of the grain size distribution - $S_0 = 0.50\%$; $Q = 210$ l/s; $e_d = 40$ mm

WITH MR SPACING **4°**	WITH MR SPACING **2°**
0°	0°
15°	15°
30°	30°
45°	45°
60°	60°
75°	75°
90°	90°

APPENDIX 11

VELOCITY DISTRIBUTIONS IN THE CROSS SECTIONS

This Appendix gives the velocity measurements in the channel. All presented velocity measurements were made at an initial bed slope of 0.50%. The influence of the macro-roughness is shown for a discharge of 210 l/s. The velocity profiles are located every 15° at cross sections from 10° to 85°. Due to the big number of measurement points over the depth (128 points), only every 4th point was used for the vector plots to facilitate the reading.

The first part (Appendix 11.1 and 11.4) shows the tangential velocities. The irregularities (stair-like behaviour) next to the ground are due to the interpolation of the data points.
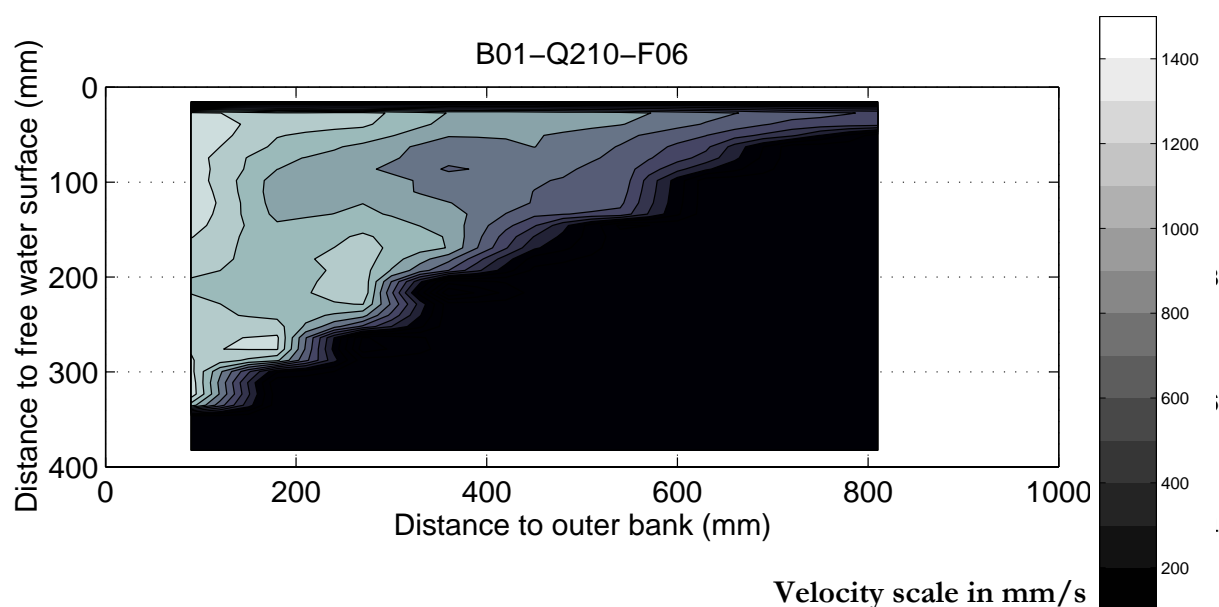
Appendix 11

The second part (Appendix 11.2 and 11.5) presents the velocity vector in the cross section (radial and vertical velocity components. The plot gives a view in downstream direction.

B01–Q210–F06
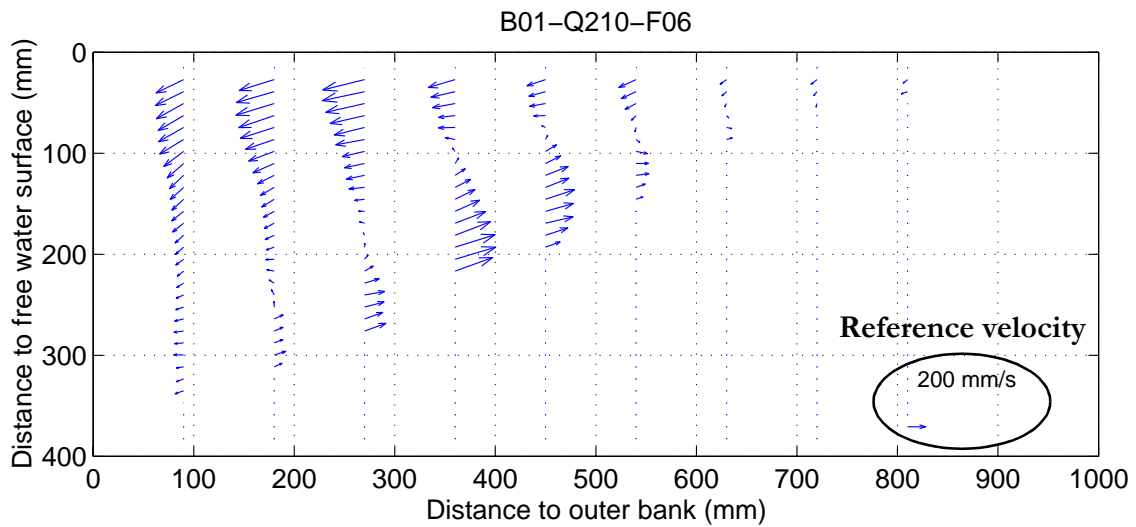
The last part gives the 3D-velocity vectors in the bend. The bend is represented as a prismatic block:

B02–Q210
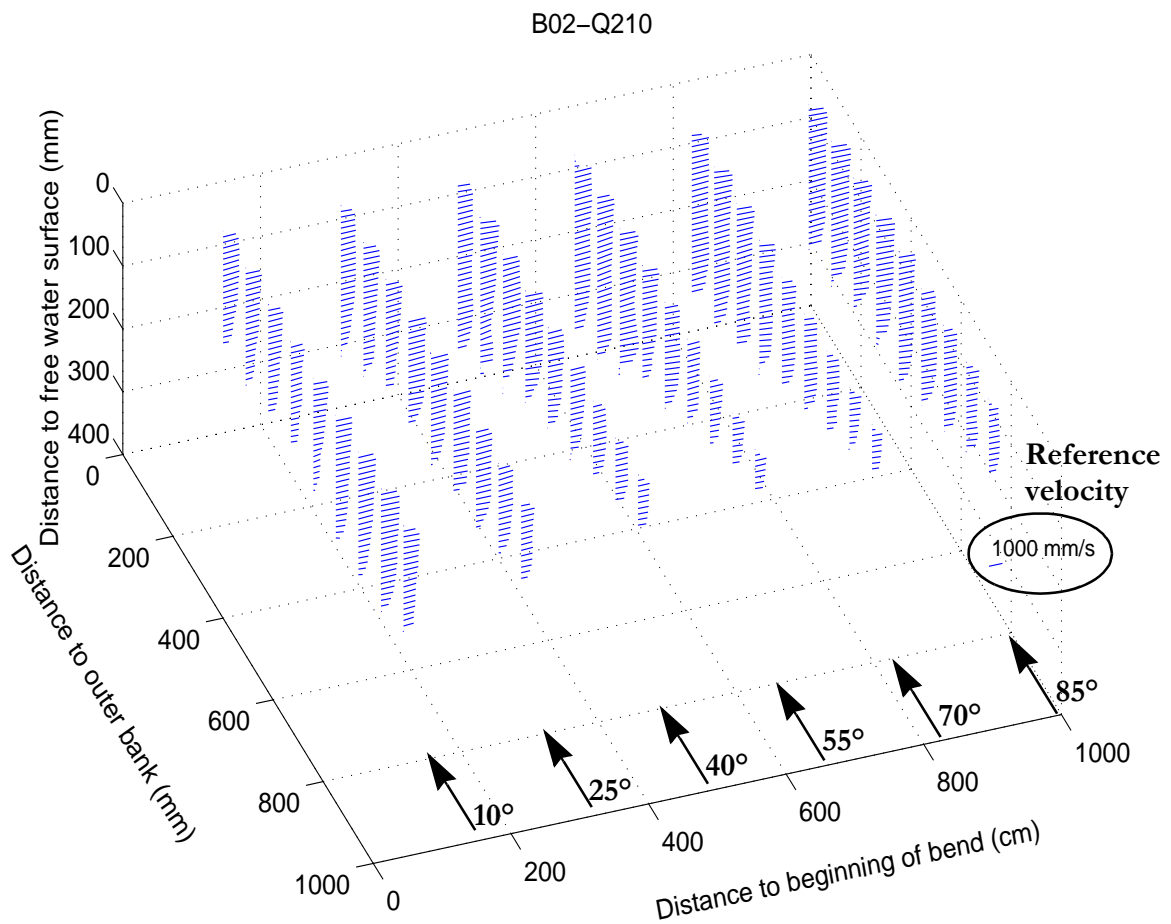
Additional information can be found in the report in Chapter 5.3.1 and 6.6.

11.1 Tangential velocities without macro-roughness
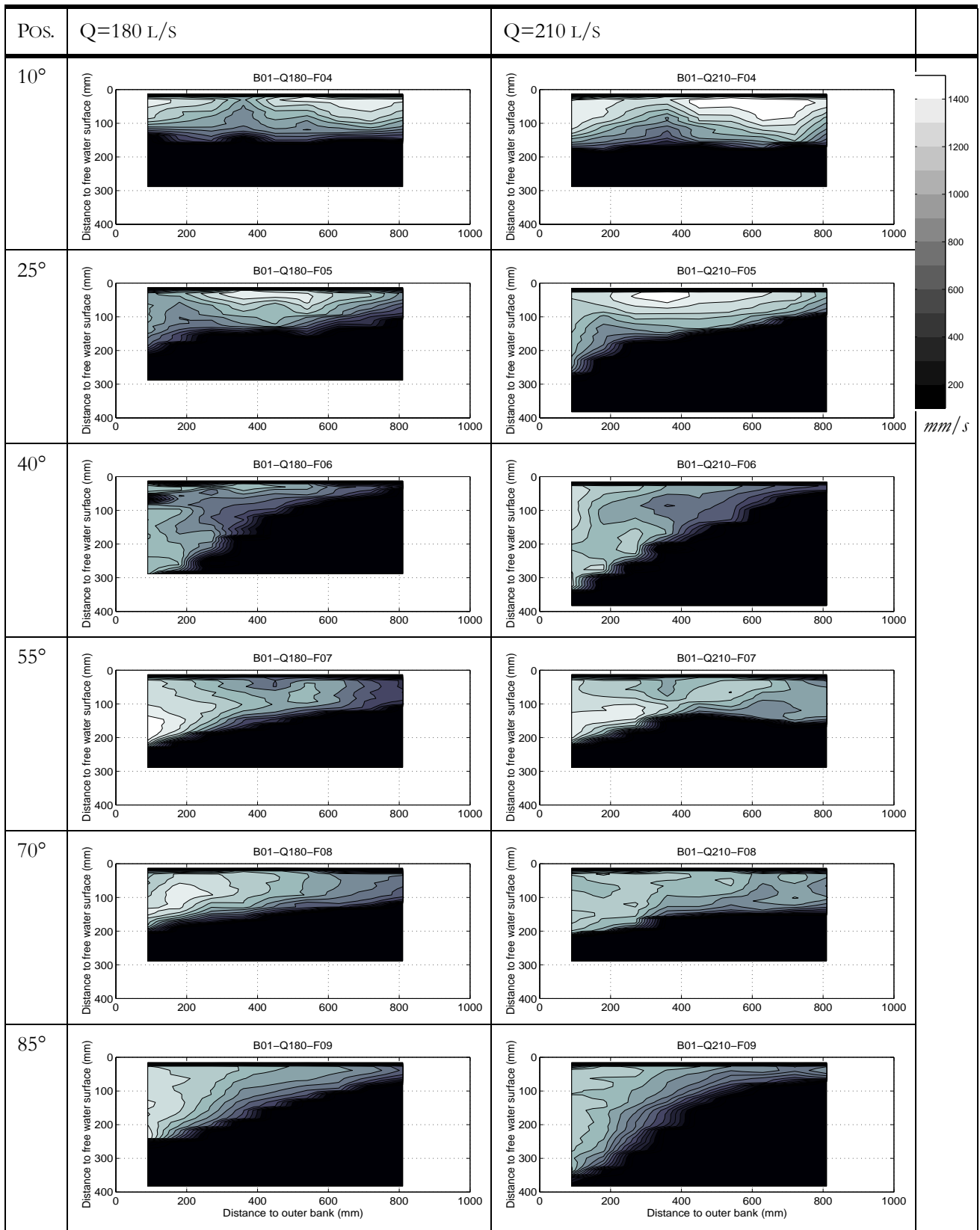
Table 11.1: Tangential velocities, without macro-roughness, $S_0 = 0.50\%$

11.2 Cross section velocities without macro-roughness
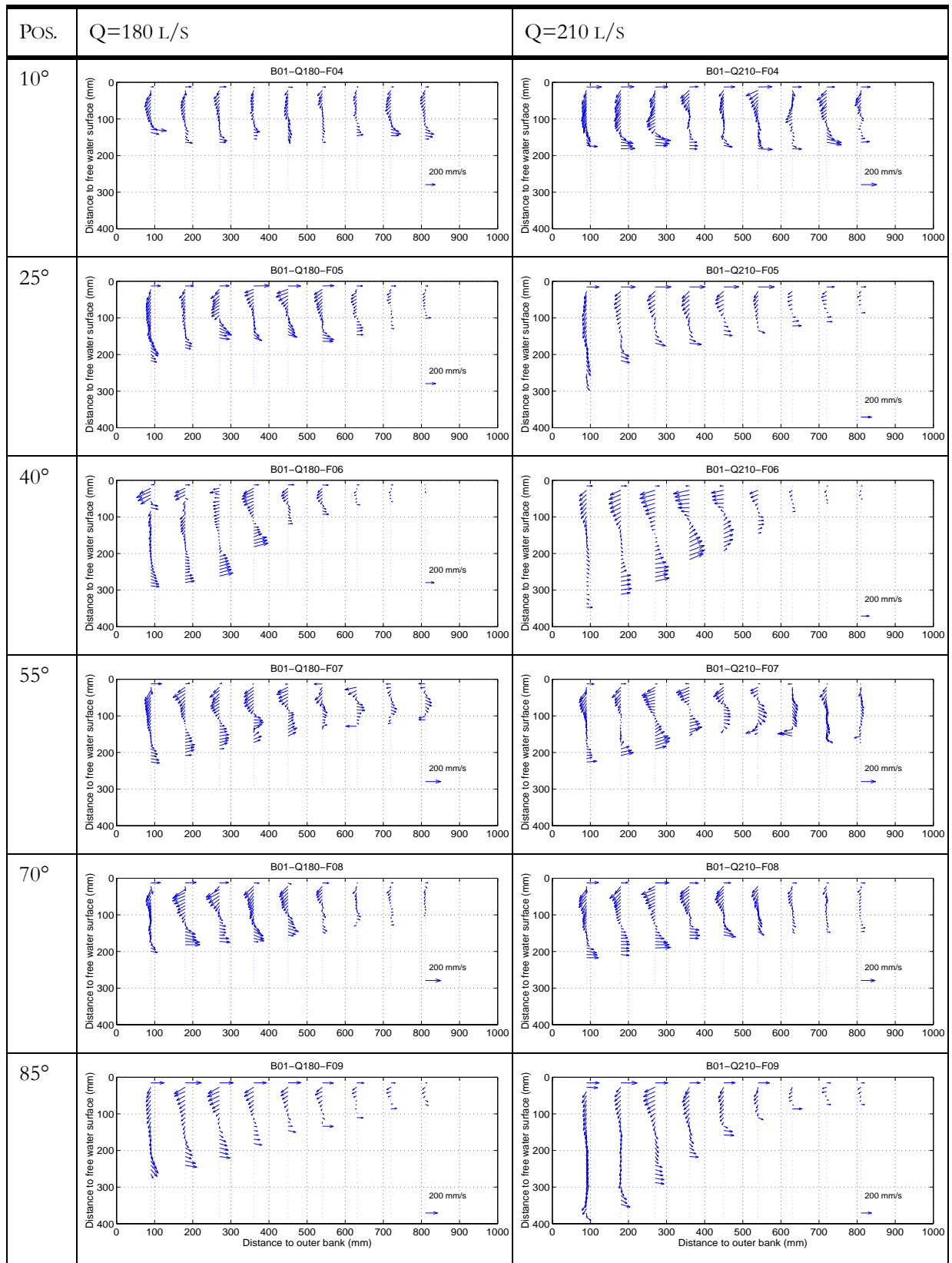
Table 11.2: Velocities in the cross section, without mr, $S_0 = 0.50\%$

11.3 3D-Velocities without macro-roughness
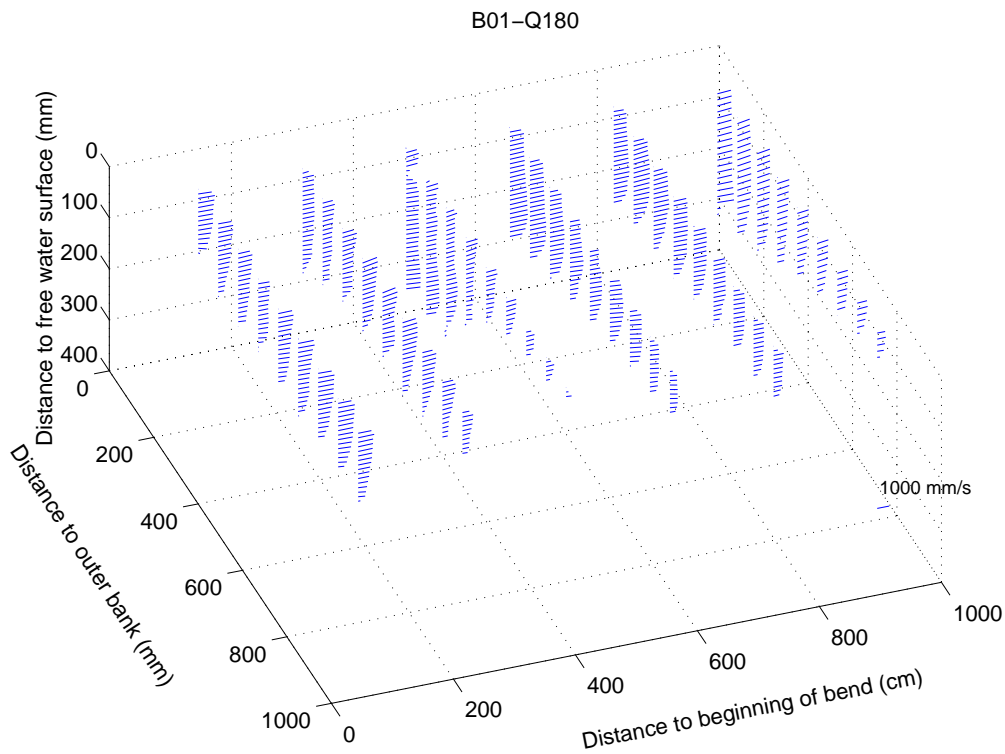
Figure 11.1: 3D-velocity field, $S_0 = 0.50\%$, without macro-roughness, Q=180 l/s
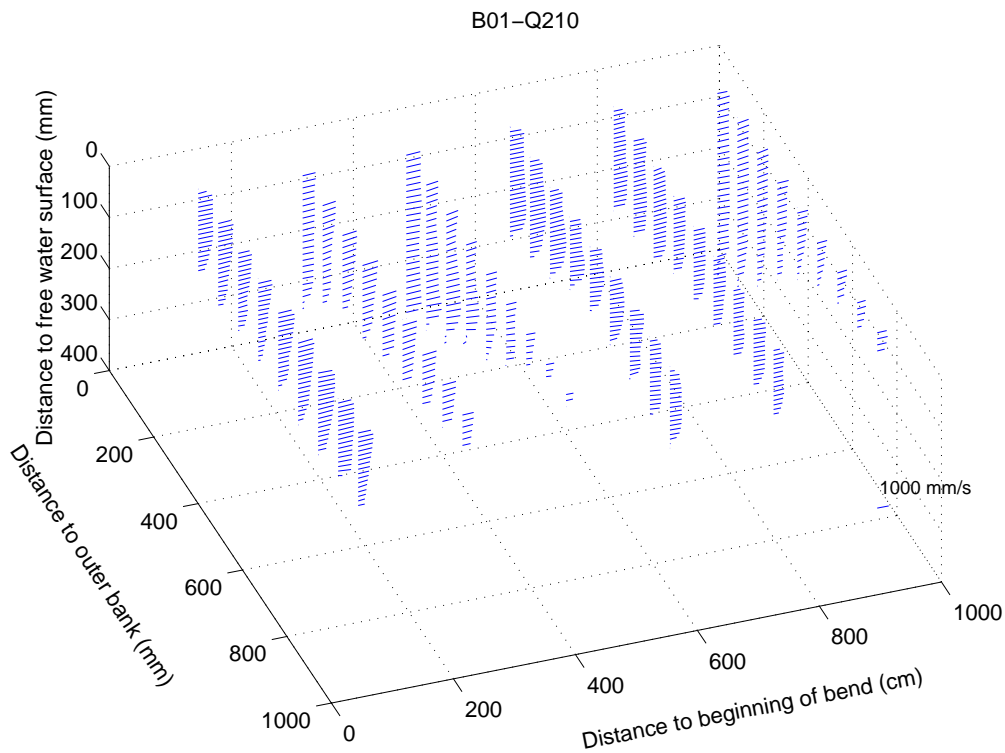
Figure 11.2: 3D-velocity field, $S_0 = 0.50\%$, without macro-roughness, Q=210 l/s

11.4 Tangential velocities with macro-roughness

POS.	WITHOUT MR	MR-SPACING 4°
10°	B01–Q210–F04	B02–Q210–F04
25°	B01–Q210–F05	B02–Q210–F05
40°	B01–Q210–F06	B02–Q210–F06
55°	B01–Q210–F07	B02–Q210–F07
70°	B01–Q210–F08	B02–Q210–F08
85°	B01–Q210–F09	B02–Q210–F09
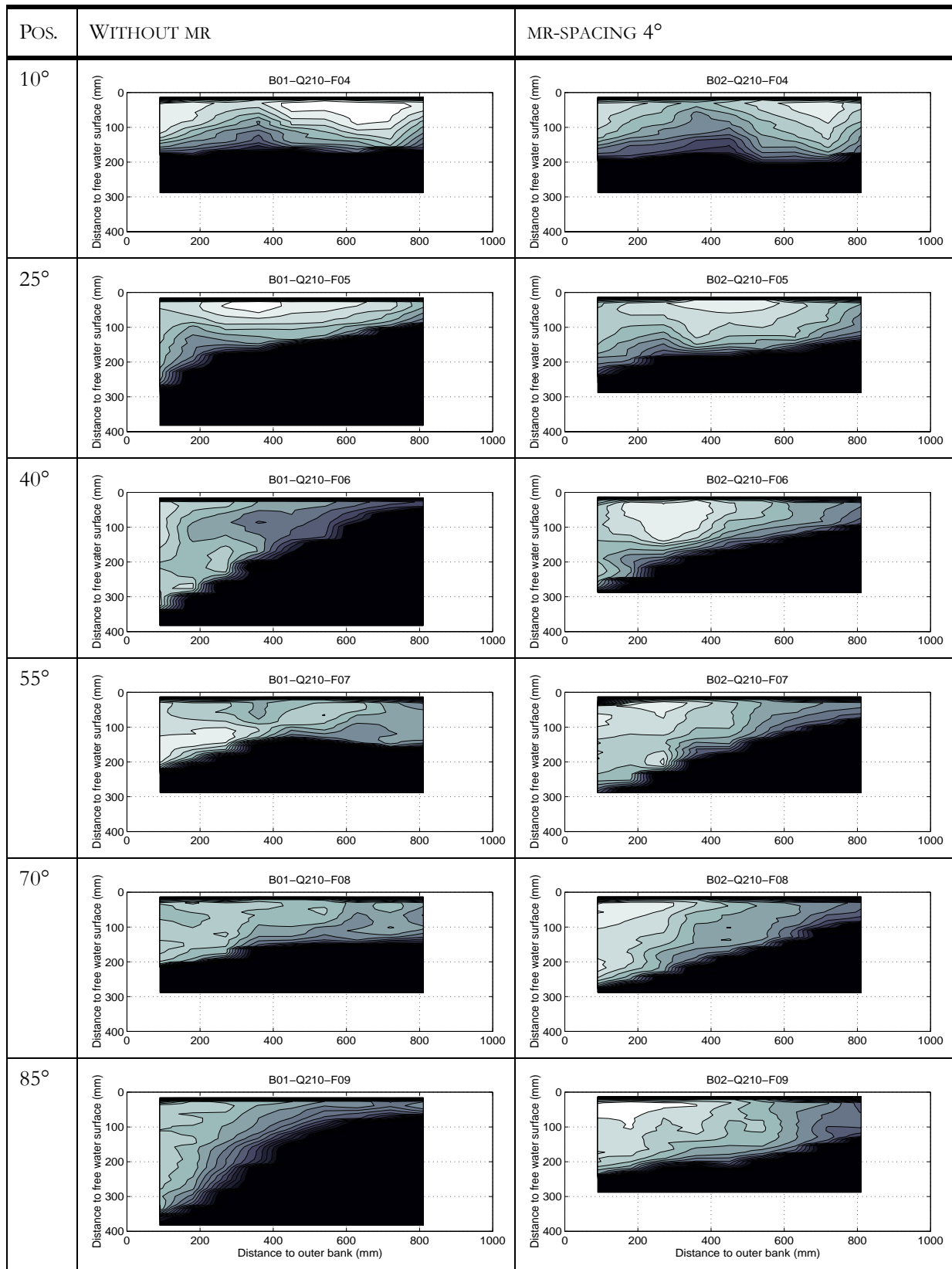
Table 11.3: Tangential velocities, $S_0 = 0.50\%$, Q=210 l/s

Tangential velocities, $S_0 = 0.50\%$, Q=210 l/s

11.5 Cross section velocities with macro-roughness
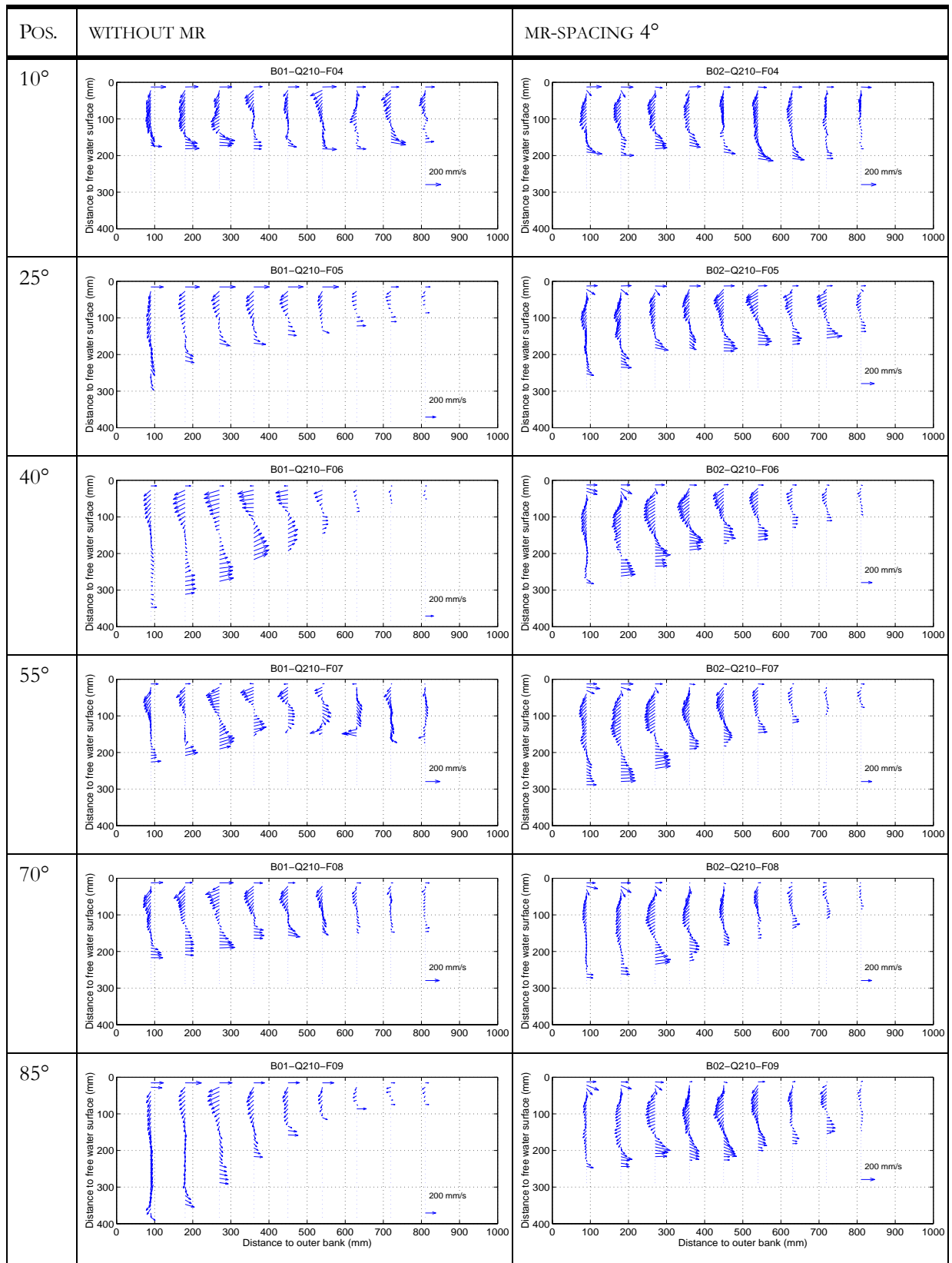
Table 11.4:   *Velocities in the cross section, $S_0 = 0.50\%$, Q=210 l/s*

MR-SPACING 2°	MR-SPACING 1°
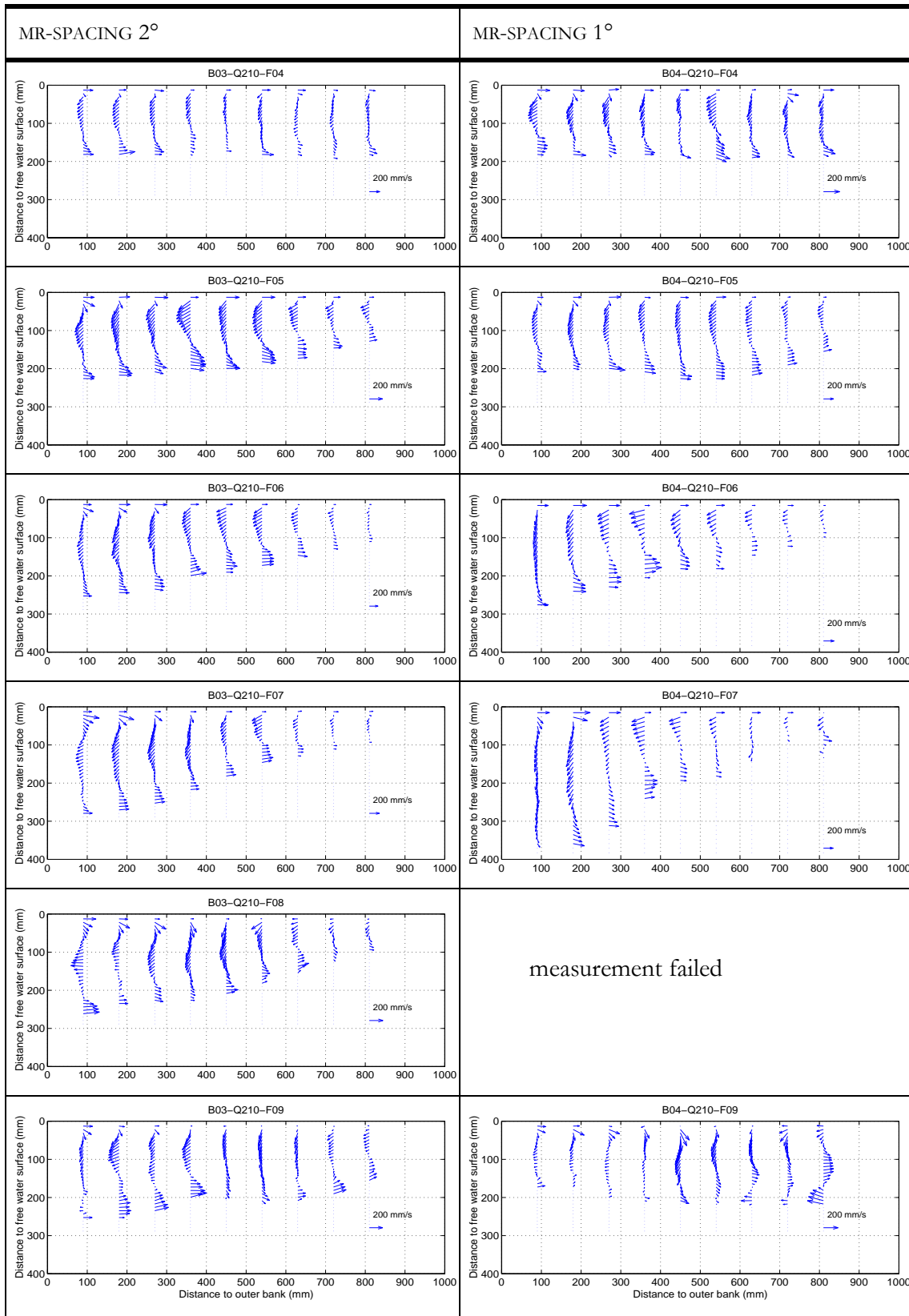
Velocities in the cross section, $S_0 = 0.50\%$, Q=210 l/s

11.6 3D-Velocities with macro-roughness
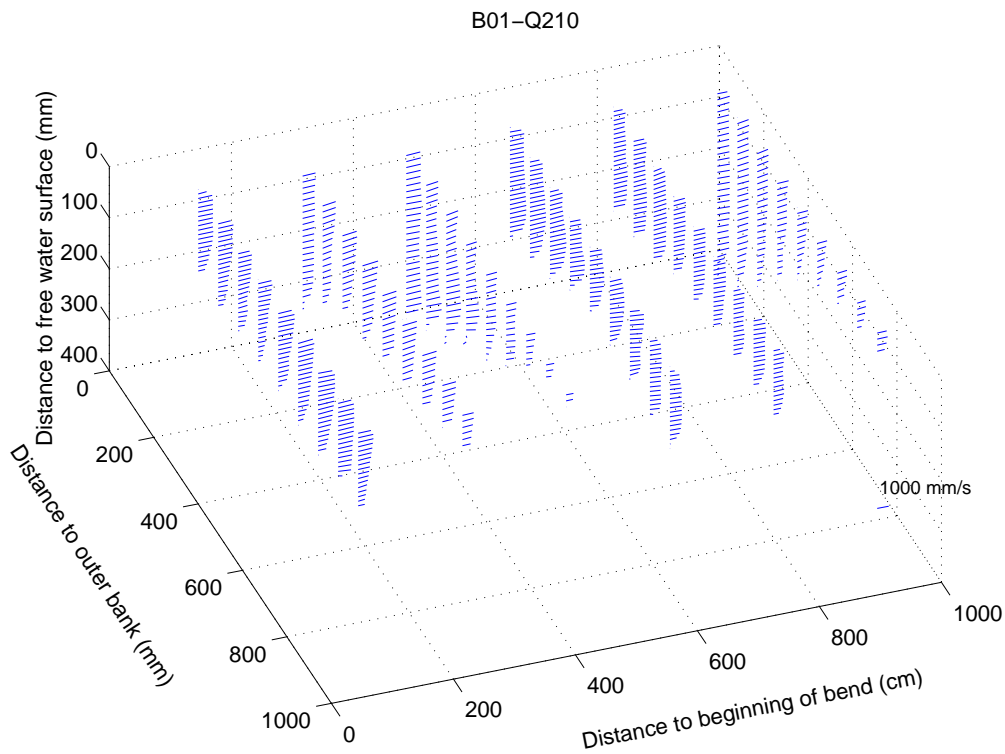
Figure 11.3: 3D-velocity field, $S_0 = 0.50\%$, Q=210 l/s, without macro-roughness
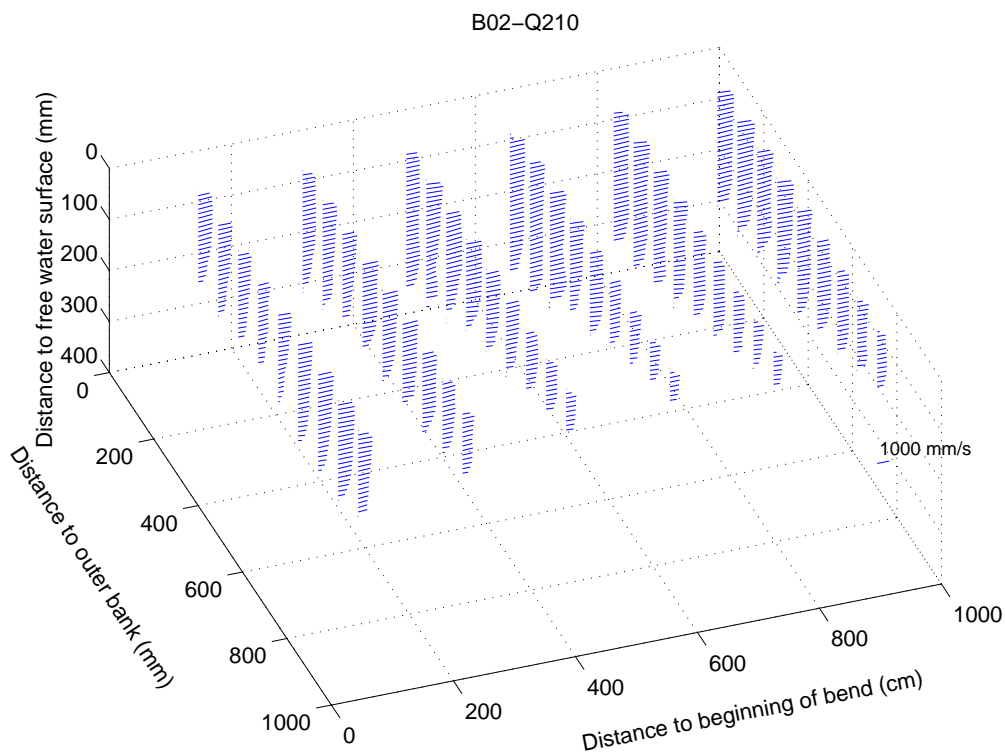
Figure 11.4: 3D-velocity field, $S_0 = 0.50\%$, Q=210 l/s, mr-spacing = 4° (about 40 cm)
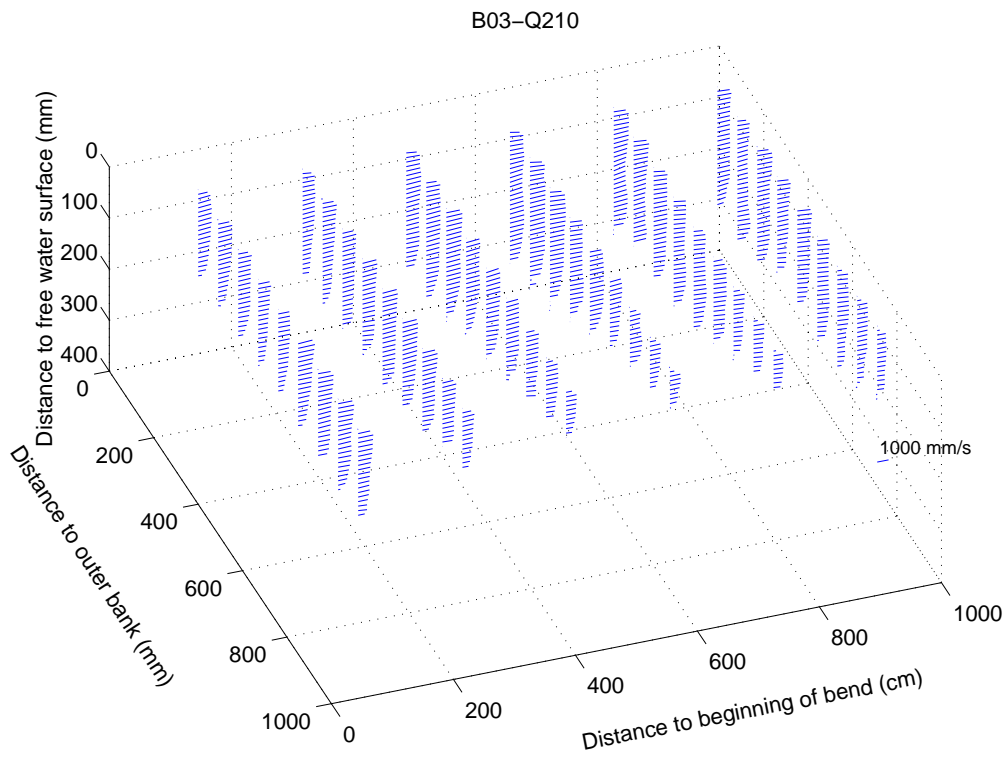
Figure 11.5: 3D-velocity field, $S_0 = 0.50\%$, Q=210 l/ s, mr-spacing = 2° (about 20 cm)
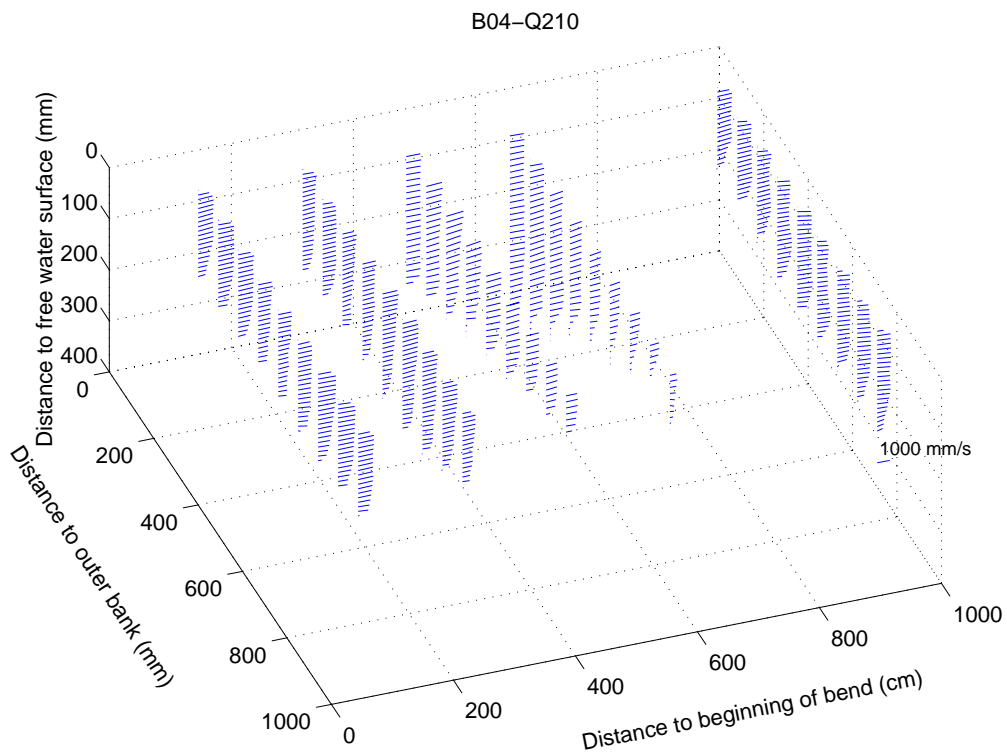
Figure 11.6: 3D-velocity field, $S_0 = 0.50\%$, Q=210 l/ s, mr-spacing = 1° (about 10 cm)

Appendix 11

A-154

APPENDIX 12

RESULTS OF THE GENETIC PROGRAMMING

This appendix gives a small subset of results obtained with the genetic programming GPKernel. Additional information can be found in the report in chapter 7.3.5.

12.1 Results obtained with the data set without mr

Target	ID	Slope	Intercept	r2	RMS	CoD	Fit p node	Hypothesis
hmax12/hm	1	1.091	-0.244	0.832	0.527	0.8323	0.2272	hmax12_hm = ((((sigma + sigma) + (hm_B + ((Fr + ((Fr + (((Fr + (Fr / sigma)) * FrD) * Rc_B)) / sigma)) / sigma)) / sigma)) * ((((d90_hm + FrStar) - hm_B) + TauStar) - hm_B) + 2)
	2	1.065	-0.296	0.830	0.5219	0.83	0.2207	hmax12_hm = (vsatr_v + (1.4909 * (((((Rc_B * FrStar) * d90_hm) + (vsatr_v + vsatr_v) + ((((((d90_hm + TauStar) / sigma) * FrD) + TauStar) / sigma) * (Rc_B * TauStar)))) / ((((TauStar + hm_B) * Rc_B) * (hm_B - TauStar)) + vsatr_v))))
	3	1.021	-0.222	0.828	0.5187	0.8287	0.2232	hmax12_hm = ((((sigma + sigma) + (((FrD + Fr) + ((Fr + ((((hm_B + (Fr * FrStar)) + (Fr / sigma)) * FrD) * Rc_B)) / sigma)) / sigma)) / sigma)) * ((((d90_hm + FrStar) - hm_B) + TauStar) - hm_B) + 2)
	4	1.076	-0.290	0.827	0.5242	0.828	0.2175	hmax12_hm = (((((d90_hm + (((d90_hm + (((d90_hm / FrStar) + FrStar) * (FrD * FrStar))) * FrD) * ((FrD * (d90_hm + (FrStar / sigma))) * (((FrStar / sigma) * Rc_B) * FrStar)))) / (hm_B + (d90_hm / Rc_B))) + 2.458) - (hm_B * Rc_B))
	5	0.987	0.108	0.826	0.5239	0.8263	0.2288	hmax12_hm = (1.5168 * (((((vsatr_v + vsatr_v) + ((Rc_B * TauStar) * (((d90_hm + TauStar) / sigma) * FrD))) + ((Rc_B * FrStar) * d90_hm)) / (((hm_B - TauStar) * (Rc_B * (vsatr_v + hm_B))) + vsatr_v)))
	6	1.177	-0.626	0.823	0.5506	0.8228	0.2279	hmax12_hm = (((((JeAll / TauStar) * (((((vsatr_v + FrStar) * (TanPhi + Rc_B)) + TanPhi) + FrD) + TanPhi)) + ((TauStar * 1.0393424) * (FrD / (TauStar + hm_B)))) / (TanPhi - TauStar)) / (TanPhi - TauStar))
	7	1.034	-0.063	0.823	0.5304	0.8228	0.2216	hmax12_hm = ((((((((TauStar * Rc_B) * (FrStar + Fr)) / sigma) / sigma) / sigma) / sigma) - hm_B * ((Fr + Fr) / vsatr_v)) + (((d90_hm + ((Fr + (sigma * FrStar)) + Fr)) + (d90_hm + Fr)) + 1.26882267))
	8	1.050	-0.134	0.822	0.5299	0.823	0.2315	hmax12_hm = (1.526 * (((((Rc_B * FrStar) * d90_hm) + (vsatr_v + vsatr_v) + (((FrD * (d90_hm + TauStar)) / sigma) * (TauStar * Rc_B)))) / (vsatr_v + ((FrStar * Rc_B) * (hm_B - TauStar)))))
	9	0.983	0.171	0.821	0.537	0.823	0.2216	hmax12_hm = (((((FrD - (hm_B / vsatr_v)) / ((FrD / FrStar) - (Rc_B + (Rc_B + (FrD - (hm_B / vsatr_v)))))) + Fr) * ((FrStar + 0.75481623) + (Fr + hm_B)) - (hm_B / vsatr_v))) + ((Fr + Fr) / Fr))
	10	1.068	-0.351	0.817	0.5412	0.8192	0.2385	hmax12_hm = (((((JeAll + ((JeAll / (FrStar / ((TauStar + Rc_B) + FrD))) + (JeAll / d90_hm))) + FrStar + (JeAll / d90_hm))) / (vsatr_v
	11	0.985	-0.015	0.814	0.5374	0.8181	0.2301	hmax12_hm = (((((JeAll * (((Rc_B / TanPhi) + Rc_B) * FrD)) + FrStar) / (0.117036738 + hm_B)) + (((Fr + (TanPhi + JeAll)) - (hm_B / vsatr_v)) + (TauStar / (d90_hm + d90_hm))) / TanPhi)

Target	ID	Slope	Intercept	r2	RMS	CoD	Fit p node	Hypothesis
hmax12/hm	12	1.072	-0.306	0.816	0.5424	0.8166	0.2335	hmax12_hm = (vstar_v + ((Fr * ((((FrStar * (FrStar + (Fr + TauStar))) * MrSpac) / (hm * TanPhi)) * TauStar)) * FrStar)) + ((Fr - (hm_B / vstar_v)) + (MrDepth_MrSpac + 2.8)))
	13	0.967	0.132	0.815	0.538	0.8152	0.2257	hmax12_hm = (((Fr * ((MrSpac / B) * (FrStar - hm_B))) + (((FrStar * ((hm_B - FrStar) - ((TauStar * (Fr / hm_B)) - hm_B))) + Fr) * ((B / MrSpac) / hm_B))) + (TauStar / TauStar))
	14	0.947	0.194	0.814	0.5411	0.8144	0.2471	hmax12_hm = (((((MrSpac / B) * (FrStar - hm_B)) * Fr) + ((B / MrSpac) / hm_B) * (Fr - (FrStar - hm_B))) + (TauStar / TauStar))
	15	0.950	0.198	0.809	0.5509	0.8095	0.2152	hmax12_hm = ((((Fr * FrStar) * FrStar) + ((Fr * ((FrStar + d90_hm) * MrSpac) / (hm * TanPhi)) * TauStar)) * FrStar)) + ((((Fr + MrDepth_MrSpac) - (hm_B / vstar_v)) + (FrStar * TauStar)) + ((Fr * (TauStar * JeAll)) + 2.6)))
	16	0.941	0.191	0.808	0.5522	0.8103	0.2406	hmax12_hm = (((Fr + ((Fr * ((((FrStar + FrStar) * MrSpac) / Rh) * TauStar)) * FrStar)) - (hm_B / vstar_v)) + (FrStar - (TauStar * 2.1))

| Target	ID	Slope	Intercept	r2	RMS	CoD	Fit p node	Hypothesis
ScourLoc1	17	0.938	2.501	0.885	4.521	0.8849	0.2324	ScourLoc1 = (JeAll - (((sigma * (d90_hm - TanPhi)) / (hm_B * (Fr + vsatr_v))) + ((((sigma * (JeAll * FrD)) / (FrD - sigma)) * (sigma - (Rc_B - 3.75))) - ((Rc_B / (Rc_B - sigma)) * (FrD - sigma)) - (FrD / vsatr_v))))
	18	1.098	-4.381	0.794	6.0545	0.7941	0.2111	ScourLoc1 = ((((((((FrD + (sigma + vsatr_v) + hm_B)) + Fr) / Fr) * (FrD - (((hm_B - d90_hm) * ((Rc_B * TanPhi) / (sigma - FrD)) + Fr)) + Rc_B)) / 0.61177) + sigma) + Rc_B) / 0.46067) + (TanPhi / hm_B))
	19	1.021	-0.910	0.759	6.4091	0.7618	0.2079	ScourLoc1 = ((vsatr_v + ((d90_hm / TauStar) * (sigma * d90_hm))) + ((((((sigma + (vsatr_v / hm_B)) / (d90_hm / TauStar)) + FrD) + TauStar) + TanPhi) / FrStar) + (((5. - (Rc_B - sigma)) / FrStar) + Rc_B))
	20	1.032	-1.402	0.757	6.4839	0.7567	0.2247	ScourLoc1 = (((sigma * FrD) * ((hm_B - -15.678) / (sigma + 0.36)) / TanPhi)) + ((TanPhi / (Fr / sigma)) + (((TanPhi / Fr) / Fr) /

Target	ID	Slope	Intercept	r2	RMS	CoD	Fit p node	Hypothesis
ScourLoc1	21	0.957	1.914	0.753	6.5398	0.7531	0.2002	ScourLoc1 = ((((2.54614568 + (sigma / Fr)) + (FrD + 1.1)) / (hm_B + FrStar)) + (JeAll + Fr) + (FrD + ((Fr + ((FrD + ((Fr + FrD) + (Fr + (FrD + ((sigma - Rc_B) / Fr))))) / Fr)) / Fr))))
	22	0.963	1.658	0.752	6.5464	0.7522	0.2	ScourLoc1 = (((FrD + (((TauStar + hm_B) + TauStar) + (sigma + ((FrStar + (FrD + FrD)) / (hm_B + FrStar))))) + ((FrD / FrStar) + ((TanPhi + sigma) - Rc_B))) + ((TanPhi + FrD) / (((hm_B + Fr) - TanPhi) + FrStar)))
	23	0.961	1.900	0.752	6.5543	0.7521	0.2053	ScourLoc1 = (((TanPhi + FrD) / (((hm_B + Fr) - TanPhi) + FrStar)) + (((FrD / FrStar) + ((TanPhi + sigma) - Rc_B) + (FrD + ((sigma + (FrStar + (FrD + FrD)) / (hm_B + FrStar))) + TauStar))))
	24	0.985	0.353	0.750	6.6149	0.7464	0.2265	ScourLoc1 = ((FrD / (((FrD + Rc_B) * TauStar) / sigma)) + ((sigma + (FrD / (Fr / FrD))) + ((FrD + 3.52) / (sigma / 3.96))))

Target	ID	Slope	Intercept	r2	RMS	CoD	Fit p node	Hypothesis
ScourLoc2	25	0.838	74.306	0.394	4.5368	0.8827	0.2319	ScourLoc2 = (((sigma + ((FrStar / ((13.22 / FrD) - FrD) / Rc_B)) + ((8.365 - Rc_B) / (hm_B + Fr)) - (sigma / ((((11.97 / FrD) - FrD) / (hm_B + (Fr + ((Fr - FrD) / Rc_B))) + Rc_B))))) + FrD) / FrStar)
	26	0.861	70.846	0.376	6.3088	0.7689	0.207	ScourLoc2 = (((vsatr_v + (vsatr_v / (FrD / sigma))) / (d90_hm + hm_B)) * (((((vsatr_v + vsatr_v) / (hm_B + (FrStar * (FrStar + Fr)))) / FrStar) + TanPhi) / FrStar)) + ((3 * (FrD * FrD)) + (FrD * 3)))
	27	0.901	71.588	0.342	6.5973	0.7474	0.2384	ScourLoc2 = ((Rc_B + (FrD / (vsatr_v + d90_hm))) + (((5.03865 + FrD) + (sigma - Rc_B)) + sigma) / (hm_B + FrStar))

Target	ID	Slope	Intercept	r2	RMS	CoD	Fit p node	Hypothesis
ScourLoc2	28	1.133	-16.0	0.676	10.05	0.6759	0.182	ScourLoc2 = ((((-1.4084041 * Rc_B) + (((((-1.4672766 * FrD) / Rc_B) + (Rc_B / -1.08963454)) / 9.73) + Rc_B)) / ((FrD + (-1.4892728 / (FrD + FrD))) + (-1.4677951 * Rc_B)) + ((FrD + (9.36 - Rc_B)) * (9.73 + Rc_B)))
	29	1.128	-13.3	0.670	10.051	0.6703	0.1856	ScourLoc2 = ((((-1.4672766 * Rc_B) + (((Rc_B / Rc_B / -1.08963454)) / 9.73) + Rc_B)) / ((FrD + (-1.4892728 / (FrD + FrD))) + (-1.4677951 * Rc_B)) + ((FrD + (9.22 - Rc_B)) * (9.73 + Rc_B)))
	30	0.976	3.038	0.665	9.9945	0.6655	0.1769	ScourLoc2 = ((12.174943 * 10.6214104) - ((((((Rc_B - FrD) / (TauStar * (Rc_B - FrD))) * Rc_B + 11.0072079)) * Rc_B) + (Fr + Rc_B) / Rc_B)) + ((TauStar + (Rc_B - FrD)) / ((Rc_B - 1.0952) - FrD))) / FrD) + vstar_v))
	31	1.004	-7.775	0.625	10.565	0.6254	0.1663	ScourLoc2 = ((((FrD + 3e+001) + (FrD + 3e+001)) / (FrD + 3e+001) + 3e+001)) - ((FrD - Rc_B) * ((d90_hm + -7.48) + (sigma + (((Rc_B - FrD) * ((sigma + (Rc_B - FrD)) + (d90_hm + -7.68))) - (FrD - Rc_B))))))
	32	0.970	3.858	0.620	10.659	0.62	0.1841	ScourLoc2 = ((((Fr + (Fr + Rc_B)) + Fr) * ((FrD + FrD) - (Fr + (Fr + Rc_B)))) + ((3.01764035 + 9.) * (8.8 + FrStar)) + 3.05906868))

Table 12.1: A small selection of results obtained with GPKernel without macro-roughness (with Peters tests)

12.2 Results obtained with the dataset with mr

Target	ID	Slope	Interc.	r2	RMS	CoD	FitPNod	Hypothesis
hmax12/hm	101	0.941	0.102	0.896	0.445	0.895	0.256	hmax12_hm = ((ed/es + (((JeAll / (ed/es + (ed/es + ((FrStar * (TanPhi - (FrStar + FrStar))) + ed/es))) * TanPhi)) * FrD) + (FrStar + (TanPhi * (Vstar/V))))) / (hm/B + (Vstar/V)))
	102	0.924	0.167	0.895	0.438	0.895	0.238	hmax12_hm = (FrD + ((((Rc/B / ((sigma * (((((hm/B * hm/B) * sigma) / TauStar) / TauStar) * ((ed/es + (d90/hm * hm/B)) * (hm/B / d90/hm)))) + d90/hm)) + (FrStar - ((sigma * (hm/B * FrD)) / d90/hm))) * d90/hm) * Fr))
	103	0.874	0.452	0.895	0.445	0.896	0.241	hmax12_hm = (FrD + ((((d90/hm - ((sigma * hm/B) / d90/hm)) + (Rc/B / ((sigma * (((ed/es + (hm/B * hm/B)) * (hm/B / TauStar)) * ((((hm/B * hm/B) * sigma) / TauStar) / TauStar))) + d90/hm)) * d90/hm) * Fr))
	104	0.894	0.328	0.894	0.440	0.893	0.247	hmax12_hm = (hm/B + ((((ed/es + (FrStar * (TanPhi - (FrStar + FrStar))) + ((JeAll / ((TanPhi * (ed/es + ((TanPhi - (FrStar + FrStar)) + FrStar))) + ed/es)) * FrD)) + FrStar) / (hm/B + (Vstar/V))))
	105	0.939	0.232	0.894	0.449	0.893	0.265	hmax12_hm = (((Vstar/V) + ((ed/es + FrStar) + (JeAll / ((((FrStar * (TanPhi - (FrStar + FrStar))) + ed/es) * TanPhi) + ed/es)) * FrD)))
	106	0.885	0.378	0.893	0.442	0.893	0.240	hmax12_hm = (2.28 + (((hm/B + Fr) + ((TauStar - hm/B) * (Rc/B + Rc/B)) * (3.09 * ((Rc/B + (2.37 * ((((FrD + hm/B) - Rc/B) - 2.32) + ((FrStar + 3.17) + TanPhi))) + FrStar)) * (FrStar - hm/B)))))
	107	0.904	0.249	0.891	0.442	0.892	0.237	hmax12_hm = ((((((FrD + (FrD / TanPhi)) * (JeAll * ((FrD / TanPhi) / TanPhi)) + TauStar) / (hm + (TauStar / (Rc/B - Fr))) + (ed/es + ed/es)) + (FrD / (sigma + (FrD * FrStar))) + ((ed/es + ed/es) + hm/B))
	108	0.883	0.326	0.889	0.448	0.889	0.246	hmax12_hm = ((hm/B + (Vstar/V)) + (((Vstar/V) + ((JeAll + FrStar) + (FrD * (JeAll / (ed/es + (TanPhi * (ed/es + (((FrStar * (TanPhi - (FrStar + FrStar))) + JeAll) + ed/es))))))) / (hm/B + (Vstar/V))))
	109	0.853	0.360	0.881	0.468	0.881	0.262	hmax12_hm = ((FrD / (sigma + sigma)) + ((FrStar + (FrStar + Fr)) / (((1.0149 + (Rc/B / (ReStar * hm/B))) / (Rc/B * Rc/B)) + (Rc/B *
	110	0.899	0.341	0.878	0.468	0.880	0.267	hmax12_hm = (((d90/hm + FrStar) * ((FrD / ((Vstar/V) / JeAll)) / (FrStar + ed/es)) + FrD)) / (hm/B + (TanPhi + (-0.621393681 +
	111	0.936	0.962	0.876	0.475	0.878	0.261	hmax12_hm = ((Fr * (((TanPhi - ((JeAll + (JeAll + TauStar)) / (ed/es + (hm/B + ed/es)))) * (((hm/B + ed/es) / hm/B) - Rc/B)) + 3)) + 2)

Target	ID	Slope	Intercep	Correlat	RMS	CoD	Fit p nod	Hypothesis
hmax12/hm	112	0.801	0.603	0.895	0.444	0.896	0.248	hmax12_hm = (((((((Vstar/V) + TauStar) * MrSpac) * ((TauStar * Fr) / 1.4)) / Rh) + ((sigma * ((FrStar - hm/B) - hm/B)) - ((((TauStar * F
	113	0.875	0.292	0.894	0.440	0.895	0.235	hmax12_hm = ((((FrStar * ((((MrSpac / Rh) + FrStar * (((MrSpac / hm) * TauStar) - ((((MrSpac / hm) * TauStar) + Vstar/V)) + TauSta
	114	0.853	0.425	0.894	0.439	0.894	0.252	hmax12_hm = (((((((sigma + (((MrSpac / Rh) + (d90/hm / TauStar) - (Vstar/V))) * Fr)) * 0.24882) * (FrStar + TauStar)) * FrStar) + (Fr +
	115	0.948	0.274	0.894	0.442	0.895	0.256	hmax12_hm = ((((((MrSpac * ((Vstar/V) + TauStar)) * ((TauStar * Fr) / 1.1)) / Rh) + (sigma * (((Vstar/V) + ((ed/es + ed/es) * (Fr * TauSt
	116	0.905	0.202	0.893	0.441	0.894	0.271	hmax12_hm = ((((((MrSpac * ((Vstar/V) + TauStar)) * ((TauStar * Fr) / 1.2)) / Rh) + (1.3 * ((FrStar - hm/B) - hm/B))) + 1.) + Fr)
	117	0.872	0.395	0.893	0.442	0.893	0.271	hmax12_hm = (d90/hm + (((Rh + (TauStar * ((MrSpac * (Fr + ((sigma * d90/hm) + d90/hm))) * (TauStar * (TauStar + 2.1))))) + hm) / h
	118	0.959	0.248	0.892	0.448	0.893	0.277	hmax12_hm = (((((((Vstar/V) + TauStar) * MrSpac) * ((TauStar * Fr) / 1.1)) / Rh) + ((FrStar - hm/B) - hm/B)) + Fr) + 1.1)
	119	0.912	0.300	0.891	0.445	0.893	0.237	hmax12_hm = (TanPhi - (((Rc/B * (Vstar/V)) - TanPhi) - ((ed/es + ((((Fr + hm/B) / (Rc/B * ((Vstar/V) * (MrSpac / Rh))) + (Vstar/V))) + (
	120	0.928	0.171	0.888	0.452	0.889	0.302	hmax12_hm = (Fr + (((((Fr * TauStar) + (Vstar/V)) / (hm / MrSpac)) * TauStar) + (TauStar + Fr)))
	121	0.886	0.307	0.886	0.452	0.887	0.301	hmax12_hm = (((TauStar * Fr) * ((((MrSpac / hm) * TanPhi) * FrStar) + (TauStar * Fr))) + 1.72925019)
	122	0.886	0.308	0.886	0.452	0.887	0.313	hmax12_hm = (((TauStar * Fr) * ((((MrSpac / hm) * TanPhi) * FrStar) + TauStar)) + 1.72925019)
	123	0.886	0.306	0.886	0.452	0.887	0.327	hmax12_hm = (((TauStar * Fr) * (((MrSpac / hm) * TanPhi) * FrStar)) + 1.72925019)

Target	ID	Slope	Intercep	Correlat	RMS	CoD	Fit p nod	Hypothesis
ScourLoc1	124	0.679	14.428	0.678	6.787	0.672	0.177	ScourLoc1 = (((((ed/es + ed/es) / ((ed/es + ed/es) + (hm/B - Fr))) + (((Vstar/V) + hm/B) + ((sigma / Fr) + ((hm/B + ((TauStar + hm/B) + ed/es)) / hm/B)))) / (Vstar/V)) - ((hm/B / (TauStar / Rc/B) + ed/es)) - 1.028))
	125	0.679	14.428	0.678	6.625	0.679	0.183	ScourLoc1 = (Rc/B + ((((0.995146334 + Rc/B) + Rc/B + (((sigma / 0.50072521) + ((-2.102943 - (0.437273562 / d90/hm)) + ((1.04013717 + 1.55438721) / (ed/es + (Vstar/V)))) * 0.440248221 + (Rc/B * (ed/es - (Vstar/V))))) / FrStar)) + (Fr / d90/hm)))
	126	0.674	14.410	0.672	6.713	0.670	0.176	ScourLoc1 = (((((ed/es * (((sigma / (Vstar/V)) + (Vstar/V)) / ((Vstar/V) + ed/es))) + FrD) / ((Fr * ((TauStar + hm/B) * TauStar)) + ed/es)) + (((13 - sigma) * ((sigma / (Vstar/V)) + (Vstar/V))) - Rc/B) - ((Vstar/V) + Rc/B))) + (8.1 / sigma))
	127	0.637	16.098	0.666	6.778	0.665	0.179	ScourLoc1 = ((((7.32664 + (((ed/es / (TauStar / d90/hm)) / (TauStar - ed/es) + ed/es)) * 9.59248) + (7.53953 / Rc/B))) * ((FrD / sigma) + sigma)) + ((((sigma * sigma) + TauStar) + (FrD / sigma)) + ed/es) / Fr))
	128	0.643	16.073	0.663	6.797	0.662	0.174	ScourLoc1 = ((((23.08 + (sigma + ((ed/es / ((ed/es + JeAll) + JeAll)) / hm/B))) + hm/B) + (((((((((FrD - hm/B) - FrStar) - FrStar) - hm/B - hm/B) - hm/B) - Fr) + (ed/es / ((ed/es + JeAll) + JeAll))) / FrStar) / FrStar)
	129	0.638	15.827	0.661	6.811	0.661	0.174	ScourLoc1 = ((1.65601122 * ((((((TanPhi + sigma) / (((FrStar + (ed/es + hm/B)) + hm/B) + d90/hm)) + FrD) * 1.08924353) + FrD) - ((ed/es + ed/es) + (Fr + sigma) + ed/es)) + (ed/es * ((sigma / (TauStar + ed/es)) / FrStar))) * 2.96379709)
	130	0.686	13.746	0.661	6.811	0.661	0.176	ScourLoc1 = (((FrD - (sigma * ((sigma - ((d90/hm / ((TauStar / Rc/B) + ed/es) * (TauStar / d90/hm) + ((Fr / (d90/hm / TauStar)) + (d90/hm / Rc/B)))) + -2.6732)) * -2.7007)) / (Fr * FrStar)) * Fr)
	131	0.632	19.457	0.661	6.845	0.658	0.173	ScourLoc1 = (3e+001 + ((((((ed/es + TauStar) * 0.5005153) + FrD) * (TauStar + 0.4463221)) / TauStar) + ((Fr * Rc/B) / (((ed/es + (TauStar + ed/es)) + ed/es) * (TauStar - (sigma + (sigma + ((ed/es + TauStar)) / (Fr * (ed/es + hm/B))))))))
	132	0.646	15.518	0.659	6.829	0.659	0.175	ScourLoc1 = ((((((TauStar / hm/B) - (Fr - (sigma + (FrD / sigma)))) + (((ed/es / TauStar) * FrD) * (d90/hm / (ed/es + (TauStar / sigma))))) * ((FrD + (sigma / (hm/B + Fr))) + (sigma + (FrD / sigma)))) + 13.35)
	133	0.617	16.927	0.655	6.876	0.656	0.172	ScourLoc1 = ((ed/es + (Vstar/V)) / ((hm/B + (Vstar/V)) * ((ed/es + ed/es) * ((ed/es + (ed/es + ed/es)) + ed/es)) + (Vstar/V))) / ((((hm/B + (TanPhi + (sigma + TanPhi))) / Fr) + (TanPhi + (TanPhi + FrD))) / (Vstar/V) + (-0.36 * (Vstar/V)))))
	134	0.635	16.853	0.649	6.949	0.649	0.173	ScourLoc1 = ((((FrD + (((ed/es / hm/B) + sigma) + (FrD + ((ed/es / (ed/es + d90/hm)) / (ed/es + d90/hm)))) + ((((FrStar / d90/hm) / Rc/B) - (d90/hm + hm/B)) + (ed/es / (ed/es + hm/B))))) / 0.692852259) + hm/B)) / FrStar)
	135	0.666	14.487	0.647	6.948	0.648	0.170	ScourLoc1 = (((TanPhi / Fr) + ((TanPhi + (((TanPhi + ((TanPhi + (TanPhi - (hm/B / ((Vstar/V) + (TanPhi * (ed/es * Rc/B)))))) / TanPhi) / TanPhi) / (Vstar/V))) - (sigma / TanPhi))) + (1.577 + sigma) / (Fr * (((Vstar/V) / TanPhi) / TanPhi)))
	136	0.672	14.652	0.646	6.963	0.646	0.172	ScourLoc1 = ((sigma + ((((FrD + ((Vstar/V) + (ed/es / (TauStar + ed/es)))) / hm/B)) + ((sigma / (hm/B + Fr)) / Fr)) / (Vstar/V) + ((0.4843 / hm/B) + (FrD + sigma))) / ((Vstar/V) + (ed/es / (TauStar + ed/es))))

Target	ID	Slope	Intercep	Correlat	RMS	CoD	Fit p nod	Hypothesis
ScourLoc1	137	0.610	17.385	0.659	6.858	0.659	0.173	ScourLoc1 = (((14 / sigma) / (-1.10085762 + Rc/B)) + ((((10.969317 + (-0.99416447 + 9.6783514)) + FrD) / sigma) + FrStar + (FrStar
	138	0.645	15.671	0.655	6.867	0.655	0.172	ScourLoc1 = (((((8.570672 + FrD) + 9.5934744) + FrD) / sigma) + (FrStar + ((sigma / FrStar) * (FrD + ((TanPhi / (((Vstar/V) - FrStar)) -
	139	0.744	11.253	0.610	7.588	0.608	0.162	ScourLoc1 = (((d90/hm / FrStar) + (((ed/es * (d90/hm / d90/hm)) + ((sigma + FrStar) / JeAll + (JeAll + (TanPhi * (JeAll + (TanPhi * ed
	140	0.524	20.729	0.505	8.236	0.505	0.133	ScourLoc1 = (((sigma + ((TanPhi - Fr) + (sigma + ((Rc/B * ed/es) + (0.1991 - hm/B) - sigma))))) / 5.87961972e-002) - (ed/es + ((Rc/B

Target	ID	Slope	Intercep	Correlat	RMS	CoD	Fit p nod	Hypothesis
ScourLoc2	141	0.621	36.726	0.718	9.775	0.718	0.189	ScourLoc2 = ((((42.6895981 + (FrD + (((FrD - Rc/B) / FrD) / ((sigma - FrD) * Rc/B)))) + ((((sigma - FrD) / (FrD - Rc/B)) / FrD) - FrD) - F
	142	0.605	38.869	0.715	9.878	0.715	0.188	ScourLoc2 = (((((FrD - ((-3.61804056 * (FrD - sigma) * (FrD - sigma) * FrD))) + ((Rc/B - sigma) * Rc/B) * Rc/B))) + ((Rc/B - sigma) /
	143	0.712	27.445	0.706	9.741	0.706	0.193	ScourLoc2 = ((((44.3062325 + (FrD + (sigma + (((FrD - Rc/B) / Rc/B) / (FrD * (sigma - FrD)))))) + ((FrD - Rc/B) - Rc/B)) + 42.8187065)
	144	0.683	31.215	0.693	9.958	0.693	0.195	ScourLoc2 = ((Rc/B - (((((5.6 + Rc/B) * (hm/B + FrD)) * ((Rc/B + (Vstar/V)) - (FrD + FrStar))) / sigma) + (sigma + FrD))) + (6.1 * (Rc/B
	145	0.660	34.474	0.691	9.991	0.691	0.184	ScourLoc2 = ((((Rc/B + (hm/B * 3.74601)) + (18 + hm/B)) + ((0.9 + (3.87632 + (hm/B * 3.74601)) - Fr)) + ((hm/B * (Fr * ((FrD - Rc/B) *

Table 12.2: A small selection of results obtained with GPKernel with macro-roughness (with Peters tests)

12.3 Computation of the scour reduction

Target	ID	Slope	Intercep	r2	RMS	CoD	Fit p no	Hypothesis
ScourRed	301	0.123	-0.166	0.117	0.1086	0.8057	0.2142	ScourRed = (((MrDepth_MrSpac * (v + (TauStar + (hm * 4.04)))) - (((((((((B / (d90 + Q)) - 4.09914) - (Q / d90_hm)) / TauStar) - TauStar) / ((TauStar + -0.9) + v)) / Re) / ((Q + TauStar) * Q))) - Q)
	302	0.218	-0.208	0.100	0.1198	0.8108	0.213	ScourRed = (((Rh - ((((1.13 + JeAll) / (Q * Q)) / ((Q - Rh) * ReStar)) * d90_hm) * (((TanPhi + MrDepth_MrSpac) / JeAll) / ((ReStar * Q) * ((JeAll + TauStar) + ((Rh * (MrDepth_MrSpac - B)) + Q))))) - (Q - MrDepth_MrSpac))
	303	0.291	-0.200	0.100	0.123	0.8239	0.2164	ScourRed = ((((MrDepth_MrSpac * v) - ((((((((B / Q) - 4.40817) - (Q / d90_hm)) / TauStar) - (v / Q)) / (v + (TauStar + -0.9))) / Re) / (Q * (Q + Q)))) - (Q + ((Q + (Q + -0.9)) * Q)))

Target	ID	Slope	Intercep	r2	RMS	CoD	Fit p no	Hypothesis
ScourRed	304	11.680	-0.306	0.119	0.2557	0.7667	0.2014	ScourRed = ((hm_B - (((d90_hm / (FrD + d90_hm) - (((hm_B + FrStar) + d90_hm) / (d90_hm / d90_hm)))) / FrStar) / FrD)) * ((d90_hm + (FrStar * MrDepth_MrSpac)) / (TauStar / (((d90_hm / ((FrD + -5.74087e-002) - (FrStar + d90_hm))) / FrStar) / FrD))))
	305	0.534	-0.227	0.112	0.1735	0.7317	0.1922	ScourRed = ((hm_B - (((d90_hm / ((MrDepth_MrSpac + FrD) - ((TauStar + d90_hm) / FrStar)) / FrStar) / FrD)) * ((d90_hm / ((FrD + hm_B) - MrDepth_MrSpac)) / FrStar) / FrD) / (TauStar / (((FrStar * MrDepth_MrSpac) + d90_hm) / (TauStar / (sigma / FrD))))))
	306	5.393	-0.310	0.102	0.2477	0.7608	0.2077	ScourRed = ((hm_B - ((d90_hm / ((FrD + -5.41769e-002) - (FrStar + d90_hm))) / FrStar) / FrD)) * (((FrStar * MrDepth_MrSpac) + (((d90_hm / FrD) / hm_B) / FrD)) / (TauStar / ((d90_hm / (FrD - MrDepth_MrSpac)) / FrStar))))

Table 12.3: Results of the computation of scour depth reduction obtained with GPKernel
The data set contained only the tests with ribs

Target	ID	Slope	Intercep	r2	RMS	CoD	Fit p no	Hypothesis 2
		Hypothesis 2						
ScourRed	201	2.003	-0.504	**0.362**	0.227	0.5212	0.1377	ScourRed = (hm_B * ((vsatr_v + MrDepth_MrSpac) * (FrD + (d90_hm / ((MrDepth_MrSpac + (vsatr_v * vsatr_v)) +
	202	2.750	-0.541	**0.334**	0.2422	0.4672	0.1284	ScourRed = ((((MrDepth_MrSpac + (JeAll + MrDepth_MrSpac)) + ((Fr * hm_B) + (JeAll / ((hm_B * TauStar) + MrDepth_MrSpac)))) +
	203	-19.52	0.428	**0.269**	0.2582	0.5023	0.1327	ScourRed = (d90_hm / ((((MrDepth_MrSpac + (1.1 + Fr)) + Fr) + (Fr / (sigma + (Re * MrDepth_MrSpac))) + (Fr / (sigma + (Re *
	204	-1.766	0.213	**0.262**	0.2691	0.5235	0.1401	ScourRed = (d90_hm / ((FrStar + (JeAll / ((hm_B * (MrDepth_MrSpac + d90_hm)) + MrDepth_MrSpac)))) + MrDepth_MrSpac))
	205	-6.469	0.362	**0.256**	0.2553	0.468	0.1269	ScourRed = (d90_hm / (((JeAll + MrDepth_MrSpac) + JeAll) + (Fr + ((MrDepth_MrSpac + (JeAll / (((JeAll + JeAll) +
	206	-14.38	0.586	**0.251**	0.2516	0.5244	0.1386	ScourRed = (d90_hm / ((d90_hm / ((MrDepth_MrSpac + vsatr_v) + MrDepth_MrSpac)) + ((MrDepth_MrSpac + (FrStar +
	207	-1.796	0.213	**0.250**	0.2621	0.5152	0.1361	ScourRed = (d90_hm / (((JeAll / ((d90_hm * hm_B) + MrDepth_MrSpac)) + (FrStar + MrDepth_MrSpac)) + (JeAll / (ReStar + Re) +

Target	ID	Slope	Intercep	r2	RMS	CoD	Fit p no	Hypothesis 2
ScourRed	208	3.186	-0.680	**0.344**	0.2253	0.5541	0.1483	ScourRed = (hm_B * (Fr + (JeAll * (((hm / dm) / (MrSpac / hm)) + (MrSpac / hm)))))
	209	3.088	-0.785	**0.330**	0.2287	0.5459	0.1501	ScourRed = ((0.2 * (JeAll + (JeAll * (MrSpac / hm)) + MrDepth_MrSpac))) + hm_B)
	210	-3.782	0.112	**0.320**	0.2511	0.5289	0.1454	ScourRed = (d90_hm / (((FrStar + (((MrSpac / Rh) * (d90_hm * d90_hm)) + MrDepth_MrSpac)) + hm_B) * FrD))
	211	-6.607	0.346	**0.311**	0.264	0.524	0.1462	ScourRed = (d90_hm / ((Fr + (MrDepth_MrSpac + hm_B)) + ((dm / hm) * ((hm_B * MrSpac) / hm))))
	212	-7.669	0.366	**0.276**	0.2533	0.5089	0.1468	ScourRed = (d90_hm / (hm_B + (vstar_v + ((MrSpac * (Fr / (MrSpac + Rc)) + (MrDepth_MrSpac + Fr)))))
	213	-7.669	0.366	**0.276**	0.2571	0.5142	0.1458	ScourRed = (d90_hm / (hm_B + (vstar_v + ((MrSpac * (Fr / (MrSpac + Rc)) + (MrDepth_MrSpac + Fr))))
	214	-34401	0.270	**0.257**	0.278	0.5122	0.1338	ScourRed = (((d90_hm + TauStar) / (d90_hm + Fr) + Re)) / (Fr + (MrDepth_MrSpac + (d90_hm + ((((d90_hm / Fr) + hm_B) / Rc) *
	215	-2.284	0.151	**0.239**	0.5903	0.5064	0.1392	ScourRed = (d90_hm / MrDepth_MrSpac + ((FrD + (MrSpac / Rc)) * FrStar)))

Table 12.4: Results of the computation of scour depth reduction obtained with GPKernel
The data set contained all tests (without Peter)

Communications du Laboratoire de constructions hydrauliques
Ecole Polytechnique Fédérale de Lausanne
Editeur: Prof. Dr A. Schleiss

ÉCOLE POLYTECHNIQUE
FÉDÉRALE DE LAUSANNE

Prof. Dr A. Schleiss
Laboratoire de constructions hydrauliques - LCH
EPFL, CH-1015 Lausanne
http://lchwww.epfl.ch
e-mail: secretariat.lch@epfl.ch